NMR Structural Aspects in Biological Systems: Analysis in Leishmaniasis, Tuberculosis and Meningitis

THESIS

Submitted in partial fulfilment
of the requirements for the degree of
DOCTOR OF PHILOSOPHY

By

SUBRAMANIAN A.R.

Under the Supervision of
Dr. Raja Roy, FNASc.

BIRLA INSTITUTE OF TECHNOLOGY AND SCIENCE
PILANI (RAJASTHAN) INDIA

2006

NMR Structural Aspects in Biological Systems: Analysis in Leishmaniasis, Tuberculosis and Meningitis

THESIS

Submitted in partial fulfilment
of the requirements for the degree of
DOCTOR OF PHILOSOPHY

By

SUBRAMANIAN A.R.

Under the Supervision of
Dr. Raja Roy, FNASc.

BIRLA INSTITUTE OF TECHNOLOGY AND SCIENCE
PILANI (RAJASTHAN) INDIA

2006

"Thou hast shown me the way
And made everything possible…"

BIRLA INSTITUTE OF TECHNOLOGY AND SCIENCE
PILANI (RAJASTHAN) INDIA

CERTIFICATE

This is to certify that the thesis entitled "**NMR Structural Aspects in Biological Systems: Analysis in Leishmaniasis, Tuberculosis and Meningitis**" submitted by **SUBRAMANIAN A.R.**, ID No. **1998PHXF006** for award of Ph.D. Degree of the Institute, embodies original work done by him under my supervision.

Signature in full of the Supervisor

Date:

_____

Dr. RAJA ROY, FNASc.
Scientist E-II
NMR Facility, Division of SAIF
Central Drug Research Institute
Lucknow (Uttar Pradesh) India

Acknowledgements

I wish to express my sincere gratitude to my supervisor & mentor Dr. Raja Roy, who introduced me to the fascinating world of NMR, for being a source of inspiration and ensuring the completion of this thesis work. The work wouldn't have reached its present shape without his active involvement, constant motivation and problem-solving approach. Most importantly, he has been by my side whenever I despaired and deviated from the track. It has been a very fulfilling journey under his guidance. I am really thankful to him for the kind of patience he showered on me, and also for giving me complete freedom to execute things in my own way and at my own pace, and this certainly enabled me to balance myself with my research work and personal life, as well as my involvement as a PS faculty. Words won't be sufficient to express my indebtedness to him, and such has been his grandeur and magnetism!

I am extremely thankful to Prof. S. Venkateswaran, Vice Chancellor, BITS, and Prof. L.K. Maheshwari, Pro Vice Chancellor and Director, BITS Pilani for giving me an opportunity to carry out the research work at a place of my choice. I wish to express my sincere gratitude to Dr. C.M. Gupta, Director, CDRI Lucknow for permitting me to do this thesis work at CDRI.

My sincere thanks are due to Prof. V.S. Rao, Deputy Director & Dean, Practice School Division, BITS Pilani for allowing me to carry out this work at CDRI through the off-campus program of BITS Pilani, and for his interest and continued moral support during this thesis work. I am highly grateful to Dr. K.P. Madhusudanan, Scientist G & Head, Division of SAIF, CDRI Lucknow for his constant enquiries and encouragement during the course of this thesis work.

I take this opportunity to specially thank Prof. Ravi Prakash, Dean, Research & Consultancy Division, BITS Pilani, Prof. R.N. Saha, Dean, FD-III, BITS Pilani, Prof. B.R. Natarajan, Dean, Distance Learning Programs Division, BITS Pilani and Prof. R. Mahesh, Group Leader, Pharmacy Group, BITS Pilani for their constant encouragement and support.

I would like to thank Dr. Zaka Imam, Head, TIILP Division, CDRI Lucknow and Dr. R.C. Tripathi, Scientist, TIILP Division for their kind support. I express my gratitude to Er. K.K. Gupta, former Head, RPBD Division, ITRC Lucknow and Shri. Bhaskar Bhattacharji, Head, RPBD Division, ITRC Lucknow for their kind support and encouragement during this work.

It has been the kind blessings, encouragement and prayers of my beloved parents that enabled me to see the completion of this thesis work, and it's indeed their long awaited dream…

I am highly grateful to my ex-mentor Dr. P. Srinivas for being so benevolent to me and motivating me with his inspiring words. He has always been there whenever I required his counseling, and his long e-mails worked wonders for me! I also wish to take this opportunity to pay reverence to (late) Prof. P. Parimoo for his guidance and kind support.

I wish to sincerely thank Dr. S.K. Mandal, Dr. Mukesh Srivastava, Dr. Anjali Nigam, Dr. U.K. Singha, Dr. Mukul Mittal, Dr. Amogh Sahasrabuddhe, Dr. R.K. Gupta and Dr. Deepak Rai for all their kind help, encouragement and support during various stages of this work. I also wish to express my sincere gratitude to Dr. Neeraj Sinha, for his kind advice, hospitality and moral support during the course of this work.

Special thanks are due to Dr. B.S. Joshi and Dr. Rajesh Grover for their kind suggestions and help during this thesis work. I profoundly thank Mr. Abhijeet Deb Roy for being there during the times of crisis and whenever I required him. The friendliness of my lab colleagues deserves a special mention, and I wish to thank Ms. Aparna Anand and Mrs. Ankita Pandey Trivedi for all their help and support. Words are insufficient to express my gratitude to Mr. Abhishek Gupta for actively taking part in the MENEXSYS development, and for sparing his precious time for a little over two years! I also would like to thank Mr. Swapnil Saxena for his participation in the expert system development during this thesis work.

My special regards and thanks to Mrs. Madhurina Roy, for her kind hospitality and good wishes during the course of this research work.

I would like to specially thank Mrs. Geetha Rajagopal for her love and support, and for constantly motivating me to stay on track throughout this thesis work.

I wish to thank Dr. K.R. Babu, Dr. W. Haq, Dr. Anil Balapure, Dr. Gautam Palit, Dr. Sanjay Batra, Dr. Atul Kumar, Dr. A.K. Shaw, Dr. S.B. Katti, Dr. Uday Bandyopadhyay, Dr. Utpal Roy, Dr. G.A. Nagana Gowda, Dr. Varsha Sinha, Dr. Tushar Srivastava, Dr. Madhushree Bhattacharya, Dr. Chitra Agarwal, Dr. B.B.L. Srivastava, Dr. Morris Waskar, Dr. T. Srinivas, Dr. S.A.V. Raghavan, Dr. K. Prakash and Dr. Kshipra Mittal for their concern and help in various aspects, both personally and professionally.

I take this opportunity to express my thanks to all PS Division members and the teaching staff of Pharmacy Group, BITS Pilani for their kind cooperation. Thanks are also due to Dr. Sanjay Pohekar, Research & Consultancy Division, BITS Pilani for his kind help and suggestions. I also wish to thank Mr. Sitaram Singh for his help and kind enquiries during the course of this work.

Special thanks are also due to all the members of the SAIF Division, CDRI Lucknow, especially Mr. Harsh Gauniyal, Mr. Ashok Pande, Mr. R.K. Verma, Mr. Sandeep Sengupta, Mrs. Krishna Kapoor, Mr. Edward Samson, (late) Mr. B.B.P. Srivastava, Mr. Sunil Arnold Singh and Mr. A.L. Vishwakarma for their wonderful company, unwavering support and kind suggestions. I would like to express my thanks to Mr. G.R. Bhatt, Mr. R.K. Purshottam, Mr. Rakesh Khanna, Mr. Sunil Verma, Mr. V.K. Kanal, Mr. Radhey Krishna and Mrs. V. Madhwar for their kind enquiries during the course of this thesis work. I also wish to thank Mr. Shrawan Kumar for his ever-readiness to offer a helping hand whenever I required during this research work.

I fall short of words to express my heartfelt gratitude to Mr. Karthikeyan Ramaswamy for being there whenever I required him and the timely help rendered in various aspects. Special thanks are also due to Mr. Krishnan Sampath for his support and encouragement. Words of gratitude certainly go to Ashish, Jadesh, Omkar and Somashekar of CBMR, SGPGIMS, Lucknow for their good wishes and help during the times of need. I also wish to thank Pankaj, Harvinder, Sathish, Ameen, Mustafa, Ashok, Amudan, Auinash, Sayee, Amrita, KVG, Pushpa, Manikandan, Malavika, Shobana, Bhaskar, Abbhi, Bharathi, Sriram, Vasu, Harish, Kripa, Subodh, Jegan, Nirupama, Ajay, Rags, Srividya, Saiprasanna, Sowmya, PVK, Leela, Kumaran and Eswar for all their concern, good wishes and wonderful company at Lucknow.

My special regards and thanks are due to my sisters and brother and their family, for all their kind encouragement, support and prayers.

Many more have helped me in this endeavor and I would like to thank them all with a due apology for not being able to accommodate their names.

Subramanian

Table of Contents

Page No.

Acknowledgements i
List of Symbols and Abbreviations/Notations vii

Chapter 1: Introduction to NMR

1. Brief History of Nuclear Magnetic Resonance 1
   1.1. Discovery of Nuclear Magnetic Resonance 1
   1.2. Evolution of Modern NMR Experiments 5
   1.3. High-resolution NMR in Solids: Development of Magic Angle Sample Spinning 8
   1.4. Development of TROSY in NMR 10
   1.5. Development of Cryoprobe for Sensitivity Enhancement in NMR 11
   1.6. Development of NMR Imaging (MRI) 11

2. Essential Concepts in Modern FT-NMR Spectroscopic Techniques 17
   2.1. Nuclear Spin and Splitting of Energy Levels in a Magnetic Field 17
   2.2. Experimental Aspects of NMR 22
   2.3. Phase Cycling in NMR 27
   2.4. Coherence Order, Coherence Transfer Pathways and Gradient Pulses in NMR 29
   2.5. Relaxation Processes 30
   2.6. Two-dimensional NMR Experiments 31

   References 36

Chapter 2: Review of Literature

1. Nuclear Magnetic Resonance in Pharmaceutical Sciences 38
   1.1. Application in Drug Discovery: Drug Design and Drug Screening 38
   1.2. Application in Pharmaceutical Analysis 42

2. Nuclear Magnetic Resonance in Biochemical Sciences 45
   2.1. Application in Biotechnology 45
   2.2. Application in Parasitology: Cellular Metabolism 48

3. Nuclear Magnetic Resonance in Biomedical Sciences 51
   3.1. Application in Medicine: Magnetic Resonance Imaging 51
   3.2. Application in the Analysis of Body Fluids and Tissue Extracts 56

4. Nuclear Magnetic Resonance in Metabonomics 60
   4.1. Application in Toxicology 63

   References 67

Chapter 3: NMR Structural Aspects in Leishmaniasis

1. Introduction 76
   1.1. Incidence of Leishmaniasis 77
   1.2. Characterization of Amastigotes and Promastigotes of *L. donovani* 78
   1.3. Problem of Drug Resistance in Leishmaniasis 79

Contents

Page No.

2. Statement of Problem 81

3. Materials and Methods 82
   3.1. Chemicals 82
   3.2. Parasite Strains 83
   3.3. Determination of Intracellular Metabolites by ^{1}H- and ^{31}P-NMR Spectroscopy 83
      3.3.1. Preparation of Neutralized PCA Extracts of the Promastigotes 83
      3.3.2. NMR Experiments for the Neutralized Promastigote PCA Extracts 83
   3.4. NMR Experiments on Live Dd8 Promastigotes 85

4. Results 87
   4.1. ^{1}H NMR Studies for the Neutralized Promastigote PCA Extracts 87
   4.2. ^{31}P NMR Study for the Neutralized Promastigote PCA Extract of the Dd8 Strain 88
   4.3. NMR Studies on Live Dd8 Promastigotes 89

5. Discussion 91
   5.1. ^{1}H and ^{31}P NMR Studies on Neutralized Promastigote PCA Extracts 91
   5.2. NMR Studies on Live Dd8 Promastigotes 95

6. Conclusions 97

7. Future Scope of the Work 98

References 99

Chapter 4: NMR Structural Aspects in Tuberculosis

1. Introduction 104
   1.1. Incidence of Tuberculosis 105
   1.2. Pathophysiology and Clinical Manifestations of Tuberculosis 106
   1.3. Diagnosis of Tuberculosis 108
      1.3.1. Active Disease 108
      1.3.2. Latent Infection 109
   1.4. Treatment of Tuberculosis 109
   1.5. Intracranial Tuberculomas due to *M. tuberculosis* 111

2. Statement of Problem 112

3. Materials and Methods 114
   3.1. Chemicals 114
   3.2. Extraction of Lipids from Tuberculoma Tissues 114
   3.3. Thin-layer Chromatography (TLC) of Tuberculoma Lipid Extracts 115
   3.4. High-performance Liquid Chromatography (HPLC) of Tuberculoma Lipid Extracts 115
   3.5. High-resolution NMR Spectroscopy 115

4. Results 117
   4.1. Chromatographic Analyses of Tuberculoma Lipid Extracts 117
   4.2. NMR Spectroscopic Identification of the Lipid Structural Components 118

5. Discussion 122
   5.1. NMR Spectroscopic Observations of the Lipid Structural Assignments 122
   5.2. NMR Assignments as Diagnostic Markers of Tuberculoma 126

6. Conclusions 130

Contents

Page No.

7. Future Scope of the Work 131

References 132

Chapter 5: NMR Structural Aspects in Meningitis

1. Introduction 138
   1.1. Incidence of Bacterial Meningitis 140
   1.2. Incidence of Tuberculous Meningitis 142
   1.3. Incidence of Viral Meningitis 144
   1.4. Diagnosis of Bacterial Meningitis in Children 146
   1.5. Diagnosis of Tuberculous Meningitis in Children 147
   1.6. Diagnosis of Viral Meningitis in Children 149

2. Statement of Problem 150

3. Materials and Methods 153
   3.1. Chemicals 153
   3.2. Cerebrospinal Fluid (CSF) 153
   3.3. NMR Experiments and Resonance Assignments 154
   3.4. Statistical Analysis 156
   3.5. Development of the Expert System MENEXSYS 157

4. Results 157
   4.1. NMR Spectroscopic Findings and Clinical Observations 157
   4.2. Multivariate Analysis 161

5. Discussion 165
   5.1. NMR Spectroscopic Findings and Clinical Observations 165
   5.2. Multivariate Analysis 168
   5.3. Operational Features of MENEXSYS 169

6. Conclusions 170

7. Future Scope of the Work 170

References 171

Summary 178

Appendices

Appendix I: MENEXSYS Modules 187
Appendix II: List of Publications and Presentations 194
Appendix III: Brief Biography of the Candidate and the Supervisor 197

List of Symbols and Abbreviations/Notations:

ν	:	Frequency of nuclear precession
μ	:	Magnetic moment
ΔE	:	Difference in energy between nuclear-spin populations
μl	:	Microliter
Δ^n	:	Di-allylic methylenes
ω_o	:	Larmor frequency
μs	:	Microsecond
^{13}C	:	Carbon-13
^{15}N	:	Nitrogen-15
18:1(n-9)	:	Oleic acid
18:2(n-6)	:	Linoleic acid
^{19}F	:	Fluorine-19
1D	:	One-dimensional
^{1}H	:	Proton
20:4(n-6)	:	Arachidonic acid
^{23}Na	:	Sodium-23
2D	:	Two-dimensional
2DG	:	2-Deoxy glucose
^{31}P	:	Phosphorous-31
^{39}K	:	Potassium-39
3D	:	Three-dimensional
5-FU	:	5-Fluorouracil
^{7}Li	:	Lithium-7
ADP	:	Adenosine diphosphate
AFB	:	Acid-fast bacilli
AIDS	:	Acquired immuno-deficiency syndrome
ANOVA	:	Analysis of variance
ATP	:	Adenosine triphosphate
ATT	:	Anti-tubercular treatment
B	:	Static magnetic field
B_1	:	Oscillating magnetic field in the form of a pulse

BCG	:	Bacille Calmette-Guérin
BM	:	Bacterial meningitis
B_o	:	Static magnetic field
BOD	:	Biological oxygen demand
BOLD	:	Blood oxygenation level dependent
C	:	Centigrade
CAT	:	Computer of average transients
CD_3OD	:	Deuterated methanol
$CDCl_3$	:	Deuterated chloroform
$CHCl_3$	:	Chloroform
cmm	:	Cubic millimeter
CNS	:	Central nervous system
CO_2	:	Carbon dioxide
COLOC	:	Correlated spectroscopy via long range coupling
COSY	:	Correlated spectroscopy
CPMG	:	Carr-Purcell-Meiboom-Gill
CSF	:	Cerebrospinal fluid
CT	:	Computed tomography
CTP	:	Cytidine triphosphate
CW	:	Continuous wave
d	:	Delay
D	:	Diffusion coefficient
D	:	Dipolar coupling
d	:	Doublet
D_2O	:	Deuterium oxide
dd	:	Double-doublet
DEPT	:	Distortionless enhancement by polarization transfer
DFA	:	Discriminant function analysis
dl	:	Deciliter
DNA	:	Deoxyribonucleic acid
DOSY	:	Diffusion ordered spectroscopy
DOTS	:	Directly observed therapy short-course
EDTA	:	Ethylenediamine tetra-acetic acid

EEG	:	Electroencephalography
ELISA	:	Enzyme-linked immunosorbent assay
ELISPOT	:	Enzyme-linked immunospot
EPI	:	Echo-planar imaging
EV	:	Enterovirus
F	:	Fisher's statistic
f	:	Friction coefficient
F_1	:	Frequency dimension-1
F_2	:	Frequency dimension-2
FCS	:	Fetal calf serum
FFT	:	Fast Fourier transform
FID	:	Free induction decay
fMRI	:	Functional magnetic resonance imaging
FT	:	Fourier transform
g	:	Rotations per minute
GABA	:	γ-Amino butyric acid
GARP	:	Globally optimized alternating phase rectangular
GHz	:	Giga Hertz
GTP	:	Guanosine triphosphate
h	:	Hour
h	:	Planck's constant
H	:	Static magnetic field
H_2O	:	Water
HEPES	:	*N*-(2-hydroxyethyl)piperazine-*N*'-ethane-sulfonic acid
HETCOR	:	Heteronuclear correlation spectroscopy
HIV	:	Human immuno-deficiency virus
HMBC	:	Heteronuclear multiple bond correlation spectroscopy
HMQC	:	Heteronuclear multiple quantum correlation spectroscopy
H_o	:	Static magnetic field
HOD	:	Deuterated water
HPLC	:	High performance liquid chromatography
HR-MAS	:	High-resolution magic angle spinning
HSE	:	Herpes simplex encephalitis

HSQC	:	Heteronuclear single quantum correlation spectroscopy
HSQMBC	:	Heternuclear single quantum multiple bond correlation
HTS	:	High-throughput screening
Hz	:	Hertz
I	:	Nuclear Spin
IgG	:	Immunoglobulin-G
IgM	:	Immunoglobulin-M
IGRA	:	Interferon-γ release assay
INADEQUATE	:	Incredible natural abundance double quantum transfer experiment
INH	:	Isonicotinic acid hydrazide
IR	:	Infrared
J	:	Coupling constant
JE	:	Japanese encephalitis
k	:	Boltzmann's constant
K	:	Kelvin
k	:	Kilo
KCl	:	Potassium chloride
kDa	:	Kilo Dalton
KH_2PO_4	:	Potassium dihydrogen phosphate
L	:	Liter
LC	:	Liquid chromatography
LMW	:	Low molecular weight
LPG	:	Lipophosphoglycan
m	:	Magnetic quantum number
M	:	Molarity
m	:	Multiplet
MAS	:	Magic angle spinning
MENEXSYS	:	Meningitis expert system
MeOH-d_4	:	Deuterated methanol
Mg	:	Magnesium
mg	:	Milligram
MHz	:	Mega Hertz
min	:	Minute

ml	:	Milliliter
mm	:	Millimeter
mM	:	Millimolar
mm^3	:	Cubic millimeter
M_o	:	Net equilibrium magnetization of a spin system in B_o
MOA	:	Mode-of-action
MR	:	Magnetic resonance
MRI	:	Magnetic resonance imaging
MRS	:	Magnetic resonance spectroscopy
MS	:	Mass spectrometry
MTB	:	*Mycobacterium tuberculosis*
N	:	Normality
NAA	:	Nucleic acid amplification
NAD	:	Nicotinamide adenine dinucleotide
NDP	:	Nucleoside diphosphate
NMP	:	Nucleoside monophosphate
NMR	:	Nuclear magnetic resonance
NMRQUANT	:	Nuclear magnetic resonance based quantification
nOe	:	Nuclear Overhauser effect
NOESY	:	Nuclear Overhauser enhancement and exchange spectroscopy
NTP	:	Nucleoside triphosphate
p	:	Pulse width
p	:	Coherence order
p	:	Probability
PBS	:	Phosphate-buffer saline
PC	:	Glycerophosphatidylcholine
PCA	:	Perchloric acid
PCA	:	Principal component analysis
PCr	:	Phosphocreatine
PCR	:	Polymerase chain reaction
PEP	:	Phosphoenol pyruvate
PET	:	Positron emission tomography
PG	:	Phosphoglycan

pH	:	Hydrogen-ion concentration
P_i	:	Inorganic phosphate
PKDL	:	Post-kala-azar dermal leishmaniasis
PLA	:	Ethanolamine plasmalogen
PP_5	:	Pentapolyphosphate
PPG	:	Proteophosphoglycan
ppm	:	Parts per million
q	:	Quartet
RF	:	Radio frequency
RNA	:	Ribonucleic acid
ROESY	:	Rotating frame nuclear Overhauser effect spectroscopy
S	:	Nuclear Spin
s	:	Second
s	:	Singlet
S/N	:	Signal-to-noise ratio
SAG	:	Sodium antimony gluconate
SE	:	Standard error of mean
SPE	:	Solid-phase extraction
SW	:	Spectral width
T	:	Absolute temperature
T	:	Tesla
t	:	Triplet
t_1	:	Evolution period
T_1	:	Spin-lattice relaxation
t_2	:	Acquisition period
T_2	:	Spin-spin relaxation
TB	:	Tuberculosis
TBM	:	Tuberculous meningitis
TCA	:	Tri-carboxylic acid cycle
TDW	:	Triple distilled water
TE	:	Echo time
TGs	:	Triglycerides
TLC	:	Thin layer chromatography

TMS	:	Tetramethyl silane
TOCSY	:	Total correlation spectroscopy
tr-nOe	:	Transferred nuclear Overhauser effect
TROSY	:	Transverse relaxation optimized spectroscopy
TSP	:	Sodium-3-(trimethylsilyl)-2,2,3,3-d_4-propionate
UDP	:	Uridine diphosphate
UDPG	:	Uridine 5'-diphosphoglucose
UTP	:	Uridine triphosphate
UV	:	Ultraviolet
v/v	:	Volume-by-volume
VE	:	Viral encephalitis
VL	:	Visceral leishmaniasis
VM	:	Viral meningitis
W	:	Words
WALTZ	:	Wideband alternating phase low-power technique for zero residue splitting
WATERGATE	:	Water attenuation by gradient tailored excitation
WHO	:	World health organization
w_i	:	Discriminant function weight
x_i	:	Discriminant function variable
Z	:	Discriminant function score
ZN	:	Ziehl-Neelsen
α-GPC	:	α-Glycerophosphorylcholine
β	:	Pulse angle
γ	:	Magnetogyric ratio

Chapter 1:

Introduction to NMR

1. Brief History of Nuclear Magnetic Resonance

1.1. Discovery of Nuclear Magnetic Resonance

In the six decades since its theoretical origins, Nuclear Magnetic Resonance (NMR) spectroscopy has matured with unprecedented speed and revolutionized the manner in which chemists and biologists conduct structural analysis. NMR has contributed not only to investigations of molecular level structures and dynamics, important in modern chemistry and biology, but also in medicine in the form of Magnetic Resonance Imaging to study the macroscopic distribution of materials found in the human body. The first demonstrations of nuclear magnetic resonance came about in the 1940's when physicists were trying to obtain a more accurate measurement of the nuclear magnetic moment. In 1944 at Harvard, Edward Purcell tackled the measurement using paraffin (Purcell et al., 1946), while Felix Bloch at Stanford chose to use water (Bloch et al., 1946). Both materials contain a high concentration of hydrogen, and the proton dipole-dipole interactions in both were predicted to broaden the NMR signals by about 5 Gauss, easily observable in the magnets then available. Purcell and Block shared the first Nobel Prize associated with the discovery and first demonstration of nuclear magnetic resonance. Subsequently, the first NMR spectroscopic innovations came in the 1950's in the form of development of commercially available high-resolution NMR spectrometers, thus providing chemists with a new tool of enormous power. The NMR spectrometer (a 60 MHz instrument) was presented, in which the chemical shift values and the ^{1}H-^{1}H coupling constants were very effective in the structural confirmation of many organic compounds. As a second revolution in the NMR field, the development of reliable superconducting magnets coupled to the application of the pulse technique and its associated Fourier transform (FT) was made, which allowed enormously greater control and manipulation of the sample's magnetization. The third spectrometry innovation came in the form of Pulse Fourier Transformation NMR spectrometry (at 100 MHz) in the 1970's, and with this development, the ^{1}H and ^{13}C NMR spectra of organic compounds could be conveniently measured, even with a small amount of the samples. Proton-proton spin decoupling methods in NMR spectrometry became helpful for the structural analysis of organic compounds. With these methodological developments of NMR (Becker et al., 1996), the stereochemistry of the organic compounds could be elucidated by new techniques such as the

nuclear Overhauser effect (nOe), and the application of NMR shift-reagents. The structural information now available to the chemists and biologists, through pulse NMR, is probably greater and more readily obtained than by any other single technique.

In 1951, two of Bloch's students, Arnold and Packard, constructed an improved instrument that had a far more homogeneous electromagnet, a much smaller sample, and a very slow sweep rate. A post-doctoral Indian organic chemist at Stanford, S. Dharmatti, provided the second turning point. Curious about how an organic compound would behave in the apparatus, he prepared several samples, one of which was ethyl alcohol, and the spectrum, shown in fig. 1, revealed the potential of NMR for determining the structures of molecules. The limitations of the early instruments and the incomplete development of theory had focused much of the earliest nuclear magnetic resonance work on studies of inter-nuclear distances in solids, a rather limited class of applications. Professor H.S. Gutowsky at the University of Illinois, Urbana, was among the first to appreciate the possibilities for chemistry. Beginning in 1951, he and his students used a permanent magnet high resolution NMR apparatus to produce data on a number of compounds. His pioneering work brought high resolution NMR to the attention of theoreticians and organic chemists in a most timely way.

Fig. 1: An oscilloscope presentation of the three chemically shifted lines in ethyl alcohol, representing the first NMR spectrum recorded (Arnold et al., 1951).

NMR differs from other spectroscopic techniques in that the energy levels involved are not a property of the spin-system but depend upon imposing an external field on the nuclei. That

makes it possible to improve the sensitivity and chemical shift dispersion indefinitely. The only limits are those imposed by the technology at hand. Trying to generate more than 20000 Gauss with an iron electromagnet leads to rapidly diminishing returns. The weight, energy consumption, and cooling requirements become prohibitive for a laboratory instrument. Further progress in field strength required a new approach, and the commercial availability of superconducting niobium-zirconium wire offered a possible opportunity. The new material, unlike earlier superconductors, could remain superconducting in a strong magnetic field. Test samples of the wire suggested that it might be possible to reach fields as high as 71 k-Gauss (300 MHz for protons). The prototype magnet that was built in the year 1962 by Harry Weaver at Varian Associates reached 46980 Gauss (200 MHz for protons) and appeared capable of maintaining that field indefinitely without significant decay, given a continued supply of liquid helium (Nelson and Weaver, 1964). If protected from local magnetic noise, it appeared to be completely stable. Homogeneity was optimized with redesigned current shims wound on cylindrical forms, and reached 0.2 Hz line widths in test samples. Sensitivity was 2.7 times better than at 100 MHz. The days of the electromagnet were numbered. With superior stability, resolution, sensitivity, and chemical shift dispersion, the superconducting magnet was a winner on all counts.

In 1964, Leland Allen, then at Yale University, proposed a method of improving the sensitivity of the NMR spectrometer, based on a computer of average transients (CAT). The signal increased by the factor *n*, while the random noise increased only as the square root of *n*. Allen proposed triggering the CAT at the beginning of the spectral scan in an NMR spectrometer, using a reference peak in the spectrum. The experiment worked, giving the expected improvement in weak signals. Varian commissioned the Nicolet Company to develop a 1024 channel accessory for NMR, the C-1024. Hundreds of them were purchased by chemists struggling to overcome the problems of analyzing small or dilute samples. Installed in the CW spectrometers, the computer improved the sensitivity by about a factor of 10, a very useful gain. The significance of the C-1024 was, however, far greater than this modest improvement suggested. It ushered in a profound change in the direction of development of NMR instrumentation by demonstrating the usefulness of digitizing the NMR signals and following with digital processing. The C-1024 was soon replaced by programmable computers, which could acquire, store, process, and display the NMR data, and also control the instrument with a speed and precision far beyond the capability of a

human operator. Freed from those limitations, the development of NMR as a structural and analytical tool soon entered an exciting new period.

The probably most important breakthrough of the 1960's was the realization of an idea that had its roots in the early 1950's. In 1965, Richard Ernst performed an experiment at Varian Associates under the direction of Wes Anderson. He applied a short, intense pulse of radiofrequency (RF), exciting the nuclei over the entire spectral range. This wide-band excitation was followed by the appearance in the receiver coil of a complex waveform in the time domain (the free induction decay, FID) that contained all of the spectral information. Fourier transformation was carried out on the digitized FID by a digital computer and yielded the familiar frequency spectrum (Ernst and Anderson, 1966). Sensitivity could be enhanced by between 30- and 100-fold. The seeds for this discovery were planted by Felix Bloch, who pointed out in his first detailed paper about NMR in 1946 that a strong RF-pulse could reorient the nuclear moments, which would then precess in the absence of a perturbing field. In 1962, Wes Anderson began construction of a device, employing a rotating drum to generate a band of frequencies and to decode the signals, but by 1965 he had realized that a train of RF-pulses would be a better way to achieve the wide-band excitation that Russell Varian (who had a clear understanding of the basic concepts of Fourier Transform (FT) NMR and of its importance) had advocated. The signals could be stored using a CAT and then Fourier-transformed using a digital computer. Richard Ernst assembled the necessary equipment and achieved the first demonstration of the concept. The first FT spectrum showed more than a 10-fold gain in sensitivity compared to a CW experiment using the same data acquisition time.

But in 1965, the new method was actually much slower because digital computers were in their infancy. The contents of the memory channels of the CAT had to be transferred to punched paper tape or cards, transported to a computing center, and when time was available the data could be printed. The mainframe computer in Varian's Accounting and Management Information System's group provided overnight service for Ernst when computer time was available. In 1969, Bruker GmbH, a German company that had recently entered the NMR business, introduced an instrument that set the direction for the 1970's. Combining the three great advances of the 1960's in a single instrument, the WH-270 offered chemists more problem-solving capability than ever

before. Combining improvements in the Dewar design with a state-of-the-art minicomputer, this FT-NMR instrument offered practical solutions to problems that had been holding up progress. Its immediate success alerted chemists all over the world to the power of NMR to solve structural problems quickly and elegantly, and launched NMR into the frenzied development and amazing accomplishments of the next thirty-four years.

1.2. Evolution of Modern NMR Experiments

As the 1970's began, Bruker demonstrated that FT-NMR spectrometers could also bring chemists the benefits of observing carbon-13 nuclei. Limited in sensitivity by its low magnetic moment and % abundance, the ^{13}C nucleus is also frequently coupled to protons through one to three bonds. The resulting multiplet patterns are split into weak, overlapping peaks, further reducing sensitivity. Richard Ernst had developed a technique for broad-band decoupling of the protons from the carbons, using noise modulation of the proton irradiation frequency (Ernst, 1970), which collapsed all of the ^{13}C peak intensity into a single sharp line and also led serendipitously to a nuclear Overhauser enhancement (Anet and Bourn, 1965) of the ^{13}C signals of up to a factor of three. Combined with pulsed FT operation, larger samples, and longer acquisition times, the technique was shown to make the acquisition of ^{13}C data practical for the chemist. Once chemists recognized the value of having information from both the protons and the carbons of a molecule, ingenious experiments to take advantage of the C-H couplings proliferated.

In 1971, Jean Jeener, a Belgian, proposed an ingenious experiment for selectively extracting information from the nuclei. In ordinary one-dimensional NMR, chemical shifts and spin-spin couplings are spread out along a single line, often badly overlapped. Jeener suggested applying two separated pulses in a series of experimental increments, increasing the pulse spacing for each new increment. After Fourier transformation, the digitized spectra would be arranged as the rows of a matrix, and a second Fourier transformation would be performed on the columns. The two types of information in the resulting spectra would determine the peak positions in a two-dimensional array. In 1971, spectrometers lacked enough data storage and computing power to perform that experiment. By 1974, however, improved computers allowed Richard Ernst to put the proposal into practice (Kumar et al., 1975; Aue et al., 1975). His success started a new

direction of development in experimental and analytical NMR, which could be called the software revolution.

Of special mention are the correlation experiments that display peaks at the chemical shift coordinates of coupled nuclei, which help in the elucidation of bonding pathways within the molecular structures. These include COSY (Aue et al., 1975), HETCOR (Bax and Morris, 1981), TOCSY (Braunschweiler and Ernst, 1983), and variations of them. Chemists and biochemists could also establish molecular conformations using the map of inter-proton distances provided by the NOESY (Jeener et al., 1979) and ROESY (Bax and Davis, 1985) experiments. Richard Ernst was awarded the Nobel Prize in Chemistry in 1991 for his role in developing FT-NMR and 2D-NMR and for systematizing entire families of 2D experiments and demonstrating their usefulness. Pulse sequence development flourished and attracted other outstanding innovators, such as Ray Freeman, Ad Bax, and Muller, to single out a few. Techniques to suppress unwanted peaks and experimental artifacts arising from imperfections in the hardware were developed and refined. With their contributions, chemical problems could be solved more elegantly and with greater confidence.

During the early and mid 1970's in Europe, Oxford Instruments and Bruker both pursued higher field strength magnets. In a rapid succession, the WH-400 and WH-470 appeared in 1974 and 1976, followed by the WH-500 in 1979. In reaching those milestones, techniques for handling the niobium-tin superconducting materials were developed and refined, and the solenoid designs were modified. Most people thought that 500 MHz (11.7 T, where T is the Tesla, equal to 10^4 Gauss) would be the maximum field for the niobium-tin compound. Consequently, the 500 MHz instrument soon became the standard for biological NMR. By the middle of the 1980's the stage was set for widespread acceptance 2D-NMR as a practical experimental technique. With adequate speed and memory, and with software to set up the experiment, acquire data, and offer convenient options for processing and plotting, organic chemists began to rely on the new technique. Because the highly selective 2D experiments provided more information, the structures of more complex molecules could be worked out with confidence, their spectral data completely assigned and understood. The design of new 2D experiments benefited greatly from the realization that the use of the Product Operator Formalism of quantum mechanics made it possible

to predict the precise behavior of the spin system. That made it easier to create a desired coherence of precessing spins and to transfer that coherence from one set of spins to another. Pulse sequences could be designed to operate more efficiently and generate fewer artifacts.

In 1977, working with Aksel Bothnerby at Carnegie Mellon Institute in Pittsburgh, Josef Dadok constructed the first 600 MHz spectrometer, using a magnet wound by Intermagnetics General Corporation with a strong, flexible tape coated with a niobium-tin film. Difficulties in making resistance-free joints made it necessary to operate the magnet in a non-persistent mode, with a continuous supply of power. That resulted in high helium consumption and a need for stabilization, both problems that could be tolerated only in a developmental instrument. However, the data generated at 600 MHz created a great demand among biochemists, and in 1987, Oxford Instruments completed the development of a 600 MHz magnet operating in a persistent mode. The benefits of increased field strength were not lost on chemists, and by the end of the decade, 600 MHz instruments were beginning to appear in pharmaceutical research laboratories and in leading academic organic chemistry departments.

In 1979, Muller developed a novel 2D pulse sequence (Muller, 1979) for correlating the chemical shifts of two coupled spins: *I*, with a strong magnetic moment, and *S*, with a weak magnetic moment. The pulse sequence made it possible to obtain the data with the full sensitivity of the *I* spins. Biochemists soon adapted this experiment for indirect detection of the weak ^{15}N nuclei in proteins. After a proton 90° pulse, ^{15}N-^{1}H spin coupling evolves, followed by a ^{15}N pulse to create double quantum coherence for the amide nitrogens and the attached protons. When converted back to single quantum coherence by a second ^{15}N pulse, the proton peaks can be detected with the sensitivity characteristic of protons, but with the peak intensities modulated at the ^{15}N chemical shift frequency. Muller's experiment was later modified to detect ^{13}C chemical shifts through detection of the protons bonded directly to the carbons (Bax and Subramanian, 1986). The resulting Heteronuclear Multiple Quantum Correlation (HMQC) 2D plot gives the same data as the carbon-detected proton-carbon chemical shift correlation 2D plot (HETCOR), but with greater sensitivity. Correlations through long-range couplings could also be mapped by using the closely related Heteronuclear Multiple Bond Correlation (HMBC) pulse sequence (Bax and Summers, 1986). Those experiments have made it possible to establish all of the observable

bonding pathways between protons and ^{13}C nuclei through two or three bonds. At the end of the decade, a general approach to total structure elucidation had been applied to at least one unknown natural product. The basis of this method was to establish a known substructure, e.g., an aromatic ring, and to obtain HMQC and HMBC 2D correlations data defining all of the observable proton-carbon bonding pathways. As the assignment of the 2D peaks proceeded, one could add additional carbons and heteroatoms to the initial fragmentary structure, weeding out inconsistencies in the assignments by using all of the observed pathways through each bond. Ultimately, a unique total structure could be built up, one carbon atom at a time. Finally, a measurement of inter-proton distances, using nOe difference or NOESY data allowed the molecular conformation to be specified. While not foolproof, the method has general applicability and can be supplemented by additional data from experiments such as DEPT, COSY, TOCSY, and 2D-INADEQUATE (Bax et al., 1981), if needed.

By the early 1980s high-resolution NMR instruments and methods had advanced to the point that very complex problems in molecular structure could be solved (Williamson et al., 1985). The vast armamentarium of 2D techniques could be brought to bear on the structure elucidation of organic molecules; inorganic systems could be studied by almost every conceivable magnetic nuclide; and biopolymers, such as proteins, nucleic acids, and complex carbohydrates, could be studied in far greater detail than heretofore (Shoolery, 1995; Emsley and Feenay, 1995). Although the data acquisition becomes lengthy sometimes, the modern NMR spectrometers can be set up to perform all of the experiments unattended.

1.3. High-resolution NMR in Solids: Development of Magic Angle Sample Spinning

The interaction Hamiltonian in the liquid state corresponds to isotropic chemical shift and scalar spin-spin interactions only, resulting in sharp lines in the spectra and providing the parameters of utmost importance in structural chemistry. In the solid state, on the other hand, anisotropic interactions, such as chemical shift anisotropy, dipole-dipole interactions, and quadrupolar interactions, are all retained in addition to the isotropic chemical shifts and indirect spin-spin couplings. The chemical shift anisotropy and the dipolar and quadrupolar interactions usually dominate the spectrum, resulting in broad lines in the solid state. The information carried by the indirect spin-spin couplings and the chemical shifts is consequently ‘buried’ under the

broad and structureless spectral patterns. With the knowledge, however, that spectra in the solid state inherently contain more information than those in the liquid state, many NMR physicists continued to seek methods to obtain spectra with sharp lines, either by eliminating some of the unwanted interactions or by reducing their dominance.

It was Raymond Andrew who first thought about spinning NMR samples in order to resolve the NMR paradox concerning observed line narrowing. He and his colleagues developed a method for spinning a solid sample about an axis inclined at an angle of 54.7° to B_o (Andrew et al., 1959). When this was reported at the AMPERE Meeting in Pisa in 1960, C.J. Gorter found the removal of dipolar broadening quite remarkable and referred to it as 'magic' and the technique was henceforth called 'magic angle spinning' (MAS). Subsequently, Andrew and his co-workers demonstrated in 1962 that high-speed rotation about the 'magic' axis removes spectral broadening arising from anisotropy of chemical shifts in polycrystalline or amorphous specimens (Andrew and Eades, 1962), and they showed the effectiveness of the high speed magic angle rotation in eliminating spectral broadening arising from anisotropy of symmetric electron-coupled nuclear spin interactions.

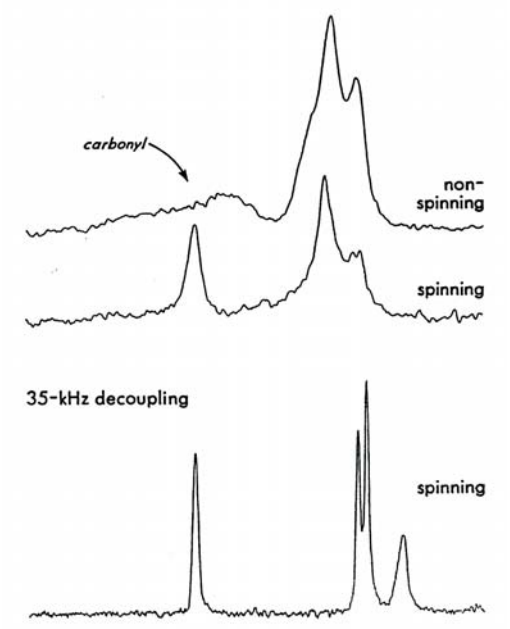

Fig. 2: Combined cross polarization and MAS applied to the ^{13}C spectrum of poly(methyl methacrylate) (Schaefer and Stejskal, 1976).

The widespread revival of MAS began largely with the work of Jacob Schaefer and Edward Stejskal, then at the Monsanto Chemical Company, who were investigating ^{13}C NMR at natural abundance in polymers with the FT methods that had become available commercially. The rapid growth of MAS experiments is the result of a variety of modifications in the rotor materials and design, and with these developments a considerable increase in spinning speeds of up to 26 kHz for a 3.5 mm rotor could be achieved. With further developments in the pulse NMR techniques involving cross polarization/high-power decoupling methods, the first ^{13}C spectra of a solid poly(methyl methacrylate) were recorded in 1975 by Jacob Schaefer and Edward Stejskal (fig. 2). Thus the advent of MAS in NMR made it possible to study the structural information of many solids (which may be poorly soluble in a solvent or not soluble at all), polymers, liquid crystals, metals, proteins, biological membranes and numerous other materials.

1.4. Development of TROSY in NMR

The development of Transverse Relaxation Optimized Spectroscopy (TROSY) technique represents one of the recent contributions that specifically address the structure determination of larger proteins, nucleic acids and their complexes using NMR. As it was theoretically predicted and proven in practice by Wuthrich and co-workers (Pervushin et al., 1997), the most efficient application of TROSY is achieved in combination with the selective or uniform deuteration of biomolecules, particularly proteins. It could be said that biomolecules with the molecular sizes exceeding 100 kDa have now become amenable for high-resolution NMR studies. Kurt Wuthrich was awarded Nobel Prize in 2002 for his pioneering contributions involving TROSY and biomolecular structure determination using NMR. Owing to its simplicity and flexibility, the TROSY method has also been integrated into many other NMR applications not necessarily targeting only larger biomolecules. An impressive range of TROSY-based NMR experiments have been developed for the detection and characterization of weak interactions, such as scalar couplings across hydrogen-bonds and residual dipolar couplings. The use of TROSY in nuclear Overhauser spectroscopy might significantly facilitate the spectral analysis by suppressing the strong diagonal peaks benefiting studies of a wide range of biomolecules. Many other TROSY applications are yet to be developed addressing the side-chain resonance assignments and various hybrid NOESY experiments for collecting structural constraints in larger proteins.

1.5. Development of Cryoprobe for Sensitivity Enhancement in NMR

The sensitivity of NMR experiment is rather low as compared to other spectroscopic techniques due to the small energy and population differences between the nuclear spin states. There are some methods by which we can enhance the sensitivity of the experiment up to a certain extent, for example: (a). increase the static magnetic field; (b). increase the sample concentration; (c). increase the sample volume and coil volume when the sample solubility is limiting; (d). reduce sample and coil volume when the amount of substance is limited; (e). increase the number of transients acquired; (f). choose the most efficient nuclear species for excitation and detection, and (g). use optimized pulse sequence for the molecular size of interest.

An entirely different and purely electronic approach for increasing NMR signal-to-noise ratio (S/N) is to reduce thermal noise within the components in the signal pathway of the NMR spectrometer. This is achieved by cooling them to extremely low temperatures. The most effective technique is to cool RF receiver coil to minimize noise directly at the site where the NMR induction signal is generated, and this principle became the mainstay behind the development of cryoprobe. The overall sensitivity gain of the cryoprobe compared to a conventional probe is about a factor of four. This substantial increase lowers the minimum sample concentration required for NMR spectroscopy by the same factor, or reduces the measurement time for a given sample by the square of this factor. Thus, it is possible to carry out the measurements on concentration limited samples that were previously inaccessible for NMR, i.e., samples from metabolic studies, proteins which tend to aggregate at higher concentration, natural products, etc.

1.6. Development of NMR Imaging (MRI)

NMR, discovered and initially developed as a technique for obtaining data of importance in physics, had been dominated from the mid-1950's by applications in chemistry, where it had revolutionized the methods used for the structure elucidation of organic molecules and biopolymers. But in the early 1970's NMR was to move into totally new areas, as methods were invented for obtaining spatial information that had immediate practical value in the fields of

biology and medicine. It was not long before a curiosity developed to stick something that was alive in the spectrometer and see what happened. Interest in living systems, however, very quickly went beyond curiosity. As NMR gained importance in biochemical investigations, there were many efforts to apply NMR as a noninvasive tool in biology.

During the 1970's, first the availability of pulse FT techniques and then the introduction of high-field superconducting magnet systems with multinuclear capability resulted in an upsurge of interest as physiological concentrations in the millimolar range became readily observable. By the early 1980's, wide-bore horizontal magnet systems that could accommodate large animals and humans, innovative probe designs such as surface coils, and localization techniques had become available, thus creating a revolution for *in vivo* NMR research. Thus, by the time it became technically feasible to perform high-resolution NMR studies on human subjects, a considerable foundation of knowledge had been built from work on perfused cells, tissues, and organs, as well as intact animal models. In September 1971, Paul Lauterbur conceived the idea of using magnetic field gradients in a more elegant way – to obtain two- or three-dimensional spatial information about the distribution of magnetic nuclei in a sample placed inside an NMR coil and thus to create a 'picture' of the object by NMR. Lauterbur proposed the use of gradients in several directions and described a way of generating two-dimensional images by back-projecting the one-dimensional 'spectra' produced from each gradient (Lauterbur, 1973). With only a standard NMR magnet available at that time, he was forced to test the method further with small objects. The first living animal to be imaged was a clam, 4 mm in diameter, which fitted into a standard 5 mm sample tube, and NMR showed the soft structure within the closed shell. By 1974, with a modified Varian DA-60 that had a larger magnet gap, he was able to display an image of the thoracic cavity of a living mouse (Lauterbur, 1974).

Following Lauterbur's works, Waldo Hinshaw developed a novel approach in which he used time-varying gradients in the x, y and z directions in which a single small volume experienced only a constant, homogeneous magnetic field. An NMR signal could be obtained only from this 'sensitive point' by taking the time integral of the FID, thus canceling out signals from time-varying fields. The sensitive point could be readily moved around the sample by varying dc currents in the three orthogonal directions and with this idea Hinshaw and his co-

workers could thus obtain a 3D image. An alternative method was proposed in 1974 by Mansfield and his co-workers, who suggested the use of a selective pulse in the presence of a field gradient to excite only a narrow band of frequencies, hence a thin slice of the sample (Garroway et al., 1974). A two-dimensional 'column' could be selected by repetition of this process, with the gradient rapidly switched to an orthogonal direction and the resultant signal read out by application of a static gradient in the third orthogonal direction. For the creation of 2D or 3D images, this method was soon supplanted by other, more efficient, techniques. In 1974 Richard Ernst realized that time-domain experiments with switched magnetic field gradients could provide an alternative to the back-projection method in obtaining NMR data across a plane or throughout a three-dimensional volume, which gave rise to the concept of 'NMR Fourier Zeugmatography' in 1975 (Kumar et al., 1975).

During the 1970's, as various methods were being tried, it became apparent that the 2D/3D FT method of Kumar et al. (1975) was an efficient procedure, but the necessity of incrementing the period for applying the phase-encoding gradient (for 2D imaging) or gradients (for 3D) could lead to distortions in the image, since inhomogeneities in the static field cause a phase error that varies as the phase-encoding time changes. By 1975, however, Mansfield and his co-workers had broadened the scope and were directing their attention to switched gradient methods with selective-pulse excitation to define a strip within the slice and obtain an image a 'line' at a time. In 1977 Mansfield published a new method, which would eventually be named 'echo-planar imaging' (EPI) (Mansfield, 1977). This technique utilized his previously developed method for slice selection but then obtained imaging information from an entire slice with one excitation pulse followed by a string of echoes that resulted from a very rapid and repeated switching of field gradients. Within a year, Mansfield and Pykett had obtained crude images of a phantom and of anatomical features (Mansfield et al., 1980).

Each of the imaging methods began with the study of inanimate objects, often tubes of water ('phantoms' in medical parlance). Fruits and vegetables became the object of study in many laboratories since their internal structures were already well known and precise details could be readily verified after completion of the NMR experiment. It was Mansfield and Maudsley who recorded the first live human NMR image, when they used a line scan to examine the internal

anatomy of a finger, an appendage small enough to be inserted into a standard NMR magnet. Serious application to most anatomical studies required a magnet capable of holding a human being. The necessary scale-up from traditional NMR sample sizes was dramatic, but the magnitude of the magnetic field was reduced correspondingly. Most early efforts were directed toward electromagnets with an air core, designed for a field of about 0.1 T (4 MHz for ^{1}H NMR). With this low-field, the image resolution was understandably poor, but major features such as the heart and lungs could be readily identified. Mansfield and his co-workers went on to record the first image of the human abdomen (Mansfield et al., 1978), while Clow and Young reported the first NMR image of a section through a human head (Clow and Young, 1978). Features such as the eyeballs and ventricles in the brain were clearly visible, and these pioneering works thus represented the beginning of commercial development of NMR imaging.

By 1980, Moore and his colleagues at Nottingham were able to demonstrate one advantage of NMR imaging over X-ray computed tomography (CT) in showing the first sagittal and coronal sections of a human head (Holland et al., 1980). They also demonstrated that NMR images could reveal a wide range of pathology in the head and commented on the dramatic new advance in neuroradiological capability with its potential impact on clinical management. Their clinical results provided examples that included tumors, aneurysms, circulatory malformations, and chronic sinus infection. By 1981, Ordidge and his co-workers had presented the first real-time moving images, which demonstrated the potential for 'freezing' cardiac motions (Ordidge et al., 1982). Mansfield and his group continued to make incremental improvements in the methods, and with the development of actively shielded gradients they were able to overcome many of the practical problems associated with rapidly switched gradients. Thus in the early 1990's EPI began to compete commercially with the more conventional methods based on spin warp FT zeugmatography. With further technological developments, Magnetic Resonance Imaging (MRI) – as NMR imaging came to be known latter, has now become widely available and is regarded as an indispensable diagnostic modality. New generations of magnets have been developed at both higher and lower magnetic fields for specific purposes. Faster scanning methods have become available and the quality of images has steadily improved. Moreover, imaging methods have been used to study function as well as anatomy, and imaging principles have been used for localized *in*

vivo NMR spectroscopy. It is for these outstanding contributions involving the development of MRI, Paul Lauterbur and Peter Mansfield shared the Nobel Prize in 2003.

To summarize, the overview of the whole processes towards the discovery and development of NMR thus illustrates the synergistic effect of the improvements that have occurred over the last sixty years. The overall developments that have happened so far for this fascinating technique of NMR spectroscopy could be summarized in the form of a flow-diagram as shown in fig. 3.

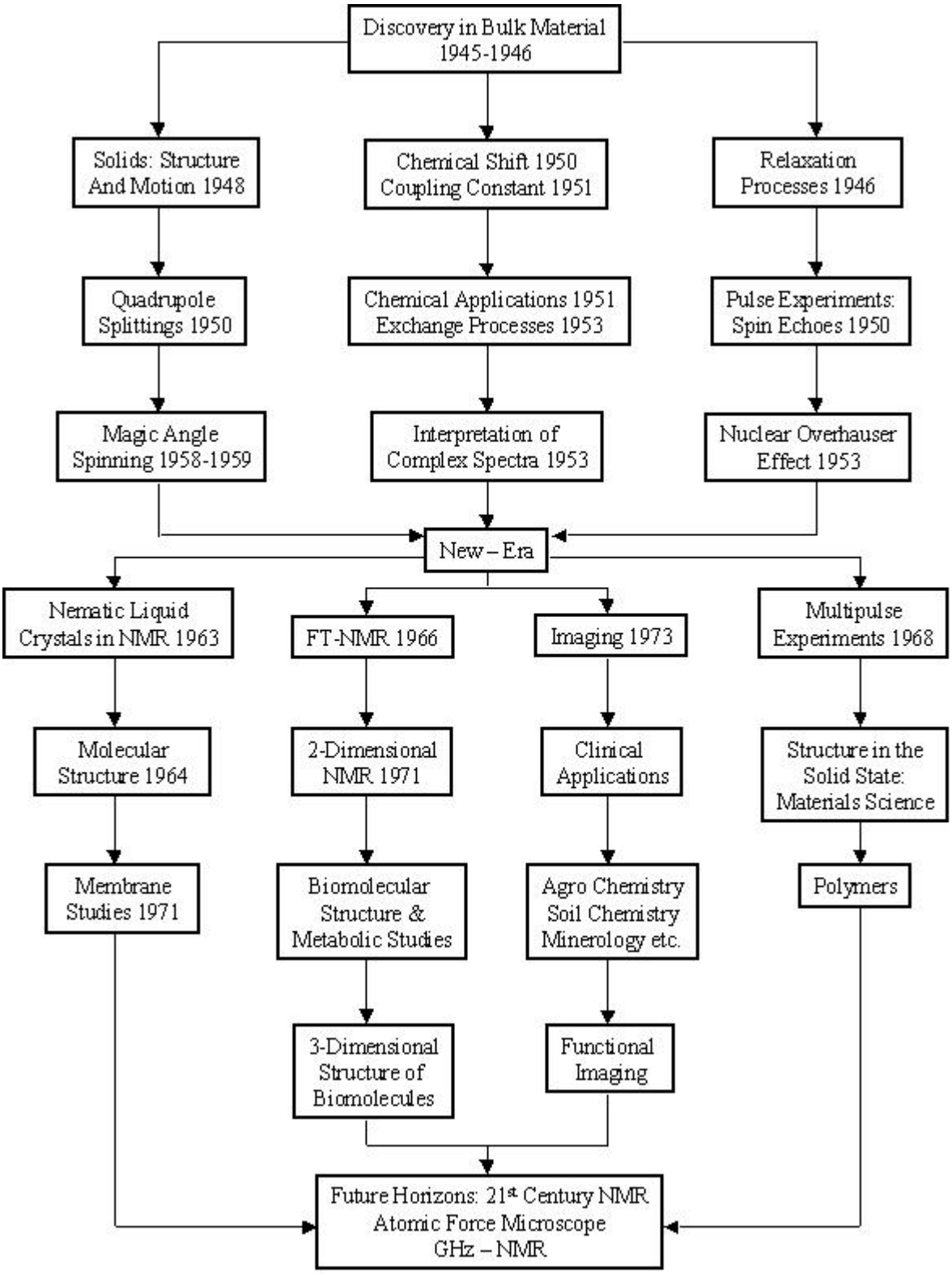

Fig. 3: Methodological developments in NMR.

2. Essential Concepts in Modern FT-NMR Spectroscopic Techniques

2.1. Nuclear Spin and Splitting of Energy Levels in a Magnetic Field

Subatomic particles (electrons, protons and neutrons) can be imagined as spinning on their axes. In many atoms (such as ^{12}C) these spins are paired against each other, such that the nucleus of the atom has no overall spin. However, in some atoms (such as ^{1}H and ^{13}C) the nucleus does possess an overall spin. The rules for determining the net spin of a nucleus are as follows:

- If the number of neutrons and the number of protons are **both even**, then the nucleus has **no spin**. Alternatively, if both the atomic number and the mass number of a nucleus are even, then the nucleus has no spin, e.g., ^{12}C, ^{16}C.

- If the number of neutrons plus the number of protons is **odd**, then the nucleus has a **half-integer spin**, i.e., 1/2, 3/2, 5/2. Alternatively, if the mass number is odd and the atomic number is either odd or even, then the nucleus has half-integer spin, e.g., ^{1}H, ^{31}P, ^{23}Na.

- If the number of neutrons and the number of protons are **both odd**, then the nucleus has an **integer spin**, i.e., 1, 2, 3. Alternatively, if the mass number is even and the atomic number is odd, then the nucleus has integer spin, e.g., ^{2}H, ^{14}N.

Since a nucleus is a charged particle in motion, it will develop a magnetic field. ^{1}H and ^{13}C have nuclear spins of 1/2 and so they behave in a similar fashion to a simple, tiny bar magnet. In the absence of a magnetic field, these are randomly oriented but when a field is applied they line up parallel to the applied field, either spin aligned or spin opposed. The more highly populated state is the lower energy spin state spin aligned situation. Two schematic representations of these arrangements are shown in fig. 4.

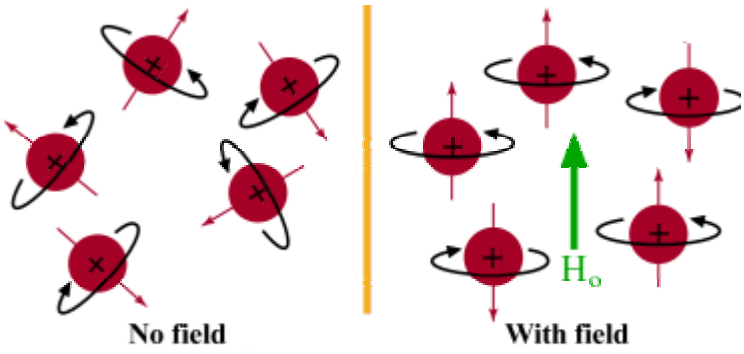

Fig. 4: Influence of the applied magnetic field on nuclear spins.

The overall spin, *I*, is important. Quantum mechanics tells us that a nucleus of spin *I* will have (2*I* + 1) possible orientations. A nucleus with spin 1/2 will have 2 possible orientations, and can align **with** or **against** the external magnetic field yielding two spin states (fig. 5). In the absence of an external magnetic field, these orientations are of equal energy. If a magnetic field is applied, then the energy levels split. Each level is given a magnetic quantum number, *m*.

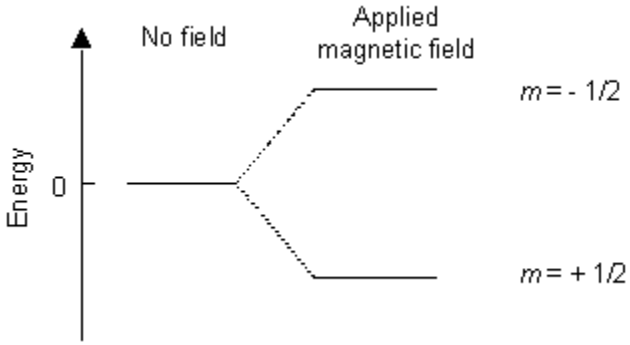

Fig. 5: Energy levels for a nucleus with spin quantum number 1/2.

Nuclei with a spin 1 have a more complex magnetic field and can have one of three orientations (1, 0, -1). In general, a nucleus will have (2*I* + 1) orientations (spin-states) with respect to the external magnetic field as shown in fig. 6.

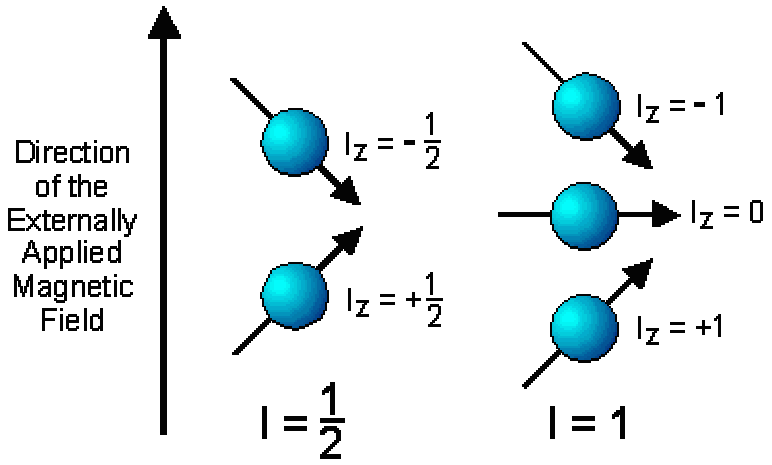

Fig. 6: Possible nuclear spin-states based on *I* in external magnetic field.

The nucleus has a positive charge and is spinning. This generates a small magnetic field. The nucleus therefore possesses a magnetic moment, μ, which is proportional to its spin, *I*.

$$\mu = \frac{\gamma I h}{2\pi}$$

The constant γ is called the *magnetogyric ratio* and is a fundamental nuclear constant. It has a different value for every nucleus and relates to the strength of the nucleus' magnetic field, and *h* is Planck's constant. The energy of a particular energy level is given by:

$$E = -\frac{\gamma h}{2\pi} m B$$

Where *B* is the strength of the magnetic field **at the nucleus**. The difference in energy between levels (the transition energy) can be found from:

$$\Delta E = \frac{\gamma h B}{2\pi}$$

This means that if the magnetic field, *B*, is increased, so is ΔE. It also means that if a nucleus has a relatively large magnetogyric ratio, then ΔE is correspondingly large. Assuming that the nucleus is spinning on its axis, and in the presence of a magnetic field this axis of rotation will *precess* around the magnetic field. The frequency of precession (ν) is termed the *Larmor frequency*, which is identical to the transition frequency and represented as:

$$\nu = \frac{\gamma H}{2\pi}$$

Another popular representation of Larmor frequency is: $\omega_o = \gamma B_o$, and it represents the energy required to induce a transition. The rotation may be clockwise or anti-clockwise, depending on the sign of the magnetogyric ratio. *H* is the strength of the externally applied magnetic field (also represented as H_o or B_o or *B*). For example, the ^{1}H atom in a magnetic field of 1.41 T has a Larmor frequency of 60 MHz.

When the nucleus is in a magnetic field, the numbers of nuclei in each spin state are described by the Boltzmann distribution:

$$\frac{N_{upper}}{N_{lower}} = e^{-\gamma_N Hh/kT}$$

The N values are the numbers of nuclei in the respective spin states, γ is the magnetogyric ratio, h is Planck's constant, H is the external magnetic field strength, k is the Boltzmann's constant, and T is the absolute temperature. In a given sample of a specific nucleus, the nuclei will be distributed throughout the various spin states available. Because the energy separation between these states is comparatively small, energy from thermal collisions is sufficient to place many nuclei into higher energy spin states. It means that the lower energy level will contain slightly more nuclei than the higher level, and it becomes possible to excite these nuclei into the higher level with electromagnetic radiation. The frequency of radiation needed is determined by the difference in energy (ΔE) between the energy levels. The energy required for the spin-flip

depends on the magnetic field strength at the nucleus. With no applied field, there is no energy difference between the spin states; but as the field increases so does the separation of energies of the spin states (fig. 7) and therefore so does the frequency required to cause the spin-flip, the phenomenon referred to as resonance.

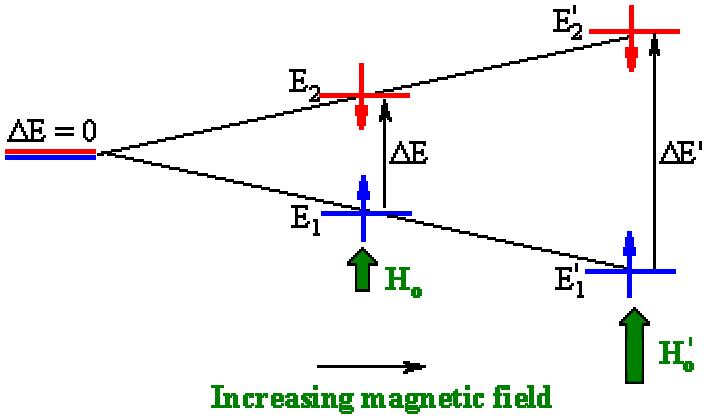

Fig. 7: Effect of applied magnetic field on ΔE of spin states.

For example, given a sample of ^{1}H nuclei in an external magnetic field of 1.41 Tesla, the ratio of populations is 0.9999382. This nearly equal population distribution has a very important consequence. In other words, the upper and lower energy spin states are almost equally populated with only a very small excess in the lower energy state. The signal intensity of any spectroscopic method depends largely on the **population difference** between the two energy levels involved. When a system is irradiated with a frequency, whose energy matches that separating the levels, transitions will be induced not only from the lower energy level to the higher, but also in the reverse direction. Upward transitions absorb energy while downward transitions release energy. The number of transitions in either direction is given by multiplying the starting level population by a probability. This probability is the same for transitions in either direction. If the energy level populations are the same, the number of transitions in either direction will also be the same. The absorption and release of energy will balance each other to zero and there will be nothing to observe. Only when the populations are not equal is there a net absorption or release of energy to observe.

The potential energy of the precessing nucleus is given by: $E = - \mu B \cos \theta$, where θ is the angle between the direction of the applied field and the axis of nuclear rotation. If energy is absorbed by the nucleus, then the angle of precession θ will change. For a nucleus of spin 1/2, absorption of radiation 'flips' the magnetic moment so that it **opposes** the applied field (the higher energy state), as shown in fig. 8.

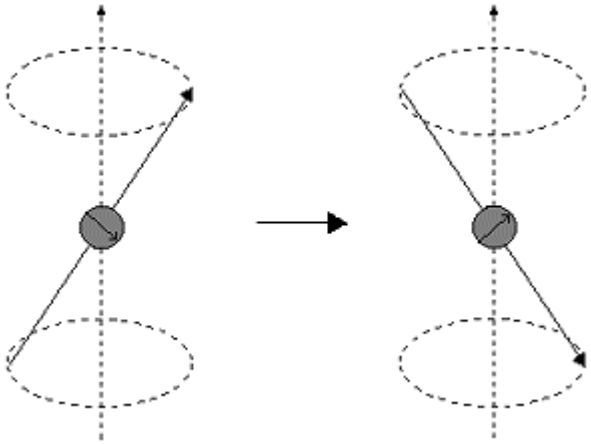

Fig. 8: Precession of a spinning nucleus after absorbing energy.

As mentioned earlier, only a small proportion of 'target' nuclei are in the lower energy state (and can absorb radiation). There is the possibility that by exciting these nuclei, the populations of the higher and lower energy levels will become equal. If this occurs, then there will be **no** further absorption of radiation. The spin system is *saturated*, meaning that the relaxation processes are given birth to, which see the nuclei return to the lower energy state.

2.2. Experimental Aspects of NMR

During an NMR experiment, electromagnetic radiation is applied to the sample with an energy exactly equivalent to the energy separation of two adjacent spin states. Some of the energy is absorbed and the alignment of one nucleus' magnetic field reorients from a lower energy to a higher energy alignment (spin transition). By sweeping the frequency, and hence the energy, of the applied electromagnetic radiation, a plot of frequency versus energy absorption can be generated, giving rise to the NMR spectrum. This simple type of experiment, where the frequency is swept across a range, is known as a continuous wave (CW) experiment. One simple variation

on this experiment is to hold the frequency of the electromagnetic radiation constant and to sweep the strength of the applied magnetic field instead. The energy separation of the spin states will increase as the external field becomes stronger. At some point, this energy separation matches the energy of the electromagnetic radiation and absorption occurs. Plotting energy absorption versus external magnetic field strength also produces the identical NMR spectrum.

Early NMR spectrometers swept the magnetic field since it was too difficult to build the very stable swept RF sources that NMR required. Technological advances have made the CW experiment obsolete and today virtually all NMR experiments are conducted using pulse methods. These methods are inherently much more sensitive, and reduce the experimental times in the order a few seconds for a single scan. In modern pulse NMR techniques, the behavior of the net magnetization, in the presence of an external magnetic field, could be explained in two ways: the first one is *Vector Approach* (Benn and Gunther, 1983) and the other is *Product Operator Formalism* (Kessler et al., 1988). The Vector Approach arises from the Bloch equation that describes the macroscopic magnetization of the sample in terms of vectors. At equilibrium the magnetization vector or simply the magnetization lies along the z-axis (fig. 9):

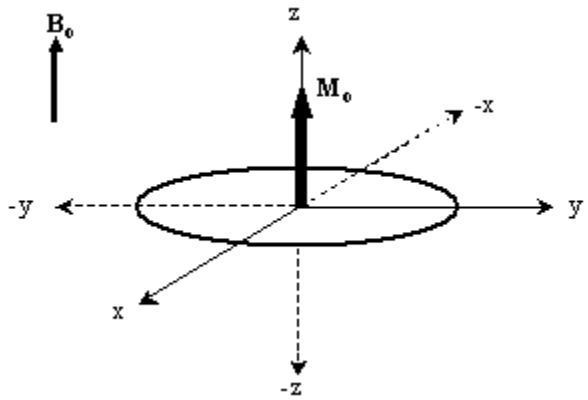

Fig. 9: Vector model depicting M_o at equilibrium.

A Pulse is a short-term high frequency oscillating magnetic field (B_1), or it is an electromagnetic wave that results from a brief application of an alternating electric current. It will be aligned in the x-y plane at 90° to the external B_o field and the magnetization. If the rotating B_1 field is turned on (in other words, a pulse), this will apply a torque to the magnetization M_o, which

will then begin to tilt. As it leaves the z-axis it will begin to precess in-phase with the B_1 field. A 90° pulse would be a rotation of the magnetization (M_o) from the z-axis to the y-axis by 90°, as shown in fig. 10.

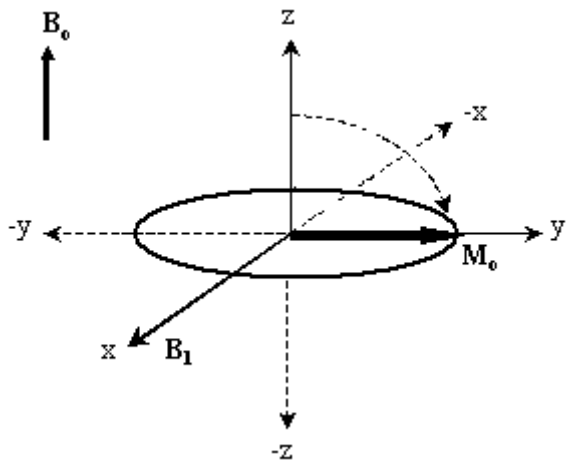

Fig. 10: Orientation of M_o after a short RF pulse.

After the B_1 field is switched off, the transverse component M_y begins to precess about the z-axis to come back to its original position. During its journey back to z-axis, the detector sees only the *difference frequency* ($\omega - \omega_o$), called as the *Chemical Shift*, where ω_o is the frequency of the rotating frame and ω is the effective frequency of a particular nuclear spin, since each chemically different nucleus has different resonance frequency. Hence, while the magnetization M_o returns back to its thermal equilibrium, two NMR parameters namely the *chemical shift* and *coupling constant* are directly observable, and the other parameter *relaxation* happens in an invisible manner. Chemical shift evolution is represented as a rotation of projected vectors on the x-y plane, as depicted in fig. 11.

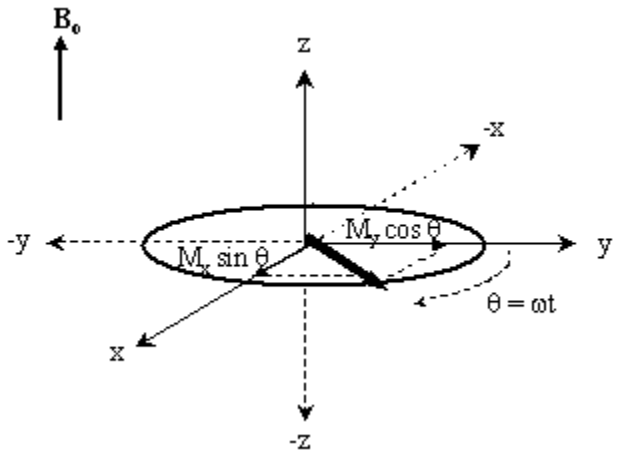

Fig. 11: Precession of M_o after a short RF pulse.

The Product Operator Formalism is a more rigorous way to describe pulse sequences than is the vector model. It is based on the quantum mechanical density matrix formalism but is much easier to use and just as general in its applicability. The great utility of the product operator formalism is its ability to deal with multiple quantum coherence, which cannot be adequately represented with the vector model. The basic idea is to describe the results of any type of evolution as a rotation via trigonometric equations. Thus, a pulse with phase *x* would be described as follows:

$$I_z \xrightarrow{\beta I_x} I_x \cos\beta - I_y \sin\beta$$

I_z refers to the equilibrium magnetization along the z-axis, β is the pulse angle, I_y is the component of the resulting magnetization in the transverse plane lying along the y-axis and I_x is the phase *x* pulse operator. The rotation of the magnetization is the opposite of that used in the vector formalism, i.e., it uses the *right hand thumb rule*. After the pulse $(\beta)_x$, the magnetization will rotate and the projection of the resultant vector in the transverse plane will be along the -y axis and have magnitude $-I_y \sin\beta$. The projection along the x-axis will be $I_x \cos\beta$, as shown in fig. 12.

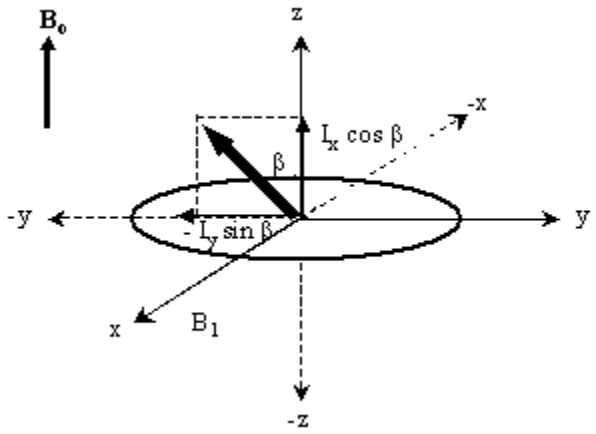

Fig. 12: Product operator formalism depicting I_z after a short RF pulse.

The pulse program is a combination of delays (d), pulses (p) and acquisition period. The delays and the type of pulse vary depending upon each NMR experiment so as to get a particular structural information. Therefore each experiment has its own pulse program like a fingerprint for that experiment. A pulse program is usually affected by the following parameters, such as:

- Spectrometer Frequency
- Pulse Width
- Acquisition Time
- Number of Points
- Sweep Width
- Relaxation Delay
- Digital Resolution

The single pulse one-dimensional (1D) FT-NMR experiment is represented in fig. 13.

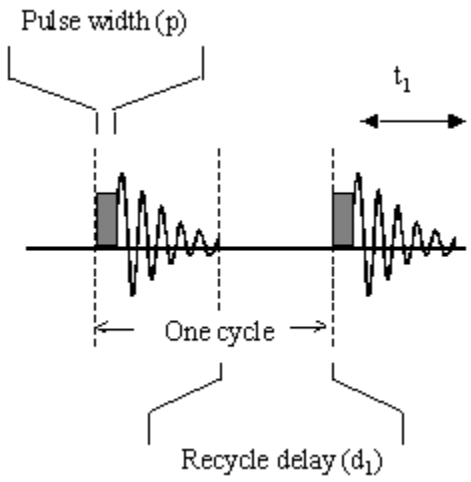

Fig. 13: A typical single pulse 1D NMR experiment.

A pulse of certain width, or in other words, a high-energy pulse is applied for a certain amount of time to the particular sample in order to flip all the spins into the x-y plane. In most modern spectrometers the 90° pulse width for a normal ^{1}H NMR experiment is about 4-10 microseconds. After giving a pulse through the sample, the magnetization vectors evolve and the acquisition of the resulting signal starts. The decaying sine wave represents the *Free Induction Decay or FID*, which is a plot of induced voltage as a function of time. The time taken to acquire the FID is usually called as the *acquisition time*. The induced voltage is digitized, i.e., the FID is taken in the form of several points along the FID curve by the computer and the *Fourier transform* of this FID (commonly referred to as FT or FFT for Fast Fourier Transform) produces the interpretable NMR spectrum, which gives intensity as a function of frequency in ppm or Hz.

2.3. Phase Cycling in NMR

Phase cycling is a method by which unwanted signals in a NMR experiment are eliminated on the basis of their phase property of the pulses. A multiple-pulse NMR experiment is designed to manipulate the spins in a certain carefully defined way so as to produce a particular spectrum. However, a given pulse sequence usually can affect the spins in several different ways and as a result the final spectrum may contain resonances other than those intended when the experiment was designed. The presence of such resonances may result in extra crowding in the spectrum, they may obscure the wanted peaks and they may also lead to ambiguities of interpretation. Those

unwanted signals might have a different phase behavior from the signal we want to sample. The unwanted signals can come from:

- Imbalance in the spectrometer hardware
- Coherent noise
- Artifacts generated by a multi-pulse experiment
- Other sources

There are two principle ways in which this selection of required signals is achieved in practice, and *Phase Cycling* is one such method, and the other is *Gradient Selection*, by which the unwanted signals in a NMR experiment are eliminated on the basis of their phase property of the pulses. *Phase Alternating Pulse Sequence* is one of the first methods for phase cycling. It consists of two transients for whom the pulse is applied on both the x-axis and –x-axis. As the magnetizations would also appear on the y-axis and –y-axis respectively, for the purpose of *Signal Averaging* the second signal must be subtracted from the first. This subtraction ensures that the NMR signals co-add while the artifacts that have not modified their phase will cancel out. The other phase cycling method is *Cyclically Ordered Phase Sequence*, which happens to be the quadrature-detection phase cycling method. During quadrature detection, two signals 90° out of phase are sampled. If there is any imbalance between the two channels, image signals would appear and to remove those artifacts the two channels need to be switched. The simplest way to do that is to acquire four transients where the phase of the pulse is varied in the order of 90° for every transient. In this way, the pulse phase cycling can be written as X, Y, -X, -Y, which tilt the magnetization along +Y, -X, -Y, -X, respectively. For encoding the phase cycling in the spectrometer, the phases are referred to as 0 1 2 3, representing the +x, +y, -x and –y-axes or 0°, 90°, 180° and 270°, respectively. The data collected from the two channels is then sent to the computer that either co-adds or subtracts, to retain the signal that is required; any artifact that does not follow this phase cycling will simply be canceled.

2.4. Coherence Order, Coherence Transfer Pathways and Gradient Pulses in NMR

Coherences can be classified by their coherence order p, which can take values 0, ±1, ±2, ±3; single quantum coherence has p = ±1, and double quantum coherence has p = ±2, and so on. At equilibrium, Z-magnetization has the same label as the zero quantum (p = 0). The receiver can only detect one of the single quantum coherences (p = -1). The other coherences can only be detected indirectly by creating them, allowing them to evolve and then retransforming them into detectable single quantum coherence. The selection of the coherence transfer pathways can be achieved by using either Phase Cycling or Gradient pulses.

A *gradient* is a *quantitative change* in some variable that occurs from one point in space to another. Such pulses are given for a brief period of time during which the magnetic field is made deliberately inhomogeneous. The first pulse creates only single quantum coherence, whereas the next pulse can create any coherence order. During a gradient pulse, the dephased coherences are apparently lost. However, the application of a subsequent pulsed field gradient can undo this dephasing and cause some of the coherences to refocus. By a careful choice of the gradient pulses within a pulse sequence, it is possible to ensure that only the coherences giving rise to the wanted signals are refocused. The dephasing and refocusing methods are based on the key concept of *coherence order* and selection of coherence transfer pathway. The crucial property of the dephasing process is that it proceeds at a different rate for different coherences. For example, the double-quantum coherence dephases twice as fast as single-quantum coherence. Thus, by applying gradient pulses of different strengths or duration it is possible to refocus coherences, which have, for example, been changed from single to double quantum by a radiofrequency pulse. Gradient pulses are introduced into the pulse sequence in such a way that only the wanted signals are observed in each experiment. Thus, in contrast to phase cycling, there is no reliance on subtraction of unwanted signals, and it can thus be expected that the level of t_1 noise will be much reduced. Again in contrast to phase cycling, no repetitions of the experiment are needed, enabling the overall duration of the experiment to be set strictly in accord with the required resolution and signal-to-noise ratio.

2.5. Relaxation Processes

During an NMR experiment, nuclear spins are promoted from a lower energy spin-state into a higher energy spin-state. This excess energy will dissipate into the surrounding environment by a variety of methods until the system is once again in its equilibrium condition. This process of shedding excess energy is called relaxation. In other words, relaxation is the process that occurs after terminating the RF pulse, in which the physical changes that were caused by the RF pulse return to the state that were in prior to the application of the pulse. There are two major relaxation processes:

- Spin - lattice (longitudinal) relaxation (T_1)
- Spin - spin (transverse) relaxation (T_2).

The return to equilibrium is an exponential process governed primarily by spin-lattice relaxation. The speed of this relaxation is described by the spin-lattice relaxation time, T_1, which is the time required for the excess energy to drop to 1/e (0.36788) of its original value (fig. 14).

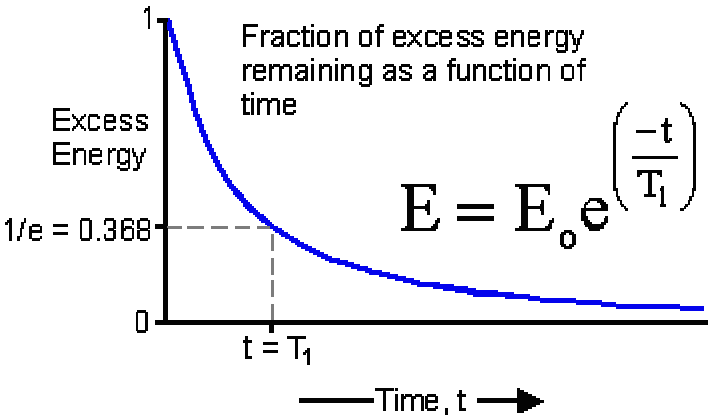

Fig. 14: Spin-lattice relaxation.

Spin-lattice relaxation (T_1) converts the excess energy into translational, rotational, and vibrational energy of the surrounding atoms and molecules (the lattice). T_1 (the average lifetime of nuclei in the higher energy state) is dependant on the magnetogyric ratio of the nucleus and the lattice (the sample in which the nuclei are held). Spin-spin relaxation (T_2) transfers the excess

energy to other magnetic nuclei in the sample. T_2 describes the interaction between neighbouring nuclei with identical precessional frequencies but differing magnetic quantum states. In this situation, a nucleus in the lower energy level will be excited, while the excited nucleus relaxes to the lower energy state. A third mechanism, quadrupolar relaxation, is very effective but only for nuclei with spin greater than 1/2. Both T_1 and T_2 affect the line widths and intensities, and correlate with the structural features of molecules. They find a role in structure elucidation, and are important in MRI techniques.

2.6. Two-dimensional NMR Experiments

Two-dimensional (2D) NMR spectroscopy has, over the past 20 years or so, made NMR spectroscopy the most powerful of the spectral analytical methods. A 2D experiment makes use of four time periods namely, preparation, evolution, mixing and detection (fig. 15).

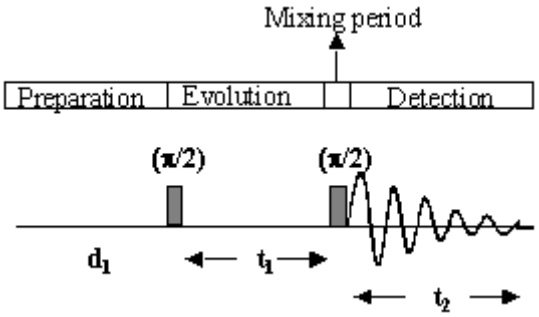

Fig. 15: A typical 2D NMR experiment.

The preparation period is necessary to bring the system to a known state, often-thermal equilibrium and to place magnetization into XY-plane frequently by application of a 90° pulse. It includes the inter-pulse delay, d_1, and the initial pulse to set up the spin system for the desired effect. The evolution period (called t_1) is the one in which there is a variable delay, d_0, which allows some part of the spin system to evolve (i.e., couplings and chemical shifts). The acquisition period (called t_2) is the time during which acquisition of the signal occurs. A series of fids are acquired, each one with a slightly longer d_0 value. The mixing period determines just what the particular 2D experiment would achieve. In some examples this period simply involves turning on or off some external perturbations (such as a decoupler) whereas, in other cases a pulse

or sequence of pulses may cause the wave functions of the spins to interact, or mix, in such a way that information from one is transferred to another. The free induction decay is then acquired as in any FT NMR experiment during the detection period (t_2). By incrementing the period t_1, the phases of the spins at the beginning of the mixing period are systematically altered, with consequences that carry over into the acquisition period. Thus each successive FID reflects the history of the spin system as a function of t_1. The NMR signal $S(t_1, t_2)$ is thus the function of two time variables and can be double Fourier transformed with respect to both t_1 and t_2, resulting in a two-dimensional frequency spectrum $S(F_1, F_2)$. In a typical homonuclear experiment, the correlation between nuclei with different chemical shifts can be displayed as off-diagonal signals, or 'cross-peaks' in a two-dimensional plot, with the F_1 and F_2 axes representing the frequencies of the same type of nuclei observed after Fourier transforming in two time-domains (fig. 16).

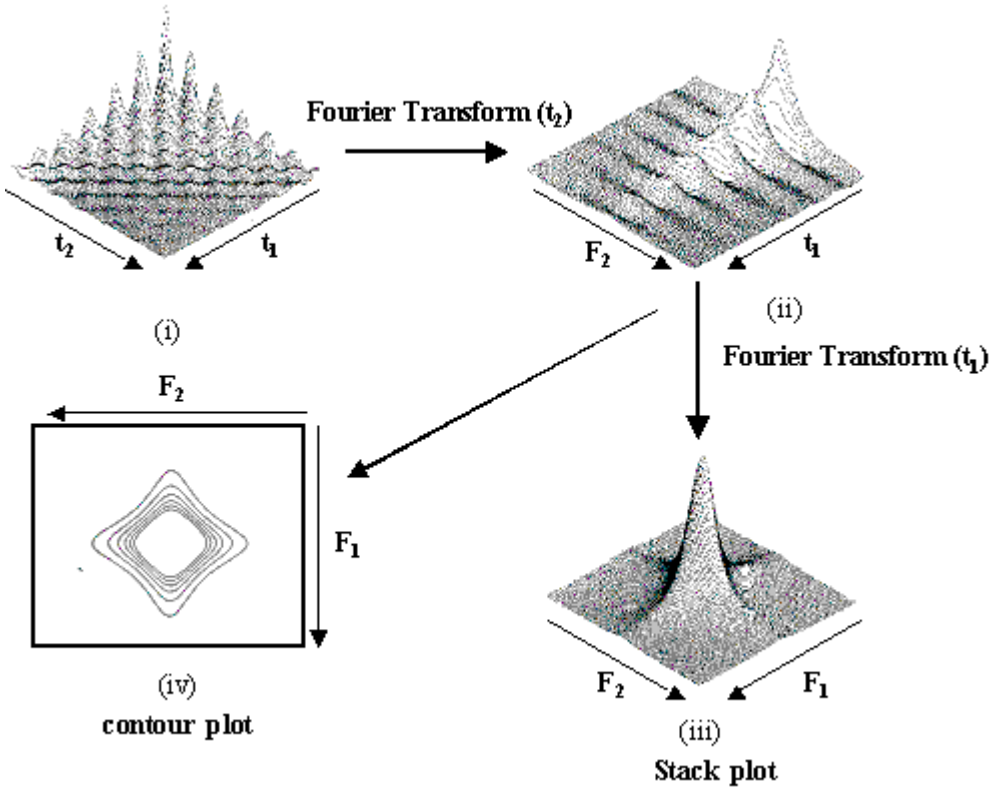

Fig. 16: Processing of data in a 2D NMR experiment.

The different NMR parameters that are usually obtained with the help of various 1D and 2D experiments are:

- **Chemical Shift** — Shift between resonance frequencies of two nuclei. Characteristic of the chemical environments.
- ***J*-Couplings** — Interaction between two nuclei via bonding electrons. Sensitive to variation in structure.
- ***D*-Couplings** — Diploar couplings through space. Contain information on internuclear distances.
- **Relaxation Times** — Define the rates at which the nuclear spins exchange energy. Useful for the study of dynamic properties, MRI, Cancer detection, state of water, blood-flow studies.
- **Quadrupole Couplings** — Present in nuclei with spin greater than 1/2. Very useful in the study of dynamic properties, e.g., Membranes and biomolecular function.

Apart from these parameters, information regarding the physical parameter *diffusion* could also be obtained with the help of NMR. Diffusion could be pictured as the motion of particles due to Brownian motion, which is closely related to molecular size as represented by the Stokes-Einstein equation:

$$D = (kT)/f$$

Where k is the Boltzmann constant, T is the temperature and f is the friction coefficient. Translational diffusion can be used to determine the size and shape of individual molecules as well as molecular aggregates. The diffusion coefficient, D, is a measure of the diffusion and can be measured by NMR. Diffusion Ordered Spectroscopy, as it is popularly called, provides an

excellent way of analyzing complex mixtures without having to physically separate out any individual molecule, and thus represents a *virtual chromatography*. The general picture of a DOSY spectrum is shown in fig. 17, which was demonstrated for a mixture containing dichlorophenol, ethanol and heptane (Viel et al., 2003).

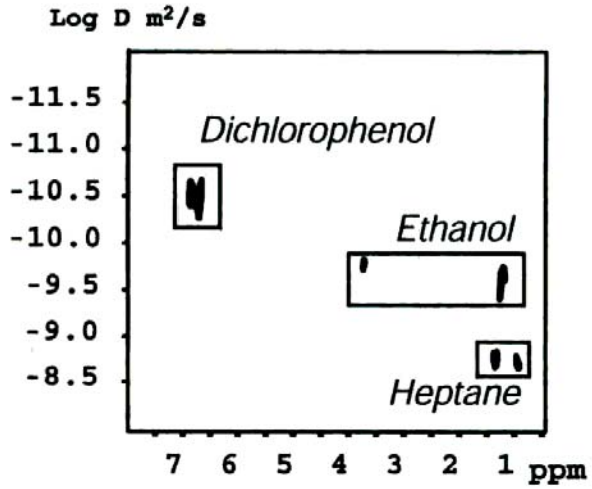

Fig. 17: DOSY spectrum of a mixture of heptane, ethanol and 3,5-dichlorophenol in silica gel.

NMR frequencies are usually presented relative to a reference frequency in dimensionless units of parts-per-million (ppm) that represent fractions of the static magnetic field. The precise resonance frequency of a nucleus is influenced by its environment, particularly the local electron density that accounts for the shielding and deshielding effects. Nuclei of the same NMR-active element in different molecules or different parts of the same molecule usually give rise to distinct NMR signals or lines. The utility of the 1D NMR methods is evident immediately upon viewing the NMR spectrum; signals arising from all magnetic, and chemically distinct, species of a NMR-active nucleus are observed simultaneously. Due to magnetic field interactions with the neighboring NMR-active nuclei, the signal for a nucleus in a particular magnetic environment may be split to form a doublet or a triplet and so on; for example, the ^{1}H-^{1}H spin-spin coupling results in a characteristic multiplicity pattern, which provides valuable information concerning the neighboring NMR-active nuclei and hence the molecular composition. Further, a full recipe can be drawn from various two-dimensional *J*-correlated and dipolar-correlated NMR experiments, which help in the complete structure elucidation of bioorganic molecules as summarized in fig. 18.

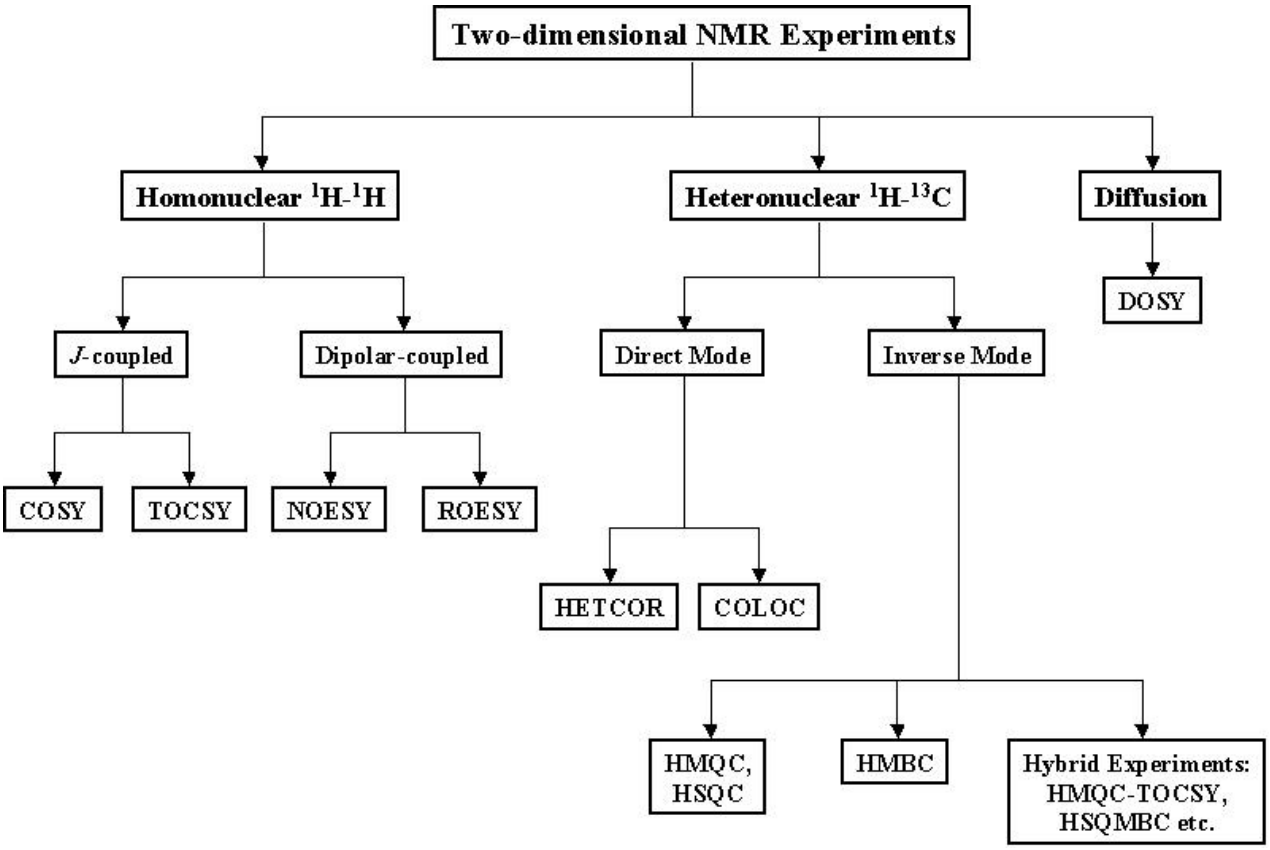

Fig. 18: Two-dimensional NMR experiments used in structure elucidation.

References

Andrew ER, Bradbury A, Eades RG (1959) *Nature* 183:1802.

Andrew ER, Eades RG (1962) *Discuss Faraday Soc* 34:38.

Anet FAL, Bourn AJR (1965) *J Am Chem Soc* 87:5270.

Arnold LT, Dharmatti SS, Packard ME (1951) *J Chem Phys* 19:507.

Aue WP, Bartholdi E, Ernst RR (1975) *J Chem Phys* 64:2229.

Bax A, Davis DG (1985) *J Magn Reson* 63:207.

Bax A, Freeman R, Frienkiel TA (1981) *J Am Chem Soc* 103:1202.

Bax A, Morris GA (1981) *J Magn Reson* 42:501.

Bax A, Subramanian S (1986) *J Magn Reson* 67:565.

Bax A, Summers MF (1986) *J Am Chem Soc* 108:2093.

Becker ED, Fisk CL, Khetrapal CL (1996) The Development of NMR. In *Encyclopaedia of NMR (Vol. 1)*. Eds, DM Grant and RK Harris. New York: John Wiley & Sons, pp 1-158.

Benn R, Gunther H (1983) *Angew Chem Int Ed Engl* 22:350.

Bloch F, Hansen WW, Packard ME (1946) *Phys Rev* 69:127.

Braunschweiler L, Ernst RR (1983) *J Magn Reson* 53:521.

Clow H, Young IR (1978) *New Scientist* 588.

Emsley JW, Feeney J (1995) *Prog Nucl Magn Reson Spectr* 28:1.

Ernst RR (1970) *J Magn Reson* 3:10.

Ernst RR, Anderson WA (1966) *Rev Sci Instrum* 37:93.

Garroway AN, Grannell PK, Mansfield P (1974) *J Phys C* 7:L457.

Holland GN, Hawkes RC, Moore WS (1980) *J Comput Assist Tomogr* 4:429.

Jeener J, Meier BH, Bachmann P, Ernst RR (1979), *J Chem Phys* 71:4546.

Kessler H, Gehrke M, Griesinger C (1988) *Angew Chem Int Ed Engl* 27:490.

Kumar A, Welti D, Ernst RR (1975) *J Magn Reson* 18:69.

Lauterbur PC (1973) *Nature* 242:190.

Lauterbur PC (1974) *Pure Appl Chem* 40:149.

Mansfield P (1977) *J Phys C* 10: L55.

Mansfield P, Morris PG, Ordidge RJ, Pykett IL, Bangert V, Coupland RE (1980) *Philos Trans R Soc London* 289:503.

Mansfield P, Pykett IL, Morris PG, Coupland RE (1978) *Br J Radiol* 51:921.

Muller L (1979) *J Am Chem Soc* 101:4481.

Nelson FA, Weaver HE (1964) *Science* 146:223.

Ordidge RJ, Mansfield P, Doyle M, Coupland RE (1982) *Radiology* 142:244.

Pervushin K, Rick R, Wider G, Wuthrich K (1997) *Proc Natl Acad Sci USA* 94:12366.

Purcell EM, Torrey HC, Pound RV (1946) *Phys Rev* 69:37.

Schaefer J, Stejskal EO (1976) *J Am Chem Soc* 98:1031.

Shoolery JN (1995) *Prog Nucl Magn Reson Spectr* 28:37.

Viel S, Ziarelli F, Caldarelli S (2003) *Proc Natl Acad Sci USA* 100:9696.

Williamson MP, Havel T, Wuthrich K (1985) *J Mol Biol* 182:195.

Chapter 2:

Review of Literature

1. Nuclear Magnetic Resonance in Pharmaceutical Sciences

1.1. Application in Drug Discovery: Drug Design and Drug Screening

In more than a half-century since its discovery, nuclear magnetic resonance (NMR) has become the single most powerful form of spectroscopy in both chemistry and structural biology. NMR, now 60 years old, has long been an invaluable analytical method in industry for verification of chemical synthesis and compound characterization. The range of molecular information accessible through NMR, however, offers a far larger horizon of applications. Of these, ligand screening by NMR has emerged as a very promising new method in drug discovery, and has recently attained heightened importance throughout the pharmaceutical industry. Its unmatched screening sensitivity, combined with the abundance of available information on the structure and nature of molecular binding, justifies the growing interest in this dynamically expanding NMR application (Diercks et al., 2001). Recent past has seen a dramatic improvement in genomic and proteomic research, numerous biophysical methods, combinatorial chemistry and screening technologies such as *in silico* screening methods. In combination with these methods, nuclear magnetic resonance spectroscopy has become a powerful tool that can provide valuable information to every step of drug development (Schwardt et al., 2003). Appropriately used, these techniques are highly complementary and synergistic, significantly enhancing the pace of the discovery process and the quality of compounds selected for further development (Muchmore and Hajduk, 2003). In recent years, advances in both methodology and hardware have broadened its range of applications and pushed back practical limitations, leading to the growing importance of NMR screening as a tool in industrial drug research (Coles et al., 2003).

The process of pre-clinical drug discovery consists of two steps: finding of initial hits (binding ligands to a medicinal relevant target, usually a protein) and lead optimization. During the structure-based lead optimization, NMR provides insight into the structural and dynamical properties of the target-ligand complex. New NMR techniques coupled in combination with high throughput screening (HTS), have lead to an efficient screening of libraries composed of small molecules (Heller and Kessler, 2001). Flow NMR techniques are now well accepted and widely used in many areas of drug discovery, and has been shown to be a potentially useful tool in

combinatorial chemistry (Keifer, 2003). Specifically, interfacing liquid chromatography with parallel NMR and mass spectrometry (LC-NMR-MS) gives comprehensive structural data on metabolites of novel drugs in development. With recent innovations to improve NMR detection limits, such as Cryo-Flow-Probes and on-line solid-phase extraction (LC-SPE-NMR), these state-of-the-art analytical platforms are widely being explored for identifying novel candidate drugs from diverse complex mixtures within a drug discovery strategy (Corcoran and Spraul, 2003). NMR screening can be applied at various points in a drug discovery program, ranging from very early in the process, when new targets can be screened long before an HTS enzymatic assay is developed, to later in the process, as in the case where no useful hits have been detected by HTS using biological assays (Fejzo et al., 2003). Moreover, screening using NMR offers significant advantages in comparison to HTS. The quantity of compounds in libraries for NMR screening may be significantly smaller than those used for HTS (Jacoby et al., 2003).

NMR methods have long been used for studying molecular interactions. One of the prime merits of NMR as a tool for lead finding in drug discovery research is its sensitivity and robustness to detect weak protein-ligand interactions (Jahnke et al., 2003). Classical examples exist in the literature that illustrate how NMR experiments could be used to characterize ligand binding to both screen for novel compounds during the process of lead generation, as well as provide structural information useful for lead optimization during the latter stages of a discovery program (Fejzo et al., 1999; Moore, 1999; Roberts, 2000). Recent improvements in gradient technology and the coupling of NMR to various chromatography methods will provide new opportunities in drug discovery to determine the receptor-bound conformations of small organic ligands (Hicks, 2001). Advances in protein NMR such as isotope-labelling techniques have extended the size limit for the structure determination and mapping of protein-ligand interactions, the extent the pathways of protein folding processes could be followed and the structures of molecules from membranes could be determined (Cooke, 1997). The drug discovery process often involves the screening of compound libraries to identify drug candidates capable of binding to target macromolecules. Besides this, it also relies on characterizing structure-activity relationships, since specific ligand-target interactions often result in important biological functions. Measuring diffusion coefficients by nuclear magnetic resonance spectroscopy is a useful way to study ligand binding (Price, 2003), because changes can be detected when a small

ligand interacts with a macromolecular target. The transferred nuclear Overhauser effect (tr-nOe) selectively influences the measured signals of binding ligands and can be used to gain insight into ligand-protein interactions. These phenomena have been studied for caffeine and L-tryptophan, which bind to human serum albumin, and the antimalarial agent trimethoprim, which interacts with dihydrofolate reductase (Lucas et al., 2003). Characterizing the binding of ligands to macromolecular receptors in solution is important to many areas of chemistry, biology, and nanobiotechnology, besides drug development. Very recent developments have considerably increased the fraction of therapeutic targets that can be tackled by NMR and significantly reduced the amount of sample required for analysis (Salvatella and Giralt, 2003). An efficient and rapid method termed as 'extraction-NMR' has recently been reported to obtain structural information on metabolites without prior separation (Gerhard et al., 2003). Recent advances in NMR spectroscopy such as affinity NMR techniques, which detect binding of a small molecule with a receptor, have been shown to be valuable tools to perform rapid screening of compounds for biological activity (Zartler et al., 2003). These NMR observable events include relaxation, chemical shift perturbations, translational diffusion, and magnetization transfer. NMR screening methods are divided into those that detect interactions by observation of either macromolecule NMR parameters or small molecule NMR parameters. In the case of macromolecules, the parameters that can be monitored are limited to chemical shifts. Additionally, the ligand-receptor interactions could be monitied by techniques such as tr-nOe, nOe pumping, reverse nOe pumping and saturation transfer experiments (Stockman and Dalvit, 2002).

The diversity and robustness of NMR based screening methods make these techniques highly attractive as tools for target-based drug discovery. Advances in NMR instrumentation and methodology have already paved the road for NMR based screening to become a high throughput technique. NMR appears to be a method of choice since it yields detailed information about the location of the binding site. In this way, ligand-based NMR screening methods can be used for protein targets of virtually any size, but are restricted in the ligand's binding affinity range, and sufficient ligand-protein dissociation rates are needed since only binding of ligands with low (millimolar) to intermediate (micromolar) affinities is detectable. Identifying a large ensemble of medium affinity ligands may not only aid in building a binding site pharmacophore model, but also may yield crucial information for overcoming tissue availability, toxicity, or even intellectual

property related problems. With the application of new cryo-cooled NMR probes, ^{15}N-^{1}H-HSQC based screening could now be considered as a high throughput method, and certainly protein and ligand concentrations can be lowered drastically and experiment times can be shortened with increased sensitivity. It remains to be seen whether ^{15}N-^{1}H-TROSY based screening techniques will prove useful for larger protein targets, especially considering the added effort needed for spectral assignment and the increased complexity due to spectral overlap. The spectral overlap will be of major concern when mixtures of up to 100 compounds are to be screened. Not only can NMR readily reveal the binding site (^{1}H-^{15}N HSQC screening) or the conformation of the bound ligand through tr-nOe, but it can also supply information that enables precise docking of the ligand to the protein's binding pocket (isotope-filtered NOESY). NMR data can therefore provide a natural connection between experimental HTS and combinatorial chemistry techniques with computational methods such as 3D-database searching, virtual screening (*in silico* docking) and structure-based ligand design (Hajduk and Burns, 2002; Vogtherr and Fiebig, 2003; Watt et al., 2003). It is hoped that this NMR-based approach in combination with other techniques would deliver leads with improved physicochemical properties as compared to leads generated from a traditional HTS program (Van Dongen et al., 2002; Wyss et al., 2002).

The field of NMR spectroscopy has grown beyond expectations from the first historic observation of nuclear magnetic resonance in 1946 by Bloch and Purcell, to the first generation of protein structures 25 years ago, to the present where NMR structures now represent 15 to 20% of those submitted to the Protein Data Bank. Since NMR is a non-invasive technique that provides a wealth of information about structure and dynamics, it is an ideal analytical method that is now being used in every step of the drug discovery and development process. Nuclear magnetic resonance techniques have become critically important in the design of new pharmaceuticals, the characterization of drug-receptor interactions and metabolite identification. Advances in solvent suppression, coherent and incoherent magnetization transfer pathway selection, isotope editing and filtering, and diffusion filtering have made it possible to examine the interactions between small molecules and proteins or nucleic acids in great detail. Multiple schemes for high-throughput lead compound identification, metabolite screening and drug disposition have been proposed and have been applied to practice. The coupling of NMR with other analytical methods, especially HPLC, combines the structural and dynamic detail available from NMR with the resolution and sensitivity

of other analytical techniques (Pochapsky and Pochapsky, 2001). Indeed, NMR is undergoing a renaissance in the pharmaceutical industry as a plethora of new applications have been developed, ranging from *in vitro* screening methods in early stage discovery to *in vivo* MRI techniques used to assess drug efficacy in clinical trials. This proves that the applications of NMR go far beyond structure determination, which has undoubtedly revolutionized the high-throughput structural characterization of protein-ligand interactions (Sem and Pellecchia, 2001). The following flow-diagram summarizes the role of NMR in various aspects of New Drug Development (fig. 1):

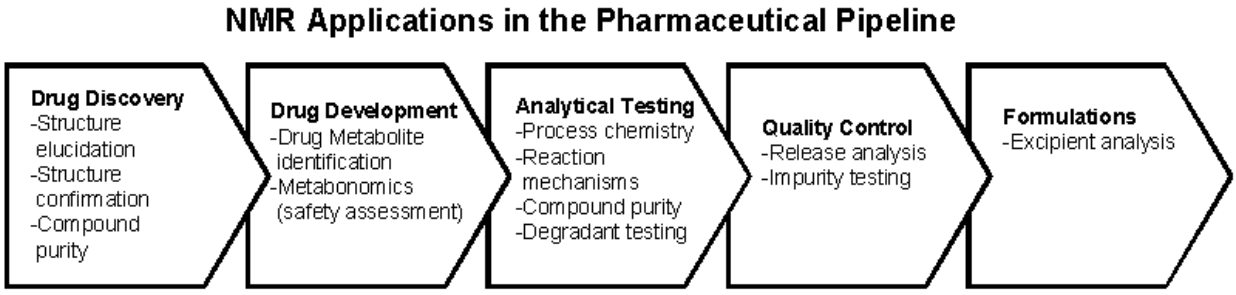

Fig. 1: NMR in Drug Development.

1.2. Application in Pharmaceutical Analysis

NMR methods have been introduced to quantitative analysis in order to determine the impurity profile of a drug, to characterize the composition of drug products, and to investigate metabolites of drugs in body fluids. For pharmaceutical technologists, solid-state measurements can provide information about polymorphism of drug powders, conformation of drugs in tablets etc. Another important MR technique, microimaging, could be used to study the dissolution of tablets (Holzgrabe et al., 1998). European pharmacopoeia mostly uses NMR spectroscopy for the identification of drugs and reagents. In the cases of tobramycin and hydrocortisone sodium phosphate, the NMR spectra replace the normally used IR spectra. Due to heavy signal overlapping, the spectra of these compounds are very complicated, and their assignment is only possible by 2D experiments. In a similar way, an increasing number of reagents, e.g., adenine, butoxycaine, aesculin etc., are identified by ^{1}H and ^{13}C NMR spectra in many national and international pharmacopoeias. Thus, the ^{1}H NMR spectra are used in the same manner as IR spectra, which can be described as a sort of pattern recognition (Holzgrabe et al., 1998). Low molecular weight (LMW) heparins (molecular weight < 8000), attracting interest in the

management of thromboembolic diseases, are obtained from different depolymerization procedures of heparin, a polysulfated glycosaminoglycan. ^{13}C NMR spectroscopy is used in international pharmacopoeias to identify LMW heparins. The possibility of exact characterization of these molecules was demonstrated by means of ^{1}H and ^{13}C NMR spectroscopy (Neville et al., 1990). ^{1}H and ^{13}C NMR could be used to characterize the polymers. In addition to a quantitative determination of polymers based on their ^{1}H NMR spectra, it has been reported that ^{13}C NMR spectra could help to understand the type of polymerization, e.g. block- or mixed-polymerization, the type and ratio of end-groups and the stereochemistry in polyethyleneglycols (tactic or atactic) (Tonelli, 1996).

The characterization of drugs in dosage forms by means of NMR spectroscopy is an interesting goal, because the identity and quantity can be determined simultaneously. It was reported that the analysis of chlorpheniramine maleate in tablets and injection, even when using only a 90 MHz spectrometer, to be as accurate as a HPLC analysis (Hanna and Lau-Cam, 1993). Thus, it was demonstrated that NMR could be a simple and reliable means of quantifying a substance no matter whether it exists in a drug or in dosage forms. Furthermore, it is possible to identify and quantify a mixture of ingredients in a dosage form using NMR (Schmedake and Welch, 1996). ^{31}P NMR spectroscopy could be used to differentiate between the various phospholipids, and is the ideal method for testing the stability of liposome containing formulations in pharmaceutical products. The amount of the different phospholipids can be calculated from their integral areas. Separation of the various phospholipids is not necessary as the phospholipids are characterized by their different resonance frequencies. Many HPLC methods for phospholipids have been developed, but chromatographic resolution and dynamics of detection are not always satisfactory. For each source of phospholipids, special standards are needed due to the different distribution of fatty acids. These standards are expensive and in some cases they are not available. The International Lecithin and Phospholipid Society has chosen the ^{31}P NMR method as the reference method, and has been tested world-wide by round robin tests in comparison to various HPLC and TLC methods (De Kock, 1993). The analysis of silicone products like simethicone can also be performed with good selectivity, using ^{1}H NMR spectroscopy. Structural data such as chain length and the viscosity, end groups (-OH, $-OCH_3$ etc.) or functional groups within the silicone chains, can be detected and quantified by means of ^{1}H NMR spectroscopy

(Holzgrabe et al., 1998). ^{19}F NMR has found a place in the analysis of dental care products, in which inorganic phosphates and fluorides are used. The combination of ^{19}F NMR spectroscopy and ^{31}P NMR spectroscopy makes it possible to simultaneously determine the content of fluoride and monofluorophosphate in presence of *ortho*-, *meta*- and pyrophosphate. The amount of monofluorophosphate could be known from the ^{31}P NMR analysis, while the fluoride content could be determined from the integral areas of the fluoride and the monofluorophosphate signals in the ^{19}F NMR spectrum (Holzgrabe et al., 1998).

There are several examples that describe the structure elucidation of drug impurities by means of NMR spectroscopy. Mostly, the impurities were collected, purified and an NMR spectrum recorded and assigned. For example, the impurity profile of production batches of fluorine-containing drugs can be characterized efficiently using ^{19}F NMR spectroscopy. This yields the number and proportions of impurities in the bulk drug to a level of approximately equal 0.1 mole % in a few minutes of NMR experiment time. This approach has been exemplified using a partially purified batch of the steroidal product fluticasone propionate, the impurities in which include a number of dimeric species. Further distinction between the monomer and dimer impurities has been achieved through high-resolution chemical shift-resolved NMR measurement of molecular diffusion coefficients on the intact mixture using ^{19}F NMR spectroscopy. The ability of NMR-based diffusion coefficient determination to distinguish between monomeric and dimeric substances was validated using a standard mixture of authentic materials containing both monomers and dimmers (Mistry et al., 1999). The NMR methods have been found to be a suitable alternative to the conventional HPLC methods for the characterization and quantification of impurities arising from synthetic processes or degradation of drugs such as dequalinium chloride (Boschetti et al., 1995), captopril (Casy and Dewar, 1994), betamethasone (Chan et al., 1996) and vitamin-E mixture (Baker and Myers, 1991). The degradation process of flurazepam dihydrochloride in different media at various temperatures had been characterized using ^{1}H-, ^{13}C- and ^{19}F NMR spectroscopy (Dawson et al., 1995). Similar studies have been described for several drugs, e.g., the alkaline hydrolysis of cefotaxime which was elucidated and the kinetic of the reaction observed by means of ^{1}H NMR spectroscopy (Vilanova et al., 1994), or the decomposition process of bispyridinium aldoximes, acetylcholine esterase reactivators, at different pH values and various temperatures (Inkmann et al., 1997), the process of photo-decomposition of

the calcium channel blocker nifedipine (Sadane and Ghogare, 1991). Some drugs are not stable in aqueous solutions and undergo equilibrium reactions, which could be observed by NMR spectroscopy. Similarly in combination with HPLC methods, ^{1}H NMR has been increasingly explored for the determination of optical purity or enantiomeric excess of an asymmetric synthesis by derivatisation with chiral (enantiomerically pure) reagents (Staubach and Buddrus, 1996). These examples impressively demonstrate the high potential of NMR spectroscopy in quantitative analysis.

2. Nuclear Magnetic Resonance in Biochemical Sciences

2.1. Application in Biotechnology

In biological research, NMR provides a means for studying crucial questions at a molecular level, including three-dimensional structures at atomic resolution, dynamics and folding. Today, NMR with biological macromolecules in solution is one of the principal experimental techniques in structural biology. Of all methods currently available for obtaining high-resolution structures of biological macromolecules, NMR is the only one that can provide this information in solution under near-physiological conditions. NMR has found its application in the areas of relevance to biotechnology, including protein engineering and protein design (Norton, 1990). A variety of NMR techniques had been developed for the comprehensive analysis of cell metabolism, which could be successfully extended for the analysis of immobilized cell bioreactors (Zupke and Foy, 1995). It was also reported that the levels of ATP and inorganic phosphate in metabolically active Chinese hamster lung fibroblasts could be monitored noninvasively by ^{31}P NMR under a variety of conditions (Knop et al., 1984). In such procedures, the cells are embedded in a matrix of agarose gel in the form of fine threads, which are then continuously perfused in a standard NMR tube. The small diameter of the thread allows rapid diffusion of metabolites and drugs into the cells. This gel-thread perfusion method had been proposed to enable routine NMR studies of cellular metabolism, besides other potential biological applications. Recently, in-cell NMR procedure has been explored to monitor the process of selective incorporation of ^{15}N in live cells (Serber et al., 2001), and this method has been proposed to have a role in monitoring protein conformations inside the living cells.

Pulsed field gradient NMR can be a valuable tool in many fields of environmental biotechnology such as biofilm, bioreactor and membrane engineering, soil and groundwater bioremediation, and wastewater treatment for investigating processes such as transport, flow, diffusivity and mass transfer processes (Humbert, 2001). Another interesting application of NMR lies in the characterization of alcoholic beverages such as beer. The beer contains a very complex mixture of nutrients that display a strongly overlapped peaks arising from several carbohydrates in the ^{1}H NMR spectrum. A principal component analysis (PCA) based approach was demonstrated to the ^{1}H NMR spectra of 50 beers differing in label and type (ale, lager, alcohol-free), to identify the spectral parameters that may provide rapid information about factors affecting beer production (Duarte et al., 2004). Moreover, it has been shown that NMR, when integrated with pattern recognition methods, has a great potential as a rapid and informative quality control tool in beer production (Duarte et al., 2002), in the detection of adulteration of orange juice with pulp wash (Le Gall et al., 2001) and to identify the fatty acid content of milk from different animal species (Andreotti et al., 2000). Another interesting application of NMR techniques in food industry is the direct characterization of juice from various fruits during their ripening stage, thus allowing a noninvasive study of the overall biochemistry of whole fruit. Liquid-state and solid-state NMR techniques were used to follow the compositional changes in mango juice and intact mango pulps (Gil et al., 2000).

The receptor gene-expression and regulation could be visualized by NMR imaging. This was demonstrated for the human transferrin receptor, wherein it was hypothesized that it might be possible to image gene transfer *in vivo* (Moore et al., 1998). Among other applications, a functionally and metabolically interesting class of cell lipid, such as a membrane lipid microdomain, was observed by ^{1}H NMR *in situ*. It was shown that observation of resonances specific to malignancy and cell death is possible, but also that of markers associated with the benign processes, such as cell activation and proliferation (Hakumaki and Kauppinen, 2000). This bears novel implications for the understanding and assessment of lipid biochemistry in the life and death of cells. In another study, ^{1}H-MRS was used to investigate the membranes of macrophages activated by γ-interferon *in vitro* and by *Listeria monocytogenes in vivo*, highlighting the usefulness of NMR in studies of immunological relevance (King et al., 1991). NMR techniques

have been explored for their unique capabilities for probing specific interactions of enzymes with substrates and substrate analogues, for characterizing the multiple conformations of the complexes such as dihydrofolate reductase (Feeney, 2000), and for measuring rates of a wide range of dynamic processes in these systems.

The relationship between organic phosphorus status of soils, soil-based microorganisms and dominant plant species of typical natural ecosystems was evaluated using ^{31}P NMR spectroscopy (Makarov et al., 2005). The development of NMR-based flow-imaging techniques to measure fluid flow in a cell-free hollow fiber bioreactor had been reported, suggesting that this non-invasive method could be used to design more efficient cell bioreactors or membrane separation devices (Hammer et al., 1990). Both NMR and MRI have found their place in the field of environmental science and engineering, pertaining to the biodegradation and biotransformation of soluble and solid organic matter, removal of nutrients and xenobiotics, fate of heavy metal ions, and transport processes in bioreactor systems (Lens and Hemminga, 1998). Further, the commercial exploitation of the fruits of recombinant DNA and cell fusion technologies has been significantly limited by the lack of fundamental metabolic information on the cell lines of interest, whether these are plant, animal, insect, or microbial cells. It has been proposed that NMR could help to provide this information and thereby improve bioreactor design and operation (Dale and Gillies, 1991).

NMR-based metabolic flux analysis using ^{13}C-labeled substrates has become an important tool in bio-metabolic engineering. It allows the detailed quantification of all intracellular fluxes in the central metabolism of a microorganism. The method has strongly evolved in recent years by the introduction of new experimental procedures, measurement techniques, and mathematical data evaluation methods (Wiechert, 2001). The main focus has been to understand the biosynthetic and energetic or redox needs of cells, and/or additional strategies in the adaptive capacity of micro-organisms to face variation in environmental conditions. The extension of ^{13}C NMR techniques to study cellular metabolism has provided valuable data supporting the occurrence, diversity and extent of carbon cycling in the carbohydrate metabolism of micro-organisms (Portais and Delort, 2002). In combination with statistical techniques such as nonlinear least squares fitting approach, the intra- and extra-cellular metabolic flux could be estimated for the cells grown on ^{13}C-labeled

substrate using NMR. In a recent study involving *Synechocystis* species, the labeling patterns of the amino acids were measured using 2D ^{1}H-^{13}C HMQC experiment, and the technique was used to investigate the central carbon metabolism (Yang et al., 2002). Further, NMR offers the possibility to map metabolites in plant tissues non-invasively using micro-imaging. Major metabolites such as sucrose and amino acids could be observed with high spatial resolution. Stable isotope tracers, such as ^{13}C-labelled metabolites can be used to measure the *in vivo* conversion rates within a metabolic network (Kockenberger, 2001).

2.2. Application in Parasitology: Cellular Metabolism

NMR investigations on parasite metabolism have not only confirmed results of investigations using traditional methods but have yielded new insights into the nature of parasite metabolism. Because of their capacity for facultative anaerobiosis and resultant accumulation of metabolic end-products, parasites are particularly suitable for NMR spectroscopic investigation. Such NMR applications should prove extremely valuable for studying parasite biochemistry and effects of anthelmintic drug action on parasite metabolism, as well as pathophysiology in the host. The potential of NMR applications in parasitology was briefly outlined, and more specific applications on parasitic protozoa, cestodes, nematodes, trematodes, and hymenopterous insect parasites were reported by using NMR and MRI investigations on the pathophysiology of the host (Thompson, 1991). Further, *in vivo* localization techniques may enable *in vivo*-*in vivo* spectroscopic studies, i.e., investigations on parasites within the host itself. NMR spectroscopy also provides unique opportunities for investigating pharmacokinetics and the effects of anthelmintics in the host at the cellular and molecular level (Thompson, 1991). The utility of NMR in understanding the parasite biochemistry and host-parasite interactions has been highlighted in several reports. Using ^{13}C and ^{2}H NMR, glucose degradation via glycolysis was demonstrated in the trypanosomatid *Crithidia fasciculate* maintained under anaerobic conditions (De Los Santos et al., 1985). ^{1}H and ^{31}P NMR was employed for studying the metabolic end-products in incubation medium of *Crithidia luciliae* (Gilroy et al., 1988). Similarly, carbohydrate metabolism and substrate cycling in *Fasciola hepatica* was reported by ^{1}H and ^{13}C NMR analysis of the end-products excreted by adult parasites into an incubation medium containing $^{13}C_1$-glucose (Matthews et al., 1986). The metabolic excretory products of *Hymenolepis diminuta* were examined by ^{13}C NMR techniques after incubation of intact adult parasites with [^{13}C]U-glucose

(Blackburn et al., 1986). The usefulness of ^{31}P NMR to examine the effects of mebendazole on the energy status of intact *Hymenolepis diminuta* perfused under hypoxic conditions was demonstrated (Thompson et al., 1987). The high-energy phosphorus metabolites of *Steinernema carpocapsae* were studied *in vivo* using flow-NMR spectroscopy (Thompson et al., 1990).

Following these lines, metabolite mapping of human filarial parasite *Brugia malayi* was carried out *in vitro* as well as *in situ* in host *Mastomys coucha* by ^{31}P NMR spectroscopy, giving a non-invasive assessment of tissue bioenergetics and phospholipid metabolism (Shukla-Dave et al., 1999). In combination with MRI techniques, the parasites could be detected by visualizing the contrast spots due to pathologic changes. Major metabolites of adult *B. malayi* observed by ^{31}P-NMR spectroscopy were of sugar phosphates, phosphomonoesters, glycerophosphorylethanolamine, glycerophosphorylcholine, phosphoenolpyruvate, inorganic phosphate, nucleoside diphosphosugar and nucleotides-mono, -di and -tri phosphates. The ^{31}P-NMR spectra of testis of *B. malayi* infected animal also indicated changes in the carbohydrate and lipid metabolism of filaria infected testis. Overall, the *in vivo* ^{31}P MRS provided a non-invasive assessment of tissue bioenergetics and phospholipid metabolism. In another study, the uptake and metabolism of a well-known glucose antimetabolite, 2-deoxy glucose (2DG) widely used in chemotherapy of cancer along with radiation, was evaluated as an antifilarial agent by ^{31}P NMR (Shukla-Dave et al., 2000). An unusually long retention time of the active metabolite of 2DG within these parasites was observed on continuous ^{31}P NMR monitoring, along with a decrease in ATP levels. Recently, to address the issue of parasitic infection in schistosomiasis, a ^{1}H NMR based metabolic profiling and multivariate pattern recognition technique has been demonstrated with a *Schistosoma mansoni* mouse-model (Wang et al., 2004a). Further, *in vivo* ^{31}P NMR spectroscopy provides unique opportunities to study the biochemistry of an organ within the intact animal in a totally non-invasive way (Brauer and Ling, 1991). ^{31}P NMR *in vivo* spectra of *Echinococcus multilocularis* cysts growing subcutaneously in *Meriones unguiculatus* showed prominent signals due to phosphomonoesters, phosphodiesters, inorganic phosphate and the phosphate groups of ATP (Novak et al., 1992). ^{1}H-NMR spectra of cyst extracts revealed that parasites grown in the abdominal cavity contained significantly less glucose but significantly more succinate, acetate, alanine and β-hydroxybutyrate.

Spin-echo MRI was employed to image the larvae of the tapeworm *Taenia crassiceps* in the mouse peritoneal cavity to develop a rapid, quantitative assay for parasite load. Since the vesicular fluid of the human parasite *Taenia solium* has a long T_2 of 600 ms, a suitable spin-echo MRI could be used to image this parasite for diagnosis of human cysticercosis (Haselgrove et al., 1987). High-field NMR imaging has the advantages of sensitivity, spatial resolution, and tissue contrasts based on longitudinal and transverse relaxations, magnetic susceptibility differences and blood flow. Highlighting these issues of NMR imaging, micro-images of the kidney and liver were recorded at 9.4 T in intact mouse, *Schistosoma mansoni*-infected mouse, and lupus nephritis in a mouse model (Kosaka et al., 2000). Besides exhibiting its potential in metabolic profiling to enhance the understanding of biological responses to parasitic infections, NMR holds promise as a basis for novel diagnostic tests with high sensitivity and specificity and for improved disease surveillance and control.

Since the NMR investigations are influenced by the spectroscopic sensitivity and natural abundance of the nuclei under study, the parasitological investigations concerning the energy metabolism often utilize enriched substrates, for example, ^{13}C-enriched glucose. This facilitates in the identification of the metabolic products in which the ^{13}C label has been incorporated, often leading to valuable information concerning the precursors and biosynthetic pathways. In case of ^{31}P NMR, under appropriate conditions, the metabolites observed reflect the absolute amount present, and ^{31}P NMR is commonly used for analysis of high-energy phosphorus metabolites and energy metabolism. The 100% natural abundance of the ^{31}P nuclei also makes it feasible to determine the intracellular pH. Since the resonance frequencies of several biological phosphates, including the inorganic phosphate (P_i), vary sharply within the physiological pH range, the chemical shift of P_i has been viewed as an indicator of pH. Coupled with various 1D ^1H-NMR and 2D NMR techniques, the metabolic end-products that accumulate in parasites could be easily detected both in *in vivo* (whole cells) and *in vitro* (cell-extracts) conditions. Despite the fact that most spectra are dominated by the proton resonance of H_2O, methods are available for suppressing or eliminating the contribution of water, and make it feasible for the *in vivo* or *in vitro* analyses, including the unique application of ^1H NMR imaging.

3. Nuclear Magnetic Resonance in Biomedical Sciences

3.1. Application in Medicine: Magnetic Resonance Imaging

In 1959, Dr. Erik Odeblad, a physician, wrote about nuclear magnetic resonance: "NMR really seems to possess extensive possibilities to help study, in a non-invasive way, many problems in biology and medicine. When instruments for NMR become more common and available at medical laboratories, we may expect direct routine clinical diagnosis with this new technique". This 1959 prediction became a reality in 1995, when examinations using MR spectroscopy (MRS) and MR imaging (MRI) have been allowing physicians to carry out routine clinical diagnoses that were previously unobtainable by other radiologic or clinical tests (Cousins, 1995).

NMR offers a powerful new probe of the body's internal anatomy and function (Bottomley, 1984). The technique utilizes a combination of static and radio frequency magnetic fields to excite a weak resonant magnetic field emission from various selected naturally abundant nuclei in the body such as hydrogen (^{1}H), phosphorus (^{31}P) and carbon (^{13}C). The emissions can be spatially encoded by application of magnetic field gradients, to enable the generation of high-resolution anatomical images, which reflect the nuclear density distribution, and/or spatial variations in the molecular level and chemical environments of the nuclei as measured by the NMR relaxation times and chemical shifts. In other words, by applying non-uniform magnetic fields across a section of the body, hydrogen nuclei in different elemental volumes in the section are tagged with different frequencies and their signals can be processed to give an image of the chosen section. In contrast to computed tomographic scanning, NMR has particularly powerful application in the imaging of soft tissues (Bradbury et al., 1983). NMR imaging modality combines the advantages of X-ray computed tomography by giving high resolution tomograms, and has become a useful clinical tool in the study of brain, spinal cord, pelvis, and has also been promising in the study of heart, kidneys, adrenals, liver, pancreas and spleen (Margulis et al., 1983).

NMR imaging techniques have found exciting new noninvasive applications in medicine by allowing imaging in any desired plane, thus offering information about physiology and metabolic processes. NMR imaging is valuable for the diagnosis of a variety of diseases and traumas since a high level of lesion and soft tissue contrast is possible in most types of pathology (Chilton and Ekstrand, 1984). Additionally, blood oxygenation level dependent (BOLD) functional magnetic resonance imaging (fMRI) has become a most widely utilized technique that makes use of the metabolic effects of brain activation (Nakada, 1997; Price et al., 2002). ^{1}H NMR relaxation time images are proving useful for the detection of a wide spectrum of disorders, whilst spatially localized ^{31}P and ^{13}C NMR chemical shift spectra measure directly the metabolic status of living tissues. *In vivo* ^{31}P NMR spectroscopy helps in the identification and quantification of the more abundant phosphate metabolites in various tissues. Changes in the levels of these metabolites and in intracellular cytoplasmic pH can be followed in various ischemic and hypoxic conditions to monitor metabolic response to stress situations and to diagnose inborn errors of metabolism (Kressel, 1983).

Due to the wide availability of MRI equipments in research laboratories and hospitals, MRS has become a serious competitor with Positron Emission Tomography (PET) to define normal body composition and its perturbation by pharmacological and pathological events (Ross and Bluml, 2001). Applications of the different MRS modalities (^{1}H, ^{31}P, ^{19}F, ^{7}Li, ^{13}C and ^{23}Na) to various neuropsychiatric disorders such as Alzheimer's disease, Schizophrenia and Affective disorders deserve a special mention (Boesch, 1999; Passe et al., 1995). It could be added that the advantage of MRI and MRS is the versatility and non-invasiveness of the techniques, which is of relevance from a statistical, economical and even the animal welfare point of view, allowing a comprehensive characterization of a diseased state and of the drug intervention. Apart from fMRI, MR has found application in imaging of the cardiovascular system and monitoring of the blood-flow. NMR angiography could be viewed as a novel concept in vascular imaging, since it is noninvasive and contrast agents are not required, and similar to vascular ultrasound, the blood flow and the arterial wall dynamics can be studied (Lanzer and Bohning, 1990). Moreover, *in vivo* oxygen concentration measurements are of crucial importance for monitoring the energetic metabolism from a physiological and pathological point of view. A tremendous amount of work is currently being done using this blood oxygen level dependent (BOLD) effect. The transverse

relaxation time (T_2) of water protons is decreased by the paramagnetism of deoxyhaemoglobin, which is inversely related to the blood oxygen concentration. The exchangeable imidazole proton of the proximal histidine of haemoglobin yields a more specific signal, which is directly related to the paramagnetism of deoxyhaemoglobin and reflects the oxygen concentration more accurately than the T_2 of water protons (Grucker, 2000). The important advantages of cardiac MRI are the large field of view (which includes extra cardiac structures), choice of slice-width and orientation, good resolution and the simultaneous evaluation of morphology, functional parameters, flow phenomena and some differentiation between tissues. Presently, MRI is indicated in problem cases, e.g., aortic aneurysm, dissecting aneurysm, constrictive pericarditis, cardiac and paracardiac tumors. Additionally, MRI also provides useful complementary information in valvular regurgitation, congenital malformations, cardiomyopathies and intracavitary thrombi (Schicha et al., 1989).

MRS has the potential to measure brain medication levels and simultaneous effects on neurochemistry. A number of studies applying MRS to the neurochemistry of schizophrenia have been reported, which encompass a range of patient populations, states of medication, anatomic regions, nuclear species, and MRS techniques (Kegeles et al., 1998). The use of ^{19}F NMR as a noninvasive probe to measure directly the pharmacokinetics of drugs at their target site(s) was illustrated by human studies with 5-fluorouracil (5-FU). This drug, and several of its metabolites, have been measured *in vivo* in animals and in patients using standard clinical MRI systems. The ^{19}F NMR studies have now been extended to other fluoropyrimidines, some of which are prodrugs of 5-FU, and other molecules where the fluorine atoms are on the ribose ring. These studies reveal information that has both scientific and clinical significance, and have a potential usefulness of ^{19}F MRS in patient management and in drug development (Wolf et al., 2000). Similar to ^{19}F MRS, the application of ^{7}Li MRS in biology and experimental medicine has been progressing steadily. The interest derives primarily from the clinical use of Li salts to treat mania and manic-depressive illness, which necessitates the development of a noninvasive, *in vivo* analytical tool to measure brain Li concentrations in humans, both as an adjunct to treatment and as a mechanistic probe (Komoroski, 2000).

^{31}P or ^{1}H NMR spectroscopy *in vivo* can provide a noninvasive probe of high-energy compounds, amino acids, and compounds of phospholipid metabolism (Komoroski et al., 1991). Several successful and potential applications of MRI and MRS in stroke, rheumatoid and osteo-arthritis, oncology, cardiovascular disorders, heart wall motion, perfusion MRI, tracer uptake and clearance studies and neuronal activation have been reported. It has been observed that selecting the appropriate neuroimaging technique can improve diagnosis and management of childhood neurodevelopmental disorders (Hoon and Melhem, 2000). One of the most important contributions of ^{1}H MRS to clinical neurology is its ability to quantify neuronal loss and to demonstrate reversible neuronal damage. Both MRI and CT identify early developmental malformations, including neural tube defects, callosal dysgenesis, neuronal migration disorders, posterior fossa malformations, and hydrocephalus. With this application of MR, neurochemical research has advanced through identification and non-invasive assay of specific neuronal N-acetylaspartate, glial markers such as *myo*-inositol, energetics and osmolytes, and neurotransmitters such as glutamate and GABA. Many disease states could be recognized, including birth injury and Alzheimer's disease, by measuring the tissue levels of the aforesaid metabolites using MR. Moreover, addition of stable isotopes of carbon (in man) or nitrogen (in experimental animals) has provided *in vivo* assays of enzyme flux through glucose transport, glycolysis, TCA-cycle, and the glutamine-glutamate-GABA system (Ross et al., 1997).

NMR as a whole has contributed as much to the study and treatment of epilepsy as to any branch of medicine. Recent examples of such progress include seizure-related brain water diffusion changes, brain metabolic abnormalities in epileptic patients, and pharmacologic manipulation of brain γ-aminobutyric acid (Prichard, 1997). Spectroscopic studies have also been useful in localizing the epileptogenic zone in intractable focal epilepsies (Novotny et al., 1998). In infants and children with genetic metabolic diseases, various applications of nuclear magnetic resonance such as diffusion-weighted imaging, MR spectroscopy and functional MRI have important diagnostic roles (Hoon and Melhem, 2000). Within pediatric neurology, proton MRS studies have been used to assist in the prediction of outcome in a variety of settings of acquired brain injuries such as perinatal asphyxia, near-drowning. Application of MR methods also holds promise for the characterization of respiratory, gastro-intestinal and skin diseases, as well as for the characterization of transgenic and knock-out animals, which have become a key technology in

modern pharmaceutical research (Rudin et al., 1999). Gradient-enhanced ^{1}H MRS techniques combined with a simple slice positioning and perfusion technique have been shown to yield a high-quality spectra from single 400 microns rat forebrain or neocortical-hippocampal slices within 15 min of data acquisition time (Gasparovic et al., 1999). In addition to greater anatomical resolution on brain slice biochemistry, single slice MRS also presents the possibility of correlating, within the same slice, ^{1}H MRS-detectable metabolite levels with other physiological measurements commonly performed on single brain slices. Many animal studies have shown that MRS monitors metabolic changes in various models of human disease. For example, conditions such as anoxia, ischemia, and infarction produce rapid loss of high-energy phosphates and accumulation of hydrolysis products (Bore et al., 1981; Gupta et al., 1983; Weiner, 1987). In such cases, the important metabolites involved in cell energetics could be noninvasively measured by MRS techniques. These metabolites include phosphocreatine, ATP, inorganic phosphate, pH, and lactate.

NMR techniques could also be extended to studies regarding exercise-induced muscle injury, to map tissue biochemistry and precise anatomical visualization of soft tissue structures. In a related study, MRS measurements had demonstrated an increase in the ratio of inorganic phosphate to phosphocreatine (P_i/PCr) 1-7 days after eccentric exercise (McCully et al., 1992). It was observed that this increase in P_i/PCr might be due to either an increase in extracellular P_i or a small increase in resting muscle metabolism. The study proposed that an increase in P_i/PCr seen during training programs might indicate persistent muscle injury. MRI findings had further shown an increased proton T_2 relaxation times following eccentric exercise that lasted up to 80 days after injury, which could be considered to indicate muscle edema and lasting changes in the characteristics of cell water.

The drive behind NMR imaging has been limited clinically to fields of up to 1.5 T (60 MHz) although higher field magnets less than 4.0 T are being approved. There may be benefits to imaging at higher fields, since the signal increases as the square of the magnetic field. To highlight this fact further, the first NMR images of a single cell were recorded with a 9.4 T microimaging system, demonstrating the advent of the NMR imaging microscope (Aguayo et al., 1986). The NMR microscope is expected to have considerable impact in the areas of biology,

medicine and materials science, and may also serve as a precursor to obtaining such resolutions on human subjects. It is also expected that human MRS will be increasingly used for clinical investigation and eventually for medical diagnosis.

3.2. Application in the Analysis of Body Fluids and Tissue Extracts

In the clinical laboratory, NMR can analyze the complex mixtures of body fluids, intact cells, tissues, and their extracts. The most attractive feature of MRS is the noninvasive and nondestructive measurement of chemical compounds in intact tissues. Assisted by pattern recognition methods, the *in vitro* high-resolution MRS of body fluids, biopsy samples and surgery specimens has been shown to provide clinically relevant information in several disease states, and hence could be viewed as a multiparametric, fast and relatively inexpensive analytical method (De Certaines, 1996). The method provides quantitative, qualitative and dynamic information on the metabolic status of the interstitial and plasma compartments under a variety of pathophysiological conditions. Further, using ^{13}C labeled compounds or magnetization transfer techniques, metabolic fluxes may be measured *in vivo* during virtually all normal and abnormal physiological conditions (Petroff, 1988). The simultaneous detection and quantification by NMR spectroscopy of numerous compounds of the intermediary metabolism offers a new insight in the understanding of the milieu interior. The technique offers a unique way to define and monitor the global metabolic homeostasis in humans, with a focus on diseases like cancer, hereditary metabolic disorders, organ transplantation and neurological diseases (Vion-Dury et al., 1992).

The determination of metabolite concentrations is straightforward for fluids with a low protein content such as urine. In fluids with a high protein content such as blood plasma, it is possible to detect not only small molecules but also mobile regions of macromolecules, and to demonstrate the interaction of anions such as lactate with proteins (Bell et al., 1989). The intensities of NMR spectral patterns of biological samples, such as blood plasma and tissues, can be related to the onset and recovery from a toxic lesion in both time- and dose-related fashion. Although the ^{1}H NMR spectra such samples are information rich, they represent a complex data owing to superposition of the resonances from a multitude of different chemical entities in multiple-phase compartments, hampering detection and subsequent resonance assignments. Several spectral-editing experiments have been introduced combining spin-relaxation filters with

both one-dimensional and two-dimensional NMR spectroscopy, which help to overcome these problems. These techniques enable the separation of NMR resonances based on their relaxation times and allow simplification of the complex spectra. This approach has been put into practice using a control human blood plasma, which is a complex mixture of proteins, lipoproteins and small-molecule metabolites (Tang et al., 2004).

NMR methods have significant application to diagnostic pathology, and allow unusually detailed studies of certain metabolic derangements and toxic ingestions. *In vitro* NMR has been applied to diagnosing inborn errors of metabolism such as glycogen storage disease, monitoring growth and regression of tumors, and assessing tissue viability (Bock, 1989). In recent times, the use of high-resolution magic angle spinning (HR-MAS) NMR spectroscopy, in conjunction with diffusion and relaxation weighting, has become a technique-of-choice to probe the metabolic compartmentation within a range of tissues. The first application of HR-MAS ^{1}H NMR was demonstrated for a sample of intact rat liver (ca. 8 mg), and a range of 2D MAS-NMR experiments were performed to enable assignments from α- and β-glucose, glycerol, alanine, glutamate, glycine, dimethylglycine, lysine and threonine, together with phosphocholine, choline, lactate, trimethylamine-N-oxide and certain fatty acids (Bollard et al., 2000). The application of HR-MAS NMR techniques often holds promise in demonstrating the impact of choline-containing metabolites in a number of disorders, including malignant cell growth. As observed in a study, ^{1}H NMR was employed to monitor metabolite changes during cell transfection, wherein an increase in phosphocholine was detected (Griffin et al., 2001). HR-MAS NMR techniques had also been utilized for the study of inter-species metabolism, which demonstrated that the metabolic data acquired on laboratory animals does not correspond to the information obtained on wild species (Griffin et al., 2000b). As shown in a study, the technique holds promise to characterize the underlying biochemistry of the testis and the process involved in the production of spermatozoa and their maturation into sperm. By using diffusion ordered NMR spectroscopy (which uses bipolar gradients to measure apparent diffusion coefficients), many low molecular weight metabolites could be characterized including relatively high amount of uridine and creatine in the testis, wherein the substantial proportion of creatine was identified from the extracellular matrix (Griffin et al., 2000a).

It has been shown that in complex biofluids, the combination of diffusion- and relaxation-editing brings about considerable spectral simplification leading to an easier resonance assignment process. By measuring a diffusion-edited ^{1}H-^{1}H TOCSY NMR spectrum of plasma, it is possible to obtain signals from only the macromolecular components such as blood lipoproteins, since such analysis of the lipid pattern of blood may also be useful as a diagnostic tool (Liu et al., 1996). Besides this, the detailed analysis of lipids, especially phospholipids, has become progressively important, since these molecules represent intercellular messenger molecules and are involved in a number of diseases. Unfortunately, suitable methods of phospholipid analysis are often time-consuming and tedious, since most of them include a variety of separation and derivatization steps. High-resolution ^{31}P NMR spectroscopy is a convenient and precise analytical tool for the phospholipid analysis of extracts from biological samples such as tissues and body fluids (Adosraku et al., 1994; Schiller and Arnold, 2002). The analysis of perfused rat liver by natural abundance ^{13}C NMR illustrates the potential of the method for a non-invasive study of lipid and carbohydrate metabolism in living systems (Cozzone et al., 1985). Also, ^{1}H and ^{13}C NMR techniques have been used to evaluate the degree of unsaturation and the cholesterol/cholesteryl ester ratio on the total lipid fractions obtained from human renal and cerebral tissues, and may be of relevance in brain tumor biology (Tosi et al., 2003).

^{31}P NMR based observations of levels of phosphorus compounds have indicated that the tissue energy status usually changes during exercise, fatigue, recovery, hypometabolism, anesthesia, hypoxia, hypercapnia and osmotic stress. In a study on wound healing, ^{31}P NMR analysis was performed on biopsy samples to explore the energy status of two chronic non-healing leg ulcers, before and after the first week of treatment with two low-pH hydrocolloid materials. It was observed that ^{31}P NMR spectroscopic measurements of chronic wound biochemistry yield rapid knowledge of whether a wound is generating, storing, or using energy. The findings state that ^{31}P NMR spectroscopy may provide a real-time biochemical fingerprint in wound-healing, and may also help the clinicians to understand the healing status of a questionable wound (Ennis and Meneses, 1996).

The biological NMR experiments preserve the tissues and can be repeated with a temporal resolution of seconds to several minutes in a reproducible fashion. A ^{1}H NMR based

methodology of tissue biopsies coupled with multivariate analysis for the diagnosis of human cancer, at high levels of accuracy, sensitivity and specificity has been reported (Smith and Blandford, 1998). As a marker of the intermediary metabolism, ^{31}P, ^{13}C, ^{1}H, ^{19}F, ^{14}N, ^{23}Na and ^{39}K isotopes are commonly observed in both pre-clinical and clinical spectroscopic studies of cancer for studying the tumor biochemistry and physiology (Robinson et al., 1997). In this regard, the biochemical changes in tissue lipid for soft tissue sarcoma were demonstrated with novel quantitative *ex vivo* NMR methods, in which the biochemical changes in tissue lipid were found to correlate with sarcoma cellularity, growth rate, and differentiation (Singer, 1999). Additionally, NMR spectroscopy has much to offer to the future understanding of the relationship between renal biochemistry and function. Since renal cortex and medulla have a different T_1 relaxation time possibly due to differences in lipid composition, human renal cancers show a unique ^{31}P NMR spectrum and a very acidic environment. Cancer chemotherapy may alter this and detection of such changes with NMR offers a method of therapeutic monitoring with significance beyond nephrology (Ross et al., 1986).

Multinuclear NMR spectroscopy involving ^{1}H, ^{13}C and ^{31}P of biological samples reflects their metabolic composition, and could be used for the structural identification of xenobiotic metabolites in complex biological matrices such as plasma, urine and bile. The analysis of high field and high-resolution spectra of body fluids, cell and biopsy extracts requires no separation of a complex mixture into individual metabolites. Combined with pattern recognition methods, NMR observations could be used to classify normal and pathological samples (Leibfritz, 1996; Reglinski and Watson, 1996), although it is advantageous to include a separation step in the experiment by directly coupling HPLC and NMR to simplify the spectra (Sidelmann et al., 2001). Studies have shown that ^{1}H NMR can rapidly analyze complex mixtures of metabolites found in body fluid and biopsy specimens, and could also serve as a method to screen for organic substances (and metabolites). For example, in a study involving 25 patients who presented with clinical indications of a drug overdose, NMR was most successful in identifying analgesics and antiepileptic drugs with a sensitivity of 83-100%, at a field-strength of 300 MHz (Komoroski et al., 2000). It was reported that ^{1}H NMR could give an overview of the low molecular weight metabolites present in ovarian cyst fluid samples, indicating that the metabolic composition of cyst fluid differs significantly between benign and malignant ovarian tumors (Boss et al., 2000). As an

important application, the use of ^{1}H NMR for estimating post-mortem time was suggested based on the ^{1}H NMR analysis of tissue extracts of various organs (Harada et al., 1984).

It could be stated that the MR methods have helped in the elucidation of hitherto unrecognized causes of disease, and yielded new ideas about the control of bioenergetics *in vivo* (Radda, 1986). The first inborn error of metabolism discovered by use of *in vitro* ^{1}H NMR spectroscopy of body fluids had been reported (Moolenaar et al., 1999), which was followed by the diagnosis of inborn errors of purine- and pyrimidine-metabolism at ^{1}H NMR field-strengths of 500 and 600 MHz (Wevers et al., 1999). Further, the NMR profiles of serum and urine samples of patients have been shown to play a role in the diagnosis of inborn errors of metabolism (Moolenaar et al., 2003). The NMR technique has the advantage of minimal sample pretreatment and does not require extraction or derivatization step, besides exhibiting a sensitivity limit of low micromolar range. With the completion of the human genome sequencing projects, there has been an active search for technologies that can provide insights into the genetic basis for physiological variation, and to interpret gene expression in terms of phenotype at the whole organism level in order to understand the pathophysiology of disease. ^{1}H NMR spectroscopic analyses of the metabolic composition of urine in experimental animals under various normal physiological conditions have revealed that inter-animal and diurnal variation, gender, age, diet, species, strain, hormonal status and stress play a role on the biochemical composition of urine (Bollard et al., 2005). These reports have been shown that NMR spectroscopy has potential applications to investigate several issues underlying human diseases, non-invasively.

4. Nuclear Magnetic Resonance in Metabonomics

Since the completion of the human genome project, there has been a tremendous requirement to move towards an understanding of the functional effects of a given gene. Understanding the relationships between human genetic factors, the risks of developing major diseases and the molecular basis of drug efficacy and toxicity has been one of the fundamental problems in modern biology. Predicting biological outcomes on the basis of genomic data is a major challenge because of the interactions of specific genetic profiles with numerous

environmental factors that may conditionally influence disease risks in a nonlinear fashion. Moreover, the increase in the diversity of therapeutic targets in the pharmaceutical industry in recent years has led to a greater diversity of toxicological effects. Hence, an understanding of the metabolic fate of a xenobiotic and the metabolic/biochemical pathways involved is very essential so as to minimize drug-induced toxicity as well as to establish a better drug-safety profile in the drug development phase. As a result, the accelerated pace of drug discovery requires the development of new technologies for the rapid elucidation of toxicological mechanisms. This has led to the emergence of many '-omic' technologies, including genomics (or transcriptomics), proteomics and metabonomics. The pharmaceutical industry has embraced these '-omic' technologies over the past decade with a view to minimize the attrition-rate and expand the drug development pipelines (Holmes and Antti, 2002). Genomics measures the entire genetic makeup of an organism and proteomics measures all the proteins expressed under given conditions, while metabonomics measures the complete metabolic response of an organism to an environmental stimulus or genetic modification. The term metabolomics is used to refer to metabonomics at the level of a single cell type, rather than a larger system. Metabonomics can be viewed as the process of defining multivariate metabolic trajectories that describe the systemic response of organisms to physiological perturbations through time (Keun et al., 2004). It is a systems approach for studying *in vivo* metabolic profiles, which promises to provide information on drug toxicity, disease processes and gene function at several stages in the discovery-development process (Nicholson et al., 2002). Taken together, 'global systems biology' attempts to integrate multivariate biological information to better understand the interaction of genes with the environment (Nicholson et al., 2004).

Metabonomics may be the most recently named of the omics, but it dates back to old-fashioned biochemistry, with its emphasis on metabolism, the sum of the processes to acquire and use energy in an organism, to biosynthesize cellular components, and to catabolize wastes. Hence it could be said that metabonomics is more closely related to things in the clinical world than either genomics or proteomics, owing to the fact that metabonomic signatures reflect both genetic information and environmental influences. Metabonomics uses a combination of data-rich analytical chemical methods such as NMR spectroscopy and Mass spectrometry together with chemometrics for profiling metabolism and interpreting metabolic fingerprints in complex

biological systems. It is well documented that high-resolution ^{1}H NMR spectroscopy is an ideal technique for monitoring low molecular weight metabolites in biofluids, tissue extracts and, with recent advances, intact tissues. In conjunction with computer based pattern recognition, the information can be reduced to a metabolic profile characteristic of the disease/pathology being investigated. These methods have been applied in many areas of relevance to pharmaceutical research and development, including drug safety assessment, characterization of genetically modified animal models of disease, diagnosis of human disease, understanding physiological variation and drug therapy monitoring (Lindon et al., 2004a; Lindon et al., 2004c). Recently, a Consortium for Metabonomic Toxicology (COMET) has been formed between six pharmaceutical companies such as Pfizer, Pharmacia, Hoffmann-La Roche, Novo Nordisk, Bristol-Myers Squibb, Eli Lilly and Imperial College, London with an objective of defining the methodologies and to apply metabonomic data generated using ^{1}H NMR spectroscopy of urine and blood serum involving a range of model compounds with well-known toxic effects for the preclinical toxicity screening of several candidate drugs (Lindon et al., 2003b). While metabonomics is still a relatively new technology in comparison to the other 'omics', published results indicate its potential impact in the drug discovery process by enabling the incorporation of safety endpoints much earlier in the drug discovery process, thereby reducing the likelihood and cost of later-stage attrition (Griffin, 2003; Nicholson et al., 1999; Robosky et al., 2002).

With the recent technological advances of NMR, cryogenic probe technology can significantly compensate for the inherently low sensitivity of nuclei such as ^{13}C. The natural abundance ^{13}C NMR involving cryoprobe technology now permits its routine use in the analysis of biofluids, such as urine or plasma, with acquisition times that enable a high throughput of samples. Information-rich ^{13}C NMR spectra of rat urine could be obtained using appropriately short acquisition times when using a cryogenic probe, followed by an automated pattern recognition analysis of the data, as shown in a study of metabolic response to the model hepatotoxin hydrazine (Stoyanova et al., 2004). Other technological advances include the application of 1 mm ^{1}H-^{13}C-^{15}N microlitre NMR probe with a Z-gradient for metabolic profiling of biofluids. With this probe, spectral profiles of rat blood plasma could be obtained using only approximately 2 μl of fluid, by employing different solvent suppression techniques (Griffin et al., 2002). Further, metabonomic analysis of high-resolution ^{1}H NMR spectra of biofluids has

provided a means of monitoring the progression of toxicity and recovery, thereby allowing the identification of novel biomarkers of a particular lesion (Nicholls et al., 2001).

Ex vivo metabolic profiling, in combination with multivariate data analysis, offers great potential in comparative biology to understand the species similarities. The use of high-resolution NMR spectroscopy in this regard has been highlighted in a recent study involving three *Eisenia* species *Eisenia fetida*, *Eisenia andrei* and *Eisenia veneta*, to distinguish them via their metabolic phenotype (metabotype) using tissue extracts and coelomic fluid analysis (Bundy et al., 2002). This study has also shown that two morphologically undistinguishable species (*E. fetida* and *E. andrei*) differ markedly in their biochemical profiles despite apparently occupying the same ecological niche, and indicated that metabolic phenotype profiling could be used as a powerful functional genomics tool. In similar lines, a novel metabonomic approach was reported for the investigation of genetic influences on metabolic balance and metabolite excretion patterns in two phenotypically normal mouse models. Differences in tricarboxylic acid cycle intermediates and methylamine pathway activity were observed, and a new metabotype concept was proposed, which would be of value in relating the quantitative physiological and biochemical data to both phenotypic and genetic variation in animals and man (Gavaghan et al., 2000).

Metabonomics has found its application in agricultural sciences too, and holds promise in the quality control and authentication of phytomedicines (Wang et al., 2004b). The biochemical mode-of-action (MOA) for herbicides and other bioactive compounds could be rapidly and simultaneously classified by automated pattern recognition of the metabonome that is embodied in the ^{1}H NMR spectrum of a crude plant extract. In a recent study, some of the prominent and most interesting MOAs of herbicides have been characterized and automatically classified using the metabonomic technologies (Ott et al., 2003).

4.1. Application in Toxicology

High-resolution ^{1}H NMR spectroscopy of biofluids and tissues is not only useful in disease diagnosis, but can also provide complementary data for use in toxicological screening when coupled with appropriate chemometric analysis of drugs *in vivo*. In combination with the multivariate analysis of complex biological profiles generated from spectroscopic instruments,

metabonomic technology has enabled the construction of successful expert systems for toxicity screening and disease diagnosis (Henry, 2002). The evolution of chemometric and bioinformatic methodologies to accommodate the multi- and mega-variate data generated by high resolution NMR spectroscopy of biofluids, tissues and cell cultures, and to explore their potential role in mining, modeling and predicting the metabolic data has recently been reported (Holmes and Antti, 2002). The metabonomic approach usually involves two main analytical approaches, namely, NMR spectroscopy and mass spectrometry; however, most literature on mammalian systems pertains to NMR spectroscopy. The application of these methodologies has been demonstrated in relation to other -omics pertaining to drug safety assessment, characterization of genetically modified animal models of disease, diagnosis of human disease and drug therapy monitoring (Lindon et al., 2003a; Lindon et al., 2004b). A recent study based on the ^{1}H NMR spectra of urine and liver tissue samples obtained from rats has demonstrated the utility of metabonomics in drug safety assessment. The analysis has further confirmed the practicality of this approach for resolving toxicity issues to characterize an ill-defined mechanism of drug-induced toxicity for drugs in discovery and development phase (Mortishire-Smith et al., 2004).

It has been shown extensively that chemometric investigations of ^{1}H NMR spectra of rat urine taken from animals dosed with model toxins produce characteristic patterns of metabolic responses and that this permits the identification of biomarkers of toxic response and regeneration. Based on this approach, the identification of 'biomarkers' using ^{1}H NMR spectra of urine has recently been reported for a study of liver toxicity in rats following administration of a model hepatotoxin hydrazine (Stoyanova et al., 2004). NMR spectroscopic information could be used to examine metabolic compartmentation between the cytosol and mitochondria as well as to identify the biomarkers of mitochondrial dysfunction (Bollard et al., 2003). In conjunction with Principal Component Analysis (PCA), subtle changes in the metabolic profiles of a tissue specimen could be selectively amplified using different spectral editing techniques such as the Carr-Purcell-Meiboom-Gill spin-echo, diffusion editing and skyline projection of a 2D *J*-resolved HR-MAS spectrum. This has been demonstrated in a recent study involving the liver tissues to distinguish between control and hydrazine-treated rats, where the effects of the toxin on rat liver biochemistry could be directly observed and characterized by depleted levels of liver glycogen, choline, taurine,

trimethylamine N-oxide, and glucose and by elevated levels of lipids and alanine (Wang et al., 2003).

HR-MAS ^{1}H NMR is increasingly being used to monitor metabolic abnormalities and many toxicological insults within cells, subcellular organelles such as mitochondria and intact tissues. The spectral information obtained for the mitochondria of the rat heart has revealed the presence of lactate, alanine, taurine, choline, phosphocholine, creatine, glycine and lipids. MAS-NMR spectroscopy requires minimal sample preparation and, unlike ^{1}H NMR spectroscopy of tissue extracts, does not discriminate metabolites based on their solubility in a particular solvent and so this is a particularly useful exploratory tool in biochemical toxicology (Waters et al., 2002). In another study, ^{1}H NMR spectroscopy was used to characterize the time-related changes in the urinary metabolite profiles of laboratory rats treated with 13 model toxins and drugs that predominantly affect liver or kidney. Using the ^{1}H NMR spectral data and a probabilistic neural networks (PNN) approach, the 13 classes of toxicity, together with the variations associated with strain, were distinguishable to >90% (Holmes et al., 2001). This study has highlighted the value of PNN in developing accurate NMR-based metabonomic models for the prediction of xenobiotic-induced toxicity in experimental animals. It has been shown in a recent study that by using spectra where the peak intensities are edited according to their molecular diffusion coefficients, it is possible to improve differentiation of control animals and those treated with a model hepatotoxin, alpha-naphthylisothiocyanate (ANIT) (Beckwith-Hall et al., 2003). By using diffusion-edited spectroscopy, the plasma lipid moieties were less attenuated than those from small endogenous metabolites, and thus the toxin-induced changes to the lipoprotein profiles could be more easily detectable. Further, in another study, the ^{1}H HR-MAS NMR and PCA analysis allowed direct detection of all of the ANIT-induced tissue perturbations, enabling metabolic characterization of the lesion, which included steatosis, bile duct obstruction and altered glucose/glycogen metabolism (Waters et al., 2002).

The metabonomic analysis of biofluids and tissues utilizing high-resolution NMR spectroscopy and chemometric techniques has thus proven valuable in characterizing the biochemical response to toxicity for many xenobiotics. To assess the analytical reproducibility of metabonomic protocols, a study was conducted at two sites (involving 500 MHz and 600 MHz

NMR systems) using two identical (split) sets of urine samples from an 8-day acute study of hydrazine toxicity in the rat, and the NMR data were collected under identical conditions. Despite the difference in spectrometer operating frequency, both datasets were extremely similar when analyzed using PCA and gave near-identical descriptions of the metabolic responses to hydrazine treatment, with an analytical error comparable to normal physiological variation in concentration (4-8%) (Keun et al., 2002). This excellent analytical reproducibility and robustness obtained for the metabonomic techniques are highly competitive and are in significant contrast to the best proteomic and genomic techniques, both of which are complementary techniques for predictive and mechanistic toxicology.

The present thesis work has focused on the Biochemical and Biomedical Applications of NMR, involving the analysis of cells, tissue extracts and body fluids. The potential role of NMR, as described in this review, has been put into practice to gain an understanding regarding the biochemistry of *Leishmania donovani* promastigotes, followed by its application as a potential diagnostic tool in characterizing human intracranial tuberculomas due to *Mycobacterium tuberculosis*, and to distinguish the three major forms of meningitis in children in combination with other routine clinical features. The details are being described in the respective chapters.

References

Adosraku RK, Choi GT, Constantinou-Kokotos V, Anderson MM, Gibbons WA (1994) *J Lipid Res* 35:1925-1931.

Aguayo JB, Blackband SJ, Schoeniger J, Mattingly MA, Hintermann M (1986) *Nature* 322:190-191.

Andreotti G, Trivellone E, Lamanna R, Di Luccia A, Motta A (2000) *J Dairy Sci* 83:2432-2437.

Baker JK, Myers CW (1991) *Pharm Res* 8:761-770.

Beckwith-Hall BM, Thompson NA, Nicholson JK, Lindon JC, Holmes E (2003) *Analyst* 128:814-818.

Bell JD, Brown JC, Sadler PJ (1989) *NMR Biomed* 2: 246-56.

Blackburn BJ, Hutton HM, Novak M, Evans WS (1986) *Exp Parasitol* 62:381-388.

Bock JL (1989) *Am J Clin Pathol* 91:S19-26.

Boesch C (1999) *Mol Aspects Med* 20:185-318.

Bollard ME, Garrod S, Holmes E, Lindon JC, Humpfer E, et al. (2000) *Magn Reson Med* 44:201-207.

Bollard ME, Murray AJ, Clarke K, Nicholson JK, Griffin JL (2003) *FEBS Lett* 553:73-78.

Bollard ME, Stanley EG, Lindon JC, Nicholson JK, Holmes E (2005) *NMR Biomed* 18:143-162.

Bore PJ, Chan L, Gadian DG, Radda GK, Ross BD, et al. (1981) *Kroc Found Ser* 15:527-535.

Boschetti C, Fronza G, Fuganti C, Grasselli P, Magnone AG, Mele A, Pellegatta C (1995) *Arzneim Forsch Drug Res* 45:1217-1221.

Boss EA, Moolenaar SH, Massuger LF, Boonstra H, Engelke UF, et al. (2000) *NMR Biomed* 13:297-305.

Bottomley PA (1984) *Comput Radiol* 8:57-77.

Bradbury EM, Radda GK, Allen PS (1983) *Ann Intern Med* 98:514-529.

Brauer M, Ling MF (1991) *Magn Reson Med* 20:100-112.

Bundy JG, Spurgeon DJ, Svendsen C, Hankard PK, Osborn D, et al. (2002) *FEBS Lett* 521:115-120.

Casy AF, Dewar GH (1994) *J Pharm Biomed Anal* 12:855-861.

Chan ATM, Evans KA, Belsky EA, Ditnfeld DJS, Tsai AT, McPhail A (1996) *Magn Res Chem* 34:1025-1030.

Chilton HM, Ekstrand KE (1984) *Am J Hosp Pharm* 41:763-768.

Coles M, Heller M, Kessler H (2003) *Drug Discovery Today* 8:803-810.

Cooke RM (1997) *Current Opinion In Chemical Biology* 1:359-364.

Corcoran O, Spraul M (2003) *Drug Discov Today* 8:624-631.

Cousins JP (1995) *AJR Am J Roentgenol* 164:1337-1347.

Cozzone PJ, Canioni P, Bernard M, Desmoulin F, Galons JP (1985) *Annales d'Endocrinologie* 46:239-247.

Dale BE, Gillies RJ (1991) *Biotechnology* 17:107-118.

Dawson BA, Black DB, Neville GA (1995) *J Pharm Biomed Anal* 13:395-407.

De Certaines JD (1996) *Anticancer Res* 16:1325-1331.

De Kock J (1993) *Fat Sci Technol* 95:352-355.

De Los Santos C, Buldain G, Frydman B, Cannata JJB, Cazzulo JJ (1985) *Eur J Biochem* 149:421-429.

Diercks T, Coles M, Kessler H (2001) *Curr Opin Chem Biol* 5:285-291.

Duarte IF, Barros A, Belton PS, Righelato R, Spraul M, et al. (2002) *J Agric Food Chem* 50:2475-2481.

Duarte IF, Barros A, Almeida C, Spraul M, Gil AM (2004) *J Agric Food Chem* 52:1031-1038.

Ennis WJ, Meneses P (1996) *Adv Wound Care* 9:21-26.

Feeney J (2000) *Angew Chemie Int Ed Engl* 39:290-312.

Fejzo J, Lepre CA, Peng JW, Bemis GW, Ajay, et al. (1999) *Chem Biol* 6:755-769.

Fejzo J, Lepre C, Xie X (2003) *Curr Top Med Chem* 3:81-97.

Gasparovic C, King D, Feeney DM (1999) *Brain Res Brain Res Protoc* 4:97-102.

Gavaghan CL, Holmes E, Lenz E, Wilson ID, Nicholson JK (2000) *FEBS Lett* 484:169-174.

Gerhard U, Thomas S, Mortishire-Smith R (2003) *J Pharm Biomed Anal* 32:531-538.

Gil AM, Duarte IF, Delgadillo I, Colquhoun IJ, Casuscelli F, et al. (2000) *J Agric Food Chem* 48:1524-1536.

Gilroy FV, Edwards MR, Norton RS, O'Sullivan WJ (1988) *Mol Biochem Parasitol* 31:107-115.

Griffin JL, Troke J, Walker LA, Shore RF, Lindon JC, Nicholson JK (2000a) *FEBS Lett* 486:225-229.

Griffin JL, Walker LA, Garrod S, Holmes E, Shore RF, Nicholson JK (2000b) *Comp Biochem Physiol B Biochem Mol Biol* 127:357-367.

Griffin JL, Mann CJ, Scott J, Shoulders CC, Nicholson JK (2001) *FEBS Lett* 509:263-266.

Griffin JL, Nicholls AW, Keun HC, Mortishire-Smith RJ, Nicholson JK, Kuehn T (2002) *Analyst* 127:582-584.

Griffin JL (2003) *Curr Opin Chem Biol* 7:648-654.

Grucker D (2000) *Prog Nucl Magn Reson Spectr* 36:241-270.

Gupta RK, Gupta P, Yushok WD, Rose ZB (1983) *Physiol Chem Phys Med NMR* 15:265-280.

Hajduk PJ, Burns DJ (2002) *Comb Chem High Throughput Screen* 5:613-621.

Hakumaki JM, Kauppinen RA (2000) *Trends Biochem Sci* 25:357-362.

Hammer BE, Heath CA, Mirer SD, Belfort G (1990) *Biotechnology (N Y)* 8:327-330.

Hanna GM, Lau-Cam CA (1993) *J Pharm Biomed Anal* 11:855-859.

Harada H, Maeiwa M, Yoshikawa K, Ohsaka A (1984) *Forensic Science Int* 24:1-7.

Haselgrove J, Grun J, Owen CS, Larralde C (1987) *Magn Reson Med* 4:517-525.

Heller M, Kessler H (2001) *Pure Appl Chem* 73:1429-1436.

Henry CM (2002) *Chem Eng News* 80:66-70.

Hicks RP (2001) *Curr Med Chem* 8:627-650.

Holmes E, Nicholson JK, Tranter G (2001) *Chem Res Toxicol* 14:182-191.

Holmes E, Antti H (2002) *Analyst* 127:1549-1557.

Holzgrabe U, Diehl BWK, Wawer I (1998) *J Pharm Biomed Anal* 17:557-616.

Hoon AH, Jr., Melhem ER (2000) *J Dev Behav Pediatr* 21:291-302.

Humbert F (2001) *J Ind Microbiol Biotechnol* 26:53-61.

Inkmann E, Hesse KF, Holzgrabe U (1997) *Pharmazie* 52:764-774.

Jacoby E, Davies J, Blommers MJJ (2003) *Curr Top Med Chem* 3:11-23.

Jahnke W, Florsheimer A, Blommers MJ, Paris CG, Heim J, et al. (2003) *Curr Top Med Chem* 3:69-80.

Kegeles LS, Humaran TJ, Mann JJ (1998) *Biol Psychiatry* 44:382-398.

Keifer PA (2003) *Curr Opin Chem Biol* 7:388-394.

Keun HC, Ebbels TM, Antti H, Bollard ME, Beckonert O, et al. (2002) *Chem Res Toxicol* 15:1380-1386.

Keun HC, Ebbels TM, Bollard ME, Beckonert O, Antti H, et al. (2004) *Chem Res Toxicol* 17:579-587.

King NJC, Ward MH, Holmes KT (1991) *FEBS Lett* 287:97-101.

Knop RH, Chen CW, Mitchell JB, et al. (1984) *BBA Mol Cell Res* 804:275-284.

Kockenberger W (2001) *J Exp Botany* 52:641-652.

Komoroski EM, Komoroski RA, Valentine JL, Pearce JM, Kearns GL (2000) *J Anal Toxicol* 24:180-187.

Komoroski RA (2000) *Magn Reson Imaging* 18:103-116.

Komoroski RA, Pappas A, Hough A (1991) *Hum Pathol* 22:1077-1084.

Kosaka M, Owatari N, Seo Y, Kawakubo H, Harada S, et al. (2000) *Jpn J Physiol* 50:463-467.

Kressel HY (1983) *Radiat Med* 1:197-204.

Lanzer P, Bohning D (1990) *Z Kardiol* 79:247-260.

Le Gall G, Puaud M, Colquhoun IJ (2001) *J Agric Food Chem* 49:580-588.

Leibfritz D (1996) *Anticancer Res* 16:1317-1324.

Lens PN, Hemminga MA (1998) *Biodegradation* 9:393-409.

Lindon JC, Holmes E, Nicholson JK (2003a) *Anal Chem* 75:A384-391.

Lindon JC, Nicholson JK, Holmes E, Antti H, Bollard ME, et al. (2003b) *Toxicol Appl Pharmacol* 187:137-146.

Lindon JC, Holmes E, Bollard ME, Stanley EG, Nicholson JK (2004a) *Biomarkers* 9:1-31.

Lindon JC, Holmes E, Nicholson JK (2004b) *Expert Rev Mol Diagn* 4:189-199.

Lindon JC, Holmes E, Nicholson JK (2004c) *Curr Opin Mol Ther* 6:265-272.

Liu M, Nicholson JK, Lindon JC (1996) *Anal Chem* 68:3370-3376.

Lucas LH, Yan J, Larive CK, Zartler ER, Shapiro MJ (2003) *Anal Chem* 75:627-634.

Makarov MI, Haumaier L, Zech W, Marfenina OE, Lysak LV (2005) *Soil Biol Biochem* 37:15-25.

Margulis AR, Crooks LE, Kaufman L (1983) *Eur J Radiol* 3:236-238.

Matthews PM, Foxall D, Shen L, Mansour TE (1986) *Mol Pharmacol* 29:65-73.

McCully K, Shellock FG, Bank WJ, Posner JD (1992) *Med Sci Sports Exerc* 24:537-542.

Mistry N, Ismail IM, Farrant RD, Liu M, Nicholson JK, Lindon JC (1999) *J Pharm Biomed Anal* 19:511-517.

Moolenaar SH, Poggi-Bach J, Engelke UF, Corstiaensen JM, Heerschap A, et al. (1999) *Clin Chem* 45:459-464.

Moolenaar SH, Engelke UF, Wevers RA (2003) *Ann Clin Biochem* 40:16-24.

Moore A, Basilion JP, Chiocca EA, Weissleder R (1998) *BBA* 1402: 239-249.

Moore JM (1999) *Biopolymers* 51:221-243.

Mortishire-Smith RJ, Skiles GL, Lawrence JW, Spence S, Nicholls AW, et al. (2004) *Chem Res Toxicol* 17:165-73.

Muchmore SW, Hajduk PJ (2003) *Curr Opin Drug Discov Devel* 6:544-549.

Nakada T (1997) *Rinsho Shinkeigaku* 37:1155-1157.

Neville GA, Racey TJ, Rej RN, Perlin AS (1990) *J Pharm Sci* 79:425-427.

Nicholls AW, Holmes E, Lindon JC, Shockcor JP, Farrant RD, et al. (2001) *Chem Res Toxicol* 14:975-987.

Nicholson JK, Lindon JC, Holmes E (1999) *Xenobiotica* 29:1181-1189.

Nicholson JK, Connelly J, Lindon JC, Holmes E (2002) *Nat Rev Drug Discov* 1:153-161.

Nicholson JK, Holmes E, Lindon JC, Wilson ID (2004) *Nat Biotechnol* 22:1268-1274.

Norton RS (1990) *Aust J Biotechnol* 4:114-120.

Novak M, Hameed N, Buist R, Blackburn BJ (1992) *Parasitol Res* 78:665-670.

Novotny E, Ashwal S, Shevell M (1998) *Pediatr Res* 44:1-10.

Ott KH, Aranibar N, Singh B, Stockton GW (2003) *Phytochemistry* 62:971-985.

Passe TJ, Charles HC, Rajagopalan P, Krishnan KR (1995) *Prog Neuropsychopharmacol Biol Psychiatry* 19:541-563.

Petroff OA (1988) *Comp Biochem Physiol B* 90:249-260.

Pochapsky SS, Pochapsky TC (2001) *Curr Top Med Chem* 1:427-441.

Portais JC, Delort AM (2002) *FEMS Microbiol Rev* 26:375-402.

Price RR, Allison J, Massoth RJ, Clarke GD, Drost DJ (2002) *Medical Physics* 29:1892-1912.

Price WS (2003) *Austral J Chemistry* 56:855-860.

Prichard JW (1997) *Curr Opin Neurol* 10:98-102.

Radda GK (1986) *Science* 233:640-645.

Reglinski J, Watson ID (1996) *Ann Clin Biochem* 33:290-307.

Roberts GC (2000) *Drug Discov Today* 5:230-240.

Robinson SP, Barton SJ, McSheehy PM, Griffiths JR (1997) *Br J Radiol* 70:S60-69.

Robosky LC, Robertson DG, Baker JD, Rane S, Reily MD (2002) *Comb Chem High Throughput Screen* 5:651-662.

Ross B, Freeman D, Chan L (1986) *Kidney Int* 29:131-141.

Ross BD, Bluml S, Cowan R, Danielsen E, Farrow N, Gruetter R (1997) *Biophys Chem* 68:161-172.

Ross B, Bluml S (2001) *Anat Rec* 265:54-84.

Rudin M, Beckmann N, Porszasz R, Reese T, Bochelen D, Sauter A (1999) *NMR Biomed* 12:69-97.

Sadane GS, Ghogare AB (1991) *J Pharm Sci* 80:895-898.

Salvatella X, Giralt E (2003) *Chem Soc Rev* 32:365-372.

Schicha H, Sechtem U, Theissen P, Hilger HH (1989) *Z Kardiol* 78:123-130.

Schiller J, Arnold K (2002) *Med Sci Monit* 8:MT205-222.

Schmedake TA, Welch LE (1996) *J Chem Educ* 73:1045-1048.

Schwardt O, Kolb H, Ernst B (2003) *Curr Top Med Chem* 3:1-9.

Sem DS, Pellecchia M (2001) *Curr Opin Drug Discov Devel* 4:479-492.

Serber Z, Ledwidge R, Miller SM, Dotsch V (2001) *J Am Chem Soc* 123:8895-8901.

Shukla-Dave A, Degaonkar M, Roy R, Murthy PK, Murthy PS, et al. (1999) *Magn Reson Imaging* 17:1503-1509.

Shukla-Dave A, Roy R, Bhaduri AP, Chatterjee RK (2000) *Physiol Chem Phys Med NMR* 32:1-12.

Sidelmann UG, Bjornsdottir I, Shockcor JP, Hansen SH, Lindon JC, Nicholson JK (2001) *J Pharm Biomed Anal* 24:569-579.

Singer S (1999) *Semin Surg Oncol* 17:11-22.

Smith IC, Blandford DE (1998) *Biochem Cell Biol* 76:472-476.

Staubach B, Buddrus J (1996) *Angew Chem Int Ed Engl* 108:1443-1445.

Stockman BJ, Dalvit C (2002) *Prog Nucl Magn Reson Spectr* 41:187-231.

Stoyanova R, Nicholson JK, Lindon JC, Brown TR (2004) *Anal Chem* 76:3666-3674.

Tang H, Wang Y, Nicholson JK, Lindon JC (2004) *Anal Biochem* 325:260-272.

Thompson SN, Lee RWK (1987) *J Parasitol* 73:64-76.

Thompson SN, Platzer EG, Lee RWK (1990) *Mol Biochem Parasitol* 22:45-54.

Thompson SN (1991) *J Parasitol* 77:1-20.

Tonelli AE (1996) The NMR spectra and the microstructures of polymers. In *Polymer Spectroscopy*. Ed, AH Fawcett. Chichester: Wiley, pp 55-95.

Tosi MR, Trinchero A, Poerio A, Tugnoli V (2003) *Ital J Biochem* 52:141-144.

Van Dongen M, Weigelt J, Uppenberg J, Schultz J, Wikstrom M (2002) *Drug Discov Today* 7: 471-478.

Vilanova B, Munoz F, Donoso J, Frau J, Blanco FG (1994) *J Pharm Sci* 83:322-327.

Vion-Dury J, Nicoli F, Torri G, Torri J, Kriat M, et al. (1992) *Biochimie* 74:801-807.

Vogtherr M, Fiebig K (2003) *EXS*: 183-202.

Wang Y, Bollard ME, Keun H, Antti H, Beckonert O, et al. (2003) *Anal Biochem* 323:26-32.

Wang Y, Holmes E, Nicholson JK, Cloarec O, Chollet J, et al. (2004a) *Proc Natl Acad Sci USA* 101:12676-12681.

Wang Y, Tang H, Nicholson JK, Hylands PJ, Sampson J, et al. (2004b) *Planta Med* 70:250-255.

Waters NJ, Holmes E, Waterfield CJ, Farrant RD, Nicholson JK (2002) *Biochem Pharmacol* 64:67-77.

Watt AP, Mortishire-Smith RJ, Gerhard U, Thomas SR (2003) *Curr Opin Drug Discov Devel* 6:57-65.

Weiner MW (1987) *Ann New York Acad Sci* 508:287-299.

Wevers RA, Engelke UF, Moolenaar SH, Brautigam C, de Jong JG, et al. (1999) *Clin Chem* 45:539-548.

Wiechert W (2001) *Metab Eng* 3:195-206.

Wolf W, Presant CA, Waluch V (2000) *Adv Drug Deliv Rev* 41:55-74.

Wyss DF, McCoy MA, Senior MM (2002) *Curr Opin Drug Discov Devel* 5:630-647.

Yang C, Hua Q, Shimizu K (2002) *J Bioscience Bioengineering* 93:78-87.

Zartler ER, Yan J, Mo H, Kline AD, Shapiro MJ (2003) *Curr Top Med Chem* 3:25-37.

Zupke C, Foy B (1995) *Curr Opin Biotechnol* 6:192-197.

Chapter 3:

NMR Structural Aspects In Leishmaniasis

1. Introduction

Leishmaniasis is not a single entity but a collection of diseases, each with its own clinical manifestations and epidemiology. The disease most commonly manifests either in a cutaneous (skin) form or in a visceral (internal organ) form. The five most common species involved are: *L. major*, *L. tropica*, *L. aethiopica*, *L. donovani* and *L. infantum*. The first three are predominantly agents of cutaneous leishmaniasis, an infection that is limited to the skin and the last two are agents of visceral leishmaniasis. Cutaneous leishmaniasis is characterized by one or more skin sores that develop over a period of time after a person is bitten by infected sand-flies. The parasitic protozoan members of genus *Leishmania* are responsible for the most severe pathologies associated with visceral leishmaniasis (VL) in humans, caused by *Leishmania donovani* and *Leishmania infantum*. VL is an infection of the liver and spleen that can be fatal, which if untreated in time may cause morbidity with high rate of mortality. The manifestations of visceral leishmaniasis, such as fever, enlargement of the spleen and liver, and anemia, typically develop after months or in some cases years, once a person becomes infected.

The disease is usually transmitted by the bite of some species of sand-flies (female phlebotamine mosquitoes, the small blood-feeding insects) where they exist in the form of extracellular, flagellated promastigotes in the gut of the 'sand-fly vector' that usually happen to be the transmitting medium. The parasite is found to exist in two main morphological forms, termed 'amastigotes' and 'promastigotes' where, amastigotes are ovoid, non-motile, largely intracellular stages, and promastigotes are elongated, motile, largely extracellular stages. *Leishmania* cycle between sandfly vectors, where they exist as multiplicative 'procyclic' promastigotes and infective 'metacyclic' promastigotes, and their mammalian host, where they exist as intracellular amastigotes living predominantly in the phagolysosome of macrophages. The form introduced into the skin of the mammalian host is a promastigote, which subsequently gets transformed into intracellular amastigotes in the macrophage phagolysosomes of the mammalian host (Molyneaux and Killick-Kendrick, 1987), and this transformation occurs within 12-24 hours. Thereafter, the parasite remains in the amastigote form for the duration of the mammalian phase of life cycle. These cells grow and divide within their host cells, intermittently bursting out and infecting new

macrophages. This phase is chronic and can last from months to years, even a lifetime depending upon the host species involved, and there is a strong influence of host genetics on the susceptibility to infection.

1.1. Incidence of Leishmaniasis

Leishmaniasis occurs in approximately 90 tropical and subtropical countries around the world (Herwaldt, 1999; Olliaro et al., 2005). It also occurs in some of the following regions: the Americas (from northern Argentina to southern Texas in the United States), northern Asia, the Middle East, and Africa (particularly east and north Africa). Leishmaniasis is usually more common in rural than urban areas. People of all ages are at risk for leishmaniasis if they live or travel where leishmaniasis is found. Like many other tropical diseases, the leishmaniasis has been related to economic development and man-made environmental changes, which increase the exposure to the sand-fly vector. Risk is highest for people who are outdoors in leishmaniasis-endemic areas. Adventure travelers, Peace Corps volunteers, missionaries, ornithologists, other people who do research outdoors at night, and soldiers are examples of people who might have an increased risk for leishmaniasis.

It has been estimated that 12 million new cases of leishmaniasis occur each year worldwide, making it the second largest protozoal disease next to malaria (Chang, 1985). It has also been reported that 350 million of people are at risk of infection across 88 countries, and 90% of worldwide cases are from Bangladesh, Bihar State (India), Nepal, Sudan and northeastern Brazil (Guerin et al., 2002). The situation in India is grave, particularly in eastern India (Bihar State) where an official estimate of more than 4,30,000 cases were reported between 1985-1996 (Lira et al., 1999), although it is believed that the actual number of cases currently exceeds this figure by at least five folds (Sundar et al., 2002). Current epidemic, which started in early seventies, continues to take its toll, and for the last three decades, every year thousands of lives are lost due to this disease alone. Recent trends indicate that there are 5,00,000 cases per year of visceral leishmaniasis, which occurs primarily in the Indian subcontinent (Davies et al., 2003; Olliaro et al., 2005).

WHO had included leishmaniasis among the six major diseases targeted for intensive research and control efforts, yet very little has been possible regarding effective treatment strategies with drugs, and to understand the intermediary metabolism of the causative organism, partially owing to the complexities of the disease and patient factors. In leishmaniasis, almost all untreated patients die; the standard anti-leishmanial drugs such as sodium antimony gluconate (SAG) and pentamidine are parenterally administered, and the development of an effective oral treatment is still underway. The risk regarding leishmaniasis also lies in the fact that vaccines and drugs for preventing the infections are not currently available, and the (only) possible way is to take preventive measures by reducing the contact with sand-flies. Sand-fly activity in an area can easily be underestimated because sand-flies are noiseless fliers, and rare bites might not be noticed. Although sand-flies are primarily nighttime biters, infection can be acquired during the daytime if the resting sand-flies are disturbed.

1.2. Characterization of Amastigotes and Promastigotes of *L. donovani*

There is little information regarding the energy metabolism of *Leishmania* amastigotes. Previous studies indicated qualitative differences in the energy metabolism of the two forms (Hart and Coombs, 1982; Rainey and Mackenzie, 1991), because of differences in their natural environment, i.e., promastigotes reside in the digestive tract of the sand-flies, whereas amastigotes reside within the parasitophorous vacuoles of host macrophages. Furthermore, promastigotes are regarded as aerobic organisms, but amastigotes are anaerobic.

Several attempts have been made to culture amastigote-like forms of different *Leishmania* species (Doyle et al., 1991; Pan et al., 1993; Castilla et al., 1995; Hodgkinson et al., 1996), mostly using temperature and in some cases, pH as the trigger for *in vitro* parasite transformation. Earlier studies have also shown the biochemical changes in the heat-stressed promastigotes of *L. donovani* (Goyal et al., 1995). Successful demonstration of an *in vitro* axenic culture of *L. donovani* (strain Dd8) amastigotes has been demonstrated for the causative agent of Indian kala-azar (Gupta et al., 1996a), followed by studies on the characterization of several of their membrane parameters (Gupta et al., 1996b). The results revealed a remarkable similarity between the axenic and intracellular amastigotes. Promastigotes can be cultured axenically at temperatures below 28°C in defined or semi-defined commercially available media (Hendricks et al., 1978),

thus explaining the numerous biochemical, immunological and molecular studies on this form of the parasite. This contrasts with the relatively fragmentary data available on the amastigote, which is the ultimate causative form for all the clinical manifestations of leishmaniasis. Studies on amastigotes have been hampered due to difficulties in obtaining/isolating the purified parasite from animal lesion or macrophage cultures, and the inability to culture them axenically (Bates, 1993).

1.3. Problem of Drug Resistance in Leishmaniasis

It has been speculated that the increasing number of treatment failures in India might be due to the emergence of drug-resistant strains as the main cause of SAG unresponsiveness in Bihar (Lira et al., 1999). All the three available anti-leishmania drugs, SAG, Pentamidine and Amphotericin-B have to be administered parenterally for long periods, and all three are toxic with treatment-related fatalities (Sundar and Benjamin, 2003). Antimonials inhibit glycolytic enzymes and fatty acid oxidation in amastigotes of leishmania, and there is a dose-dependent inhibition in net formation of ATP and GTP. Pentamidine is a polyamine, and acts probably by inhibition of kinetoplast DNA function. Amphotericin-B and other azole antifungals inhibit the biosynthesis of ergosterol like sterols, which are membrane sterols for both fungi and *Leishmania*. Amphotericin-B also increases the membrane permeability of *Leishmania* leading to its death. It is believed that the real breakthrough is likely to be provided by the successful development and commercial availability of oral miltefosine. Although liposomal amphotericin-B has been reported to be very effective in such unresponsive cases, its high cost restricts the treatment in developing countries (Sundar et al., 2001a). This drug has also been proposed to be helpful in regions where parasites are resistant to current agents (Sundar et al., 2001a). Miltefosine (Croft et al., 1987), which was proposed to be the first oral drug for leishmaniasis, has been under clinical trials in India and is expected to change the scenario of unresponsiveness for VL (Jha et al., 1999; Murray, 2002; Sundar et al., 2002). Clinical trials in India have also been performed comparing miltefosine with the most effective standard treatment, amphotericin-B (Sundar et al., 2002). The novelty of miltefosine lies in the fact that it is a choline-based analog (1-*O*-hexadecylphosphocholine; fig. A), and has been speculated to interfere with the cell-signaling pathways and membrane synthesis of *L. donovani*, causing the death of the parasite by membrane rupture (Jha et al., 1999). The clinical trails have pointed out that oral miltefosine is an effective and safe treatment for Indian visceral

leishmaniasis and may be helpful in regions where the parasite is resistant to current agents (Sundar et al., 2002; Sundar, 2003).

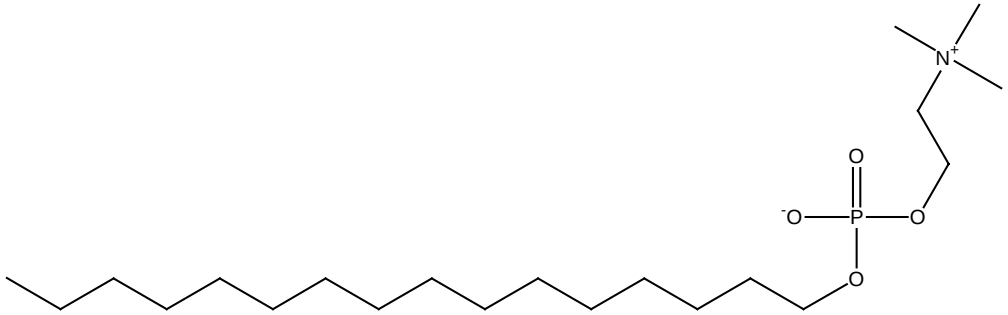

Fig. A: Chemical structure of Miltefosine.

The mechanism of drug-resistance in kala-azar is still not well understood. A collective study of host and parasite factors is needed to understand the basic mechanisms behind drug-resistance, and this has become really essential especially in relation to management and future perspective of this dreaded disease. From the reports of a large number of primary resistant cases, it appears that this resistance is getting transmitted (Lira et al., 1999; Sundar et al., 2000; Sundar, 2001b). It has been observed that in Bihar there is also a regional variation in unresponsiveness; in certain parts, more than 90% of cases still responded to 30 days regimen of SAG, and in some areas almost all cases have emerged resistant to SAG (Lira et al., 1999; Sundar, 2001). This might indicate that, besides the parasite-related factors that cause unresponsiveness, host-related mechanisms might also play a role among other factors. As the mechanism of action is different for each class of anti-leishmanial drugs, the mechanism of resistance also might be different, and in most resistant cases, amphotericin-B is used to treat such patients. Although several methods are currently employed for characterizing unresponsiveness in leishmaniasis (Singh et al., 2003; Sundar et al., 2001b; Legare et al., 1997), it is apparent that in-depth parasitological investigations and new approaches will be necessary to fully understand the exact extent of drug resistance in leishmaniasis.

Characterization of the cellular metabolic profiles of *L. donovani* parasites has been attempted in recent times to account for any possible causes of drug resistance. A comprehensive knowledge regarding the metabolic capabilities of *Leishmania* strains may be essential at least for

the following reasons: (a). such information may provide insights about various biochemical pathways, which play a key role in the life-cycle of the parasite and for its survival in different (host) environments; (b). these biochemical pathways, especially if they are essential or unique to the organism and play some important pathophysiologic role in the host-parasite relationship, could provide targets for innovative therapeutic strategies and form the basis of development of future techniques for investigation and also drug-designing, and (c). the quantitative estimation of these metabolites might be useful in the differentiation of various strains/species of *Leishmania*.

2. Statement of Problem

Besides the various laboratory diagnostic methods that are currently in practice (Sundar and Benjamin, 2003), the characterization of drug responsive and unresponsive strains of *L. donovani* has been a topic of interest. Several reports exist in literature regarding the biochemical, molecular biological and immunological aspects of *L. donovani* (Glew et al., 1988; Santhamma and Bhaduri, 1995; Marr and Berens, 1985; Hwang and Ullman, 1997; Langford et al., 1994; Meade et al., 1984; Kumar et al., 2001), the possible resistance-causing mechanism involved (Turco et al., 2001; Perez-Victoria et al., 2003; Singh et al., 2003; Prasad and Dey, 2000), and regarding the role of trypanothione and its component parts in causing drug resistance (Mittal et al., 2005; Wyllie et al., 2004; Carter et al., 2003; Drummelsmith et al., 2003; Mukhopadhyay et al., 1996). In addition to the current procedures, the utility of other bio-analytical techniques such as NMR spectroscopy in understanding the biochemistry of *Leishmania* has been explored in recent times. In particular, ^{1}H, ^{13}C and ^{31}P NMR spectroscopic techniques have become the methods-of-choice to obtain a variety of structural information regarding the metabolites in cellular systems and their bioenergetics (Lindon et al., 2004; Griffin, 2003; Grivet et al., 2003; Thompson, 1991) in a single metabolic window, and these can be mapped and quantitated from a single experiment (Gilroy et al., 1988; Learmonth et al., 1987; Kinoshita and Yokota, 1997; Subramanian et al., 2005). Moreover, it has been recently documented that the absolute quantitative information obtained through proton NMR spectroscopy is highly reproducible with an accuracy of 95% (Keun et al., 2002). Despite the scarcity of the ^{13}C nucleus (1.1%), natural-abundance ^{13}C NMR studies have been reported to be useful for monitoring the progress of

fermentation process (Lohmeier-Vogel et al., 1995), while ^{31}P NMR provides a non-invasive information pertaining to the physiological status of cells (Lundberg et al., 1990).

The potential usefulness of NMR in understanding the biochemistry of *Leishmania* species has been demonstrated for the characterization of the products of glucose metabolism in *L. pifanoi* amastigotes and promastigotes (Rainey and MacKenzie, 1991), and to characterize various phosphate entities in *L. major* using ^{31}P NMR (Moreno et al., 2000). Further, ^{13}C NMR has been employed to characterize the products of *in vitro* tryptophan catabolism in *L. donovani* promastigotes (Leelayoova et al., 1992), and a ^{1}H NMR based lipid-profile of the *L. donovani* promastigotes has been demonstrated (Adosraku et al., 1993). The end products of glycolysis in both the promastigote and short-term cultured amastigote-like forms of *L. donovani* (strain LRC133) have been characterized using ^{1}H NMR to probe into their strategies for energy utilization (Castilla et al., 1995). Reports from our laboratory had revealed that proton NMR spectroscopy could aid in obtaining metabolic information in *L. donovani* promastigotes (Singha et al., 1996), as well as to obtain a comparative metabolites profile in intracellular amastigotes, axenic amastigoes and promastigotes, in order to understand their biochemical similarities (Gupta et al., 1999). However, there has been no report available regarding a comprehensive metabolic profiling of intracellular metabolites in these strains, which may account for drug responsiveness/unresponsiveness. In continuation to the earlier efforts, the present investigation has been undertaken with an objective of mapping important intracellular metabolites using ^{1}H NMR spectroscopy in the promastigote PCA extracts of six cultured strains of *L. donovani*. An attempt has been made to understand the metabolic information of the live Dd8 promastigotes (WHO reference strain) under different conditions, to arrive at any possible clues regarding the biochemical pathways in *L. donovani*.

3. Materials and Methods

3.1. Chemicals

$^{13}C_1$-glucose (99 atom% ^{13}C-enriched), D_2O (99.96 atom% deuterium-enriched), *N*-(2-hydroxyethyl)piperazine-*N'*-ethane-sulfonic acid (HEPES) and di-sodium salt of ethylenediamine

tetra-acetic acid (EDTA) were purchased from Sigma-Aldrich Inc. (St. Louis, MO, USA). All other chemicals used were of reagent grade with the highest purity commercially available, unless otherwise mentioned.

3.2. Parasite Strains

The six *L. donovani* strains, namely, PKDL, S-lal, RMRI, Ag-83, #5 and Dd8 (Table-1) were cultured as promastigotes in the Division of Biochemistry, CDRI, Lucknow. The strain Dd8 (reference strain, as per WHO standards) was originally obtained as promastigotes from the late Professor P.C.C. Garnham (Imperial College, London), and has been maintained at CDRI *in vivo* in golden hamsters (*Mesocricetus auratus*) and *in vitro* in promastigote form in RPMI-1640 medium with 10% FCS at 26 ± 1°C. Mass cultivation of all the strains was undertaken in RPMI-1640 medium (100-150 ml), which was seeded with 0.5 x 10^6 promastigotes/ml, and maintained at 26 ± 1°C in a BOD incubator. The cells were harvested at stationary phase of growth depending upon the parasite strain based on the growth-curve profiles of the *L. donovani* promastigotes as reported earlier (Singha et al., 1996).

3.3. Determination of Intracellular Metabolites by ^{1}H- and ^{31}P-NMR Spectroscopy

3.3.1. Preparation of Neutralized PCA Extracts of the Promastigotes

Stationary phase promastigote cells were harvested through centrifugation at 1,500 x *g* for 10 min at 4°C and were washed three times with pre-chilled normal saline to remove FCS, if any. 2 x 10^9 cells/ml of each strain were used for the preparation of PCA extract. The neutralized perchloric acid (PCA) extracts of the parasite samples were prepared as described elsewhere (Singha et al., 1996; Gupta et al., 1999). The washed cells were suspended in 0.6 ml of ice-cold 14% PCA (0.75 N, Merck) and sonicated at 4°C using a ultrasonicator (Sonics, USA) with a 6 mm-diameter tip by applying low power three times (3 min each, duty cycle, 20% of maximum power) followed by centrifugation at 16,000 x *g* for 10 min at 4°C. The pH of the supernatant obtained was adjusted to 6.8 by adding potassium hydroxide solution (10 N), kept on ice for 1 h to allow precipitation of potassium perchlorate and centrifuged (6,000 x *g*, for 10 min). The supernatant obtained was lyophilized, and re-suspended in 600 μl of D_2O, centrifuged at 45,000 x

Table-1: Information regarding the *L. donovani* strains.

Sample Code	WHO Reference Code	Strain Status[#]
Dd8	MHOM/IN/80/Dd8	VL
#5	MHOM/IN/80/Dd8/#5	VL
Ag-83	MHOM/IN/83/Ag-83	VL
RMRI	MHOM/IN/90/RMRI-188	VL
S-lal	MHOM/IN/94/S-lal	VL
PKDL	MHOM/IN/94/PKDL	PKDL

[#]VL: Visceral Leishmaniasis; PKDL: Post-kala-azar Dermal Leishmaniasis.

g for 20 min. The pellet obtained was discarded and the final supernatant was taken for the ^{1}H NMR studies, wherein the pH of the prepared sample was not measured thereafter.

For ^{31}P NMR experiment the sample preparation essentially remained the same as described above, wherein the supernatant obtained for the strain Dd8 was lyophilized and taken separately instead of re-dissolving it in D_2O. The material obtained was dissolved in a buffer solution containing 5.9 mg HEPES (pH 7.0) and 0.9 mg EDTA in 400 µl TDW, and to this solution 100 µl of D_2O was added for the purpose of internal locking and taken further for ^{31}P NMR studies (Shukla et al., 1995).

3.3.2. NMR Experiments for the Neutralized Promastigote PCA Extracts

All NMR spectra were recorded at 298K unless otherwise stated, using a Bruker (Fallanden, Switzerland) *Avance* DRX 300 MHz FT-NMR spectrometer (7.2 T, 54 mm vertical-bore magnet) equipped with a 5 mm multinuclear inverse-probehead with a Z-shielded gradient, operating at a proton frequency of 300.13 MHz. The spectrometer was operated from a Silicon Graphics Indy workstation and controlled by Bruker's XWINNMR software (version 2.6). The ^{1}H NMR experiment was run using a standard water-suppression pulse-sequence and the spectra were recorded between 0 to 10 ppm in all samples with the following acquisition parameters: spectral width of 3.491 kHz, 32768 data points, total relaxation time of 8.13 s, 32 free-induction decays (FIDs) were accumulated and 0.3 Hz line-broadening was used prior to Fourier transformation. The two-dimensional COSY experiment with water-suppression was performed using Bruker's standard pulse-program library, with 1024 data-points using 256 t_1 increments with a repetition time of 2 s, and 128 transients per t_1 increment. The raw data was zero-filled up to 512 W in F_1 using sine-bell window function prior to double Fourier transformation. Metabolite assignments were carried out based on the standard literature available (Wuthrich, 1986; Gribbestad et al., 1994; Sitter et al., 2002), and were with respect to the chemical shift position of the terminal methyl of alanine (doublet) at 1.48 ppm that served as an internal chemical shift reference.

The ^{31}P NMR spectrum was recorded at 121.49 MHz between –30 to 30 ppm for the PCA extract of one of the representative *L. donovani* strains (Dd8) to observe the phosphate resonances.

The experimental parameters were as follows: spectral width of 8.169 kHz, 32768 data points, pulse width 90° (3.8 μs), relaxation delay 2 s, composite pulse decoupling using WALTZ-16, 18000 FIDs were accumulated to obtain a reasonably good signal-to-noise ratio, and a line-broadening of 1.0 Hz was used prior to Fourier transformation. The chemical shifts were calibrated with respect to the ^{31}P signal of NTP (β-P) assigned at -21.21 ppm, taking into consideration the likely influence of pH on many of the commonly assigned ^{31}P signals of the metabolites (Moreno et al., 2000).

3.4. NMR Studies on Live Dd8 Promastigotes

The live Dd8 promastigotes were harvested during the stationary phase of growth as mentioned earlier for the promastigote PCA extracts. The cell-count was adjusted approximately to 1 x 10^8 cells/ml, and centrifuged at 1,500 rpm at 4°C for 10 min, re-suspended with 0.6 ml phosphate-buffer saline (PBS) and washed at least thrice with the same solution to remove FCS, if any. The pellet obtained was re-suspended in PBS with a total volume of 200 μl, and was taken for the NMR studies. A concentration of 10% D_2O was added into the PBS buffer for the purposes of internal locking in the NMR spectrometer prior to the suspension of the promastigotes. The study was divided into two major categories: (a). Dd8 promastigotes in PBS without $^{13}C_1$-glucose (180 μl PBS + 20 μl 100% D_2O), and (b). Dd8 promastigotes in PBS supplemented with $^{13}C_1$-glucose as the energy source. For the second category, a concentration of 5.3 mg/ml $^{13}C_1$-enriched glucose (0.03 M, > 99 atom% ^{13}C) in 100% D_2O was prepared, and a volume of 20 μl of the $^{13}C_1$-glucose-D_2O mixture was added into the buffer prior to the suspension of the cells (180 μl PBS + 20 μl $^{13}C_1$-glucose-D_2O mixture).

NMR experiments were separately carried out by suspending the Dd8 promastigotes in N_2-bubbled (to mimic hypoxic or anaerobic conditions) and in O_2-bubbled (to mimic normoxic or aerobic conditions) PBS along with $^{13}C_1$-glucose to observe the metabolic changes, if any, based on a standard protocol as reported earlier (Lohmeier-Vogel et al., 1995). Anaerobic conditions were induced in PBS by bubbling N_2 at a rate of 25-ml/min, whereas O_2 bubbling at a rate of 25-ml/min defined aerobic conditions. The cells suspended in the buffer were transferred into a 5 mm NMR tube (Wilmad Glass, USA) containing low-gelling agarose up to a height of 1.5 cm, to

prevent sedimentation of the cells beyond the sensitivity region of the receiver coil (Kotitschke et al., 1994). Once the cells were transferred into the NMR tube, the whole setup was kept in ice and brought to the spectrometer. The NMR experiments were started within approximately 30 min once the samples were prepared, and were continued up to 12 hours depending upon the experimental conditions. Once the NMR experiments were over, the cell viability was checked microscopically using a haemocytometer; the promastigotes were found to be motile and alive up to approximately 5 hours while they were maintained in PBS without any external energy-source, and were alive up to approximately 18 hours beyond the NMR experimentation when they were maintained in PBS with $^{13}C_1$-glucose as the external energy-source.

For the live Dd8 promastigotes, the experimental parameters of the ^{1}H NMR with water pre-saturation essentially remained the same as mentioned above for the PCA extracts. The probe-head temperature was initially maintained at 277K (4°C) for some of the experiments in order to prevent cells from becoming anaerobic and to minimize the metabolic rate, thereby prolonging the viability of the Dd8 cells within the NMR tube. The temperature was later maintained at 298K (25°C) in certain cases, wherever required. The experimental parameters were: spectral width of 3.491 kHz, 32,768 data points, total relaxation time of 4.69 s, 128 FIDs were accumulated and 2.00 Hz line-broadening was used prior to Fourier transformation. The ^{1}H Carr-Purcell Meiboom-Gill (CPMG) experiments were performed mainly to minimize the resonance contribution of membrane lipid components of the Dd8 cells as well as to help in the ^{1}H resonance assignments. The acquisition parameters for the CPMG experiment were: relaxation delay 2 s, τ = 0.6 ms, repetition rate 1600 times, 128 FIDs were accumulated and 3.0 Hz line-broadening was used prior to Fourier transformation. The Hahn spin-echo experiments were performed for the spectral editing of longer T_2 components and to observe the phase reversal of *J*-coupled multiplets, with an echo-time (TE) of 160 ms. Proton chemical shift assignments of the metabolites were carried out with respect to the terminal methyl of alanine (doublet) at 1.48 ppm, as done for the PCA extracts.

^{13}C NMR experiments were performed at 75.47 MHz for one of the samples incubated with $^{13}C_1$-glucose to observe the ^{13}C-labeled metabolite resonances, with the following experimental parameters: spectral width of 19.96 kHz, 32768 data points, pulse width 90° (10 μs),

relaxation delay 2 s, composite pulse decoupling using WALTZ-16, 22000 FIDs were accumulated to obtain a reasonably good signal-to-noise ratio, and a line-broadening of 3.0 Hz was used prior to Fourier transformation. The ^{13}C chemical shifts of the metabolites were referred to the C1α of glucose at 92.3 ppm. The 'user-defined' 300/75 MHz gradient ^{1}H-^{13}C HSQC experiments with water-presaturation pulse-sequence were also recorded for the live Dd8 promastigotes incubated with $^{13}C_1$-glucose as the sole carbon source, which were maintained in the phosphate-buffer saline under normal, hypoxic and normoxic buffer conditions.

4. Results

4.1. ^{1}H NMR Studies for the Neutralized Promastigote PCA Extracts

The representative ^{1}H NMR spectrum for one of the *L. donovani* strains (S-lal) has been given in fig. 1a-b to highlight the intracellular metabolites assigned at 300 MHz, and the detailed assignments are given in Table-2. The metabolites in the ^{1}H NMR spectra were further identified by the cross-peak mapping of two-dimensional COSY contour plot for the strain S-lal (fig. 2a-b). Since all strains in the present study displayed nearly similar ^{1}H NMR spectrum profiles (fig. 3), the standard assignments in Table-2 were utilized to identify the metabolites in the remaining *L. donovani* strains. ^{1}H resonance signals occurring due to the presence of valine, lactate, alanine, arginine, citrulline, acetate, acetoacetate, glutamate, succinate, citrate, choline, α-glycerophosphorylcholine (α-GPC), betaine, mannose, tyrosine, phenyl alanine, formate, uracil, cytosine, guanine, adenine, UTP/UDP, CTP, GTP, NAD/NADH and ATP/ADP were assigned in all promastigote PCA extracts.

^{1}H resonance signals arising from the ribose sugars bound to uracil, cytosine, guanine and adenine, and in the forms of UTP/UDP, CTP, GTP, NAD/NADH, ATP/ADP (as nucleotides) were found to be highly abundant in all ^{1}H NMR spectra of the promastigote PCA extracts of the *L. donovani* strains (fig. 3). The *J*-correlations for the sugar resonances in the COSY spectrum (fig. 2a-b) further indicated that only ribose units might be present in these nucleotides. This has also been substantiated by the fact that only uracil could be assigned along with adenine, guanine and cytosine. The chemical shift assignments of these nucleic acid bases and their sugars have

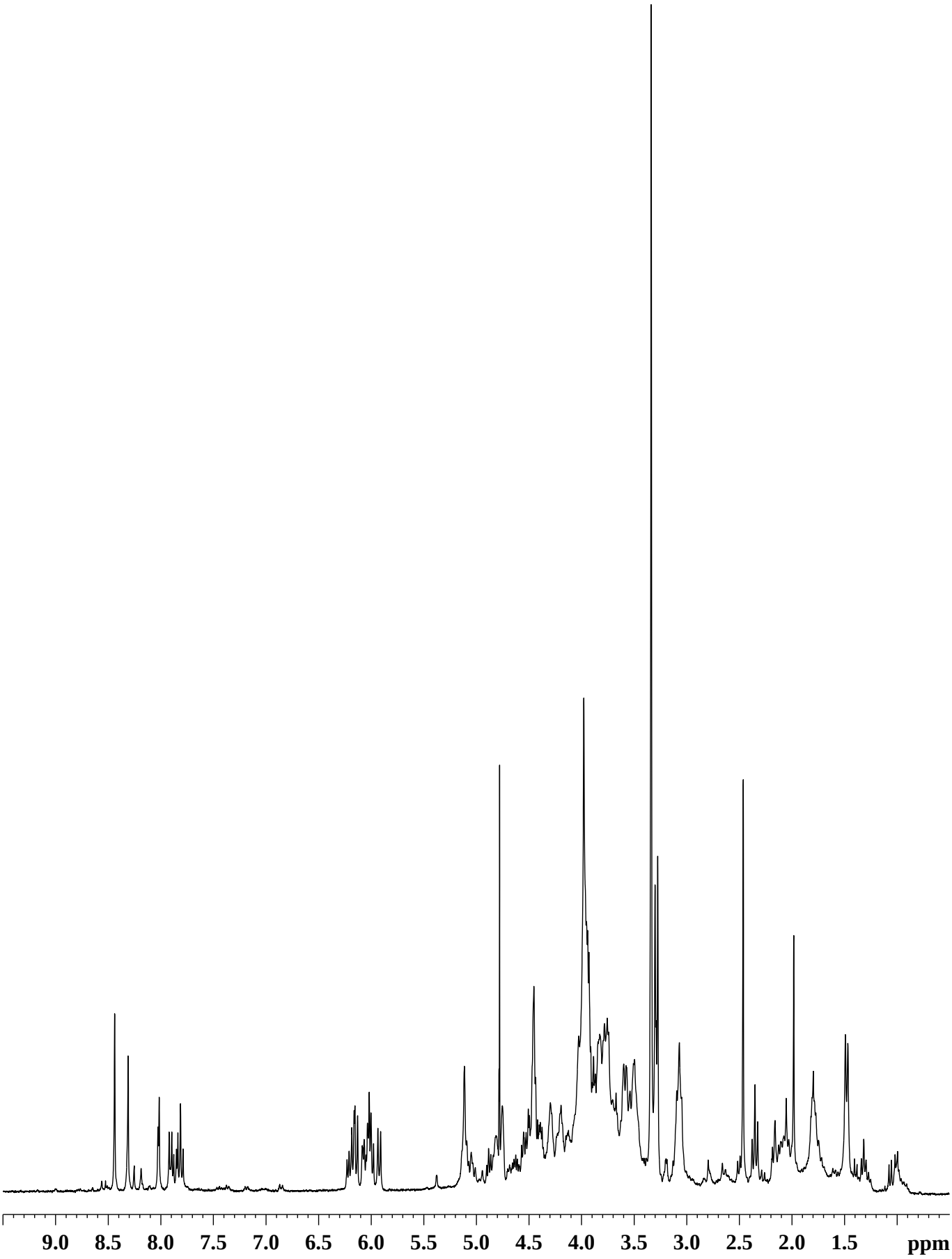

Fig. 1a: ^{1}H NMR spectrum of the promastigote PCA extract of a representative *L. donovani* strain (S-lal).

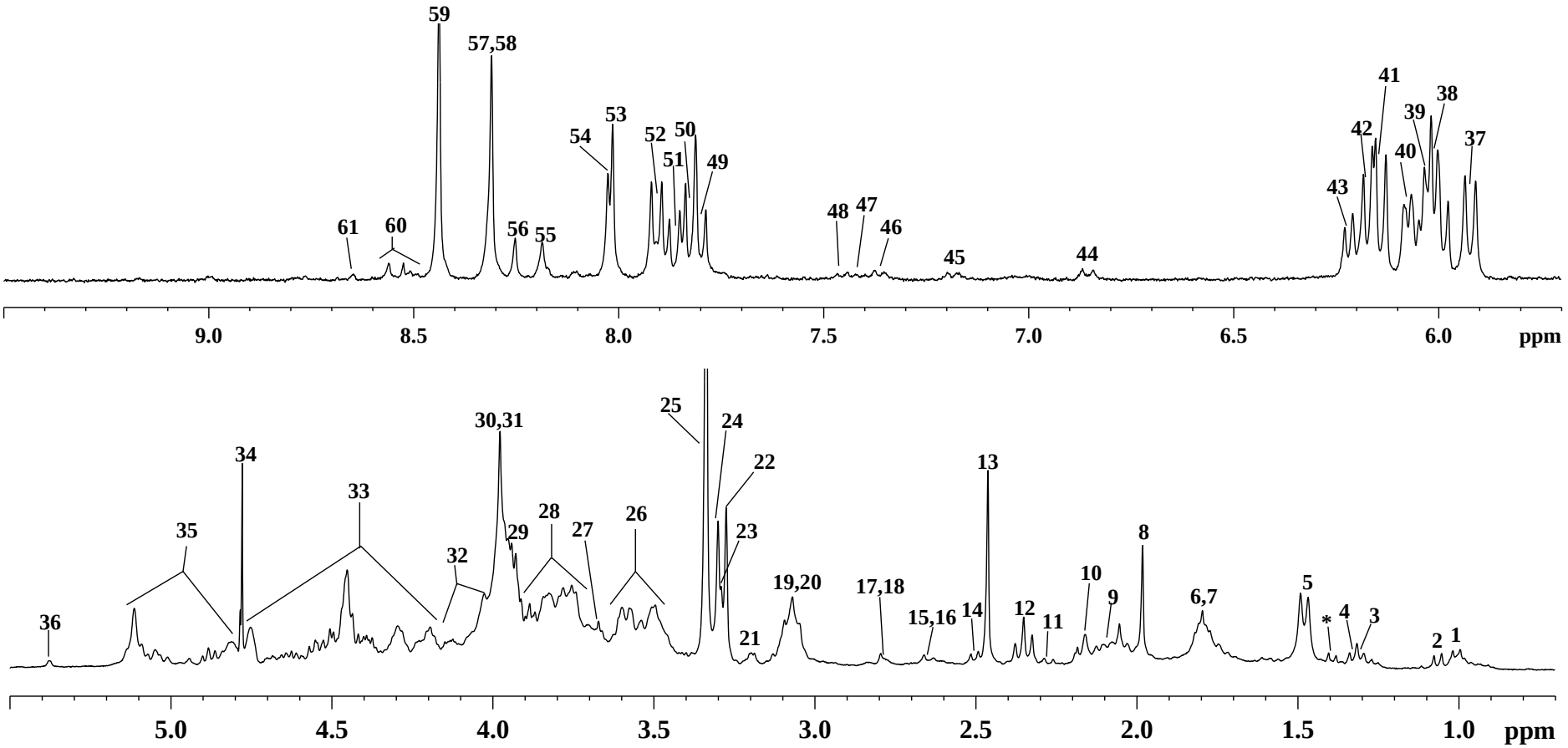

Fig. 1b: Expansions of the ^{1}H NMR spectrum of the promastigote PCA extract of a representative *L. donovani* strain (S-lal), highlighting the resonance assignments between 0.7-5.5 ppm and 5.7-9.5 ppm. The labeled assignments of the metabolites are as given in Table-2.

Table-2: Proton chemical shift assignments of the metabolites, as seen in the ^{1}H NMR spectrum of the promastigote PCA extract of the *L. donovani* strain S-lal. The chemical shift referencing has been done with respect to the terminal -CH_3 of alanine (doublet) at 1.48 ppm. Minor variations in the chemical shift assignments are as expected due to the influence of pH. The ^{1}H multiplicity is denoted as, s: singlet; d: doublet; dd: double doublet; t: triplet; m: multiplet. Resonances marked as * are unassigned.

Metabolite	**Chemical Shift (δ, ppm)**		**Assignment Number**	**^{1}H Multiplicity**
Valine	γCH_3	1.01	1	d
Valine	$\gamma' CH_3$	1.06	2	d
Threonine	γCH_3	1.31	3	d (overlapped)
Lactate	CH_3	1.33	4	d (overlapped)
Alanine	βCH_3	1.48	5	d
Arginine	$\beta,\gamma CH_2$	1.65-1.86	6	m
Citrulline	$\beta,\gamma CH_2$	1.65-1.86	7	m
Acetate	CH_3	1.98	8	s
Glutamate	βCH_2	2.08	9	m (overlapped)
Glutamine	βCH_2	2.15	10	m (overlapped)
Valine	βCH	2.27	11	m
Glutamate	γCH_2	2.35	12	t
Succinate	$\alpha,\beta CH_2$	2.46	13	s
Glutamine	γCH_2	2.41-2.48	14	m (overlapped)
Citrate	αCH_2	2.64	15	d (overlapped)
Aspartate	βCH	2.64	16	d (overlapped)
Citrate	$\alpha' CH_2$	2.78	17	d (overlapped)
Aspartate	$\beta' CH$	2.78	18	d (overlapped)
Arginine	δCH_2	2.99-3.14	19	m
Citrulline	δCH_2	2.99-3.14	20	m
Threonine, Tyrosine	βCH, 1/2 βCH_2	3.19-3.23	21	d (broad)
Choline	$N^+(CH_3)_3$	3.27	22	s
Phosphocholine	$N^+(CH_3)_3$	3.28	23	s (overlapped)
α-GPC	$N^+(CH_3)_3$	3.30	24	s
Betaine	$N^+(CH_3)_3$	3.34	25	s
Myo-inositol, Cholines, Ribose sugars	CH, CH_2	3.43-3.63	26	overlapped signals
Glutamate, Glutamine	αCH	3.67	27	t
Ribose sugars, Alanine, Aspartate, Citrulline	CH, αCH	3.71-3.95	28, 29	overlapped signals

Metabolite	Chemical Shift (δ, ppm)		Assignment Number	^{1}H Multiplicity
Lactate	CH	3.97	30	m (overlapped)
Betaine	αCH_2	3.98	31	s
Myo-inositol, Cholines, Threonine	CH, CH_2, αCH	4.00-4.16	32	overlapped signals
Mannose, Ribose sugars, Glycerol-backbone	CH, CH_2	4.16-4.75	33	overlapped signals
Water, residual	HOD	4.77	34	s
Ribose sugars, Glycerol backbone	CH, CH_2	4.81-5.17	35	overlapped signals
Mannose	αCH (anomeric)	5.38	36	s (broad)
Uracil (bound)	5H (C5 ring)	5.92	37	d
Ribose sugar	CH	6.01	38	d (overlapped)
Ribose sugar	CH	6.03	39	d (overlapped)
Ribose sugar	CH	6.07	40	dd
Cytosine (bound)	5H (C5 ring)	6.14	41	d
Ribose sugar	CH	6.17	42	d
Ribose sugar	CH	6.22	43	d
Tyrosine	3,5H (C3,5 ring)	6.85	44	d
Tyrosine	2,6H (C2,6 ring)	7.18	45	d
Phenylalanine	2,6H (C2,6 ring)	7.36	46	d
Phenylalanine	4H (C4 ring)	7.41	47	d
Phenylalanine	3,5H (C3,5 ring)	7.45	48	d
Uracil (bound)	6H (C6 ring)	7.80	49	d
Uracil (bound)	6H (C6 ring)	7.83	50	d
Cytosine (bound)	6H (C6 ring)	7.86	51	d
Cytosine (bound)	6H (C6 ring)	7.91	52	d
Adenine (bound)	2H (C2 ring)	8.01	53	s
Adenine (bound)	2H (C2 ring)	8.02	54	s
Inosine	2H (C2 ring)	8.18	55	s
ADP and ATP	2H (C2 ring)	8.25	56	s
Adenine (bound)	8H (C8 ring)	8.31	57	s
Guanine (bound)	8H (C8 ring)	8.31	58	s
Formate	$HCOO^-$	8.44	59	s
ADP and ATP	8H (C8 ring)	8.51-8.58	60	s
NADH	4H (N4 ring)	8.65	61	d (broad)

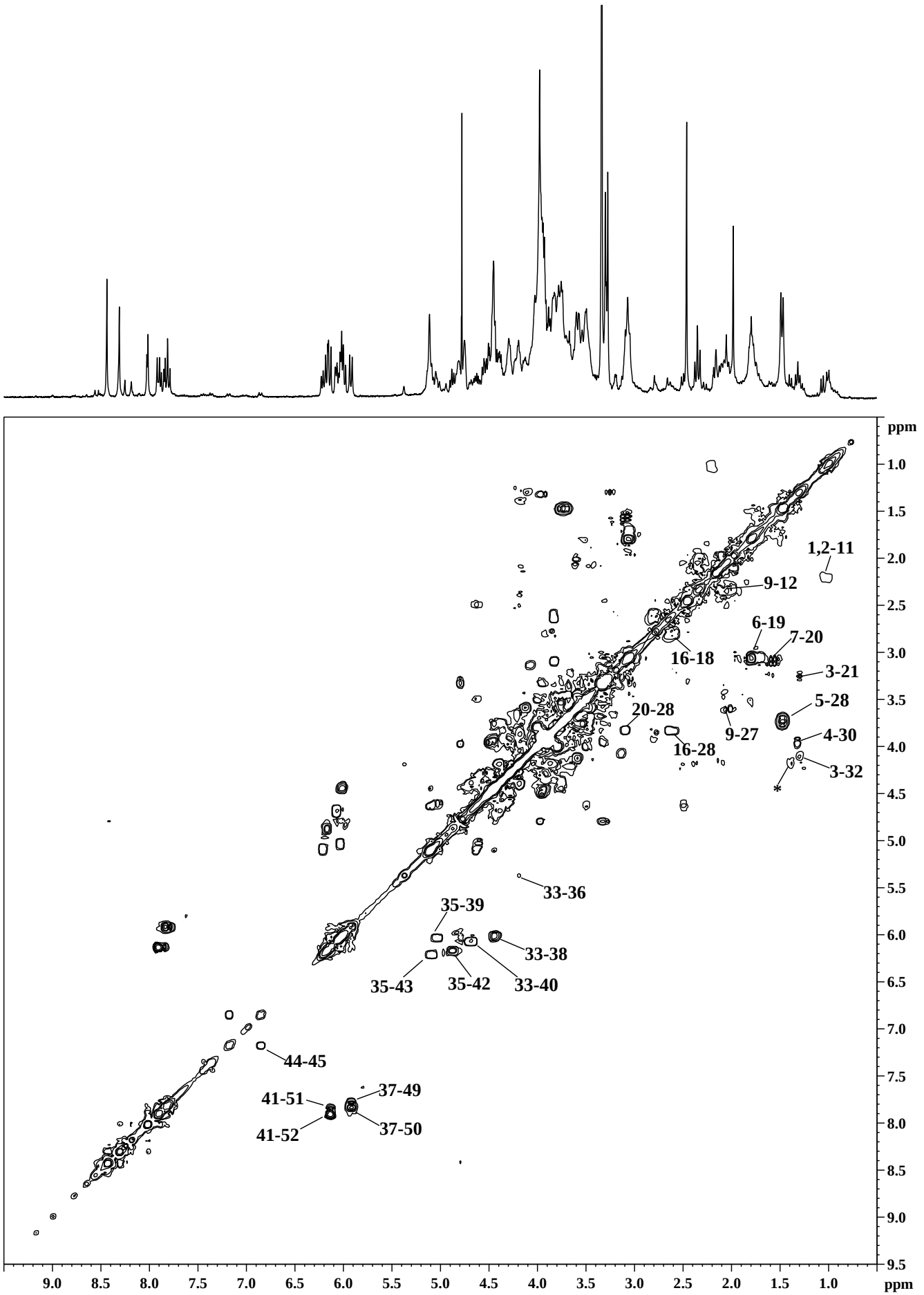

Fig. 2a: ^{1}H-^{1}H COSY of the promastigote PCA extract of a representative *L. donovani* strain (S-lal). The labeled assignments are as given in Table-2.

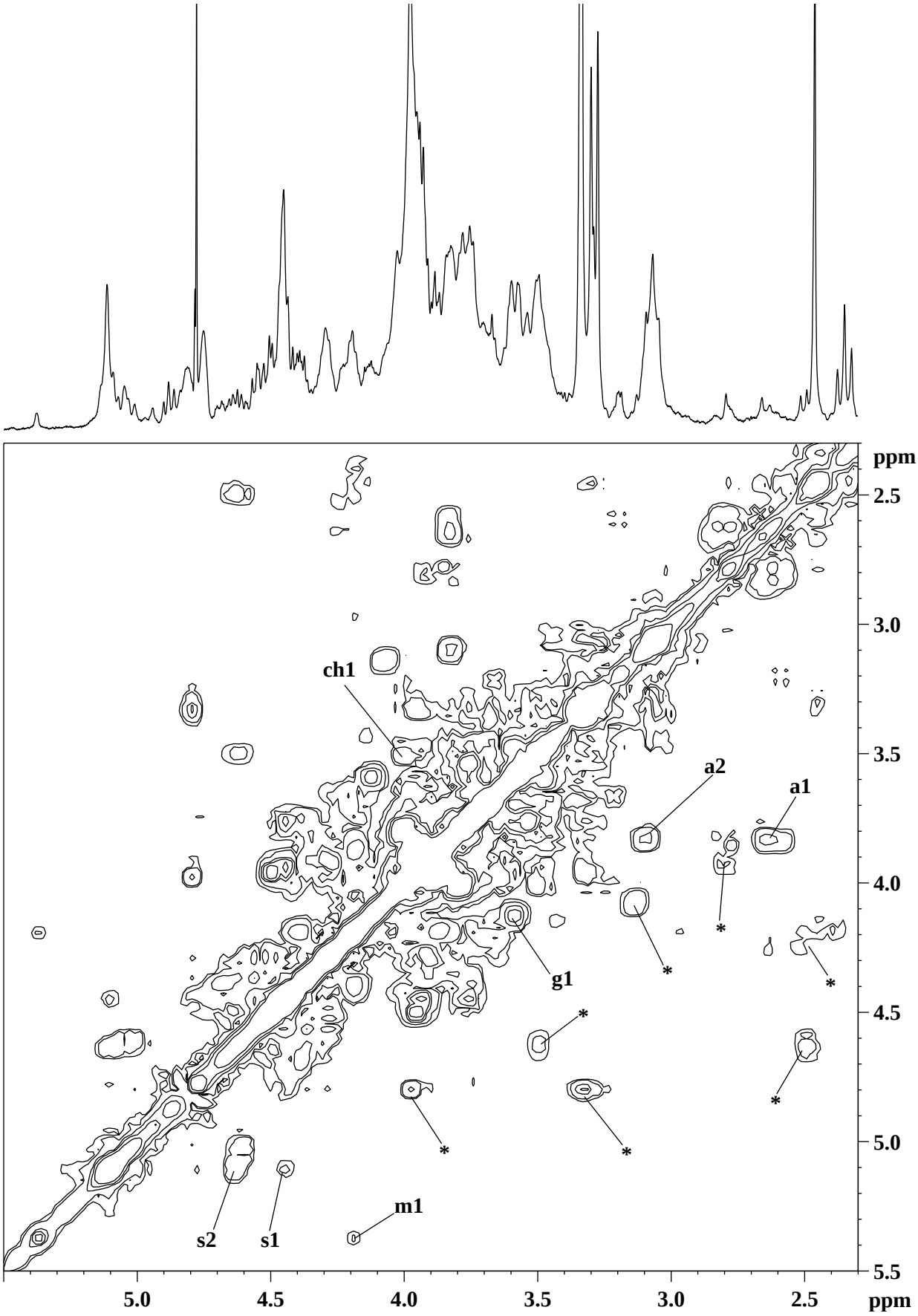

Fig. 2b: Expansion of the ^{1}H-^{1}H COSY spectrum of the promastigote PCA extract of a representative *L. donovani* strain (S-lal), highlighting the resonance assignments between 2.3-5.5 ppm. The labeled assignments are: a1, a2. arginine; ch1. choline; g1. α-GPC; m1. mannose; s1, s2. sugar units of PG; * is unassigned.

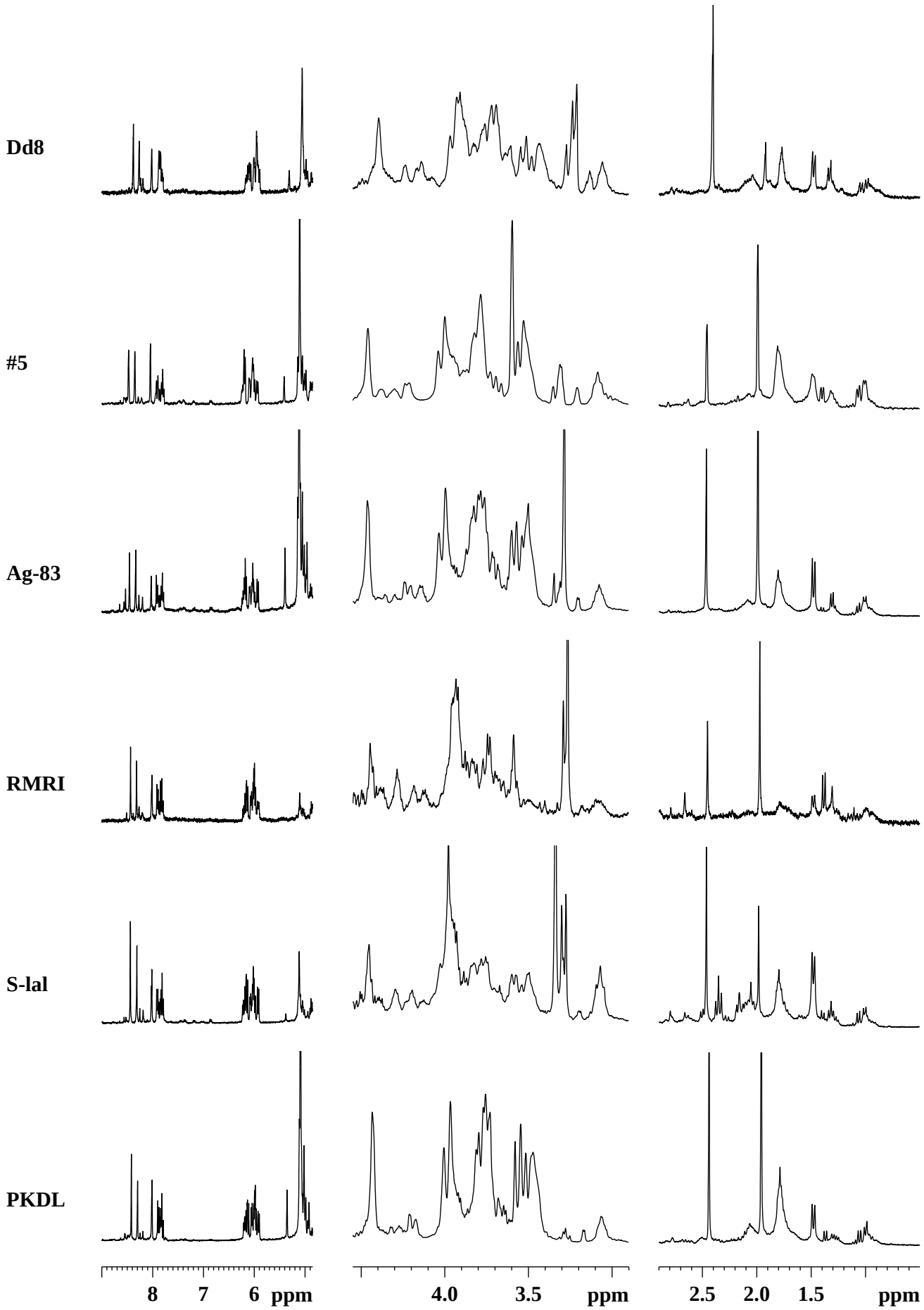

Fig. 3: Stack plot of the ^{1}H NMR spectra of the promastigote PCA extracts of *L. donovani* strains, showing the relative abundance of the metabolite resonances.

been demonstrated for the first time using ^{1}H NMR in the PCA extracts of *L. donovani* promastigotes. In addition to this, presence of mannose-based sugar components possibly arising from the cell membrane portion of the *L. donovani* promastigotes has been observed in all strains of the present study, although the exact resonance assignments could not be carried out due to severe overlapping of the ^{1}H resonances as seen in the expanded region (3.0-5.5 ppm) of the COSY spectrum (figs. 2b), which consisted of signals from the methylenes of the choline head-groups (Loening et al., 2005) and sugar units, as mentioned above.

4.2. ^{31}P NMR Study for the Neutralized Promastigote PCA Extract of the Dd8 Strain

Presence of high-energy phosphate entities and nucleotides in *L. donovani* promastigotes has been established by performing ^{31}P NMR experiment for one of the strains (Dd8), and the chemical shift assignments are shown in fig. 4a-b (Table-3). The chemical shifts of some of the ^{31}P resonances fluctuate in response to pH, while others are sensitive to the level of free magnesium (Mg^{2+}) (Lohmeier-Vogel et al., 1995). The influence of Mg^{2+} could be eliminated by adding EDTA, which acts as a chelating agent. Resonance signals arising from NTP, NDP, NMP (adenosine-, guanosine-, cytidine- and uridine- mono-, di-, and tri-phosphates), pentapolyphosphate, pyrophosphate, glycerophosphorylethanolamine, glycerophosphorylcholine, inorganic phosphate, phosphorylcholine, phosphorylethanolamine, 3-phosphoglycerate, glycerol 3-phosphate and glucose 6-phosphate could be assigned based on the ^{31}P chemical shifts as reported earlier (Moreno et al., 2000; Rager et al., 1999; Miranda et al., 1997; Lohmeier-Vogel et al., 1995). In the present study, the nucleoside tri-, di-, mono-phosphates have been collectively represented as NTP, NDP, NMP, respectively, since it is not possible to selectively identify their individual contributions in the ^{31}P spectra obtained from cell suspensions, perfused cells and human or animal tissues. The total NTP pool is frequently used as an indicator of ATP concentration because NTP predominantly consists of ATP (Lutz et al., 2002).

Elevated levels of pentapolyphosphate (-20.21, -5.32 ppm) and pyrophosphate (-6.09 ppm) could be observed from the ^{31}P spectrum of the promastigote PCA extract of the Dd8 strain, followed by phosphorylcholine (3.53 ppm) and phosphorylethanolamine (4.00-4.09 ppm). A few of the phosphorylated intermediates of glycolysis could be assigned, namely, fructose-6-phosphate (3.81 ppm), 3-phosphoglycerate (4.17 ppm), glycerol 3-phosphate (4.32 ppm), fructose 1,6-

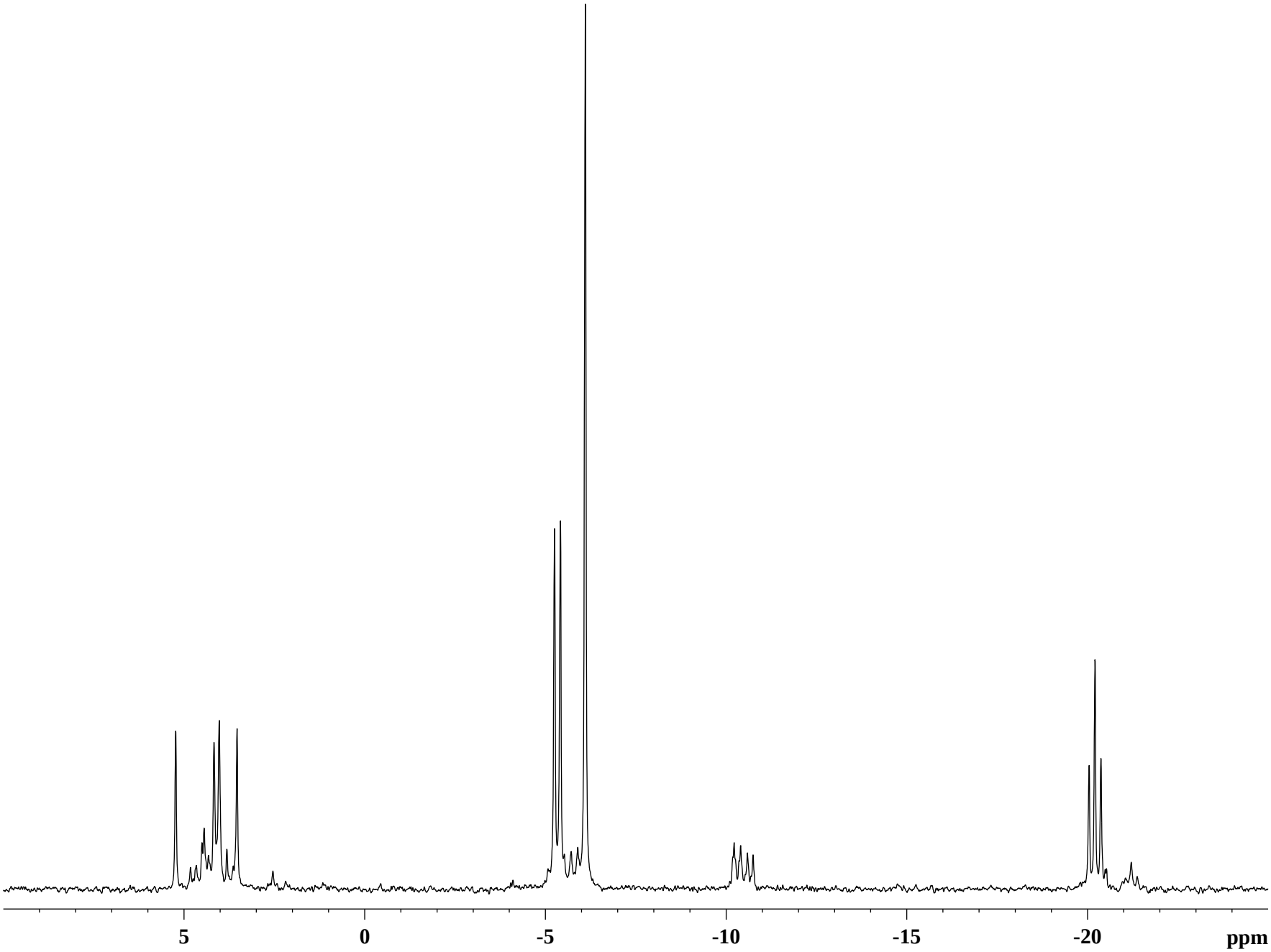

Fig. 4a: ^{31}P NMR spectrum of the promastigote PCA extract of the *L. donovani* strain Dd8.

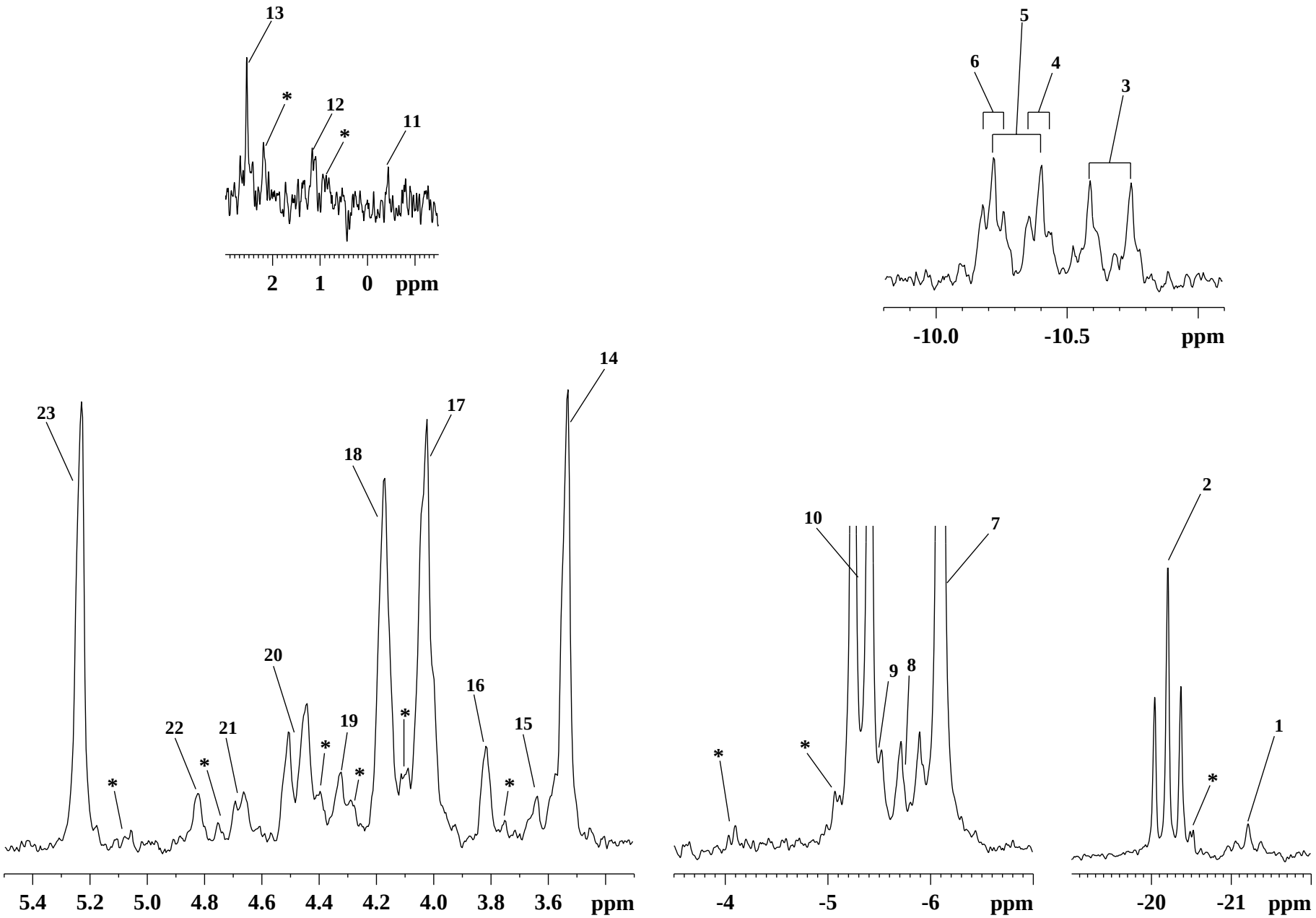

Fig. 4b: Expansion of the ^{31}P NMR spectrum of the promastigote PCA extract of the *L. donovani* strain Dd8, highlighting the resonance assignments between (-22.0)-(-19.0) ppm, (-11.0)-(-9.8) ppm, (-7.0)-(-3.5) ppm, (-1.5)-3.0 ppm and 3.3-5.5 ppm. The labeled assignments are as given in Table-3.

Table-3: ^{31}P chemical shift assignments of the phosphate metabolites, as seen in the ^{31}P NMR spectrum of the promastigote PCA extract of the *L. donovani* strain Dd8. The chemical shifts were calibrated with respect to the ^{31}P signal of NTP (β-P) assigned at -21.21 ppm, taken as an internal reference. Minor variations in the chemical shift assignments are as expected due to the influence of pH. The ^{31}P assignments of the nucleoside- mono-, di- and tri-phosphates have been collectively represented as NMP, NDP and NTP, respectively. The ^{31}P multiplicity is denoted as, s: singlet; d: doublet; t: triplet. Resonances marked as * are unassigned.

Metabolite Assigned	**Chemical Shift (δ, ppm)**	**Assignment Number**	**^{31}P multiplicity**
β-P of NTP	-21.21	1	t
β-P of pentapolyphosphate (PP_5)	-20.21	2	t
α-P of NTP	-10.66	3	d
Uridine 5'-diphosphoglucose (UDPG)	-10.39 (merged with 5)	4	d (overlapped)
α-P of NDP	-10.30 (merged with 4,6)	5	d (overlapped)
NAD^+-UDPG	-10.21 (merged with 5)	6	d (overlapped)
Pyrophosphate	-6.09	7	s
β-P of NDP	-5.79	8	d
γ-P of NTP	-5.43 (merged with 10)	9	d (overlapped)
α-P of PP_5	-5.32	10	d
α-Glycerophosphorylethanolamine	-0.44	11	s
α-Glycerophosphorylcholine	1.12	12	s
Inorganic phosphate (P_i)	2.54	13	s
Phosphorylcholine	3.53	14	s
NMP	3.64	15	s
Fructose 6-phosphate	3.81	16	s
Phosphorylethanolamine + 2-Phosphoglycerate	4.00-4.09	17	s (broad)
3-Phosphoglycerate	4.17	18	s
Glycerol 3-phosphate	4.32	19	s
Fructose 1,6-diphosphate (major)	4.44-4.53 (two forms)	20	s
Fructose 1,6-diphosphate (minor)	4.63-4.71 (two forms)	21	s
Glucose 6-phosphate	4.83	22	s
6-Phosphogluconate	5.23	23	s

diphosphate (4.44-4.71 ppm), glucose 6-phosphate (4.83 ppm) and 6-phosphogluconate (5.23 ppm). The ^{31}P resonances of 2-phosphoglycerate and phosphorylethanolamine were assigned as overlapped signals, which appeared as a broad signal at 4.00-4.09 ppm (fig. 4b). The visual examination of the ^{31}P spectra has also revealed that the intracellular levels of 3-phosphoglycerate, 2-phosphoglycerate and 6-phosphogluconate to be elevated than the other intermediates.

4.3. NMR Studies on Live Dd8 Promastigotes

To ascertain further the details of the metabolism in *L. donovani* promastigotes, NMR experiments were done on the live cells of Dd8 strain obtained at the stationary phase of their growth. The study was divided into two categories: in the first category the live Dd8 promastigotes were suspended in normal PBS without any nutrient and subjected to the NMR studies, and in the second category the parasites were incubated with $^{13}C_1$-glucose under different buffer conditions. For the second category, the conditions involved suspending the cells in normal PBS with $^{13}C_1$-glucose, followed by the incubation with $^{13}C_1$-glucose under hypoxic (anaerobic, N_2-bubbled) and normoxic (aerobic, O_2-bubbled) conditions.

Figs. 5a1-d represent the ^1H NMR along with the ^1H spin-echo and COSY spectra of the live cells without any external energy-source. Signals pertaining to ethanol, lactate, alanine, acetate, acetoacetate, succinate, and resonances pertaining to betaine and choline-containing compounds could be readily assigned for the cells maintained under starved conditions. Resonances of the aliphatic cytosolic amino acids such as valine, leucine and isoleucine could also be identified using 2D ^1H-^1H COSY spectrum (fig. 5d). The levels of lactate, acetate and alanine were pronounced as indicated by the corresponding ^1H resonance-signal intensities, followed by moderately intense signals from acetoacetate, succinate and ethanol (figs. 5a1-c2). The high-field region of the ^1H NMR spectra (1.2-1.4 ppm) also showed the presence of lipid components such as fatty acids, possibly arising due to the membrane rupture of the cells (figs. 5a1-c2).

When the cells were maintained in normal PBS with $^{13}C_1$ glucose at 4°C, there was an increased production of acetate and succinate as seen in the ^1H normal and spin-echo spectra (figs. 6a1, 6b1) than the usually observed high levels of lactate as observed for the cells under starved conditions (figs. 5a1-c2). The cells exhibited a similar ^1H metabolic profile when the temperature

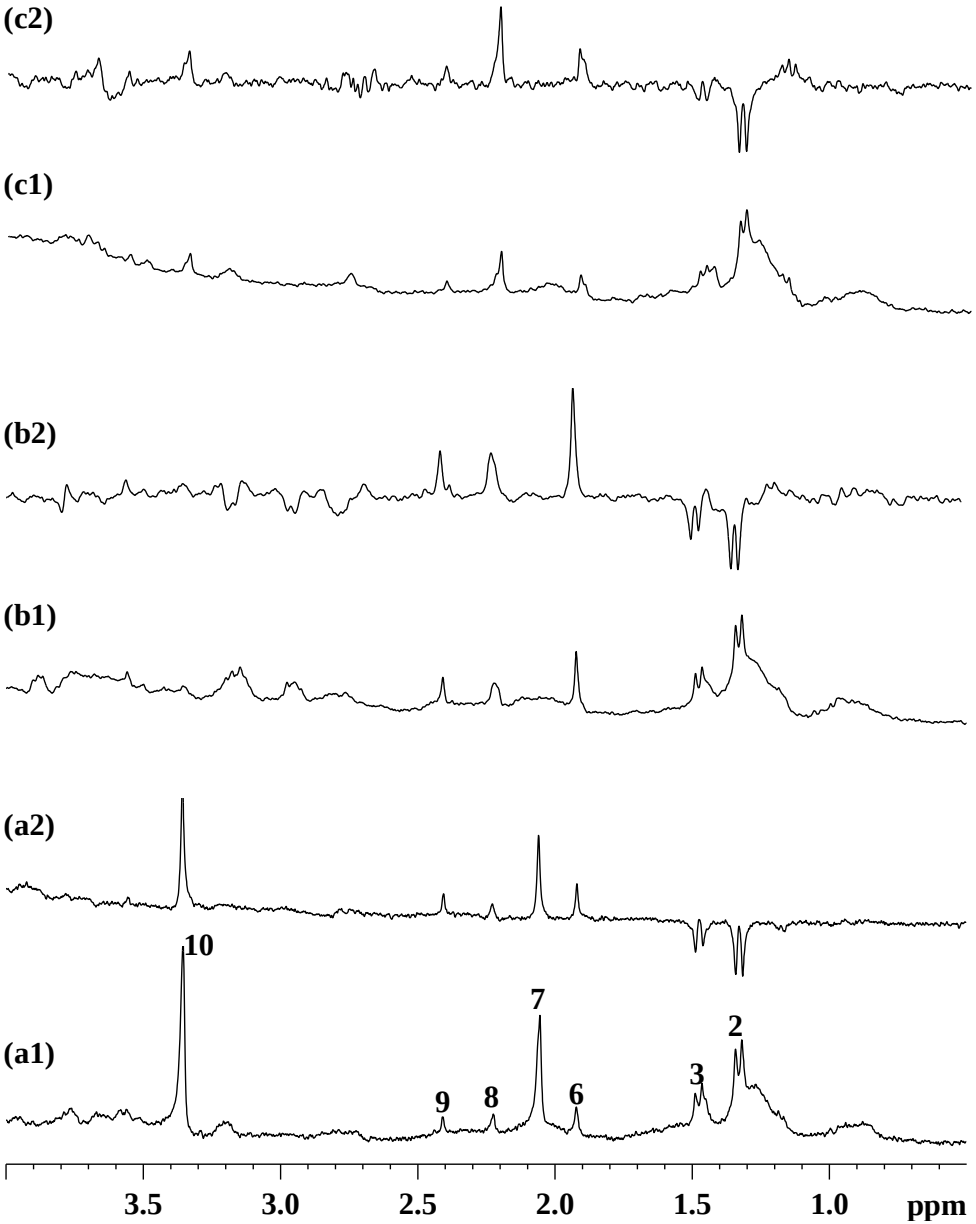

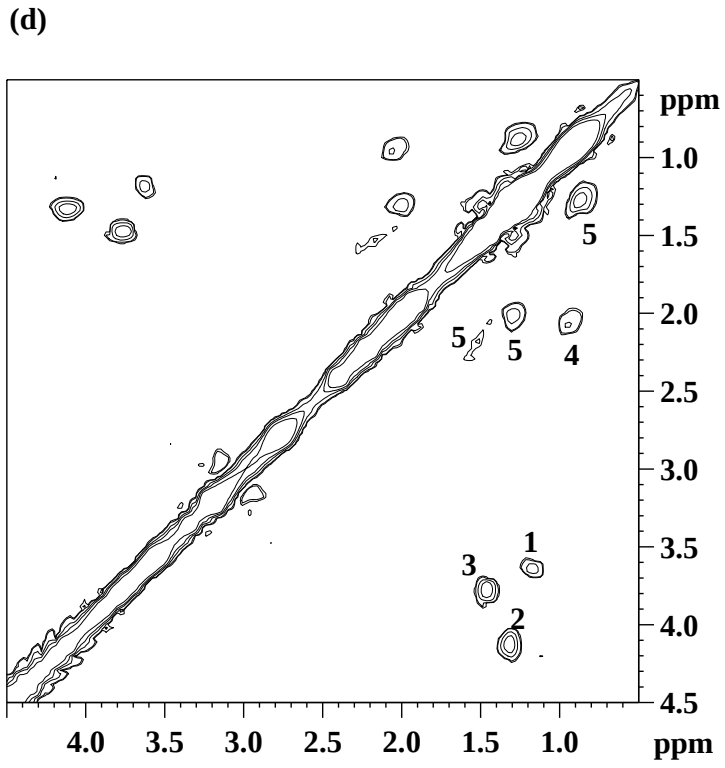

Fig. 5: (**a1**-**c2**). Stack plot of the ^{1}H normal and spin-echo spectra, and (**d**). ^{1}H-^{1}H COSY spectrum of the live Dd8 promastigotes in PBS under starved conditions. The labeled assignments are: 1. ethanol; 2. lactate; 3. alanine; 4. valine/leucine/isoleucine; 5. resonances from the lipids; 6. acetate; 7. resonance from an N-acetyl portion; 8. acetoacetate; 9. succinate; 10. choline-containing compounds.

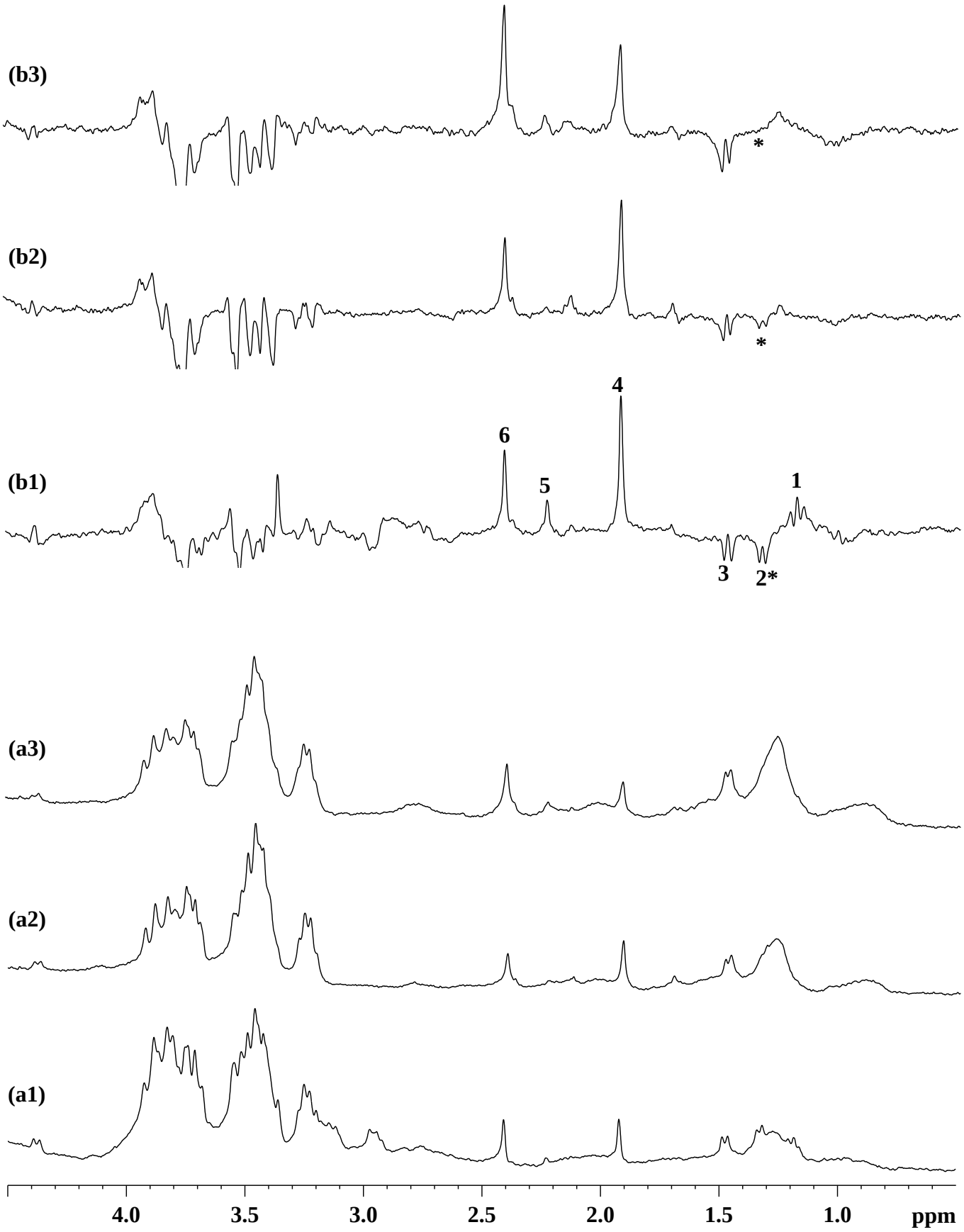

Fig. 6: Stack plot of the ^{1}H normal and spin-echo spectra of the live Dd8 promastigotes incubated with $^{13}C_1$-glucose in: **a1**, **b1**: Normal PBS; **a2**, **b2**: N_2-bubbled PBS; **a3**, **b3**: O_2-bubbled PBS. The labeled assignments are: 1. ethanol; 2. lactate; 3. alanine; 4. acetate; 5. acetoacetate; 6. succinate.

was maintained at 25°C, which was subsequently carried over for the ^{13}C experiments. Upon incubating the promastigotes with $^{13}C_1$-glucose, the ^{13}C resonances of both α- and β-anomers of glucose ($C_1\alpha$: 92.3 ppm; $C_1\beta$: 96.2 ppm) were readily observed; after 18 hours of $^{13}C_1$-glucose incubation, the NMR-observable incorporation of ^{13}C-enrichment was observed to be maximum for succinate and alanine, followed by a moderate labeling of glycerol-based intermediate and acetate, and a minimum labeling of lactate as confirmed from the ^{13}C NMR and ^{1}H-^{13}C HSQC spectra (figs. 7a-c).

When the live Dd8 promastigotes were subjected to anaerobic and aerobic conditions with $^{13}C_1$ glucose available as the energy-source, signals pertaining to succinate, alanine and acetate were mainly observed from the respective ^{1}H-^{13}C HSQC spectra (figs. 6a2-b3, 8a-b). Interestingly, the ^{1}H NMR spectrum of the live Dd8 promastigotes maintained under anaerobic conditions showed a weak lactate signal after 45 min of incubation with $^{13}C_1$ glucose, which was not ^{13}C-labeled (in the C_3 position) as seen in the HSQC spectra (fig. 8a), while no lactate signal could be observed for the cells maintained under aerobic conditions (figs. 6a3, 6b3). Further, the presence of membrane lipid components could be confirmed from the ^{1}H NMR spectra of the cells incubated with $^{13}C_1$-glucose as seen in the high-field region (1.2-1.4 ppm), which hampered the resonance assignments of lactate and ethanol (figs. 6a1-b3). The ambiguity regarding the resonance assignments of lactate and ethanol could be readily resolved with the help of the CPMG experiment, wherein the signals of lactate and ethanol appeared to have merged with the terminal methyl signal(s) arising from lipid components as shown in fig. 9.

5. Discussion

5.1. ^{1}H and ^{31}P NMR Studies on Neutralized Promastigote PCA Extracts

The present investigation using ^{1}H NMR analysis of the promastigote PCA extracts of six *L. donovani* strains has indicated that all the strains have undergone similar biochemical pathways, but with different metabolic activities. A collective visual examination of the ^{1}H NMR spectra revealed no exclusive marker signals that could distinguish the strains (fig. 3), overall indicating a similar spectral pattern in all of them. Although major differences could be observed in the signal

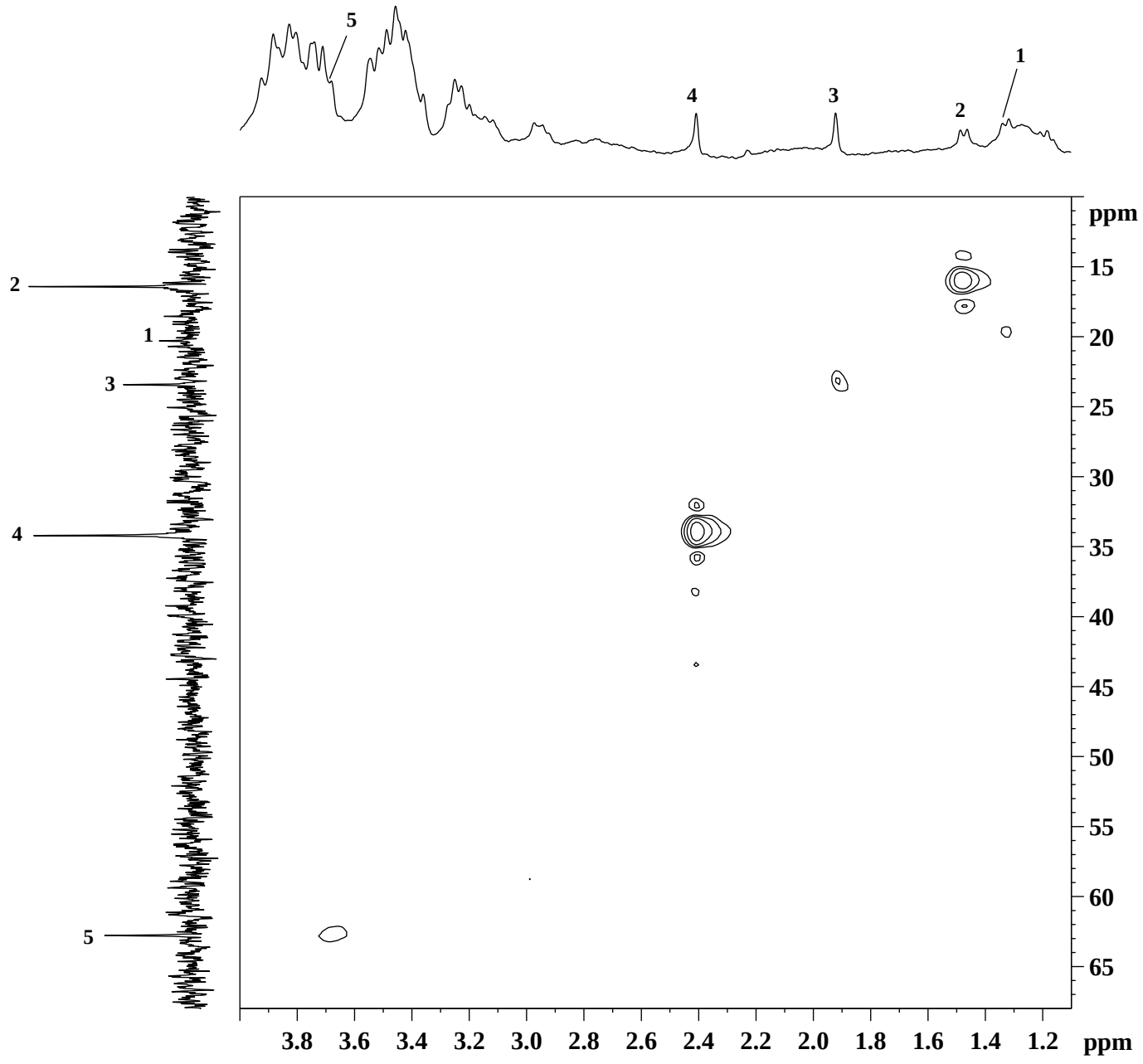

Fig. 7a: ^{1}H-^{13}C HSQC spectrum of the live Dd8 promastigotes in normal PBS incubated with $^{13}C_1$-glucose, highlighting the assignments and relative abundance of the ^{13}C-labeled metabolites. The labeled assignments are: 1. lactate; 2. alanine; 3. acetate; 4. succinate; 5. glycerol-based intermediate (glycerol-3-phosphate).

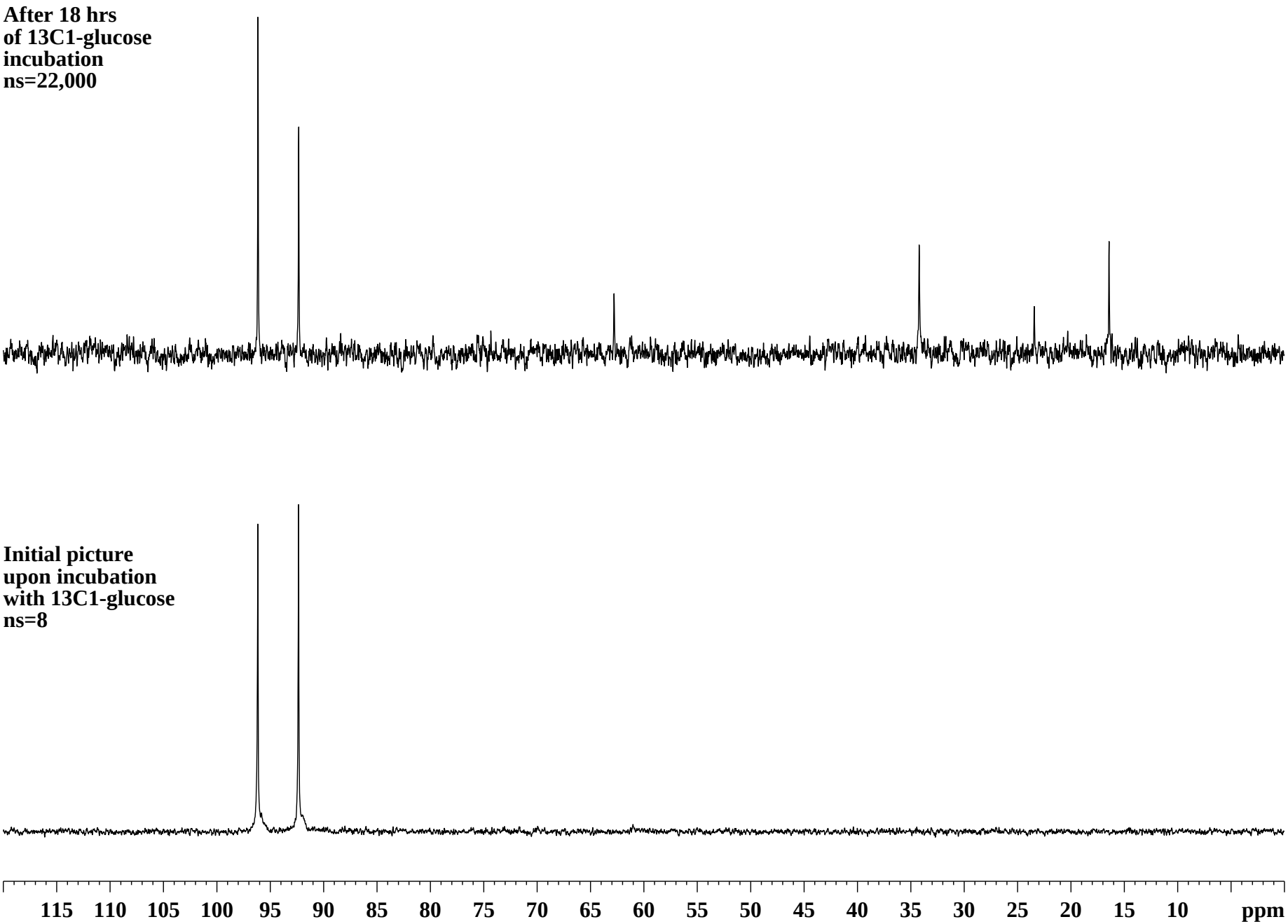

Fig. 7b: Stack plot of the ^{13}C NMR spectra of the live Dd8 promastigotes in normal PBS incubated with $^{13}C_1$-glucose.

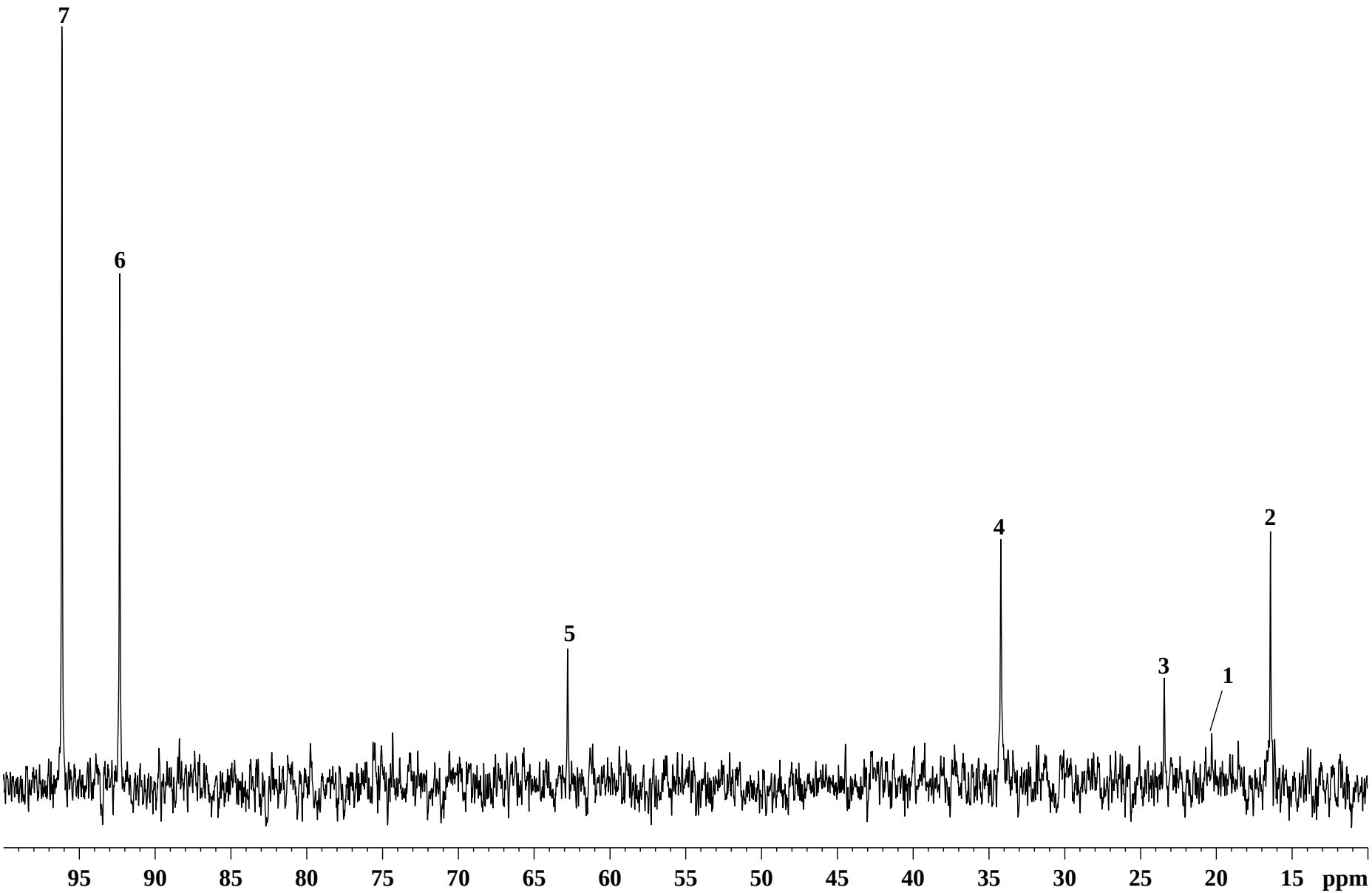

Fig. 7c: Expansion of the ^{13}C NMR spectrum of the live Dd8 promastigotes in normal PBS incubated with $^{13}C_1$-glucose, highlighting the resonance assignments between 10.0-100.0 ppm. The labeled assignments are: 1. lactate; 2. alanine; 3. acetate; 4. succinate; 5. glycerol-based intermediate (glycerol-3-phosphate); 6: β-glucose (C_1); α-glucose (C_1).

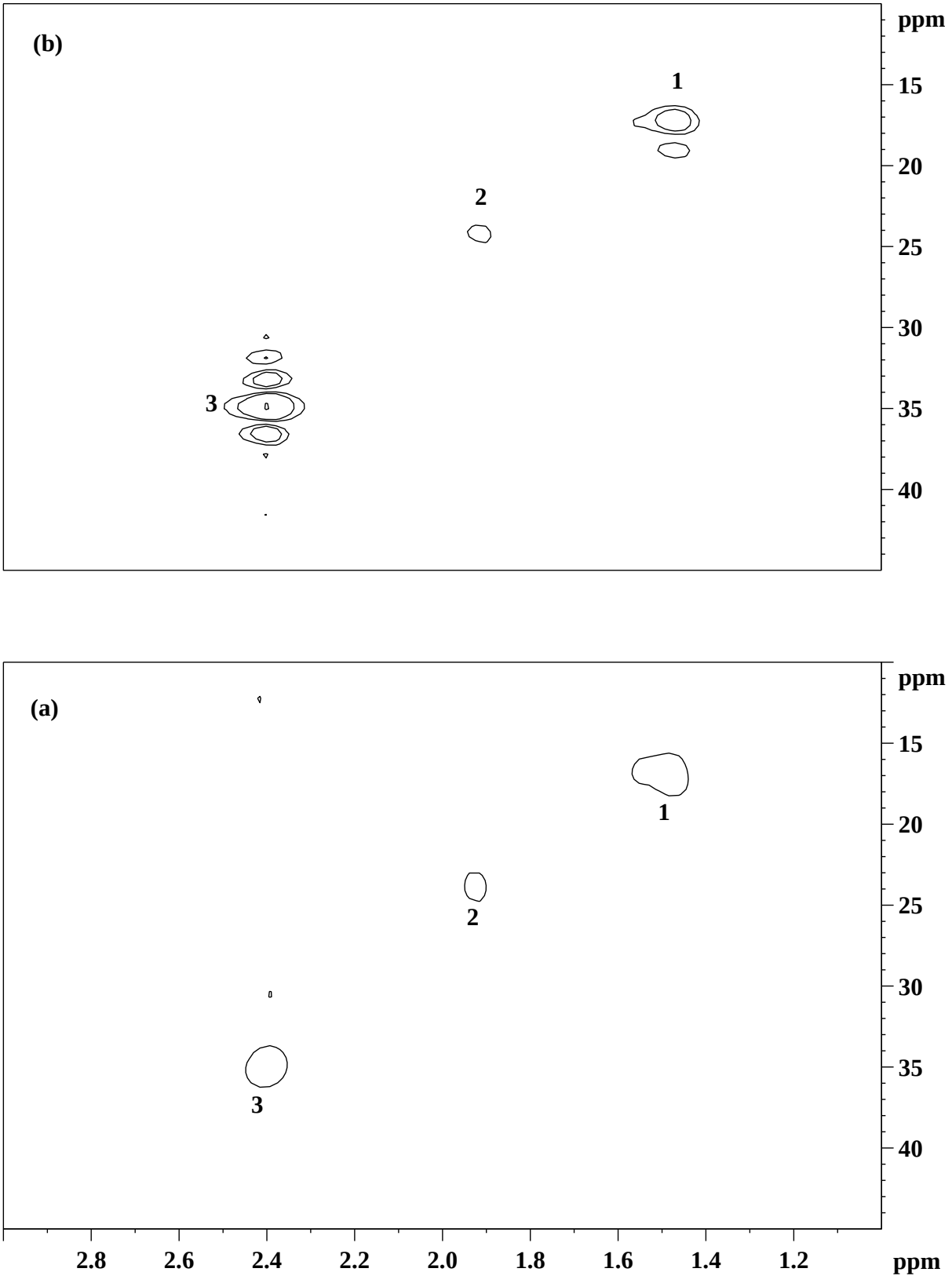

Fig. 8: ^{1}H-^{13}C HSQC spectrum of the live Dd8 promastigotes highlighting the assignments and relative abundance of the ^{13}C-labeled metabolites when incubated with $^{13}C_1$-glucose in: **a**. N_2-bubbled PBS; **b**. O_2-bubbled PBS. The labeled assignments are: 1. alanine; 2. acetate; 3. succinate.

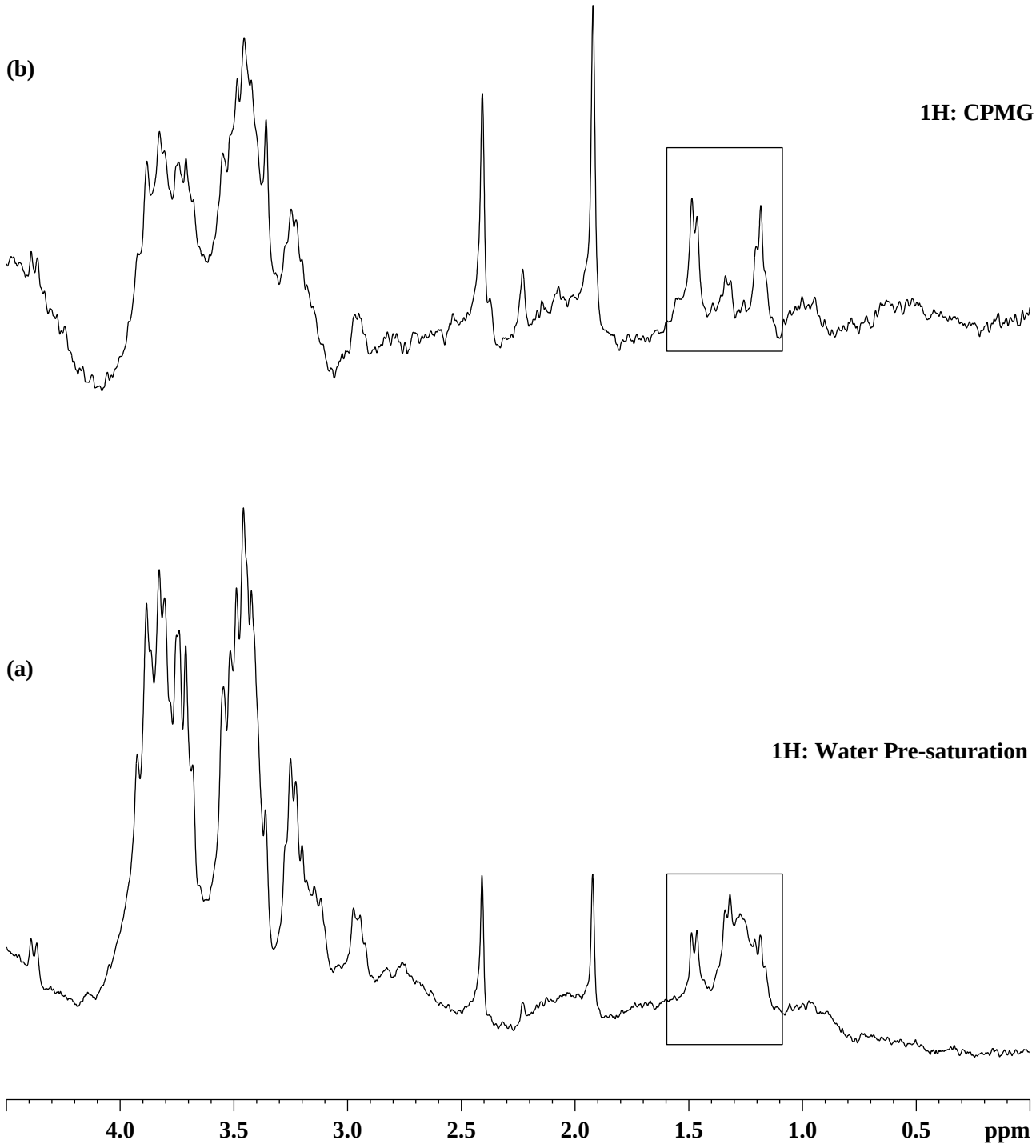

Fig. 9: Stack plot of the ^{1}H normal and CPMG spectra of the live Dd8 promastigotes incubated with $^{13}C_1$-glucose in normal PBS, highlighting the overlapping resonance contribution of lipids.

intensity profiles of the metabolites, such as succinate, acetate and choline-containing compounds (fig. 3), they could not be treated as 'strain specific' markers.

^{1}H NMR signals arising from citrate, succinate, acetate, lactate and formate were assigned (fig. 1a-b; Table-2) during the course of the present investigation. Metabolic studies have demonstrated that glucose, though a substrate of secondary importance is consumed by *Leishmania* promastigotes grown in tissue culture medium. The final products of glucose catabolism by *Leishmania* spp. have been previously characterized (Chatterjee et al., 1973; Cazullo, 1992). It has also been observed that carbohydrates were metabolized primarily by aerobic fermentation in the promastigotes, wherein they oxidize sugars incompletely to a mixture of organic acids (e.g., succinate, acetate, and pyruvate), lactate and CO_2 (Chatterjee et al., 1973; Glew et al., 1988; Janovy, 1987; Crowther et al., 1954). Based on the studies done on the carbohydrate metabolism of *Leishmania* spp., glucose is most likely converted to triose phosphates by a combination of the pathway of glycolysis and the pentose phosphate pathway (Berens et al., 1980). Triose phosphates are metabolized to pyruvate via the intermediary of phosphoenol pyruvate (PEP); pyruvate is converted to oxaloacetate, most likely by means of the pyruvate carboxylase reaction, and oxaloacetate is converted sequentially to malate, fumarate, and succinate (Berens et al., 1980). It was observed that no NMR-observable glucose signals could be assigned in the ^{1}H NMR spectra of the promastigote PCA extracts of *L. donovani* in the present study, which implies that glucose could have been broken down to some of the metabolic products as cited above. The fermentation-based conversion of glucose to PEP could have resulted in succinate, where PEP was simultaneously converted to pyruvate, finally resulting in lactate. The formation of succinate could have also resulted from the citric-acid cycle, with the entry of pyruvate formed in glycolysis; conversion of pyruvate might have further resulted in the production of NMR-observable alanine, acetate and formate as shown in fig. 1a-b.

Earlier studies done on different species of *Leishmania* have shown that although all the major metabolites of promastigotes are common to different species but their relative abundance varies from species to species, for example, *L. major* produces mainly succinate and acetate and much smaller quantities of alanine and pyruvate, whereas acetate and alanine are the major metabolites observed in *L. donovani* (Rainey and MacKenzie, 1991; Castilla et al., 1995). It was

also reported earlier that four major species of *Leishmania* form D-lactate under anaerobic conditions (Darling et al., 1988). In the present study, among the products of glucose metabolism, succinate and acetate were observed in relatively higher levels than lactate. It has been reported that the concentration of intracellular lactate in axenic and intracellular amastigotes is 3–4-fold increased than promastigotes, possibly due to their likely preference for the anaerobic catabolism (Gupta et al., 1999). Darling and co-workers (1987) hypothesized that the survival of *Leishmania* species under anaerobic conditions may be mediated by the increased production of D-lactate, which generates NAD^+ from NADH. While the chirality of lactate was not determined in the present study, it could be pointed out that the level of anaerobic respiration varied from strain to strain, which further prompted the present study to be aimed at the biochemical implications associated with lactate production involving live Dd8 promastigotes.

It was reported that *Leishmania* promastigotes rely mainly on amino acids as their primary fuel sources instead of fatty acids or glucose (Marr, 1980), providing an information that glucose is a substrate of secondary importance and metabolized only by the stationary-phase cells. It was also reported that rates of amino acid utilization in general were higher in promastigotes than in amastigotes; proline was a poor substrate for both (Hart and Coombs, 1982). Based on the ^1H NMR observations of the present study, it could be stated that all *L. donovani* strains have utilized both glucose and certain amino acids as efficient substrates, as seen in the respective ^1H NMR spectra of the PCA extracts (figs. 1a-b, 3). Only a few of the amino acids could be assigned, which included arginine, glutamate, alanine, valine and tyrosine (figs. 1a-b, 2a-b). It was also observed that the relative levels of amino acids such as tyrosine and valine were found to be less than the levels of products of glucose metabolism in all strains. Among amino acids that were assigned, the relative levels of arginine and alanine were found to be higher in almost all strains than tyrosine and valine (fig. 3).

Arginine is utilized by *Leishmania* for metabolic functions (Blum, 1992) and has been shown to induce oxygen consumption in *L. donovani* promastigotes at rates comparable to those of D-glucose (Bera, 1987). As reported by Bera (1987), it could be reasoned that the pronounced levels of arginine, followed by succinate, could have occurred due to the assimilation of L-arginine by *L. donovani* promastigotes through the α-ketoglutarate pathway, which involves the

intermediary of γ-guanidinobutyramide and the enzyme L-arginine decarboxyoxidase that finally converts L-arginine to succinate. On the other hand, pronounced level of glutamate could be observed in only one strain, while it was present in very low abundance in others (fig. 3). Although the reason for this is not clear, it might be reasoned that the biosynthesis of glutamate in this strain had occurred in a pronounced manner from the α-ketoglutarate that was produced via the citric-acid cycle. This high abundance of glutamate in one of the promastigote PCA extracts (S-lal) has been demonstrated in fig. 10.

It is well known that the protozoan parasite *Leishmania* has a remarkable ability to survive and proliferate in extreme microbicidal environments during its digenetic life cycle in the sand-fly vector and the human host. All life-cycle stages of *Leishmania* species produce a unique class of glycoconjugates named phosphoglycans in abundance ($> 10^7$ copies/cell) (Turco et al., 2001). These include the most abundant cell-surface molecule lipophosphoglycan (LPG) expressed by the infectious promastigote stage and proteophosphoglycans (PPG) secreted by the intracellular amastigote form of the parasite. These phosphoglycans (PG) have been found to have a critical role in subverting the host immune system, help in binding of the parasite to the sandfly midgut epithelial cells and to human macrophages, and in receptor-mediated phagocytosis via direct interaction with carbohydrate binding sites (Mengeling et al., 1997). The presence of mannose as an integral component of LPG could be ascertained from the ^{1}H resonance signal at 5.38 ppm (anomeric -CH) in all strains, although further chemical shift assignments of the LPG units could not be carried out due to complex coupling-network pattern of overlapped signals, as seen in the COSY spectrum (fig. 2b).

Besides mannose, choline-containing compounds and betaine have been assigned in the present study (figs. 1b, 2b; Table-2). Choline is a vital component of cell membranes in most eukaryotes; it is an essential nutrient required by the body to make several important compounds necessary for healthy cell membranes. Among its various functions, it serves as a methyl donor and checks the cell-proliferation process since methyl units are essential for RNA and DNA replication, a process ongoing in every cell of the body. Another major role of choline in a living system is in the formation of betaine (trimethylglycine), an important methyl donor, which is

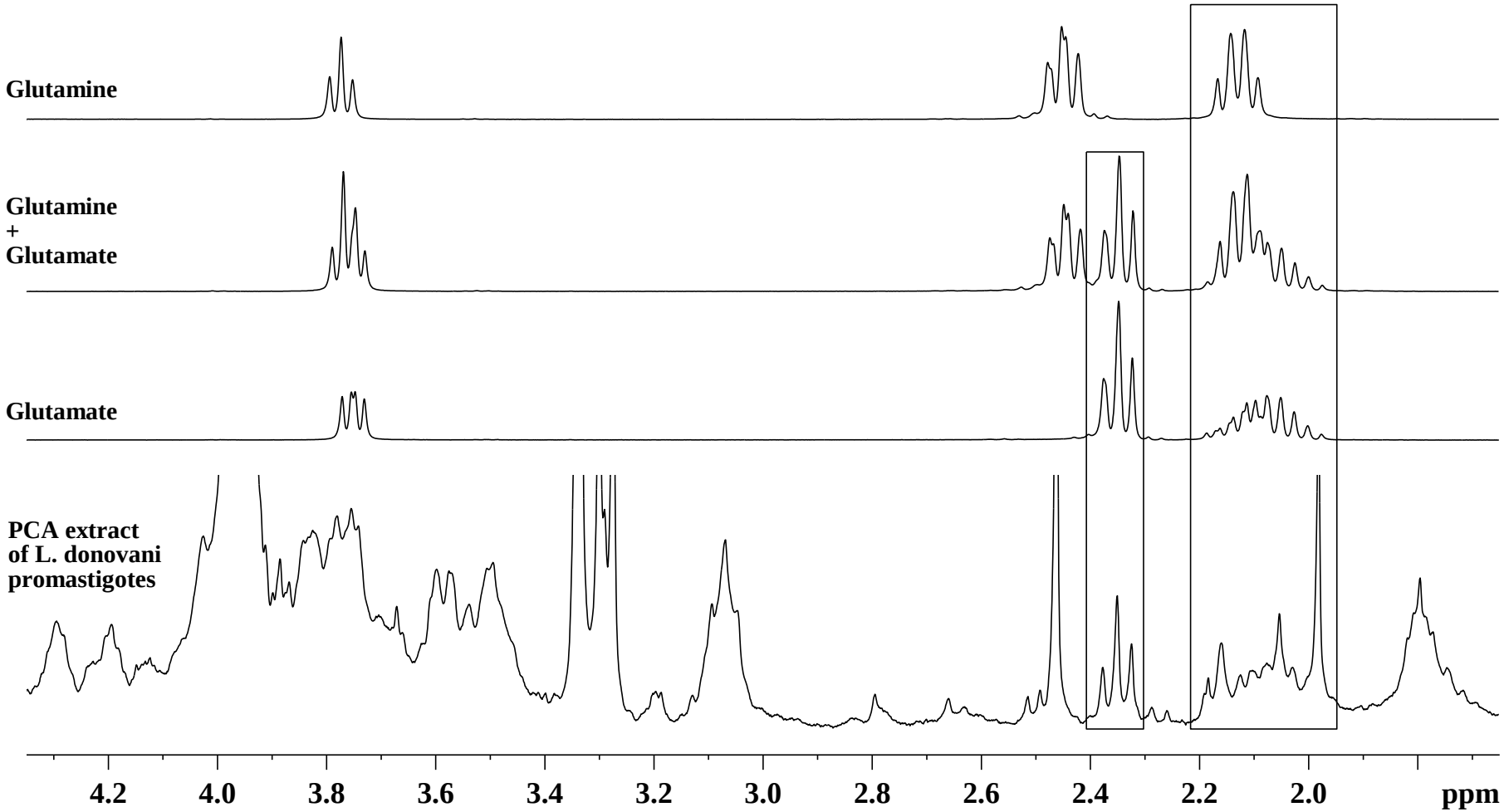

Fig. 10: Confirmation of the chemical shift assignments of glutamate in the ^{1}H NMR spectra of promastigote PCA extract of a *L. donovani* strain (S-lal), highlighting the relative abundance of glutamate (as marked in the rectangular boxes) based on the comparison of the individual spectra of glutamate and glutamine.

synthesized during the glycine biosynthesis from choline. Betaine is found in a variety of plant and animal sources, and serves as a substrate in one of the two recycling pathways that convert homocysteine to L-methionine. Apart from choline and betaine, the presence of α-GPC as one of the major cellular products in *L. donovani* promastigotes is of considerable interest. α-GPC has been defined as one of the most important metabolic reservoir of phospholipids, the orthomolecules that are the structural and functional foundation of cell membranes, besides serving as an effective source of choline. It could be stated that the biosynthesis of α-GPC possibly arises from phosphatidylcholine or lysolecithin by the action of phospholipase-A_2 (Adosraku et al., 1993). Considering the biochemical implications of α-GPC into consideration, it could be proposed that along with mannose it may participate in maintaining the integrity of the cell membrane (membrane-bound phospholipids) in *L. donovani*. The relative levels of choline-containing compounds and betaine have been observed to vary in the *L. donovani* strains in the present study (fig. 3), which might be attributed to the difference in the lipid catabolism and the likely differences in the mitochondrial structure and enzyme abundance of the promastigotes (Gupta et al., 1999).

The NMR assignments of nucleic acid bases such as adenine, guanine, cytosine and uracil, as well as their presence in the form of nucleosides/nucleotides have formed an important aspect during the course of the present investigation. Since *Leishmania* species appear to be incapable of synthesizing the purine nucleus *de novo* and therefore require exogenous purines for growth (Marr and Berens, 1985), the pronounced occurrence of nucleic acids might have occurred due to either increased uptake or increased metabolic activity involving these nucleic acid bases. The ^{31}P assignments of NTP, NDP, NMP and various metabolic intermediates of glycolysis such as glucose 6-phosphate, fructose 6-phosphate, fructose 1,6-diphosphate, glycerol 3-phosphate, 3-phosphoglycerate, 2-phosphoglycerate and 6-phosphogluconate have given a preliminary insight regarding the possible energy machinery in *L. donovani* strains, which has been explored further by using live Dd8 cells in the present investigation. Combined together, the ^{1}H and ^{31}P NMR observations (figs. 1b, 4b) have indicated that the nucleic acid bases might be present in ribose-bound phosphorylated forms during the infective (metacyclic) promastigote stage, and may play a

role in the phosphorylation of certain amino acids and/or proteins in *L. donovani* strains (Singh et al., 2003; Prasad and Dey, 2000).

5.2. NMR Studies on Live Dd8 Promastigotes

In addition to the abovementioned observations for the promastigote PCA extracts, it was essential to explore the possible mechanisms/pathways that might be operative in *L. donovani* promastigotes using NMR. The NMR experiments involving the live Dd8 cells revealed significant results; in particular, consistent production of lactate was observed for the cells maintained under starved conditions (figs. 5a1-d). While lactate was produced to a varying degree when incubated with $^{13}C_1$-glucose and maintained under normal and anaerobic PBS conditions (figs. 6a1, 6b1, 6a2, 6b2), the extent of lactate production appeared to be almost nil when the parasites were suspended in O_2-bubbled PBS enriched with $^{13}C_1$-glucose (aerobic condition), as seen in the ^{1}H normal and spin-echo spectra (figs. 6a3, 6b3).

The ^{1}H and ^{13}C NMR observations regarding the metabolism of $^{13}C_1$-glucose, by the live Dd8 promastigotes, have indicated that the cells consume both the β-anomer (^{13}C signal at 96.2 ppm) and the α-anomer (^{13}C signal at 92.3 ppm) (figs. 7b-c). Consumption of glucose was accompanied by the appearance of the ^{13}C-labeled resonance signals of $^{13}C_2$ and $^{13}C_3$ succinate (34.2 ppm), $^{13}C_2$-acetate (23.4 ppm), $^{13}C_3$-alanine (16.4 ppm) and $^{13}C_3$-lactate (20.3 ppm), with the prominent distribution of the ^{13}C-label favored towards succinate and alanine as seen in the ^{1}H-^{13}C HSQC contour plots (figs. 7a, 8a-b). It could be stated that, excluding alanine and a glycerol-based intermediate (possibly $^{13}C_1$ of glycerol 3-phosphate, ^{13}C signal at 62.8 ppm), lactate and ethanol were observed to be the major end products of glucose metabolism; succinate and acetate might be the end products or might act as the substrates for further metabolic reactions. Apart from lactate, ethanol was produced as a metabolic end product in the cells under starved conditions (figs. 5a1-d) as well as in the cells maintained with $^{13}C_1$ glucose in normal PBS (figs. 6a1, 6b1). As reported earlier for *P. shigelloides* (Rager et al., 2000), these observations and the labeling pattern of the metabolites in live Dd8 promastigotes have given an indication that glucose was most likely converted via the Embden-Meyerhof-Parnas glycolytic pathway, with the associated conversion of pyruvate to succinate, alanine and acetate. This was further supported by

the ^{31}P NMR performed on the promastigote PCA extract of the Dd8 strain, wherein many of the metabolic intermediates and high-energy phosphates of the proposed pathway could be observed (fig. 4b; Table-3).

While the live Dd8 promastigotes under starved conditions exhibited enhanced lactate production (figs. 5a1-d), the *L. donovani* strains subjected to the PCA extract method showed markedly low levels of lactate than alanine, acetate and succinate (fig. 3). This corresponded to the decreased level of lactate in live Dd8 cells under anaerobic conditions upon incubation with $^{13}C_1$-glucose (figs. 6a2, 6b2). Although this lactate signal could be observed in the ^{1}H spin-echo spectrum (fig. 6b2), it could not be detected in the corresponding HSQC spectrum for the live cells under anaerobic conditions (fig. 8a), possibly due to the fact that lactate was not ^{13}C-labeled at C_3 position. This is in contrast to the observations made for the cells under normal conditions, in which lactate was ^{13}C-labeled at C_3 position, as seen in the corresponding HSQC spectrum (fig. 7a). Since lactate was observed under anaerobic conditions, but was not ^{13}C-labeled, it might be likely that lactate was not solely derived through the metabolic conversion of $^{13}C_1$-glucose. In other words, while glycolysis and citric-acid cycle could still be the primary metabolic pathways in *L. donovani* promastigotes, an alternative biochemical mechanism or reserve energy-source utilization might be essentially responsible for the production of lactate under the said conditions.

The markedly elevated ^{1}H NMR signals of lactate for live Dd8 cells under starved conditions indicated that the parasites had experienced a high-degree of anaerobic condition (possibly due to endogenous respiration). The likely influence of the osmotic stress coupled with high density of the cells in PBS (200 μl) might have automatically rendered the medium highly anaerobic, ultimately producing increased lactate as the end product of metabolic conversion of the reserve energy-source. In contrast to this observation, when the parasites were incubated with $^{13}C_1$-glucose (in normal PBS) they seemed to rely on the external energy-source available in the form of glucose, in addition to the reserve energy-source. The signal intensity of lactate in this case was almost similar to that of alanine, while it was less than succinate and acetate (figs. 6a1, 6b1). Since lactate was only partially ^{13}C-labeled (figs. 7a-b), the utilization of reserve energy-source could not ruled out. Taken together, the decreased ^{1}H signal intensity of lactate with a partial ^{13}C labeling, an increased ^{1}H signal intensity of succinate and acetate, an increased ^{13}C

labeling in succinate and alanine, followed by a moderate ^{13}C labeling in acetate, seem to justify the role of both glycolysis and citric acid cycle when the promastigotes were maintained in PBS with glucose as the external energy-source. In addition to this, the ^{13}C-labeling of lactate and a glycerol-based intermediate (possibly glycerol 3-phosphate) could be observed only for the cells under normal buffer conditions (figs. 7a-b), and seemed to be absent for the cells under anaerobic and aerobic conditions as seen in their corresponding HSQC spectra (figs. 8a-b).

It could be summarized that lactate production was different under different conditions; when starved, the promastigotes were found to use the endogenous reserve energy-source (possibly glycogen), producing high levels of lactate followed by acetate and ethanol (figs. 5a1-c2). When the promastigotes were provided an external energy-source in the form of $^{13}C_1$ glucose, utilization of the reserve energy-source decreased; the level of lactate was decreased, while the levels of succinate and acetate were pronounced. The weak ^{13}C-labeling of lactate indicated that the parasites (in normal PBS) had utilized the external energy-source and metabolized it partially to lactate; the majority of lactate was produced by the metabolic conversion of the reserve energy-source. The cells under anaerobic conditions relied on the reserve energy-source but to a lesser extent, which was accounted for the production of lactate; they predominantly utilized $^{13}C_1$-enriched glucose as the external energy-source, and thus produced the metabolic intermediates specifically succinate and acetate. Lastly, when the cells were maintained under aerobic conditions with $^{13}C_1$-glucose, they did not produce lactate and seemed to utilize only the $^{13}C_1$-enriched glucose and not the reserve energy-source. No NMR-observable lactate was produced by the cells under aerobic conditions, which seemed to justify that the cells met their energy demands mainly by the metabolic conversion of glucose via other biochemical pathways such as citric-acid cycle. These unique observations in *L. donovani* promastogites are to be explored further using other conventional biochemical techniques.

6. Conclusions

^{1}H NMR studies on the promastigote PCA extracts have highlighted that the *L. donovani* strains have undergone similar biochemical pathways, but with different metabolic activities. The

^{31}P assignments of the metabolic intermediates have given a preliminary insight regarding the possible energy machinery in *L. donovani* promastigotes, which has been explored further in live Dd8 cells. NMR studies involving live *L. donovani* Dd8 promastigotes have indicated the possible existence of a reserve energy-source that might help the parasites for their survival under different conditions.

7. Future Scope of the Work

The work paves way for further studies on live Dd8 cells under different conditions using NMR and other conventional biochemical techniques so as to under the bioenergetics of *L. donovani* promastigotes. Further, a comprehensive metabolic profiling of intracellular metabolites involving the field-isolates (samples collected from kala-azar patients) could be carried out using NMR, which may aid in characterizing drug responsiveness and/or unresponsiveness.

References

Adosraku RK, Anderson MM, Anderson GJ, Choi G, Croft SL, Yardley V, Phillipson JD, Gibbons WA (1993) *Mol Biochem Parasitol* 62:251-262.

Bates PA (1993) *Parasitol Today* 9:143-146.

Bera T (1987) *Mol Biochem Parasitol* 23:183-192.

Berens RL, Deutsch-King LC, Marr JJ (1980) *Exp Parasitol* 49:1-8.

Blum JJ (1992) *J Protozool* 39:613-618.

Carter KC, Sundar S, Spickett C, Pereira OC, Mullen AB (2003) *Antimicrob Agents Chemother* 47:1529-1535.

Castilla JJ, Sanchez-Moreno M, Mesa C, Osuna A (1995) *Mol Cell Biochem* 142:89-97.

Chang KP, Fong D, Bray RS (1985) Biology of Leishmania and Leishmaniasis. In *The Leishmaniasis*. Eds, KP Chang and RS Bray. Amsterdam: Elsevier Biomedical Press, pp 1-30.

Chatterjee T, Dutta AG (1973) *Exp Parasitol* 33:138-146.

Croft SL, Neal RA, Pendergast W, Chan JH (1987) *Biochem Pharmacol* 36:2633-2636.

Crowther S, Fulton JD, Joyner LP (1954) *Biochem J* 56:182-185.

Darling TN, Davis DG, London RE, Blum JJ (1987) *Proc Natl Acad Sci USA* 84:7129-7133.

Darling TN, Balber AE, Blum JJ (1988) *Mol Biochem Parasitol* 30:253-258.

Davies CR, Kaye P, Croft SL, Sundar S (2003) *BMJ* 326:377-382.

Doyle PS, Engel JC, Pimenta PFP, DaSilva PP, Dwyer DM (1991) *Exp Parasitol* 73:326-334.

Drummelsmith J, Brochu V, Girard I, Messier N, Ouellette M (2003) *Mol Cell Proteomics* 2:146-155.

Gilroy FV, Edwards MR, Norton RS, O'Sullivan WJ (1988) *Mol Biochem Parasitol* 31:107-115.

Glew RH, Saha AK, Das S, Remaley AT (1988) *Microbiol Rev* 52:412-432.

Goyal N, Singh AK, Guru PY, Rastogi AK (1995) *Ind J Exp Biol* 33:222-226.

Gribbestad IS, Petersen SB, Fjosne HE, Kvinnsland S, Krane J (1994) *NMR Biomed* 7:181-194.

Griffin JL (2003) *Curr Opin Chem Biol* 7:648-654.

Grivet JP, Delort AM, Portais JC (2003) *Biochimie* 85:823-840.

Guerin PJ, Olliaro P, Sundar S, Boelaert M, Croft SL, Desjeux P, Wasunna MK, Bryceson AD (2002) *Lancet Infect Dis* 2:494-501.

Gupta N, Mittal N, Goyal N, Maitra SC, Rastogi AK (1996a) *Trop Med* 38:39-50.

Gupta N, Goyal N, Kumar R, Agarwal AK, Seth PK, Rastogi AK (1996b) *Trop Med Int Health* 1:495-502.

Gupta N, Goyal N, Singha UK, Bhakuni V, Roy R, Rastogi AK (1999) *Acta Trop* 73:121-133.

Hart DT, Coombs GH (1982) *Exp Parasitol* 54:397-409.

Hendricks LD, Wood DE, Hajduk ME (1978) *Parasitology* 76:309-316.

Herwaldt BL (1999) *Lancet* 354:1191-1199.

Hodgkinson V, Soong L, Duboise SM, McMahon-Pratt D (1996) *Exp Parasitol* 83:94-105.

Hwang HY, Ullman B (1997) *J Biol Chem* 272:19488-19496.

Janovy J (1987) Physiology and biochemistry. In *The Leishmaniasis in Biology and Medicine*. Eds, W Peters and R Killick-Kendrick. London: Academic Press, pp 178-210.

Jha TK, Sundar S, Thakur CP, Bachmann P, Karbwang J, Fischer C, Voss A, Berman J (1999) *N Engl J Med* 341:1795-1800.

Keun HC, Ebbels TM, Antti H, Bollard ME, Beckonert O, Schlotterbeck G, Senn H, Niederhauser U, Holmes E, Lindon JC, Nicholson JK (2002) *Chem Res Toxicol* 15:1380-1386.

Kinoshita Y, Yokota A (1997) *NMR Biomed* 10:2-12.

Kotitschke K, Jung H, Nekolla, Haase A, Bauer A, Bogdahn U (1994) *NMR Biomed* 7: 111-120.

Kumar R, Pai K, Sundar S (2001) *Clin Exp Immunol* 124:262-265.

Langford CK, Burchmore RJ, Hart DT, Wagner W, Landfear SM (1994) *Parasitology* 108:S73-S83.

Learmonth MP, Euerby MR, Jacobs DE, Gibbons WA (1987) *Mol Biochem Parasitol* 25:293-298.

Leelayoova S, Marbury D, Rainey PM, Mackenzie NE, Hall JE (1992) *J Protozool* 39:350-358.

Legare D, Papadopoulou B, Roy G, Mukhopadhyay R, Haimeur A, Dey S, Grondin K, Brochu C, Rosen BP, Ouellette M (1997) *Exp Parasitol* 87:275-282.

Lindon JC, Holmes E, Bollard ME, Stanley EG, Nicholson JK (2004) *Biomarkers* 9:1-31.

Lira R, Sundar S, Makharia A, Kenney R, Gam A, Saraiva E, Sacks D (1999) *J Infect Dis* 180:564-567.

Loening NM, Chamberlin AM, Zepeda AG, Gonzalez RG, Cheng LL (2005) *NMR Biomed* 18:413-420.

Lohmeier-Vogel EM, Hahn-Hagerdal B, Vogel HJ (1995) *Appl Environ Microbiol* 61:1414-1419.

Lundberg P, Harmsen E, Ho C, Vogel HJ (1990) *Anal Biochem* 191:193-222.

Marr JJ (1980) Carbohydrate metabolism in Leishmania. In *Biochemistry and Physiology of Protozoa*. Eds, M Levandowsky and SH Hunter. New York: Academic Press, pp 313-338.

Marr JJ, Berens RL (1985) Purine and pyrimidine metabolism in *Leishmania*. In *The Leishmaniasis*. Eds, KP Chang and RS Bray. Amsterdam: Elsevier Biomedical Press, pp 65-78.

Meade JC, Glaser TA, Bonventre PF, Mukkada AJ (1984) *J Protozool* 31:156-161.

Mengeling BJ, Beverley SM, Turco SJ (1997) *Glycobiology* 7:873-880.

Miranda M, Ramos A, Veiga-da-Cunha M, Loureiro-Dias MC, Santos H (1997) *J Bacteriol* 179:5347-5354.

Mittal MK, Misra S, Owais M, Goyal N (2005) *Protein Expr Purif* 40:279-286.

Molyneaux DH, Killick-Kendrick R (1987) Morphology and ultrastructure. In *The Leishmania in Biology and Medicine*. Eds, W Peters and R Killick-Kendrick. London: Academic Press, pp 122-176.

Moreno B, Urbina JA, Oldfield E, Bailey BN, Rodrigues CO, Docampo R (2000) *J Biol Chem* 275:28356-28362.

Mukhopadhyay R, Dey S, Xu N, Gage D, Lightbody J, Ouellette M, Rosen BP (1996) *Proc Natl Acad Sci USA* 93:10383-10387.

Murray HW (2002) *N Engl J Med* 347:1793-1794.

Olliaro PL, Guerin PJ, Gerstl S, Haaskjold AA, Rottingen JA, Sundar S (2005) *Lancet Infect Dis* 5:763-774.

Pan AA, Duboise SM, Eperon S, Rivas L, Hodgkinson V, Traub-Cseko Y, McMahon-Pratt D (1993) *J Eukaryot Microbiol* 40:213-223.

Perez-Victoria FJ, Castanys S, Gamarro F (2003) *Antimicrob Agents Chemother* 47:2397-2403.

Prasad V, Dey CS (2000) *Parasitol Res* 86:876-80.

Rager MN, Binet MRB, Bouvet OMM (1999) *Eur J Biochem* 263:695-701.

Rager MN, Binet MRB, Ionescu G, Bouvet OMM (2000) *Eur J Biochem* 267:5136-5141.

Rainey PM, MacKenzie NE (1991) *Mol Biochem Parasitol* 45:307-315.

Santhamma KR, Bhaduri A (1995) *Mol Biochem Parasitol* 75:43-53.

Shukla A, Roy R, Bhaduri AP, Chatterjee RK (1995) *Ind J Pharmacol* 27:106-110.

Singh N, Singh RT, Sundar S (2003) *J Infect Dis* 188:600-607.

Singha UK, Bhakuni V, Ali V, Roy R (1996) *Mol Cell Biochem* 162:17-22.

Sitter B, Sonnewald U, Spraul M, Fjosne HE, Gribbestad IS (2002) *NMR Biomed* 15:327-337.

Subramanian A, Gupta A, Saxena S, Gupta A, Kumar R, Nigam A, Kumar R, Mandal SK, Roy R (2005) *NMR Biomed* 18:213-225.

Sundar S, More DK, Singh MK (2000) *Clin Infect Dis* 31:1104-1107.

Sundar S (2001) *Trop Med Int Health* 6:849-854.

Sundar S (2003) *J Postgrad Med* 49:29-30.

Sundar S, Benjamin B (2003) *J Assoc Physicians India* 51:195-201.

Sundar S, Agrawal G, Rai M, Makharia MK, Murray HW (2001a) *BMJ* 323:419-422.

Sundar S, Pai K, Kumar R, Pathak-Tripathi K, Gam AA, Ray M, Kenney RT (2001b) *Am J Trop Med Hyg* 65:193-196.

Sundar S, Jha TK, Thakur CP, Engel J, Sindermann H, Fischer C, Junge K, Bryceson A, Berman J (2002) *N Engl J Med* 347:1739-1746.

Thompson SN (1991) *J Parasitol* 77:1-20.

Turco SJ, Spath GF, Beverley SM (2001) *Trends Parasitol* 17:223-226.

Wuthrich K (1986) In *NMR of proteins and nucleic acids*. New York: John Wiley & Sons, pp 13-25.

Wyllie S, Cunningham ML, Fairlamb AH (2004) *J Biol Chem* 279:39925-39932.

Chapter 4:

NMR Structural Aspects In Tuberculosis

1. Introduction

In 1993, the World Health Organization (WHO) declared tuberculosis (TB) to be a global emergency, the first infectious disease to be recognized as such (Raviglione et al., 1995). TB still remains one of the foremost among infectious diseases in the world, which causes maximum death from a single microorganism (Frieden et al., 2003). Approximately one third of the world's population has been infected with the causative organism *Mycobacterium tuberculosis* (MTB), eight million become sick with TB every year, and globally it accounts for almost 3 million deaths annually (Ginsburg et al., 2003; Collins and Kaufmann, 2001). One fifth of all deaths of adults in developing countries results is due to TB, which is a re-emergent problem particularly in many industrialized countries. In 1990s, nearly 90 million new cases were predicted, and in 1991 it was estimated that 1,700 million people are infected with MTB (Ellner et al., 1993). It was reported that around 19-43% of the world's population might get infected with MTB between 2000 and 2020 if control measures are not strengthened further (Raviglione et al., 1995). Not only is there a global increase in the disease itself, there is a worrying rise in the number of cases resistant to the two principal antituberculosis drugs, isoniazid and rifampicin (Zumla and Grange, 2001). Further, immunodeficiencies occurring under conditions of malnutrition, deterioration of general health or after the HIV infection have become responsible for an increase in the incidence of central nervous system (CNS) TB (Gupta et al., 1996; Schutte et al., 1996).

Tuberculosis poses a major threat to the health of people living in South East Asia, especially India. At least one in three people living in this part of the world are infected with TB, and every year 1 million people die from TB. India has been particularly hit by the dual threat of HIV and TB (Sharma et al., 2005). The treatment plan of TB consists of a combination of Isoniazid or isonicotinic acid hydrazide (INH), Rifampicin and pyrazinamide to be administered for the first two months, followed by a follow-up therapy involving INH and rifampicin for four months (Bass et al., 1994). Strains of *M. tuberculosis* resistant to INH were noted soon after the introduction of the drug, and multi-drug-resistant *M. tuberculosis* strains have since emerged, which further necessitated the inclusion of ethambutol in the WHO-recommended treatment regimens (Frieden et al., 2003).

The re-emergence of TB is mainly due to the compromise of immune mechanisms, and particularly in HIV-infected individuals the risk is more. The HIV infection and the evidence of an association between TB and HIV infection has caused marked increases in the incidence of TB in many countries (Sharma et al., 2005; Gallant et al., 1994). Not only do many developed countries face the gloomy scenario of increasing TB incidence, but also the problem of multi-drug-resistant TB that has emerged in several major urban centers of countries worldwide (Lane et al., 1994; Bastian et al., 2003; Frieden et al., 2003; Ted et al., 2003; Caminero, 2005). It could be stated that TB is currently a global disaster on an unprecedented scale. Things are getting worse due to the lack of proper TB control programs, co-existence of HIV infection, population growth and poverty. Tuberculosis has resurged as an opportunistic infection in immuno-compromised patients, and new drugs are needed to control this global epidemic. The alarming statistics reveal the need for urgent action by both basic scientists and pharmaceutical companies to prevent a global catastrophe (Kaufmann, 2000).

1.1 Incidence of Tuberculosis

Tuberculosis has probably killed 100 million people over the past 100 years (Iseman, 2000), and is the world's second commonest cause of death from infectious disease, after HIV/AIDS. There were an estimated 8-9 million new cases of tuberculosis in 2000, fewer than half of which were reported; 3-4 million cases were sputum-smear positive, the most infectious form of the disease (Corbett et al., 2003). Most cases (5-6 million) are in people aged 15-49 years. Sub-Saharan Africa has the highest incidence rate (290 per 1,00,000 population), but the most populous countries of Asia have the largest numbers of cases: India, China, Indonesia, Bangladesh, and Pakistan together account for more than half the global burden. 80% of new cases occur in 22 high-burden countries (WHO Report, 2003).

Every minute of every day 15 people in the world develop, and six people die from, tuberculosis; this translates into 8 million new cases each year from which 2-2.5 million will die (Collins and Kaufmann, 2001). As if these figures were not alarming enough, it is estimated that only 45% of actual tuberculosis cases are detected and reported (WHO Report, 2001). As with the other two top infectious disease killers, AIDS and malaria, the biggest burden of morbidity and mortality is in developing countries; however, industrialized nations across Europe and in the

USA, the incidence of tuberculosis is on the increase. There have been striking increases in countries of the former Soviet Union and in sub-Saharan Africa (Dye et al., 1999).

Tuberculosis remains a serious public-health problem in India accounting for nearly one-third of the global burden, and it has been estimated that 3.5 million of the population are infected with TB (Granich et al., 2003; Sharma, 2003). Despite the introduction of the National Tuberculosis Control Programme in 1962, India has about 2 million new cases every year, of which nearly 1 million are infectious smear-positive pulmonary cases (Dye et al., 1999). One person dies from tuberculosis in India every minute – more than 1000 every day and 4,50,000 every year (Khatri et al., 2000). India's tuberculosis problem is further compounded by an estimated 3.97 million people infected with HIV (De Cock and Weiss, 2000), tuberculosis being the most common opportunistic disease amongst HIV-infected people.

1.2 Pathophysiology and Clinical Manifestations of Tuberculosis

Tuberculosis is spread by airborne droplet nuclei, which are particles of 1-5 μm in diameter that contain *M. tuberculosis*. Because of their small size, the particles can remain airborne for minutes to hours after expectoration by people with pulmonary or laryngeal tuberculosis during coughing, sneezing, singing, or talking (Riley et al., 1959). The infectious droplet nuclei are inhaled and lodged in the alveoli in the distal airways. *M. tuberculosis* is then taken up by alveolar macrophages, initiating a cascade of events that results in either successful containment of the infection or progression to the active form of disease (Pieters and Gatfield, 2002). *M. tuberculosis* can persist within an infected individual for extended periods of time without causing overt, clinical disease, in a state normally referred to as latent or chronic tuberculosis (Bentrup and Russell, 2001). Most people are exposed to infection early in life but the infection can remain latent and reactivate at any time point, especially under conditions of immunosuppression. The risk of development of the active form of TB varies according to time since infection, age and host immunity (Comstock et al., 1974; Sutherland, 1976).

After being ingested by alveolar macrophages, *M. tuberculosis* replicates slowly but continuously and spreads via the lymphatic system to the hilar lymph nodes. In most infected individuals, cell-mediated immunity develops 2-8 weeks after infection. Activated T-lymphocytes

and macrophages form granulomas that limit further replication and spread of the micro-organism (Schluger and Rom, 1998). *M. tuberculosis* is in the centre of the characteristically necrotic (caseating or cheese-like) granulomas, but it is usually not viable. Unless there is a subsequent defect in cell-mediated immunity, the infection generally remains contained and active disease may never occur; in other words, active disease occurs when the host immune response cannot contain the replication of *M. tuberculosis* associated with initial infection. This development is most common in children under 5 years old and adults with advanced immunosuppression (e.g., AIDS). This primary progressive disease can manifest in almost any organ system, but it occurs most frequently in the parenchyma of the mid and lower lung, in the hilar lymph nodes, or as generalized lesions resulting from haematogenous dissemination (Iseman, 2000). Several studies have suggested a genetic predisposition to tuberculosis, while other conditions can also compromise the immune system and predispose to development of active disease, such as, poorly controlled diabetes mellitus, renal failure, underlying malignant disease, chemotherapy, extensive corticosteroid therapy, malnutrition and deficiency of vitamin D or A (Karyadi et al., 2002; Wilkinson et al., 2000).

The discrete disease states observed during the course of TB are products of both the host and the infecting microorganism. In a naive host, following initial infection of the macrophages in the lung, the bacteria undergo a period of rapid expansion in the absence of a specific, limiting immune response. However, once the host becomes 'aware' of the infection, the immune system responds and limits dissemination of infection by developing granulomas or tubercles around the infection foci. The stratified structure of the granuloma is such that it benefits both host and pathogen. From the host's perspective, the granuloma limits dissemination of infection by walling it off, yet this benefits the pathogen as well, because the T-cells capable of releasing macrophage-activating cytokines are restricted to the periphery of the granuloma, away from the infected macrophages. The formation of the granuloma involves both innate and acquired immune responses, and bacterial cell wall components such as trehalose dimycolate (cord factor) are potent initiators of the response (Lima et al., 2001). The bacterial cell wall lipids are shed actively during phagocytosis by viable intracellular mycobacteria, and travel from cell to cell spreading the influence of the bacterium (Beatty et al., 2000). The ability to synthesize and export peripheral cell wall lipids has a major impact on bacterial colonization and persistence (Cox et al., 1999).

The most common clinical manifestation of tuberculosis is pulmonary disease (Frieden et al., 2003). Extrapulmonary tuberculosis accounts for about 20% of disease in HIV-seronegative people but is more common in HIV-seropositive individuals (Shafer and Edlin, 1996). Among people not infected with HIV, extrapulmonary disease such as lymphatic tuberculosis is particularly common in women and young children (Rieder and Snider, 1990). Pleural tuberculosis occurs as a result of either primary progressive *M. tuberculosis* infection or reactivation of the latent infection (Frieden et al., 2003).

1.3. Diagnosis of Tuberculosis

1.3.1. Active disease

Criteria for the diagnosis of active tuberculosis vary according to the setting (Frieden et al., 2003; Drobniewski et al., 2003). Patients with persistent cough (e.g., lasting longer than 2 weeks) should be assessed for tuberculosis. Other common symptoms include fever, night sweats, weight loss, shortness of breath, haemoptysis, and chest pain. Among children, important diagnostic clues are a history of previous exposure to an individual with tuberculosis or evidence of tuberculosis infection (e.g., a positive tuberculin skin test). To improve the diagnostic yield in children, diagnostic algorithms and point scoring systems are often used, particularly in less developed countries (Hesseling et al., 2002).

Tests for the diagnosis of tuberculosis vary in sensitivity, specificity, speed, and cost. Even if additional tests are done, culture is required for definite diagnosis and is essential for drug-susceptibility testing. Routine cultures are generally neither practicable nor necessary for disease control. The sputum smear is an inexpensive test that can be carried out rapidly; fluorochrome, Ziehl-Neelsen and Kinyoun staining methods can be used (Frieden et al., 2003). In countries with a high prevalence of tuberculosis, a positive direct smear is due to *M. tuberculosis* in more than 95% of patients suspected of having tuberculosis (Crampin et al., 2001).

Nucleic-acid amplification assays can be used directly on clinical specimens; they are most reliable in smear-positive respiratory samples from patients with previously untreated tuberculosis. In such samples, the sensitivity and specificity can be as high as 95% and 98%, respectively

(Frieden et al., 2003). However, widespread implementation of nucleic-acid amplification assays has been limited by high cost and potential for poor performance under field conditions. Amplification tests do not replace the sputum smear (which provides a gauge of infectiousness) or culture (which is necessary for drug-susceptibility testing). The assays can still give positive results after effective treatment because of detection of residual genetic material, so they may not be as useful in people with previous disease or in monitoring response to therapy.

1.3.2. Latent infection

The intradermal administration of tuberculin has been used as a diagnostic test for tuberculosis infection since the early 1900s; the more consistent form of tuberculin (standardized purified protein derivative) has been used to assess latent *M. tuberculosis* infection since 1939 (Lee and Holzman, 2002). Although the tuberculin skin test is the best available way to diagnose latent *M. tuberculosis* infection, it has limitations, including low sensitivity in immunocompromised patients, cross-reactivity with bacille Calmette-Guérin (BCG) vaccine and environmental mycobacteria (resulting in decreased specificity), and a requirement that patients must return 48-72 h after the test is done to know the result (Huebner et al., 1993).

Recent research has used defined antigens for an accurate and rapid test for tuberculosis infection based on the detection of T-cells sensitized to *M. tuberculosis* either by blood tests *in vitro* or skin tests *in vivo* (Andersen et al., 2000). A whole-blood interferon-γ release assay (IGRA), like the tuberculin skin test, assesses cell-mediated immunity to tuberculin (Mazurek and Villarini, 2003). Although it has been reported that the IGRA is less sensitive and specific than the tuberculin skin test (Bellete et al., 2002), responses are less affected by previous BCG vaccination (Mazurek et al., 2001). An enzyme-linked immunospot (ELISPOT) assay has recently been developed that is relatively sensitive and specific in detecting latent *M. tuberculosis* infection (Ewer et al., 2003).

1.4. Treatment of Tuberculosis

BCG, an attenuated strain derived from *M. bovis* developed by the French scientists Calmette and Guérin, has been in use in human beings since 1921 and has been administered to more than 3 billion individuals worldwide. It is generally accepted that this vaccine appreciably

protects children from meningeal and miliary tuberculosis. Unfortunately all available evidence reveals that this vaccine is insufficient. Protection of adults from pulmonary tuberculosis, the most common form of the disease, varies considerably from 80% in the UK to 0% in south India (Colditz et al., 1994). The case fatality rate of untreated tuberculosis is approximately 50%. Problems with treatment arise, as resistance rapidly develops against single antibiotics, necessitating a complex and long-term regimen of drug treatment combining at least two different compounds for a minimum of 4 months. To implement successful drug treatment, the World Health Organization initiated directly observed therapy short-course (DOTS), which is currently adopted by 119 countries including all 22 high-burden countries that contain 80% of all estimated cases (WHO Report, 2001).

Despite the availability of effective therapy for almost 50 years, future treatment of tuberculosis will depend, at least in part, on the development of new anti-tuberculosis drugs. By contrast with other infectious diseases, there are relatively few antimicrobial agents clinically effective against *M. tuberculosis*. Currently, tuberculosis treatment requires lengthy courses of medication due to the ability of *M. tuberculosis* to enter a dormant, persistent, anti-microbial resistant phase. Furthermore, adherence to treatment of tuberculosis is limited by a multitude of clinical, social, financial and behavioural factors. Consequently, there is a need for new agents not only to improve the treatment of multi-drug resistant TB, but also to augment the efficacy of current approaches to both latent and active tuberculosis (O'Brien and Nunn, 2001; Ginsburg et al., 2003).

It may be mentioned that the current state of tuberculosis diagnosis, treatment, and control reveals striking contrasts. The mainstays of diagnosis remain the sputum smear and culture, both 100 years old. No new first-line drugs have been discovered for several decades, and two-thirds of patients who develop tuberculosis are not effectively diagnosed, treated, or monitored. Further progress will require continued rigorous and dedicated application of current technology and will be greatly facilitated by the discovery and widespread application of new diagnostic techniques, drugs and prevention strategies (Frieden et al., 2003).

1.5. Incracranial Tuberculomas due to *M. tuberculosis*

The extrapulmonary manifestation of tuberculosis, involving the central nervous system, is the most serious clinical manifestation of tuberculosis. Such involvement can include inflammation of the meninges (intracranial and intraspinal meningitis), as well as space-occupying lesions (tuberculomas) of the brain (cerebral or cord tuberculoma). Tuberculoma is the intracranial form of tuberculosis and causes a mass effect related to its localization. Tuberculomas arise because of tuberculous bacilli reaching the brain via the blood supply. In the CNS, they will eventually give rise to intracerebral mass lesions (intracerebral tuberculomas) or will rupture, discharging the organism into the subarachnoid space thereby giving rise to meningitis. Tuberculomas are solid, granulomatous masses, and caseous degeneration occurs at the centre of granulomas and causes granulomatous inflammation with surrounding vasogenic oedema (Gurses and Aydin, 1992; Gupta et al., 1988). Spinal cord tuberculomas and spinal meningitis are much less frequent but may occur as a result of the same pathogenetic mechanism. In such patients with tuberculoma, surgery becomes essential to avoid mass effect and hydrocephalus. The CT scan and contrast-enhanced MRI of the brain typically shows hydrocephalus and basillar enhancement in such patients (Gupta et al., 1988).

Granulomas are often large, spherical masses with a peripheral enhancing rim, central hypointensity and surrounding vasogenic oedema in the early stages. As tuberculoma improves, the peripheral rim gets thinner and the central hypodense area gets smaller. In due course of time, calcium accumulates on the wall and slightly hyperintense images could also be seen. Finally evident calcification occurs and oedema regresses. The lesion looks isointense with grey matter on T_1-weighted images, while central hyperintensity can be seen on T_2-weighted images (Gupta et al., 1988). The clinical manifestations are due to the presence of *M. tuberculosis* as well as the inflammatory host immune response. Neurological manifestations can include cranial-nerve palsies and motor, sensory, and cerebellar defects, according to the location of the tuberculomas; seizures can also occur. Additional manifestations involving the spine are discitis and spondylitis. Each of these entities may constitute the clinical presentation of previously undiagnosed TB.

2. Statement of Problem

Proper antitubercular treatment to patients suffering from tuberculoma of brain, if at all diagnosed by MRI, becomes an essential requirement (Gupta et al., 1996), and ultimately in such cases the imaging modalities fail to differentiate whether it is a malignant, non-malignant or an infectious lesion. The diagnosis of tuberculomas is usually based on the characteristic histological features, which at times may overlap with other infective or non-infective granulomas, and the gold-standard culture method is very time-consuming and is often insensitive. As a result, there is an increasing requirement for the development of newer and additional diagnostic techniques for the CNS form of TB.

The characteristics of intracranial tuberculoma on computed tomography (CT) and magnetic resonance imaging (MRI) are still not well known (Wasay et al., 2003); a recent report has highlighted an intracranial tuberculoma case in which the diagnosis could be confirmed only after surgical excision (Tewary et al., 2005). Diagnostic dilemma has been reported in tuberculomas, and very often other CNS disorders such as tumors, cysticercosis and bacterial abscesses have been reported to interfere in the differential diagnosis (Gupta et al., 1999; Gupta et al., 2001). Despite their pathogenetic and epidemiologic similarities, tuberculous meningitis and CNS tuberculoma and their spinal equivalents are clinically separate diseases, being associated with the other only infrequently. The incidence of tuberculoma of brain was found to be 2% in a study involving 214 cases with tuberculous meningitis (Yaramis et al., 1998). The frequency of brain complications is higher in infants and young children, and often a proper diagnostic methodology such as computed tomography or contrast-enhanced MRI is required in such cases if intracranial tuberculoma is suspected. In this regard, the diagnostic utility of CT and MRI in intracranial tuberculomas had been highlighted (Gupta et al., 1990; Ceylan and Gencer, 2005), and the imaging features of the tuberculomas were observed to be distinct from those of abscesses, metastases and gliomas (Gupta et al., 1988; Gupta et al., 1999; Gupta et al., 2001). Improved MR techniques (Gupta et al., 2005; Gupta et al., 2002; Poonnoose et al., 2004) coupled with *in vivo* proton MRS (Poptani et al., 1995; Gupta et al., 1995; Gupta et al., 2001; Kaminogo et al., 2002) have been explored in recent times to aid in selective diagnosis of tuberculomas. Once the

tuberculoma is diagnosed, surgical removal of the intracranial lesion becomes essential followed by histopathological investigation in order to initiate timely antitubercular treatment in such patients; otherwise the condition may become fatal. The diagnostic utility of histopathology may not be foolproof in certain cases since purulent exudates of the lesions may give rise to a diagnostic confusion, thus calling for other alternative procedures.

The findings of proton MRS have suggested that the lipid components of tuberculomas as well as the causative organism have a role in assisting differential diagnosis (Poptani et al., 1995; Gupta et al., 1995; Gupta et al., 1996). It is well known that MTB possesses a unique array of lipid structural components in its membrane, which provide protection and support for the cell and also contain the mechanisms that allow (or prevent) traffic of substances between the bacterial cell and its environment (Besra and Chatterjee, 1996; Chatterjee, 1997). Hence, the characterization of such lipid structural components pertaining to the diagnosis of tuberculomas might become important for at least two reasons: (a). Cellularity or cellular proliferation as seen in pathlogical conditions such as tumors, which also include conditions like tuberculoma, has often been associated with lipid components; (b). The lipid components identified under certain pathological condition could be correlated to those identified for a particular causative organism, and may help to identify the fingerprint diagnostic markers, if any.

Multinuclear MR spectroscopy has been found to offer a convenient methodology in the analysis of lipids obtained from biological systems (Sparling et al., 1988). Numerous reports are available in literature regarding the ^{1}H, ^{13}C and ^{31}P assignments of lipids in biological systems (Tosi et al., 2003; Schiller and Arnold, 2002; Holmback et al., 2001; Sonnewald et al., 1993; Meneses and Glonek, 1988). With other methods such as Gas Chromatography-Mass Spectrometry-Selective Ion Monitoring, TLC and HPLC, a suitable derivative and/or a suitable chromatographic medium must be prepared for the specific compounds to be assayed, and often the derivatization procedure is time-consuming (Sparling et al., 1988; Metz and Dunphy, 1996). Although Mass Spectrometry, a technique much sensitive than NMR, helps one to characterize the components, often the spectra gives rise to a mixed pattern of fragments information and this complexity of the data makes it too difficult to be used as a routine technique.

The earlier work from our laboratory has revealed that one could fingerprint the membrane lipid components of *Mycobacterium tuberculosis* in the lipid extract of intracranial tuberculomas, despite the fact that NMR analysis may not always show any diagnostic marker signals from MTB in more than 60% of proven cases suffering from CNS tuberculosis (Gupta et al., 1996). In continuation to this work, and in order to explore further the diagnostic utility of NMR, detailed ^{1}H, ^{13}C and ^{31}P NMR studies of the lipid extract of intracranial tuberculomas have been carried out in the present investigation. The main objective was to characterize various lipid structural components in tuberculoma and to look for any possible specific diagnostic markers that may aid in the differentiation of tuberculomas from the tumors of brain.

3. Materials and Methods

3.1. Chemicals

D_2O (99.96 atom% deuterium-enriched, with traces of TMS) was purchased from Sigma-Aldrich Inc., USA (Sigma Chemicals, St. Louis, MO, USA). For lipid extraction, HPLC grade chloroform (Merck, India) and methanol (Qualigens, India) were used. All other chemicals used were of reagent grade with the highest purity commercially available, unless otherwise mentioned.

3.2. Extraction of Lipids from Tuberculoma Tissues

Proven cases of excised intracranial tuberculomas were obtained from twelve patients while they were undergoing surgery at Department of Neurosurgery, King George's Medical University, Lucknow, India. The samples were snap frozen in liquid nitrogen in order to stall metabolism, and stored at –85°C until lipid extraction. The lipid extraction was done as per the standard protocol described in the literature (Folch et al., 1957; Adosraku et al., 1994). About 60-100 mg of the frozen tissue was taken for the extraction of lipids and ground under liquid nitrogen. The samples were divided into two groups: the first group consisted of samples from seven cases for the purpose of carrying out ^{1}H and ^{13}C NMR experiments, while the second group consisted of samples from five cases for obtaining ^{31}P NMR information. The crushed tuberculoma tissue sample was taken in 10 ml chloroform:methanol mixture (2:1 v/v) and homogenized at 4°C using a ultrasonicator (Sonics, USA) with a 6 mm-diameter tip by applying low power three times (3

min each, duty cycle, 20% of maximum power). The sample was vigorously vortexed for 1 min at 25°C (Spinix Vortexer) and left in the refrigerator overnight to enable complete extraction of lipids. The supernatant was separated and the lipids were re-extracted again in 10 ml chloroform:methanol mixture (2:1 v/v), followed by 10 ml chloroform:methanol mixture (1:1 v/v) and finally in 5 ml chloroform, vortexed for 1 min followed by the separation of the organic layers. The organic layers were combined and treated twice with an equal volume of 0.2 M aqueous KCl solution to remove non-lipid entities. The separated organic layer was subsequently removed under a stream of nitrogen to give the oily lipid extract (ca. 15-25 mg), which was re-dissolved in deuterated chloroform:methanol (2:1 v/v) mixture, and kept at –20°C till the NMR experiments were performed.

3.3. Thin-layer Chromatography (TLC) of Tuberculoma Lipid Extracts

Ascending TLC was run using silica gel G (Merck, India) coated aluminum plates (10 cm x 8 cm) in a solvent mixture of chloroform:methanol:acetic acid in a ratio of 190:9:1 v/v (Stewart and Downing, 2001) for a portion of the pooled tuberculoma lipid extracts. The chromatogram was visualized by spraying 50% sulphuric acid, followed by heating the developed plate to 220°C on a hot plate.

3.4. High-performance Liquid Chromatography (HPLC) of Tuberculoma Lipid Extracts

A portion of the pooled tuberculoma lipid extracts was injected onto a Whatman Partisil ODS-3 column and run with a gradient of 5 mM KH_2PO_4 into acetonitrile (flow rate 0.6, 0-20% at 30 min), on a Waters HPLC instrument (Adosraku et al., 1994). Ultraviolet (UV) detection at 240 nm (determined using a Perkin-Elmer UV spectrophotometer, prior to running the HPLC) was mainly used to monitor the lipid separation.

3.5. High Resolution NMR Spectroscopy

The NMR experiments were performed using a Bruker's (Fallanden, Switzerland) *Avance* DRX 300 MHz FT-NMR spectrometer (7.2 T, 54 mm vertical-bore magnet) equipped with a 5 mm multinuclear inverse-probehead with a Z-shielded gradient, operating at a proton frequency of 300.13 MHz. All the NMR spectra were recorded at 298K unless otherwise stated, in a non-

spinning mode by dissolving the lipids in $CDCl_3$:CD_3OD solvent system, taken in a ratio of 2:1 (v/v), with a total sample volume of 600 μl in the 5 mm NMR tube (Wilmad, USA). The ^1H NMR spectra were acquired with the following experimental parameters: 32768 data-points, spectral width of 3.591 kHz, and 128 free-induction decays (FIDs) were averaged with a recycle delay of 2 s. ^{13}C NMR experiments were performed at 75.47 MHz with the following experimental parameters: spectral width of 19.96 kHz, 32768 data points, pulse width 90° (10 μs), relaxation delay 2 s, composite pulse decoupling using WALTZ-16, 20000 FIDs were accumulated to obtain a reasonably good signal-to-noise ratio, and a line-broadening of 3.0 Hz was used prior to Fourier transformation. ^1H decoupled, ^{13}C-edited DEPT135 and DEPT90 experiments were performed using the standard experimental parameters as mentioned for the ^{13}C experiment. The chemical shifts were calibrated with respect to the solvent peak of CD_3OD at 3.30 ppm in ^1H NMR, and at 49.04 ppm in the ^{13}C spectra to aid in the resonance assignments of the lipid components.

Standard two-dimensional ^1H-^1H COSY 90°, phase-sensitive ^1H-^1H TOCSY, ^1H-^{13}C HMQC and ^1H-^{13}C HMBC experiments were carried out using the Bruker's standard pulse program library. The spectral widths of COSY and TOCSY were 3.591 kHz in both dimensions, and 256 t_1 increments with 2.143 s recycle delay per scan were set. For each t_1 step, 128 transients were added with 1024 data points. The data points were zero-filled up to 512 W in F_1 dimension and were weighted with sine-bell (in case of COSY) and 90° shifted sine-bell (in case of TOCSY) window functions in both dimensions prior to double Fourier transformation. In case of TOCSY, the spin-locking time was set to 90 ms, which included a duration of 2.5 ms for the trim-pulses.

Heteronuclear two-dimensional ^1H-^{13}C chemical shift correlations were measured in the ^1H-detected mode via multiple quantum coherence (HMQC). The 2D HMQC experiment was performed in gradient mode with a spectral width of 3.591 kHz in F_2 dimension and 14.340 kHz in F_1 dimension, 256 t_1 increments with 1.7 s recycle delay. For each t_1, 88 transients were added with 2048 data points. GARP decoupling (Shaka et al., 1985) was employed in the ^{13}C domain during the t_2 period for all HMQC spectra. The data were weighted with sine-bell window functions in both dimensions prior to double Fourier transformation. The 2D HMBC experiment was performed in gradient mode with the following experimental parameters: a spectral width of

3.591 kHz in F_2 dimension and 18.113 kHz in F_1 dimension, 256 t_1 increments with 1.7 s recycle delay, and 71 ms delay was set for the evolution of long-range couplings. For each t_1, 88 transients were added with 4096 data points. GARP decoupling was employed in the ^{13}C domain during the t_2 period for all HMBC spectra. The data were weighted with 90° shifted cosine-bell window function in F_1 dimension and sine-bell window function in F_2 dimension prior to double Fourier transformation.

The ^{31}P spectra were acquired at 121.49 MHz in proton decoupling mode for the pooled tuberculoma lipid extracts between –30 and 30 ppm to observe the phospholipid resonances. The lipid extract was dissolved in a solvent system containing $CDCl_3$:MeOH-d_4:D_2O:EDTA as described in the literature, so as to resolve the phosphorus resonances (Meneses and Glonek, 1988; Branca et al., 1995; Tyagi et al., 1996). The experimental parameters were as follows: spectral width of 7.44 kHz, 32768 data points, pulse width 90° (3.8 μs), relaxation delay 1 s, composite pulse decoupling using WALTZ-16, 4500 FIDs were accumulated to obtain a reasonably good signal-to-noise ratio, and a Gaussian line-broadening of -1.0 Hz was used prior to Fourier transformation. The chemical shifts were calibrated with respect to the ^{31}P signal of the highly abundant glycerophosphatidylcholine (PC) assigned at 2.63 ppm as described in the literature (Lutz et al., 2002).

4. Results

4.1. Chromatographic Analyses of Tuberculoma Lipid Extracts

The developed TLC chromatogram of the lipid extract of a representative human tuberculoma sample is shown in fig. 1a. Further, the UV absorption profile (fig. 1b) indicated that the lipid mixture contains olefinic functionalities. The TLC and HPLC analyses were carried out mainly to confirm the possibility of existence of mixtures in the lipid extract. The HPLC profile (fig. 1c) indicated that there is a mixture of components in the lipid extract.

Fig. 1a: Thin-layer chromatogram of the tuberculoma lipid extracts. 1-3: Tuberculoma lipid extracts; 4. Cholesteryl acetate standard; 5. Sphingomyelin standard.

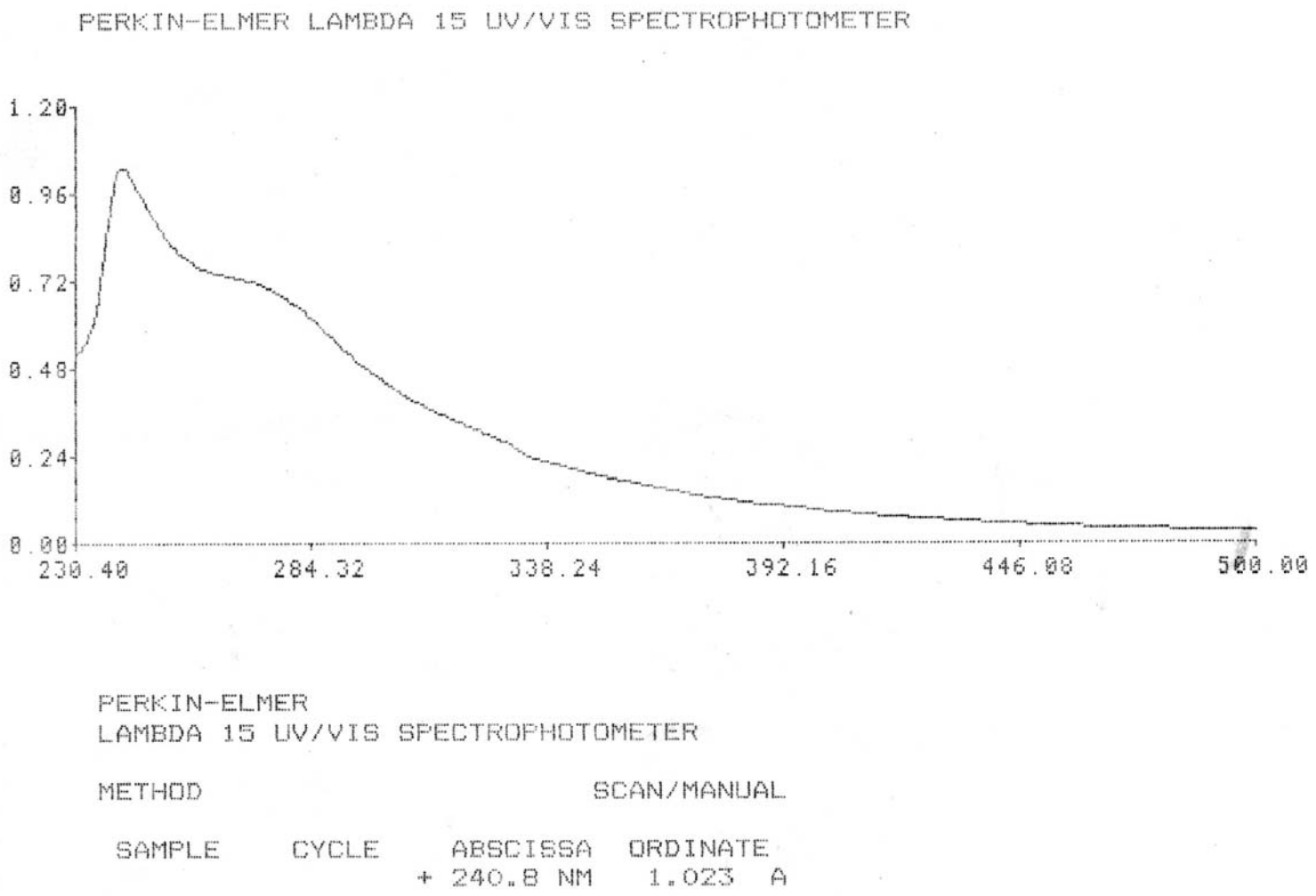

Fig. 1b: UV absorption profile of the tuberculoma lipid extracts.

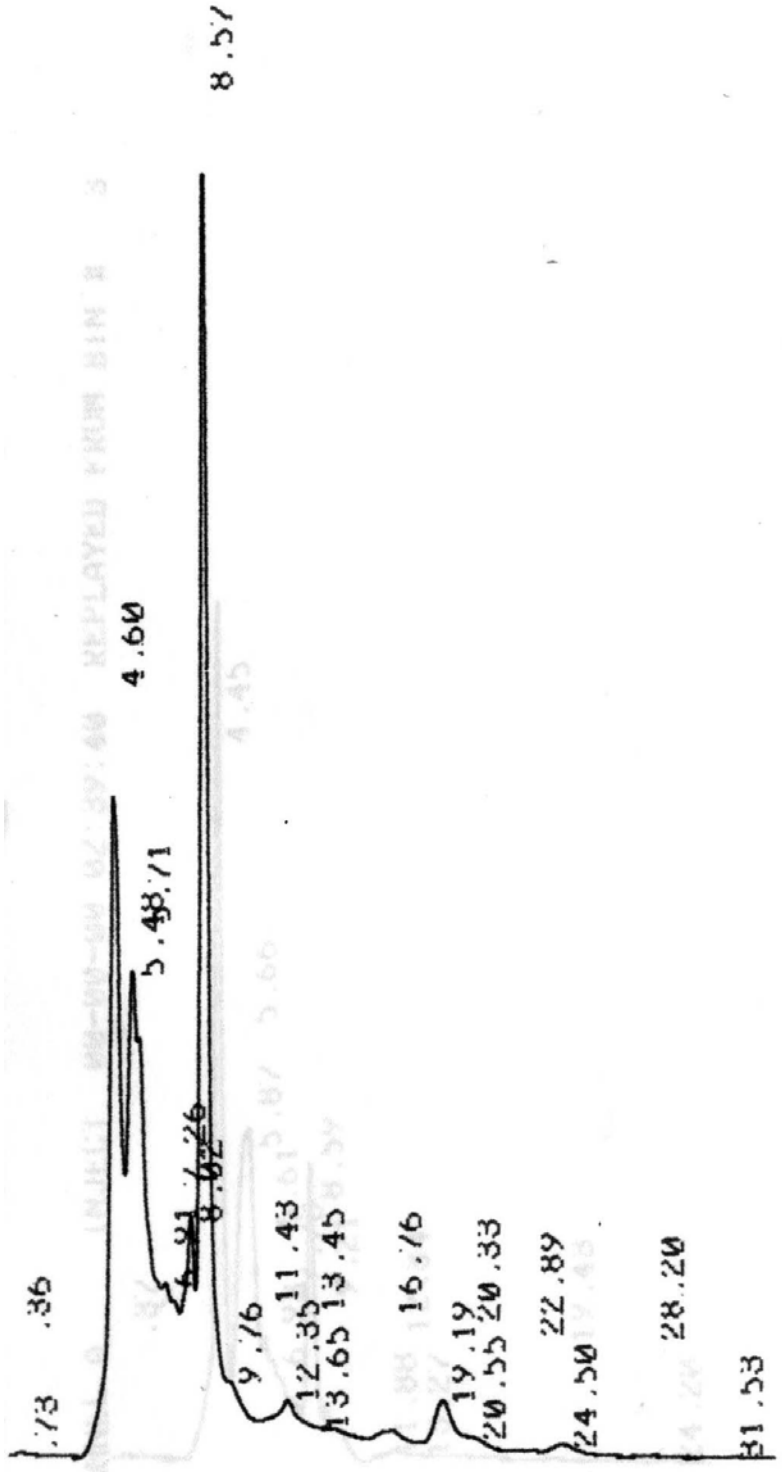

Fig. 1c: HPLC profile of the tuberculoma lipid extracts.

4.2. NMR Spectroscopic Identification of the Lipid Structural Components

A representative ^{1}H, ^{13}C, ^{1}H-^{1}H COSY, ^{1}H-^{1}H TOCSY, ^{1}H-^{13}C HMQC, ^{1}H-^{13}C HMBC and ^{31}P NMR spectra of the lipid extracts of the human tuberculoma samples under study are shown in figs. 2a, 3a, 4a-d and 11a, respectively. In ^{1}H NMR, the region between 0.5 ppm and 6.0 ppm consisted of contribution from three major entities (Casu et al., 1991): (a). Methyl and methylene protons of sterol and fatty chain at 0.5-2.9 ppm; (b). Proton resonances from the head group of phospholipid and the glycerol backbone at 3.00-4.45 ppm, and (c). The olefinic proton signals of sterol and fatty chain at 5.15-6.00 ppm. The ^{1}H and ^{13}C resonance assignments of various lipid entities have been carried out as described in the literature (Sze and Jardetzky, 1990; Gunstone, 1992; Kriat et al., 1993; Adosraku et al., 1994; Tosi et al., 2003; Tugnoli et al., 2003), and all the respective resonance assignments are marked in the ^{1}H, ^{13}C, DEPT135 and DEPT90 spectra (figs. 2b, 3b-d) and are listed in Tables 1 and 2. The overlapped ^{1}H assignments of the individual lipid classes could be resolved by the combined use of various 2D NMR experiments such as COSY (fig. 5a-c) and TOCSY (fig. 6a-c), while the corresponding ^{1}H-^{13}C assignments were carried out using heteronuclear experiments such as HMQC (figs. 7a-e, 8a-d) and HMBC (figs. 9a-h, 10a-g). Based on the ^{1}H, ^{13}C and ^{31}P NMR spectroscopic observations, the following lipid components have been assigned: cholesterol, cholesterol ester (as oleate), glycerophosphatidylcholine, glycerophosphatidylethanolamine, glycerophosphatidalethanolamine or plasmalogen, sphingomyelin, glycerophosphatidylinositol, glycerophosphatidylserine, triglycerides, phenolic glycolipids, phosphatidylglycerol and phosphatidic acid.

Glycerophosphatidylcholine and sphingomyelin were identified as the two major choline-containing phospholipids in the present study. The characteristic $-N^{+}(CH_3)_3$ proton signal from these two lipid entities appeared as a broad singlet at 3.16 ppm. Further, the two choline head group methylene protons ($-PO-CH_2-$ and $-CH_2-N^{+}(CH_3)_3$) were identified by their 2D COSY cross-peaks resonating at 3.54 ppm and 4.19 ppm, as shown in figs. 5a-c. A similar cross-peak coupling pattern was observed between two proton resonances at 3.06 ppm and 4.02 ppm, which were assigned to be the ethanolamine head group methylene protons ($-PO-CH_2-$ and $-CH_2-NH_2$). The broad signal at 3.06 ppm also indicated a mixture of ethanolamine phospholipids, which were later identified as glycerophosphatidylethanolamine and plasmalogen (PLA) based on the 2D

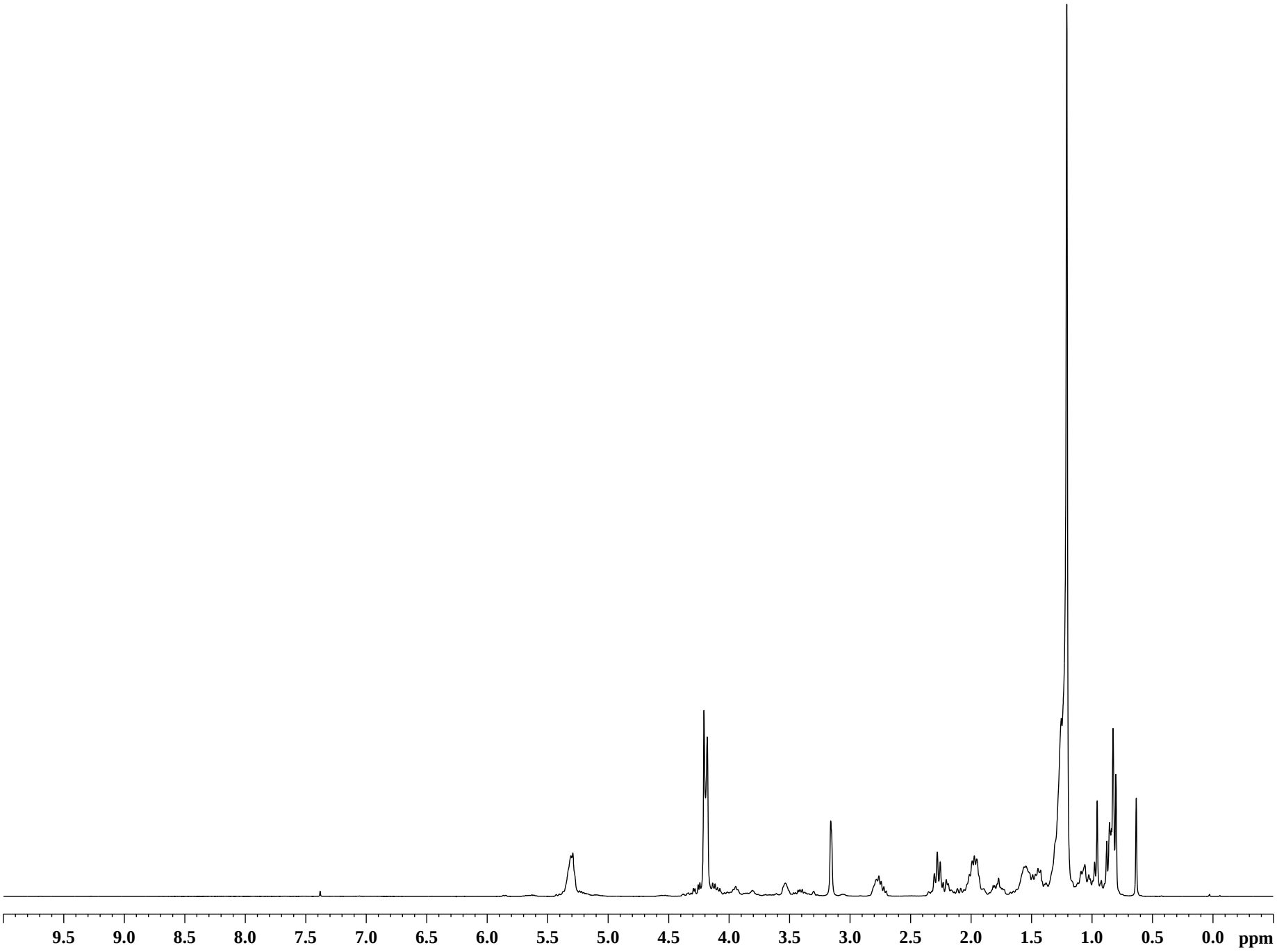

Fig. 2a: ^{1}H NMR spectrum of the lipid extract of a representative human tuberculoma sample.

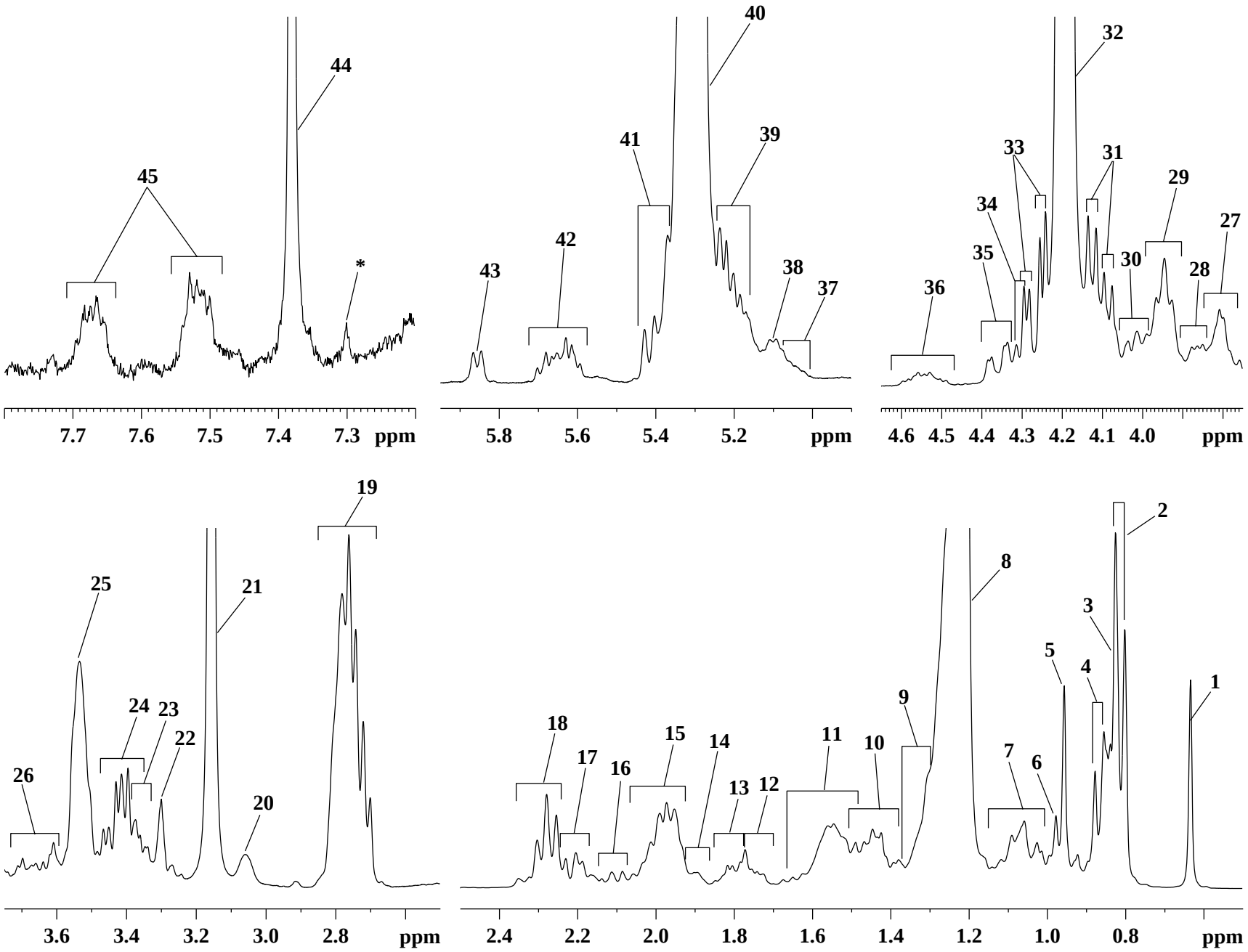

Fig. 2b: Expansions of the ^{1}H NMR spectrum of the lipid extract of the representative human tuberculoma sample, highlighting the resonance assignments between 0.5-2.5 ppm, 2.5-3.75 ppm, 3.75-4.65 ppm, 4.90-5.95 ppm and 7.20-7.80 ppm. The labeled assignments of the lipid components are as given in Table-1.

Table-1: Proton chemical shift assignments of the lipid components, as seen in the ^{1}H NMR spectra of human tuberculoma lipid extracts. The chemical shifts were calibrated with respect to the residual undeuterated methanol resonance at 3.30 ppm. Resonances marked as * are unassigned.

Assignment Number	**Lipid Components Assigned**		**Chemical Shift (δ, ppm)**
1	Cholesterol	18-CH_3	0.63
	Cholesterol ester		
2	Cholesterol	26-CH_3, 27-CH_3	0.81
	Cholesterol ester		
3	Fatty acid chain (methyls)	C**H$_3$**-CH_2-y	0.83
4	Cholesterol	21-CH_3, 9-CH	0.87
	Cholesterol ester		
5	Cholesterol	19-CH_3	0.96
6	Cholesterol ester	15-CH_2, 19-CH_3	0.94-1.00, 0.98
	Cholesterol	15-CH_2	
	Fatty acid chain (methylenes)	x-C**H$_2$**-$(CH_2)_n$-C**H$_2$**-y	
7	Fatty acid chain (methylenes)	x-C**H$_2$**-$(CH_2)_n$-C**H$_2$**-y	1.00-1.14
	Cholesterol	1-CH_2, 14-CH, 17-CH, 22-CH_2, 23-CH_2, 24-CH_2	
	Cholesterol ester	1-CH_2, 14-CH, 17-CH, 23-CH_2, 24-CH_2	
8	Fatty acid chain (methylenes)	x-CH_2-(C**H$_2$**)$_n$-CH_2-y	1.15-1.30
9	Fatty acid chain (methylenes)	x-C**H$_2$**-$(CH_2)_n$-C**H$_2$**-y	1.30-1.36
	Cholesterol	16-CH_2, 20-CH, 23-CH_2	
	Cholesterol ester	16-CH_2, 20-CH, 22-CH_2, 23-CH_2	
10	Fatty acid chain (methylenes)	x-C**H$_2$**-$(CH_2)_n$-C**H$_2$**-y	1.37-1.50
	Cholesterol	2-CH_2, 4-CH_2, 11-CH_2	
	Cholesterol ester	11-CH_2	
11	Fatty acid chain (β-methylenes)	x-CH_2-C**H$_2$**-CH_2-CO-y	1.48-1.67
	Cholesterol	7-CH_2, 15-CH_2, 25-CH	
	Cholesterol ester	2-CH_2, 4-CH_2, 7-CH_2, 15-CH_2, 25-CH	
12	Cholesterol	2-CH_2	1.70-1.77
13	Cholesterol	1-CH_2	1.77-1.85
	Cholesterol ester	2-CH_2	
14	Cholesterol	7-CH_2, 8-CH	1.86-1.92
	Cholesterol ester		
15	Fatty acid chain (mono-allylic methylenes)	x-C**H$_2$**-CH=CH-y, x-C**H$_2$**-CH=CH-C**H$_2$**-CH_2-y	1.92-2.06
	Sphingomyelin (mono-allylic methylene)	x-C**H$_2$**-CH=CH-CHOH-y	
	Plasmalogen (mono-allylic methylene)	x-C**H$_2$**-CH=CH-O-y	

Assignment Number	Lipid Components Assigned		Chemical Shift (δ, ppm)
	Cholesterol	12-CH_2, 16-CH_2	
	Cholesterol ester		
16	Fatty acid chain (mono-allylic methylenes)	x-C**H$_2$**-CH=CH-y, x-C**H$_2$**-CH=CH-C**H$_2$**-CH_2-y	2.07-2.14
	Cholesterol ester	1-CH_2	
17	Cholesterol	4-CH_2	2.16-2.24
18	Fatty acid chain (α-methylenes)	x-CH_2-CH_2-C**H$_2$**-CO-y	2.24-2.36
	Cholesterol ester	4-CH_2	
19	Fatty acid chain (di-allylic methylenes)	x-CH=CH-(C**H$_2$**-CH=CH)$_n$-y	2.68-2.86
20	Glycerophosphatidylethanolamine	x-CH_2-C**H$_2$**-NH_2	3.06
	Plasmalogen		
21	Glycerophosphatidylcholine	-$N^+(CH_3)_3$	3.16
	Sphingomyelin		
22	Methanol-d_4 (solvent)	CH_3-OH	3.30
23	Glycolipid sugars	-CH, -CH_2	3.33-3.38
	Inositol in phosphatidylinositol	-CH	
24	Glycolipid sugars	-CH, -CH_2	3.35-3.47
	Cholesterol	3-CH	
25	Glycolipid sugars	-CH, -CH_2	3.49-3.58
	Glycerophosphatidylcholine	x-CH_2-C**H$_2$**-$N^+(CH_3)_3$	
	Sphingomyelin		
26	Glycolipid sugars	-CH, -CH_2	3.59-3.72
27	Glycolipid sugars	-CH, -CH_2	3.77-3.84
	Inositol in phosphatidylinositol	-CH	
28	Glycolipid sugars	-CH, -CH_2	3.84-3.89
	Plasmalogen	C**H$_2$**OR_1-$CHOR_2$-CH_2-x	
	Sphingomyelin	x-CHOH-C**H**R-CH_2-O-y	
29	Glycolipid sugars	-CH, -CH_2	3.90-3.98
	Glycerophospholipids (phosphatidylcholine, phosphatidylethanolamine, plasmalogen, phosphatidylserine, phosphatidylinositol)	CH_2OR_1-$CHOR_2$-C**H$_2$**-x	
30	Glycolipid sugars	-CH, -CH_2	3.98-4.05
	Glycerophosphatidylethanolamine	x-C**H$_2$**-CH_2-NH_2	
	Plasmalogen		
	Sphingomyelin	x-C**H**OH-CHR-CH_2-O-y	
31	Glycerophospholipids (phosphatidylcholine, phosphatidylethanolamine, phosphatidylserine, phosphatidylinositol)	C**H$_2$**OR_1-$CHOR_2$-CH_2-x	4.06-4.15
	Sphingomyelin	x-CHOH-CHR-C**H$_2$**-O-y	

Assignment Number	Lipid Components Assigned		Chemical Shift (δ, ppm)
32	Water, residual	HOD	4.15-4.23
	Glycerophosphatidylcholine	x-C**H$_2$**-CH$_2$-N$^+$(CH$_3$)$_3$	
	Sphingomyelin		
33	Glycerophospholipids (phosphatidylcholine, phosphatidylethanolamine, phosphatidylserine, phosphatidylinositol)	C**H$_2$**OR$_1$-CHOR$_2$-CH$_2$-x	4.23-4.30
	Triglycerides	C**H$_2$**OR$_1$-CHOR$_2$-C**H$_2$**OR$_3$	
34	Plasmalogen (olefinic)	x-CH$_2$-C**H**=CH-O-y	4.29-4.33
35	Triglycerides	C**H$_2$**OR$_1$-CHOR$_2$-C**H$_2$**OR$_3$	4.33-4.40
36	Cholesterol ester	3-CH	4.54
37	Glycolipid sugars (cerebrosides)	-CH (anomeric)	5.00-5.07
38	Glycolipid sugars (cerebrosides)	-CH (anomeric)	5.07-5.13
	Plasmalogen	CH$_2$OR$_1$-C**H**OR$_2$-CH$_2$-x	
39	Glycerophospholipids (phosphatidylcholine, phosphatidylethanolamine, phosphatidylserine, phosphatidylinositol)	CH$_2$OR$_1$-C**H**OR$_2$-CH$_2$-x	5.16-5.25
	Triglycerides	CH$_2$OR$_1$-C**H**OR$_2$-CH$_2$OR$_3$	
40	Fatty acid chain (olefinic)	x-C**H**=C**H**-(CH$_2$-C**H**=C**H**)$_n$-y, x-CH$_2$-C**H**=C**H**-y, x-CH$_2$-C**H**=C**H**-CH$_2$-CH$_2$-y	5.25-5.36
	Cholesterol	6-CH	
	Cholesterol ester		
41	Sphingomyelin (olefinic)	x-CH$_2$-CH=C**H**-CHOH-y	5.36-5.45
42	Sphingomyelin (olefinic)	x-CH$_2$-C**H**=CH-CHOH-y	5.65
43	Plasmalogen (olefinic)	x-CH$_2$-CH=C**H**-O-y	5.86
44	Chloroform-d (solvent)	CHCl$_3$	7.38
45	Phenolic glycolipids	-CH (ring)	7.49-7.55, 7.64-7.71

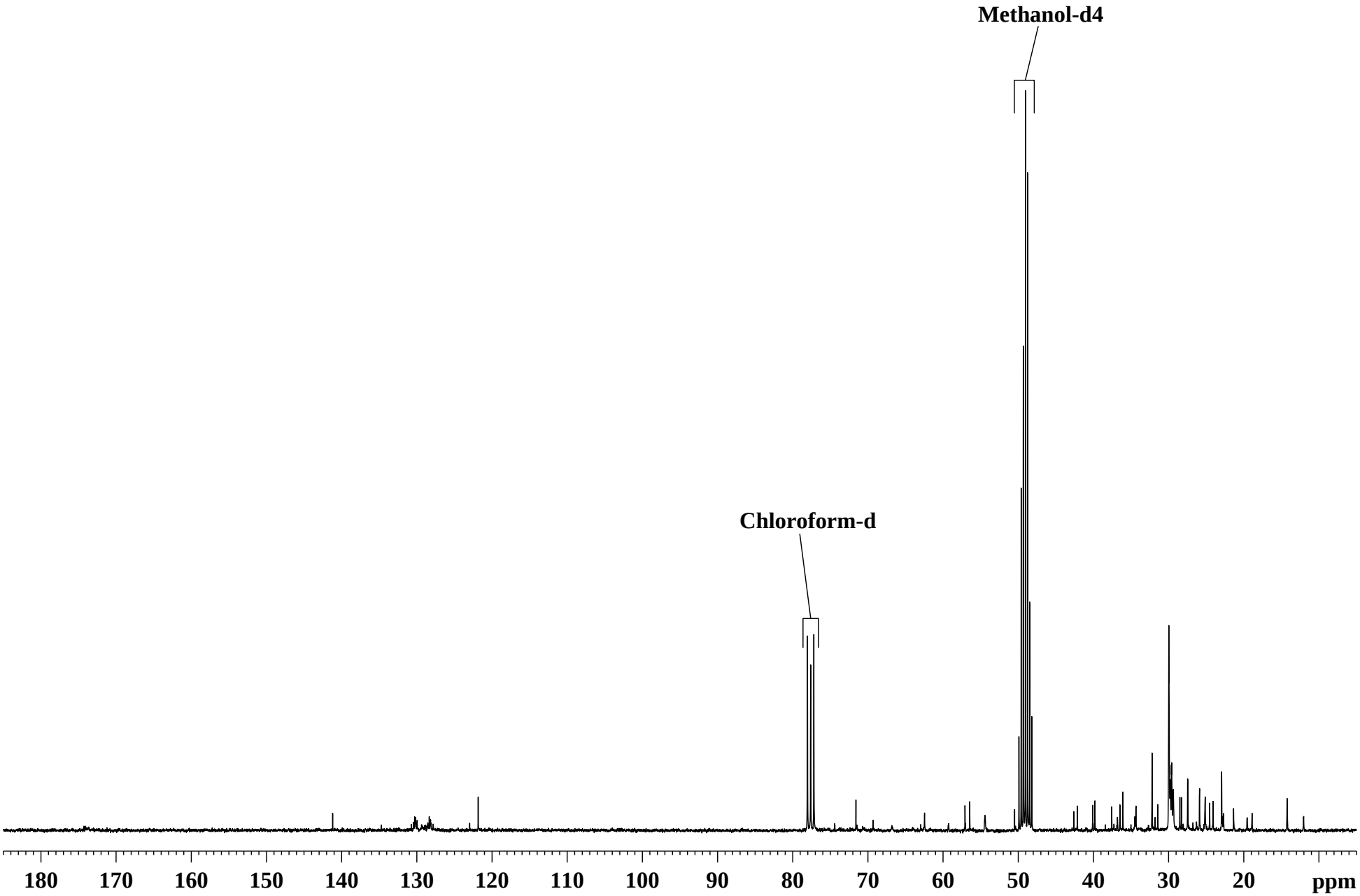

Fig. 3a: ^{13}C NMR spectrum of the lipid extract of a representative human tuberculoma sample.

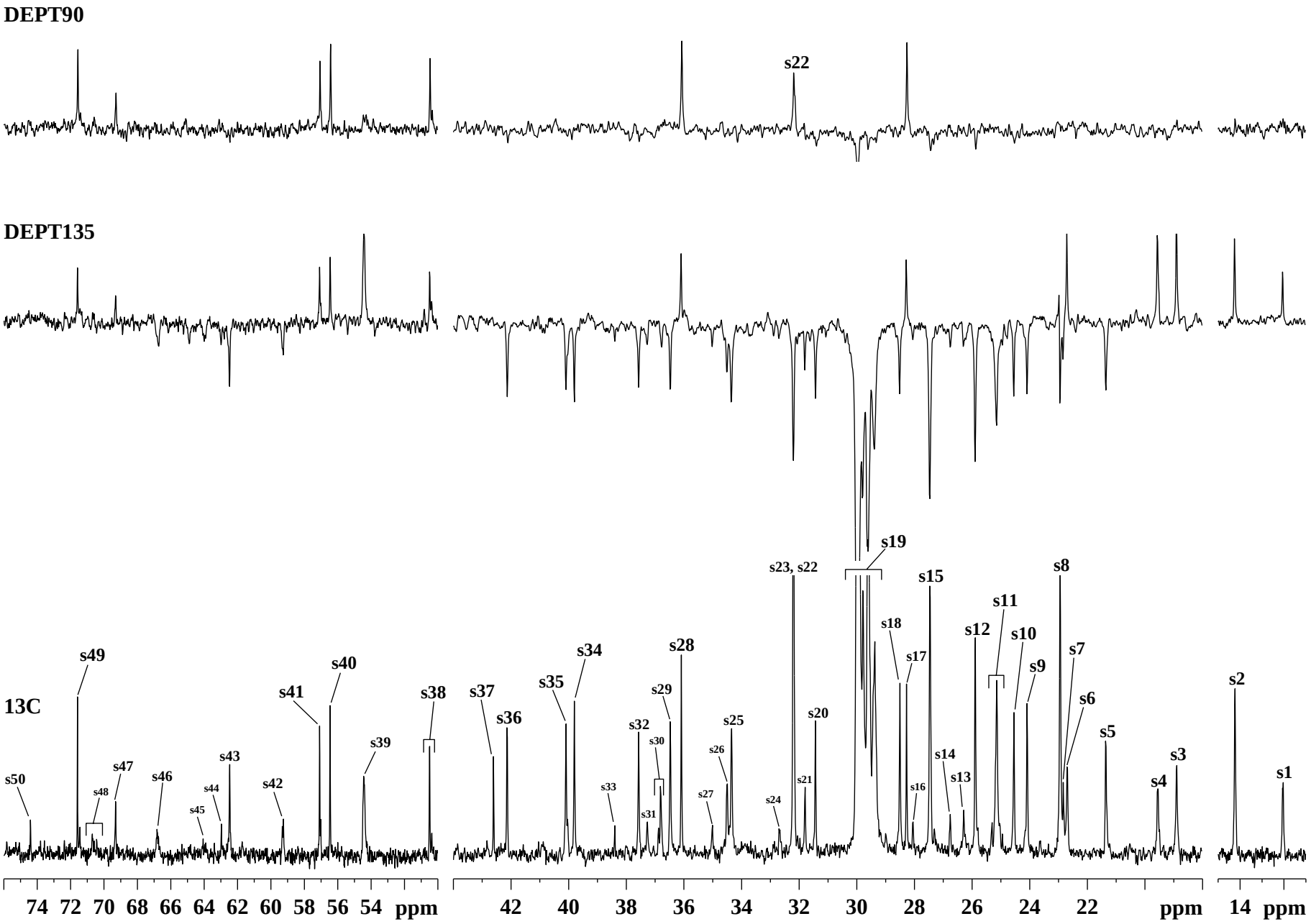

Fig. 3b: Expansions of the ^{13}C, DEPT135 and DEPT90 NMR spectra of the lipid extract of the representative human tuberculoma sample, highlighting the resonance assignments between 11.0-15.0 ppm, 18.0-44.0 ppm and 50.0-76.0 ppm. The labeled assignments of the lipid components are as given in Table-2.

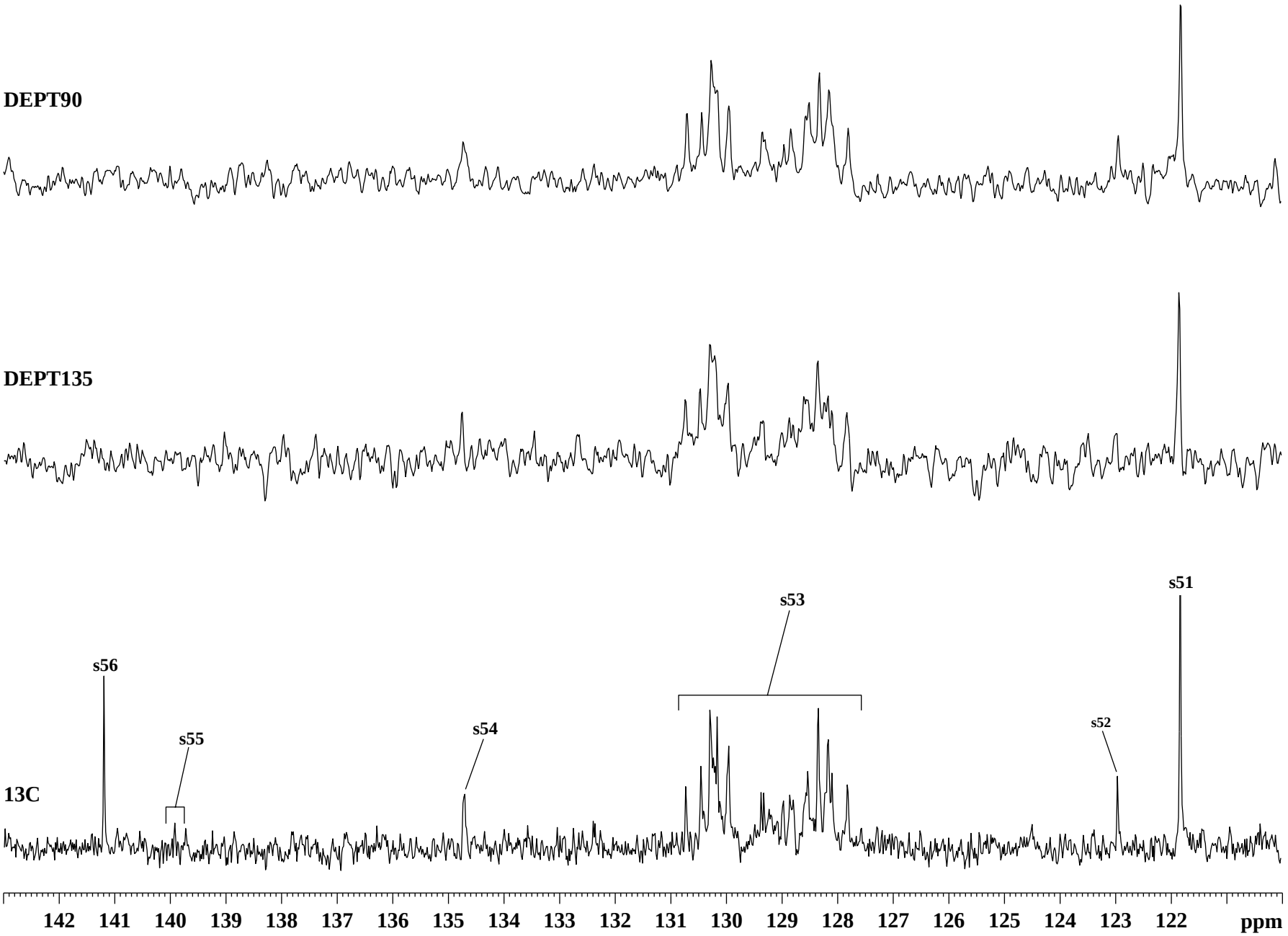

Fig. 3c: Expansion of the ^{13}C, DEPT135 and DEPT90 NMR spectra of the lipid extract of the representative human tuberculoma sample, highlighting the resonance assignments between 120.0-143.0 ppm. The labeled assignments of the lipid components are as given in Table-2.

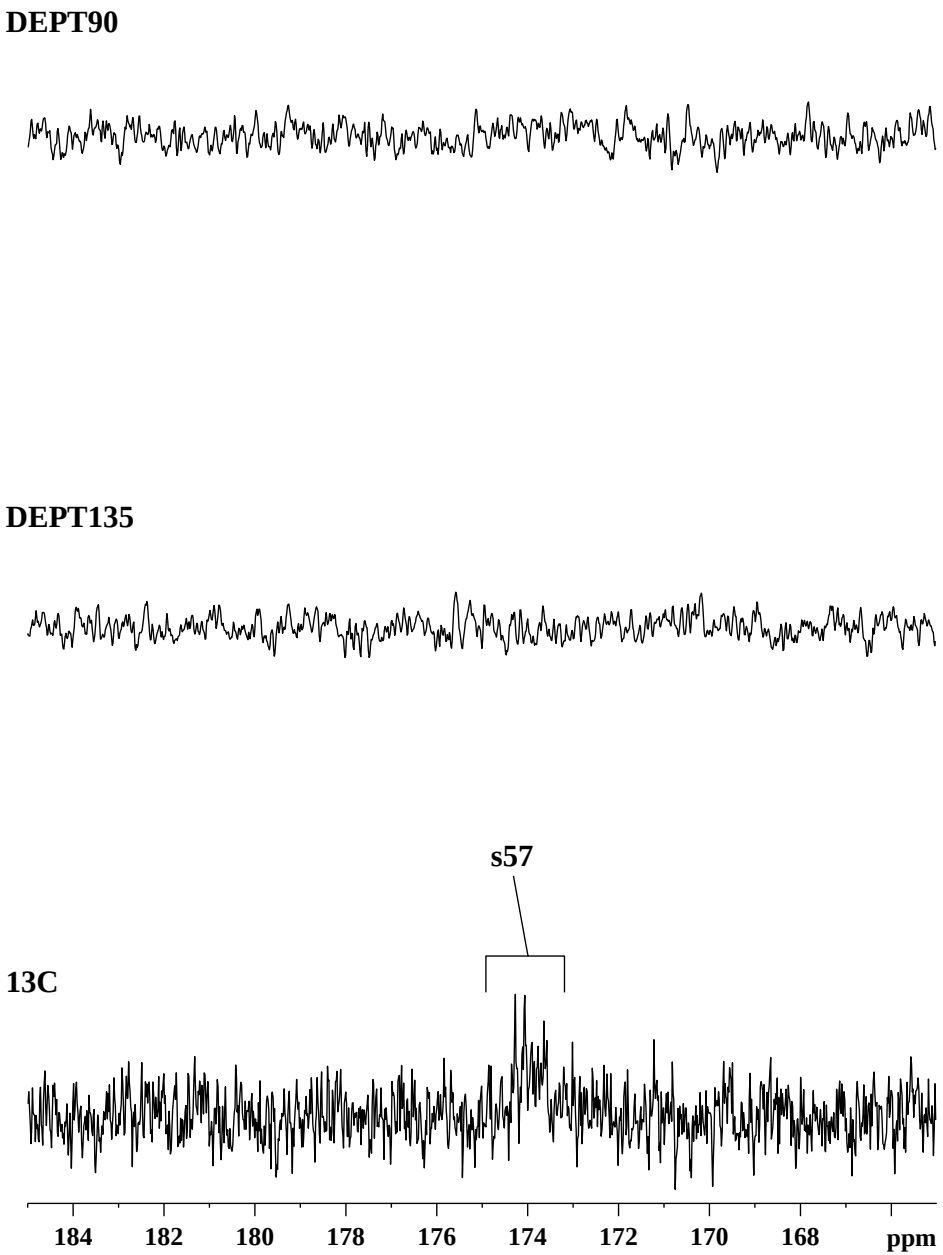

Fig. 3d: Expansion of the ^{13}C, DEPT135 and DEPT90 NMR spectra of the lipid extract of the representative human tuberculoma sample, highlighting the resonance assignments between 165.0-185.0 ppm. The labeled assignments of the lipid components are as given in Table-2.

Table-2: Carbon-13 chemical shift assignments of the lipid components, as seen in the ^{13}C NMR spectra of human tuberculoma lipid extracts. The chemical shifts were calibrated with respect to the methanol (solvent) resonance at 49.04 ppm. Resonances marked as * are unassigned.

Assignment Number	Lipid Components Assigned		Chemical Shift (δ, ppm)
s1	Cholesterol	18-CH_3	12.0
	Cholesterol ester		
s2	Fatty acid chain (methyls)	**C**H_3-CH_2-y	14.2
s3	Cholesterol	21-CH_3	18.9
	Cholesterol ester		
s4	Cholesterol	19-CH_3	19.6
	Cholesterol ester		
s5	Cholesterol	11-CH_2	21.4
	Cholesterol ester		
s6	Cholesterol	26-CH_3, 27-CH_3	22.7
	Cholesterol ester		
s7	Fatty acid chain (methylenes)	x-**C**H_2-$(CH_2)_n$-**C**H_2-y	22.8
s8	Fatty acid chain (methylenes)	x-**C**H_2-$(CH_2)_n$-**C**H_2-y	22.9
s9	Cholesterol	23-CH_2	24.1
	Cholesterol ester		
s10	Cholesterol	15-CH_2	24.5
	Cholesterol ester		
s11	Fatty acid chain (β-methylenes)	x-CH_2-**C**H_2-CH_2-CO-y	25.1
s12	Fatty acid chain (di-allylic methylenes)	x-CH=CH-(**C**H_2-CH=CH)$_n$-y	25.9
s13	Fatty acid chain (mono-allylic methylenes)	x-**C**H_2-CH=CH-y, x-**C**H_2-CH=CH-**C**H_2-CH_2-y	26.3
	Sphingomyelin (mono-allylic methylene)	x-**C**H_2-CH=CH-CHOH-y	
	Plasmalogen (mono-allylic methylene)	x-**C**H_2-CH=CH-O-y	
s14	Fatty acid chain (mono-allylic methylenes)	x-**C**H_2-CH=CH-y, x-**C**H_2-CH=CH-**C**H_2-CH_2-y	26.7
	Sphingomyelin (mono-allylic methylene)	x-**C**H_2-CH=CH-CHOH-y	
	Plasmalogen (mono-allylic methylene)	x-**C**H_2-CH=CH-O-y	
s15	Fatty acid chain (mono-allylic methylenes)	x-**C**H_2-CH=CH-y, x-**C**H_2-CH=CH-**C**H_2-CH_2-y	27.5
	Sphingomyelin (mono-allylic methylene)	x-**C**H_2-CH=CH-CHOH-y	
	Plasmalogen (mono-allylic methylene)	x-**C**H_2-CH=CH-O-y	
s16	Cholesterol ester	2-CH_2	28.1
s17	Cholesterol	25-CH	28.3
	Cholesterol ester		

Assignment Number	Lipid Components Assigned		Chemical Shift (δ, ppm)
s18	Cholesterol	16-CH_2	28.5
	Cholesterol ester		
s19	Fatty acid chain (methylenes)	x-**C**H_2-(**C**H_2)$_n$-**C**H_2-y	29.2-30.1
s20	Cholesterol	2-CH_2	31.4
s21	Fatty acid chain (methylenes)	x-**C**H_2-(CH_2)$_n$-**C**H_2-y	31.8
s22	Cholesterol	8-CH	32.1
	Cholesterol ester		
s23	Cholesterol	7-CH_2	32.2
	Cholesterol ester		
	Fatty acid chain (methylenes)	x-**C**H_2-(CH_2)$_n$-**C**H_2-y	
s24	Fatty acid chain (methylenes)	x-**C**H_2-(CH_2)$_n$-**C**H_2-y	32.7
s25	Fatty acid chain (α-methylenes)	x-CH_2-CH_2-**C**H_2-CO-y	34.3
s26	Fatty acid chain (α-methylenes)	x-CH_2-CH_2-**C**H_2-CO-y	34.5
s27	Fatty acid chain (α-methylenes)	x-CH_2-CH_2-**C**H_2-CO-y	35.0
s28	Cholesterol	20-CH	36.1
	Cholesterol ester		
s29	Cholesterol	22-CH_2	36.5
	Cholesterol ester		
s30	Cholesterol	10-C	36.8
	Cholesterol ester		
s31	Cholesterol ester	1-CH_2	37.3
s32	Cholesterol	1-CH_2	37.6
s33	Cholesterol ester	4-CH_2	38.4
s34	Cholesterol	24-CH_2	39.8
	Cholesterol ester		
s35	Cholesterol	12-CH_2	40.1
	Cholesterol ester		
s36	Cholesterol	4-CH_2	42.1
s37	Cholesterol	13-C	42.6
	Cholesterol ester		
s38	Cholesterol	9-CH	50.5
	Cholesterol ester		
s39	Glycerophosphatidylcholine	-N^+(**C**H_3)$_3$	54.4
	Sphingomyelin		
s40	Cholesterol	17-CH	56.5
	Cholesterol ester		
s41	Cholesterol	14-CH	57.1
	Cholesterol ester		
s42	Glycerophosphatidylcholine	x-**C**H_2-CH_2-N^+(CH_3)$_3$	59.3
	Sphingomyelin		
	Glycerophosphatidylethanolamine	x-**C**H_2-CH_2-NH_2	
	Plasmalogen		

Assignment Number	Lipid Components Assigned		Chemical Shift (δ, ppm)
s43	Glycerophospholipids (phosphatidylcholine, phosphatidylethanolamine, plasmalogen, phosphatidylserine, phosphatidylinositol)	**C**H_2OR_1-$CHOR_2$-CH_2-x	62.5
	Triglycerides	**C**H_2OR_1-$CHOR_2$-**C**H_2OR_3	
	Sphingomyelin	x-CHOH-CHR-**C**H_2-O-y	
	Glycolipid sugars	-CH_2	
s44	Glycerophospholipids (phosphatidylcholine, phosphatidylethanolamine, plasmalogen, phosphatidylserine, phosphatidylinositol)	**C**H_2OR_1-$CHOR_2$-CH_2-x	62.9
	Triglycerides	**C**H_2OR_1-$CHOR_2$-**C**H_2OR_3	
	Sphingomyelin	x-CHOH-CHR-**C**H_2-O-y	
	Glycolipid sugars	-CH_2	
s45	Glycerophospholipids (phosphatidylcholine, phosphatidylethanolamine, plasmalogen, phosphatidylserine, phosphatidylinositol)	CH_2OR_1-$CHOR_2$-**C**H_2-x	64.0
s46	Glycerophosphatidylcholine	x-CH_2-**C**H_2-$N^+(CH_3)_3$	66.8
	Sphingomyelin		
	Glycerophosphatidylethanolamine	x-CH_2-**C**H_2-NH_2	
	Plasmalogen		
s47	Glycolipid sugars	-CH	69.3
	Inositol in phosphatidylinositol		
	Glycerophospholipids (phosphatidylcholine, phosphatidylethanolamine, plasmalogen, phosphatidylserine, phosphatidylinositol)	CH_2OR_1-**C**HOR_2-CH_2-x	
	Triglycerides	CH_2OR_1-**C**HOR_2-CH_2OR_3	
	Sphingomyelin	x-CHOH-CHR-CH_2-O-y	
s48	Glycolipid sugars	-CH	70.7
	Inositol in phosphatidylinositol		
	Glycerophospholipids (phosphatidylcholine, phosphatidylethanolamine, plasmalogen, phosphatidylserine, phosphatidylinositol)	CH_2OR_1-$CHOR_2$-CH_2-x	
	Triglycerides	CH_2OR_1-$CHOR_2$-CH_2OR_3	
	Sphingomyelin	x-**C**HOH-**C**HR-CH_2-O-y	
s49	Cholesterol	3-CH	71.5
s50	Cholesterol ester	3-CH	74.4
s51	Cholesterol	6-CH	121.8

Assignment Number	Lipid Components Assigned		Chemical Shift (δ, ppm)
s52	Cholesterol ester	6-CH	122.9
s53	Fatty acid chain (olefinic)	x-**C**H=**C**H-(CH_2-**C**H=**C**H)$_n$-y	127.6-130.8
	Fatty acid chain (olefinic)	x-CH_2-**C**H=**C**H-y, x-CH_2-**C**H=**C**H-CH_2-CH_2-y	
	Sphingomyelin (olefinic)	x-CH_2-**C**H=**C**H-CHOH-y	
	Phenolic glycolipids	-CH (ring)	
	Plasmalogen (olefinic)	x-CH_2-**C**H=CH-O-y	
s54	Plasmalogen (olefinic)	x-CH_2-CH=**C**H-O-y	134.7
s55	Cholesterol ester	5-C	139.9
s56	Cholesterol	5-C	141.2
s57	Cholesterol ester	-O**C**OR	173.2-174.7
	Fatty acid esters		

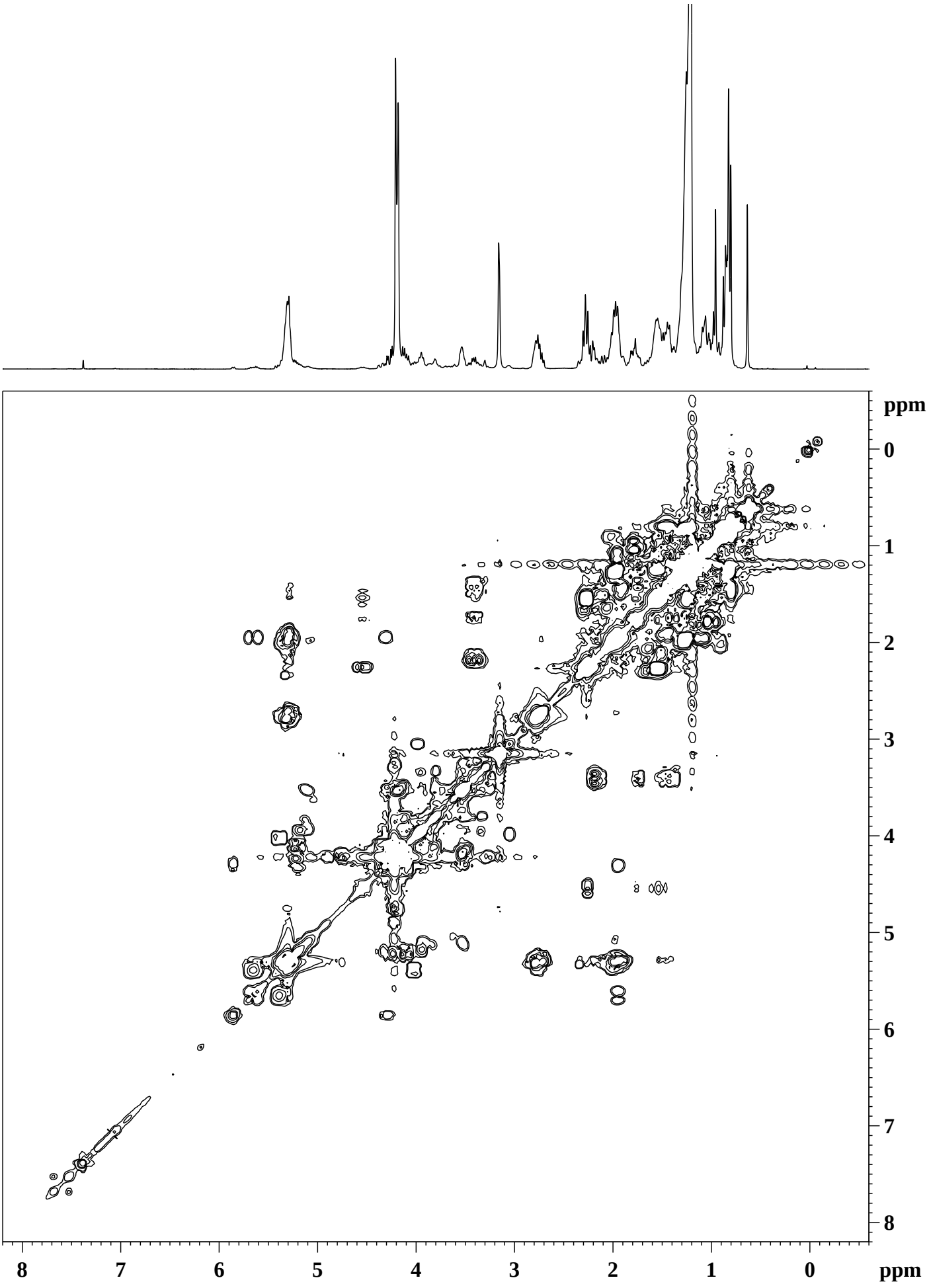

Fig. 4a: ^{1}H-^{1}H COSY spectrum of the lipid extract of a representative human tuberculoma sample.

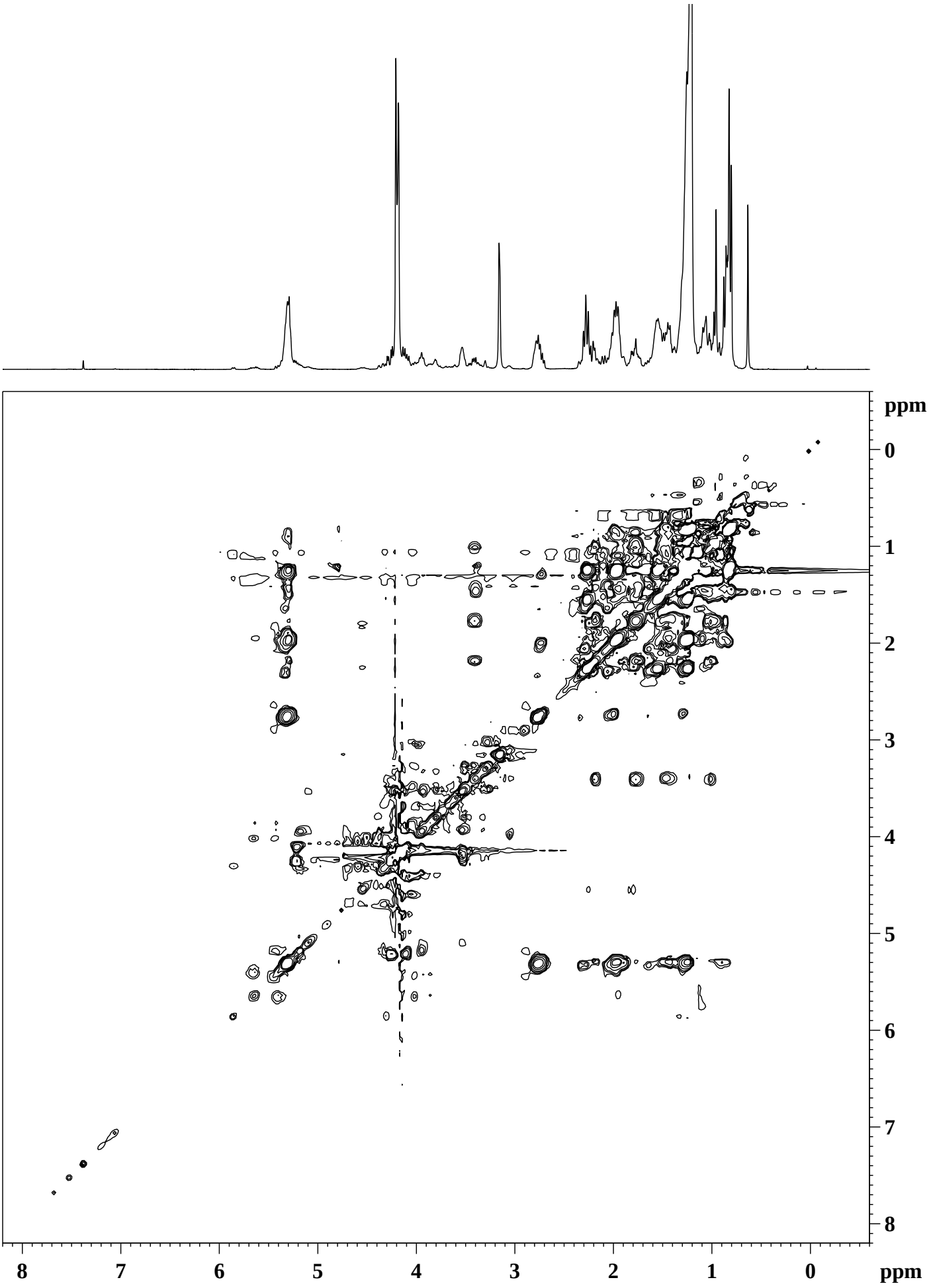

Fig. 4b: ^{1}H-^{1}H TOCSY spectrum of the lipid extract of a representative human tuberculoma sample.

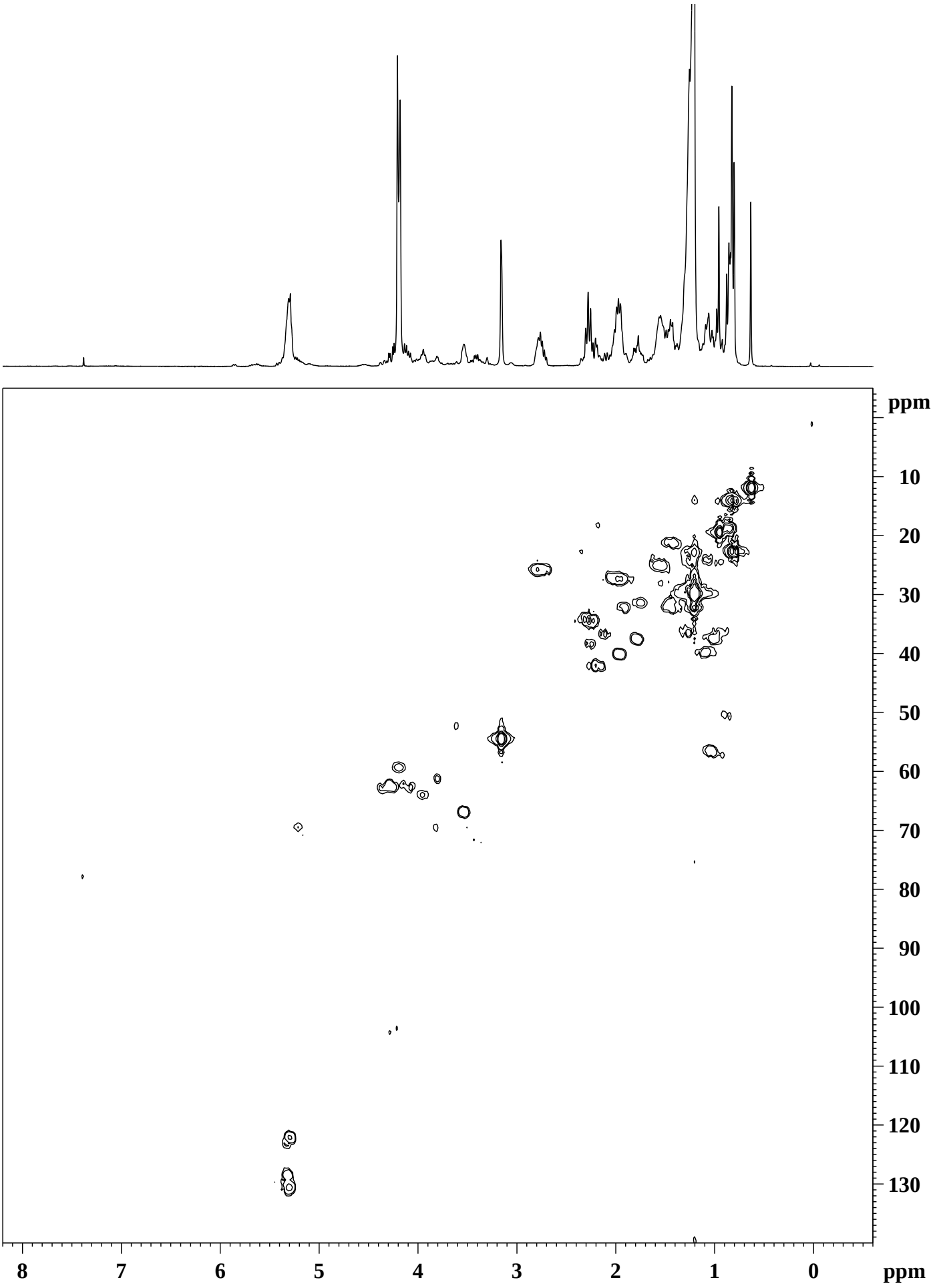

Fig. 4c: ^{1}H-^{13}C HMQC spectrum of the lipid extract of a representative human tuberculoma sample.

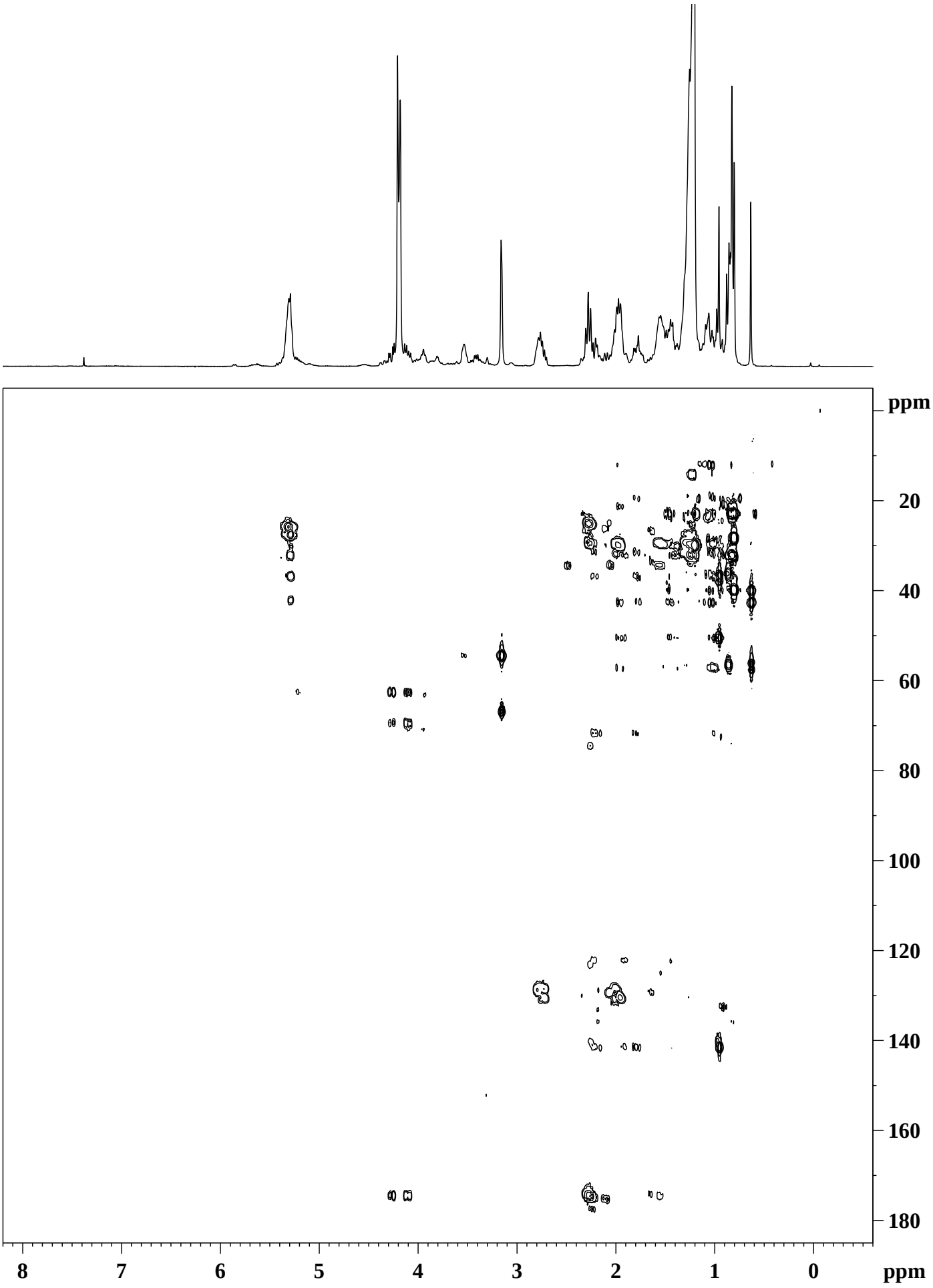

Fig. 4d: ^{1}H-^{13}C HMBC spectrum of the lipid extract of a representative human tuberculoma sample.

COSY and TOCSY coupling patterns (figs. 5a-c, 6a-c). Further, the olefinic proton correlations at 4.30 ppm and 5.86 ppm, and the long-range correlation of the resonance signal at 5.86 ppm with the methylene signal resonating at 1.97 ppm gave an indication that an olefinic ether linkage (-O-CH=CH-CH_2-) was present that belonged to the PLA (fig. 5b). The sphingolipids in the tuberculoma mainly comprised of sphingomyelin, which was identified by the characteristic vinyl proton resonances at 5.65 ppm (multiplet) and 5.39 ppm (-CH=CH-, double-doublets), as confirmed by their cross-peak coupling information from the 2D COSY and TOCSY spectra (figs. 5a-c, 6a-c).

The assignments of the choline head-group could be carried out by the combined use of HMQC and HMBC experiments. In the ^{1}H-^{13}C HMQC spectra (figs. 7b, 8b), the choline head-group -$N^{+}(CH_3)_3$ protons at 3.16 ppm gave a characteristic cross-peak correlation with the corresponding ^{13}C signal at 54.4 ppm. Further, the two methylenes of the phosphocholine head-group gave their respective ^{13}C correlations with the signals at 59.3 ppm and 66.8 ppm in the HMQC spectra (figs. 7b, 8b). The -$N^{+}(CH_3)_3$ signal also gave a HMBC correlation with one of the phosphocholine head-group methylenes at 66.8 ppm (figs. 9c, 10c), thus confirming the assignments of phosphocholine head-group.

The glycerol backbone of the diacylglycerophospholipids was assigned by the cross-peaks between the protons resonating at 4.10 ppm and 4.27 ppm, both corresponding to the sn-1 (geminal) methylene protons of glycerol backbone, which are magnetically inequivalent. These protons, together with the protons at 3.95 ppm (corresponding to the sn-3 methylene protons of glycerol backbone linked to the phosphocholine-phosphoethanolamine-phosphoinositol-phosphoserine head groups) gave cross-peak correlations with the proton at 5.21 ppm (corresponding to the sn-2 proton of the diacylglycerol backbone) as seen in the 2D COSY and TOCSY spectra (figs. 5a-c, 6a-c), thereby helping in the assignments of the diacylglycerol backbone. It has not been possible to selectively identify the individual resonance assignments for the abovementioned glycerophospholipids, due to spectral overlapping of the lipid components (Kriat et al., 1993). Further, the proton signal centered at 4.33 ppm (double-doublet) gave a clear indication for the presence of triglycerides (TGs), although the sn-1 and sn-3 (geminal) methylenes of TGs were observed to be overlapped with the sn-1 (geminal) methylene protons of

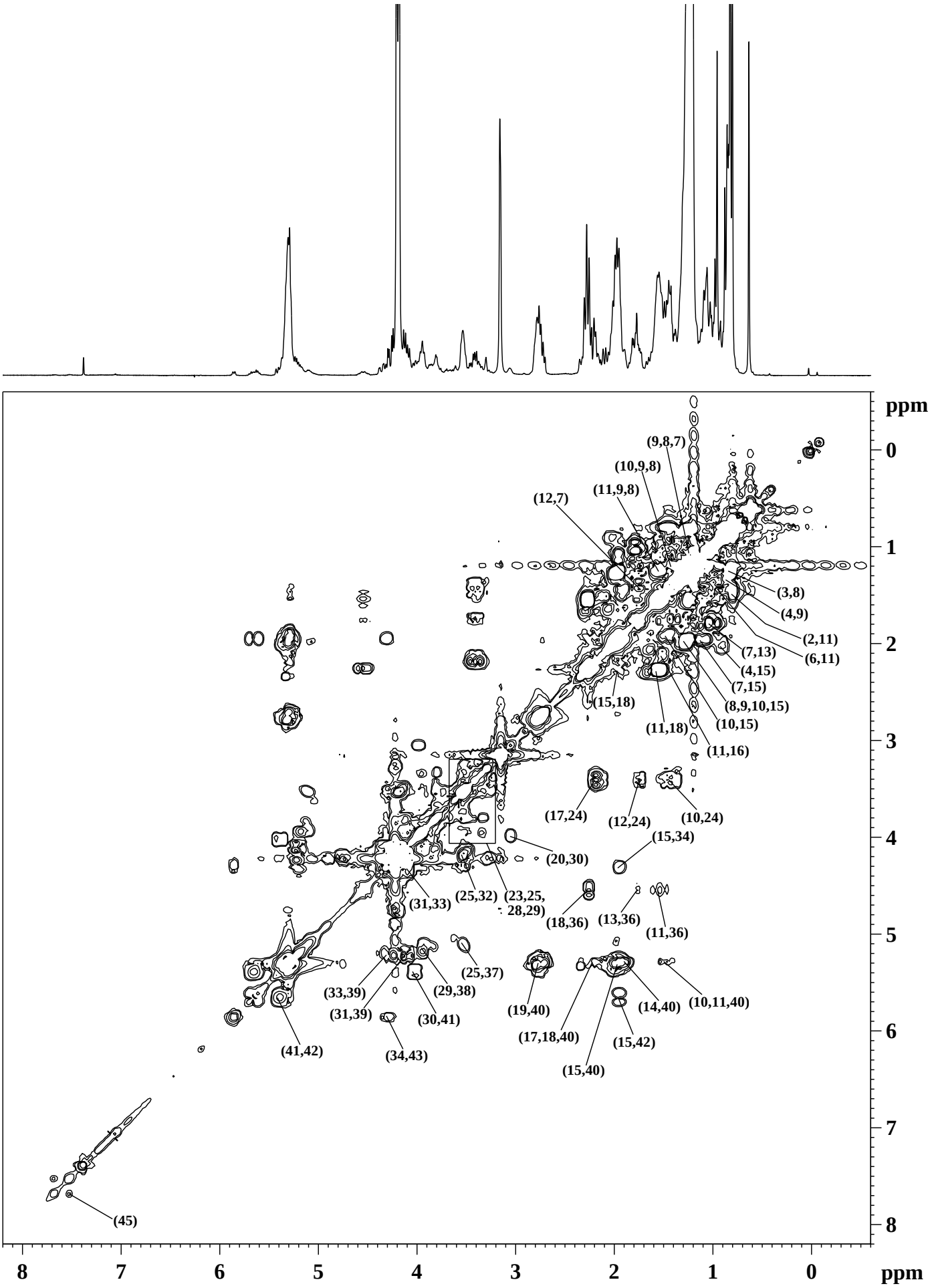

Fig. 5a: ^{1}H-^{1}H COSY spectrum of the lipid extract of a human tuberculoma sample. The labeled assignments are as given in Table-1.

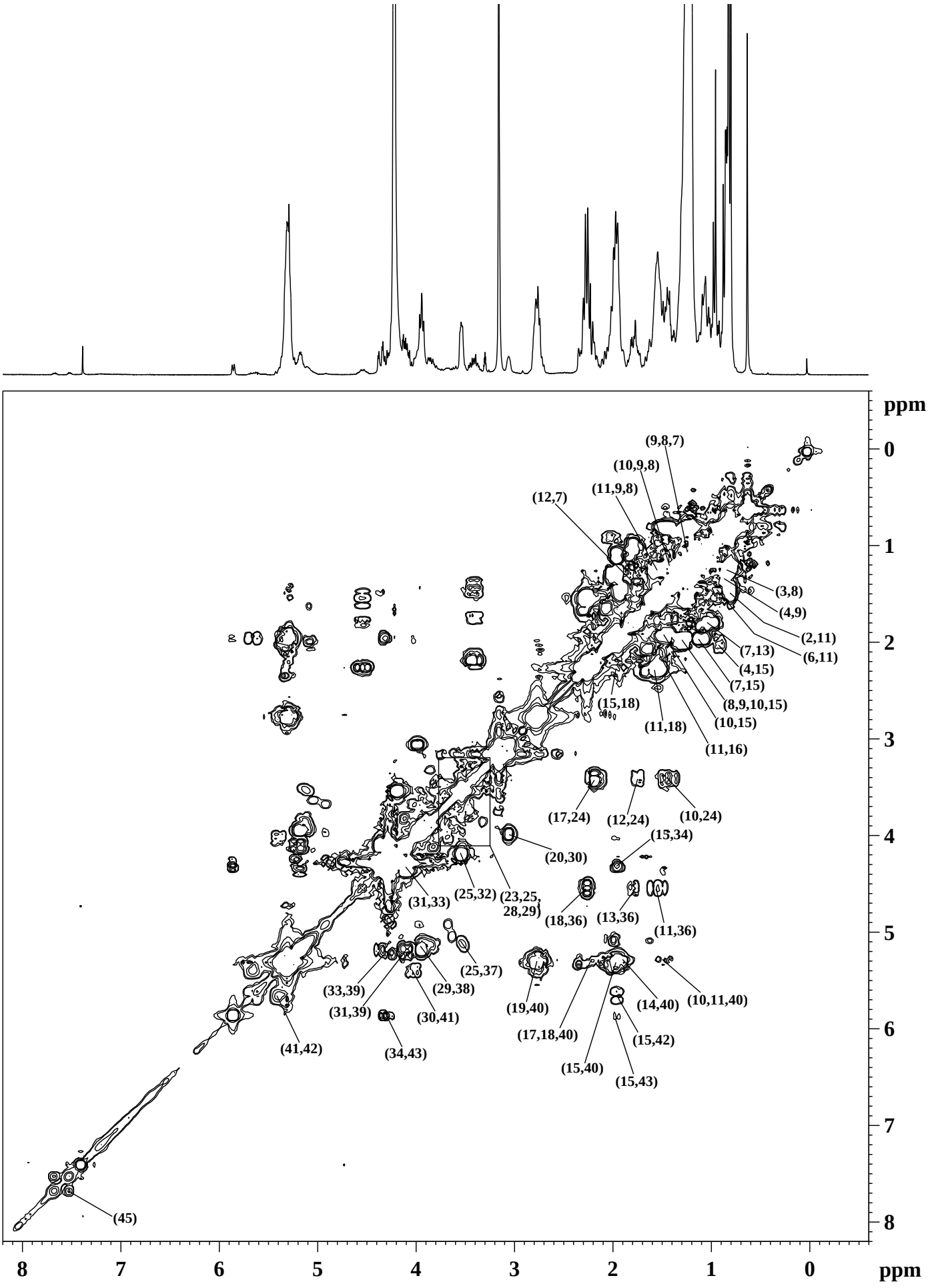

Fig. 5b: ^{1}H-^{1}H COSY spectrum of the lipid extract of a human tuberculoma sample. The labeled assignments are as given in Table-1.

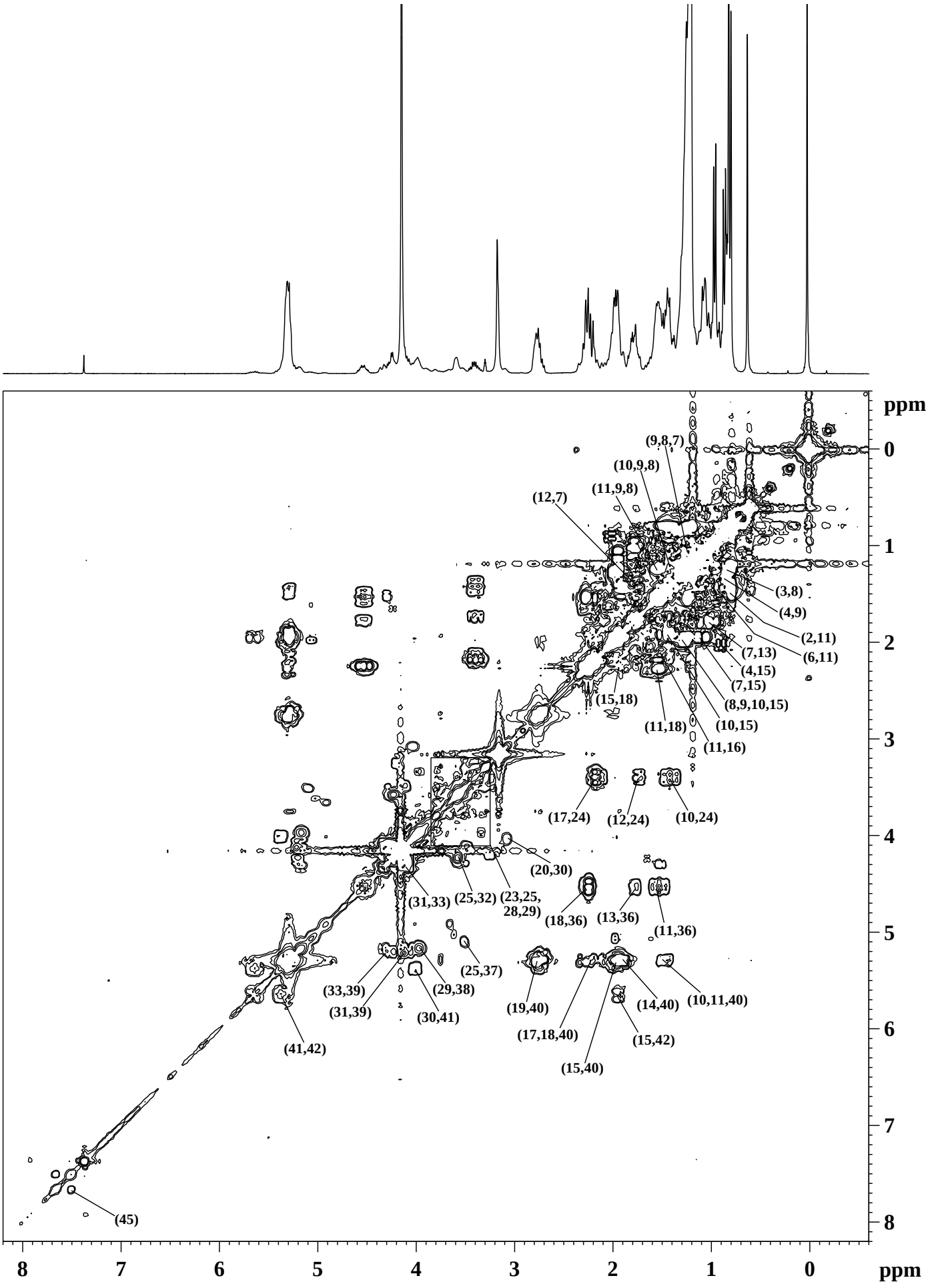

Fig. 5c: ^{1}H-^{1}H COSY spectrum of the lipid extract of a human tuberculoma sample. The labeled assignments are as given in Table-1.

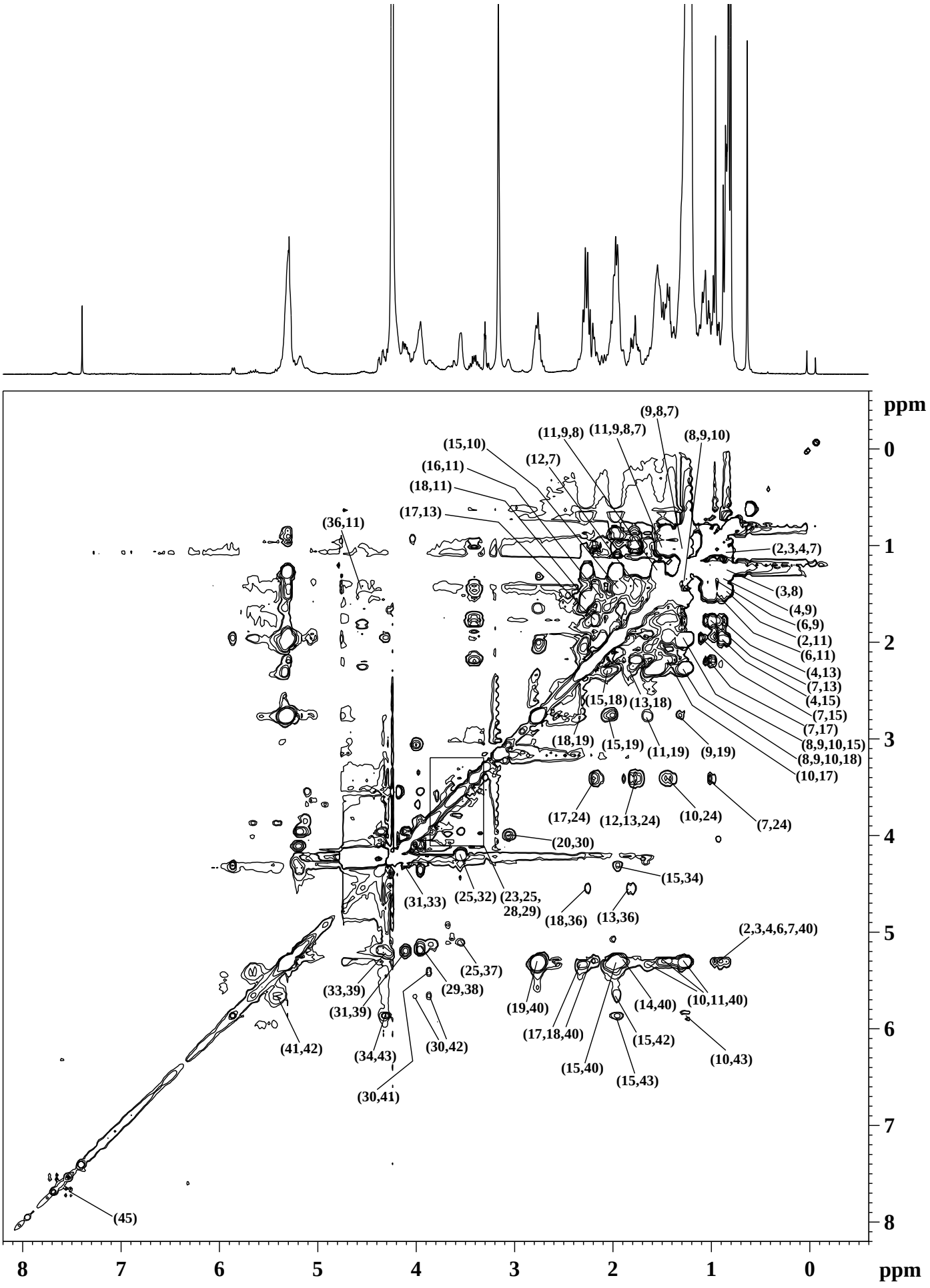

Fig. 6a: ^{1}H-^{1}H TOCSY spectrum of the lipid extract of a human tuberculoma sample. The labeled assignments are as given in Table-1.

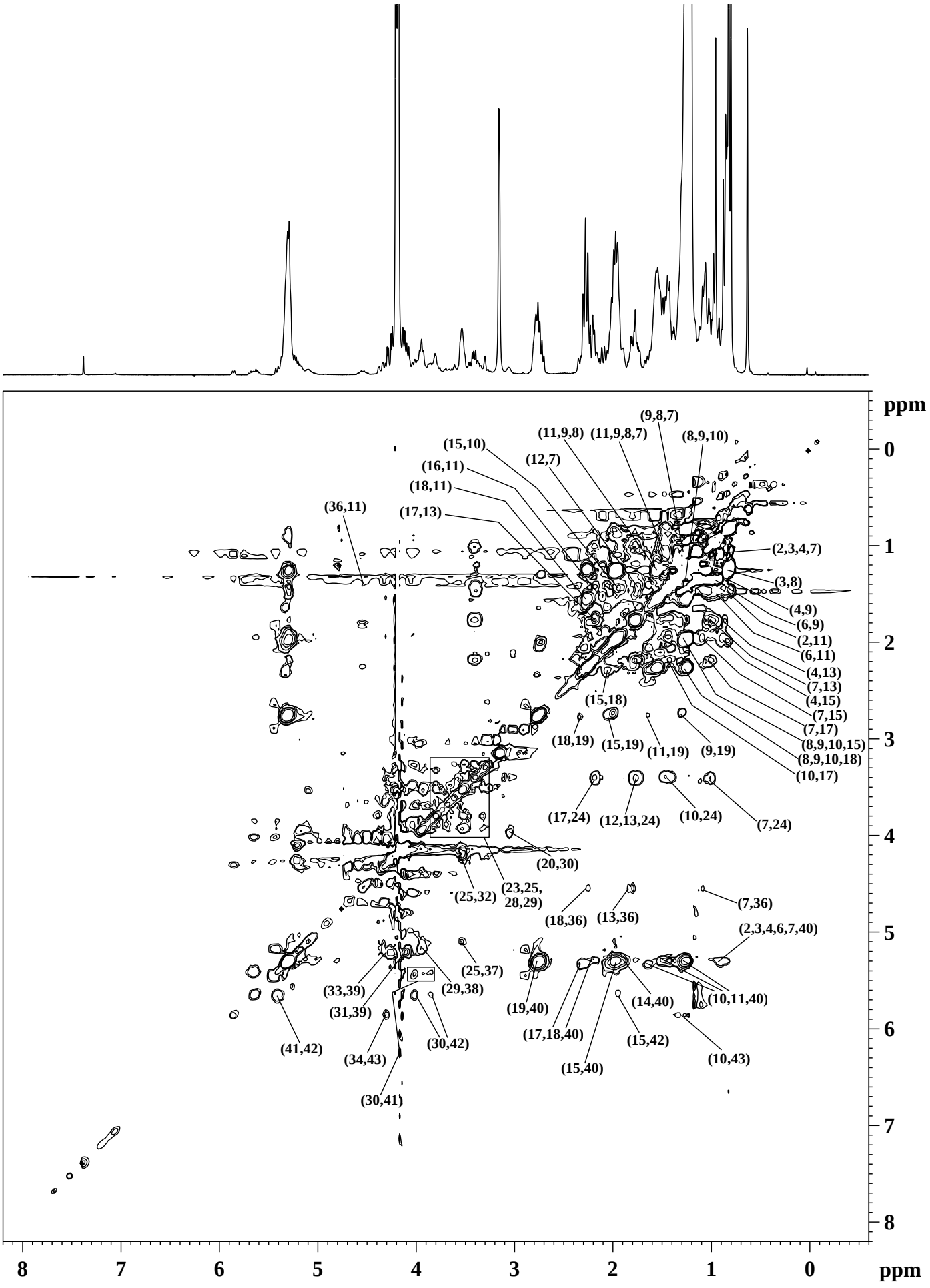

Fig. 6b: ^{1}H-^{1}H TOCSY spectrum of the lipid extract of a human tuberculoma sample. The labeled assignments are as given in Table-1.

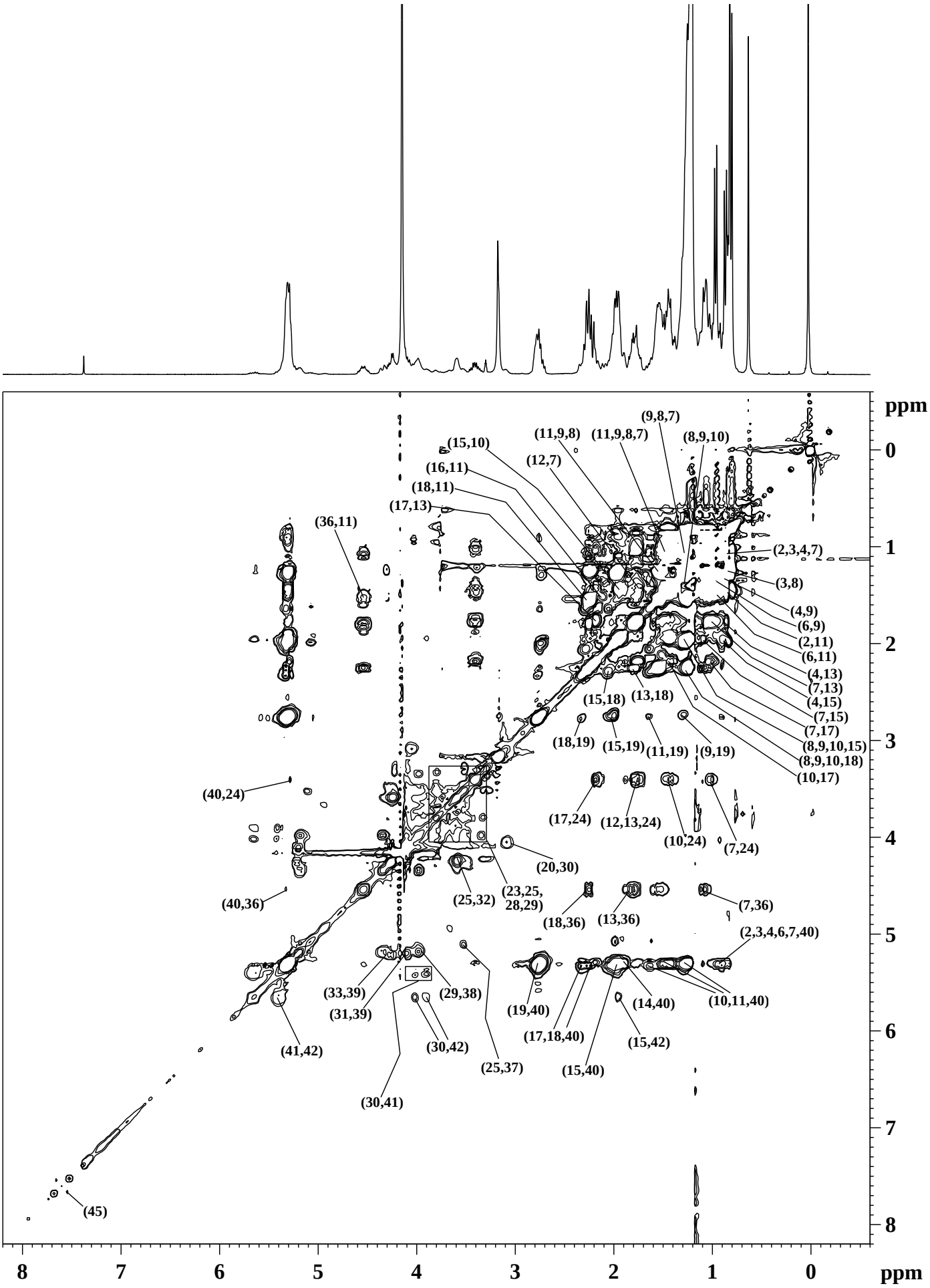

Fig. 6c: ^{1}H-^{1}H TOCSY spectrum of the lipid extract of a human tuberculoma sample. The labeled assignments are as given in Table-1.

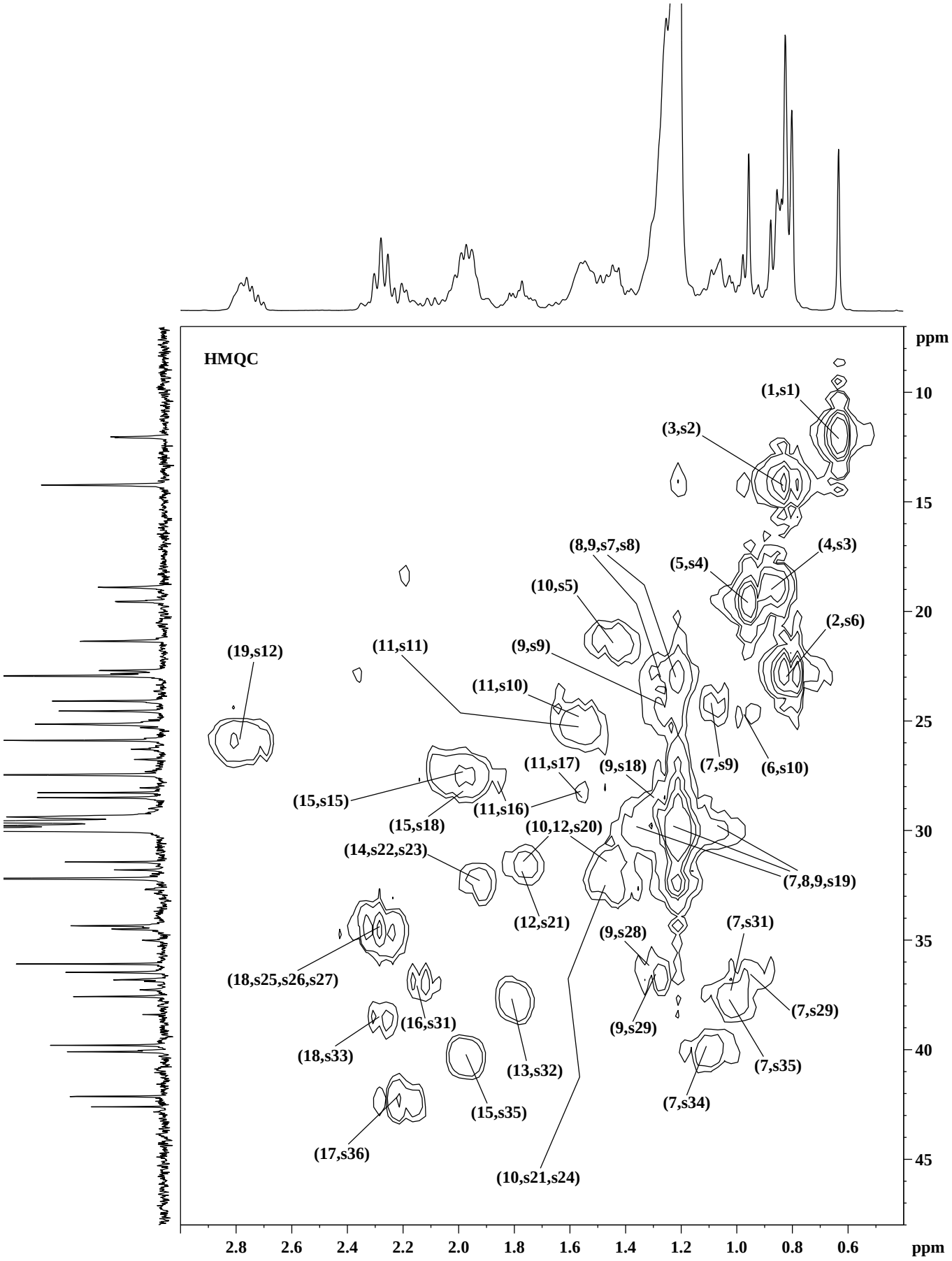

Fig. 7a: Expansion of the ^{1}H-^{13}C HMQC spectrum of the lipid extract of a human tuberculoma sample, highlighting the resonance assignments between 7.0-48.0 ppm in the F1 dimension (^{13}C) and 0.4-3.0 ppm in the F2 dimension (^{1}H). The labeled assignments are as given in Tables 1 and 2.

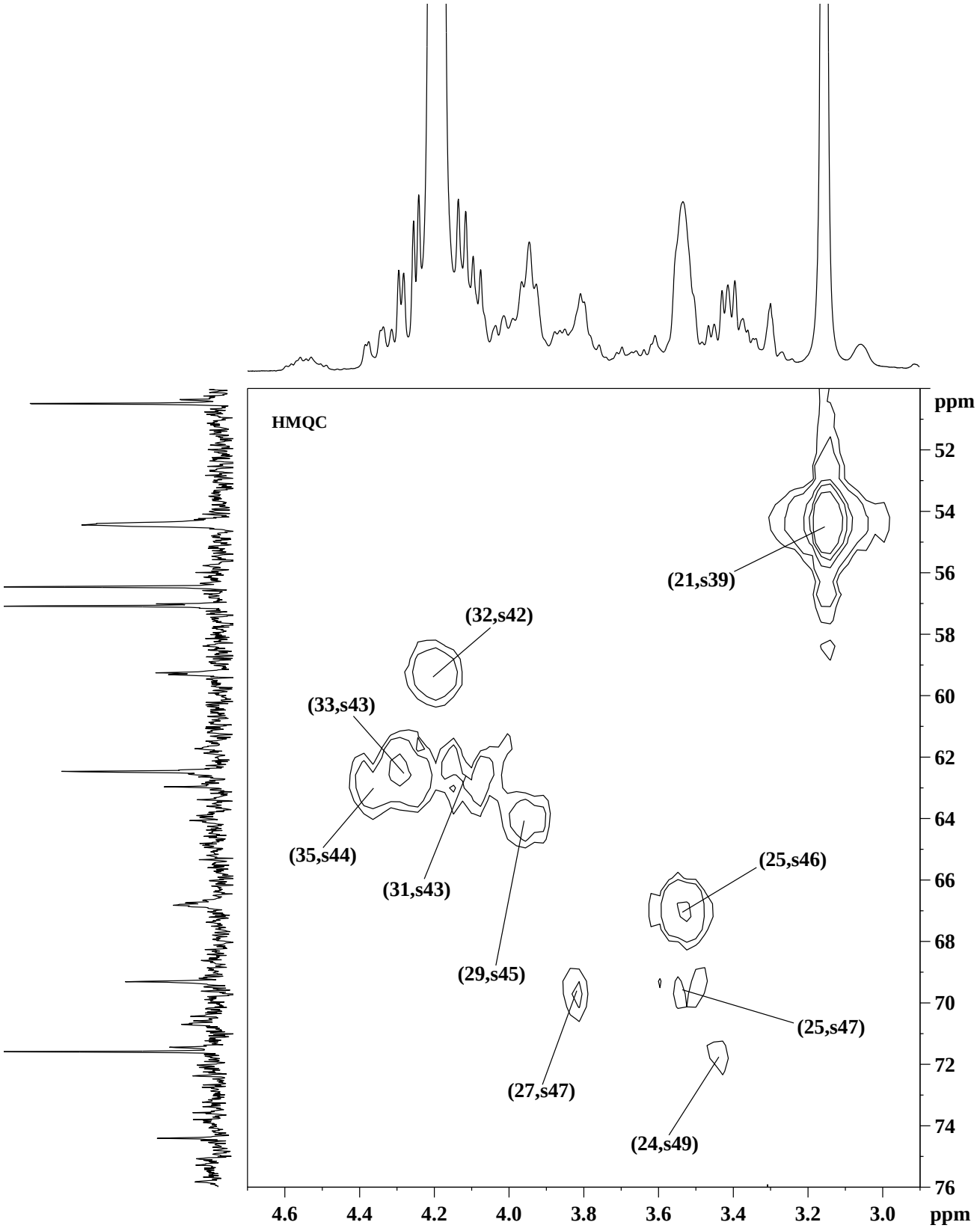

Fig. 7b: Expansion of the ^{1}H-^{13}C HMQC spectrum of the lipid extract of a human tuberculoma sample, highlighting the resonance assignments between 50.0-76.0 ppm in the F1 dimension (^{13}C) and 2.9-4.7 ppm in the F2 dimension (^{1}H). The labeled assignments are as given in Tables 1 and 2.

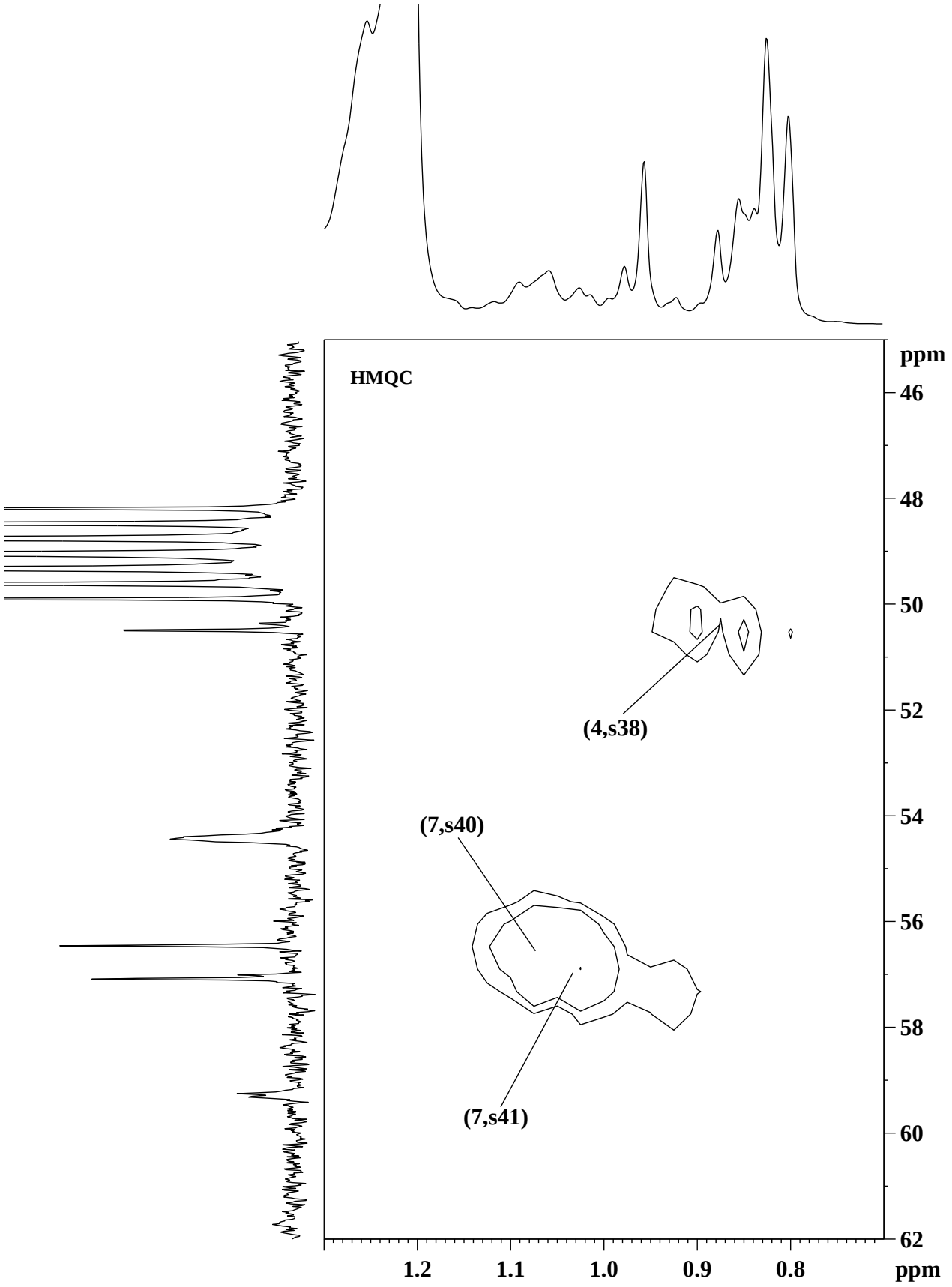

Fig. 7c: Expansion of the ^{1}H-^{13}C HMQC spectrum of the lipid extract of a human tuberculoma sample, highlighting the resonance assignments between 45.0-62.0 ppm in the F1 dimension (^{13}C) and 0.7-1.3 ppm in the F2 dimension (^{1}H). The labeled assignments are as given in Tables 1 and 2.

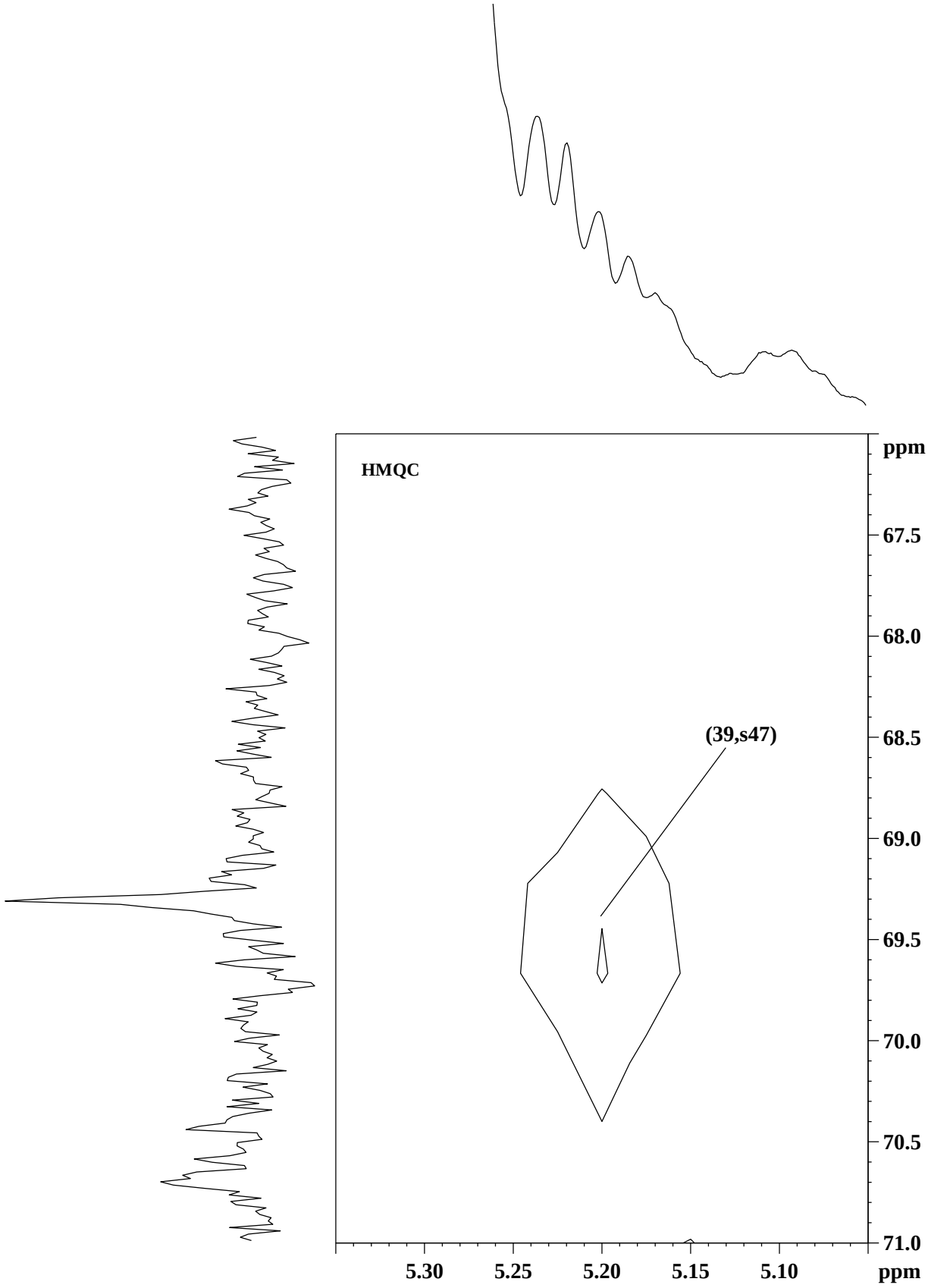

Fig. 7d: Expansion of the ^{1}H-^{13}C HMQC spectrum of the lipid extract of a human tuberculoma sample, highlighting the resonance assignments between 67.0-71.0 ppm in the F1 dimension (^{13}C) and 5.05-5.35 ppm in the F2 dimension (^{1}H). The labeled assignments are as given in Tables 1 and 2.

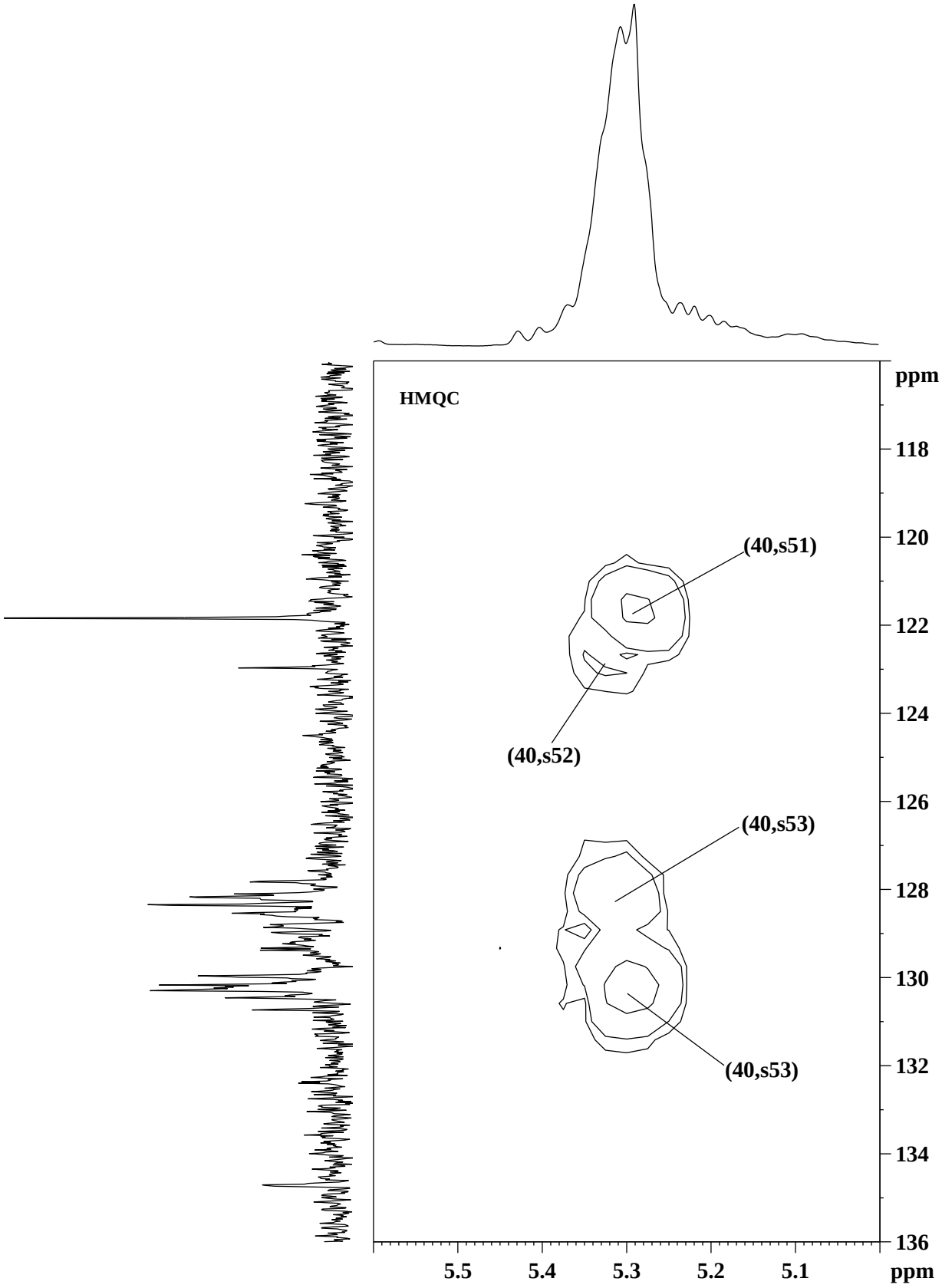

Fig. 7e: Expansion of the ^{1}H-^{13}C HMQC spectrum of the lipid extract of a human tuberculoma sample, highlighting the resonance assignments between 116.0-136.0 ppm in the F1 dimension (^{13}C) and 5.0-5.6 ppm in the F2 dimension (^{1}H). The labeled assignments are as given in Tables 1 and 2.

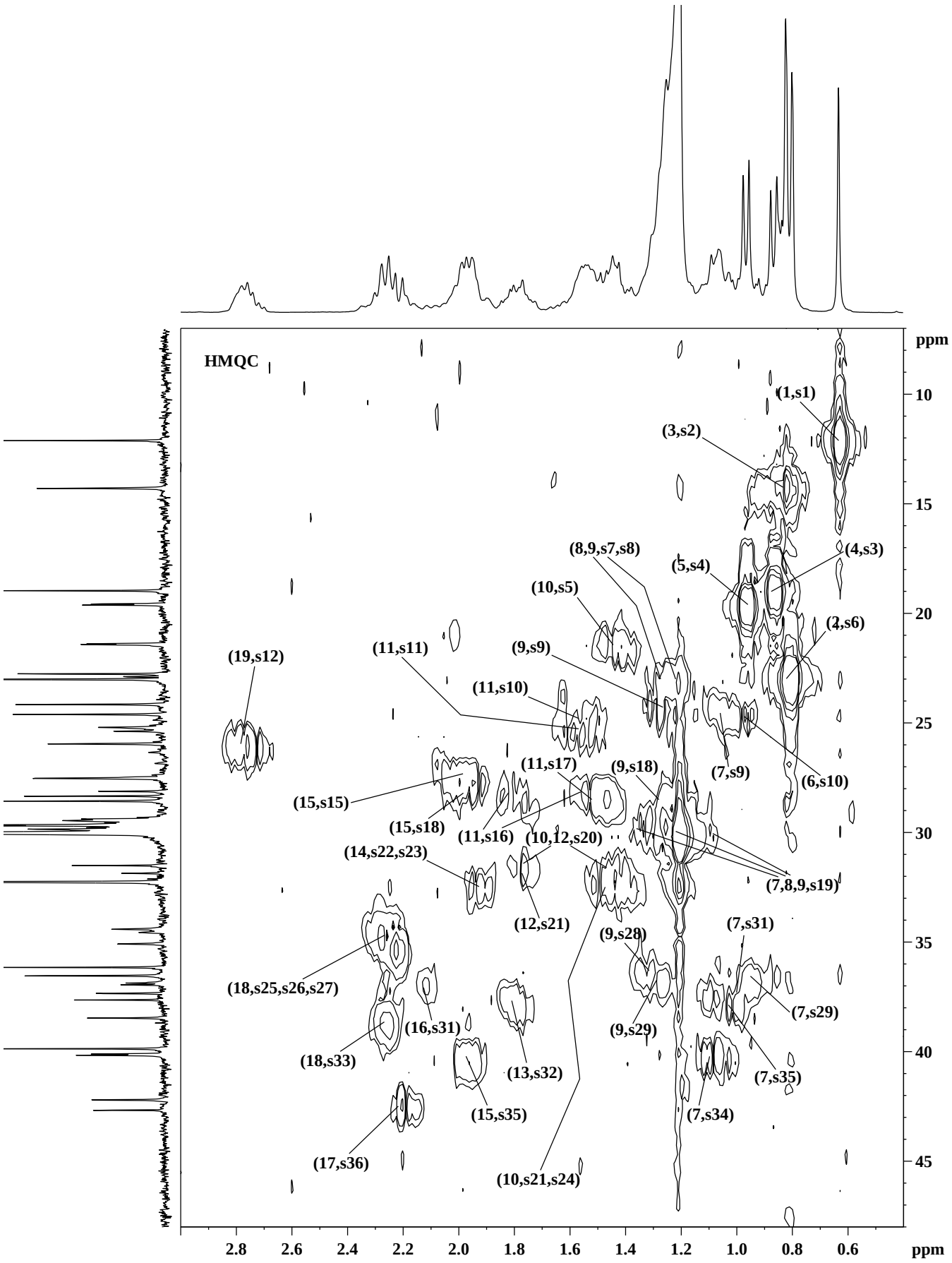

Fig. 8a: Expansion of the ^{1}H-^{13}C HMQC spectrum of the lipid extract of a human tuberculoma sample, highlighting the resonance assignments between 7.0-48.0 ppm in the F1 dimension (^{13}C) and 0.4-3.0 ppm in the F2 dimension (^{1}H). The labeled assignments are as given in Tables 1 and 2.

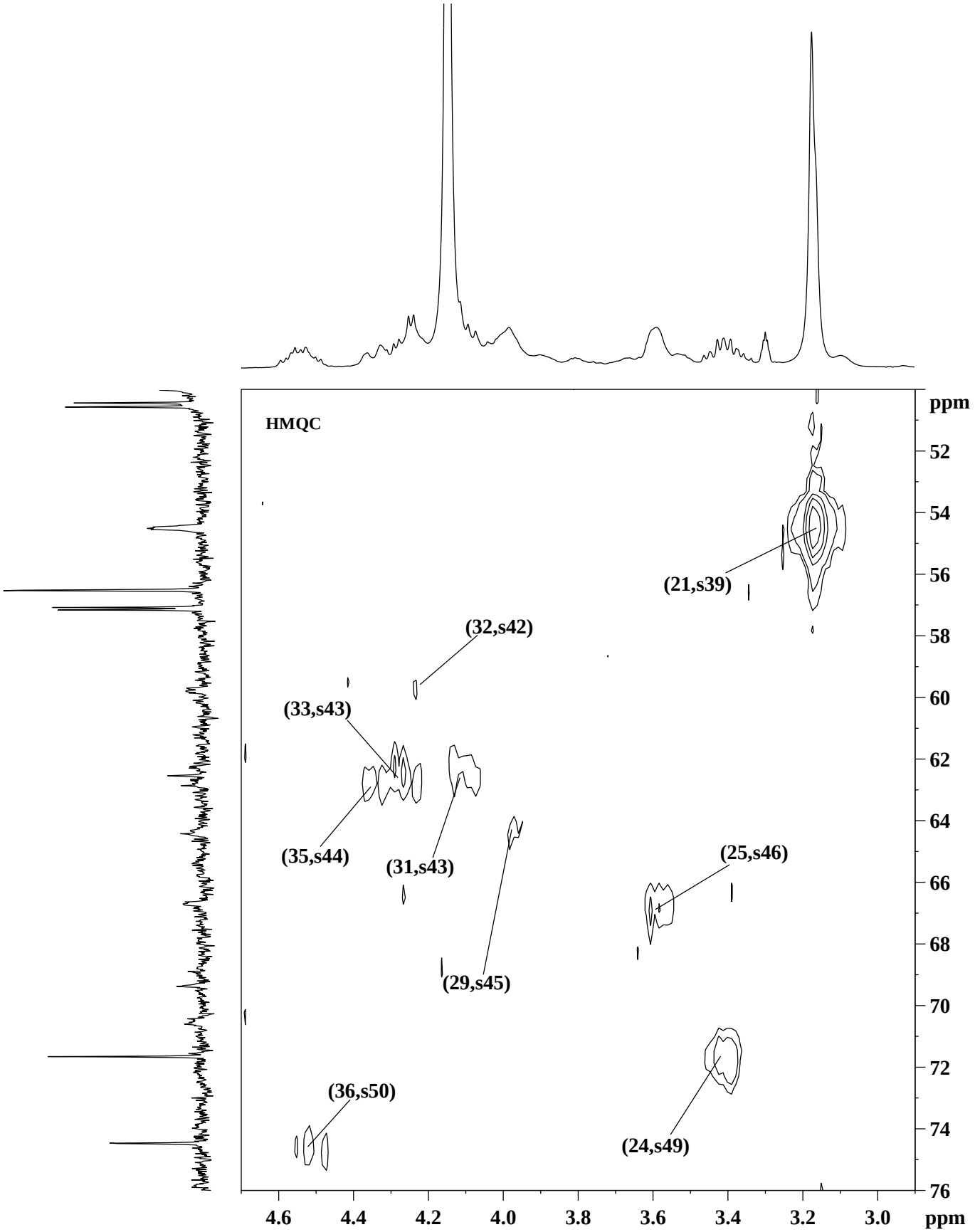

Fig. 8b: Expansion of the ^{1}H-^{13}C HMQC spectrum of the lipid extract of a human tuberculoma sample, highlighting the resonance assignments between 50.0-76.0 ppm in the F1 dimension (^{13}C) and 2.9-4.7 ppm in the F2 dimension (^{1}H). The labeled assignments are as given in Tables 1 and 2.

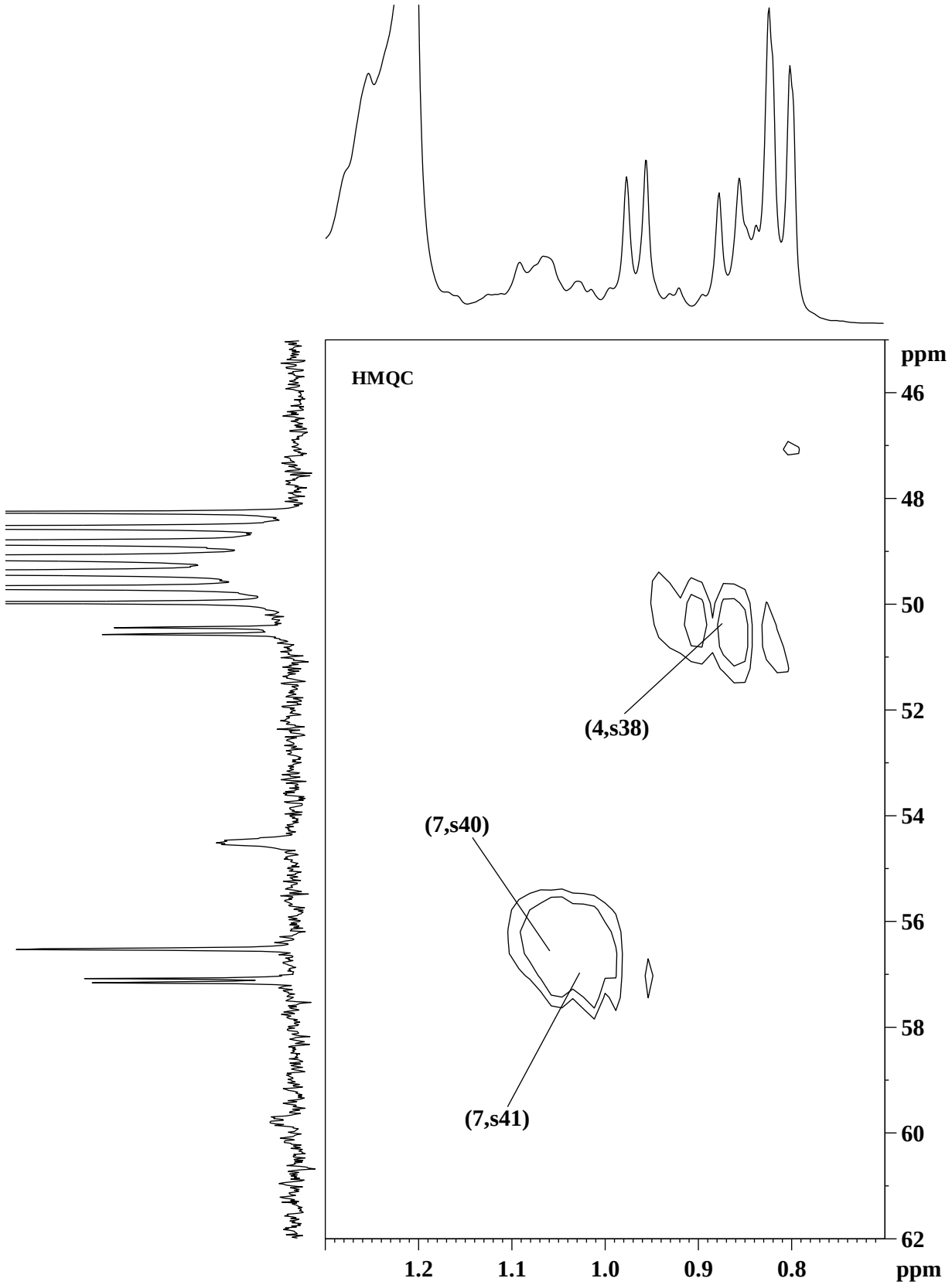

Fig. 8c: Expansion of the ^{1}H-^{13}C HMQC spectrum of the lipid extract of a human tuberculoma sample, highlighting the resonance assignments between 45.0-62.0 ppm in the F1 dimension (^{13}C) and 0.7-1.3 ppm in the F2 dimension (^{1}H). The labeled assignments are as given in Tables 1 and 2.

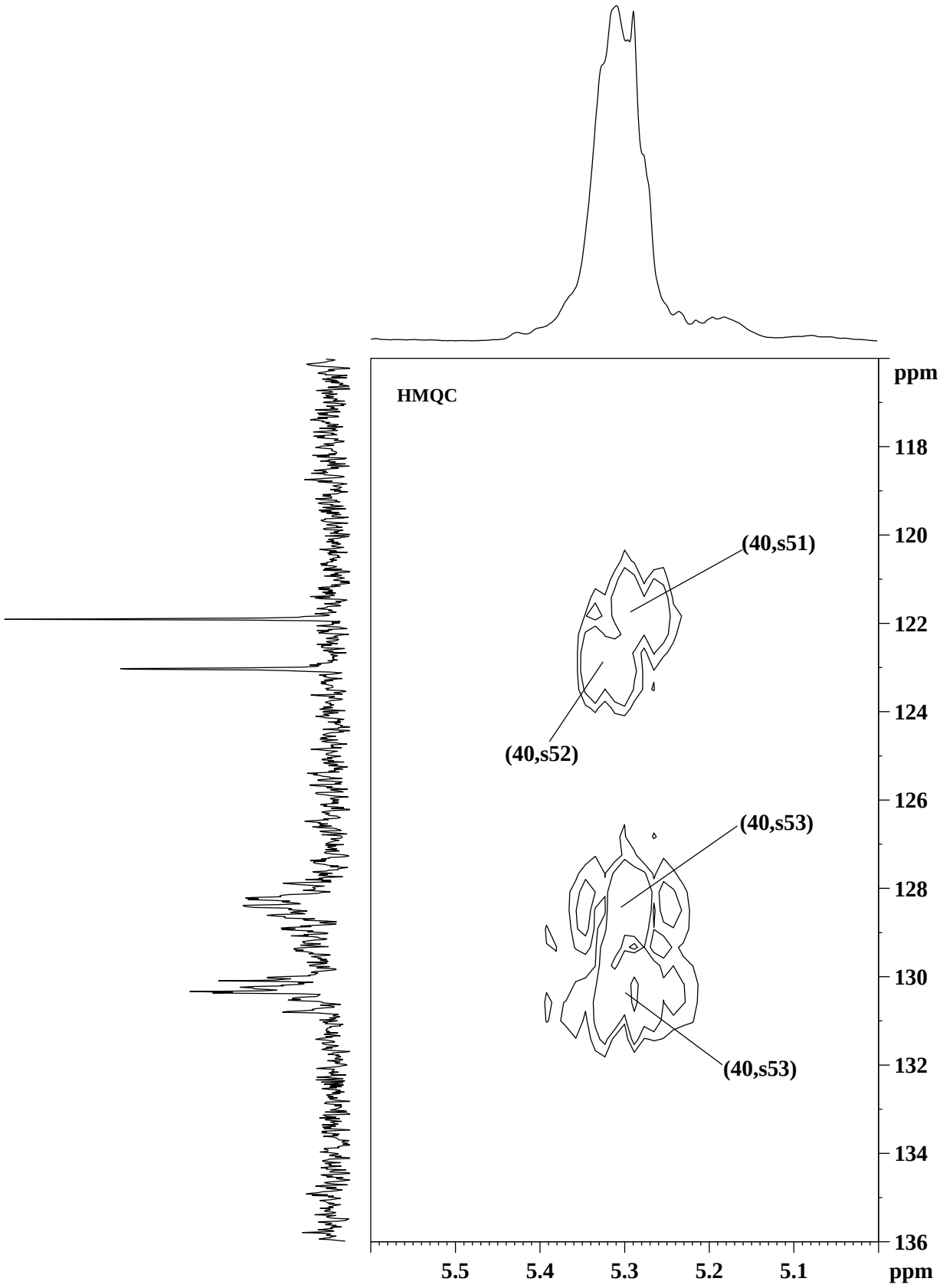

Fig. 8d: Expansion of the ^{1}H-^{13}C HMQC spectrum of the lipid extract of a human tuberculoma sample, highlighting the resonance assignments between 116.0-136.0 ppm in the F1 dimension (^{13}C) and 5.0-5.6 ppm in the F2 dimension (^{1}H). The labeled assignments are as given in Tables 1 and 2.

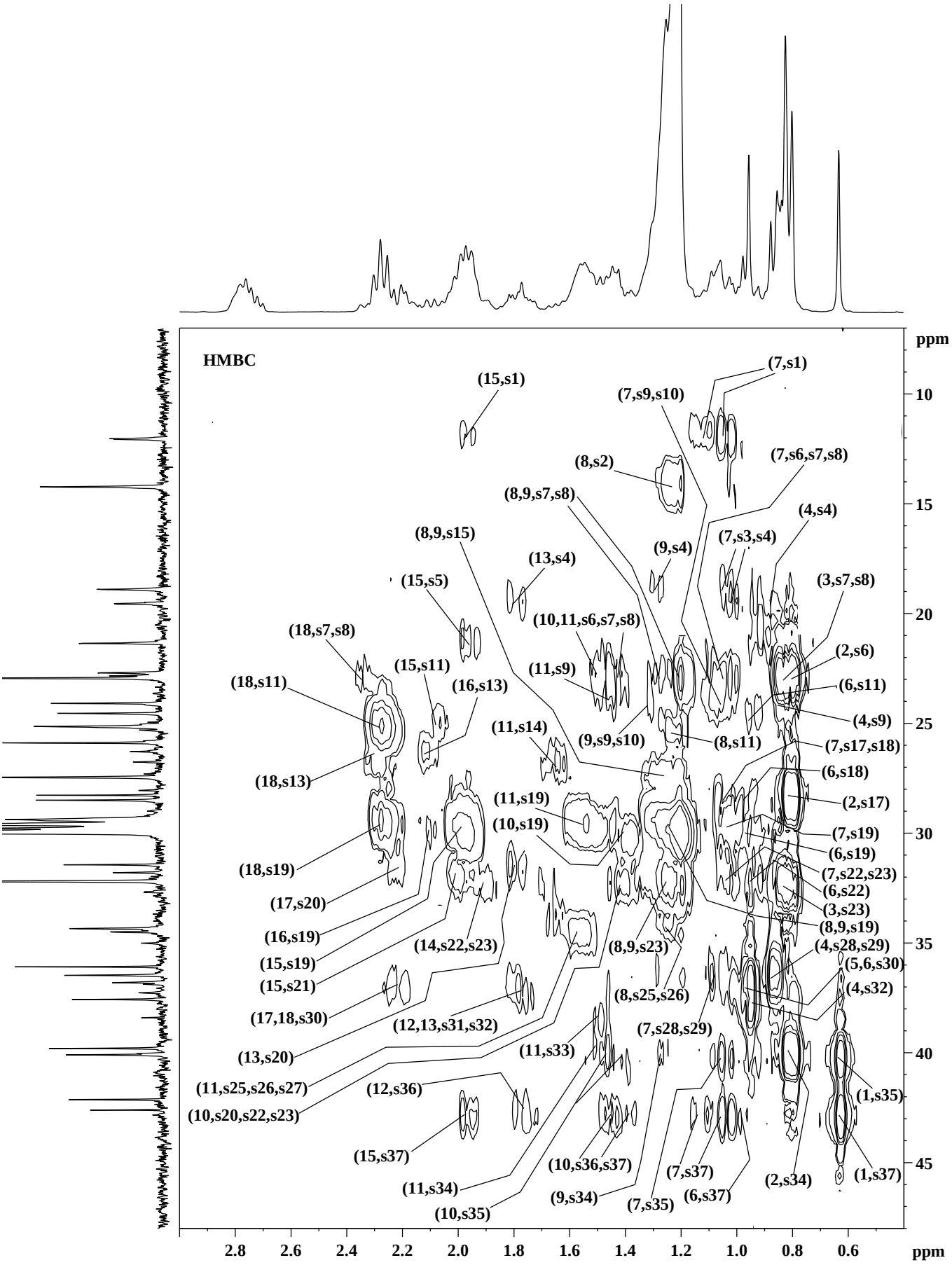

Fig. 9a: Expansion of the ^{1}H-^{13}C HMBC spectrum of the lipid extract of a human tuberculoma sample, highlighting the resonance assignments between 7.0-48.0 ppm in the F1 dimension (^{13}C) and 0.4-3.0 ppm in the F2 dimension (^{1}H). The labeled assignments are as given in Tables 1 and 2.

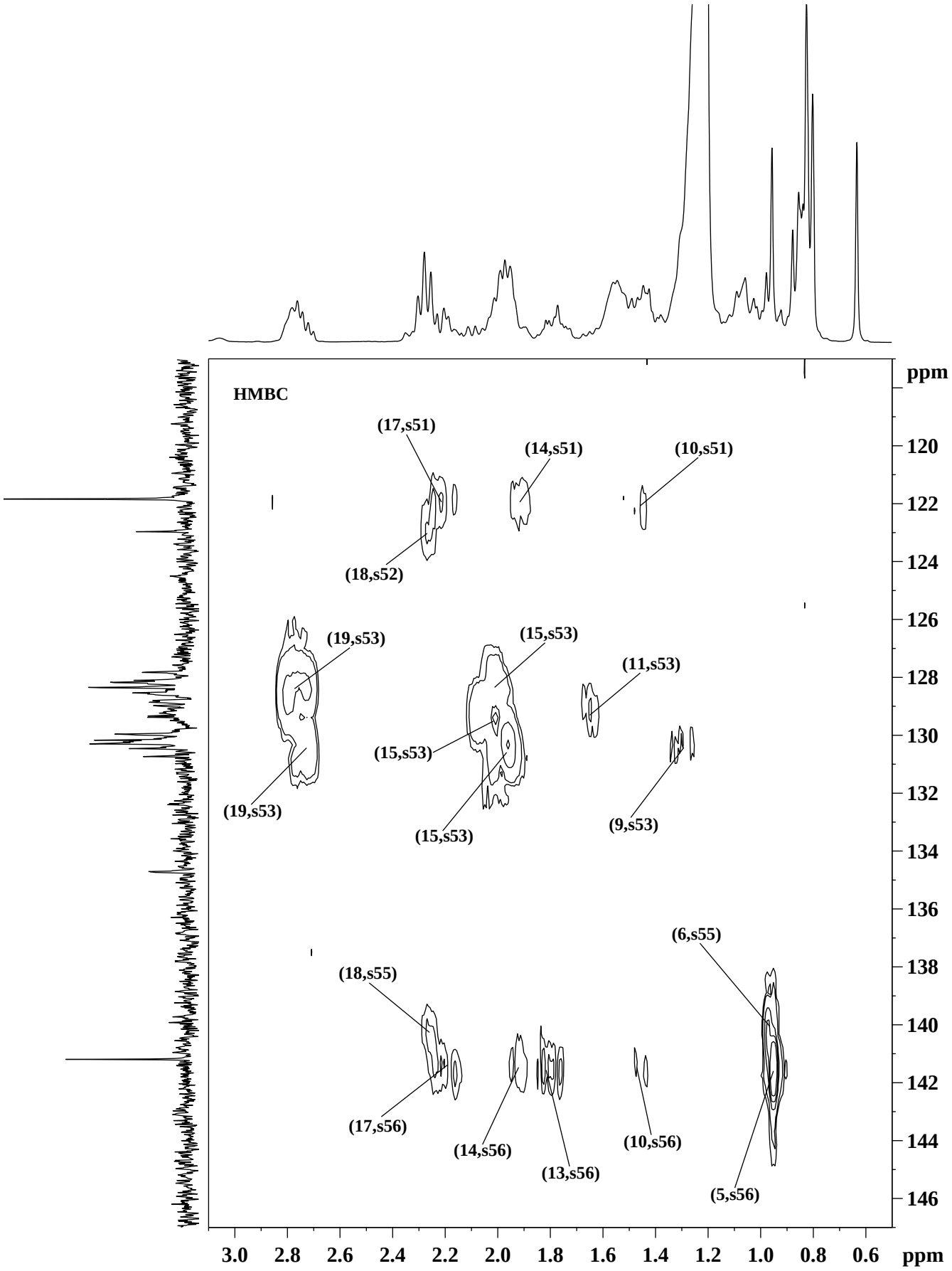

Fig. 9b: Expansion of the ^{1}H-^{13}C HMBC spectrum of the lipid extract of a human tuberculoma sample, highlighting the resonance assignments between 117.0-147.0 ppm in the F1 dimension (^{13}C) and 0.5-3.1 ppm in the F2 dimension (^{1}H). The labeled assignments are as given in Tables 1 and 2.

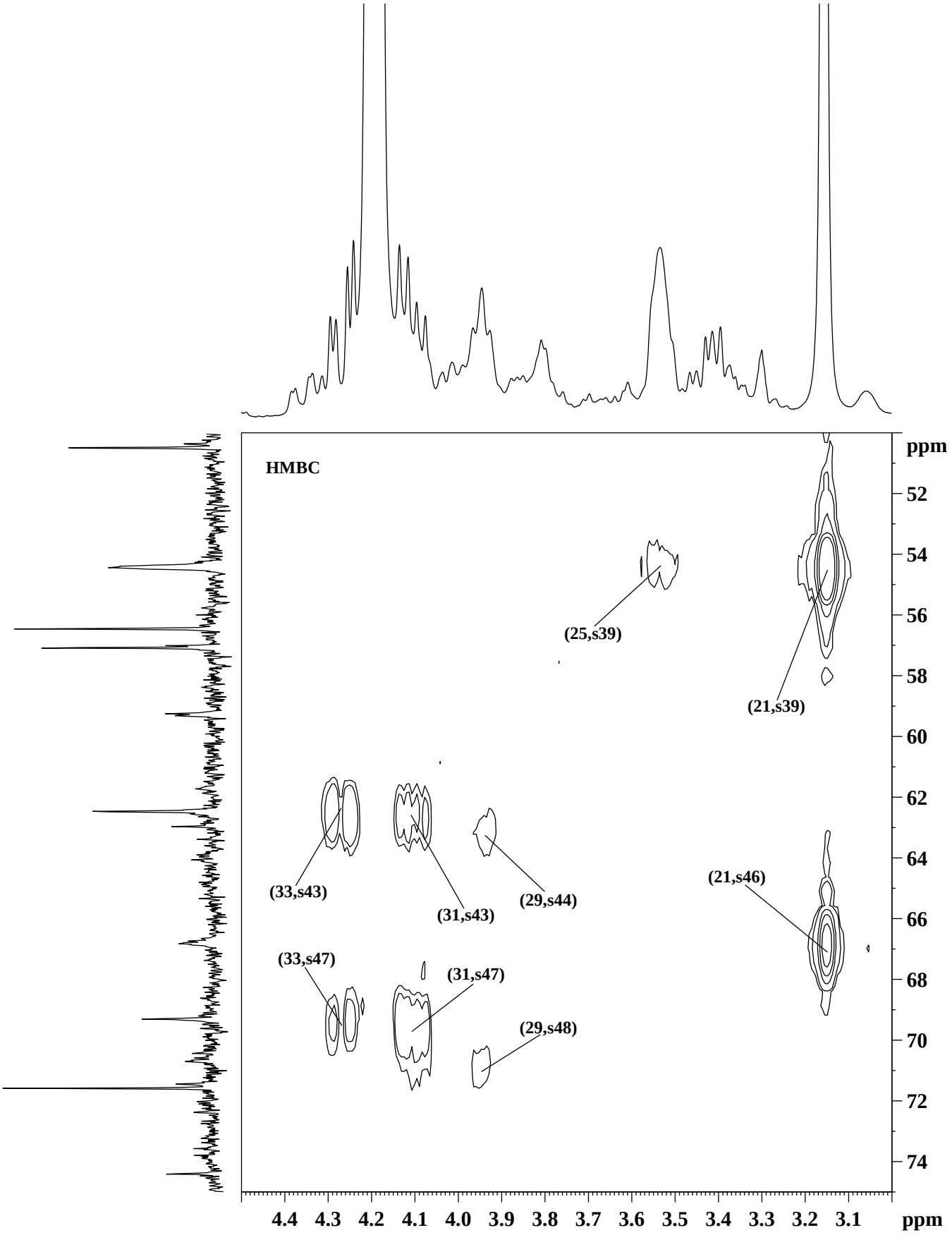

Fig. 9c: Expansion of the ^{1}H-^{13}C HMBC spectrum of the lipid extract of a human tuberculoma sample, highlighting the resonance assignments between 50.0-75.0 ppm in the F1 dimension (^{13}C) and 3.0-4.5 ppm in the F2 dimension (^{1}H). The labeled assignments are as given in Tables 1 and 2.

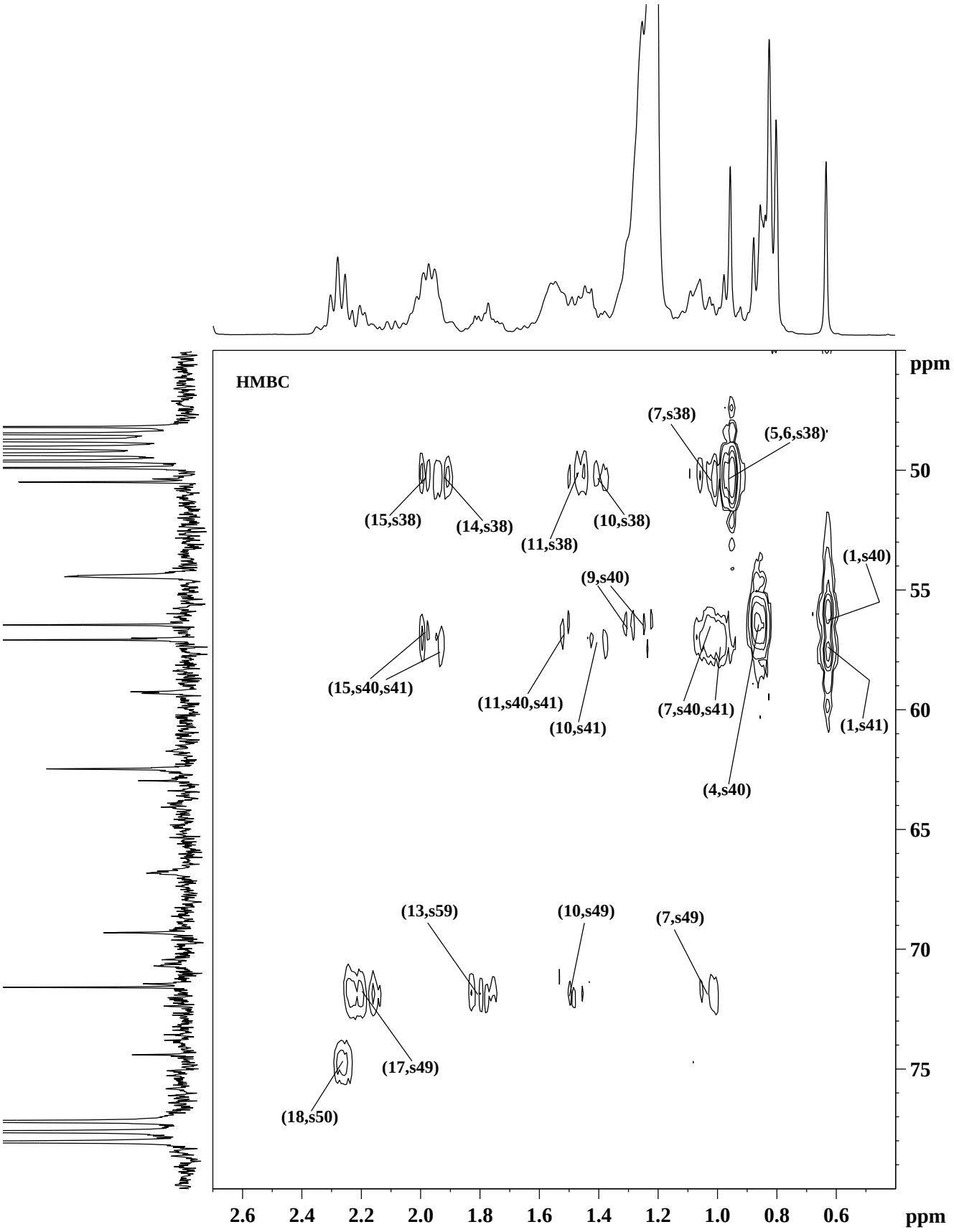

Fig. 9d: Expansion of the ^{1}H-^{13}C HMBC spectrum of the lipid extract of a human tuberculoma sample, highlighting the resonance assignments between 45.0-80.0 ppm in the F1 dimension (^{13}C) and 0.4-2.7 ppm in the F2 dimension (^{1}H). The labeled assignments are as given in Tables 1 and 2.

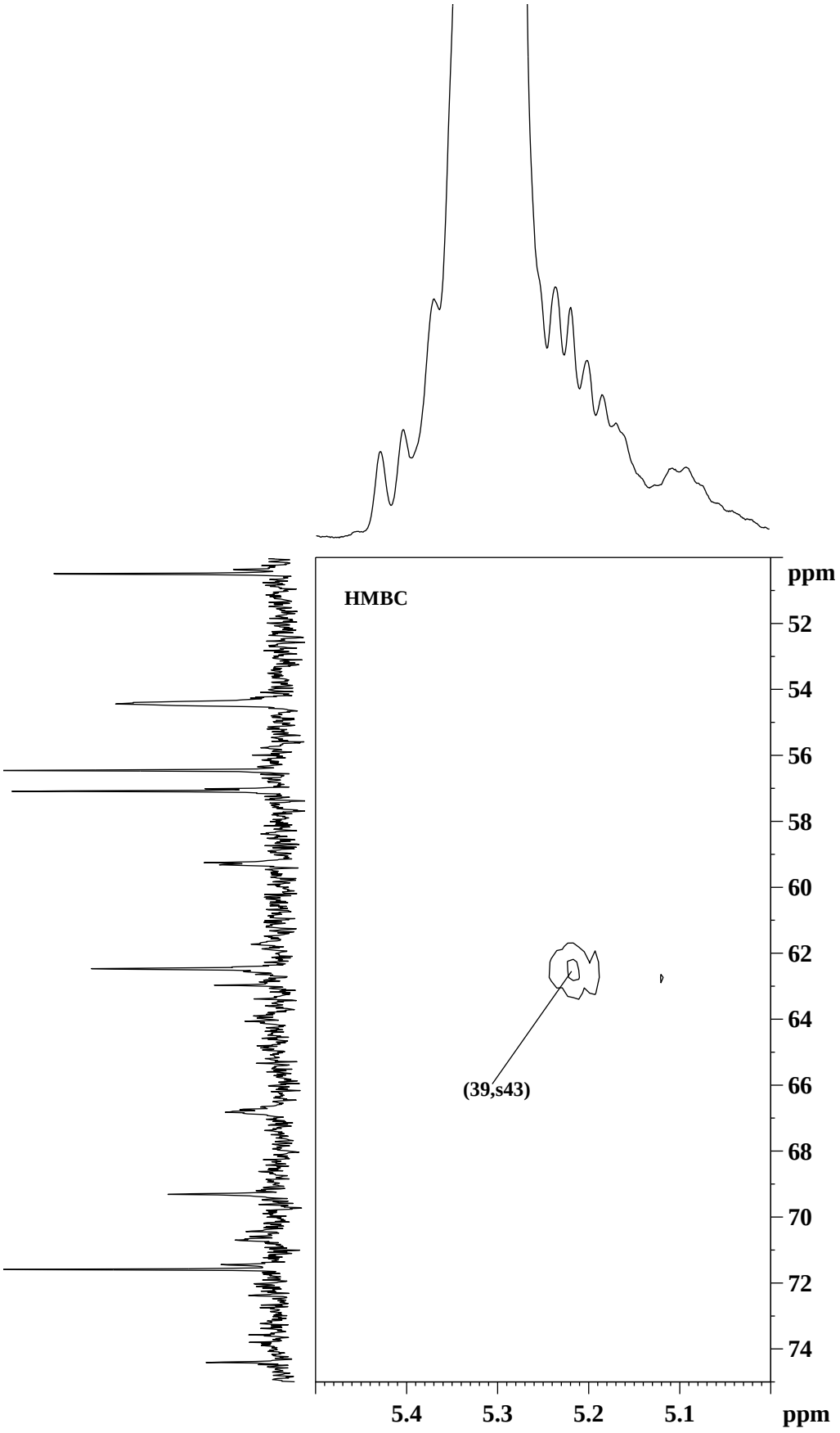

Fig. 9e: Expansion of the ^{1}H-^{13}C HMBC spectrum of the lipid extract of a human tuberculoma sample, highlighting the resonance assignments between 50.0-75.0 ppm in the F1 dimension (^{13}C) and 5.0-5.5 ppm in the F2 dimension (^{1}H). The labeled assignments are as given in Tables 1 and 2.

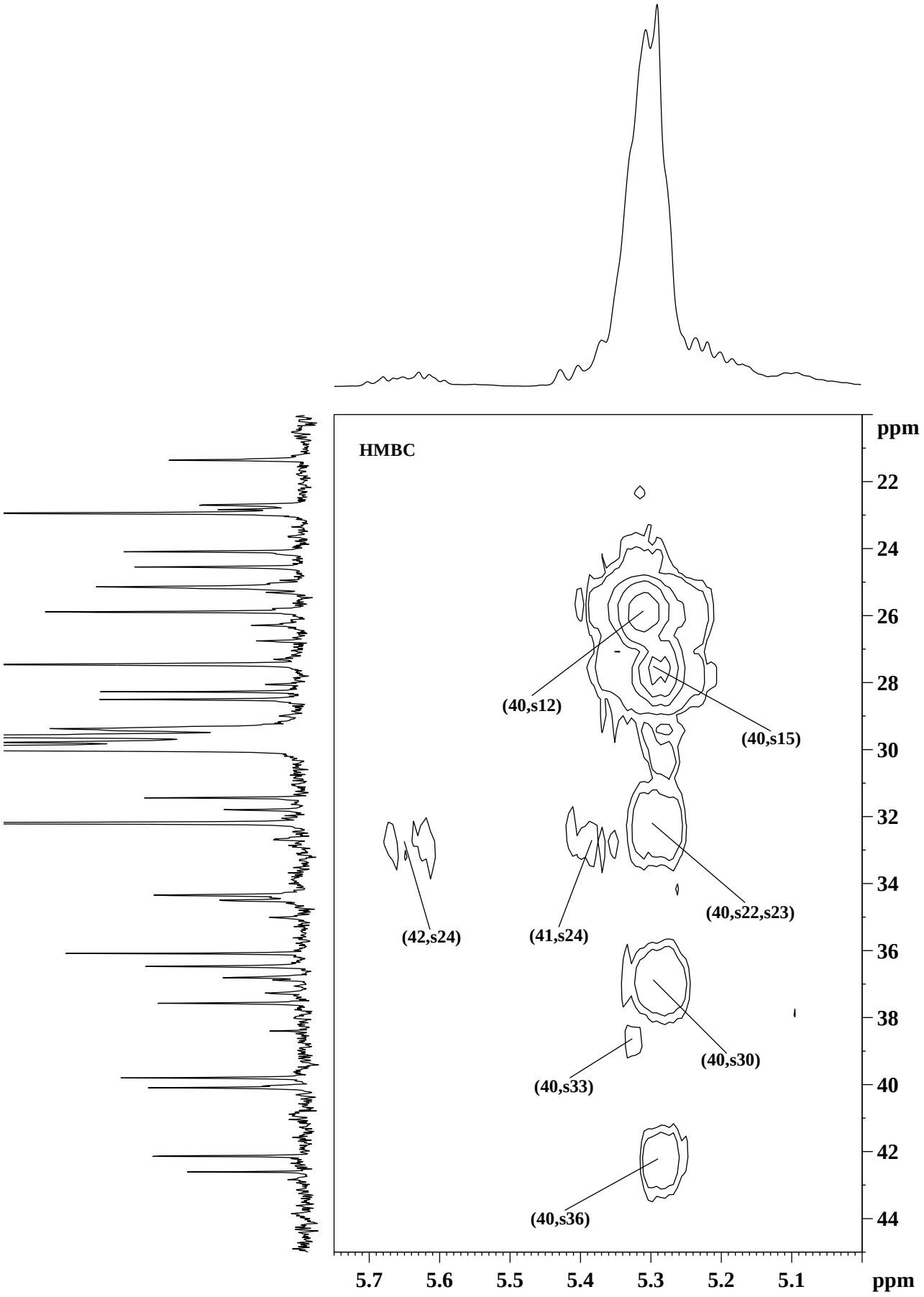

Fig. 9f: Expansion of the ^{1}H-^{13}C HMBC spectrum of the lipid extract of a human tuberculoma sample, highlighting the resonance assignments between 20.0-45.0 ppm in the F1 dimension (^{13}C) and 5.0-5.75 ppm in the F2 dimension (^{1}H). The labeled assignments are as given in Tables 1 and 2.

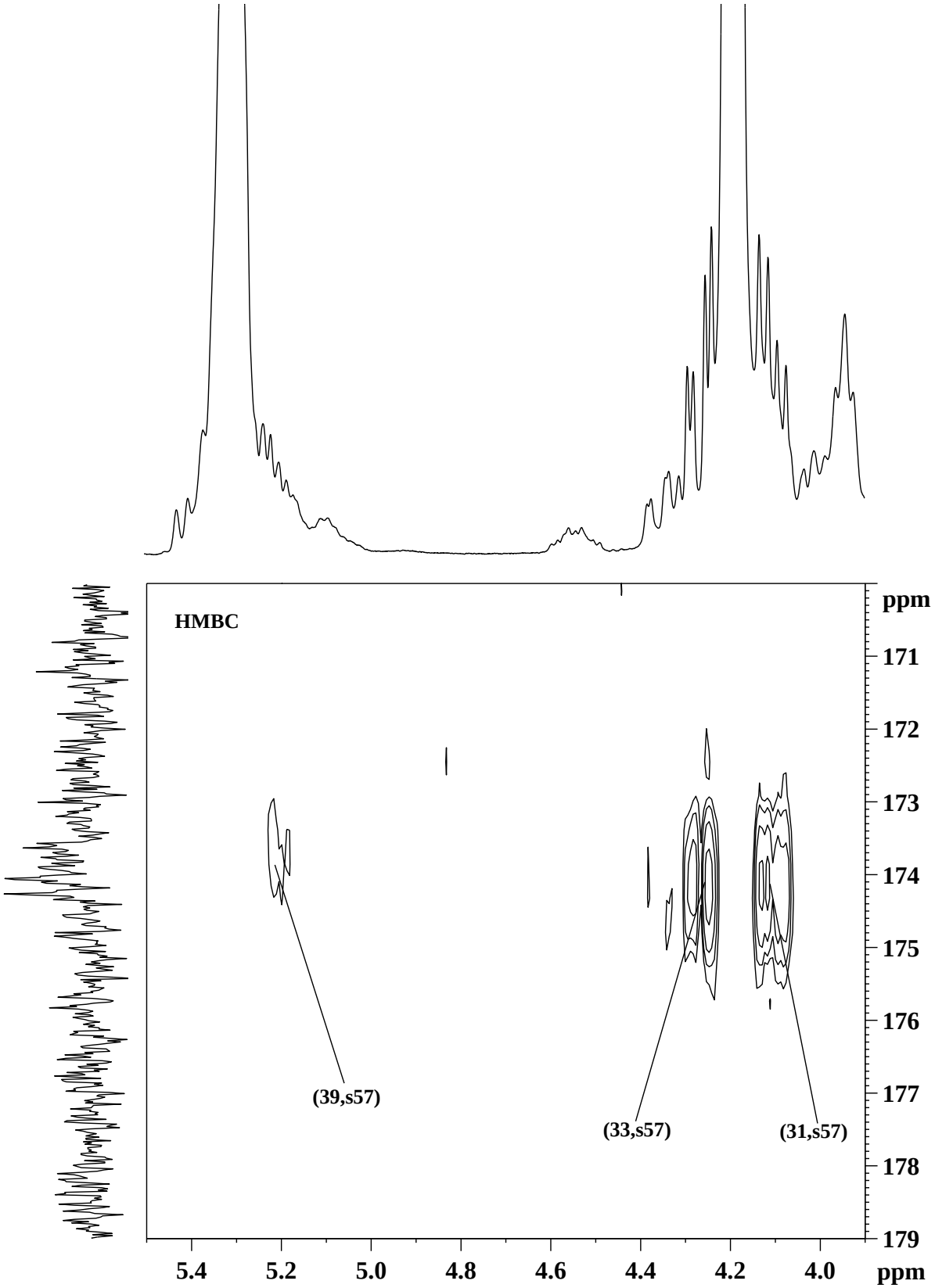

Fig. 9g: Expansion of the ^{1}H-^{13}C HMBC spectrum of the lipid extract of a human tuberculoma sample, highlighting the resonance assignments between 170.0-179.0 ppm in the F1 dimension (^{13}C) and 3.9-4.5 ppm in the F2 dimension (^{1}H). The labeled assignments are as given in Tables 1 and 2.

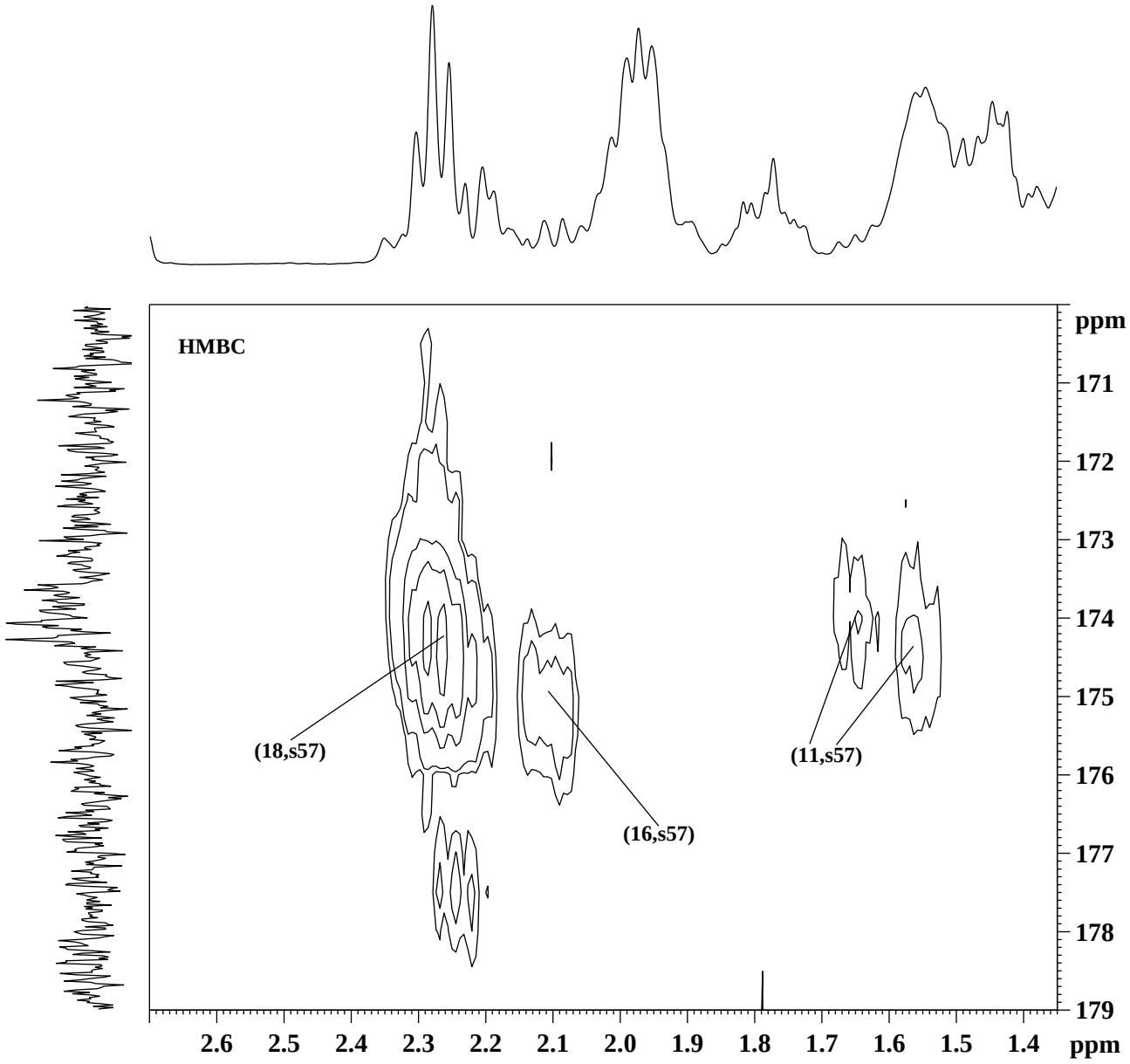

Fig. 9h: Expansion of the ^{1}H-^{13}C HMBC spectrum of the lipid extract of a human tuberculoma sample, highlighting the resonance assignments between 170.0-179.0 ppm in the F1 dimension (^{13}C) and 1.35-2.70 ppm in the F2 dimension (^{1}H). The labeled assignments are as given in Tables 1 and 2.

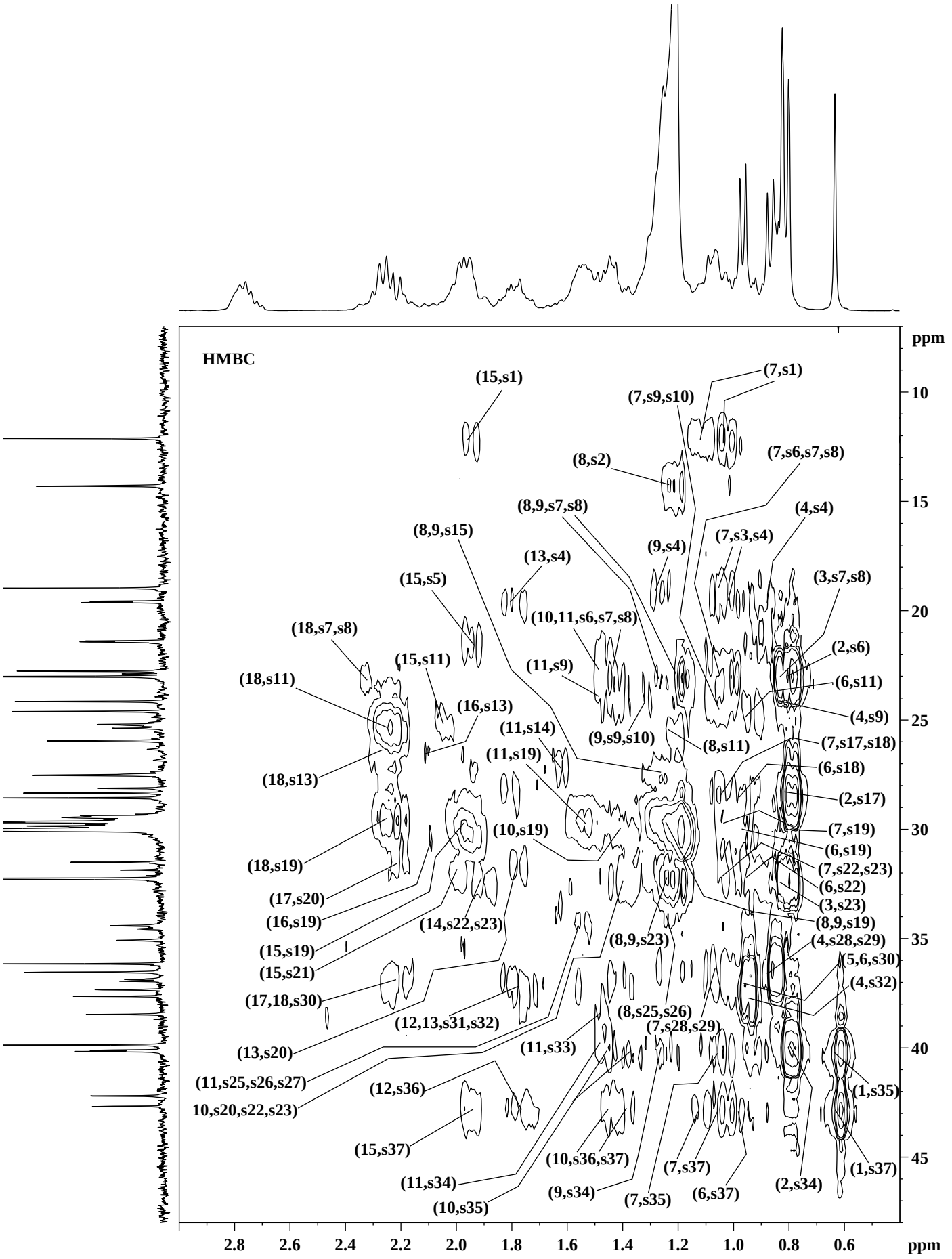

Fig. 10a: Expansion of the ^{1}H-^{13}C HMBC spectrum of the lipid extract of a human tuberculoma sample, highlighting the resonance assignments between 7.0-48.0 ppm in the F1 dimension (^{13}C) and 0.4-3.0 ppm in the F2 dimension (^{1}H). The labeled assignments are as given in Tables 1 and 2.

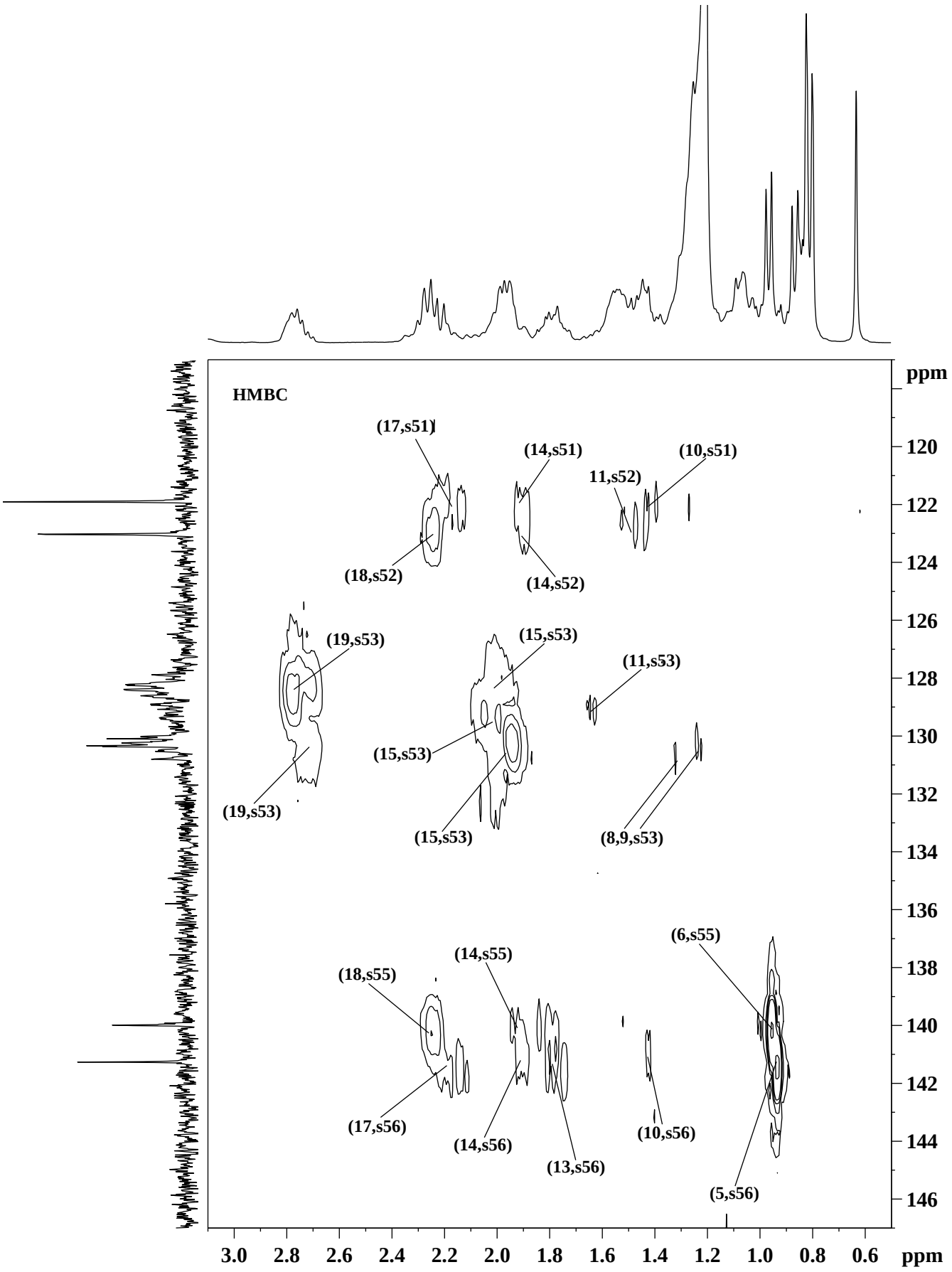

Fig. 10b: Expansion of the ^{1}H-^{13}C HMBC spectrum of the lipid extract of a human tuberculoma sample, highlighting the resonance assignments between 117.0-147.0 ppm in the F1 dimension (^{13}C) and 0.5-3.1 ppm in the F2 dimension (^{1}H). The labeled assignments are as given in Tables 1 and 2.

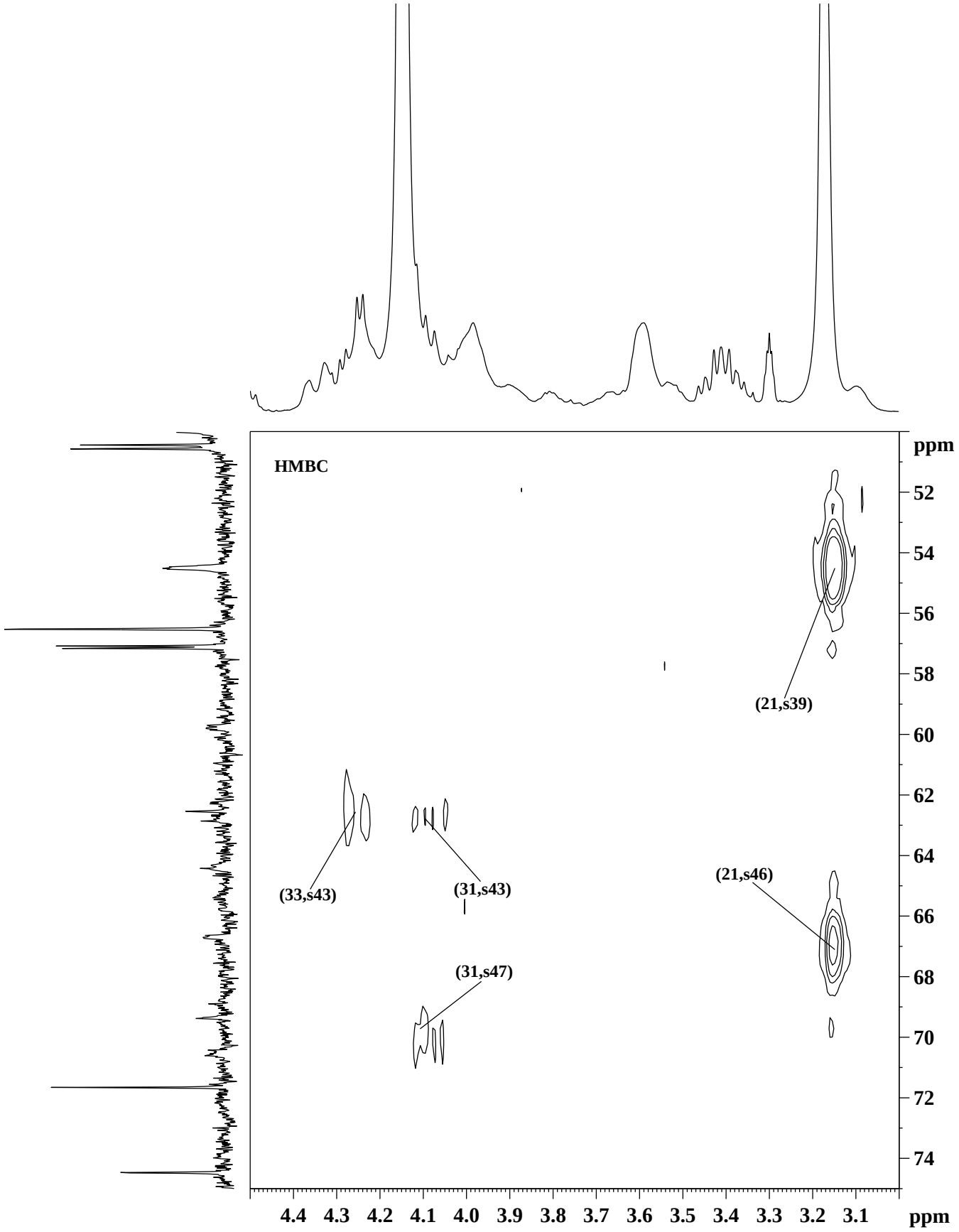

Fig. 10c: Expansion of the ^{1}H-^{13}C HMBC spectrum of the lipid extract of a human tuberculoma sample, highlighting the resonance assignments between 50.0-75.0 ppm in the F1 dimension (^{13}C) and 3.0-4.5 ppm in the F2 dimension (^{1}H). The labeled assignments are as given in Tables 1 and 2.

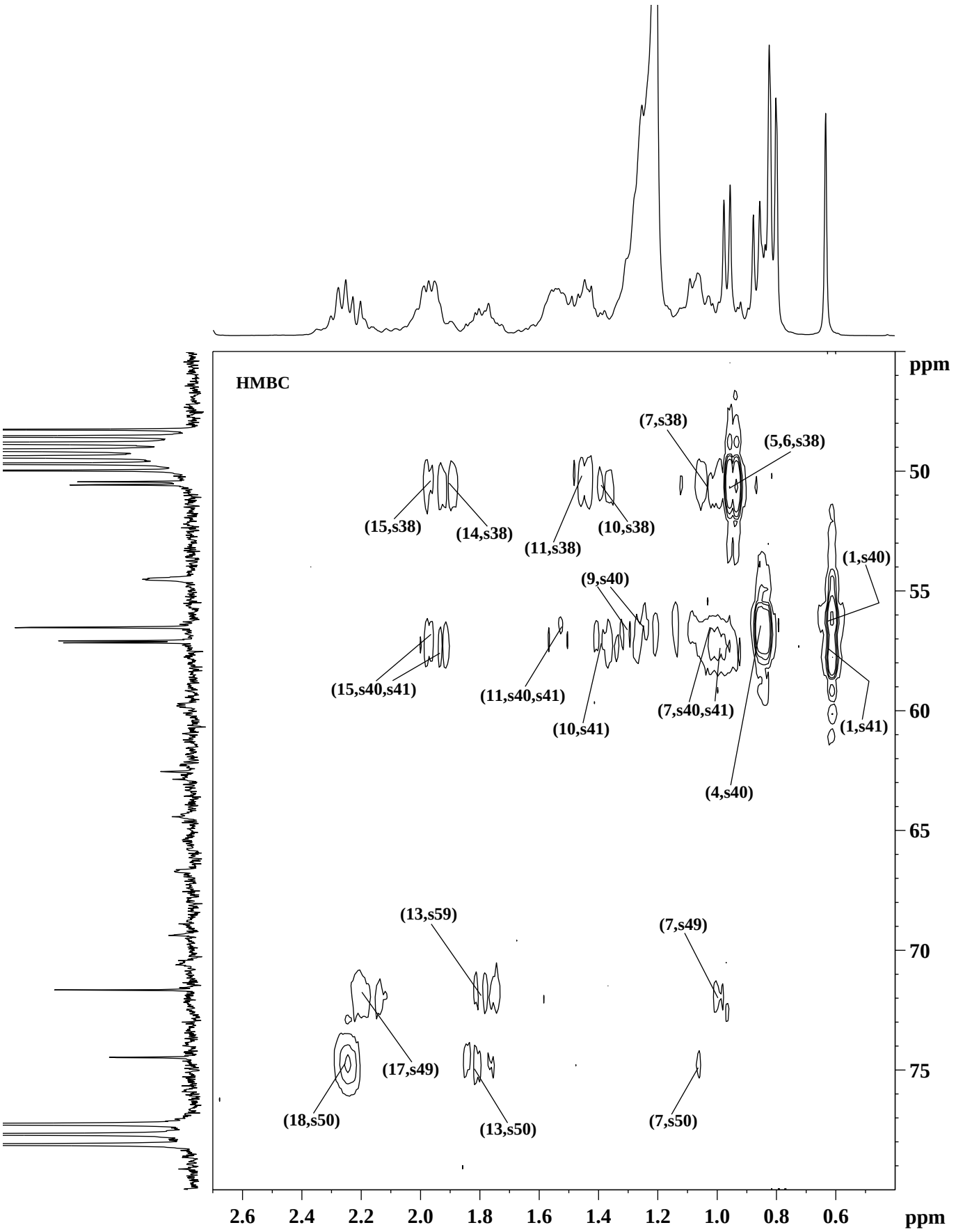

Fig. 10d: Expansion of the ^{1}H-^{13}C HMBC spectrum of the lipid extract of a human tuberculoma sample, highlighting the resonance assignments between 45.0-80.0 ppm in the F1 dimension (^{13}C) and 0.4-2.7 ppm in the F2 dimension (^{1}H). The labeled assignments are as given in Tables 1 and 2.

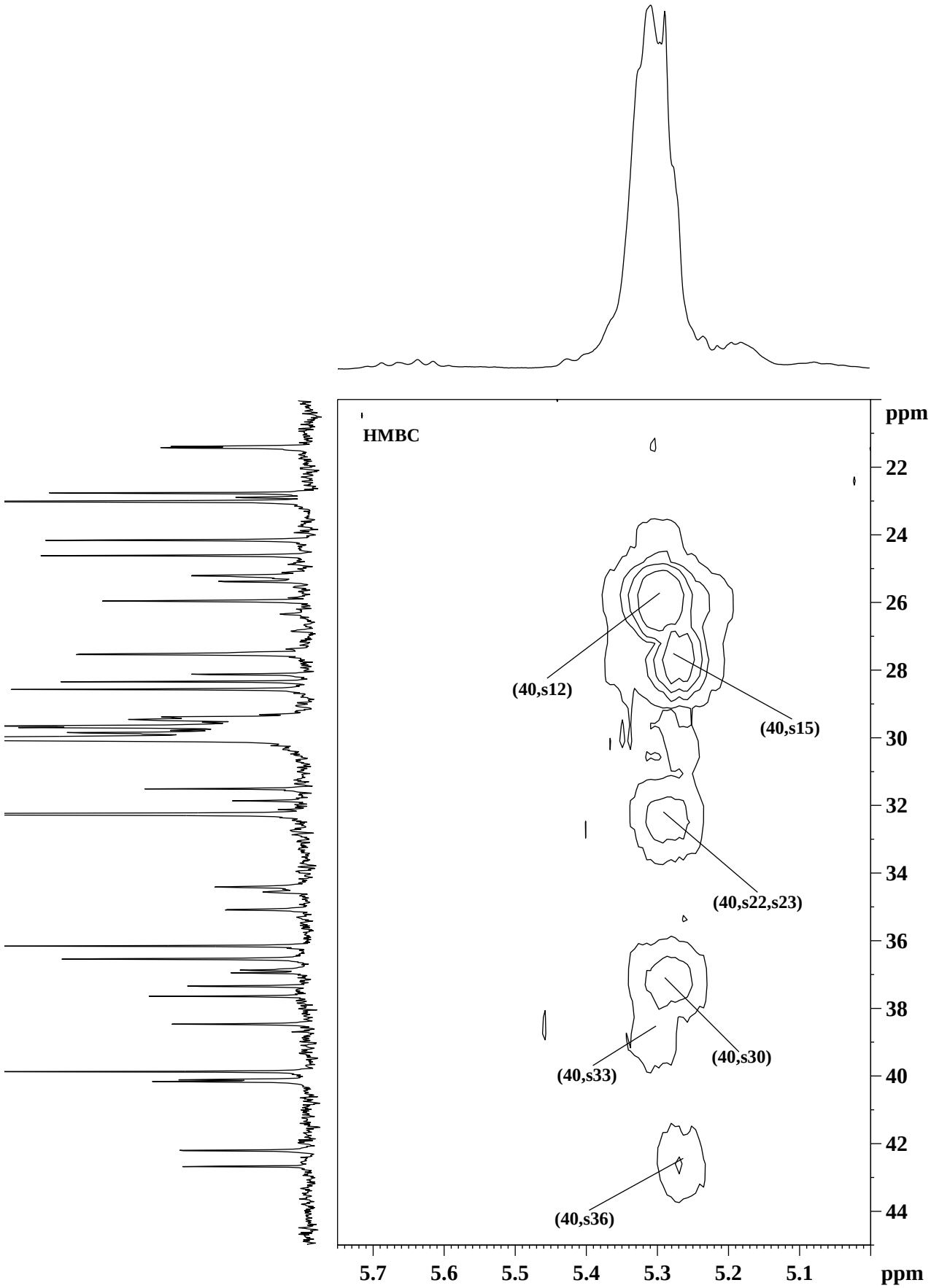

Fig. 10e: Expansion of the ^{1}H-^{13}C HMBC spectrum of the lipid extract of a human tuberculoma sample, highlighting the resonance assignments between 20.0-45.0 ppm in the F1 dimension (^{13}C) and 5.0-5.75 ppm in the F2 dimension (^{1}H). The labeled assignments are as given in Tables 1 and 2.

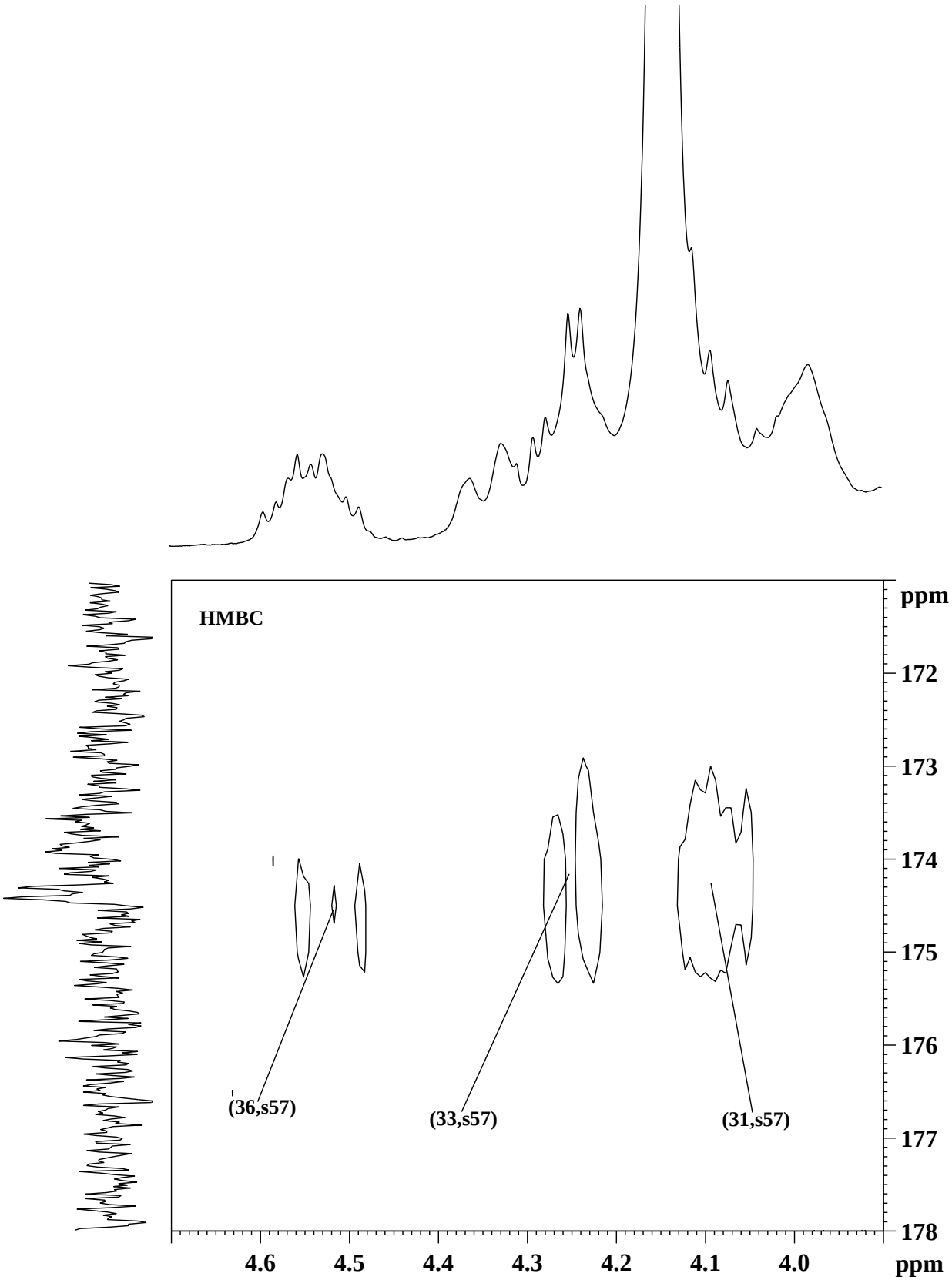

Fig. 10f: Expansion of the ^{1}H-^{13}C HMBC spectrum of the lipid extract of a human tuberculoma sample, highlighting the resonance assignments between 170.0-179.0 ppm in the F1 dimension (^{13}C) and 3.9-4.5 ppm in the F2 dimension (^{1}H). The labeled assignments are as given in Tables 1 and 2.

other diacylglycerophospholipids centered at 4.27 ppm, as seen in the 2D COSY cross-peak correlations (figs. 5a-c).

In case of ether phospholipids, the signal at 5.10 ppm that was overlapped with the resonances arising from sugar residues gave cross-peak correlations with the protons resonating at 3.95 ppm and 3.86 ppm, which were subsequently assigned to be the sn-2, sn-3 and sn-1 protons of ether phospholipids such as PLA (figs. 5a-c), respectively. The overlapped proton multiplet resonance at 3.80 ppm, which is characteristic for one or more of the inositol ring triplets (Casu et al., 1991; Adosraku et al., 1994), gave an indication for the presence of the inositol head group of phosphatidylinositol. It was not possible to selectively identify the serine head group protons of phosphatidylserine due to signal overlap in the ^{1}H NMR spectra and also due to their low abundance in the tuberculoma lipid extracts. The inositol proton signal at 3.80 ppm had contribution from other overlapping resonances, possibly from glycolipid sugars. Overall, the sn-1, sn-2 and sn-3 protons of the glycerol backbone gave their corresponding HMQC and HMBC correlations at 62.5 ppm, 69.3 ppm, 63.9 ppm, respectively (figs. 7b, 8b, 9c). Additionally, the sn-1 and sn-2 glycerol backbone protons gave the required HMBC correlations with the ^{13}C signal of fatty acid ester linkage (-OCOR) at 174.2 ppm (fig. 9g), thus confirming the presence of diacylglycerophospholipids. Further, a set of ortho-coupled protons at 7.52 ppm and 7.68 ppm indicated the presence of phenolic glycolipids from *M. tuberculosis* (Daffe and Servin, 1989; Watanabe et al., 1994; Villeneuve et al., 2003) in the tuberculoma lipid extracts as observed earlier (Gupta et al., 1996).

The ^{31}P NMR helped in confirming the presence of phospholipids in the tuberculoma lipid extracts, and the following could be assigned based on the ^{31}P chemical shifts of phospholipids (Kriat et al., 1993; Branca et al., 1995; Culeddu et al., 1998; Metz and Dunphy, 1996; Moesgaard et al., 1999; Merchant et al., 1999; Schiller and Arnold, 2002): diacylphosphatidylcholine (2.63 ppm), 1-alkyl-2-acyl-phosphatidylcholine (2.69 ppm), phosphatidylinositol (3.10 ppm), *lyso*-phosphatidylcholine (3.24 ppm), phosphatidylserine (3.34 ppm), diacylphosphatidylethanolamine (3.44 ppm), 1-alkyl-2-acyl-phosphatidylethanolamine (3.47 ppm), plasmalogen (3.56 ppm), sphingomyelin (3.60 ppm), *lyso*-phosphatidylethanolamine (3.67 ppm), diphosphatidylglycerol/phosphatidylglycerol (3.88 ppm) and phosphatidic acid (4.00 ppm) (Table-

3). The relative abundance of diacylphosphatidylcholine was observed to be higher than the rest of the phospholipid components, followed by diacylphosphatidylethanolamine in the pooled tuberculoma lipid extracts (figs. 11a, 11b).

Both cholesterol and its esterified derivative were assigned with the help of ^{1}H and ^{13}C NMR experiments in the current study. Among the proton resonances that account for these sterols, the sharp proton singlets at 0.64 ppm (corresponding to the C-18 methyl protons), 0.96 ppm and 0.98 ppm (corresponding to the C-19 methyl protons of cholesterol and its ester derivative), the C-3 proton multiplets at 3.41 ppm for cholesterol and 4.54 ppm for cholesterol ester helped in the initial confirmation of the presence of these entities in the lipid extracts. The detailed assignments for these two sterols are marked in figs. 1b, 2b-d and are listed in Table-1. The fatty acid chain in case of esterified cholesterol was assigned to be oleic acid as described in literature (Tugnoli et al., 2001; Tosi et al., 2003; Tugnoli et al., 2003), based on the characteristic olefinic protons (-CH=CH-) in the ^{13}C and DEPT NMR spectra, between 127 ppm and 131 ppm (figs. 2b-d). The 3-CH proton of the esterified cholesterol at 4.54 ppm gave a characteristic HMBC correlation with the ^{13}C signal of fatty acid ester linkage (-OCOR) at 174.2 ppm, which was observed due to its increased abundance in one of the tuberculoma lipid extracts (fig. 10f).

The ^{1}H and ^{13}C NMR assignments of fatty acid chains indicated that the lipids consisted of both mono-unsaturated and poly-unsaturated fatty acids. The highly intense proton multiplet signal at 5.30 ppm had the collective contributions from vinyl (-CH=CH-) protons in the fatty acid chains and from sterols. Further, a broad multiplet signal at 2.76 ppm reinforced the presence of Δ^{n} methylenes (-CH=CH-(CH_2-CH=CH)$_n$-; $n \geq 1$) in the fatty acid chain. The fatty acid chains have been observed to be the integral structural component of the glycerophospholipids, as seen in the HMBC correlations of the sn-1 and sn-2 methylenes of the glycerol backbone to the corresponding -OCOR linkage of the fatty acid chains (fig. 9g).

The overlapped signal of the terminal methyl protons of the fatty acid chains could be assigned based on the HMQC and HMBC correlations (figs. 7a, 8a, 9a, 10a), at 0.83 ppm in the ^{1}H NMR and at 14.3 ppm in the ^{13}C NMR spectra. Further, the -(CH_2)$_n$- protons were found to occur as a highly intense and broad signal at 1.17-1.29 ppm. Based on the HMQC and HMBC

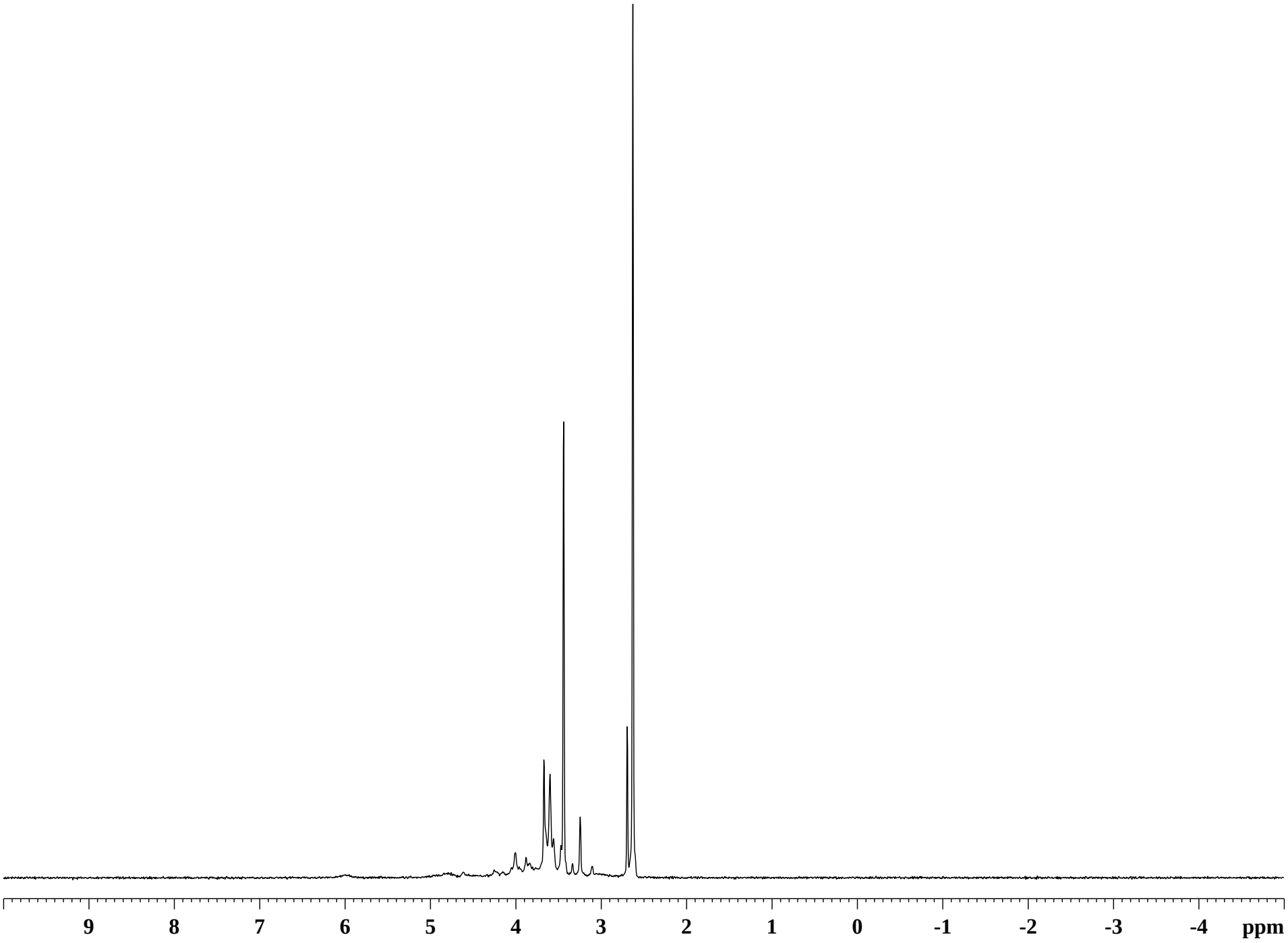

Fig. 11a: ^{31}P NMR spectrum of the pooled lipid extracts of human tuberculoma samples.

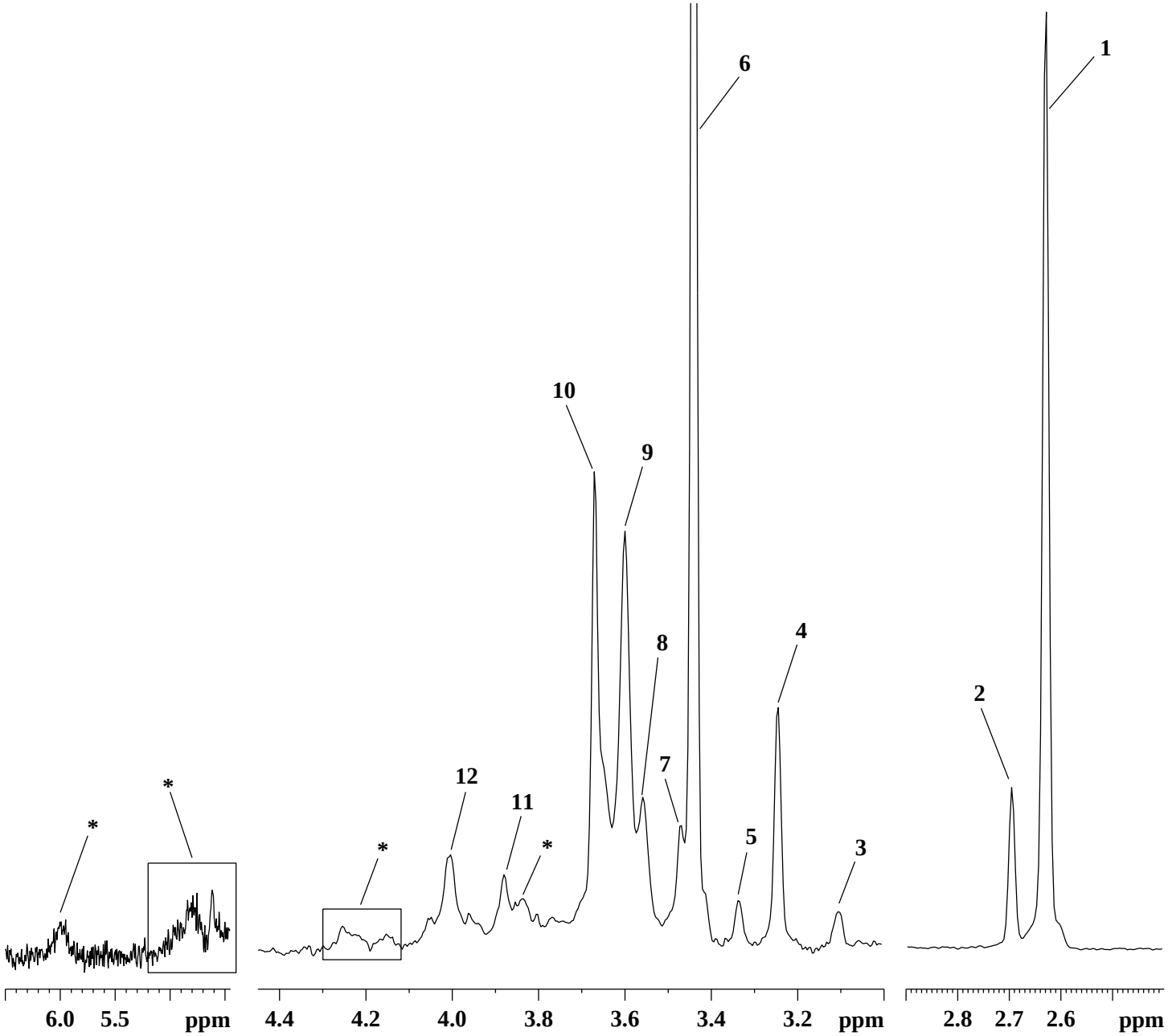

Fig. 11b: Expansions of the ^{31}P NMR spectrum of the pooled lipid extracts of human tuberculoma samples, highlighting the resonance assignments between 2.4-2.9 ppm, 3.00-4.45 ppm and 4.45-6.50 ppm. The labeled assignments of the lipid components are as given in Table-3.

Table-3: ^{31}P chemical shift assignments of the phospholipids, as seen in the ^{31}P NMR spectrum of the pooled tuberculoma lipid extracts. The chemical shifts were calibrated with respect to the ^{31}P signal of diacylphosphatidylcholine assigned at 2.63 ppm. Resonances marked as * are unassigned.

Phospholipid Assigned	**Assignment Number**	**Chemical Shift (δ, ppm)**
Phosphatidylcholine (diacyl)	1	2.63
1-alkyl-2-acyl-phosphatidylcholine	2	2.69
Phosphatidylinositol	3	3.10
Lyso-phosphatidylcholine	4	3.24
Phosphatidylserine	5	3.34
Phosphatidylethanolamine (diacyl)	6	3.44
1-alkyl-2-acyl-phosphatidylethanolamine	7	3.47
Plasmalogen	8	3.56
Sphingomyelin	9	3.60
Lyso-phosphatidylethanolamine	10	3.67
Diphosphatidylglycerol (cardiolipin), Phosphatidylglycerol	11	3.88
Phosphatidic acid	12	4.00

correlations, the α- and β-methylenes of the fatty acid chains were assigned at 2.27 ppm, 1.55 ppm in the ^{1}H NMR, and at 34.4 ppm, 25.2 ppm in the ^{13}C NMR spectra, respectively. The allylic methylenes of type -CH_2-CH=CH- were assigned at 1.97 ppm in the ^{1}H NMR and at 27.5 ppm in the ^{13}C NMR spectra, while the Δ^n methylenes were assigned at 25.9 ppm in the ^{13}C NMR spectra and were observed to give the HMBC correlations with the olefinic -CH protons between 127.6-130.9 ppm (figs. 9b, 10b). The olefinic -CH's (at 5.30 ppm) gave the corresponding ^{13}C correlations between 127.6-130.9 ppm, as seen in the HMQC spectra (figs. 7e, 8d), as well as correlations with both Δ^n methylenes at 25.9 ppm and allylic methylenes at 27.5 ppm, as seen in the HMBC spectra (figs. 9f, 10e). Both α- and β-methylenes of the fatty acid chains gave their corresponding HMBC correlations with the -OCOR linkage at 174.2 ppm, as seen in the HMBC spectra (figs. 9h, 10g). When the 2D COSY spectra were examined, coupling between the terminal methyl (0.83 ppm) and adjacent methylene protons (1.24 ppm), α- and β-methylenes of the fatty acid chains (2.27 ppm and 1.55 ppm), and between the allylic (-CH_2-CH=CH-, 1.97 ppm) and vinyl protons (-CH=CH-, 5.30 ppm) could be observed (figs. 5a-c). Further, these olefinic -CH protons showed ^{1}H-^{1}H coupling with the Δ^n methylenes at 2.76 ppm, while the allylic methylenes at 1.97 ppm showed coupling with the adjacent methylenes (linked to the -$(CH_2)_n$ of the fatty acid chain) at 1.28 ppm (figs. 5a-c). The olefinic ^{13}C signal at 134.7 ppm was found to be present in all samples except one, which has been tentatively assigned as the -OCH signal of the plasmalogen (fig. 3c). The possible ^{1}H total correlations of the assigned lipid components could be elucidated with the help of ^{1}H-^{1}H TOCSY experiments, as shown in figs. 6a-c.

5. Discussion

5.1. NMR Spectroscopic Observations of the Lipid Structural Assignments

In the present study, the detailed ^{1}H and ^{13}C NMR spectroscopic assignments of the lipid extracts of tuberculous granulomas have been carried out using one- and two-dimensional NMR techniques, mainly to address the role of lipid components as possible diagnostic markers with an aim to discriminate intracranial tuberculomas from CNS tumors. A comparison of the ^{1}H NMR spectra of the lipid extracts showed that all had identical spectral pattern, except for the signal of the residual water, which showed a slight shift in the signal profile (fig. 12a). The relative

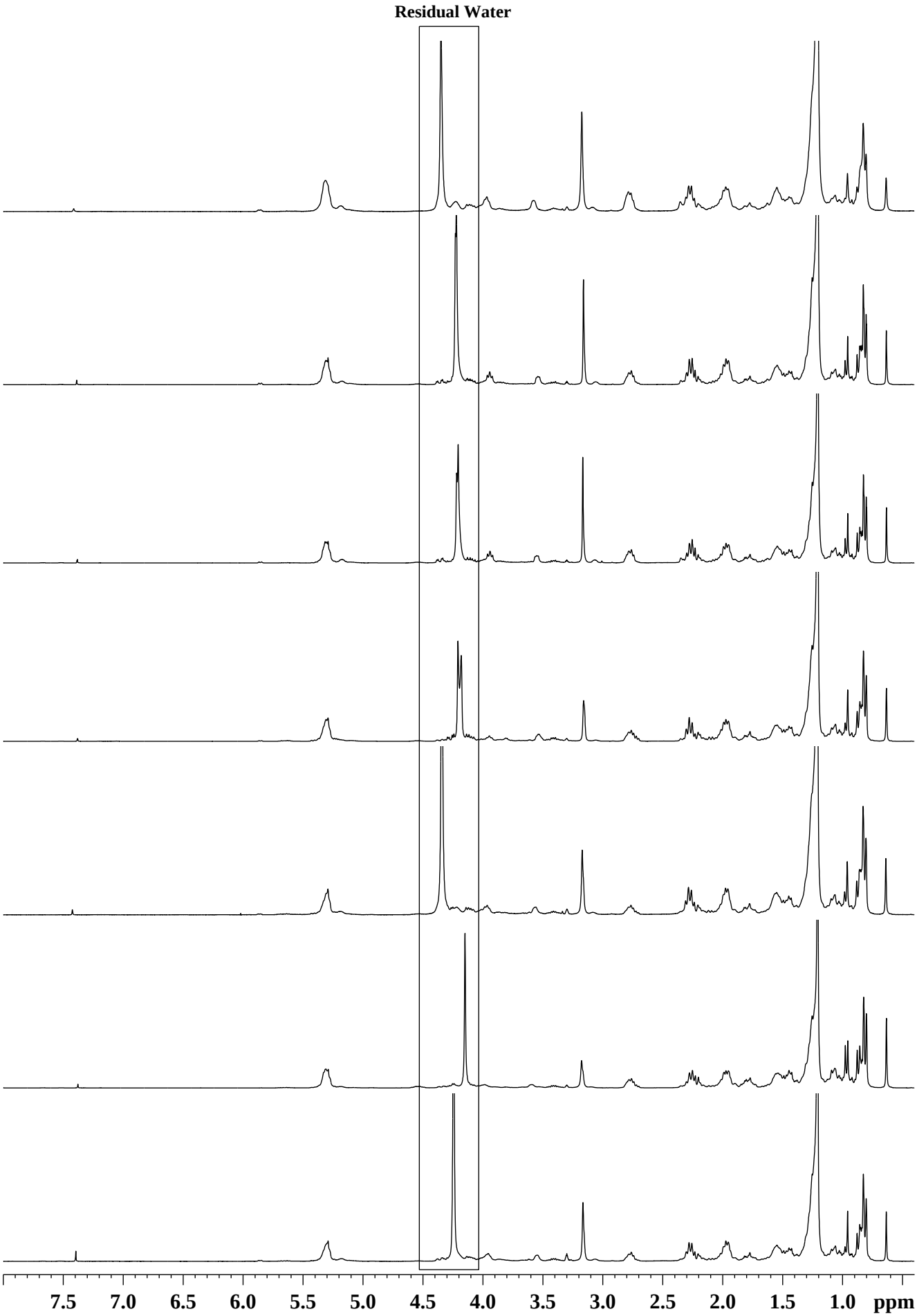

Fig. 12a: Stack plot of the ^{1}H NMR spectra of the lipid extracts of human tuberculoma samples. The relative variation in the chemical shift of residual water has been highlighted.

abundance of a few of the assigned lipid components were found to be either increased or decreased, such as cholesterol, cholesterol ester, sphingomyelin, plasmalogen and phenolic glycolipids (fig. 12b). A comparison of the ^{13}C NMR spectra of two lipid extract samples further confirmed the ^{1}H NMR observations regarding the presence of assigned lipid components, besides resolving the overlapping resonance contributions arising due to the presence of cholesterol and cholesterol ester (figs. 13a-b). It could be pointed out that the decrease in some of the ^{13}C signal intensities of the assigned lipid components might have occurred either due to their low abundance or due the sensitivity at 300 MHz, as was the case with the 3-CH and 5-C signals of cholesterol ester (fig. 13a).

The comparison of the ^{1}H NMR spectra of the lipid extracts further showed certain important features. The signal of plasmalogen was found to be present in all samples except one, as confirmed by the ^{1}H NMR spectra of the lipid extracts as shown in figs. 14 and 15. Further, elevated level of cholesterol ester was observed in the sample in which the -OCH proton signal of plasmalogen had been absent. The possible link for this absence of plasmalogen and the abnormal increase in cholesterol ester, if any, remains to be investigated. Further, when the ^{1}H NMR was repeated after a span of 1-4 months (after performing the initial set of NMR experiments) for a few samples (in which plasmalogen was present), an interesting phenomenon was observed pertaining to the -OCH proton signal of plasmalogen. The decrease in the intensity of -OCH proton signal at 5.86 ppm has been shown for a representative tuberculoma lipid sample (fig. 16). It was further observed that a decrease in the intensity of this -OCH proton signal at 5.86 ppm had a correlation with the development of an unidentified signal at 4.92 ppm as shown in fig. 17. The unidentified proton signal at 4.92 ppm gave correlations with the proton signals at 3.65 ppm and 4.00 ppm in the COSY spectra (figs. 5b and 5c), and has thus given rise to a possible structural change in plasmalogen during sample preservation that remains to be investigated.

Since the assigned lipid components were found to be present in all tuberculoma lipid extracts, it was possible to quantify their relative levels based on the integral areas so as to compare them with the available literature data (Adosraku et al., 1994; Kriat et al., 1993; Singer et al., 1996; Willker and Leibfritz, 1998). This task was first adopted for one of the representative tuberculoma samples as shown in figs. 18a-c, which was subsequently carried out for the ^{1}H NMR

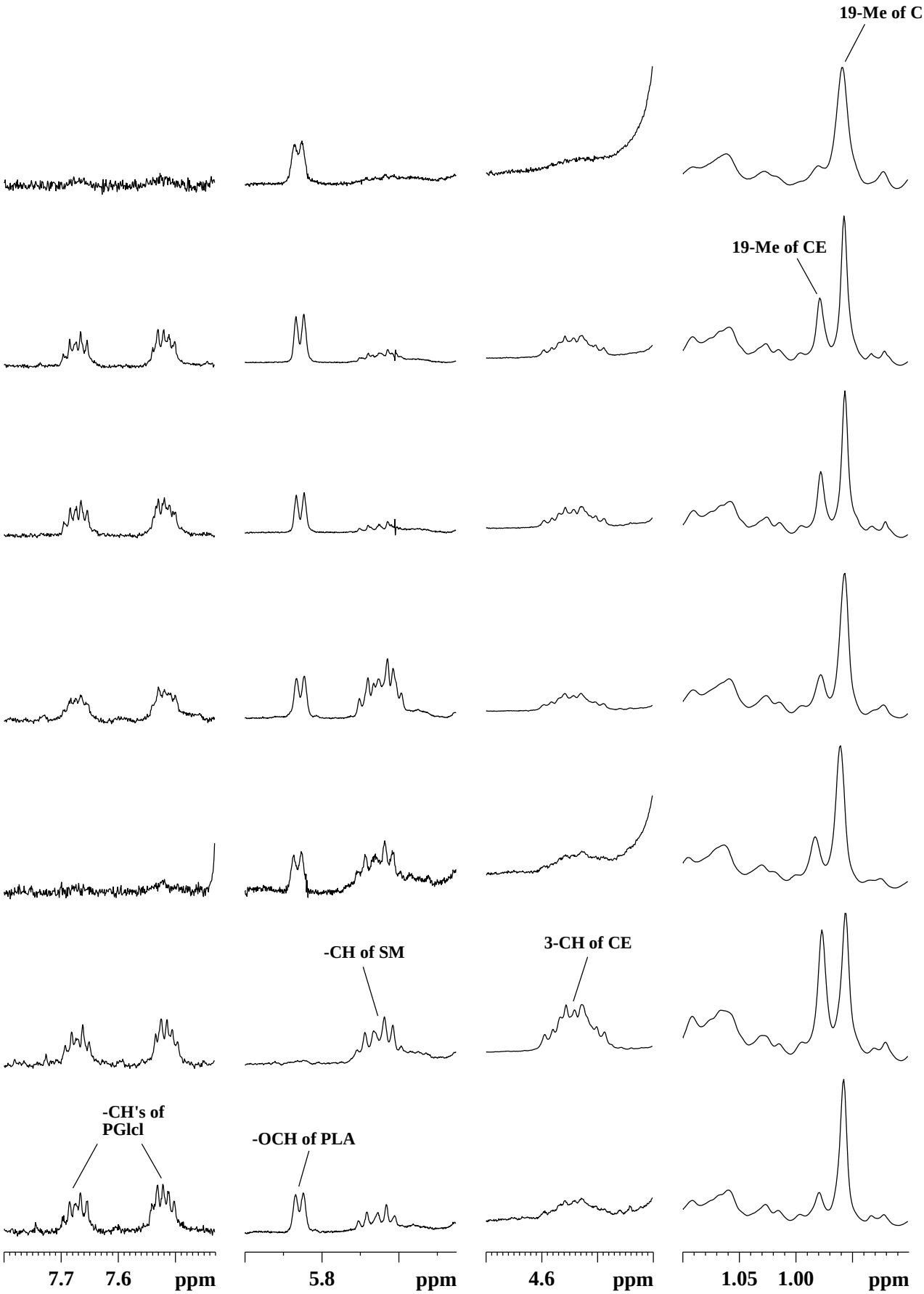

Fig. 12b: Stack plot of the ^{1}H NMR spectra of the lipid extracts of human tuberculoma samples, highlighting the relative abundance between 0.9-1.1 ppm, 4.4-4.7 ppm, 5.45-6.00 ppm and 7.43-7.80 ppm. The labeled assignments are: C: Cholesterol; CE: Cholesterol ester; SM: Sphingomyelin; PLA: Plasmalogen; PGlcl: Phenolic Glycolipids.

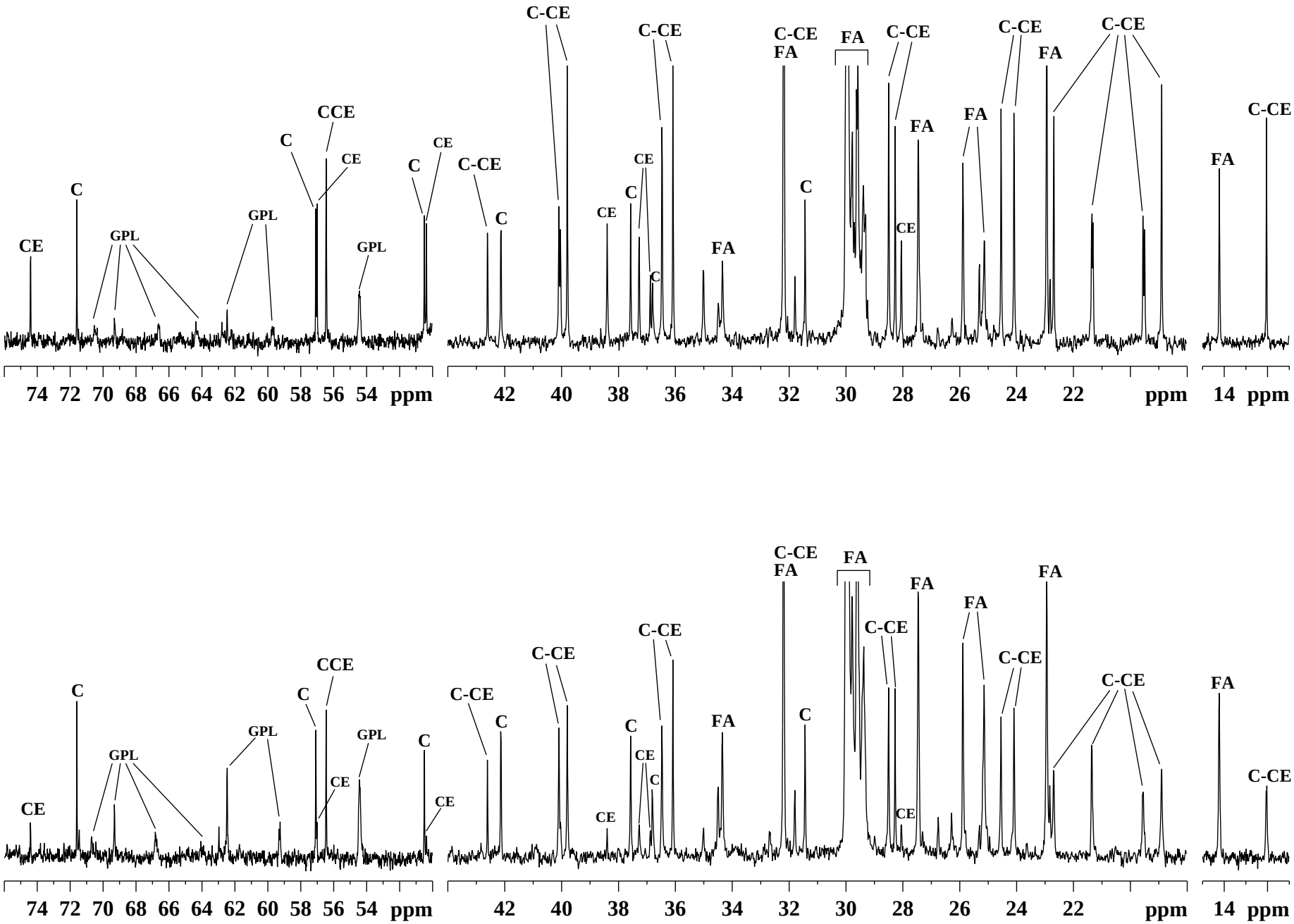

Fig. 13a: Expansions of the ^{13}C NMR spectra of the lipid extracts of human tuberculoma samples, highlighting the resonance assignments between 11.0-15.0 ppm, 18.0-44.0 ppm and 50.0-76.0 ppm. The labeled assignments are: C: Cholesterol; CE: Cholesterol ester; FA: Fatty acid backbone of the lipids; GPL: Glycerophospholipids.

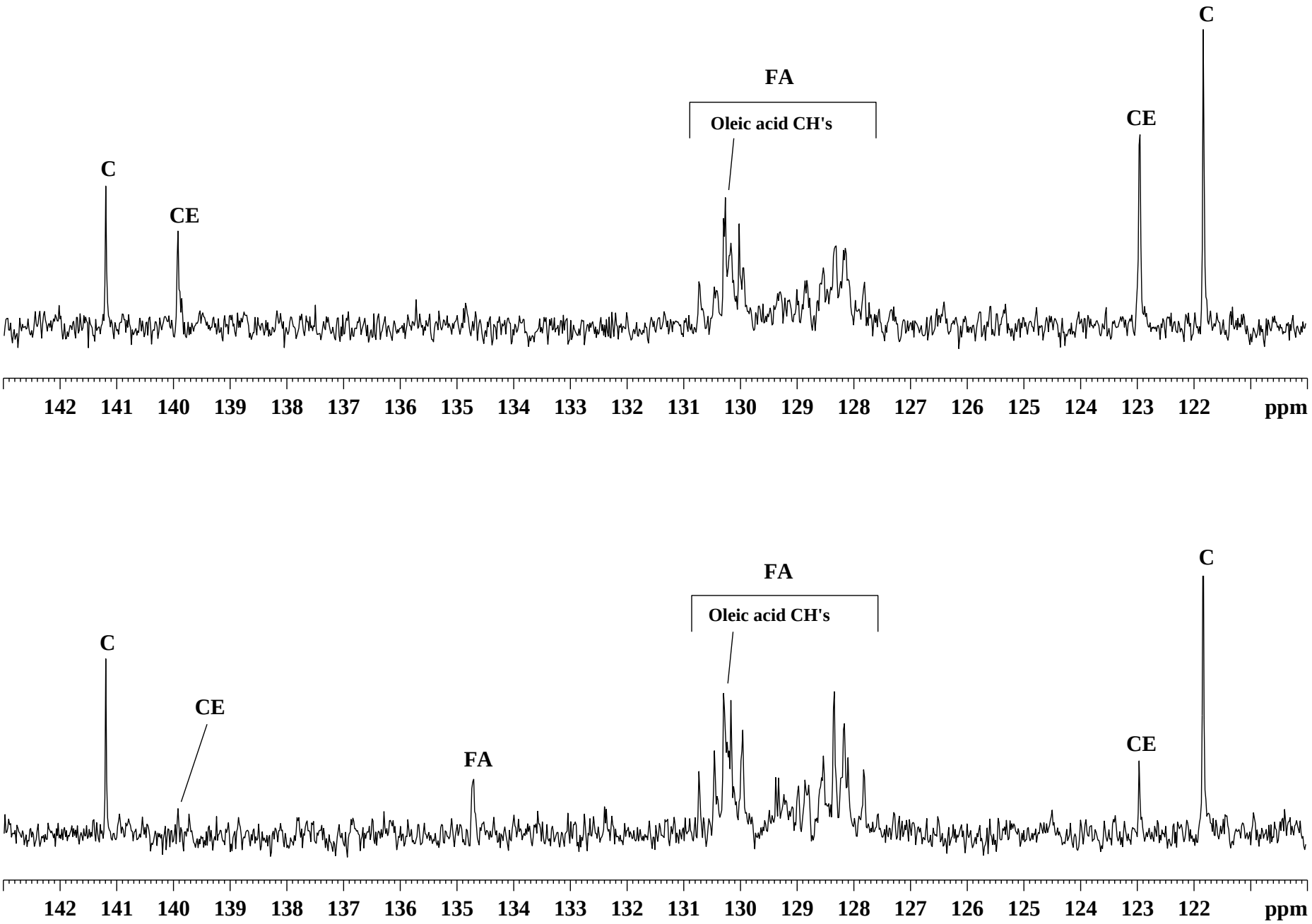

Fig. 13b: Expansions of the ^{13}C NMR spectra of the lipid extracts of human tuberculoma samples, highlighting the resonance assignments between 120.0-143.0 ppm. The labeled assignments are: C: Cholesterol; CE: Cholesterol ester; FA: Fatty acid backbone of the lipids.

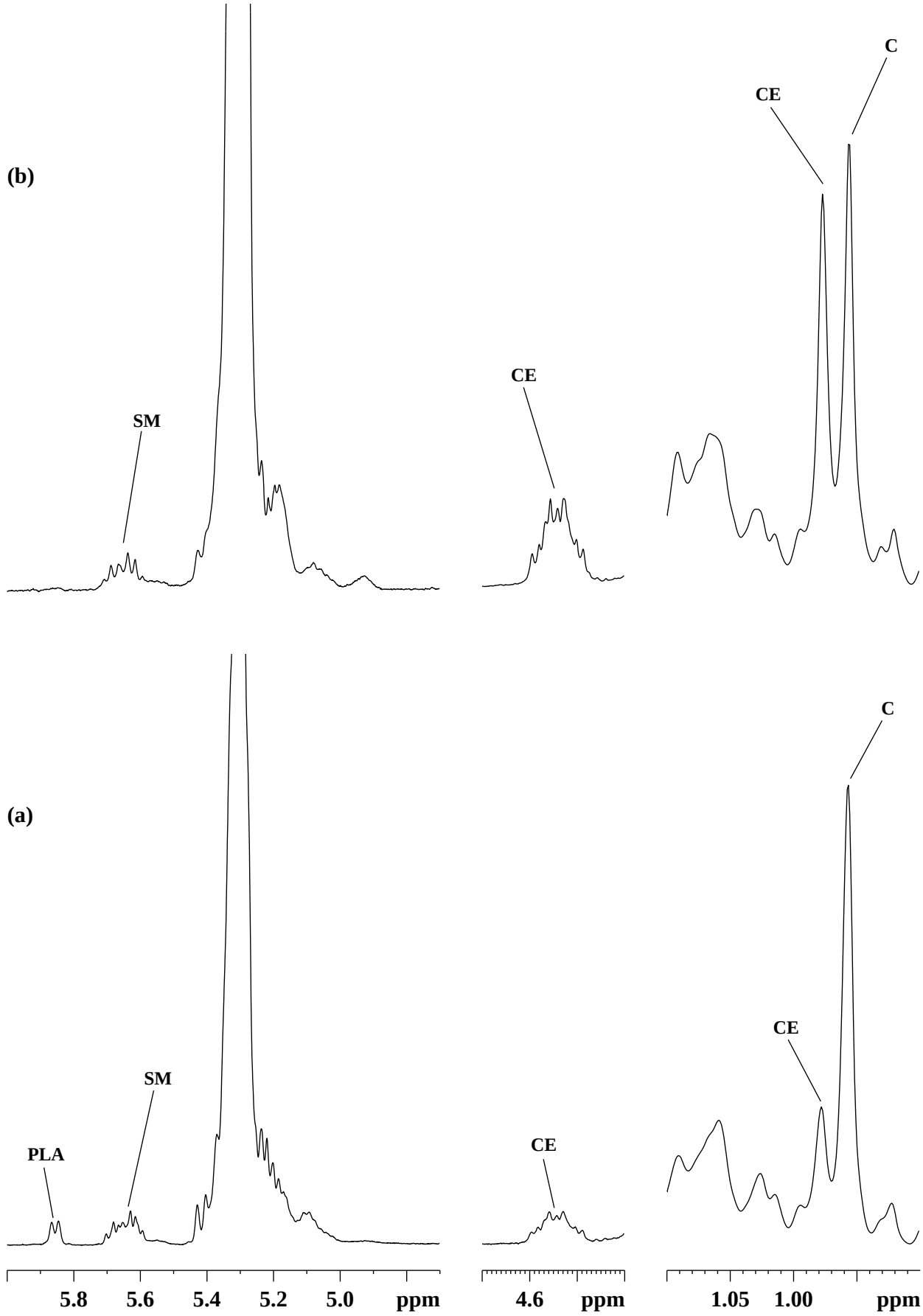

Fig. 14: Stack plot of the ^{1}H NMR spectra of the lipid extracts of two human tuberculoma samples, highlighting the relative abundance between 0.9-1.1 ppm, 4.4-4.7 ppm and 4.7-6.0 ppm. The labeled assignments are: C: Cholesterol; CE: Cholesterol ester; SM: Sphingomyelin; PLA: Plasmalogen.

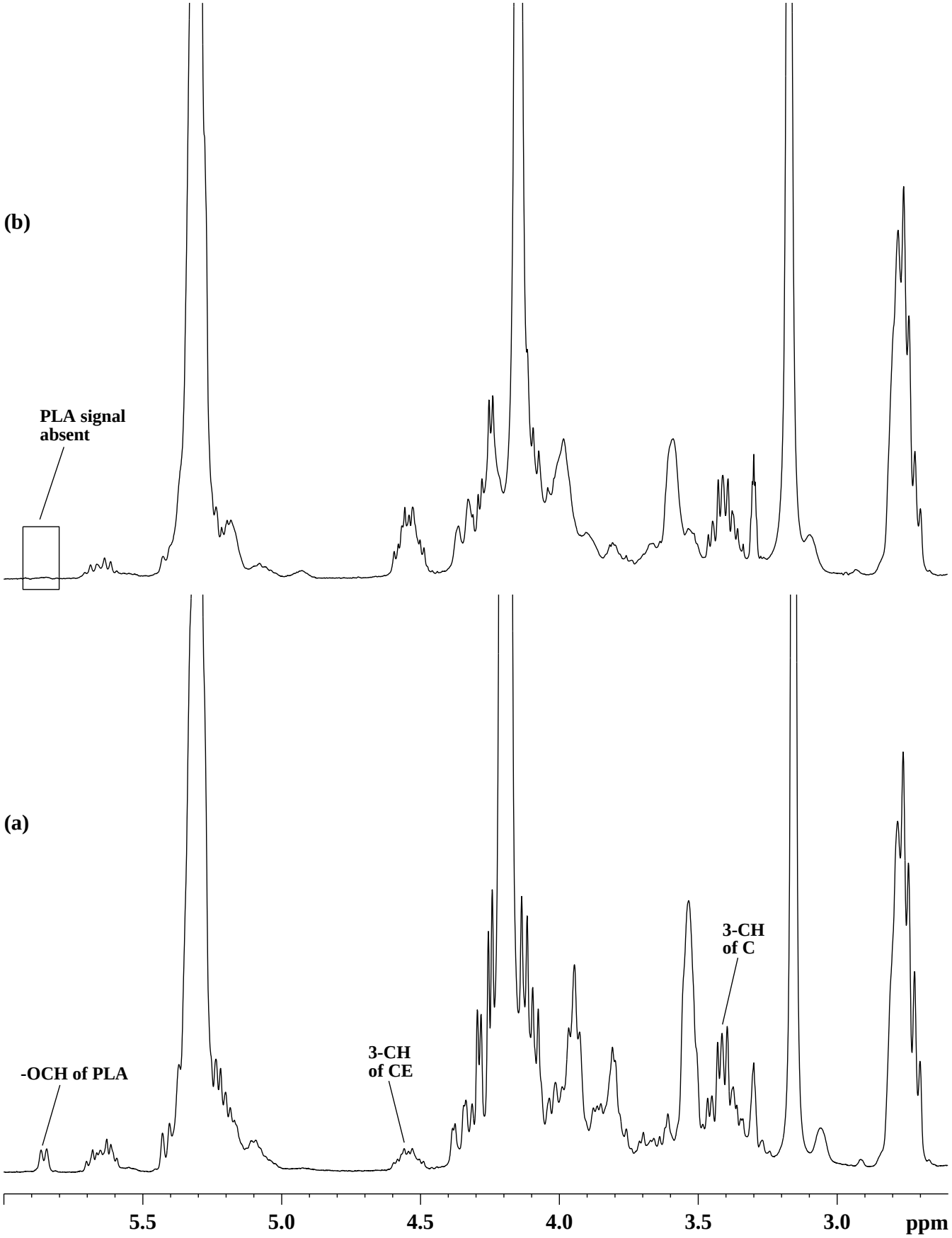

Fig. 15: Stack plot of the ^{1}H NMR spectra of the lipid extracts of two human tuberculoma samples, highlighting the relative abundance between 2.6-6.0 ppm. The labeled assignments are: C: Cholesterol; CE: Cholesterol ester; PLA: Plasmalogen.

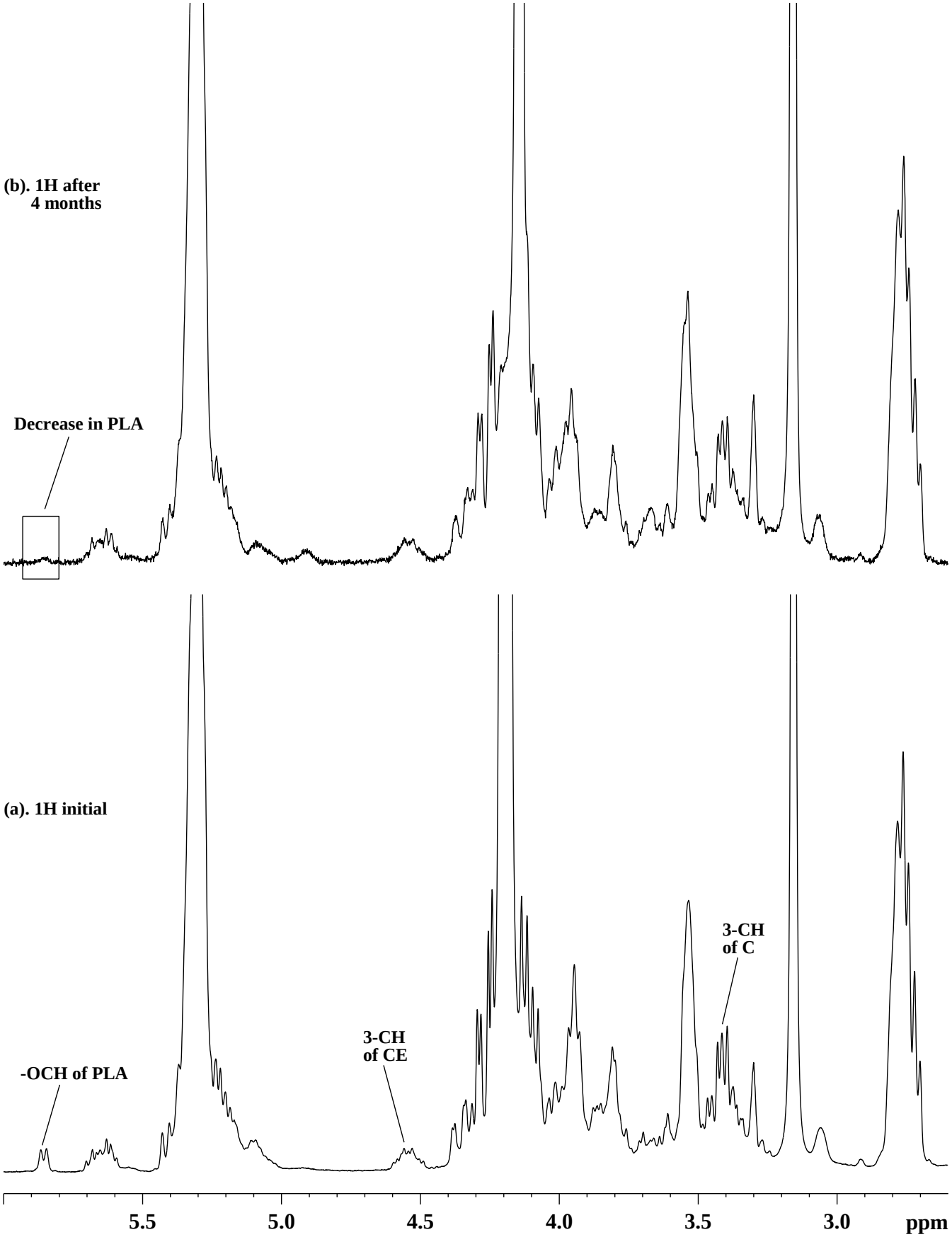

Fig. 16: Stack plot of the ^{1}H NMR spectra of the lipid extract of a human tuberculoma sample, highlighting the relative abundance between 2.6-6.0 ppm. The labeled assignments are: C: Cholesterol; CE: Cholesterol ester; PLA: Plasmalogen.

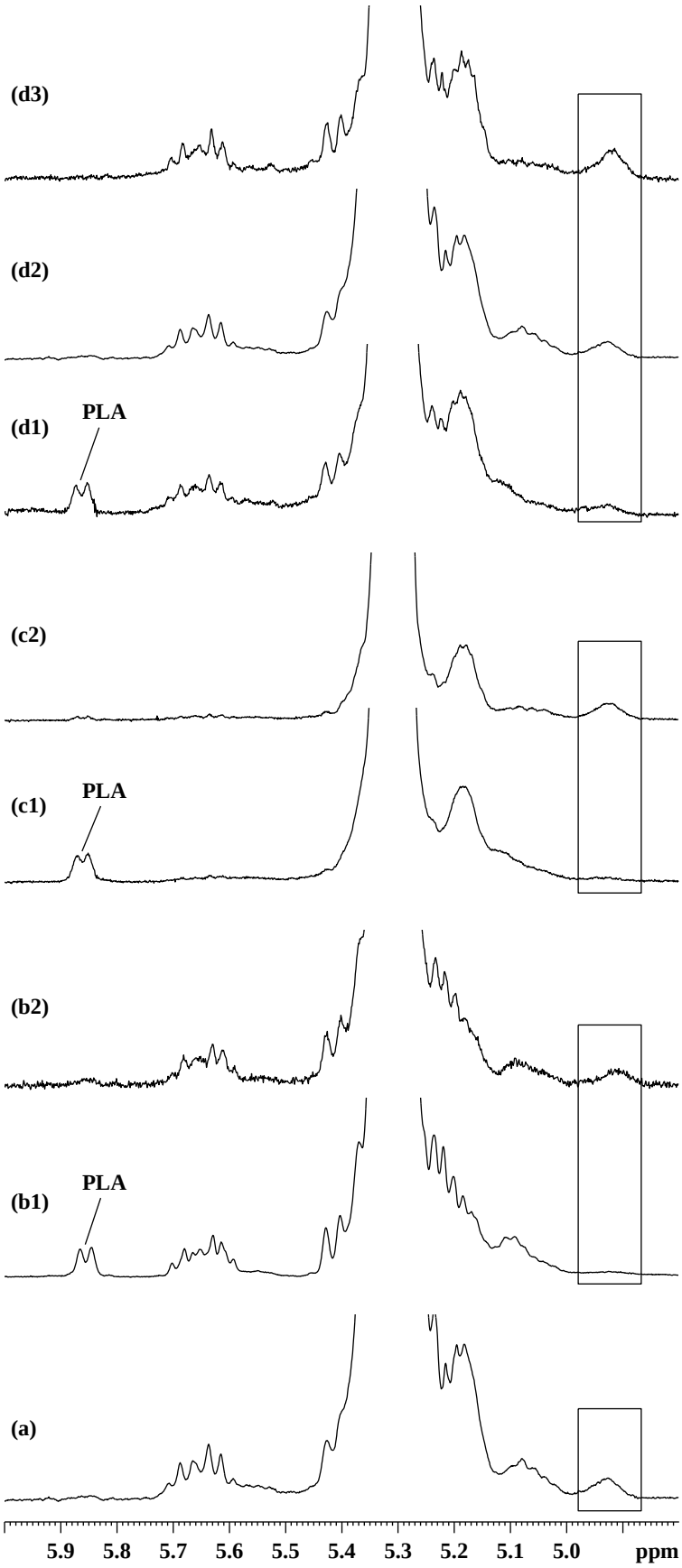

Fig. 17: Stack plot of the ^{1}H NMR spectra of lipid extracts of human tuberculoma samples (between 4.8-6.0 ppm) done in different time intervals, to highlight the variation in the signal intensities of PLA, which had an associated increase in the intensity of the unassigned signal at 4.93 ppm (inside the box). Spectra (a), (b1), (c1), (d1) denote the initial ^{1}H NMR experiments, (b2) denotes the ^{1}H NMR done after 4 months, (c2) and (d2) denote the ^{1}H NMR done after 1 month, (d3) denotes the ^{1}H NMR done after 2 months.

spectra of other samples. The semi-quantitative values of the lipid components thus obtained are summarized in Tables 4 and 5. When the integral value of the olefinic -CH of sphingomyelin at 5.65 ppm was set to one, the integral value of the choline $-N^{+}(CH_3)_3$ signal at 3.16 ppm corresponded to a value of forty-five. Since the contribution for the choline peak was expected mainly from sphingomyelin and phosphatidylcholine in the present study, the integral value obtained for the choline signal indicated that the majority of the choline head group corresponded to phosphatidylcholine of the order of around three times more than that of sphingomyelin. In a similar manner, the ethanolamine-containing compounds, identified to be phosphatidylethanolamine (PE) and PLA in the present study were resolved based on their integral area contributions. The contribution of ethanolamine methylene protons at 3.06 ppm was resolved by calibrating the integral value of PLA -OCH signal at 5.86 ppm to one. The total integral value for the signal at 3.06 ppm corresponded to eighteen, which had the contribution from two PLA ethanolamine methylene protons and two phosphatidylethanolamine methylene protons. Since PLA -OCH integral value was calibrated to one and the corresponding integral contribution of PLA methylene protons at 3.06 ppm would be two, the remaining would correspond to the methylene protons of PE, thus giving them a value of sixteen. This has indicated that the relative level of phosphatidylethanolamine is around eight times more than that of PLA.

The major contributions for the sn-1, sn-2 and sn-3 methylene protons of the glycerol backbone were from TGs, phosphatidylcholine, phosphatidylethanolamine, and PLA, although contributions from other minor forms of glycerophospholipids such as phosphatidylinositol, phosphatidylserine, phosphatidylglycerol and phosphatidic acid could not be ruled out in the present investigation. The main contributions for the sn-1 and sn-3 glycerol protons could be accounted by calibrating the PLA -OCH signal at 5.86 ppm to one. The double-doublet signal at 4.36 ppm was observed mainly due to the presence of sn-1 and sn-3 methylenes of TGs, which had coupling with the other set of sn-1 and sn-3 methylenes (geminal) at 4.27 ppm. The corresponding integral value of twenty-four for this signal indicated that TGs were present around twelve times more than that of PLA (figs. 18a-c).

Based on the integral area of 3-CH proton at 4.54 ppm, esterified cholesterol was found to be around five times more than PLA when the integral value of -OCH of PLA at 5.86 ppm was set

Table-4: Relative signal intensities of lipid components based on the integral area of sphingomyelin olefinic -CH proton at 5.65 ppm set to 1.0.

Lipid Component(s)	**Chemical Shift (δ, ppm)**	**Relative Integral Areas (Mean ± SE)**
Plasmalogen (-OCH)	5.86	1.37 ± 0.54
Olefinic CH's	5.25-5.36	121.29 ± 31.27
Cholesterol ester (3-CH)	4.54	2.44 ± 0.97
Triglycerides (sn-1 and sn-3 -CH_2's)	4.33-4.40	14.04 ± 4.83
Glycerophospholipids (sn-3 -CH_2's)	3.90-3.98	35.77 ± 11.77
Sphingomyelin + Phosphatidylcholine (-$N^+(CH_3)_3$)	3.16	104.61 ± 32.89
Plasmalogen + Phosphatidylethanolamine (-CH_2's)	3.06	8.96 ± 3.07
Di-allylic methylenes (-CH=CH-(CH_2-CH=CH)$_n$-)	2.68-2.86	66.87 ± 20.63
Mono-allylic methylenes (-CH_2-CH=CH-)	1.92-2.06	129.62 ± 28.37
Methylenes (-(CH_2)$_n$-)	1.15-1.36	1159.22 ± 270.24
Methyls (-CH_3)	0.78-0.91	288.86 ± 56.59
Cholesterol ester + Cholesterol (18-CH_3)	0.63	42.78 ± 7.38

Table-5: Ratios of relative ^{1}H signal integral areas of the lipid components.

Lipid Component Variables	**Ratios of ^{1}H Integral Areas (Mean ± SE)**
Plasmalogen : Phosphatidylethanolamine	0.43 ± 0.14
Sphingomyelin : Phosphatidylcholine	0.16 ± 0.041
Plasmalogen : Phosphatidylcholine	0.11 ± 0.028
Phosphatidylethanolamine : Phosphatidylcholine	0.24 ± 0.047
Triglycerides : Phospholipids	0.42 ± 0.027
Choesterol ester : Cholesterol	0.25 ± 0.1
Methylenes (-$(CH_2)_n$-) : Methyls (-CH_3)	3.91 ± 0.19
Methylenes (-$(CH_2)_n$-) : Di-allylic methylenes	20.24 ± 2.17
Methylenes (-$(CH_2)_n$-) : Mono-allylic methylenes	8.89 ± 0.25
Methylenes (-$(CH_2)_n$-) : Olefinic CH's	10.07 ± 0.58
Di-allylic methylenes : Olefinic CH's	0.51 ± 0.03
Mono-allylic methylenes : Olefinic CH's	1.13 ± 0.05
Di-allylic methylenes : Mono-allylic methylenes	0.46 ± 0.042

to one, while it was around twice less than sphingomyelin with respect to the integral area of olefinic -CH at 5.65 ppm. The levels of both cholesterol and cholesterol ester could be resolved based on their contribution to the C-18 methyl signal at 0.64 ppm. When the integral value of 3-CH of cholesterol ester at 4.55 ppm was set to one, the integral value of C-18 methyl protons at 0.64 ppm corresponded to a value of forty-five (figs. 18a-c). Accounting a value of three for the C-18 methyl protons of the esterified cholesterol from this integral value, the remaining value indicated that free cholesterol was present around fourteen times more than esterified cholesterol in the tuberculoma samples, except in one sample where esterified cholesterol was present in almost equal proportion to that of free cholesterol (fig. 19). Additionally, the PLA -OCH signal was absent in this case (fig. 14), and apart from confirming the proton contributions of the ethanolamine methylenes at 3.06 ppm, the integral value at 3.06 ppm indicated a rise in the level of phosphatidylethanolamine. The levels of sterols assumed a higher proportion in this case, which might indicate the severity of the disease, as normally reported in case of malignant tumors (Tugnoli et al., 2001; Tosi et al., 2003; Tugnoli et al., 2003). Overall, the mean levels of triglycerides, glycerophospholipids, sphingomyelin and sterols were elevated in all samples when compared to plasmalogen (Table-4).

Although it has been reported in literature that the olefinic proton integral value at 5.30 ppm could be taken as a measure of the extent of unsaturation in the fatty acid chains (Adosraku et al., 1994; Singer et al., 1996; Willker and Leibfritz, 1998), it was not possible to selectively identify the individual fatty acid contributions, mainly due to the overlapping signal contributions from the olefinic and allylic protons of these lipid components, which also included the contributions from sterols. Nevertheless, the relative levels of the olefinic -CH's, di- and mono-allylic methylenes have been summarized (as a collective profile) in Table-4. Based on the characteristic ^{1}H and ^{13}C signals and as reported in literature (Willker and Leibfritz, 1998; Singer et al., 1996; Adosraku et al., 1994), it could be stated that the unsaturated fatty acids in the tuberculoma lipid extracts mainly comprised of oleic acid (18:1(n-9)), linoleic acid (18:2(n-6)) and possibly arachidonic acid (20:4(n-6)). Except oleic acid that has no di-allylic methylenes, the other two are known to have di-allyllic methylenes and thus gave a characteristic ^{1}H NMR signal patterns between 2.68 and 2.84 ppm; as for example, the di-allylic methylene of 18:2(n-6) appears as a triplet at 2.73 ppm, while the di-allylic methylenes of 20:4(n-6) appear as a triplet at 2.78 ppm

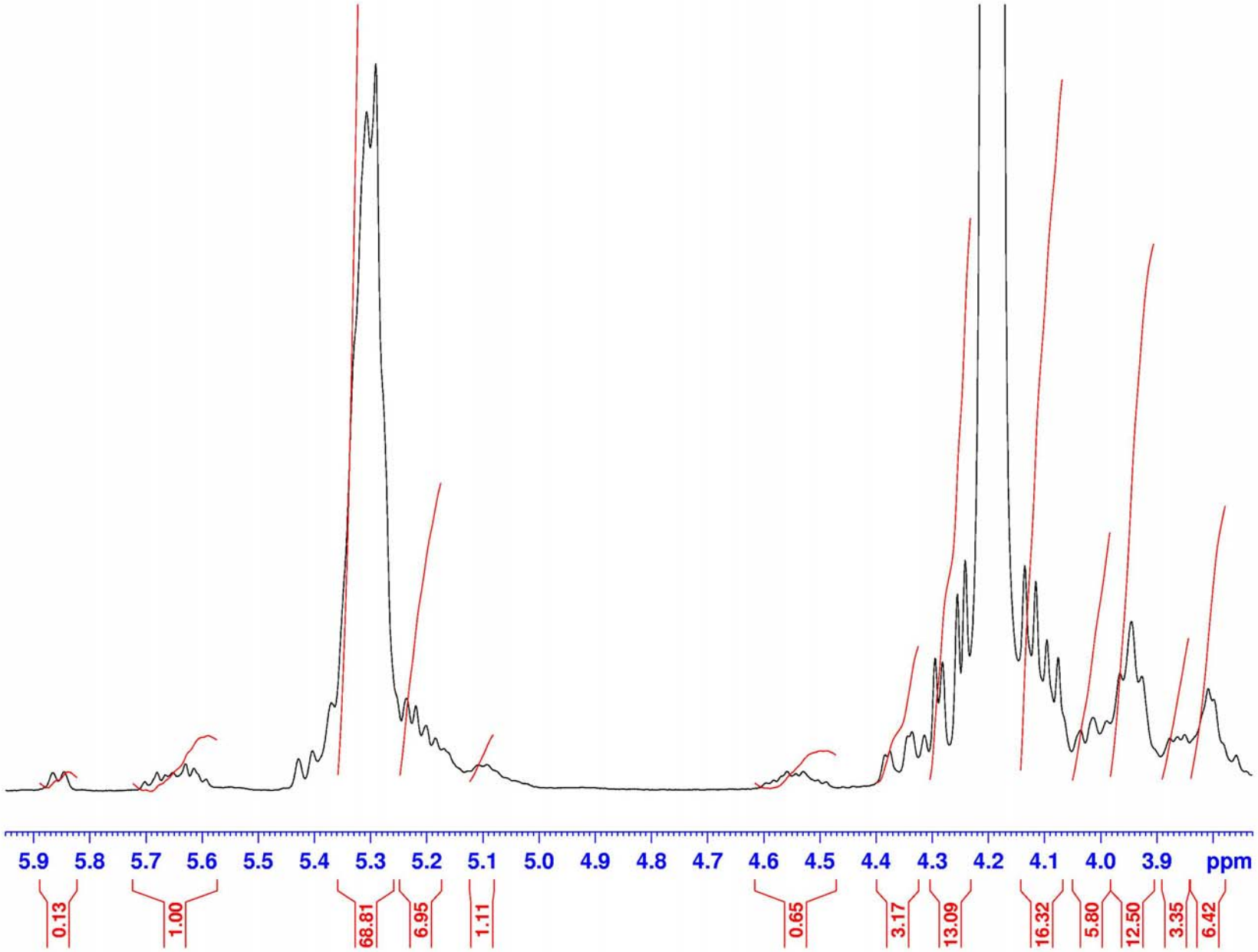

Fig. 18a: ^{1}H NMR spectrum of the lipid extract of a representative human tuberculoma sample, highlighting the relative abundance of the lipid components between 3.74-5.95 ppm, based on the integral area of the sphingomyelin -CH proton at 5.65 ppm set to 1.0.

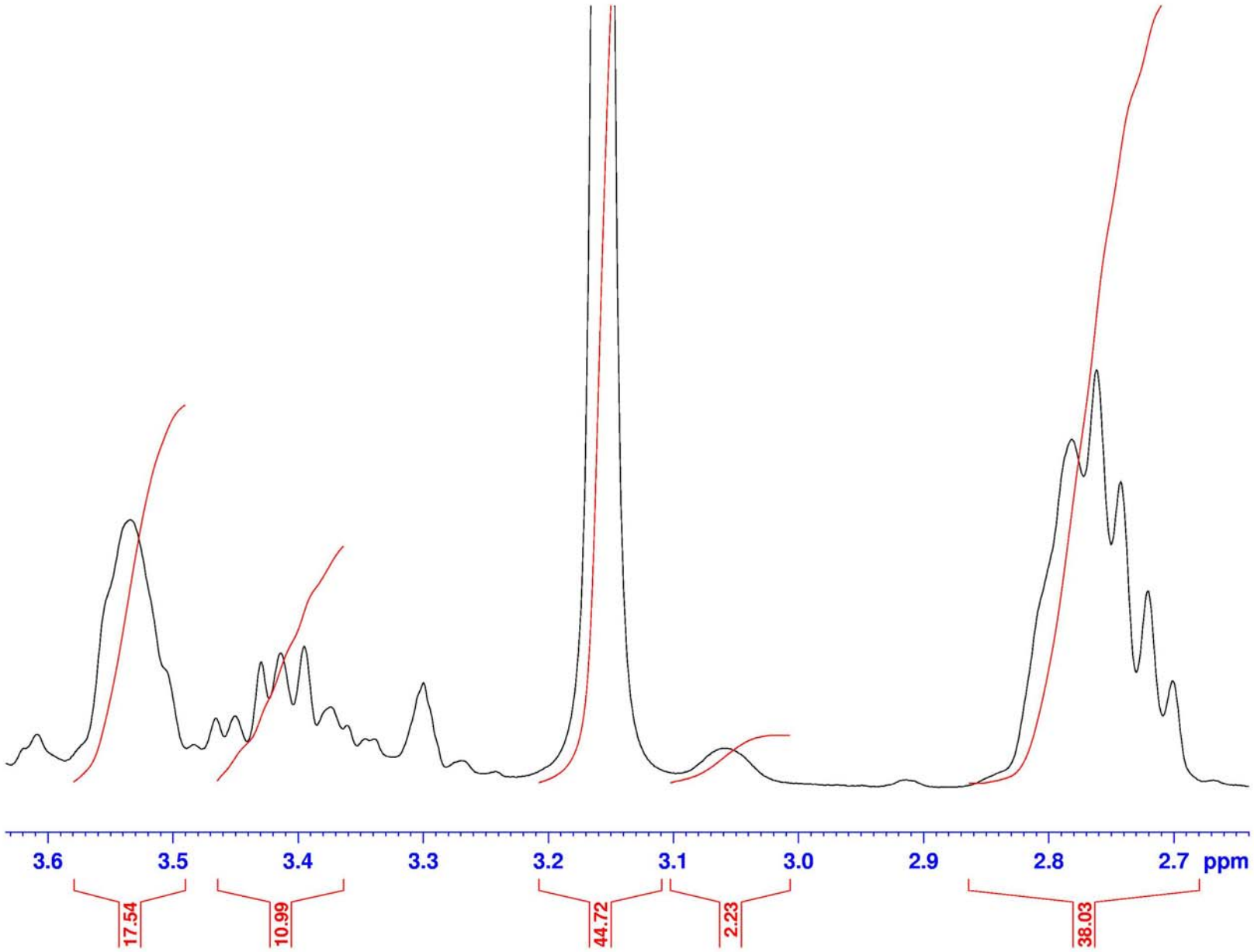

Fig. 18b: ^{1}H NMR spectrum of the lipid extract of a representative human tuberculoma sample, highlighting the relative abundance of the lipid components between 2.64-3.63 ppm, based on the integral area of the sphingomyelin -CH proton at 5.65 ppm set to 1.0.

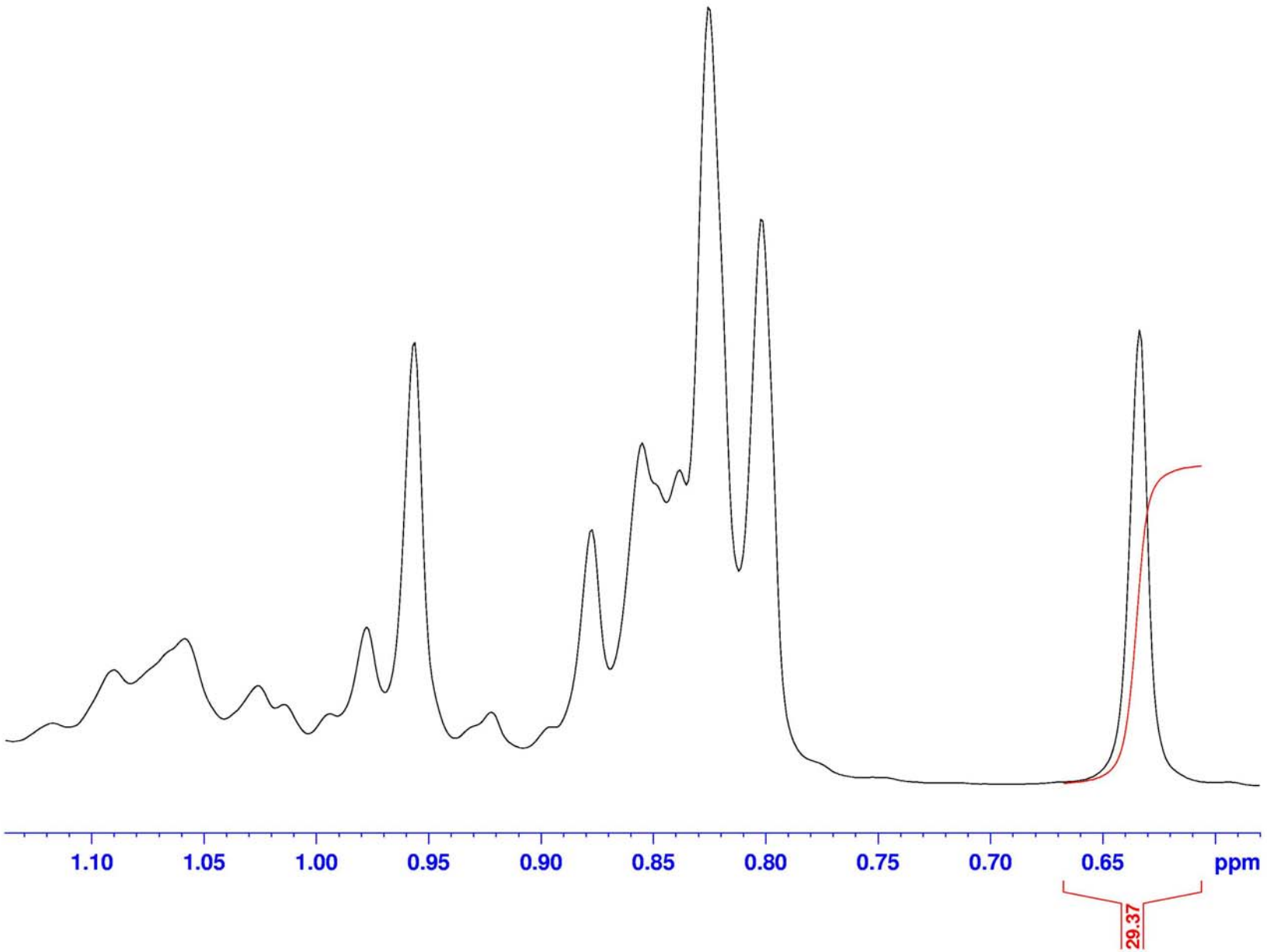

Fig. 18c: ^{1}H NMR spectrum of the lipid extract of a representative human tuberculoma sample, highlighting the relative abundance of the lipid components between 0.58-1.14 ppm, based on the integral area of the sphingomyelin -CH proton at 5.65 ppm set to 1.0.

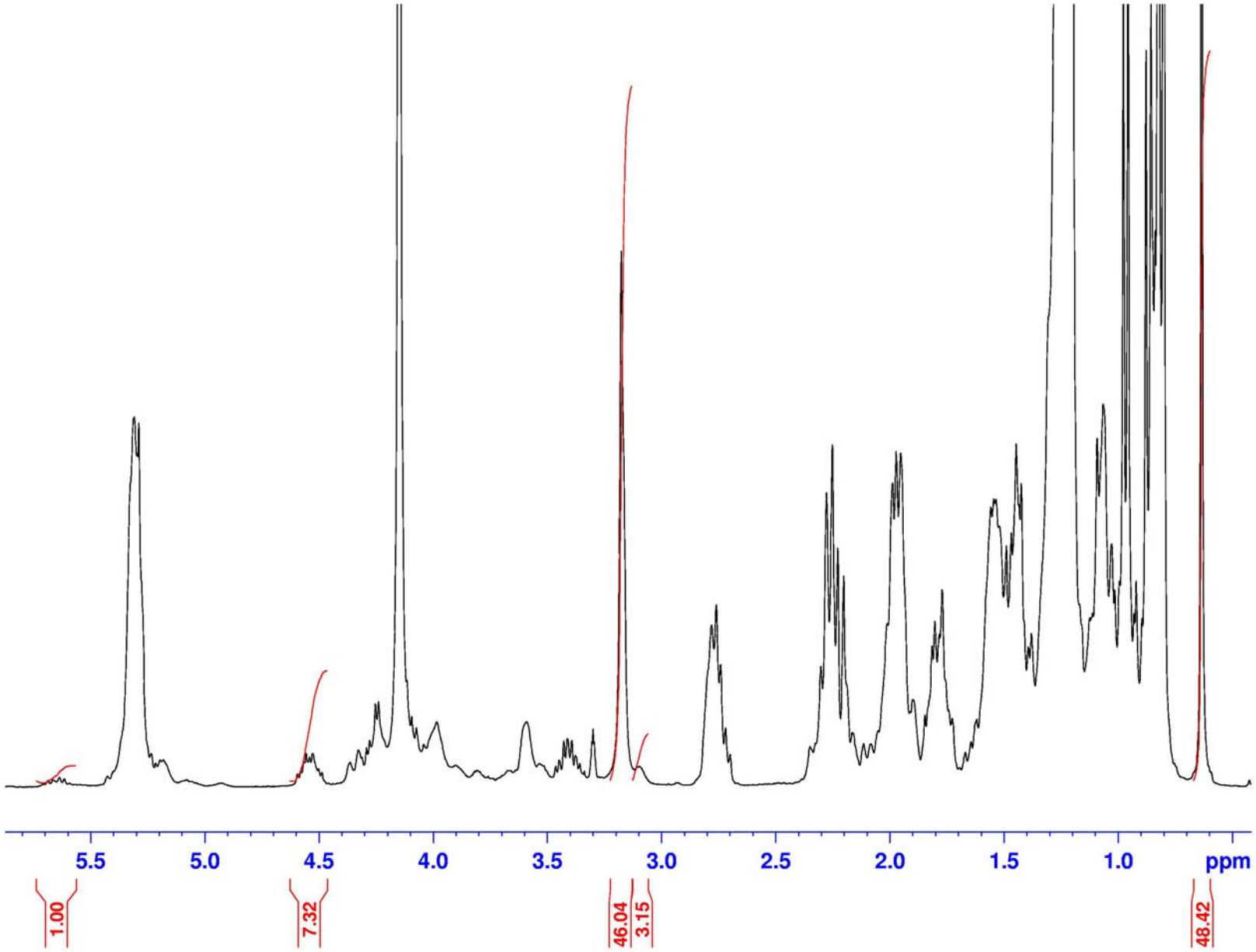

Fig. 19: ^{1}H NMR spectrum of the lipid extract of a human tuberculoma sample with high abundance of cholesterol-cholesterol ester, highlighting the relative abundance of the lipid components between 0.40-5.86 ppm, based on the integral area of the sphingomyelin -CH proton at 5.65 ppm set to 1.0.

(Willker and Leibfritz, 1998). Despite the signal overlap at 300 MHz, this type of signal pattern was observed to be present in all tuberculoma lipid extracts (figs. 2a and 12a), indicating that the di-allylic methylenes mainly belonged to the 18:2(n-6) and 20:4(n-6) types in the present study.

5.2. NMR Assignments as Diagnostic Markers of Tuberculoma

Several reports exist in the literature regarding the NMR analysis of lipids/lipid extracts and its possible role in disease diagnosis. Among these, quantification of lipids from normal and pathological thyroid tissue (Yoshioka et al., 2000), quantification of phospholipid classes in patients with renal cell carcinoma (Sullentrop et al., 2002), characterization of the phospholipid composition of tissues and body fluids (Schiller and Arnold, 2002), analysis of plasma lipids applicable to malignant tumors (Kriat et al., 1993), analysis of lipids from human erythrocytes (Adosraku et al., 1994), analysis of phosphate metabolism in thymoma cells (Lutz et al., 2002), analysis of lipids from human renal tissues (Tugnoli et al., 2003), characterization of lipids from human brain tissues (Tugnoli et al., 2001), ^{1}H NMR analysis of fatty acids in excised leiomyosarcoma (Singer et al., 1996), ^{1}H NMR analysis of lipids from human healthy and neoplastic cerebral and renal tissues (Tosi et al., 2002), ^{13}C NMR analysis of total lipid extracts from human liver (Pollesello et al., 1996) and *in vivo* and *in vitro* NMR investigations of intracranial mass (Tosi et al., 2001) are of interest. A recent report has highlighted the role of NMR in differentiating the malignant neoplastic tissues based on cholesterol and its esters (Tosi et al., 2003). There has been no report available in the literature addressing the role of NMR in differentiating intracranial tuberculomas from other CNS disorders, such as tumors, based on the NMR lipid profiles.

The semi-quantitative levels of the lipid components are of importance so as to differentiate a pathological condition from healthy or other diseased states as shown by the literature evidence (Adosraku et al., 1994; Kriat et al., 1993; Singer et al., 1996; Willker and Leibfritz, 1998). This task was carried out for the tuberculoma lipid extracts in the present study, by obtaining the ratios of arbitrary integral values of lipid components from their respective ^{1}H NMR spectra (Table-5). The mean levels obtained for the methylenes/methyls ratio, methylenes/di-allylic methylenes ratio, methylenes/olefinic ratio, di-allylic methylenes/mono-allylic methylenes ratio, triglycerides/phospholipids ratio and cholesterol ester/cholesterol ratio

were in accordance with the reported values observed in pathological states such as cancer (Kriat et al., 1993; Singer et al., 1996; Tosi et al., 2003). Despite the fact that control samples (healthy or other pathological brain tissues) could not be obtained during the course of the present investigation, the relative semi-quantitative values obtained for the tuberculoma lipid extracts corresponded well with the available literature data. Based on the observations of the present study, it could be stated that the values obtained for methylenes/methyls ratio, triglycerides/phospholipids ratio, methylenes/di-allylic methylenes ratio, methylenes/olefinic ratio and cholesterol ester/cholesterol ratio may be of importance in differentiating tuberculomas from healthy or other pathological conditions of the brain.

Among the lipid components assigned, the presence of sphingomyelin in the tuberculoma lipid extracts may assume diagnostic importance. Sphingolipids such as sphingomyelin have been known to occur in large quantities in brain and nerve tissue, and have been related to certain pathological conditions such as Niemann-Pick disease (Brady et al., 1966). It has also been reported in literature that choline-containing phospholipids mark cellularity, as seen in case of proliferating tumors (Ledwozyw and Lutnicki, 1992; Leach et al., 1998; Tugnoli et al., 2001; Lehnhardt et al., 2001). While other glycerophospholipids such as phosphatidylethanolamine, phosphatidylserine and phosphatidylinositol have also been implicated in malignant conditions (Leach et al., 1998; Podo, 1999), an earlier report from our laboratory has shown the relevance of phosphatidylserine in *M. tuberculosis* and in intracranial tuberculomas using MR techniques (Gupta et al., 1996). Apart from the diacyl form glycerophosphatidylcholine, two other minor forms, such as 1-alkyl-2-acyl-glycerophosphatidylcholine and *lyso*-phosphatidylcholine have been assigned using ^{31}P NMR during the course of the present investigation. In a similar way, diacyl form of glycerophosphatidylethanolamine followed by its minor variants, such as 1-alkyl-2-acyl-glycerophosphatidylethanolamine and *lyso*-phatidylethanolamine could be assigned using ^{31}P NMR (fig. 11b).

The presence of ethanolamine plasmalogen in the tuberculoma lipid extracts, as observed during the course of the present investigation, may also assume diagnostic significance, since literature evidence had indicated a possible role of choline plasmalogen in certain forms of tumors (Albert, 1977). Among the reports that are available, the peroxyl-radical scavenging property of

plasmalogens (Hahnel et al., 1999), and the occurrence of ethanolamine plasmalogen in human erythrocyte lipid extracts (Adosraku et al., 1994) and in esophageal tumors (Merchant et al., 1999) may highlight the biological significance of plasmalogens. While the exact role of ethanolamine plasmalogen in the disease process could not be elucidated during the present study, the relatively higher abundance of glycerophosphatidylcholine and glycerophosphatidylethanolamine, as seen in ^{1}H and ^{31}P NMR, may give an indication that the tuberculomas belong to the proliferative class and thus may mimic tumors. The difference between proliferating tumors and tuberculomas is that the latter belong to the infectious granulomatous lesions, while tumors are not. As a result, and due to the overlapping clinical diagnostic features, it has become imperative to find out the tuberculoma specific markers, if any, in the patients. Although the conventional CT, MRI techniques and routine histopathological examinations have been reported to be helpful in differentiating tuberculomas from benign/malignant tumors and other CNS disorders, they are not very specific (Gupta et al., 1990; Gupta et al., 1999; Gupta et al., 2001). The detailed NMR analyses, as carried out in the present investigation, has been an attempt to help in the clinical diagnosis and/or the finger-printing of tuberculomas based on the lipid profile, as lipid components form an important aspect of cellularity.

The earlier observations from our laboratory had pointed out a possible role of phenolic glycolipids and cyclopropane-containing lipids (such as mycolates) as fingerprint diagnostic markers (Gupta et al., 1996), as these entities have been observed to be present as integral cell-wall components of *M. tuberculosis* (Besra and Chatterjee, 1996; Chatterjee, 1997). While cyclopropane-containing lipid entities could not be characterized during the present investigation using NMR, possibly due to very low abundance in the lipid extracts, it was possible to identify phenolic glycolipids in the ^{1}H NMR spectra (fig. 2b). Moreover, it could be stated that the free-form of cyclopropane, being gaseous/volatile (Subramanian et al., 2005), might have been lost during the lipid extraction process. On the other hand, as observed by Gupta et al. (1996), the presence of phenolic glycolipids in tuberculoma lipid extracts itself could be taken to indicate an intracranial infection due to *M. tuberculosis*, or in other words as a fingerprint marker for *M. tuberculosis*.

It could be stated that the possible diagnostic value of ^{1}H NMR spectral assignments of human tuberculoma samples in the present study involved the assignments of cholesterol, cholesterol ester, phenolic glycolipids and plasmalogen. As documented in literature, the steroids such as cholesterol are often found in association with lipids (cholesterol ester) during pathological conditions such as cancer, giving rise to abnormal levels of cholesterol ester in tumors (Nygren et al., 1997; Gebhard et al., 1987). Recent studies have documented the possible implications of cholesterol and its esterified form in various forms of CNS tumors, and have shown that the brain tissues of healthy individuals exhibited only cholesterol and not its esterified form (Tugnoli et al., 2001; Tosi et al., 2003; Tugnoli et al., 2003). The ratios of the levels of cholesterol and its esterified form have been found to vary depending upon the proliferative state of the tumor – most of the benign and low-grade tumors had a low cholesterol ester/cholesterol ratio, and in many cases no cholesterol ester was observed at all (Tosi et al., 2003), while highly malignant tumors showed a higher cholesterol ester/cholesterol ratio (Tugnoli et al., 2001; Tosi et al., 2003; Tugnoli et al., 2003). The relative levels of cholesterol ester and cholesterol, as observed during the course of the present investigation, may thus be considered important in understanding the development of tuberculomas in the brain. A comparative picture of cholesterol and its esterified form (identified as cholesterol oleate) in the ^{1}H NMR spectra of tuberculoma lipid extracts (fig. 12b) has indicated that the tuberculomas were of proliferative type with a relatively lower cholesterol ester/cholesterol ratio (Table-5), and hence could be different from benign or low-grade tumors in which cholesterol ester has been reported to be absent (Tosi et al., 2003).

Moreover, prominent vascularization and cytoplasmic lipid inclusions in the *Mycobacterium* infected macrophages might have contributed to the observed levels of cholesterol ester in case of tuberculomas, as has been related to proliferative processes in different experimental models of cell proliferation and in several types of human tumors (Batetta et al., 1999). Cholesterol is an important mediator of cell proliferation and differentiation, and therefore assumes biological importance in normal and tumor cells. An increase in the synthesis of cholesterol as well as its storage in the esterified form has been observed to be the mainstay of the proliferative processes (Batetta et al., 1999). The high growth rate of tumor-like formation, such as tuberculomas when infected with *M. tuberculosis*, demands a large amount of cholesterol that is

mainly supplied through the formation of cholesterol ester, possibly due to either an uptake of cholesterol ester (transported in plasma lipoproteins) from the blood by the infected macrophages or an endogenous conversion of cholesterol (Brown et al., 1980; Nygren et al., 1997).

The NMR investigations on tuberculoma lipid extracts have further highlighted the presence of phenolic glycolipids, besides cholesterol ester and ethanolamine plasmalogen. *Mycobacterium* species are known to possess various forms of phenolic glycolipids as the integral membrane structural components (Daffe and Servin, 1989; Watanabe et al., 1994), and may have a role in the inhibition of phagocytosis by the macrophages (Villeneuve et al., 2003). It could be reasoned that the granuloma formation by MTB infected macrophages in intracranial lesions might have resulted in the NMR observable levels of phenolic glycolipids (Gupta et al., 1996) that are constantly shed by the mycobacteria within the intracellular milieu of the host during infection (Paul and Beveridge, 1994). Phenolic glycolipids thus observed in the present study could be taken to represent the component of the cell wall of either living or dead mycobacteria in a granuloma.

Tissue destruction during the tuberculosis infection often leads to cheese-like necrotic tissue formation (caseation) due to the membrane rupture of MTB during phagocytosis, which is unique to tuberculomas. The diagnosis of tuberculomas through culture (for the demonstration of MTB in the tissue) is time consuming (6-8 weeks) and the histopathology aids only if caseating granuloma is observed (Bhargava et al., 1985); often it becomes difficult to distinguish tuberculomas from non-tuberculous granulomas. Since timely diagnosis after surgery and appropriate treatment is the cornerstone of management in intracranial tuberculomas, the present study has addressed the role of NMR as an additional diagnostic tool based on the analysis of lipid extracts.

6. Conclusions

The present study has brought out a speculation that the presence of cholesterol ester along with ethanolamine plasmalogen and phenolic glycolipids may aid in the identification of

intracranial tuberculomas more authentically, and could thus differentiate them from the benign/malignant tumors of the brain. It is proposed that the presence of cholesterol ester is not only significant in case of proliferating tumors, but also in infective tuberculous granulomas of the brain.

7. Future Scope of the Work

The work paves way for comparative NMR studies involving CNS tumors, tuberculomas and healthy brain tissues, so as to practically validate the role of NMR as a potential diagnostic tool in characterizing human intracranial tuberculomas due to *M. tuberculosis*.

References

Adosraku RK, Choi GTY, Kokotos VC, Anderson MM, Gibbons WA (1994) *J Lipid Res* 35:1925-1931.

Albert DH, Anderson CE (1977) *Lipids* 12:188-192.

Andersen P, Munk ME, Pollock JM, Doherty TM (2000) *Lancet* 356:1099-1104.

Bass JB, Farer LS, Hopewell PC, O'Brien R, Jacobs RF, Ruben F, Snider DE, Thornton G (1994) *Am J Respir Crit Care Med* 149:1359.

Bastian I, Stapledon R, Colebunders R (2003) *Curr Opin Pulmonary Med* 9:186-192.

Batetta B, Pani A, Putzolu M, Sanna F, Bonatesta R, Piras S, Spano O, Mulas MF, Dessi S (1999) *Cell Prolif* 32:49-61.

Beatty WL, Rhoades ER, Ullrich HJ, Chatterjee D, Heuser JE, Russell DG (2000) *Traffic* 1:235-247.

Bellete B, Coberly J, Barnes GL, Ko C, Chaisson RE, Comstock GW, Bishai WR (2002) *Clin Infect Dis* 34:1449-1456.

Bentrup KH, Russell DG (2001) *Trends Microbiol* 9:597-605.

Besra GS, Chatterjee D (1996) Lipids and carbohydrates of *Mycobacterium tuberculosis*. In *Tuberculosis: Pathogenesis, protection and control*. Ed, BR Bloom. Washington DC: ASM Press, pp 285-306.

Bhargava DK, Shrinivas, Chawla TC, Tandon BN, Kapur BML (1985) *J Trop Med Hygiene* 88:249-252.

Brady RO, Kanfer JN, Mock MB, Fredrickson DS (1966) *Proc Natl Acad Sci USA* 55:366-369.

Branca M, Culeddu N, Fruianu M, Serra MV (1995) *Anal Biochem* 232:1-6.

Brown MS, Ho YK, Goldstein JL (1980) *J Biol Chem* 255:9344-9352.

Caminero JA (2005) *Eur Respir J* 25:928-936.

Casu M, Anderson GJ, Choi G, Gibbons WA (1991) *Magn Reson Chem* 29:594-602.

Ceylan E, Gencer M (2005) *Tohoku J Exp Med* 205:367-370.

Chatterjee D (1997) *Curr Opin Chem Biol* 1:579-588.

Colditz GA, Brewer TF, Berkey CS, Wilson ME, Burdick E, Fineberg HV, Mosteller F (1994) *JAMA* 271:698-702.

Collins HL, Kaufmann SHE (2001) *Lancet Infect Dis* 1:21-28.

Comstock GW, Livesay VT, Woolpert SF (1974) *Am J Epidemiol* 99:131-138.

Corbett EL, Watt CJ, Walker N, Maher D, Williams BG, Raviglione MC, Dye C (2003) *Arch Intern Med* 163:1009-1021.

Cox JS, Chen B, McNeil M, Jacobs WR (1999) *Nature* 402:79-83.

Crampin AC, Floyd S, Mwaungulu F, Black G, Ndhlovu R, Mwaiyeghele E, Glynn JR, Warndorff DK, Fine PE (2001) *Int J Tuberc Lung Dis* 5:994-999.

Culeddu N, Bosco M, Toþanin R, Pollesello P (1998) *Magn Reson Chem* 36:907-912.

Daffe M, Servin P (1989) *Eur J Biochem* 185:157-162.

De Cock KM, Weiss HA (2000) *Trop Med Int Health* 5:A3-9.

Drobniewski FA, Caws M, Gibson A, Young D (2003) *Lancet Infect Dis* 3:141-147.

Dye C, Scheele S, Dolin P, Pathania V, Raviglione MC (1999) *JAMA* 282:677-686.

Ellner JJ, Hinman AR, Droley SW, Fischl MA, Sepkowitz KA, Goldberger MJ, Shinnick TM, Iseman MD, Jacobs WR (1993) *J Infect Dis* 168:535-537.

Ewer K, Deeks J, Alvarez L, Bryant G, Waller S, Andersen P, Monk P, Lalvani A (2003) *Lancet* 361:1168-1173.

Folch JS, Lees M, Stanley HS (1957) *J Biol Chem* 226:497-509.

Frieden TR, Sterling TR, Munsiff SS, Watt CJ, Dye C (2003) *Lancet* 362:887-899.

Gallant JE, Moore RD, Chaisson RE (1994) *Ann Intern Med* 120:932-944.

Gebhard RL, Clayman RV, Prigge WF, Figenshau R, Staley NA, Reesey C, Bear AJ (1987) *Lipid Res* 28:1177-1184.

Ginsburg AS, Grosset JH, Bishai WR (2003) *Lancet Infect Dis* 3:432-442.

Granich R, Wares F, Suvanand S, Chauhan LS (2003) *Lancet Infect Dis* 3:535.

Gunstone FD (1992) High resolution ^{1}H and ^{13}C NMR. In *Lipid analysis: A practical approach*. Eds, RJ Hamilton and S Hamilton. Oxford: OIRL Press, pp 243-262.

Gupta RK, Jena A, Sharma A, Guha DK, Khushu S, Gupta AK (1988) *J Comput Assist Tomogr* 12:280-285.

Gupta RK, Jena A, Singh AK, Sharma A, Puri V, Gupta M (1990) *Clin Radiol* 41:120-127.

Gupta RK, Poptani H, Kohli A, Chhabra DK, Sharma B, Gujral RB (1995) *Indian J Med Res* 101:19-24.

Gupta RK, Roy R, Dev R, Hussain M, Poptani H, Pandey R, Kishore J, Bhaduri AP (1996) *Magn Reson Med* 36:829-833.

Gupta RK, Kathuria MK, Pradhan S (1999) *AJNR Am J Neuroradiol* 20:867-875.

Gupta RK, Vatsal DK, Husain N, Chawla S, Prasad KN, Roy R, Kumar R, Jha D, Husain M (2001) *AJNR Am J Neuroradiol* 22:1503-1509.

Gupta RK, Husain M, Vatsal DK, Kumar R, Chawla S, Husain N (2002) *Magn Reson Imaging* 20:375-381.

Gupta RK, Prakash M, Mishra AM, Husain M, Prasad KN, Husain N (2005) *Eur J Radiol* 55:384-392.

Gurses N, Aydin M (1992) *Microbiyol Bul* 26:163-169.

Hahnel D, Beyer K, Engelmann B (1999) *Free Radic Biol Med* 27:1087-1094.

Hesseling AC, Schaaf HS, Gie RP, Starke JR, Beyers N (2002) *Int J Tuberc Lung Dis* 6: 1038-1045.

Holmback J, Karlsson AA, Arnoldsson KC (2001) *Lipids* 36:153-165.

Huebner RE, Schein MF, Bass JB (1993) *Clin Infect Dis* 17:968-975.

Iseman MD (2000) In *A clinician's guide to tuberculosis*. Philadelphia: Lippincott, Williams & Wilkins.

Kaminogo M, Ishimaru H, Morikawa M, Suzuki Y, Shibata S (2002) *Neurol Res* 24:537-543.

Karyadi E, West CE, Schultink W, et al. (2002) *Am J Clin Nutr* 75:720-727.

Kaufmann SHE (2000) *Nat Med* 6:955-960.

Khatri GR, Frieden TR (2000) *Int J Tuberc Lung Dis* 4:193-200.

Kriat M, Vion-Dury J, Confort-Gouny S, Favre R, Viout P, Sciaky M, Sari H, Cozzone PJ (1993) *J Lipid Res* 34:1009-1019.

Lane HC, Laughton BE, Falloon J, Kovacs JA, Davey RT, Polis MA, Masur H (1994) *Ann Intern Med* 120:945-955.

Leach MO, Verrill M, Glaholm J, Smith TAD, Collins DJ, Payne GS, Sharp JC, Ronen SM, McCready VR, Powles TJ, Smith IE (1998) *NMR Biomed* 11:314-340.

Ledwozyw A, Lutnicki K (1992) *Acta Physiol Hung* 79:381-387.

Lee E, Holzman RS (2002) *Clin Infect Dis* 34:365-370.

Lehnhardt FG, Rohn G, Ernestus RI, Grune M, Hoehn M (2001) *NMR Biomed* 14:307-317.

Lima VM, Bonato VL, Lima KM, Dos Santos SA, Dos Santos RR, Goncalves ED, Faccioli LH, Brandao IT, Rodrigues-Junior JM, Silva CL (2001) *Infect Immun* 69:5305-5312.

Lutz NW, Tome ME, Aiken NR, Briehl MM (2002) *NMR Biomed* 15:356-366.

Mazurek GH, LoBue PA, Daley CL, Bernardo J, Lardizabal AA, Bishai WR, Iademarco MF, Rothel JS (2001) *JAMA* 286:1740-1747.

Mazurek GH, Villarini ME (2003) *MMWR Morb Mortal Wkly Rep* 52:15-18.

Meneses P, Glonek T (1988) *J Lipid Res* 29:679-689.

Merchant TE, Minsky BD, Lauwers GY, Diamantis PM, Haida T, Glonek T (1999) *NMR Biomed* 12:184-188.

Metz KR, Dunphy LK (1996) *J Lipid Res* 37:2251-2265.

Moesgaard B, Jerzy W, Jaroszewski, Hansen HS (1999) *J Lipid Res* 40:515-521.

Nygren C, Von'Holst H, Mansson JE, Fredman P (1997) *Br J Neurosurg* 11:216-220.

O'Brien RJ, Nunn PP (2001) *Am J Respir Crit Care Med* 163:1055-1058.

Paul TR, Beveridge TJ (1994) *Infect Immunol* 62:1542-1550.

Pieters J, Gatfield J (2002) *Trends Microbiol* 10:142-146.

Podo F (1999) *NMR Biomed* 12:413-439.

Pollesello P, Eriksson O, Hockerstedt K (1996) *Anal Biochem* 236:41-48.

Poonnoose SI, Singh S, Rajshekhar V (2004) *Neuroradiology* 46:136-139.

Poptani H, Gupta RK, Roy R, Pandey R, Jain VK, Chhabra DK (1995) *AJNR Am J Neuroradiol* 16:1593-1603.

Raviglione MC, Snider DE, Kochi A (1995) *JAMA* 273:220-226.

Rieder HL, Snider DE, Cauthen GM (1990) *Am Rev Respir Dis* 141:347-351.

Riley RL, Mills CC, Nyka W, Weinstock N, Storey PB, Sultan LU, Riley MC, Wells WF (1959) *Am J Hygiene* 70:185-196.

Schiller J, Arnold K (2002) *Med Sci Monit* 8:MT205-222.

Schluger NW, Rom WN (1998) *Am J Respir Crit Care Med* 157:679-691.

Schutte CM, Meyslen VCH, Labuscague JH, Olta D (1996) *Tubercle and Lung Dis* 77:285-286.

Shafer RW, Edlin BR (1996) *Clin Infect Dis* 22:683-704.

Shaka AJ, Barker PB, Freeman R (1985) *J Magn Reson* 64:547-552.

Sharma DC (2003) *Lancet Infect Dis* 3:265.

Sharma SK, Mohan A, Kadhiravan T (2005) *Indian J Med Res* 121:550-567.

Singer S, Sivaraja M, Souza K, Millis K, Corson JM (1996) *J Clin Invest* 98:244-250.

Sonnewald U, Westergaard N, Isern E, Muller TB, Schousboe A, Petersen SB, Unsgard G (1993) *Int J Oncol* 2:545-555.

Sparling ML, Zidovetzki R, Muller L, Chan SI (1989) *Anal Biochem* 178:67-76.

Stewart ME, Downing DT (2001) *J Lipid Res* 42:1105-1110.

Subramanian A, Gupta A, Saxena S, Gupta A, Kumar R, Nigam A, Kumar R, Mandal SK, Roy R (2005) *NMR Biomed* 18:213-225.

Sullentrop F, Moka D, Neubauer S, Haupt G, Engelmann U, Hahn J, Schicha H (2002) *NMR Biomed* 15:60-68.

Sutherland I (1976) *Adv Tuberc Res* 19:1-63.

Sze DY, Jardetzky O (1990) *BBA* 1054:198-206.

Ted C, Sommers B, Murray M (2003) *Lancet Infect Dis* 3:13-21.

Tewary RK, O'Sullivan MG, Ali TA, O'Sullivan PG (2005) *J Laryngol Otol* 119:486-488.

Tosi MR, Bottura G, Lucchi P, Reggiani A, Trinchero A, Tugnoli V (2003) *Int J Mol Med* 11:95-98.

Tosi MR, Fini G, Tinti A, Reggiani A, Tugnoli V (2002) *Int J Mol Med* 9:299-310.

Tosi MR, Ricci R, Buttura G, Tugnoli V (2001) *Oncol Rep* 8:1337-1339.

Tugnoli V, Bottura G, Fini G, Reggiani A, Tinti A, Trinchero A, Tosi MR (2003) *Biopolymers* 72:86-95.

Tugnoli V, Tosi MR, Tinti A, Trinchero A, Bottura G, Fini G (2001) *Biopolymers* 62:297-306.

Tyagi RK, Azrad A, Degani H, Salomon Y (1996) *Magn Reson Med* 35:194-200.

Villeneuve C, Etienne G, Abadie V, Montrozier H, Bordier C, Laval F, Daffe M, Parini IM, Dequeker CA (2003) *J Biol Chem* 278:51291-51300.

Wasay M, Kheleani BA, Moolani MK, Zaheer J, Pui M, Hasan S, Muzaffar S, Bakshi R, Sarawari AR (2003) *J Neuroimaging* 13:240-247.

Watanabe M, Yamade Y, Iguchi K, Minnikin DE (1994) *BBA* 1210:174-180.

WHO Report (2001) In *Global tuberculosis control: WHO report 2000*. Geneva: World Health Organization.

WHO Report (2003) In *Global tuberculosis control: surveillance, planning, financing (WHO/CDS/TB/2003.316)*. Geneva: World Health Organization.

Wilkinson RJ, Llewelyn M, Toossi Z, Patel P, Pasvol G, Lalvani A, Wright D, Latif M, Davidson RN (2000) *Lancet* 355:618-621.

Willker W, Leibfritz D (1998) *Magn Reson Chem* 36:S79-S84.

Yaramis A, Gurkan F, Elevli M, Soker M, Haspolat K, Kirbas G, Tas MA (1998) *Pediatrics* 102:E49.

Yoshioka Y, Sasaki J, Yamamoto M, Saitoh K, Nakaya S, Kubokawa M (2000) *NMR Biomed* 13:377-383.

Zumla A, Grange JM (2001) *Lancet Infect Dis* 1:199-202.

Chapter 5:

NMR Structural Aspects In Meningitis

1. Introduction

Meningitis is a severe acute infectious disease caused by several microorganisms, including viruses, bacteria, parasites and fungi, and is one of the most devastating infectious diseases of childhood in developing as well as in underdeveloped countries (Avery and First, 1994). Infection of the meninges, the membranes that surround the brain and spinal cord, is called meningitis, while encephalitis refers to the inflammation of the brain. The entire central nervous system (the brain and spinal medulla) is enclosed in three membranes or meninges (the dura mater, the arachnoid, and the pia mater), which are separated from each other by two spaces (the subdural and subarachnoid spaces) containing fluid.

The clear fluid called as cerebrospinal fluid (CSF) that bathes the brain and spinal medulla through these membranes, is mainly derived from special vascular tufts (choroid plexuses) in the cavities of the brain (ventricles) from which it escapes into the subarachnoid space. In addition to the metabolic and transport functions, it forms a protective water bath around the brain and spinal medulla, and when this CSF is infected, it causes meningitis. Meningitis causes an intense headache, fever, loss of appetite, and intolerance to light and sound, rigidity of muscles especially those in the neck, and in severe cases convulsions, vomiting, and delirium finally leading to death if not properly diagnosed and treated. It is one of the major causes of childhood mortality, morbidity and disability.

The statistical features regarding the incidence of this disease are still alarming. Fatality rates associated with this disease can be as low as 2% in infants and children, and as high as 20-30% in neonates and adults (Saez'Llorens and McCracken, 1990). A steady rise in the incidence of meningitis worldwide has recently been reported (Jodar et al., 2002). Despite the availability of several therapies, the three most common forms of meningitis, *viz*., bacterial meningitis (Singhi and Singhi, 1995; Tunkel and Scheld, 1995; Behrman, 1996; McCracken, 2002; Saez'Llorens and McCracken, 2003), tuberculous meningitis (Singhi and Singhi, 1995; Upadyaya et al., 1984; Walia and Hoskyns, 2000; Narain et al., 2000) and viral meningitis (Maxson and Jacobs, 1993; O'Meara and Ouvrier, 1996; Panagariya et al., 2001; Whitley and Gnann, 2002; Chadwick, 2005) continue

to be potentially fatal illnesses that can lead to death or permanent neurological sequelae in the child if not diagnosed at an early stage. Bacterial meningitis (BM) occurs in about 70% of children less than 5 years of age (Avery and First, 1994) with a peak incidence between 1 month to 5 years of age (Behrman, 1996), and accounts for 3-4% of hospital admissions in India. Tuberculous meningitis (TBM) accounts for 1-4% of total childhood hospital admissions in various parts of India (Upadyaya et al., 1984). The incidence of Viral meningitis (VM) in India is not known largely due to problems in establishing a viral diagnosis and the fact that a wide variety of central nervous system disorders may mimic the illness (Panagariya et al., 2001; Kabilan, 2004).

The outcome of meningitis is strongly associated with the stage of disease presentation, with a 100% cure rate if proper diagnosis and treatment are given; otherwise it leads to 50% mortality or 80% permanent handicap. Infants and children who survive bacterial meningitis are more likely to have seizures, hearing deficits, learning and behavioural problems, and lower intelligence compared with their healthy siblings who have not had meningitis thus calling for an adequate diagnostic technique followed by a timely treatment (Saez'Llorens and McCracken, 2003). Transient or permanent deafness, or other neurological sequelae, arise in up to a third of survivors (Neuman and Wald, 2001). Unfortunately, because of limited economic resources and poor living conditions, many developing countries are still affected by the devastating consequences of this life-threatening systemic infection.

A definitive diagnosis of meningitis is dependent on examination and culture of CSF, and if meningitis is suspected to be present, usually a lumbar puncture is undertaken. Indications for needle puncture of a subdural effusion include a clinical suspicion that empyema is present (prolonged fever and irritability, stiff neck coupled with CSF leukocytosis), a rapidly enlarging head circumference in a child without hydrocephalus, focal neurological findings, and evidence of increased intracranial pressure. In neonates, the procedure should be considered when sepsis is suspected, because meningitis accompanies sepsis in 20-25% of cases. In infants, fever and convulsions may be the only initial signs of meningitis. In rare instances, especially very early in the illness, the cell count can be normal despite a positive CSF culture. A glucose concentration of less than 200 mg/L in CSF is associated with a higher rate of hearing impairment. When focal

neurological signs are present, the use of cranial CT or magnetic resonance imaging is often undertaken before the lumbar puncture, to exclude a brain abscess or generalized cerebral edema, and to avoid the danger of herniation.

1.1. Incidence of Bacterial Meningitis

From its first description by Vieusseux in 1806 up to the early 20th century, acute BM has been uniformly considered to be a fatal disease (Koedel et al., 2002). BM is a serious threat to global health, accounting for an estimated 1,71,000 deaths worldwide per year (Jodar et al., 2002). At least 1.2 million cases of BM are estimated to occur each year, out of which 1,35,000 of them are fatal (WHO Report, 1998). These numbers have made BM a top-ten infectious cause of death worldwide (Koedel et al., 2002). Even with antimicrobial therapy and the availability of advanced intensive care, case fatality rates are 5-10% in industrialised countries (Laurichesse et al., 1998; Venetz et al., 1998), and are even higher in the developing world (Campagne et al., 1999). Between 10% and 20% of survivors develop permanent sequelae, such as epilepsy, mental retardation, or sensorineural deafness (Smith et al., 1988; Kirsch et al., 1996). Acute BM is caused by a variety of infectious agents, and the most common ones are *Haemophilus influenzae* type B, *Streptococcus pneumoniae*, *Neisseria meningitidis* and *Listeria monocytogenes*, and generally the first three species – *Haemophilus influenzae*, *Streptococcus pneumoniae* and *Neisseria meningitidis* – account for most cases of BM occurring after the neonatal period (Jodar et al., 2002). Although the introduction of sulfonamides and penicillins made BM curable, mortality and morbidity from the disease remain unacceptably high (Schuchat et al., 1997).

The clinical outcome of acute BM varies according to socio-economic aspects (developed- or developing-countries), age, and the causative pathogen (Hoen et al., 1993). In developed countries, *S. pneumoniae* meningitis has the highest case-fatality rate (about 20%) for community-acquired meningitis (Schuchat et al., 1997). Of the survivors, up to 30% develop long-term sequelae including hearing loss, neurological deficits, and neuropsychological impairment (Van De'Beek et al., 2002). In developing countries mortality and morbidity rates are dramatically higher than in industrialized countries. About 50% of children with pneumococcal meningitis die while in hospital and up to 60% of survivors have clinical sequelae (Goetghebuer et al., 2000),

whereas the mortality and morbidity rates of this age group in industrialized countries are about 10% and 30%, respectively (Arditi et al., 1998).

Neuropathological and clinical studies have shown that a fatal outcome of the disease is often due to central nervous system (CNS) complications including cerebrovascular involvement, brain oedema formation, and hydrocephalus resulting in increased intracranial pressure and seizure activity. It has been observed that the host defense mechanisms within the brain are notably ineffective in eliminating major meningitis pathogens, and that the inflammatory reaction to the pathogen, rather than the pathogen itself, is largely responsible for the damage that results from BM (Pfister and Scheld, 1997). The spectrum of causes of deaths attributed to BM is known to be broad (McMillan et al., 2001), ranging from systemic (e.g., septic shock) to several neurological complications (e.g., brain edema, hydrocephalus, cerebrovascular involvement, and intractable seizures).

The clinical picture of acute bacterial meningitis mainly depends on the patient's age. In general, the younger the patient, the more subtle and atypical are the signs and symptoms (Saez'Llorens and McCracken, 2003). Classic meningitis of children and adults usually begins with fever, chills, vomiting, photophobia, and severe headache. Occasionally, the first sign of illness is a convulsion that can recur during progression of the disease. Irritability, delirium, drowsiness, lethargy, neck rigidity and coma can also develop. These signs and symptoms are common to all types of meningitis (Kaplan, 1999). Other manifestations, however, are associated with specific infections. Petechial and purpuric eruptions are usually indicative of meningococcaemia, although they can be present in *H. influenzae* meningitis. Rashes very rarely occur with pneumococcal infections. Implication of the joints suggests infection with meningococci or *H. influenzae*, and can arise early (suppurative arthritis) or late (reactive arthritis) in the illness. The presence of a chronically draining ear or a history of head trauma with or without skull fracture is most likely to be associated with pneumococcal meningitis. Some patients with BM may not present with the classic symptoms or signs. Neonates, as well as infants, may present with a change in affect or state of alertness, temperature instability (hypothermia or hyperthermia), listlessness, high-pitched crying, fretfulness, lethargy, refusal to

feed, weak suck, irritability, jaundice, vomiting, diarrhoea, or respiratory distress (Tunkel and Scheld, 1995).

Complications of acute BM can develop early in the course of illness, either before diagnosis or several days after starting treatment. Profound shock usually develops early in the course of the illness and, if untreated, progresses rapidly to a fatal outcome. In some patients, treatment with antibiotics can initially aggravate these systemic problems, probably as a result of release of active components such as endotoxin from the cell walls or membranes of rapidly lysed microorganisms (Saez'Llorens et al., 1990). Focal neurological findings such as hemiparesis, quadriparesis, facial palsy, and visual field defects arise early or late in about 10-15% of patients with meningitis, and can correlate with persistent neurological abnormalities (Kaplan, 1999). Presence of focal signs can be associated with cortical necrosis, occlusive vasculitis, or thrombosis of the cortical veins. Inflammation of the cochlear aqueduct and the auditory nerve can lead to reversible or permanent deafness in 5-30% of patients (Auslander and Meskan, 1988). Hydrocephalus, of either the communicating or obstructive type, is occasionally seen in patients in whom treatment has been either sub-optimal or delayed, arising more often in younger infants. Joints can be affected initially or during the course of BM; early occurrence suggests direct invasion of the joint by the microorganism, usually *H. influenzae* type-B, whereas arthritis that develops after the fourth day of treatment is thought to be an immunecomplex-mediated event that affects several joints, and is most frequently seen with meningococcal infections (Kaplan, 1999). Concentrations of glucose and protein in CSF usually remain abnormal for several days despite effective treatment in BM. The amount of bacteria or their products correlates with an increased host production of inflammatory mediators such as tumor necrosis factor, interleukin-1, and prostaglandins. The greater the host's inflammatory response in the subarachnoid space to the microorganism and its products, the greater is the likelihood of permanent sequelae.

1.2. Incidence of Tuberculous Meningitis

TBM or CNS tuberculosis continues to be a medical emergency, which carries significant morbidity and mortality (Farinha et al., 2000). Two of the most severe manifestations of tuberculosis (TB), namely, miliary disease and tuberculous meningitis (TBM) are significantly more common in children (Walls and Shingadia, 2004), and among these two, the highest

mortality and morbidity occurs with TBM (Kumar et al., 1997). TBM is a potentially fatal form of extrapulmonary TB with serious long-term consequences. Studies from developing countries have reported fatality rates as high as 44-69% (Hosoglu et al., 1998). The post-HIV era has further complicated the situation, often resulting in devastating consequences making the diagnosis difficult (Narain et al., 2000; Berenguer et al., 1992). Early and accurate diagnosis has thus become crucial for preventing morbidity and mortality due to TBM. Meningitis is the most feared complication of TB in children, particularly due to neurological sequelae including blindness, deafness, intracranial calcification, diabetes incipidus and mental retardation. It usually occurs within 3-6 months of initial infection and is most common in the younger children (0-4 years of age) accounting for 80% of meningitis cases (Lobato et al., 1998).

It many instances, the presenting clinical features of TBM in children are similar to those of other meningoencephalitides, which result in frequent diagnostic confusion. The most frequent presenting signs were alterations in consciousness and the presence of focal neurological signs, although these may overlap with other types of meningitis. The CT scan of the head in TBM typically shows hydrocephalus, and basilar enhancement when contrast is given (Kingsley et al., 1987); the incidence of hydrocephalus increases with the duration of illness (Bhargava et al., 1982). Diagnostic uncertainty arises commonly in patients who present with a few days of headache, fever, photophobia and neck-stiffness; undefined treatment in the community; a low concentration of glucose in cerebrospinal fluid, and neutrophils and lymphocytes in the cerebrospinal fluid (Thwaites et al., 2002).

CNS TB is usually characterized by fever, headache, drowsiness, meningism, and confusion over a period of approximately 2-3 weeks, and other non-specific symptoms such as fatigue, malaise and myalgia. Tremor is the most common movement disorder seen in the course of TBM. In a smaller percentage of patients, abnormal movements have been observed, more so in children than in adults. As per a recent study, the main clinical symptoms and signs observed in 38 children with TBM on admission were alteration in consciousness in 30 patients (79%), focal neurological signs in 25 (66%) and fever in 25 (66%). Seizures were observed in 20 patients (53%) and meningism in 18 (47%). The overall mortality of patients was 13%, while permanent neurological sequelae were observed in 47% of the patients (Farinha et al., 2000).

1.3. Incidence of Viral Meningitis

Similar to BM and TBM, inflammation of the brain due to invasion by a viral agent is an important cause of death and permanent neurological disability in children and adults (Bale, 1993). Viral infections of the CNS, such as *Herpes simplex* encephalitis (HSE) and arthropod-borne encephalitis cause some of the most severe and feared diseases in children (Griffin and Hardwick, 1999). Encephalitis is a term that theoretically applies for any inflammatory condition involving the brain. VM and Viral encephalitis (VE) are overlapping syndromes, some viruses predominantly producing a picture of encephalitis and others that of meningitis. VM and VE are usually caused by enteroviruses, which are present in mucus, saliva, and feces and can be transmitted through direct contact with an infected person or an infected object or surface. Other viruses that cause meningitis include *Varicella zoster* (the virus that causes chicken pox and can appear decades later as shingles), influenza, mumps, HIV, and *Herpes simplex* type 2 (genital herpes) as well as other incidental nervous system pathogens such as orthomyxo viruses, paramyxo viruses and adeno viruses. Encephalitis due to *Herpes simplex* virus type 1 can affect any age group but is most often seen in persons under age 20 or over age 40.

Several thousand cases of encephalitis are reported each year, but many more may actually occur since the symptoms may be mild to non-existent in most patients. Most cases of encephalitis in the USA are caused by enteroviruses, *Herpes simplex* virus types 1 and 2, a bite from a rabid animal (rabies virus), or arboviruses, which are transmitted from infected animals to humans through the bite of an infected tick, mosquito, or other blood-sucking insect. Besides VE, VM is the most common form of meningitis in the USA. About 1000-2000 cases of VE/VM are reported to the Center for Disease Control, Atlanta annually (Bale, 1993). HSE is responsible for about 10 percent of all encephalitis cases, with a frequency of about 2 cases per million persons per year. About 30 percent of cases result from the initial infection with the *Herpes simplex* virus; the majority of cases are caused by reactivation of an earlier infection. Several factors such as age, geographical location, season, climate and host immunocompetence affect the epidemiology of VE. Arboviruses are known for their diverse geographical distributions, influenced by the activity of their insect vectors. HSE tends to occur sporadically worldwide with little seasonal

variation (Whitley, 1990). Mumps and measles encephalitis have been largely eradicated from many developed countries due to vaccination, as has rabies (Bale, 1993).

In Indian scenario, the prevalence of VM/VE may vary from region to region and also depending upon the diagnostic workup. The paucity of data stems from the fact that a wide variety of agents can cause encephalitis and also virological investigations are complex, expensive and time-consuming, and are largely not available across the country (Kumar, 1999; Kumar et al., 1990; Kabilan, 2004). Japanese encephalitis (JE) is probably the commonest form of VE in India, and occurs in epidemics over large parts of the country (Kumar et al., 1993; Kumar et al., 1991). Rabies is another form of viral encephalitis, which poses a public health problem in the country and elsewhere (Kumar, 1999; Rupprecht et al., 2002). In almost all forms of VM/VE, the symptoms are noticed within 7-10 days, and may include headache with increasing severity, sudden fever, nausea, vomiting, general flu-like muscle pains, confusion, partial paralysis, seizure, and coma. Permanent neurological damage with or without signs of meningeal irritation occurs in about half of all cases, and death in about 10-15 percent of all cases. Children under age 16, particularly those under 12 months of age, are affected more severely than adults and may have permanent neurologic damage. In immunocompromized patients the VM/VE follow a chronic course and present with cognitive signs and mental alterations progressing to dementia over months, rather than with focal neurological deficits. They may also follow a chronic course independently of the immune status of the patients. Examples include subacute sclerosing panencephalitis, a disease caused by a defective measles virus and occurring several years after measles infection, and progressive rubella panencephalitis a similar disease caused by rubella virus.

VM and VE are often dramatic in their rapid onset and progression to coma or paralysis and death (Kabilan et al., 2000). Similar to other common forms of meningitis, in those who survive, permanent neurological deficits, such as mental retardation, paralysis and Parkinsonism, are often the residua of infection (Huy et al., 1994; Chadwick, 2005). For each of these virus-induced diseases, neurons are the primary cells that are infected in the CNS. There is considerable evidence that both fatal disease and long-term sequelae in those who survive are caused by virus-induced death of neurons; for example, polio virus infects motor neurons, causing paralysis,

Herpes simplex virus infects temporal lobe neurons, causing seizures and changes in personality, and Japanese encephalitis virus often targets basal ganglia neurons, causing Parkinsonism symptoms. Altered consciousness is a prominent finding and reflects the inflammation of the cerebral parenchyma and induction of cerebral edema either by the agent itself or by the host response (Bale, 1993). Severe cases may be associated with life-threatening rise in intracranial tension, decerebration or flaccid coma. Typically this stage lasts for 7-10 days after which there is gradual recovery with or without sequelae (Cherry, 1993).

1.4. Diagnosis of Bacterial Meningitis in Children

It has been reported that the diagnosis of acute BM in children is difficult (Berkley et al., 2001). First, the clinical features are not specific, especially in young children. In regions such as sub-Saharan Africa there is also substantial overlap in the clinical features of acute BM and malaria (Molyneux et al., 1998). Second, there is no gold-standard laboratory test. CSF culture is specific but lacks sensitivity, especially when antibiotics have been given before the lumbar puncture is done. In many instances, antimicrobial therapy must be started empirically because no causative agent can be identified in advance. Conventional diagnostic methods for BM are frequently not rapid or sensitive enough to guide initial antimicrobial therapy. Examination of CSF for glucose, protein, cells, and organisms is necessary for accurate diagnosis, but in many parts of the world facilities do not exist to do so. Reagent strips that measure glucose and protein concentrations in blood or urine have been used to evaluate CSF with varying results (Muller and Donald, 1987; Moosa et al., 1995). Incidentally, the sensitivities of current bacterial antigen tests in CSF samples vary from 50% to 100% dependent on the commercial assays used and the organisms studied (Gray and Fedorko, 1992). Despite the limitations, a rapid antigen test in the CSF and urine of patients with suspected BM was proposed, and was found to be highly sensitive and specific for the detection of pneumococci (Marcos et al., 2001).

The diagnosis of BM is usually based on examination of CSF (Feigin et al., 1992). Examination of the CSF of a patient with acute BM characteristically reveals a cloudy fluid, consisting of an increased white blood cell count and predominance of polymorphonuclear leucocytes, a low glucose concentration in relation to serum value, a raised concentration of protein, and a positive stained smear and culture for the causative microorganism (Klein et al.,

1986). The CSF white cell count is usually in the range 1000-5000/μl with a neutrophilic predominance. About 10% of patients with acute BM present with a lymphocytic predominance, this pattern being seen more often in the newborn with gram-negative bacillary meningitis and in patients with *L. monocytogenes* meningitis. Patients with very low CSF white cell counts (0-20/μl) despite high CSF bacterial concentrations tend to have a poor prognosis. A decreased CSF glucose (below 40 mg/dl) is found in 60% of patients, and the CSF:serum glucose ratio is below 0.31 in 70% of cases (Marton and Gean, 1986). The CSF protein is raised (100-500 mg/dl) in virtually all patients with BM (Tunkel and Scheld, 1995).

The CSF Gram stain is positive in 60-90% of cases of acute BM, and has a specificity of nearly 100%. However, the probability of detecting the organism by Gram stain may decrease to 40-60% in patients who have already been given an antibiotic, and the yield of CSF cultures similarly falls to below 50% from 70-85% (Tunkel and Scheld, 1995). In patients whose CSF protein, glucose, and cell count pattern is consistent with acute BM but whose CSF Gram stain is negative, a latex agglutination test is used to detect the bacterial antigen in CSF (Gray and Fedorko, 1992). Currently available tests detect *H. influenzae* type B, *S. pneumoniae*, *N. meningitidis*, *E. coli* K1, and *S. agalactiae*. Although the sensitivity of latex agglutination test ranges from 50% to 100%, with a high specificity, a negative test never rules out meningitis caused by a specific meningeal pathogen (Tunkel and Scheld, 1995). The polymerase chain reaction (PCR) has been used to amplify DNA from patients with meningococcal meningitis (Ni et al., 1992), but further refinements are needed to confirm the usefulness of this technique in patients with BM in whom the CSF Gram stain, bacterial antigen tests, and culture are negative.

1.5. Diagnosis of Tuberculous Meningitis in Children

It has been reported that the diagnosis of TBM is difficult (Thwaites et al., 2002). Conventional tests are not always helpful in making a diagnosis of TBM (Pai et al., 2003). Discrimination of cases from those of BM by clinical features alone is often impossible, and current laboratory methods remain inadequate or inaccessible in many developing countries. Delays in diagnosis and treatment have been regarded as the major contributing factors for high mortality in TBM (Hosoglu et al., 1998). However, about 30% of patients with TBM die despite

anti-tuberculosis chemotherapy (Thwaites et al., 2000). Because of the non-specific clinical features, and the deadly consequences of a missed diagnosis, accurate, early confirmation of diagnosis is an essential component in the management of TBM. Furthermore, there are potentially serious side-effects as well as costs associated with the treatment of patients incorrectly diagnosed (Pai et al., 2003).

The diagnostic workup for TBM involves detection of acid-fast bacilli (AFB) in the CSF by microscopy (smear) and culture. The sensitivity of acid-fast staining and TB culture of CSF is directly dependent on the number and volume of CSF samples examined (Farinha et al., 2000). Direct Ziehl-Neelsen (ZN) staining of the CSF for acid-fast bacilli remains the cornerstone of rapid diagnosis, but this technique lacks sensitivity (Thwaites et al., 2000). These conventional tests are often unhelpful in making the diagnosis since TBM is a paucibacillary form of TB. Microscopy, although rapid and inexpensive, has very low sensitivity (10-20%) (Thwaites et al., 2002; Thwaites et al., 2000). Culture, another established method, is not very sensitive (<50%) to aid clinical decision-making, and results are not available for weeks (Thwaites et al., 2002; Thwaites et al., 2000). Further, a diagnosis of TBM cannot be made nor excluded on the basis of clinical features (Thwaites et al., 2002; Thwaites et al., 2000). There is some evidence that a combination of clinical data (age, duration of history) and simple laboratory data (white blood cell count, total CSF white cell count, and CSF neutrophil proportion) might help in the diagnosis of adult tuberculous meningitis (Thwaites et al., 2002).

In developed countries such as USA, nucleic acid amplification (NAA) tests have emerged with the intended goal of enabling clinicians to make a rapid and accurate diagnosis of TBM. But the newer diagnostic techniques based on PCR have not been assessed completely (Pfyffer, 1999), and are not possible in most settings in the developing world where most cases of TBM are seen (Foulds and O'Brien, 1998). Although it has been found that all NAA tests amplify target nucleic acid regions that uniquely identify the *Mycobacterium tuberculosis* complex in a rapid manner (about 3-6 h from receipt of specimen) (Pai et al., 2003), they are expensive for a wide use in many developing countries. Consequently, the decision to treat a patient for TBM is frequently empirical, irrespective of the diagnostic facilities available to clinicians (Thwaites et al., 2002).

The routinely used criteria for the diagnosis of TBM are (Farinha et al., 2000): (a). The presence of increased lymphocytes (>10/mm^3) in the CSF, with high protein (>40 mg/dl) and low CSF/serum glucose ratios (<0.6); (b). Positive culture of CSF or other body fluids or tissues for *Mycobacterium tuberculosis*; (c). Positive microscopy for AFB from CSF, gastric aspirate, sputum or sterile body tissue (ZN stain); (d). Positive Mantoux reaction; (e). Epidemiological evidence of TB contact, e.g., close family member with active tuberculous disease, and (f). Response to anti-tuberculous therapy.

1.6. Diagnosis of Viral Meningitis in Children

VM in children is often suspected to arise due to an enterovirus (EV) (Chadwick, 2005). The typical presentation of enteroviral meningitis in children is with vomiting, anorexia, rash or respiratory symptoms as well as meningism, often preceded by flu-like symptoms and a sore throat (Dagan et al., 1988). The clinical and CSF picture can be confusing, but a diagnosis can be made based on the detection of EV RNA by PCR in the CSF (Jeffery et al., 1997). Even in advanced centers, viral diagnosis has been possible in only a small proportion of clinically suspected cases (Xu et al., 1996). Electroencephalography (EEG) is used to diagnose some of the neurological manifestations seen in specific CNS viral infections, such as HSE (Panagariya et al., 2001). Confirmation of HSE is also carried out by the demonstration of Immunoglobulin-M (IgM) and Immunoglobulin-G (IgG) in CSF and serum (Kennedy, 1995; Kumar, 2005). Further, the confirmation of VM/VE has been carried out using routine CSF analysis, EEG, CT scan and MRI, besides the determination of specific viral antibody estimation in CSF and blood using ELISA (Panagariya et al., 2001).

Pronounced occurrence of symptoms such as altered sensorium and seizures are commonly seen in viral meningitis (80-100%). In the acute stage, blood counts usually reveal a polymorphonuclear leucocytosis. Examination of CSF may show a pleocytosis of up to 1000 cells per cmm, which can be either predominantly lymphocytic or polymorphonuclear, with slightly raised protein and normal sugar level. It was reported that CSF pleocytosis occurred in only half of patients with clinically suspected encephalitis (Kennedy, 1995). EEG findings are seldom specific except in HSE, and cranial CT is often normal or may show diffuse low attenuation, but

may show specific abnormalities in HSE (Misra and Kalita, 1998; Panagariya et al., 2001; Tyler, 2004).

The diagnostic workup in VM/VE usually includes a viral culture in appropriate transport media of respiratory secretions, throat swab, CSF, blood, urine and stool taken as early as possible during the illness (Kennedy, 1995; Kumar, 2005). Like in other forms of meningitis, PCR provides a rapid, accurate diagnosis of a host of viral pathogens. Measurement of interferon-α levels in CSF provides evidence of active viral infection in the CNS but this test is not widely available (Kumar, 2005). Specific IgG ratios in serum and CSF can be used to identify infection with specific viruses (Kennedy, 1995). Once VM is diagnosed, the patient is usually treated with an antiviral drug such as acyclovir. Like other forms of meningitis, mortality rate becomes higher if proper diagnosis is not carried out and if the treatment is delayed, or the presentation of the disease itself is in a severe form (Chadwick, 2005). It has been found that delayed treatment even in less severe cases produced neurological deficit in many survivors (Panagariya et al., 2001).

2. Statement of Problem

The cornerstone of management of meningitis in children depends on the rapid diagnosis and prompt treatment; however, the differential diagnosis of meningitis in children has been reported to be difficult due to various non-specific clinical features (Tunkel and Scheld, 1995; Upadyaya et al., 1984; Maxson and Jacobs, 1993). The outlook in individual patients with meningitis is correlated with many factors, including age of patient, time and clinical stability before effective treatment is begun, type of microorganism, quantity of active bacterial or viral products in CSF at the time of diagnosis, and intensity of the host's inflammatory response (Saez'Llorens and McCracken, 2003), but for this a definitive diagnosis is essential. In this direction, the diagnosis of meningitis using CSF analysis, reagent strips (Moosa, 1995), CT (Jinkins, 1991) and MRI (Pagliano, 2001; Pui and Memon, 2001) have been quite straightforward – often the diagnosis of meningitis is trivial with these techniques, but not differential diagnosis. The gold-standard culture method is usually insensitive if antibiotic treatment has already started, and it often takes a period of 6-8 weeks to confirm the tubercle bacilli. The timely treatment is

usually based on clinical symptoms and a baseline test of the CSF. Although microscopic examination is one of the best methods, it lacks sensitivity in case of TBM (Kennedy and Fallon, 1979). Due to non-specific differential diagnosis, about 50% of the patients in the present study received both antibiotics and anti-tubercular treatment (ATT) in the local hospitals at Lucknow (King George's Medical University; Sanjay Gandhi Post-Graduate Institute of Medical Sciences), where the ATT regimen was mainly a combination of pyrazinamide, ethambutol, rifampicin and isoniazid, and common antibiotics such as ampicillin, vancomycin and cephalosporins such as cefotaxime and ceftriaxone were administered.

Several new methodologies and techniques have been developed over the course of time such as the bromide partition test (Mandal et al., 1972; Wiggelinkhoizen and Mann, 1980), lactate dehydrogenase assay (Sharma et al., 1982), adenosine deaminase assay (Ribera et al., 1987), IgG assay (Pole et al., 1983) etc., but none has yet been stated to be a foolproof method. PCR, a relatively new technique for the diagnosis of TBM is also not foolproof, and is expensive for many developing countries (Pfyffer, 1999). Extensive studies have been carried out regarding a diagnostic utility for BM and TBM in adults and BM in children using an algorithm based on clinical and CSF laboratory features (Thwaites et al., 2002; Berkley et al., 2001). Very recently, Ewer et al. (2003) have reported a sensitive enzyme-linked immunospot assay to detect T-cells specific for *Mycobacterium tuberculosis* antigens and proposed that the technique offers a more accurate approach than the tuberculin skin test for the diagnosis of latent TB. Besides all these techniques, the analysis of CSF often becomes crucial for the diagnosis of neurological disorders as the chemical components of CSF reflect the state of the CNS in healthy and diseased state (Petroff et al., 1986).

High-resolution proton MR spectroscopy, beyond doubt, has become one of the most important analytical tools for obtaining the metabolic information of biological fluid or tissue extracts (Petroff et al., 1986; Learmonth et al., 1987; Gilroy et al., 1988; Bell et al., 1989; Nicholson and Wilson, 1989; Kinoshita and Yokota, 1997; Lisboa et al., 1998; Wevers et al., 1999; Boss et al., 2000; Govindaraju et al., 2000; Groenen et al., 2004). It has been well documented that NMR spectroscopy gives non-invasive, qualitative as well as quantitative information regarding the metabolic profile (Bock, 1989; Vion-Dury et al., 1992; De'Certaines,

1996; Henry, 2002; Griffin, 2003; T'Hart et al., 2003) and usually a metabolite concentration of greater than a few μM is detectable in the ^{1}H NMR spectra (Moolenaar et al., 2003) in a reasonable amount of time (^{1}H NMR; 128 scans; ca. 15 min). With the recent technological advances in NMR probe design such as microprobes and cryoprobes, the detection range and time taken reduce further by using high-field magnets like 600 MHz or higher. Moreover, it has been recently documented that the absolute quantitative information obtained through proton NMR spectroscopy is highly reproducible with an accuracy of 95% (Keun et al., 2002).

Several reports exist in the literature, which highlight the potential role of NMR in understanding the metabolic profile of CSF under various pathological conditions. Analysis of CSF by NMR has revealed the presence of methylmalonic acid from a Vitamin B_{12} deficient patient (Commodari et al., 1991). A detailed ^{1}H NMR analysis was carried out in 600 MHz for obtaining the complete resonance specific assignments of all the metabolites in CSF by using two-dimensional NMR methods (Sweatman et al., 1993). Its consecutive application had been demonstrated on human post-mortem CSF for the distinction of Alzheimer's disease, which clearly stated the importance of citrate in the disease state (Ghauri et al., 1993). In another study, several new metabolites that may have a possible role in CSF disease analysis were assigned in the high-field region of the spectrum (Lutz et al., 1998). The semi-quantitative analysis of CSF by NMR suggested a higher concentration of lactate in case of BM (Hiraoka et al., 1994), and the demonstration of the presence of ethanol in 10 out of 20 patients with cervical myelopathy (Meshitsuka et al., 2001). Despite the fact that information concerning several volatile metabolites (such as acetone) as well as exchangeable protons are lost in case of lyophilized CSF (Maillet et al., 1998), a combined study involving brain MRI, MRS and spectroscopic analysis in centrifuged, lyophilized CSF has demonstrated the evolution of multiple sclerosis metabolite patterns (Simone et al., 1996). Taking into consideration the limitations of the currently available diagnostic techniques as well as the persistent problems regarding the timely diagnosis of childhood meningitis, the present investigation has been carried out to explore the possibility of ^{1}H NMR spectroscopy as an additional diagnostic tool based on the analysis of CSF from 191 cases.

3. Materials and Methods

3.1. Chemicals

D_2O (99.96 atom% deuterium-enriched, with 0.75% sodium-3-(trimethylsilyl)-2,2,3,3-d_4-propionate (TSP)) was purchased from Sigma-Aldrich Inc. (St. Louis, MO, USA).

3.2. Cerebrospinal Fluid (CSF)

The CSF samples of children (6-12 years of age) comprising bacterial meningitis (n = 85), tuberculous meningitis (n = 47), viral meningitis (n = 35) and control cases (n = 24) were obtained by lumbar puncture over a period of five years (1998-2003) on the first day of their admission from the local hospitals at Lucknow (King George's Medical University; Sanjay Gandhi Post-Graduate Institute of Medical Sciences). Samples for the control group were obtained from children suffering from other diseases such as septicemia (n = 7), seizures (n = 6), post-measles (n = 1), acute diarrhoea (n = 2), acute respiratory tract infections coupled with urinary tract infection (n = 2), oligodendroglioma (n = 1), neurofibroma (n = 1), craniopharyngioma (n = 2), choroid plexus papilloma (n = 2) for whom the CSF was collected upon suspicion of metabolic abnormalities, if any, to serve as a base-line limit for the differentiation of the three types of meningitis. About 1 ml of CSF was collected from the patients, 700 µl of the sample was snap-frozen in liquid nitrogen after the collection and sent for NMR experiments, and the remaining amount of sample was used for routine laboratory tests (CSF cell count, protein content estimation and bacterial culture). The snap-frozen CSF sample (450 µl) was transferred to a 5 mm NMR tube (Wilmad Glass, USA) containing 50 µl of D_2O for the purpose of internal locking and immediately subjected to NMR analysis. A capillary tube containing the known concentration of 0.75% TSP in D_2O was inserted separately in all the NMR tubes to aid in the metabolite quantification.

The study was approved by the Institute's as well as the Hospitals' Scientific and Ethical Committees following established guidelines. All participants provided written informed consent after the study procedures were explained to them involving the CSF analysis. After providing informed consent, each patient underwent standard history taking, examination, and baseline

investigations (including lumbar puncture, chest radiography, and computed tomography of the head where required). Further, the patients were given an explanation regarding the study involving CSF analysis using NMR spectroscopy, and a separate informed consent was obtained from each patient's parents/guardians citing the usefulness of the study for research purposes concerning future benefits of other patients.

3.3. NMR Experiments and Resonance Assignments

The NMR experiments were performed at 298K using a Bruker (Fallanden, Switzerland) *Avance* DRX 300 MHz FT-NMR spectrometer (7.2 Tesla, 54 mm vertical-bore magnet) equipped with a 5 mm multinuclear inverse probehead with a Z-shielded gradient, operating at a proton frequency of 300.13 MHz. The spectroscopic task was controlled by a Silicongraphics Indy and the spectral plotting was obtained using the Bruker's XWINNMR 2.6. ^{1}H NMR spectra were acquired using WATERGATE (Piotto et al., 1992) water suppression pulse-sequence with 32768 data points, spectral width (SW) of 3591 Hz, 128 scans, with a total relaxation time of 7.68 s per scan, and the binomial 90° pulse was set to 32 μs. The FIDs were multiplied by an exponential function with a line-broadening of 0.30 Hz, prior to Fourier transformation. The Hahn spin-echo experiments were performed with an echo-time (TE) of 160 ms for a few native CSF samples using the water-presaturation pulse-sequence to observe the phase reversal of *J*-coupled multiplets. ^{13}C NMR experiment was performed for one lyophilized CSF sample to aid in the 2D cross-peak assignments, with the following experimental parameters: 32768 data points, SW of 18115 Hz, 16000 scans, with a relaxation delay (d1) of 2 s per scan, and the 90° pulse was set to 10 μs. The FIDs were multiplied by an exponential function with a line-broadening of 3 Hz, prior to Fourier transformation.

The quantification of the metabolites in all 191 CSF samples was carried out using the software program NMRQUANT available on the spectrometer as reported earlier (Garg et al., 2002) with respect to a known concentration of TSP (49 mg/dl) serving as an external reference. In case of glucose, the α-anomeric proton resonance was quantitated with a factor of 36/100 to get the weight of total CSF glucose, as α-glucose and β-glucose are present respectively in solution in a ratio of 36:64 under physiological conditions.

Standard 2D COSY was performed with the presaturation of the HOD signal at 4.78 ppm for a few of the native CSF samples to observe the *J*-coupled resonances with the following experimental parameters: SW of 3591 Hz in both dimensions, recycle delay of 2.143 s for each t_1 step, and 128 transients were added with 2048 data points using 400 t_1 increments. The FIDs were zero-filled to 1024 data points, and a sine-bell window function was used in both dimensions prior to double Fourier transformation. The total experimental time was 18 hours. Similarly 2D Watergate TOCSY was performed for few of the native CSF samples with a spin-lock time of 12.5 ms in order to assign the overlapping resonances. The experimental parameters used were: SW of 3591 Hz in both dimensions, 256 t_1 increments with a 2.143 s recycle delay; for each step, 128 transients were added with 1024 data points. The FIDs were zero-filled to 1024 data points, and a sine-bell window function was used in both dimensions prior to double Fourier transformation. The total experimental time was 19 hours.

Standard 300/75 MHz gradient HMQC was recorded for one of the CSF samples (1.5 ml) that was centrifuged, lyophilized with experimental parameters of: SW of 3591 Hz in F_2 dimension and 13585 Hz in F_1 dimension; relaxation delay, d1: 1.5 s; delay for creation of anti-phase magnetization, d2: 3.44 ms; 90° pulse, 6.88 μs for ^{1}H, 10 μs for ^{13}C hard-pulses and 60 μs for ^{13}C GARP decoupling with gradient ratios of GPZ1:GPZ2:GPZ3 as 50:30:40; 1024 data points in t_2; 256 experiments in t_1; linear prediction to 512; zero-filling up to 1024 data points and apodization with sine-bell window function in both dimensions prior to double Fourier transformation. The total experimental time was 17 hours. Similarly, 300/75 MHz gradient HSQC was performed for a lyophilized CSF sample to aid in the spectral assignments with the following experimental parameters: SW of 3591 Hz in F_2 dimension and 13585 Hz in F_1 dimension; relaxation delay, d1: 2 s; delay for creation of anti-phase magnetization, d24: 3.44 ms; 90° pulse, 6.50 μs for ^{1}H, 9.25 μs for ^{13}C hard-pulses and 60 μs for ^{13}C GARP decoupling with gradient ratios of GPZ1:GPZ2:GPZ3 as 30:80:20; 2048 data points in t_2; 256 experiments in t_1; linear prediction to 512; zero-filling up to 1024 data points and apodization with sine-bell window function in both dimensions prior to double Fourier transformation. The total experimental time was 18 hours.

3.4. Statistical Analysis

The percentage occurrence for eleven Clinical Symptoms is expressed along with the total number of patients (n) for whom a particular symptom was observed (Table-1(a)). The seven unquantified metabolites as seen in the NMR spectra (Table-1(b)), and the respective clinical data comprising the CSF cell-count and the CSF protein content information (Table-1(c)) are also given. The values obtained were further subjected to Kruskal-Wallis test (non-parametric ANOVA) for statistical significance followed by a post hoc Dunn's multiple comparisons test (carried out by the GraphPad INSTAT 3.0 software). The results obtained for the twelve NMR-based quantified metabolites are expressed as Mean ± SE (Table-2). The statistical significance for the quantitated metabolites was determined by one-way ANOVA followed by a post hoc Student-Newman-Keuls multiple comparisons test (carried out by the GraphPad INSTAT 3.0 software). A probability *p*-value of less than 0.05 was taken to indicate statistical significance.

The data were subsequently considered for Multivariate Analysis (Discriminant Function Analysis, DFA) so as to define important descriptors for differentiation of meningitis from the control group, followed by discrimination of three types of meningitis. In this analysis only eleven clinical symptoms (Table-1(a)) and twelve NMR-derived metabolite concentrations (Table-2) were used. All analyses were done by the software program SYSTAT 7.0.

The Discriminant Function weights (w_i) and score described by 'Z' values, were calculated according to the following equation (Armitage and Berry, 1990):

$$Z = \sum w_i x_i$$

Where, x_i represents the variable either from the NMR-data or from the clinical symptoms such as urea, headache etc., and w_i represents the corresponding discriminant function-based weights/coefficient values obtained for each metabolite/clinical symptoms variable. A stepwise-forward variable selection procedure was adopted to find out set of predictors of meningitis with discriminant function based Z-cut-off values. These predictors were assessed further by re-substitution and prospective test data methods, in which the software was being trained to provide the sensitivity and specificity values. The re-substitution method carried out as part of the

Table-1: (a). Information obtained regarding the Clinical Symptoms as observed in the patients suffering from meningitis and the control group. (b). Information obtained regarding the occurrence of other NMR-based signals based on the visual examination of the respective NMR spectra of patients from the meningitis and control groups. (c). Collective CSF cell-count (cells per cubic millimeter; cmm) and protein content information (in mg%) as obtained from the laboratory reports of patients grouped under a particular category. '**N**' represents the total number of patients grouped under a particular category, '**n**' stands for the total number of patients for whom the respective clinical symptoms were observed along with the corresponding percentage values (**%**). The *p*-values were obtained based on a non-parametric ANOVA (Kruskal-Wallis test) followed by a post hoc Dunn's multiple comparisons test.

Category	Items Scored		Bacterial Meningitis (N=85)		Tuberculous Meningitis (N=47)		Viral Meningitis (N=35)		Control Cases (N=24)	
			n	%	n	%	n	%	n	%
(a). Clinical Symptoms	**Fever**		85^{***}	100	47^{***}	100	32^{***}	91.4	9	37.5
	Headache		12	14.1	15	31.9	10	28.6	3	12.5
	Convulsions - Generalized		49	57.6	26	55.3	22	62.8	8	33.3
	Convulsions – Focal		11	12.9	8	17.0	4	11.4	0	0
	Vomiting		42	49.4	19	40.4	20^{*}	57.1	5	20.8
	Focal Weakness		$11^{\$}$	12.9	15^{*}	31.9	7	20.0	1	4.2
	Altered Sensorium		70^{**}	82.3	39^{**}	83.0	35^{***}	100	12	50.0
	Lymphadenopathy		$9^{\$\$}$	10.5	$15^{**\#}$	31.9	3	8.6	0	0
	BCG Scar		$59^{***\$\$\$}$	69.4	$15^{\#\#\#}$	31.9	30^{***}	85.7	6	25.0
	Abnormal Movements		$2^{\#\#\#\$}$	2.3	9	19.1	13^{*}	37.1	3	12.5
	Neck Rigidity		$60^{***\#\#\#}$	70.6	$35^{***\#\#\#}$	74.5	4	11.4	5	20.8
(b). Unquantified NMR Signals	**Cyclopropane**		$0^{\$\$\$}$	0	$40^{***\#\#\#}$	85.1	0	0	0	0
	Tyrosine		53	62.3	23	48.9	18	51.4	11	45.8
	***Myo*-Inositol**		78	91.8	37	78.7	31	88.6	22	91.7
	Glycine		37	43.5	21	44.7	8	22.8	7	29.2
	Choline-containing compounds		$29^{\$}$	34.1	$27^{\#\#\#}$	57.4	5	14.3	8	33.3
	Valine, Leucine & Isoleucine		81	95.3	42	89.4	33	94.3	19	79.2
	Formate		59	69.4	34	72.3	17	48.6	16	66.7
(c). CSF Investigations	**CSF cell count**	<50/cmm	$0^{***\#\#\#}$	0	$3^{***\#\#\#}$	6.4	28	80.0	21	87.5
		50-<100/cmm	$0^{\#\#\$\$\$}$	0	10	21.3	7	20.0	3	12.5
		100-<500/cmm	$61^{***\#\#\#}$	71.8	$32^{***\#\#\#}$	68.1	0	0	0	0
		>500/cmm	$24^{***\#\#\#\$\$\$}$	28.2	2	4.2	0	0	0	0
	CSF Protein	<60 mg%	$12^{***\#\#\#}$	14.1	$10^{***\#\#\#}$	21.3	30	85.7	22	91.7
		60-200 mg%	$58^{***\#\#\#}$	68.2	$33^{***\#\#\#}$	70.2	5	14.3	2	8.3
		200-1000 mg%	9	10.6	4	8.5	0	0	0	0
		>1000 mg%	6	7.1	0	0	0	0	0	0

$^{***}p < 0.001$, $^{**}p < 0.01$, $^{*}p < 0.05$ as compared to the Control group;
$^{\#\#\#}p < 0.001$, $^{\#\#}p < 0.01$, $^{\#}p < 0.05$ as compared to the VM group;
$^{\$\$\$}p < 0.001$, $^{\$\$}p < 0.01$, $^{\$}p < 0.05$ as compared to the TBM group.

Table-2: Absolute concentrations of the quantitated CSF metabolites as obtained through Bruker's NMRQUANT, with respect to a known concentration of TSP (49 mg/dl). The statistical significance for the quantitated metabolites was determined by one-way ANOVA followed by a post hoc Student-Newman-Keuls multiple comparisons test.

Metabolite Name	**Bacterial Meningitis (N=85)**	**Tuberculous Meningitis (N=47)**	**Viral Meningitis (N=35)**	**Control Cases (N=24)**
	Conc. (mg/dl) **Mean ± SE**	*Conc. (mg/dl)* **Mean ± SE**	*Conc. (mg/dl)* **Mean ± SE**	*Conc. (mg/dl)* **Mean ± SE**
Urea	12.91 ± 0.89$^{***\#\#\#}$	10.76 ± 0.91$^{*\#\#}$	7.16 ± 0.52	6.37 ± 0.73
Total Glucose	28.47 ± 1.39	30.70 ± 2.23	29.50 ± 2.78	31.07 ± 2.92
Creatine/creatinine	2.18 ± 0.13$^{\#}$	2.02 ± 0.12	1.54 ± 0.09	1.66 ± 0.25
Citrate	5.74 ± 0.27$^{**\#\#}$	5.94 ± 0.38$^{**\#}$	4.49 ± 0.32	3.96 ± 0.45
Glutamine	10.87 ± 0.52	10.24 ± 0.78	8.78 ± 0.65	9.17 ± 1.06
Pyruvate	1.72 ± 0.09$^{\#\#}$	1.46 ± 0.08	1.10 ± 0.23	1.35 ± 0.14
Acetoacetate	3.29 ± 0.42$^{\#}$	2.11 ± 0.27	1.33 ± 0.40	2.90 ± 0.63
Acetone	0.38 ± 0.02	0.39 ± 0.03	0.32 ± 0.04	0.39 ± 0.07
Acetate	1.55 ± 0.15	1.60 ± 0.21	1.51 ± 0.31	1.71 ± 0.76
Alanine	1.44 ± 0.11*	1.71 ± 0.14**	1.27 ± 0.18	0.81 ± 0.12
Lactate	27.01 ± 1.73	24.70 ± 2.07	21.80 ± 2.67	27.05 ± 5.18
β-Hydroxy butyrate	4.48 ± 0.37$^{\#\#}$	3.69 ± 0.36	2.43 ± 0.34	2.98 ± 0.41
1,2-Propanediol	6.68 ± 2.85	2.68 ± 0.40	1.09 ± 0.16	5.06 ± 1.46

*** $p < 0.001$, ** $p < 0.01$, * $p < 0.05$ as compared to the Control;
$^{\#\#\#}$ $p < 0.001$, $^{\#\#}$ $p < 0.01$, $^{\#}$ $p < 0.05$ as compared to the VM group.

validation process involved feeding the same disease and control data into the DFA model to check the correct classifications based on the discriminant function weights obtained. The prospective test data methods comprised a re-assessment of the prediction possibility by treating 75% of the disease data from each meningitis group as training sets and examining the remaining 25% of the data as test sets, which were obtained based on the Random Numbers Table by Fisher and Yates (1957). This has served as a validation of the model built based on DFA comprising three separate training sets viz., control vs. BM+TBM+VM, TBM vs. BM+VM, and BM vs. VM, and checking the percentage classifications of the remaining 25% of the patients' data treated as test sets, prior to the inclusion of all the patients' data for the purpose of MENEXSYS development.

3.5. Development of the Expert System MENEXSYS

A new expert system MENEXSYS was developed using Microsoft Visual Basic 6.0 incorporating all the ^{1}H NMR quantitative information, and clinical symptoms data of 167 meningitis and 24 control cases. The discriminant function analysis-based weights/coefficients and the mid-point cut-off values obtained based on the multivariate analysis of the entire database of 191 cases have been incorporated in the software modules to make predictions of the 'disease type' in a new childhood meningitis patient case. The classification logic that would be responsible for any future prediction of the meningitis type has been divided into three phases as: (i). Differentiation of control (non-meningitis) from disease (meningitis) groups; (ii). Differentiation of TBM from the non-TBM cases, i.e., bacterial and viral meningitis; (iii). Differentiation of BM from VM cases.

4. Results

4.1. NMR Spectroscopic Findings and Clinical Observations

The ^{1}H NMR spectrum of the CSF of a representative childhood meningitis case is displayed in fig. 1 to highlight the general metabolite pattern. The respective chemical shift assignments of the metabolites assigned in the CSF samples are listed in Table-3, and are shown separately as expansions in figs. 2-4. The representative ^{1}H NMR spectra of CSF one each from

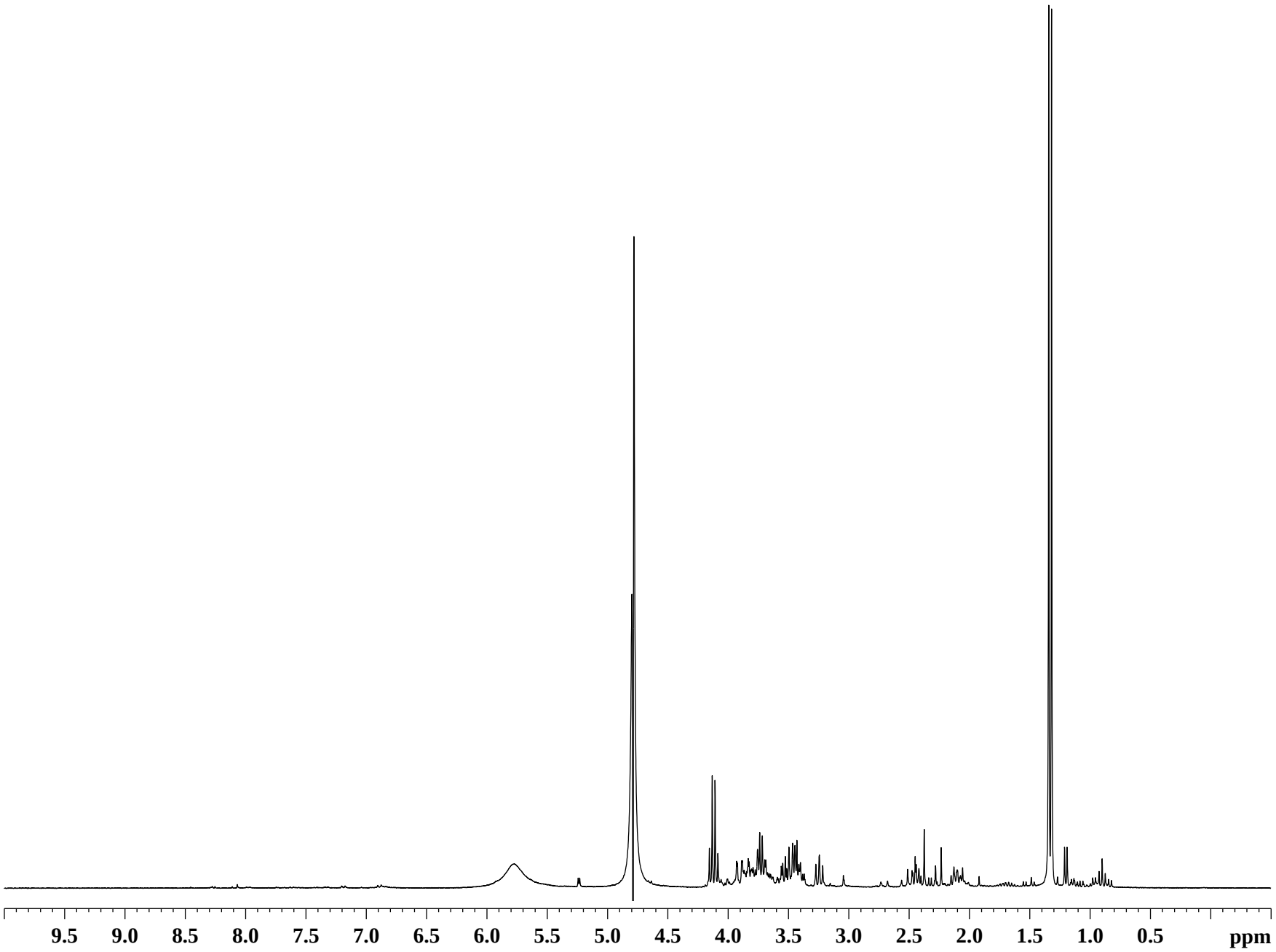

Fig. 1: ^{1}H NMR spectrum of the CSF of a representative childhood meningitis case.

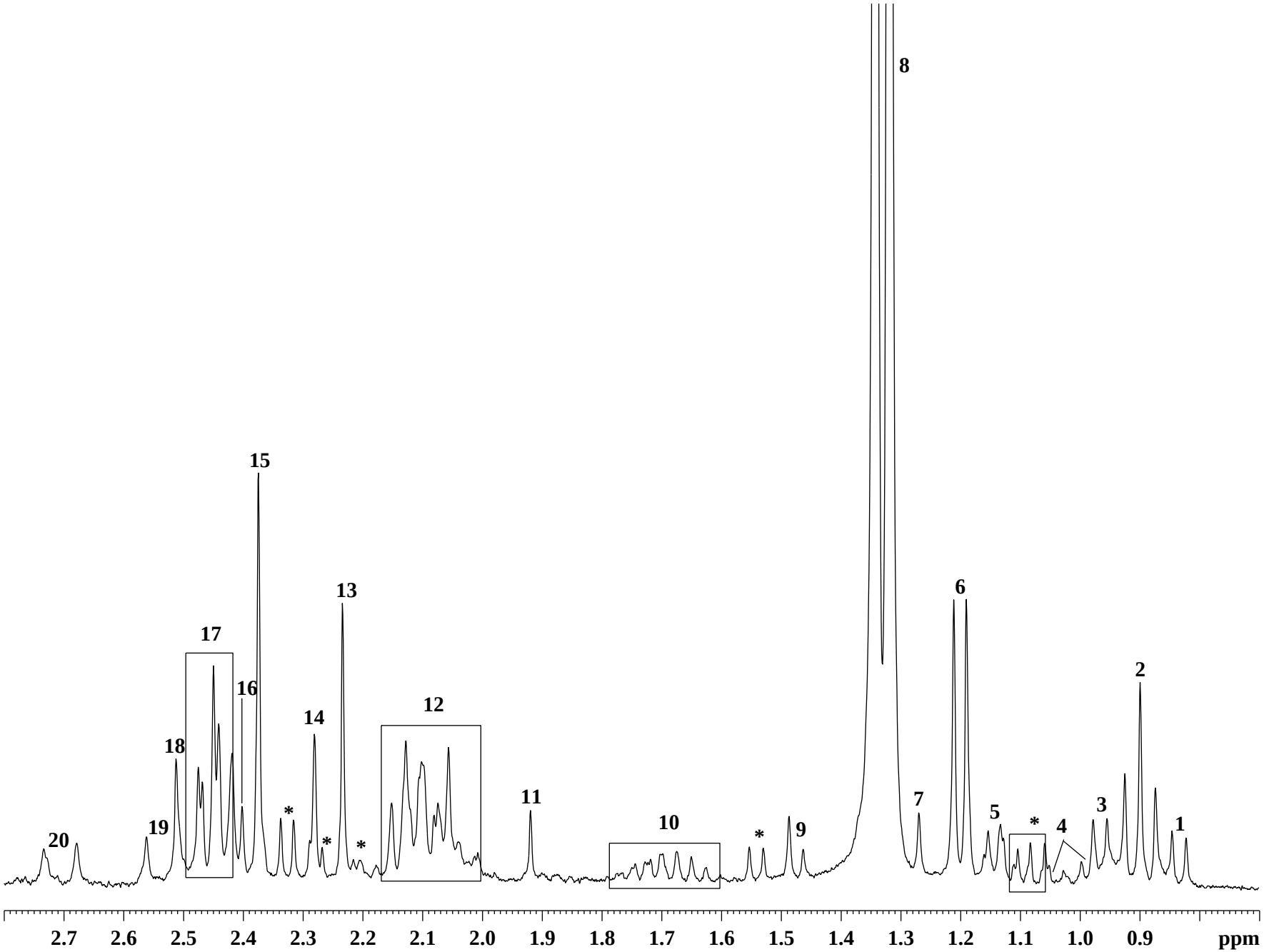

Fig. 2: Expansion of the ^{1}H NMR spectrum of the CSF of a representative childhood meningitis case, highlighting the resonance assignments between 0.0-3.0 ppm. The labeled assignments of the metabolites are as given in Table-3.

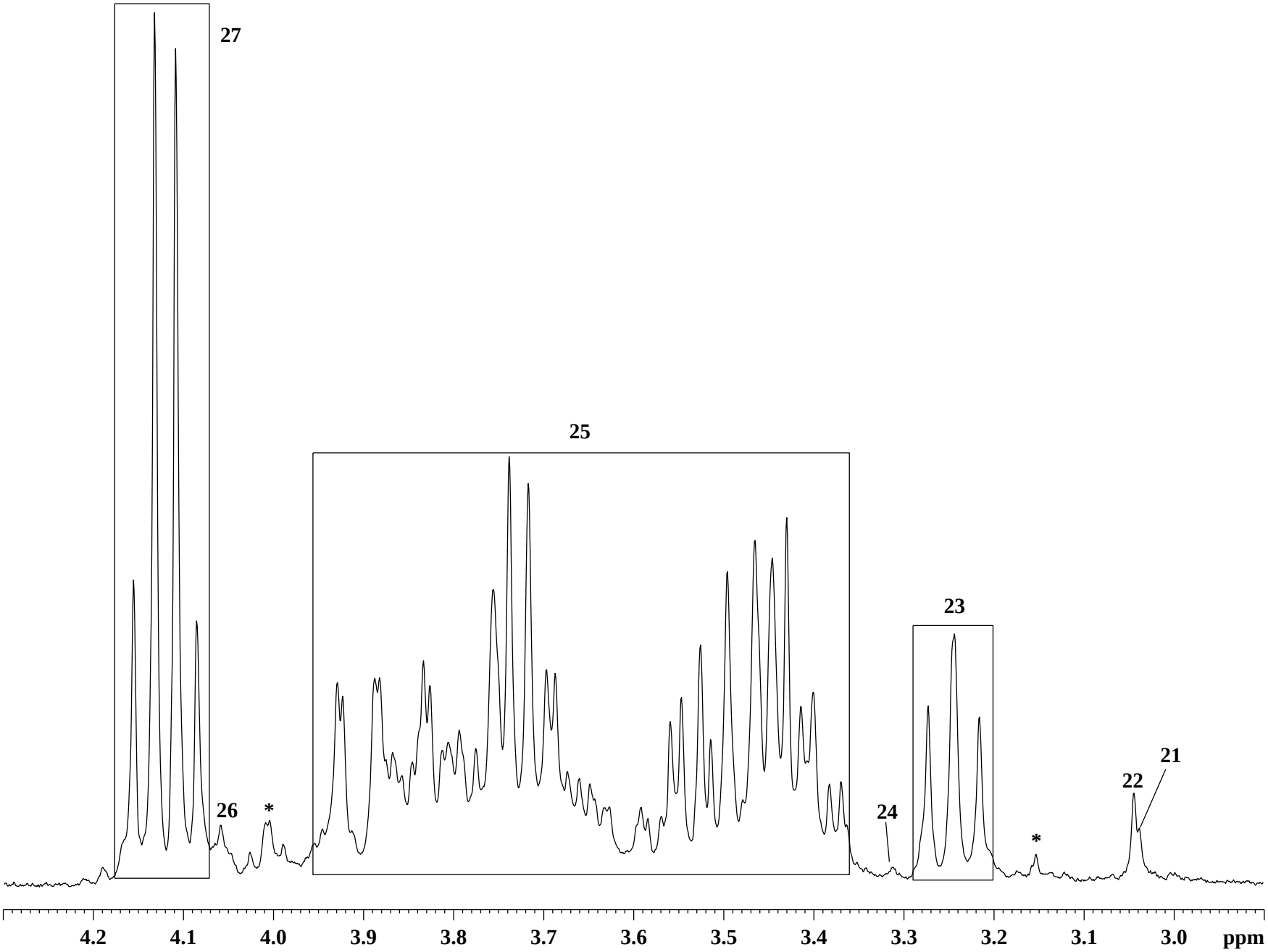

Fig. 3: Expansion of the ^{1}H NMR spectrum of the CSF of a representative childhood meningitis case, highlighting the resonance assignments between 2.9-4.3 ppm. The labeled assignments of the metabolites are as given in Table-3.

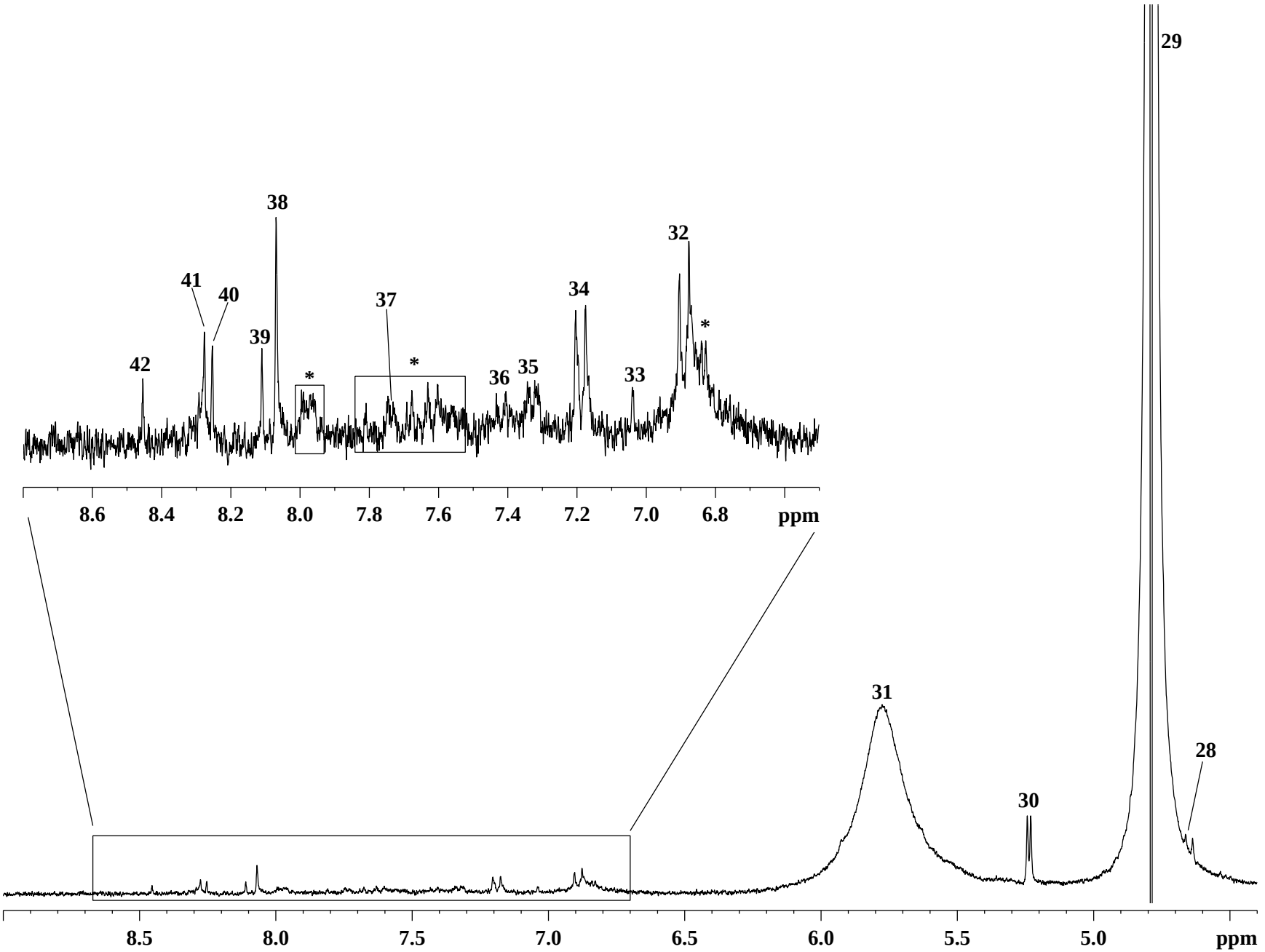

Fig. 4: Expansion of the ^{1}H NMR spectrum of the CSF of a representative childhood meningitis case, highlighting the resonance assignments between 4.4-9.0 ppm. The labeled assignments of the metabolites are as given in Table-3.

Table-3: Proton chemical shift assignments of the metabolites, as seen in the ^{1}H NMR spectrum of the CSF of children suffering from meningitis and control cases. The chemical shift referencing has been done with respect to the TSP at 0.0 ppm. The ^{1}H multiplicity is denoted as, s: singlet; d: doublet; dd: double doublet; t: triplet; q: quartet; m: multiplet. Resonances marked as * are unassigned.

Metabolite	Chemical Shift (δ, ppm)		Assignment Number	^{1}H Multiplicity
α-Hydroxy isovalerate, Isoleucine	γCH_3	0.83	1	d
α-Hydroxy butyrate	γCH_3	0.90	2	t
α-Hydroxy isovalerate, Leucine	$\gamma' CH_3$, $\delta,\delta' CH_3$	0.97	3	d
Valine	γCH_3	1.01	4	d
1,2-Propanediol	CH_3	1.14	5	d
β-Hydroxy butyrate	γCH_3	1.20	6	d
β-Hydroxy isovalerate	βCH_3	1.27	7	s
Lactate	CH_3	1.33	8	d
Alanine	βCH_3	1.47	9	d
α-Hydroxy butyrate, Leucine	βCH_2	1.60-1.80	10	m
Acetate	CH_3	1.92	11	s
Glutamine	βCH_2	2.02-2.17	12	m
Acetone	CH_3	2.23	13	s
Acetoacetate	CH_3	2.28	14	s
Pyruvate	CH_3	2.37	15	s
Succinate	$\alpha,\beta CH_2$	2.40	16	s
Glutamine	γCH_2	2.41-2.48	17	m
β-Hydroxy isovalerate	αCH_2	2.51	18	s
Citrate	αCH_2	2.53	19	d
Citrate	$\alpha' CH_2$	2.70	20	d
Creatine	CH_3	3.04	21	s (merged)
Creatinine	CH_3	3.05	22	s
β-Glucose	CH	3.24	23	t
Betaine	$N^{+}(CH_3)_3$	3.31	24	s
α, β-Glucose	CH, CH_2	3.36-3.94	25	m
Myo-inositol	CH	4.06	26	t
Lactate	CH	4.12	27	q

Metabolite	Chemical Shift (δ, ppm)		Assignment Number	^{1}H Multiplicity
β-Glucose	CH (anomeric)	4.65	28	d
Water, residual	HOD	4.79	29	s
α-Glucose	CH (anomeric)	5.24	30	d
Urea	H_2N-CO-NH_2	5.78	31	s (broad)
Tyrosine	3,5H (C3,5 ring)	6.89	32	d
Histidine	5H (C5 ring)	7.04	33	s
Tyrosine	2,6H (C2,6 ring)	7.19	34	d
Phenylalanine	2,6H (C2,6 ring)	7.33	35	d
Phenylalanine	4H (C4 ring)	7.42	36	d
Histidine	2H (C2 ring)	7.74	37	s
Adenine (bound)	2H (C2 ring)	8.07	38	s
Inosine	2H (C2 ring)	8.11	39	s
Adenine (bound)	8H (C8 ring)	8.25	40	s
Guanine (bound)	8H (C8 ring)	8.27	41	s
Formate	$HCOO^-$	8.45	42	s
NADH	4H (N4 ring)	8.68	43	d
NADH	6H (N6 ring)	8.87	44	d
NADH	2H (N2 ring)	8.94	45	s

bacterial, tuberculous, viral meningitis and control group are shown as a combined stack-plot in fig. 5 to demonstrate the metabolite patterns and chemical shift assignments. Stack-plots of some of the representative cases of CSF from meningitis and control cases are shown separately in figs. 6-9 to further highlight the metabolite pattern. Resonance signals arising due to the presence of valine, leucine, isoleucine, 1,2-propanediol, β-hydroxy butyrate, lactate, alanine, acetate, acetone, acetoacetate, pyruvate, glutamine, citrate, creatine/creatinine, α,β-glucose, glycine, *myo*-inositol, tyrosine and formate were readily assigned at 300 MHz as per the standard proton chemical shift values for CSF metabolites (Sweatman et al., 1993; Lutz et al., 1998), besides assigning urea for the first time in CSF. The chemical shift region 0.9-1.1 ppm consisted of signals from α-hydroxy butyrate, valine, leucine, isoleucine, α-hydroxyisovalerate (Lutz et al., 1998) and α-amino butyrate (Lutz et al., 1998) observed as a complex coupling-network pattern (fig. 2). The resonances in the region 3.1-4.3 ppm consisted of overlapping signals from α,β-glucose, choline-containing compounds, *myo*-inositol, lactate, α-amino acids such as alanine, glutamine and glycine that could be assigned at 300 MHz (fig. 3). The region 6.0-9.0 ppm consisted of signals arising from the aromatic amino acids such as tyrosine, histidine and phenylalanine, besides formate (fig. 4), and in a few cases signals arising from drugs such as isoniazid and pyrazinamide or some probable drug-excipients (fig. 10). The 2D experiments such as COSY, TOCSY, HMQC and HSQC were performed for a few CSF samples (native/lyophilized) so as to resolve the overlapping of resonances as seen in the ^{1}H NMR spectra, and to aid in the chemical shift assignments based on their cross-peak correlation information (figs. 11-14). ^{13}C NMR spectrum was recorded for the lyophilized CSF sample for which the 2D HSQC experiment was performed, so as to mark the carbon chemical shift assignments (fig. 15).

Stack-plots to highlight the occurrence of 1,2-propanediol in the CSF samples involving BM, TBM and Control cases are shown separately in figs. 16-18, respectively. The presence of glutamine (not as a mixture with glutamate) in the meningitis CSF samples has been established by performing the ^{1}H NMR experiments for glutamine and glutamate separately as well as by mixing them together, followed by a comparison of the respective ^{1}H NMR spectra (fig. 19). The metabolites that were ubiquitously present in all CSF samples, *viz.*, 1,2-propanediol, β-hydroxy butyrate, lactate, alanine, acetate, acetone, acetoacetate, pyruvate, glutamine, citrate,

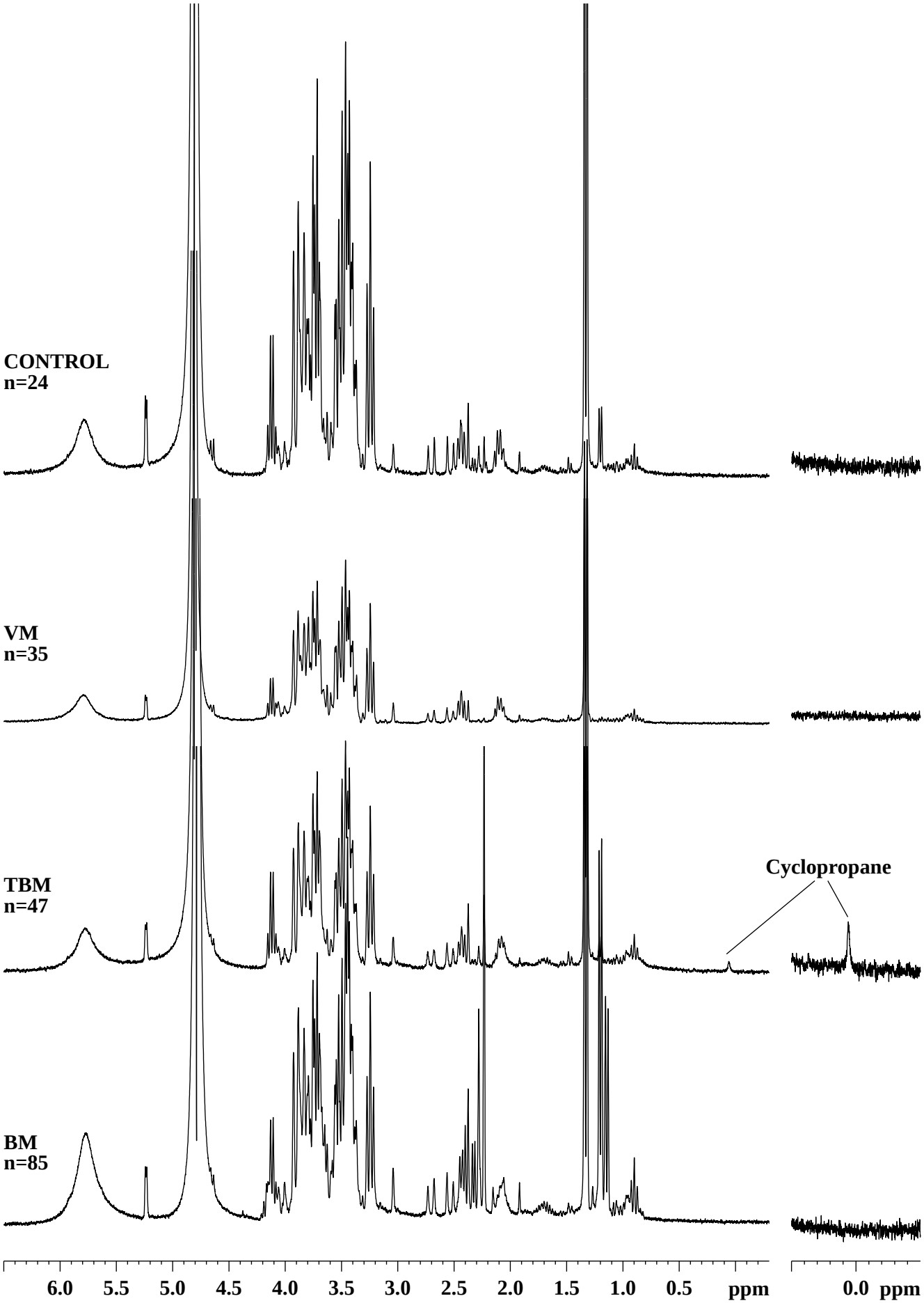

Fig. 5: Stack-plot of the ^{1}H NMR spectra of representative cases of BM, TBM, VM and Control , displaying the chemical shift region between 0-10 ppm.

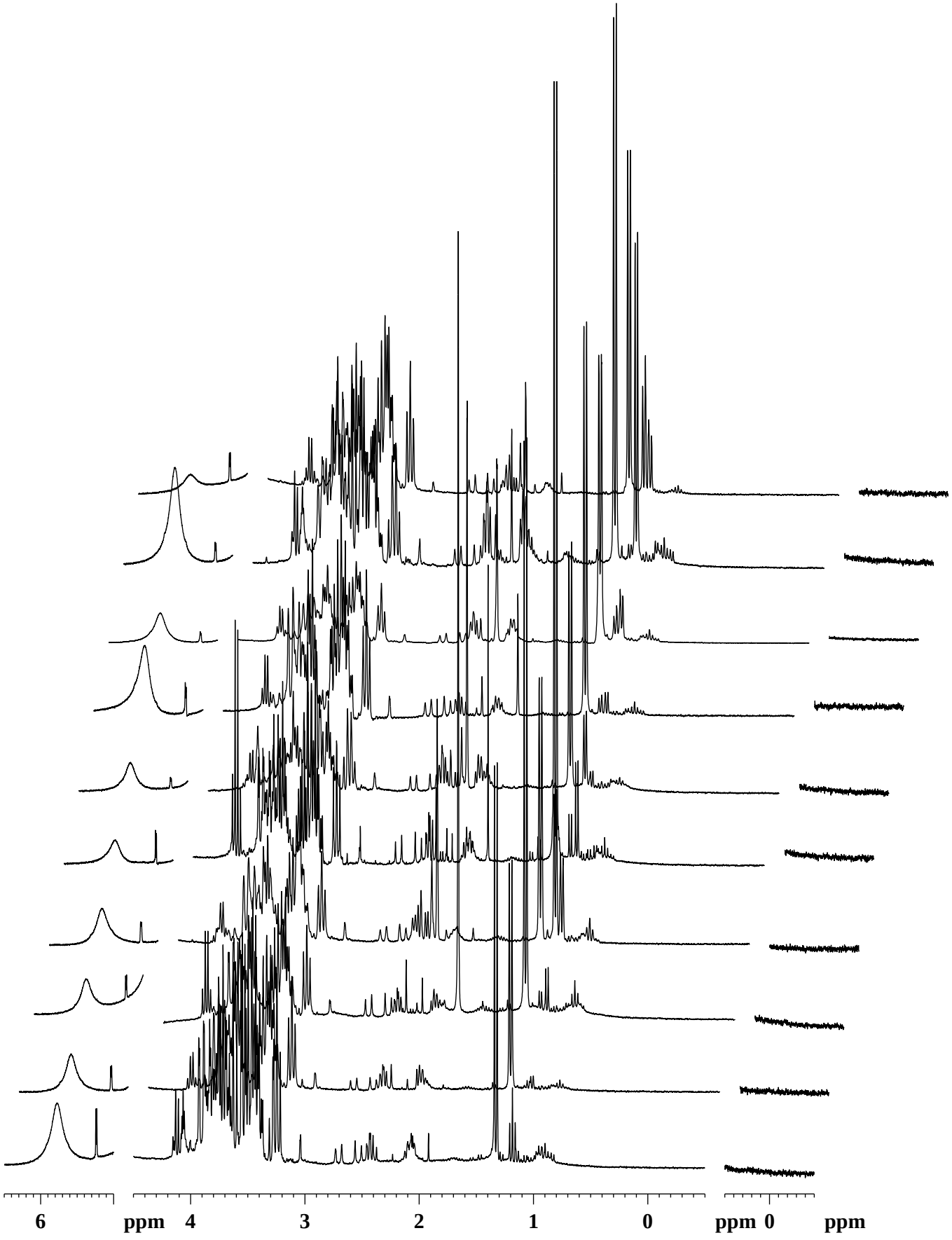

Fig. 6: Stack plot of the ^{1}H NMR spectra of representative BM cases.

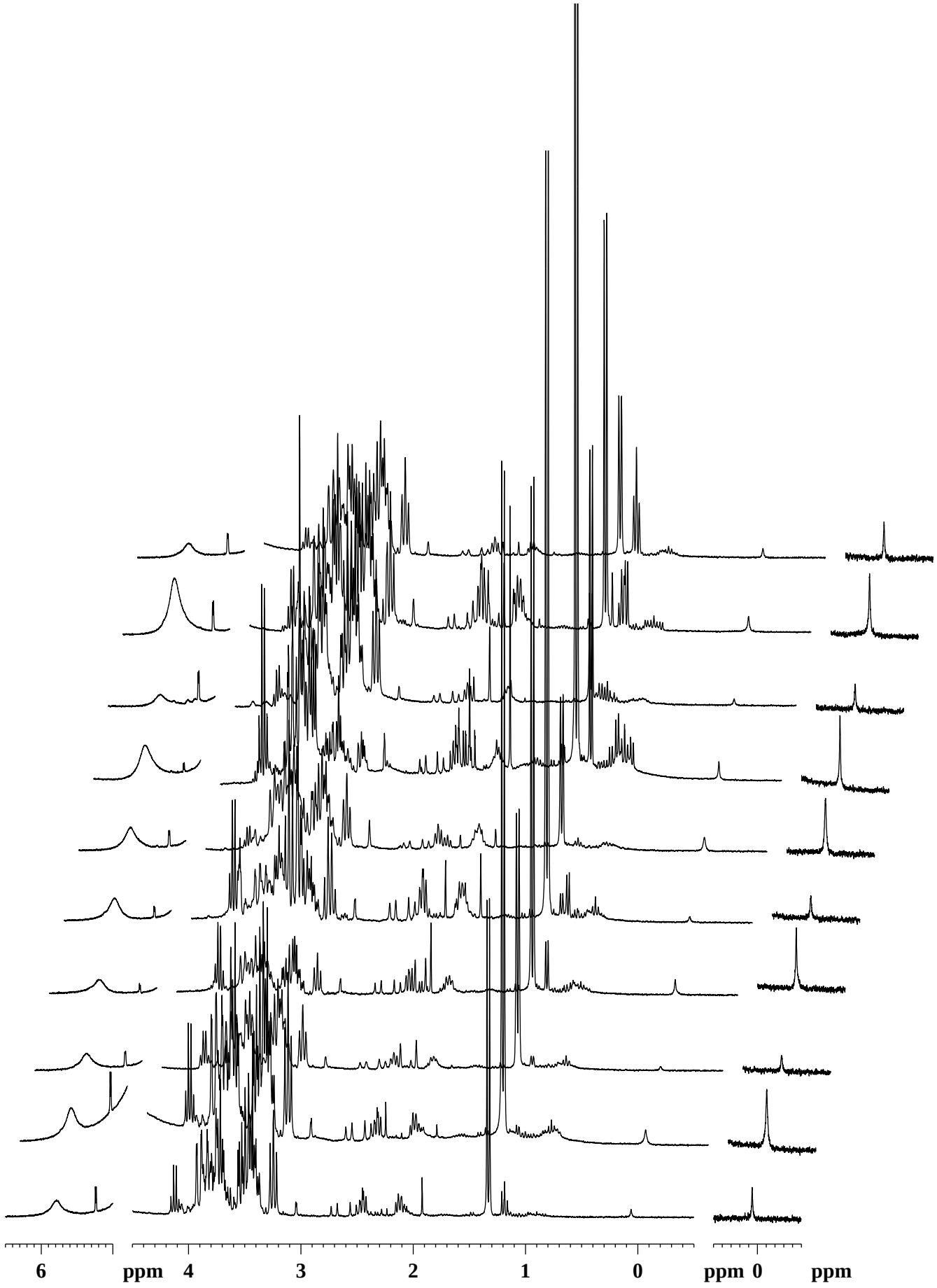

Fig. 7: Stack plot of the ^{1}H NMR spectra of representative TBM cases.

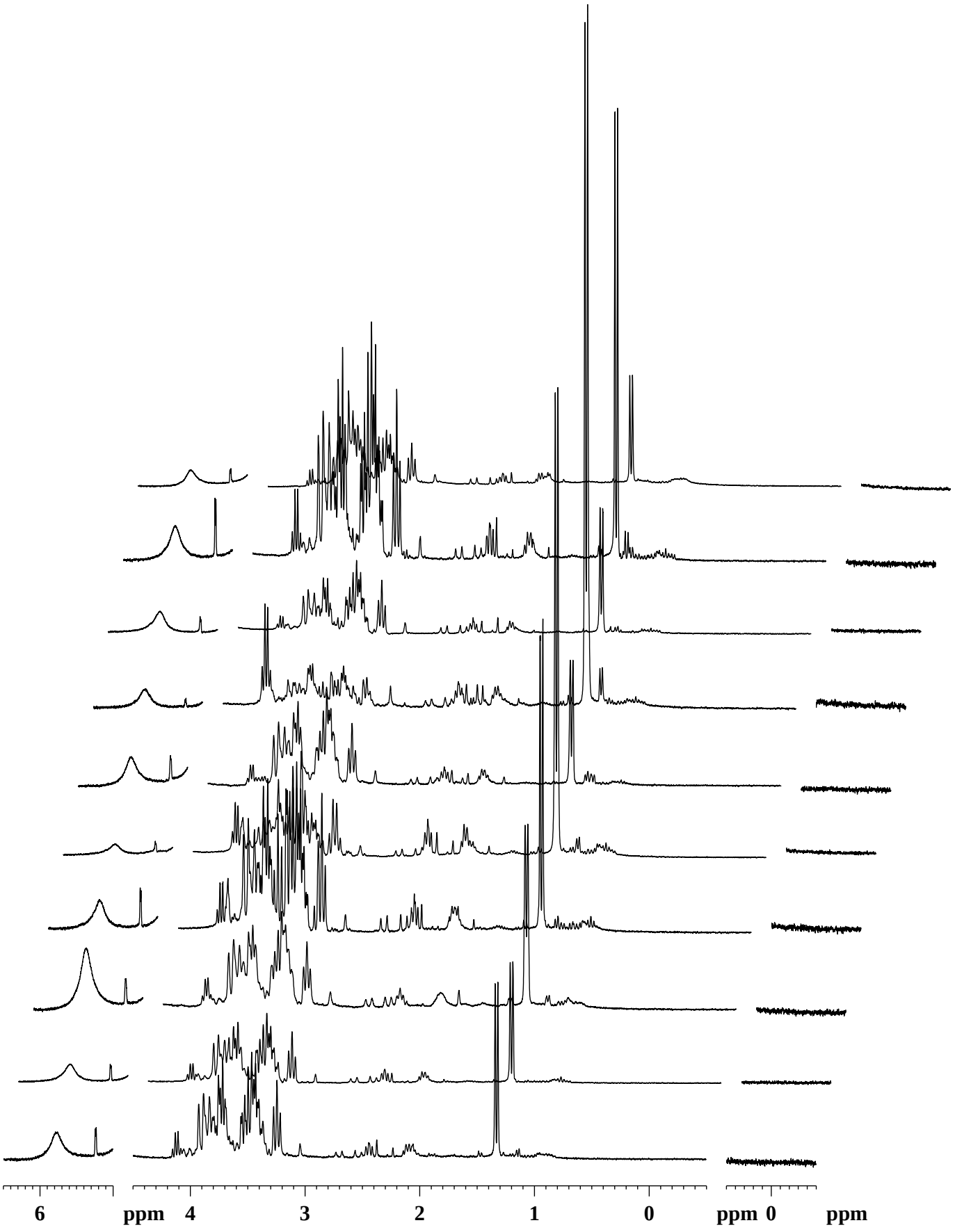

Fig. 8: Stack plot of the ^{1}H NMR spectra of representative VM cases.

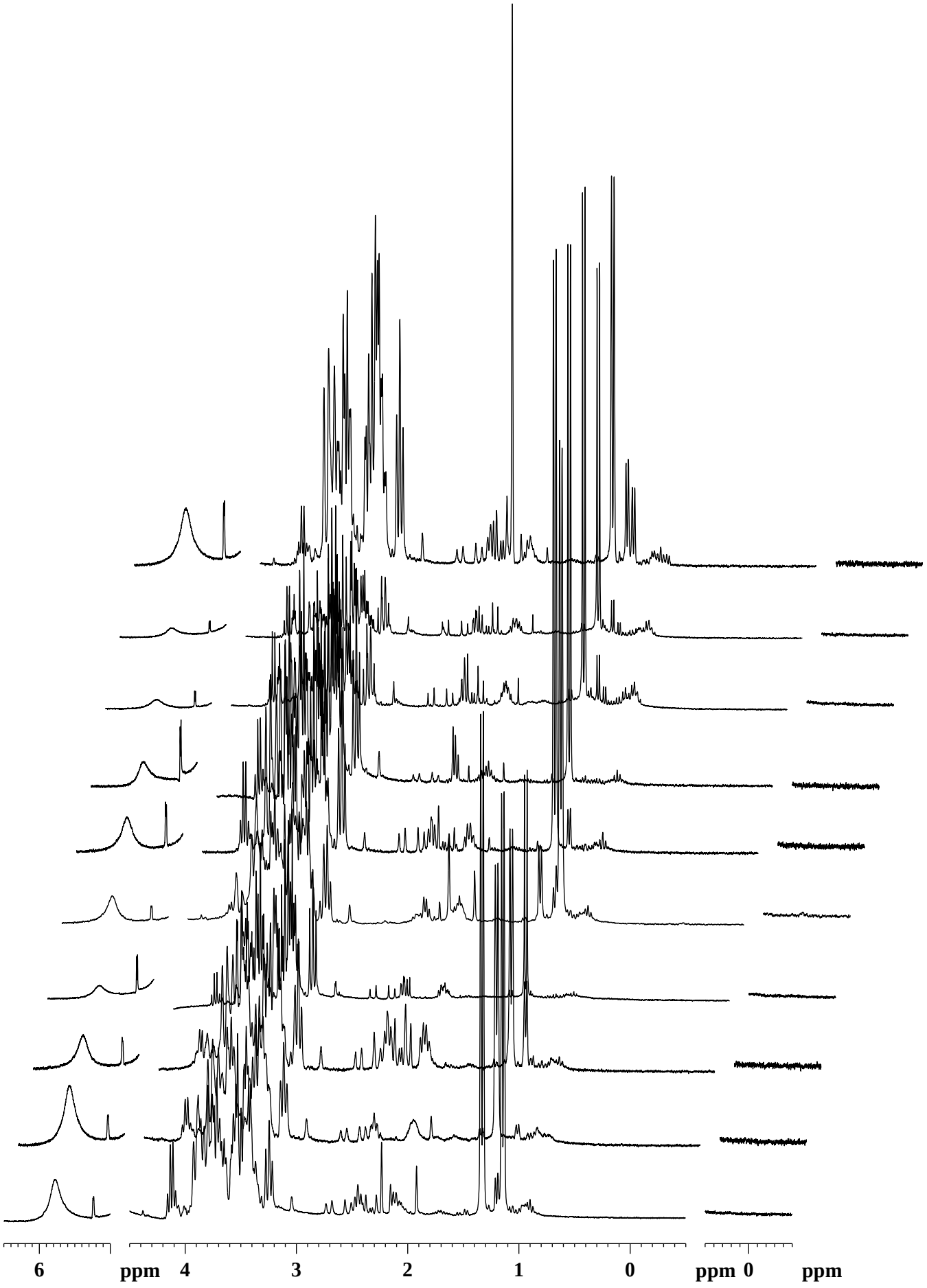

Fig. 9: Stack plot of the ^{1}H NMR spectra of representative Control cases.

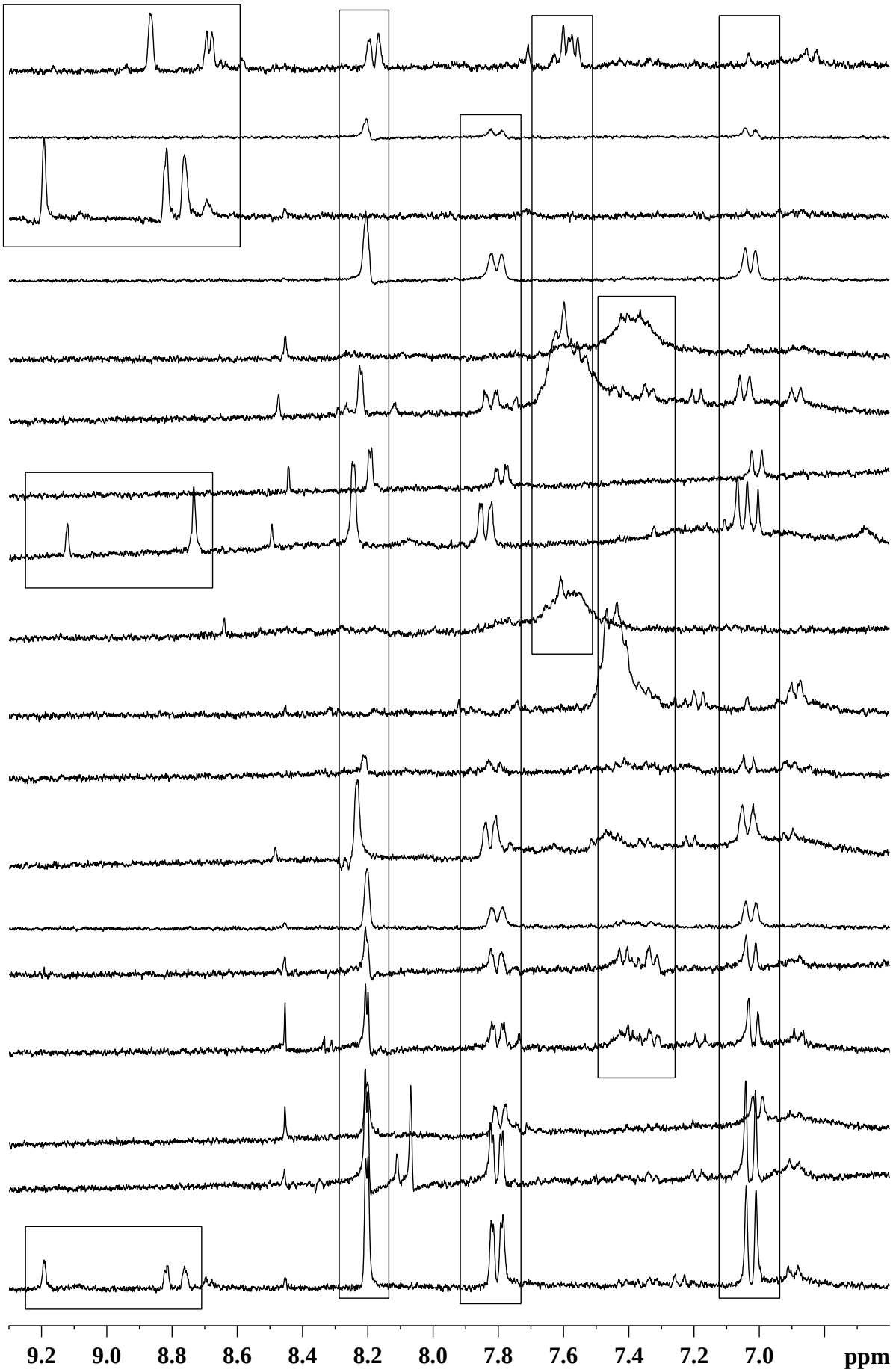

Fig. 10: Stack plot of the ^{1}H NMR spectra of the CSF of meningitis cases, highlighting the resonance signals from drug-excipients.

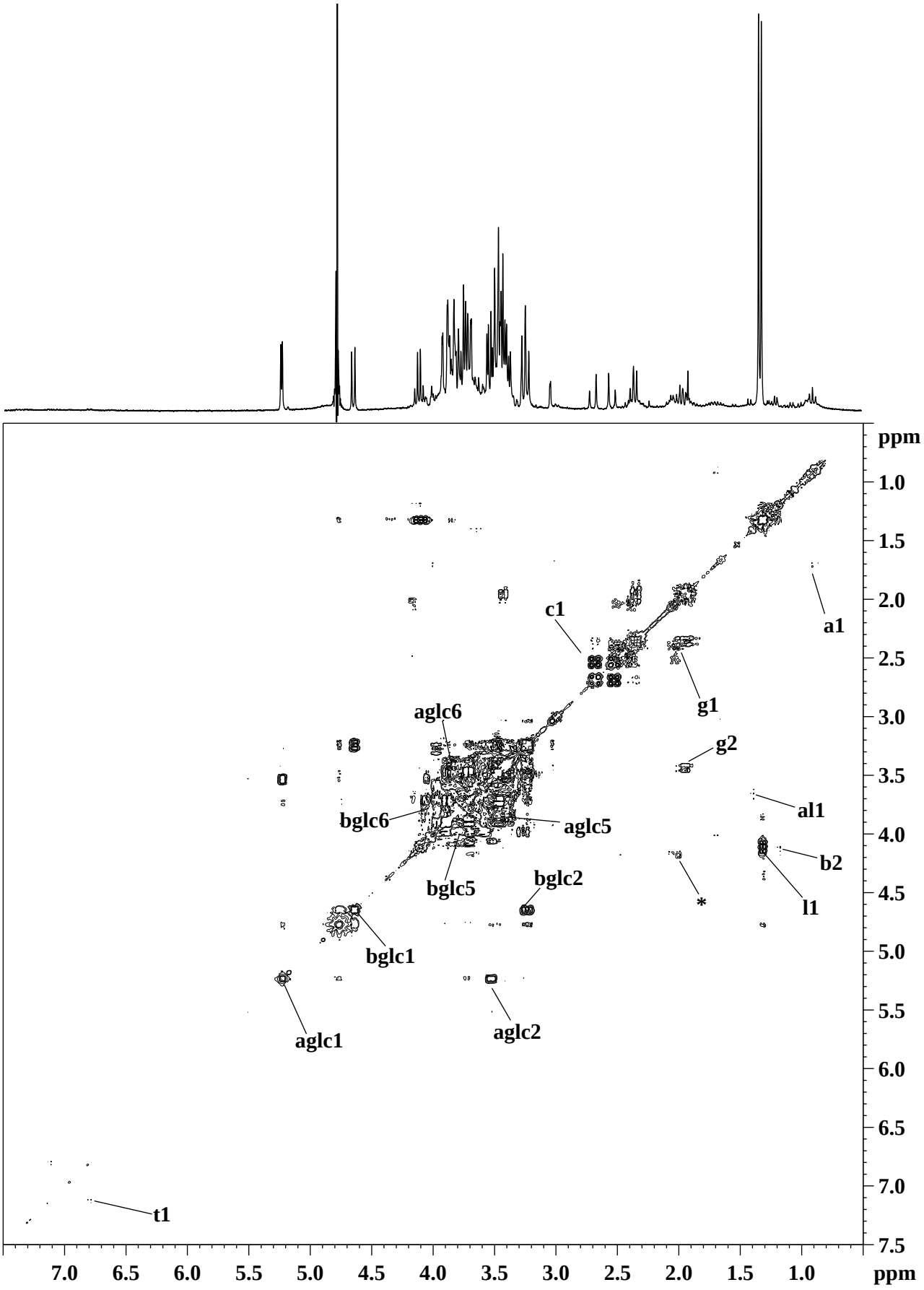

Fig. 11: ^{1}H-^{1}H COSY spectrum of a representative CSF sample (native state, Water Presaturation). The labeled assignments are: a1. α-hydroxy butyrate; al1. alanine; b2. β-hydroxy butyrate; c1. citrate; g1, g2. glutamine; l1. lactate; aglc1, aglc2, aglc5, aglc6. α-glucose; bglc1, bglc2, bglc5, bglc6. β-glucose; t1. tyrosine; * is unassigned.

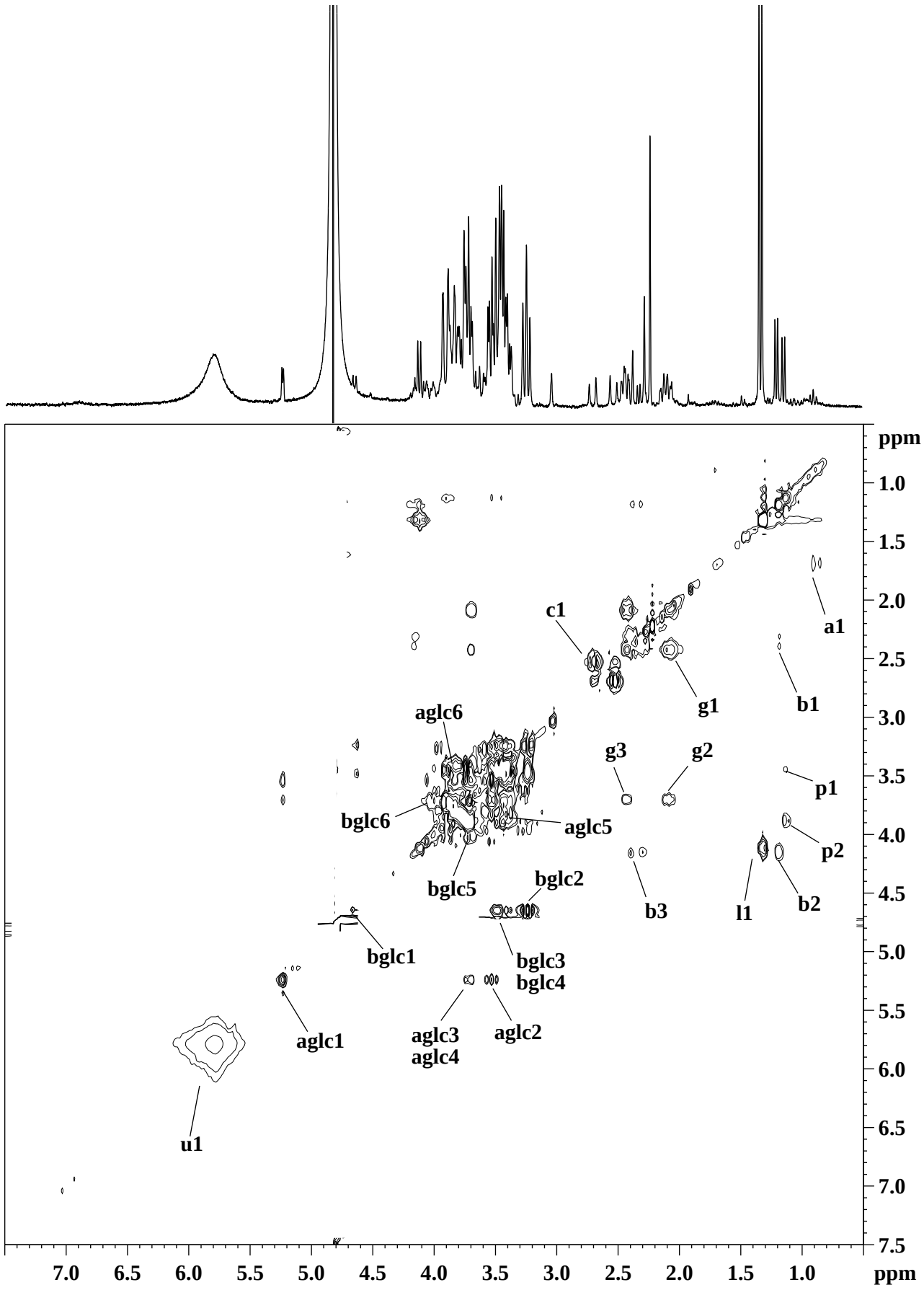

Fig. 12: ^{1}H-^{1}H TOCSY spectrum of a representative CSF sample (native state, WATERGATE). The labeled assignments are: a1. α-hydroxy butyrate; b1, b2, b3. β-hydroxy butyrate; c1. citrate; g1, g2, g3. glutamine; l1. lactate; aglc1, aglc2-aglc6. α-glucose; bglc1-bglc6. β-glucose; u1. urea.

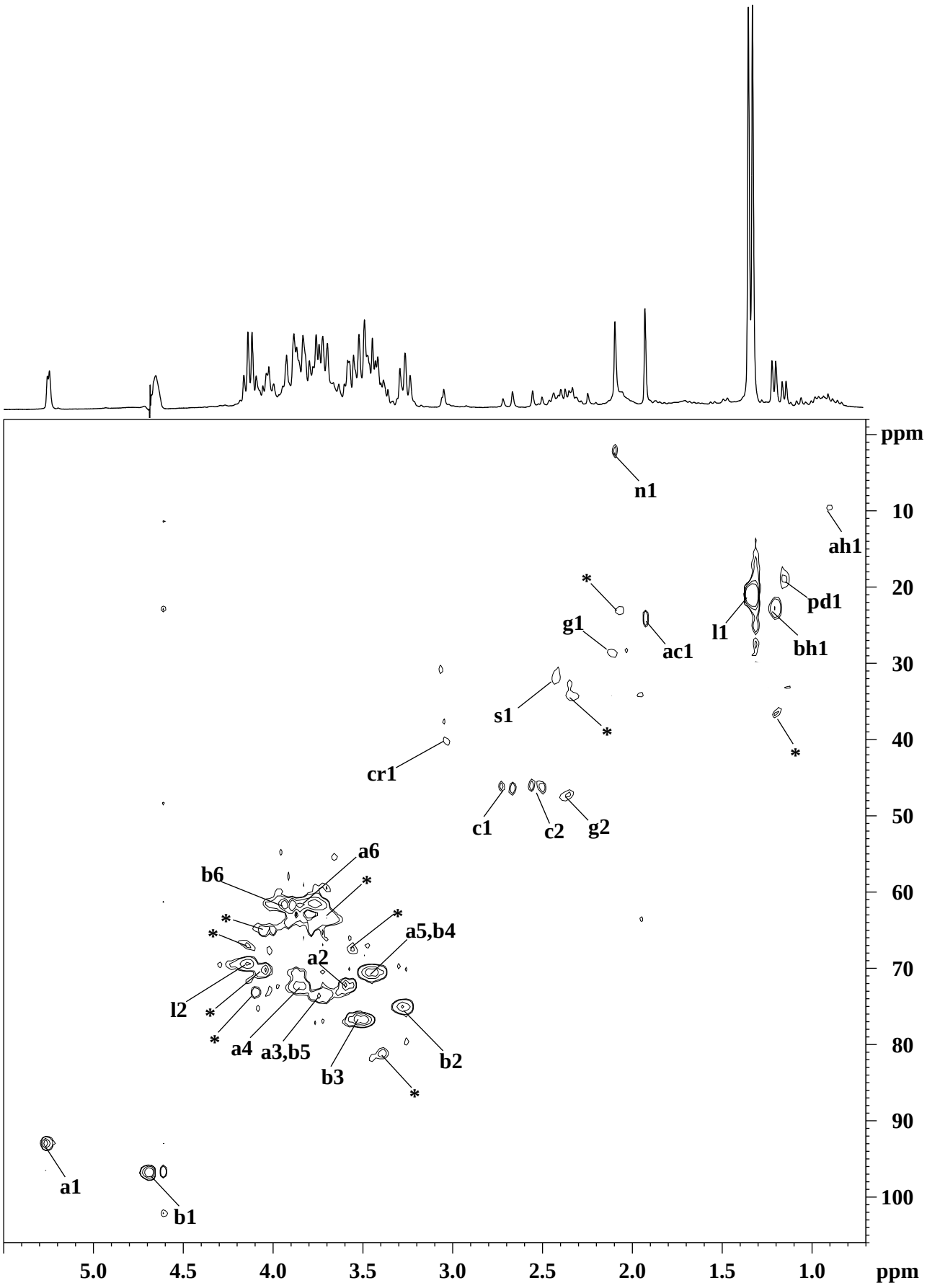

Fig. 13: ^{1}H-^{13}C HMQC spectrum of a lyophilized CSF sample. The labeled assignments are: ac1. acetate; ah1. α-hydroxy butyrate; bh1. β-hydroxy butyrate; c1, c2. citrate; cr1. creatine/creatinine; g1, g2. glutamine; l1, l2. lactate; pd1. 1,2-propanediol; s1. succinate; a1-a6. α-glucose; b1-b6. β-glucose; * is unassigned.

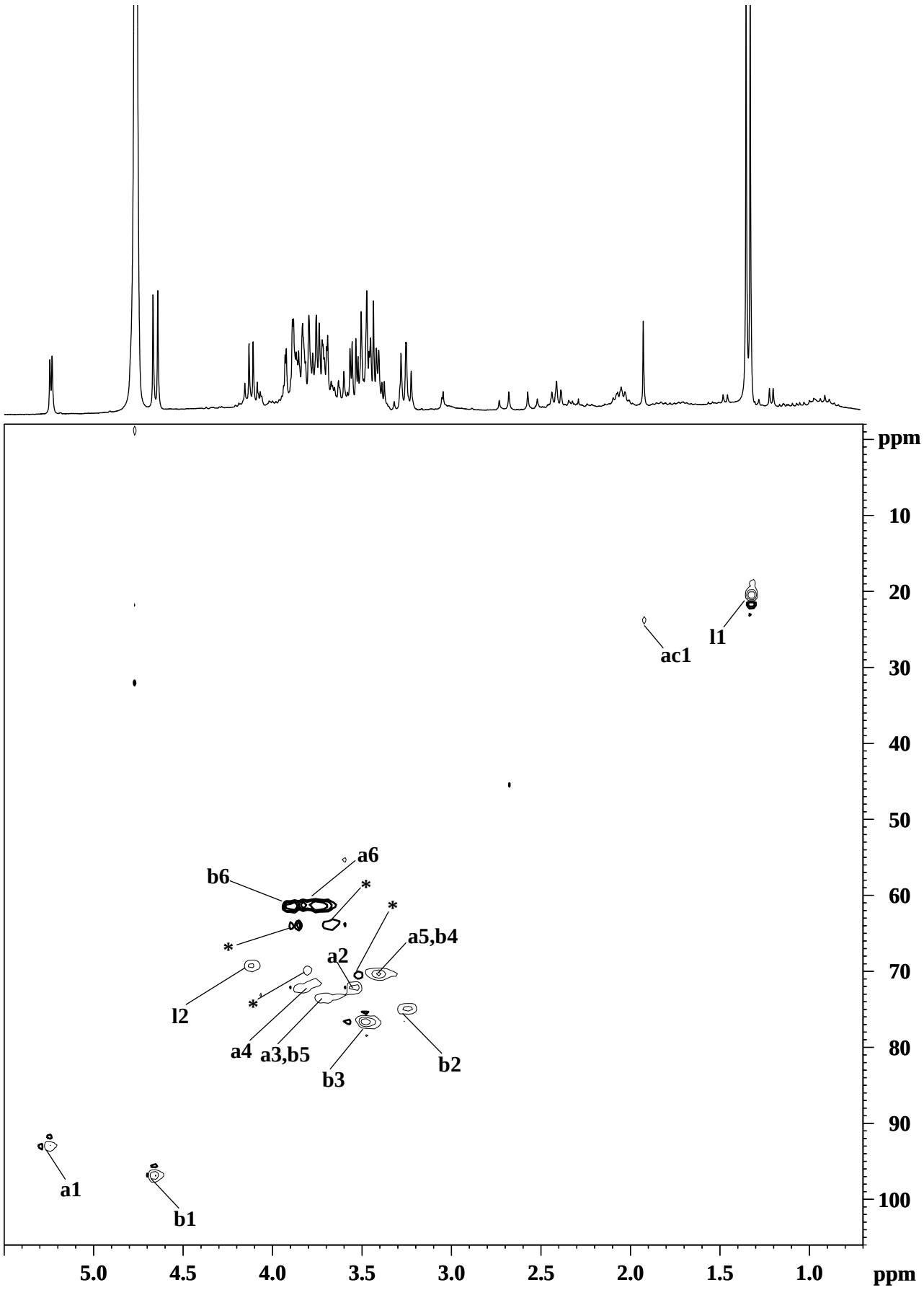

Fig. 14: ^{1}H-^{13}C HSQC spectrum of a lyophilized CSF sample. The labeled assignments are: ac1. acetate; l1, l2. lactate; a1-a6. α-glucose; b1-b6. β-glucose; * is unassigned.

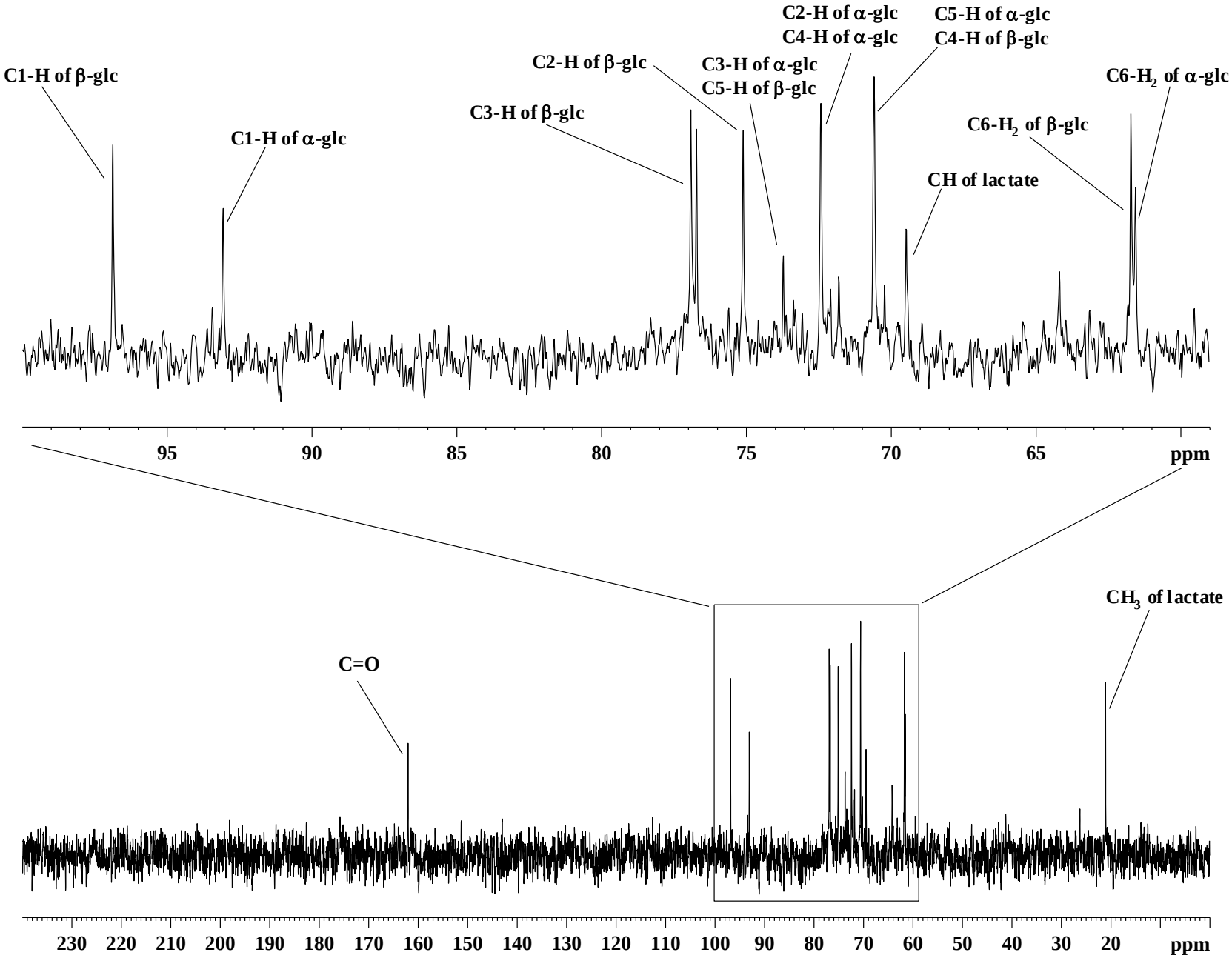

Fig. 15: ^{13}C spectrum of the lyophilized CSF, highlighting the resonance assignments between 10.0-240.0 ppm. The labeled assignments are: α-glc, α-glucose; β-glc, β-glucose.

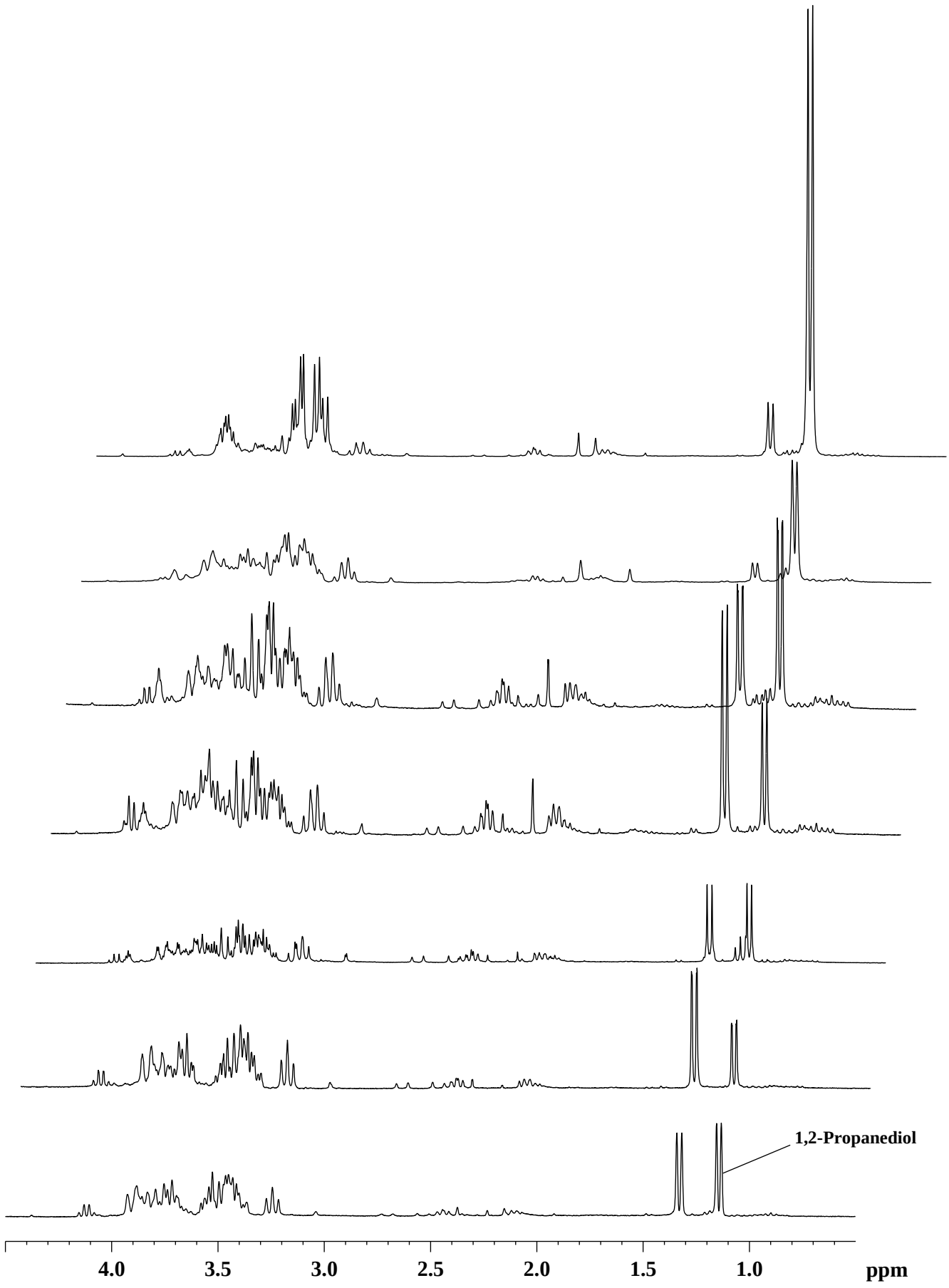

Fig. 16: Stack plot of the ^{1}H NMR spectra of representative BM cases, highlighting the occurrence of 1,2-propanediol.

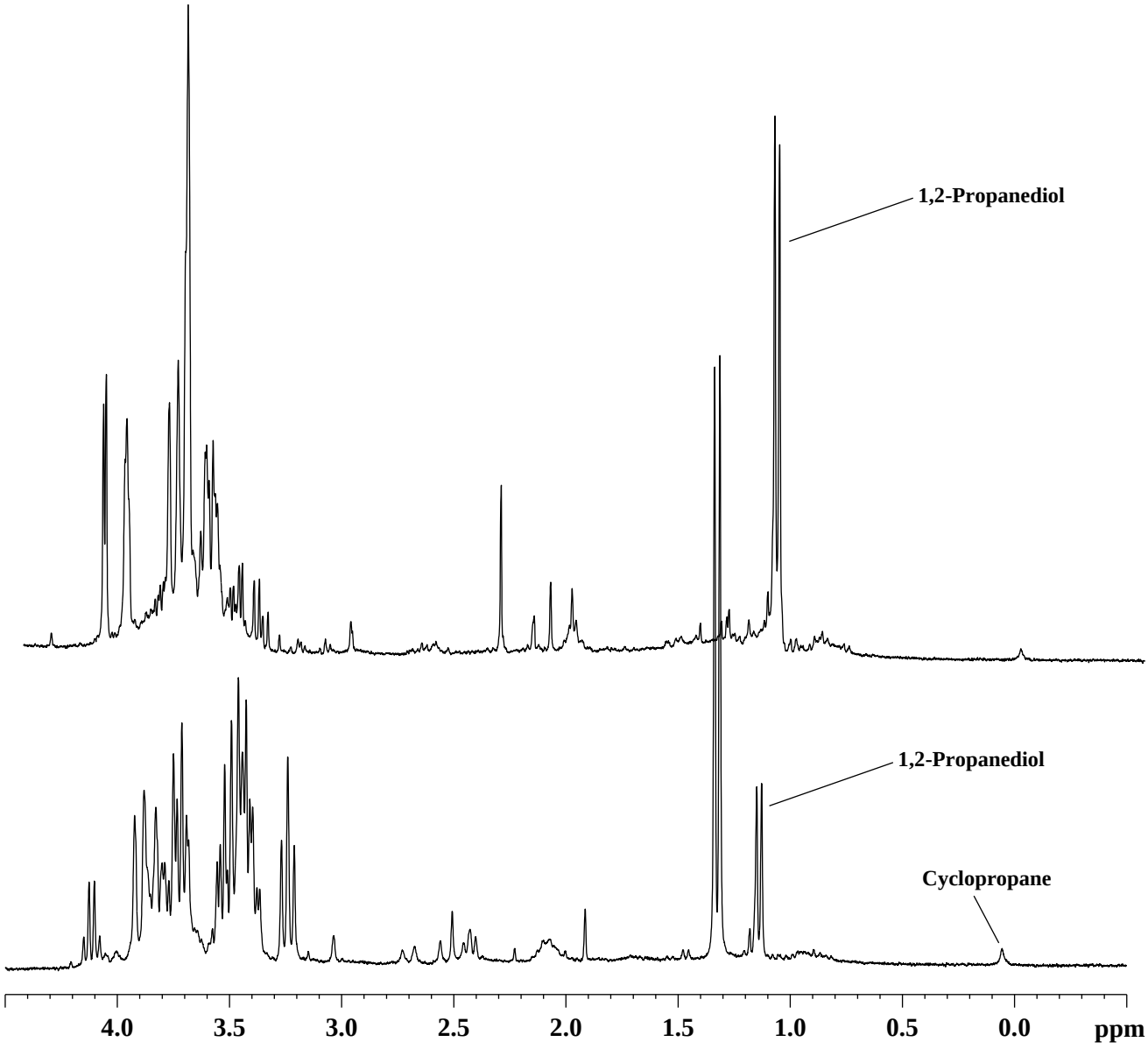

Fig. 17: Stack plot of the ^{1}H NMR spectra of representative TBM cases, highlighting the occurrence of 1,2-propanediol.

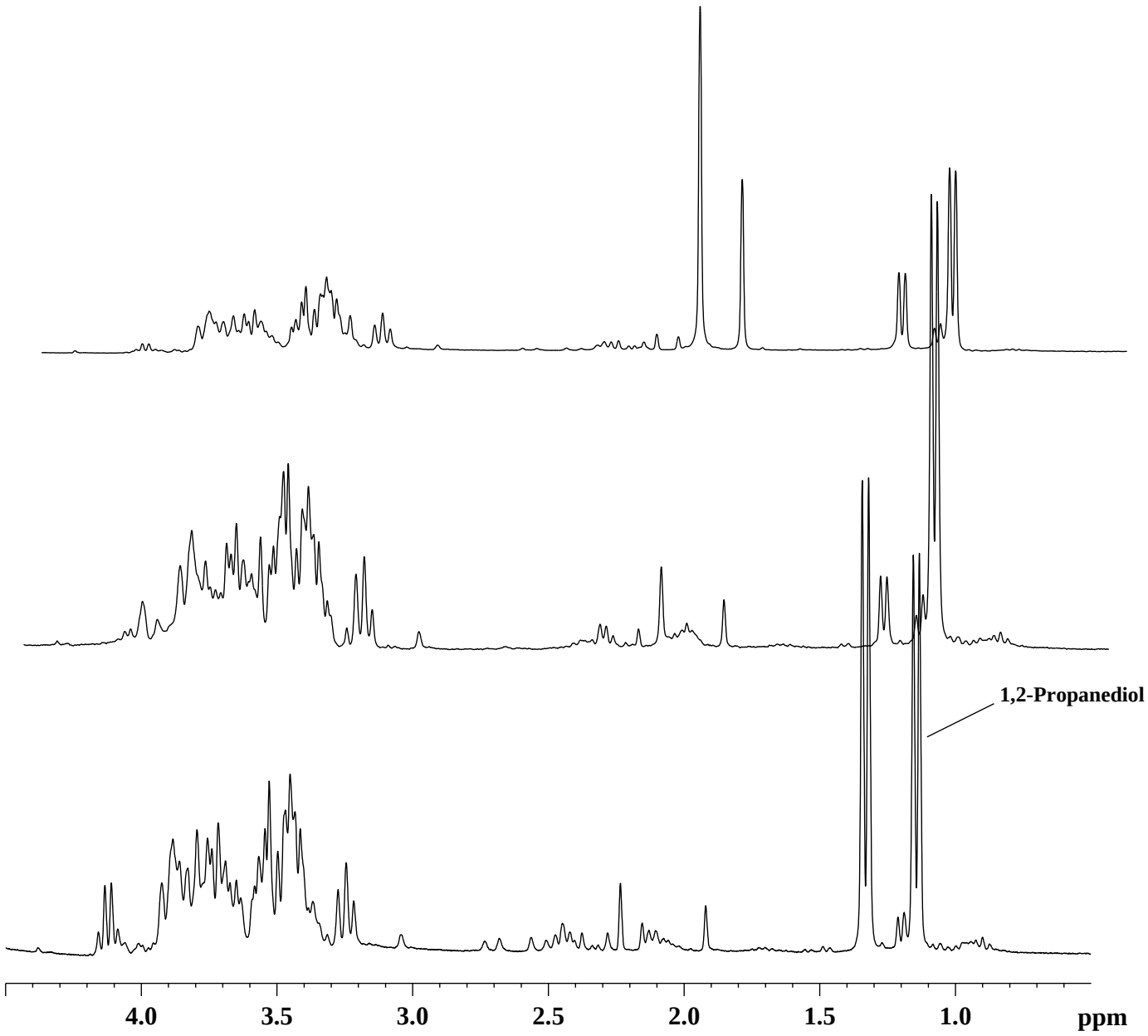

Fig. 18: Stack plot of the ^{1}H NMR spectra of representative Control cases, highlighting the occurrence of 1,2-propanediol.

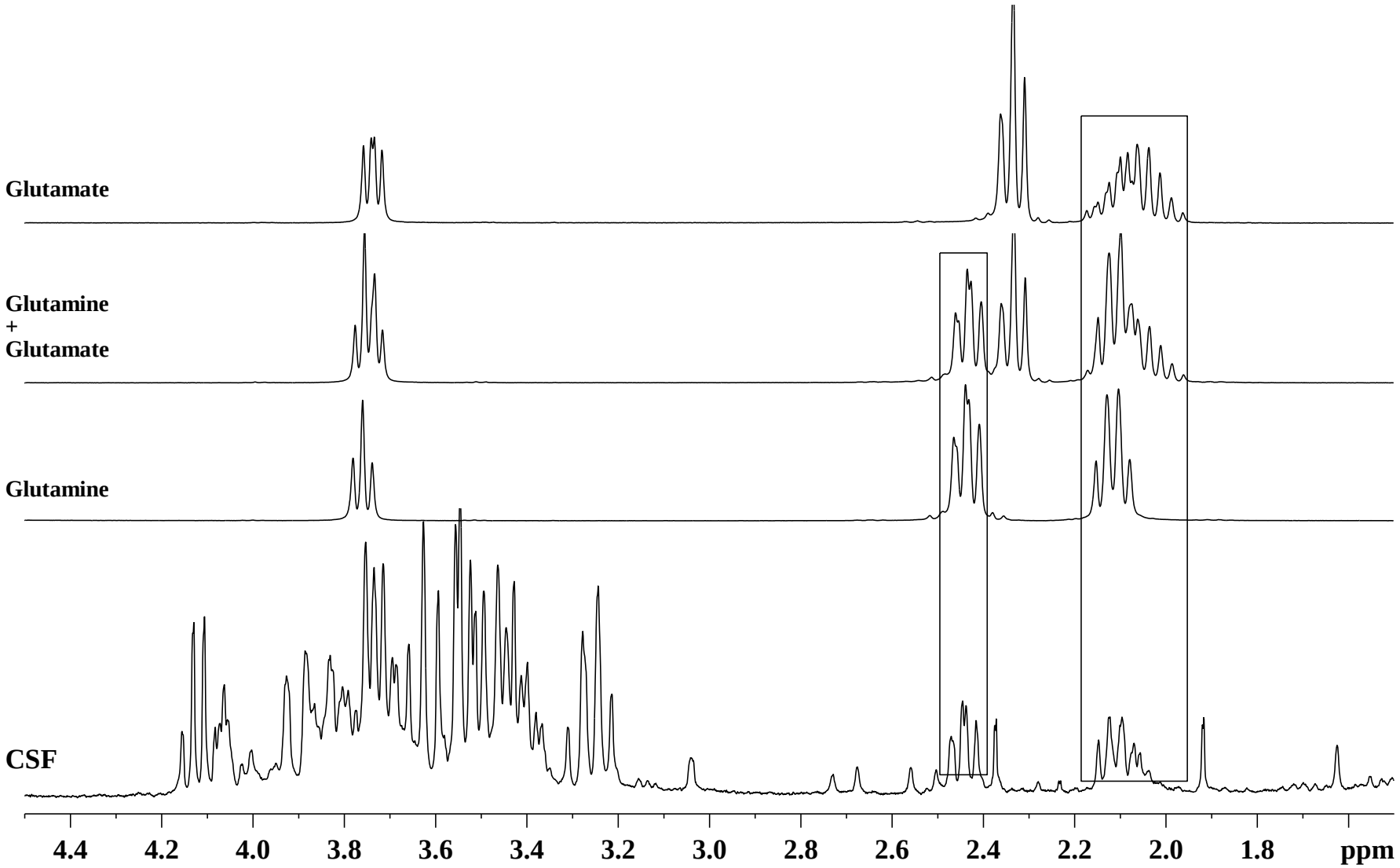

Fig. 19: Confirmation of the chemical shift assignments of glutamine in the ^{1}H NMR spectra of CSF, showing the presence of only glutamine and not glutamate (as marked in the rectangular boxes) based on the comparison of the individual spectra of glutamine and glutamate.

creatine/creatinine, glucose and urea, which could be readily assigned at 300 MHz, were chosen for the NMR-based quantification.

The information obtained regarding the clinical symptoms of the patients is summarized in Table-1(a). When the meningitis cases were compared with the control cases, the percent clinical symptoms observed were significantly increased for fever ($p < 0.001$, BM; $p < 0.001$, TBM; $p < 0.001$, VM), vomiting ($p < 0.05$, VM), altered sensorium ($p < 0.01$, BM; $p < 0.01$, TBM; $p < 0.001$, VM), lymphadenopathy ($p < 0.01$, TBM), BCG scar ($p < 0.001$, BM; $p < 0.001$, VM), abnormal movements ($p < 0.05$, VM) and neck rigidity ($p < 0.001$, BM; $p < 0.001$, TBM). Among meningitis cases, the BM and TBM groups when compared with the VM group exhibited a significant increase in lymphadenopathy for TBM ($p < 0.05$), a significant decrease in BCG scar for TBM ($p < 0.001$), a significant decrease in abnormal movements for BM ($p < 0.001$) and a significant increase in neck rigidity ($p < 0.001$, BM; $p < 0.001$, TBM). Similarly when the BM group was compared with the TBM group, a significant decrease in focal weakness ($p < 0.05$), a significant decrease in lymphadenopathy ($p < 0.01$), a significant increase in BCG scar ($p < 0.001$) and a significant decrease in abnormal movements ($p < 0.05$) were observed.

The concentrations of twelve chosen metabolites obtained through NMR-based quantification (NMRQUANT) *viz.*, β-hydroxy butyrate, lactate, alanine, acetate, acetone, acetoacetate, pyruvate, glutamine, citrate, creatine/creatinine, glucose and urea, as well as 1,2-propanediol, are presented in Table-2. A significant increase in the concentrations of urea ($p < 0.001$, BM; $p < 0.05$, TBM), citrate ($p < 0.01$, BM; $p < 0.01$, TBM) and alanine ($p < 0.05$, BM; $p < 0.01$, TBM) were observed for the BM and TBM cases when compared with the control group. Comparisons of the quantitated metabolites among the three meningitis groups showed a significant increase in the concentrations of urea ($p < 0.001$, BM; $p < 0.01$, TBM), creatine/creatinine ($p < 0.05$, BM), citrate ($p < 0.01$, BM; $p < 0.05$, TBM), pyruvate ($p < 0.01$, BM), acetoacetate ($p < 0.05$, BM) and β-hydroxy butyrate ($p < 0.01$, BM) for the BM and TBM groups when they were compared with the VM group.

The percent occurrence of other unquantified NMR-observed metabolites as obtained for the meningitis as well as the control cases has been summarized in Table-1(b). The signals arising due to the presence of tyrosine (6.80, 7.20 ppm), *myo*-inositol (4.05 ppm), glycine (3.56 ppm), choline-containing compounds (3.21-3.27 ppm), valine, leucine, isoleucine (0.90-1.10 ppm), formate (8.46 ppm) and cyclopropane (0.05 ppm, which was observed only in TBM cases), were taken in this category. These biochemicals were not considered for NMR-based quantification and were grouped separately to summarize their occurrence in the CSF samples of patients, either due to signal overlapping or they were absent in the ^{1}H NMR spectra as seen in certain cases. Comparisons among the groups showed a significant increase in the occurrence of cyclopropane for tuberculous meningitis ($p < 0.001$) when compared to the control, bacterial and viral meningitis groups, followed by a significant decrease in the occurrence of choline-containing compounds for bacterial meningitis when compared with tuberculous meningitis ($p < 0.05$) with a significant increase of the same for tuberculous meningitis ($p < 0.001$) when compared with viral meningitis group. Further, a physical examination/comparison of the ^{1}H NMR spectra of meningitis and control groups proved that the only visible differentiating factor was the presence of a small, broad singlet at 0.05 ppm assigned as cyclopropane, as seen in tuberculous meningitis cases. The chemical shift assignments of the metabolites were found to be the same for the lyophilized and reconstituted CSF samples (in D_2O) when the Watergate ^{1}H NMR was re-performed, except for the absence of cyclopropane, acetone and urea signals as they were either gaseous, volatile and/or exchangeable in nature (fig. 19).

The collective CSF cell-count and CSF protein information obtained for the total number of patients under a particular group is summarized in Table-1(c). When the meningitis cases were compared with the control cases for the CSF cell-count information, the patients under the CSF cell-count category <50/cmm were significantly lower for BM ($p < 0.001$) and TBM ($p < 0.001$) groups, but were significantly higher in the 100-<500/cmm category for both BM ($p < 0.001$) and TBM ($p < 0.001$), followed by a significant increase in the >500/cmm category for the BM group ($p < 0.001$). Among the meningitis groups, comparison of both bacterial and tuberculous meningitis with viral meningitis showed that the patients in the <50/cmm category were significantly lower for both BM ($p < 0.001$) and TBM ($p < 0.001$), as well as in the 50-<100/cmm category for the BM group ($p < 0.01$). Similarly, the patients in the 100-<500/cmm category were

found to be significantly higher for both BM ($p < 0.001$) and TBM ($p < 0.001$), as well as in the >500/cmm category for BM ($p < 0.001$). Comparisons among the BM and TBM groups indicated the patients were significantly lower in the 50-<100/cmm category ($p < 0.001$) and were significantly higher for the >500/cmm category ($p < 0.001$). Similar comparisons for the CSF protein data indicated that under the <60 mg% category, the patient score was significantly lesser for both BM ($p < 0.001$) and TBM ($p < 0.001$) when compared with control and VM groups, followed by a significantly higher patient score for the 60-200 mg% category for both BM ($p < 0.001$) and TBM ($p < 0.001$), respectively.

4.2. Multivariate Analysis

Following the univariate analysis of the data shown in Tables 1-2, the data were further subjected to multivariate analysis to see their impact on disease classification. This excluded the collective CSF cell-count and CSF protein information, as the data were not recorded for each patient and were obtained as a collective information for a particular group. As a result, only the clinical symptoms along with the NMR-based metabolites quantification information were subjected to discriminant function analysis to define which of the variables would function as important descriptors for the classification of disease and control groups, respectively. Based on the correlation-matrix observations, it was found that none of the clinical symptom variables were related to each other, and hence all symptom variables were considered for DFA. Whereas in the case of NMR-derived metabolite variables, metabolites such as creatine/creatinine, citrate, glutamine, pyruvate, acetoacetate, alanine, lactate and β-hydroxy butyrate were related to each other in all three disease groups in comparison with the control group, and this correlation permitted selection of a set of few variables for each disease groups (Table-4) needed for a successful classification.

Discriminant function analysis was carried out for the already classified data (data comprising 85 cases of BM, 47 cases of TBM, 35 cases of VM and 24 cases of control) involving these set-of-variables (clinical symptoms and NMR-derived metabolite variables) to re-validate the classification. The detailed results are summarized in Table-4. Based on DFA, for bacterial meningitis cases when pooled with the control cases, the twelve chosen NMR-derived metabolite variables alone could successfully classify overall 72.48% cases with a sensitivity of 74.12% for

Table-4: Re-validation of the data (first stage) comprising clinical symptoms and metabolite weights (obtained from NMR) from three classes of meningitis with the control data, giving the respective sensitivity and specificity values of classification using Discriminant Function Analysis. The NMR variables are: urea, glucose, creatine/creatinine, citrate, glutamine, pyruvate, acetoacetate, acetone, acetate, alanine, lactate, and β-hydroxy butyrate. The clinical symptom variables are: fever, headache, convulsions-general, convulsions focal, vomiting, focal weakness, altered sensorium, lymphadenopathy, BCG scar, abnormal movements, and neck rigidity.

Variables taken for DFA	**Bacterial Meningitis with Control**				**Tuberculous Meningitis with Control**				**Viral Meningitis with Control**			
	Sensitivity	Specificity	*F*-ratio	*p*-value	Sensitivity	Specificity	*F*-ratio	*p*-value	Sensitivity	Specificity	*F*-ratio	*p*-value
All NMR variables	74.12%	66.67%	1.58	0.11	76.60%	75.00%	2.22	0.02	88.57%	58.33%	1.37	0.21
Few NMR variables[@,#,$]	78.82%	45.83%	4.02	0.01	78.72%	62.50%	2.23	0.06	94.29%	41.67%	3.51	0.01
Clinical Symptom variables	98.44%	79.17%	17.25	< 0.001	97.37%	95.83%	12.01	< 0.001	99.00%	87.50%	6.60	< 0.001
Combined variables (NMR + Clinical)	99.00%	99.00%	4.46	0.001	97.37%	95.83%	4.97	< 0.001	99.00%	99.00%	5.67	0.002

[@]For Bacterial Meningitis Group: glucose, glutamine, acetate, alanine and lactate.
[#]For Tuberculous Meningitis Group: citrate, glutamine, acetoacetate, alanine and β-hydroxy butyrate.
[$]For Viral Meningitis Group: citrate, acetoacetate, acetate, alanine and β-hydroxy butyrate.

the bacterial meningitis and a specificity of 66.67% for the control (*F*-Ratio: 1.58, *p*-value: 0.11). Among these variables when only glucose, glutamine, acetate, alanine and lactate were selected based on their discriminant function weights and the DFA was carried out again, overall 71.56% cases could be successfully classified, with a sensitivity of 78.82% and a specificity of 45.83% (*F*-Ratio: 4.02, *p*-value: 0.01). Similarly for the same pool of BM and control cases when DFA was carried out considering eleven clinical symptom variables, overall 93.18% cases could be successfully classified with a sensitivity of 98.44% and a specificity of 79.17% (*F*-Ratio: 17.25, *p*-value: < 0.001). We have found that neither the NMR-derived metabolite variables nor the clinical symptoms could efficiently differentiate the BM group from the control, but when both clinical and NMR-derived metabolite variables were combined together and subjected to DFA, the classification was found to be improved and overall 99% cases could be successfully classified with a sensitivity of 99% and a specificity of 99% (*F*-Ratio: 4.46, *p*-value: 0.001). Thus, the discriminant function analysis involving the clinical symptom variables and the NMR-derived metabolite variables proved that for successful classification of a disease group from the control, it is necessary to combine both these classes of variables together.

Similarly when the tuberculous meningitis cases were pooled with the control cases, with the help of twelve NMR-derived metabolite variables overall 76.06% cases could be successfully classified with a sensitivity of 76.6% and a specificity of 75% (*F*-Ratio: 2.22, *p*-value: 0.02). Variables such as citrate, glutamine, acetoacetate, alanine and β-hydroxy butyrate were selected based on their discriminant function weights, and when the DFA was carried out again overall 73.24% cases could be successfully classified with a sensitivity of 78.72% and a specificity of 62.5% (*F*-Ratio: 2.23, *p*-value: 0.06). Similarly when DFA was carried with eleven clinical symptom variables, overall 96.77% cases could be successfully classified with a sensitivity of 97.37% and a specificity of 95.83% (*F*-Ratio: 12.01, *p*-value: < 0.001). As noted for BM cases, when the clinical symptom variables and the NMR-derived metabolite variables were combined together and subjected to DFA, overall 96.77% cases could be successfully classified with a sensitivity of 97.37% and a specificity of 95.83% (*F*-Ratio: 4.97, *p*-value: < 0.001).

For the viral meningitis group pooled with the control group, when all the NMR-derived metabolite variables were taken into consideration and the DFA was performed, overall 76.27%

cases could be successfully classified with a sensitivity of 88.57% and a specificity of 58.33% (*F*-Ratio: 1.37, *p*-value: 0.21). Variables such as citrate, acetoacetate, acetate, alanine and β-hydroxy butyrate were selected based on their discriminant function weights, and when the DFA was carried out again overall 72.88% cases could be successfully classified with a sensitivity of 94.29% and a specificity of 41.67% (*F*-Ratio: 3.51, *p*-value: 0.01). Further when DFA was carried out involving the clinical symptom variables alone, overall 91.67% cases could be successfully classified with a sensitivity of 99% and a specificity of 87.5% (*F*-Ratio: 6.61, *p*-value: < 0.001). As noted for BM and TBM groups when NMR-derived metabolite variables and clinical symptom variables were combined together, overall 99% cases could be successfully classified with a sensitivity of 99% and a specificity of 99% (*F*-Ratio: 5.67, *p*-value: 0.002).

It was observed that except cyclopropane, other unquantified NMR-derived metabolite variables such as tyrosine, *myo*-inositol, glycine, choline-containing compounds, valine, leucine and isoleucine, and formate do not play any major role towards classification of the disease data from the control. When these unquantified NMR-derived metabolite variables were subjected to DFA with the respective meningitis and control data, the classification pattern ranged from 67-90% with severe overlapping for bacterial and viral meningitis groups, although incorporation of cyclopropane could improve the classification up to 90.14% only in case of tuberculous meningitis. Since cyclopropane was observed overall in 85.1% cases of TBM, based on the DFA results it was therefore concluded as a fingerprint marker for this disease class.

Followed by the initial re-validation of the classified data comprising the disease and control groups using DFA, the second stage of re-validation (based on DFA) involved combining all three disease groups together and pooling them along with the control group so as to assess the classification pattern. This task was carried out solely with an aim of segregating the disease group (combining bacterial, tuberculous and viral meningitis) from the control group (non-meningitis cases), followed by the segregation of tuberculous meningitis from the non-tuberculous meningitis cases (bacterial meningitis and viral meningitis), ultimately culminating in the segregation of bacterial meningitis cases from the viral meningitis cases. As observed in the initial re-validation of the data based on DFA, a combination of the NMR-derived metabolite variables and the clinical symptom variables could successfully classify overall 96.38% cases into

the respective groups, with a sensitivity of 99% for the disease cases (BM+TBM+VM) and a specificity of 79.17% for the control group (*F*-Ratio: 10.85, *p*-value: < 0.001). Subsequently, when the non-tuberculous meningitis (BM+VM) and tuberculous meningitis cases were subjected to DFA, overall 77.19% cases could be successfully classified into the respective groups, with a sensitivity of 81.58% for the non-tuberculous meningitis category and a specificity of 68.42% for the tuberculous meningitis group (*F*-Ratio: 1.79, *p*-value: 0.03). Subjecting the bacterial meningitis and viral meningitis cases for DFA with clinical and NMR-derived metabolite variables, overall 84.21% cases could be successfully classified into the respective groups, with a sensitivity of 84.38% for the bacterial meningitis group and a specificity of 83.33% for the viral meningitis group (*F*-Ratio: 1.83, *p*-value: 0.04).

The detailed results regarding the sensitivity and specificity values obtained through the discriminant function analysis for the second stage of re-validation of the meningitis and control data are summarized in Table-5. Based on the DFA results it was observed that among the clinical symptom variables, fever was necessary to separate out the disease cases from the control group, but it was ineffective for the differentiation of the TBM from non-TBM cases as well as for the differentiation of BM from VM cases. Similarly among the NMR-derived metabolite variables, the contribution of acetoacetate was noteworthy, as this single NMR-derived metabolite variable alone (in combination with the clinical symptom variables) could successfully classify the disease cases from the control group, followed by the differentiation of TBM cases from the non-TBM cases as well as the differentiation of BM cases from VM cases (Table-5). The respective mid-point cut-off values and discriminant function weights (w_i) obtained for all the clinical symptom variables and NMR-derived metabolite variables (Table-5) were subsequently incorporated in our expert system MENEXSYS, resulting in the formulation of classification criteria (fig. 20) for the purpose of prediction of the type of any new ‘suspected to be meningitis’ case.

Table-5: Re-validation of the Classified Data (second stage) comprising clinical symptoms and metabolite weights (obtained from NMR) from three classes of meningitis with the control data based on the Discriminant Function Analysis for the construction of MENEXSYS, giving the respective sensitivity and specificity values of classification. The same methodology has been applied in the form of 'classification tree' as outlined in fig. 20 for the differential diagnosis of a new patient's case through MENEXSYS.

Variables taken for DFA	**Bacterial Meningitis + Tuberculous Meningitis + Viral Meningitis with Control**				**Tuberculous Meningitis with Bacterial Meningitis + Viral Meningitis**				**Bacterial Meningitis with Viral Meningitis**			
	Sensitivity	Specificity	*F*-ratio	*p*-value	Sensitivity	Specificity	*F*-ratio	*p*-value	Sensitivity	Specificity	*F*-ratio	*p*-value
NMR + clinical symptom variables	99%	79.17%	10.85	< 0.001	--	--	--	--	--	--	--	--
NMR + clinical symptom variables (without fever)	--	--	--	--	68.42%	81.58%	1.79	0.03	84.38%	83.33%	1.83	0.04
Acetoacetate + clinical symptom variables	99%	62.5%	21.18	< 0.001	--	--	--	--	--	--	--	--
Acetoacetate + clinical symptom variables (without fever)	--	--	--	--	60.53%	84.21%	3.33	0.001	81.25%	83.33%	2.65	0.01

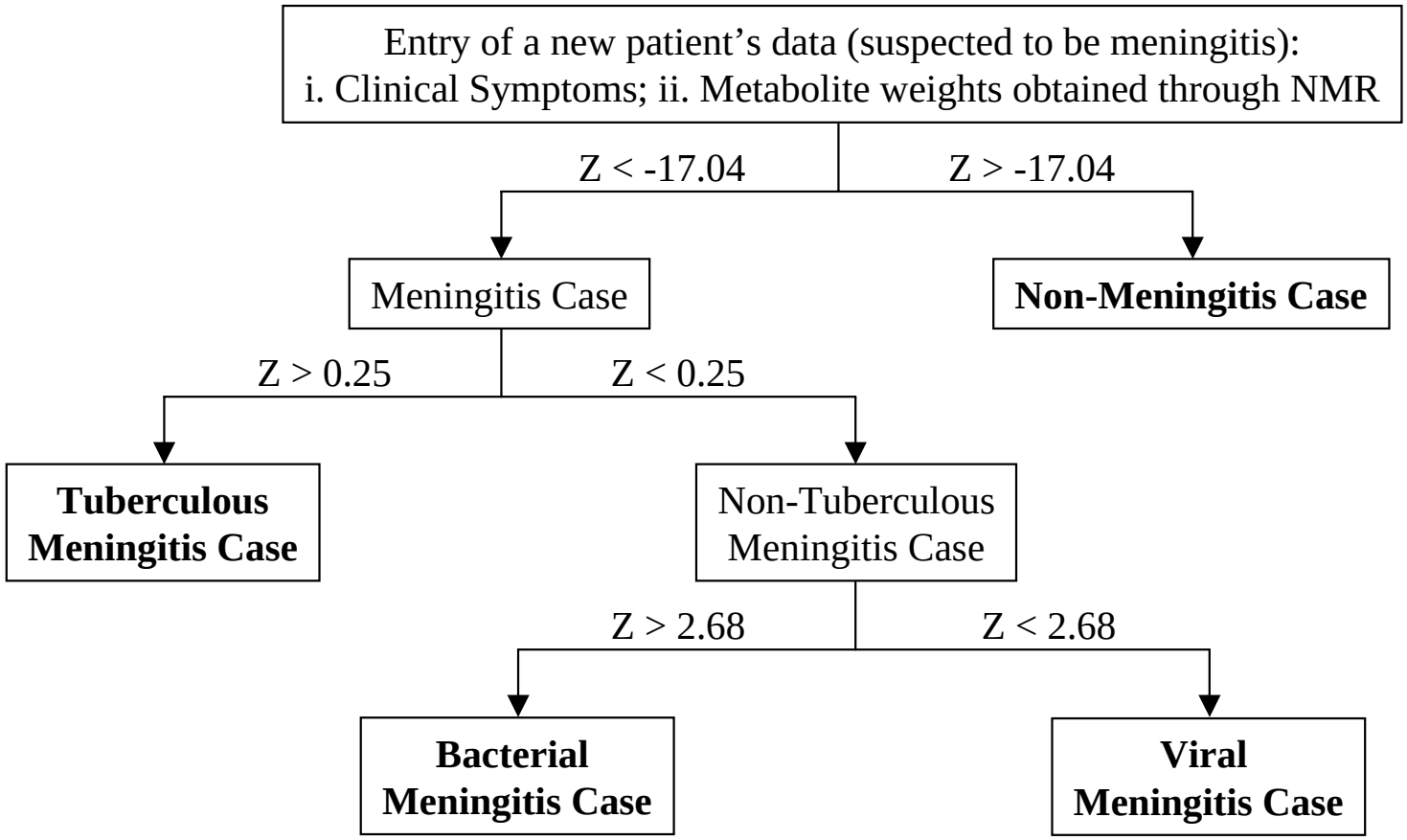

Fig. 20: Classification-tree for the differential diagnosis of a new childhood meningitis case through MENEXSYS, involving the clinical symptoms and metabolite weights data obtained through NMR.

5. Discussion

5.1. NMR Spectroscopic Findings and Clinical Observations

The metabolite concentrations of CSF play a very important role for the diagnosis of neurological diseases (Petroff et al., 1986; Hiraoka et al., 1994; Simone et al., 1996; Niroli et al., 1993). It has recently been observed that the analysis of CSF based on CSF cytology, sugar and protein content is not the primary information to serve for the purpose of differential diagnosis (Thwaites et al., 2002). As noted during the course of our present investigation, in certain cases, recording of the clinical symptoms (as observed by the clinician) was difficult to interpret and it was found that the children were unable to express themselves. Although in adults the clinical symptoms may serve as good differentiating markers for meningitis (Thwaites et al., 2002), our experience has indicated that the clinical symptoms may not be the sole differentiating markers in childhood meningitis, possibly due to the anomalies as explained above in recording the symptoms or due to any overlapping. The judicious choice is then to select a few metabolites, which are consistently present in all CSF samples along with the identification of fingerprint metabolite(s), quantify them and see whether they have any impact on disease classification. Our study has therefore involved a combination of clinical symptoms, various metabolite concentrations as observed through NMR and identification of fingerprint marker(s) as a 'method of choice' for a quick differential diagnosis in order to proceed to a better treatment of the child, otherwise it may become fatal. Since lumbar puncture is not justified in normal children, we had to compare the quantitative results obtained for meningitis cases with the CSF samples of children suffering from other disorders that were subsequently grouped as controls (n=24) as per the earlier reported works (Heiblim et al., 1978; McGale et al., 1977).

The cyclopropane signal assigned at 0.05 ppm was observed in a significant proportion of tuberculous meningitis patients and has formed an important finding in our study (fig. 5). The assignment of cyclopropane was based on an earlier NMR study involving *M. tuberculosis* strains and intracranial granuloma (Gupta et al., 1996) that showed the presence of phenolic glycolipids and cyclopropane in their lipid extracts, and was proposed as a fingerprint assignment of the integral product of mycobacterial cell-wall. It is unlikely that this resonance signal has arisen due

to any drug metabolism, since none of the drugs comprising the ATT regimen administered to the patients had the cyclopropyl group as an integral structural component. The cyclopropane signal was detected as a discrete, dissolvable gaseous form instead of the collective form (as seen in mycolic lipids), and in lyophilized CSF samples this signal was found to be absent (fig. 21). The ^{1}H NMR chemical shift of cyclopropane is known to be anomalously high and a value of 0.05 ppm is as expected. This indicated that the signal to be in dissolved gaseous form and since this signal was only observed in tuberculous meningitis samples alone, it was unequivocally assigned to be cyclopropane. Since this signal has been found to merge with the signal of TSP, the commonly used reference (fig. 22), it became necessary that the NMR experiments be performed twice, first without TSP and later with TSP (taken separately in a sealed capillary tube with a known concentration, and inserted into the NMR tube containing CSF).

The possible presence of the drugs and their metabolites or some probable drug-excipients in the CSF samples could be ascertained based on the ^{1}H NMR spectra of the drug molecules (involved in the treatment protocol, such as isoniazid and pyrazinamide), and comparing the chemical shifts along with the pattern observed in the NMR spectra of CSF (fig. 10). In addition to this observation, the presence of 1,2-propanediol, which has also been speculated as a drug excipient/vehicle besides being known as an agent involved in glycerol metabolism (Michal, 1998), was observed in the CSF spectra, but showed a much lower concentration in cases of viral meningitis (Table-2). Since the inclusion of 1,2-propanediol solely as a metabolic end product is debatable, the quantitative information obtained for only twelve metabolites (excluding 1,2-propanediol) was then used for univariate and multivariate analysis as well as for the software (MENEXSYS) development purposes.

An important observation of this study involved the assignment of urea for the first time in CSF using ^{1}H NMR, which has been primarily based on the chemical shift assignment of urea as reported for urine samples (Potts et al., 2001). Although the presence of urea in CSF was documented earlier using certain biochemical methods (Fishman, 1980), its occurrence in CSF in this study has been demonstrated as an exchangeable proton at 5.76 ppm, assigned to the amide NH_2 of urea, which could be effectively detected only by the use of Watergate ^{1}H NMR pulse sequence (fig. 23). This signal was found to either get suppressed or suffer a decrease in the signal

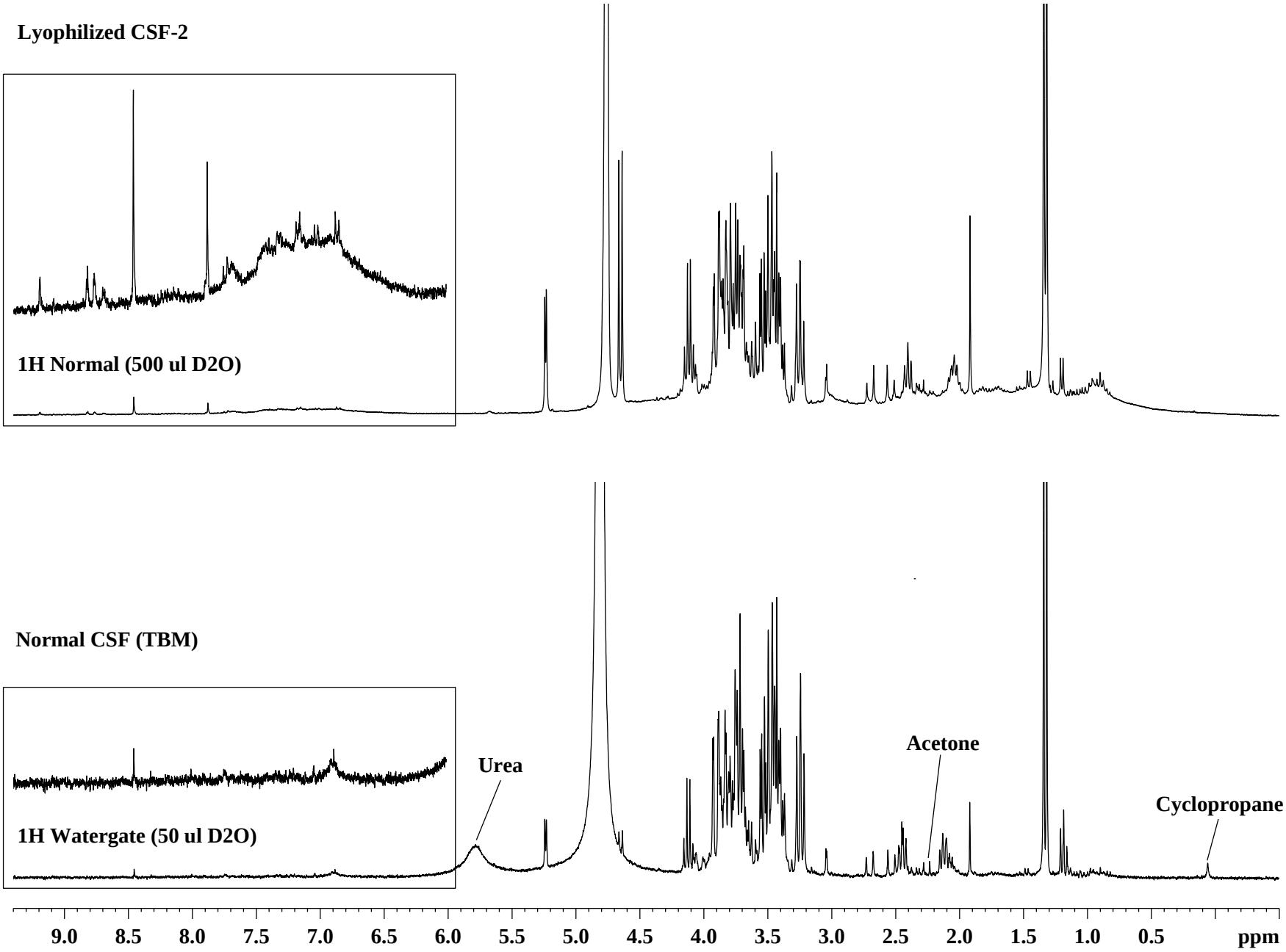

Fig. 21: ^{1}H NMR spectra of the CSF of a representative childhood meningitis case and that of the lyophilized CSF, highlighting the resonance assignments of cyclopropane, acetone and urea, which are gaseous/volatile and exchangeable in nature.

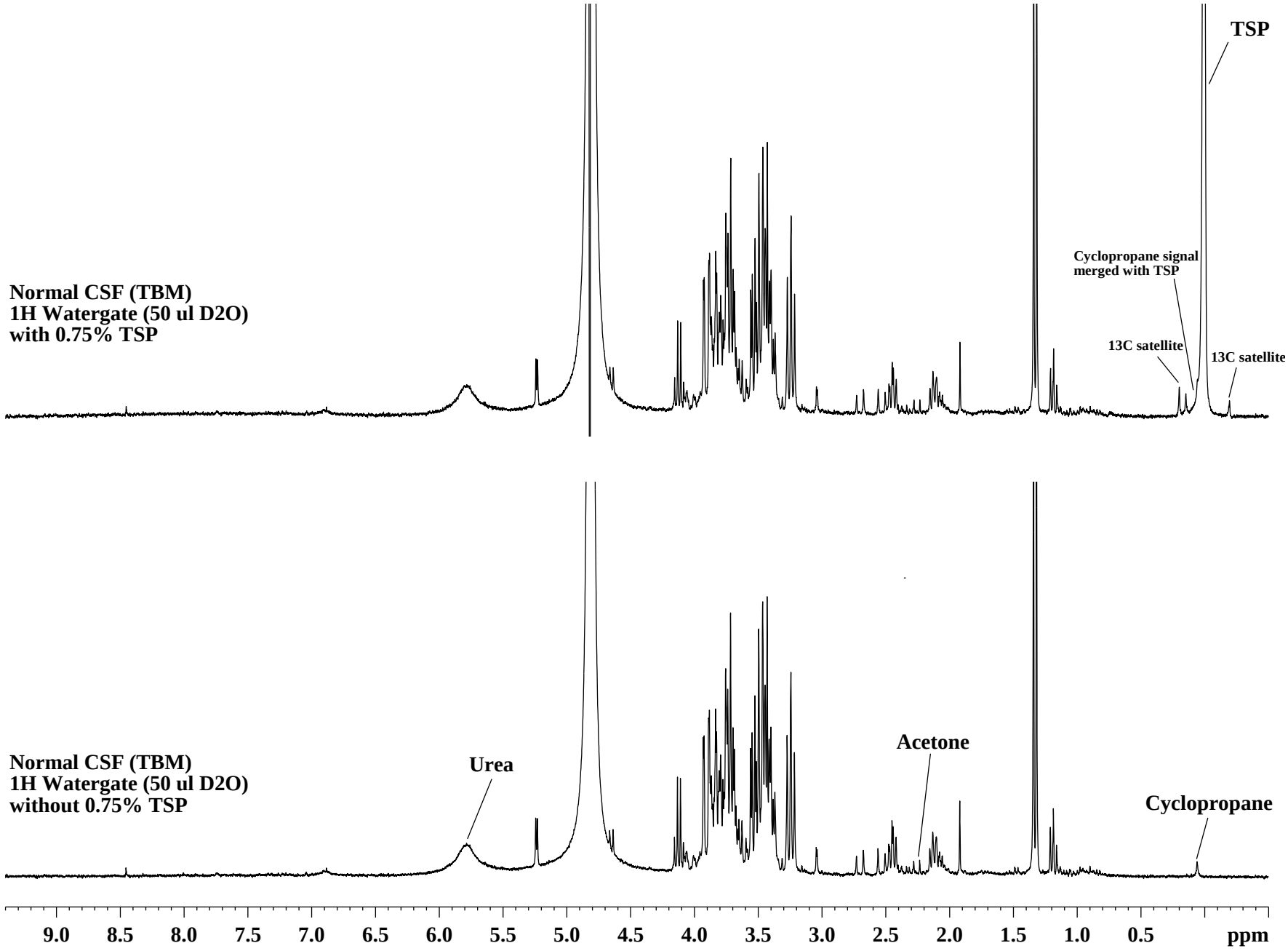

Fig. 22: ^{1}H NMR spectra of a representative tuberculous meningitis case, highlighting the resonance assignment of cyclopropane that merges with the TSP signal.

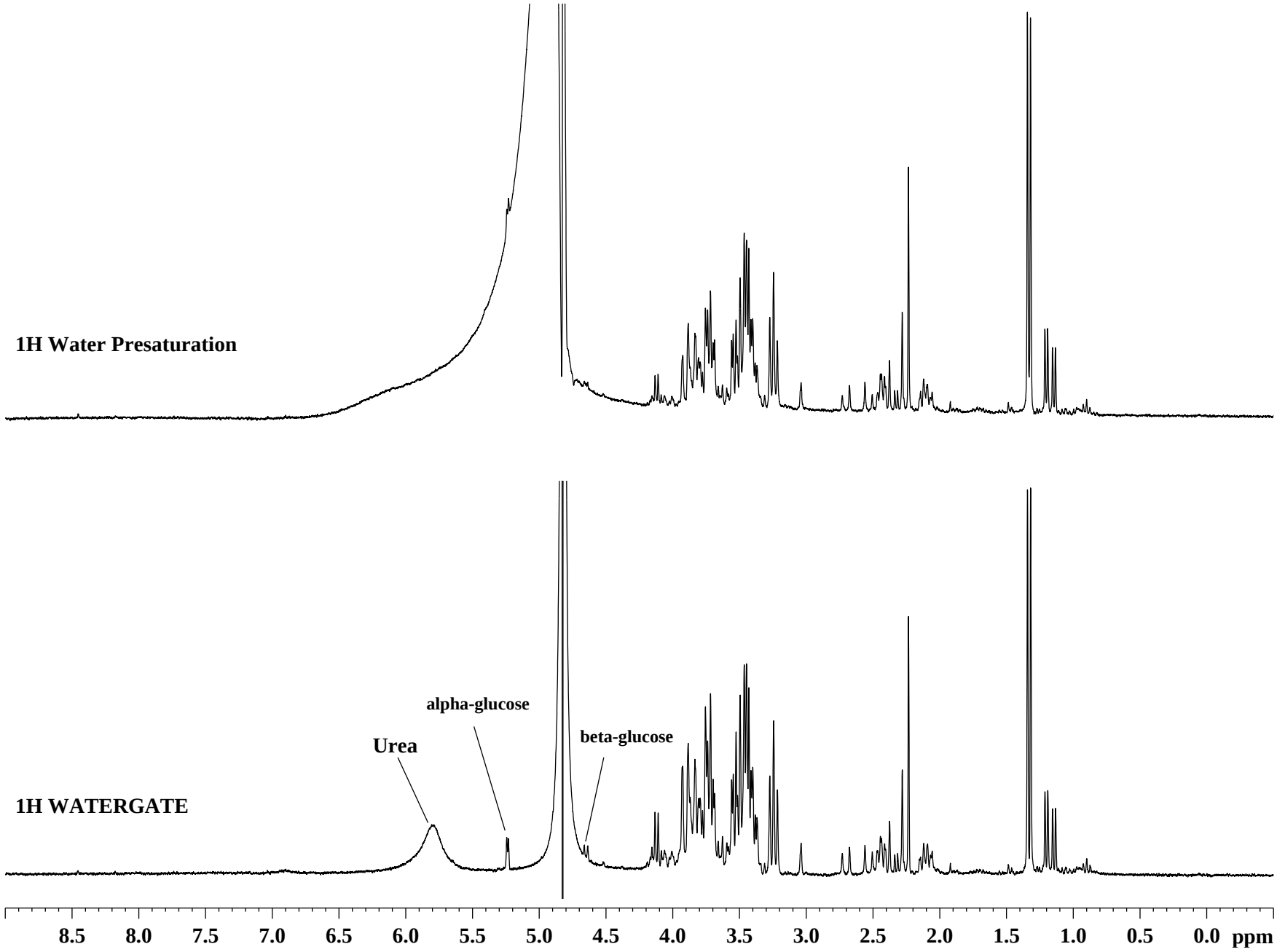

Fig. 23: Comparison of the ^{1}H NMR spectra obtained through WATERGATE and Water Presaturation techniques. Possibility of the resonance assignment of urea by the WATERGATE technique has been highlighted.

intensity due to an exchange process when the water presaturation pulse sequence was employed in native CSF samples (fig. 24), and was almost absent in case of lyophilized CSF due to complete exchange of the amide NH_2 with the deuterium in D_2O (fig. 25).

The visual examination of ^1H NMR spectra proved the distinctive presence of glutamine and the relative absence of glutamate in all 167 meningitis CSF samples, which is somewhat a striking feature. This is in sharp contrast to the findings of an earlier report that described the measurement of glutamine and glutamate in the CSF of meningitis-affected children using electrophoresis (Tucci et al., 1998). The study had demonstrated a lower concentration of glutamine and a higher concentration of glutamate due to bacterial growth and cell destruction, as confirmed earlier by an enzymatic colorimetric assay (Spranger et al., 1996). The unique observation of glutamine in our study could be attributed to the acuteness of the disease, whereas in a few control cases glutamate was found to be present based on the examination of their respective ^1H NMR spectra (fig. 26). Further, it was observed that with an increase in the concentrations of urea, there was an associated increase in the concentrations of glutamine (Table-2). It could be reasoned that the elevation in the levels of urea and glutamine could have occurred due to an increased activity of the urea cycle in the host, wherein the toxic ammonia that was produced either by the bacteria or the mononuclear cells of CSF had in turn been utilized for the conversion of glutamate into glutamine (Seiler, 2002; Suarez et al., 2002), apparently resulting in increased NMR-detectable levels of glutamine and urea, but not glutamate.

The ^1H spin-echo experiment helped in the confirmation of chemical shift assignments, which was based on the phase reversal of *J*-coupled multiplets, where the odd-order multiplets occur above the plane (same as seen in the normal ^1H spectra) while the even-order multiplets experience a phase-reversal and occur below the plane (fig. 27). Apart from the metabolite assignments and their quantification, many significant observations could be drawn from the ^1H Watergate NMR spectra of the CSF samples of the meningitis and control cases. The region 3.1-5.4 ppm in the ^1H NMR spectra had several overlapping signals, which could be resolved with the help of 2D experiments. The individual assignments of α- and β-glucose along with *myo*-inositol have been shown in the expansion of the abovementioned region in the ^1H-^1H COSY spectra (fig. 28), followed by the ^1H NMR of a meningitis CSF that had a pronounced level of *myo*-inositol

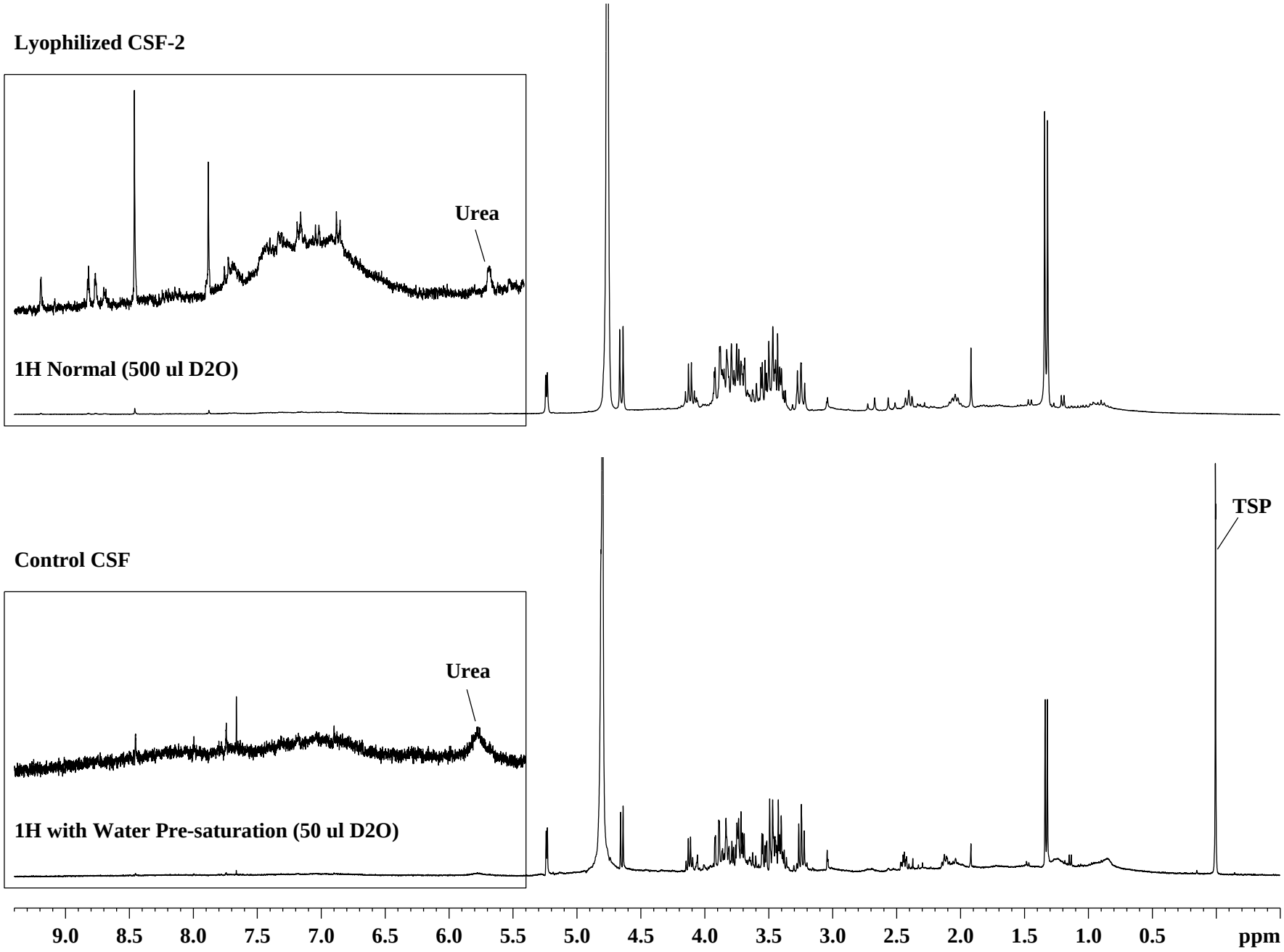

Fig. 24: ^{1}H NMR spectra of the CSF of a representative Control case and that of the lyophilized CSF, highlighting the exchangeable nature of urea -NH_2 protons (with D_2O) when the Water Presaturation technique was employed.

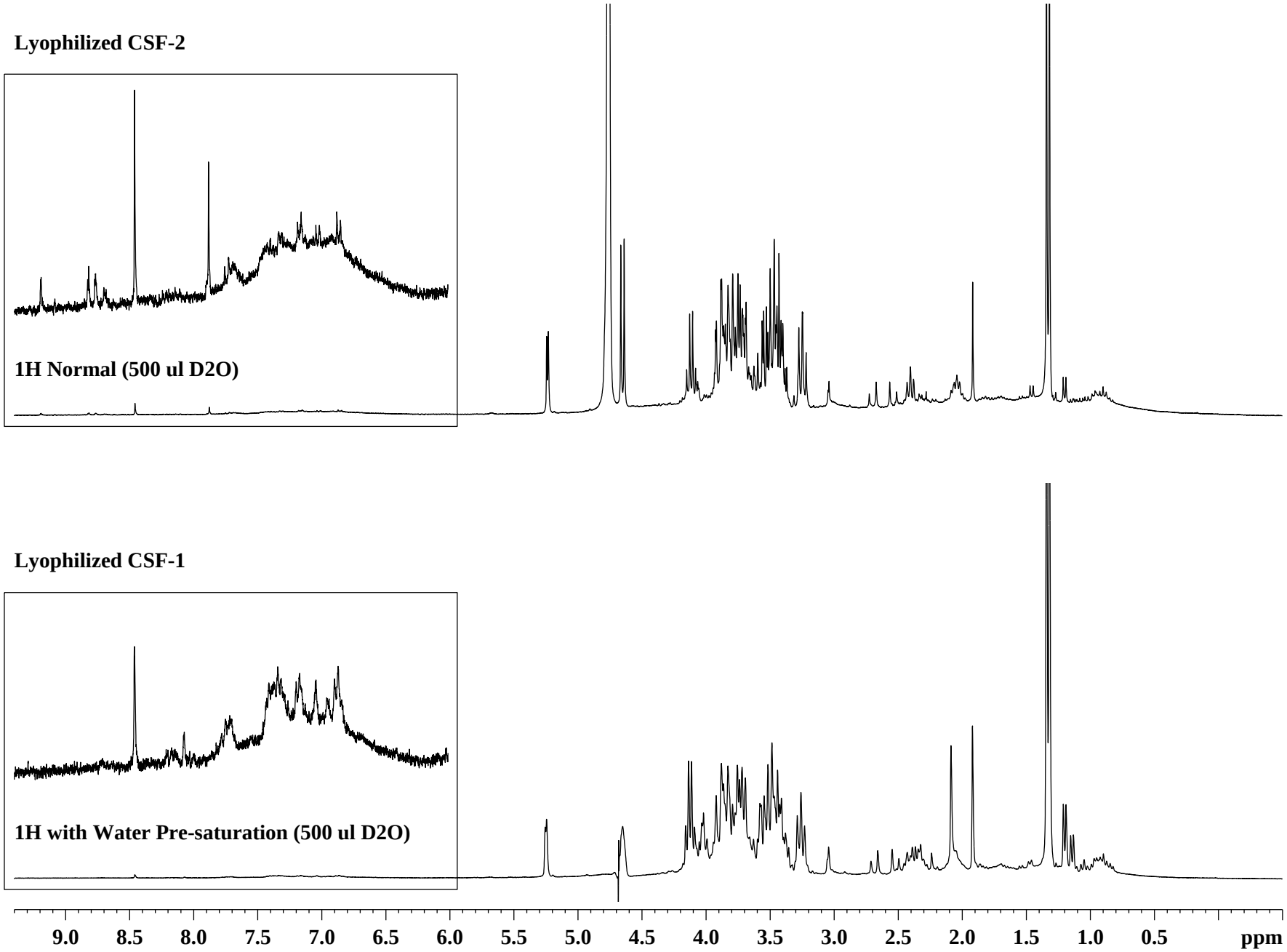

Fig. 25: ^{1}H NMR spectra of lyophilized CSF samples, highlighting the absence of urea protons due to the exchange process with D_2O.

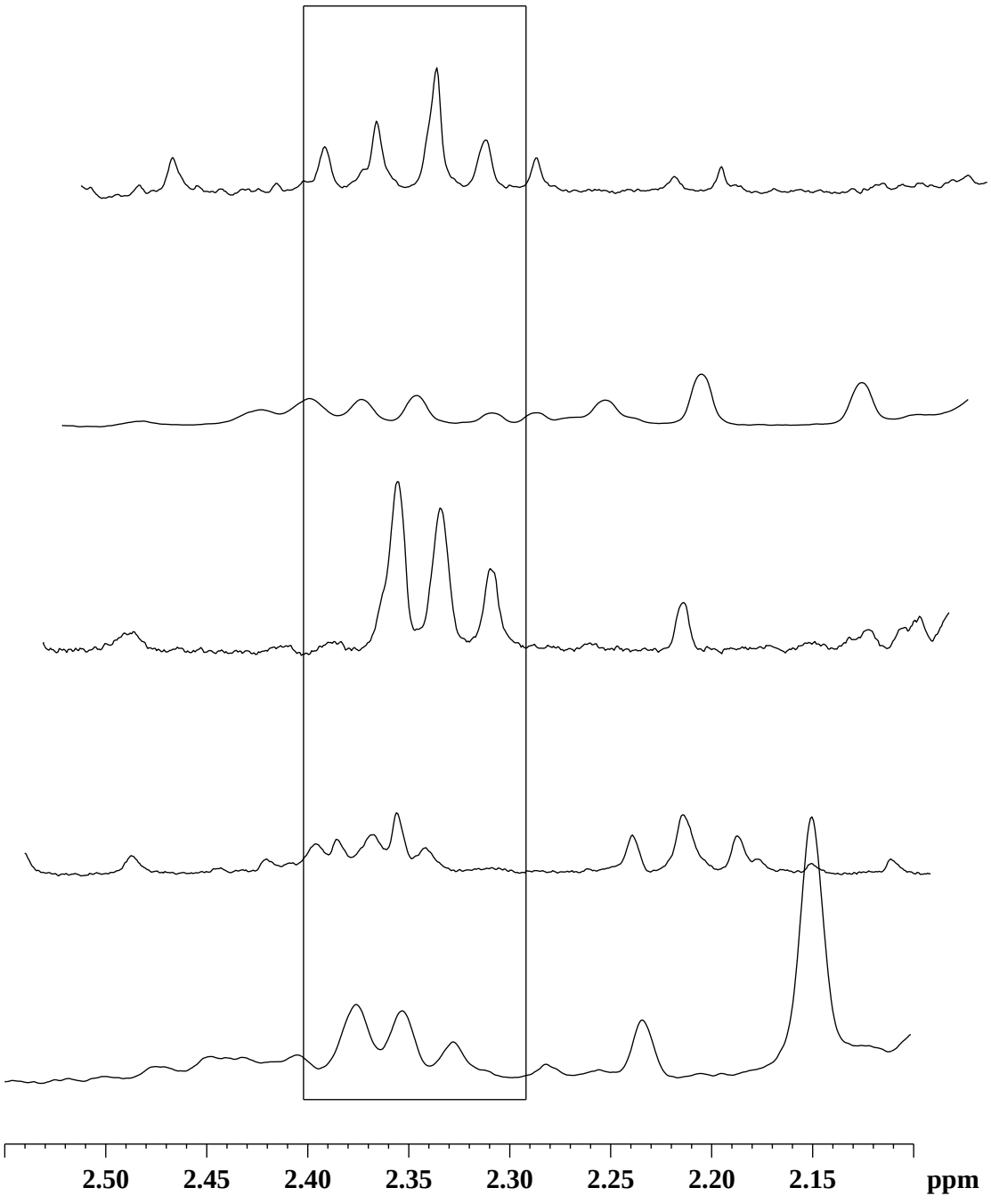

Fig. 26: Stack plot of the ^{1}H NMR spectra of representative Control cases, highlighting the occurrence of glutamate.

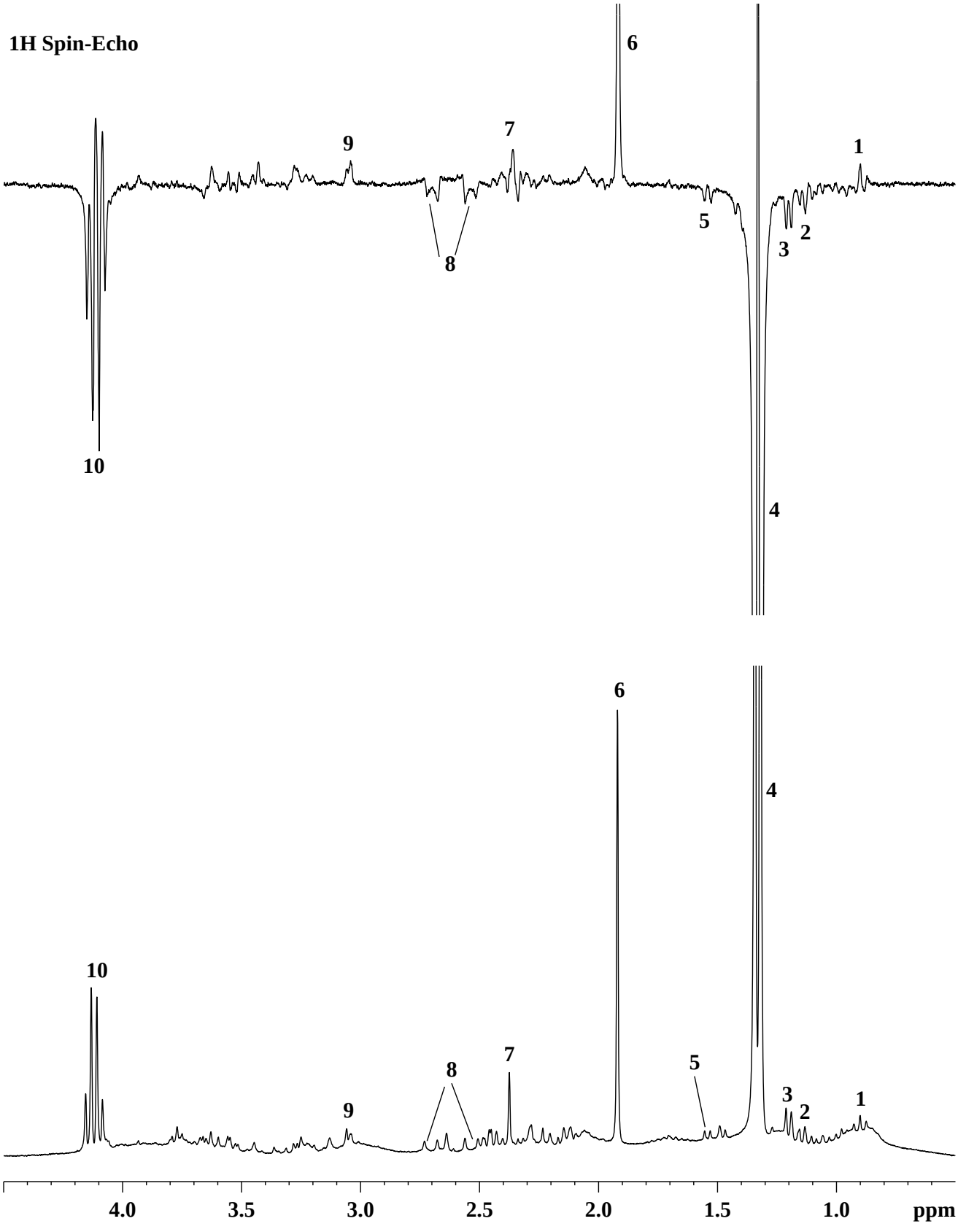

Fig. 27: ^{1}H WATERGATE and spin-echo spectra of a representative childhood meningitis case. The labeled assignments are: 1. α-hydroxy butyrate; 2. 1,2-propanediol; 3. β-hydroxy butyrate; 4. lactate; 5. alanine; 6. acetate; 7. succinate; 8. citrate; 9. creatine/creatinine; 10. lactate.

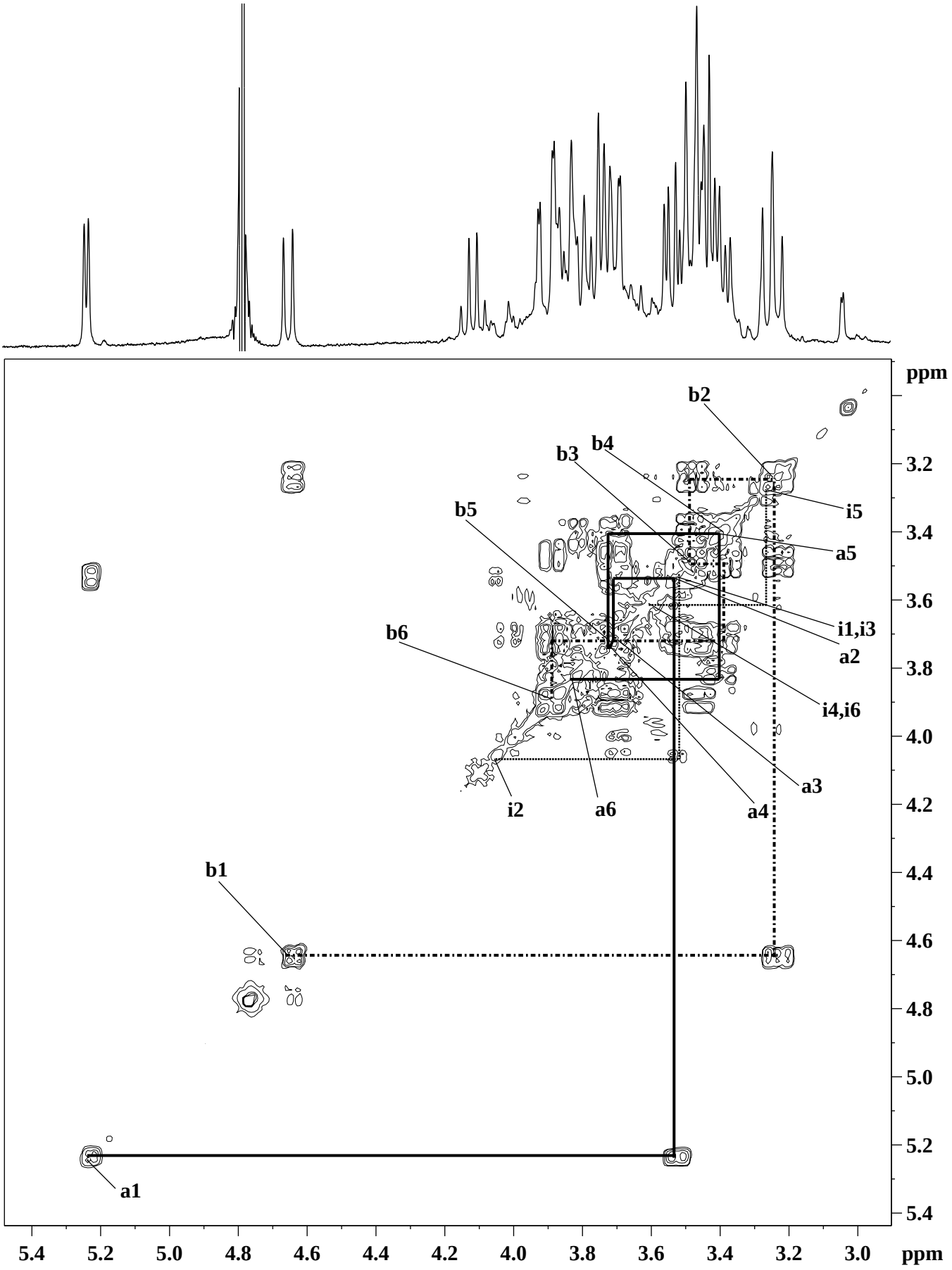

Fig. 28: Expansion of the ^{1}H-^{1}H COSY spectrum of CSF of a representative meningitis case, highlighting the resonance assignments between 2.9-5.5 ppm. The labeled assignments are: a1-a6. α-glucose; b1-b6. β-glucose; i1-i6. *myo*-inositol.

(fig. 29). Similarly, signals from mannitol had been seen to a very high degree at the same region in the ^{1}H NMR spectra especially in those cases with an increased hydrocephalus or an increased cerebral edema, and in those cases an intravenous infusion of mannitol had to be given to cause cerebral dehydration and to reduce cerebral inflammation (figs. 30-33). The downfield region of the ^{1}H NMR spectra of CSF consisted of signals from aromatic amino acids, formate and nucleic acid bases as well as some unassigned signals (fig. 34), although they were not present uniformly in all CSF samples. The visual examination of the ^{1}H NMR spectra of CSF also helped to figure out the contribution of proteins (figs. 35-37), coagulum (figs. 38-40), besides indicating abnormal metabolic profiles (figs. 41-44). In a few cases, the ^{1}H NMR profiles also predicted death of certain patients and are shown in figs. 45-47. The abnormal spectral pattern was a clear-cut evidence of severe pathophysiology associated with meningitis in those patients.

Based on the univariate statistical analysis, the significant observations were drawn as shown in Tables 1-2 and could be considered as general markers for the differentiation of the three types meningitis and the control group. The clinical symptoms *viz*., fever, vomiting, focal weakness, altered sensorium, lymphadenopathy, BCG Scar, abnormal movements and neck rigidity were helpful in segregating the meningitis cases from the control cases, while vomiting, BCG Scar and abnormal movements were the markers for viral meningitis, and focal weakness, lymphadenopathy and neck rigidity were identified as markers for bacterial meningitis and tuberculous meningitis (Table-1(a)). The cyclopropane signal proved to be a straightforward differentiating factor for the tuberculous meningitis cases based on its presence in 85.1% of cases obtained for the NMR analysis, followed by the choline-containing compounds (Table-1(b)). Quantitated metabolites like urea, citrate and alanine were identified as markers for the differentiation of bacterial meningitis and tuberculous meningitis from viral meningitis and control cases, while urea, creatine/creatinine, citrate, pyruvate, acetoacetate and β-hydroxy butyrate contributed towards the separation of bacterial meningitis cases from viral meningitis, although urea and citrate were the only markers for the differentiation of tuberculous meningitis cases from viral meningitis (Table-2).

5.2. Multivariate Analysis

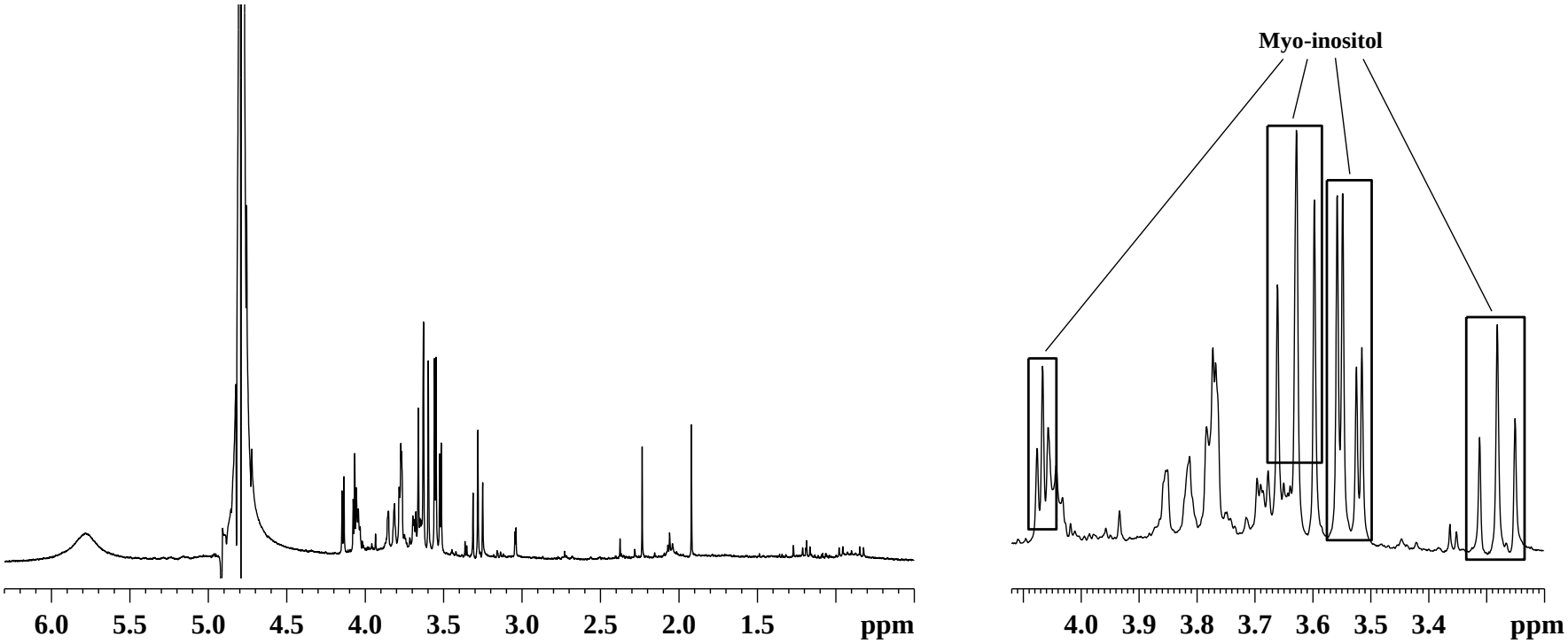

Fig. 29: *Myo*-inositol as seen in the ^{1}H NMR spectrum of a representative BM case.

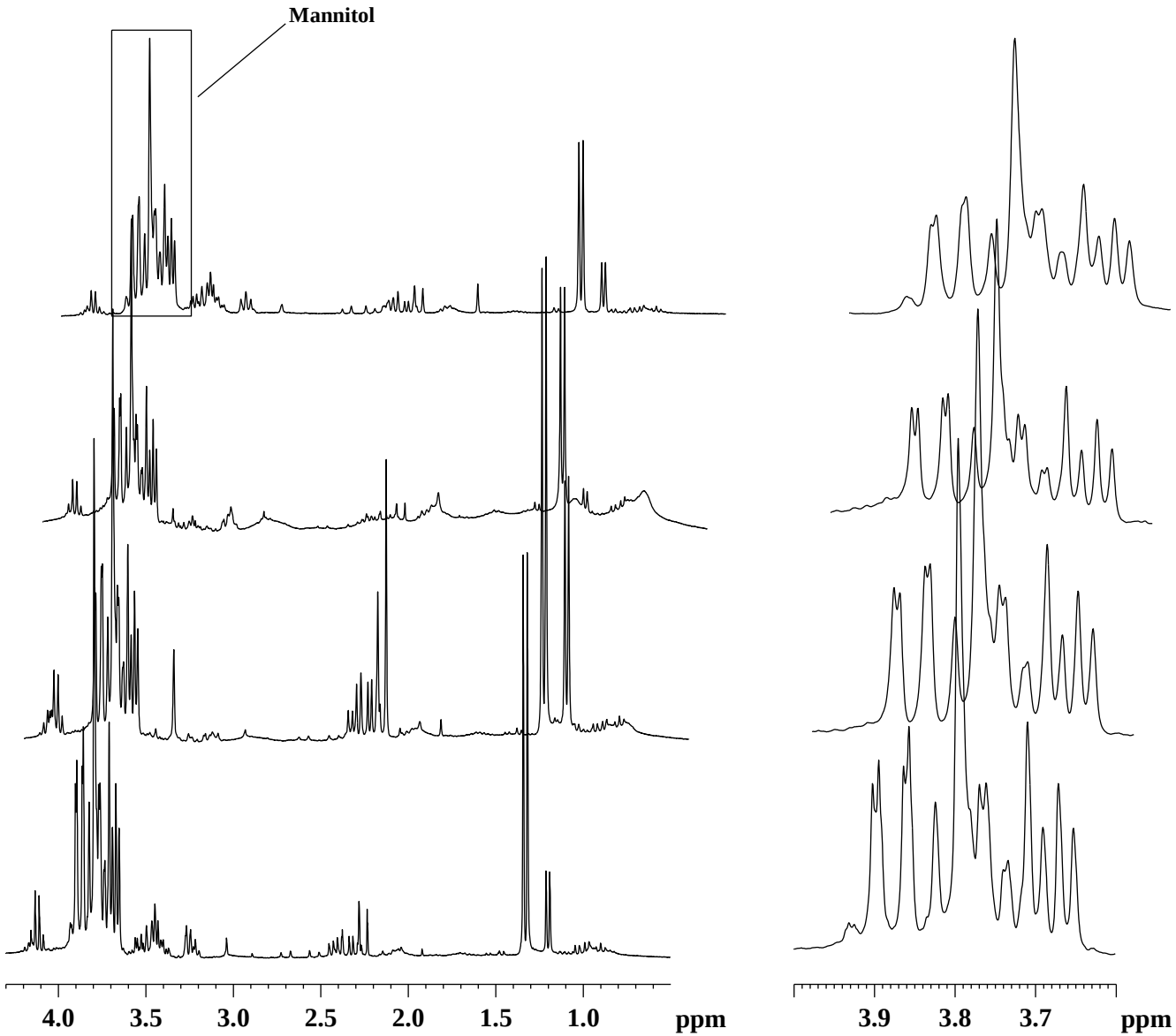

Fig. 30: Stack plot of the ^{1}H NMR spectra of representative BM cases, highlighting the resonance assignment of mannitol.

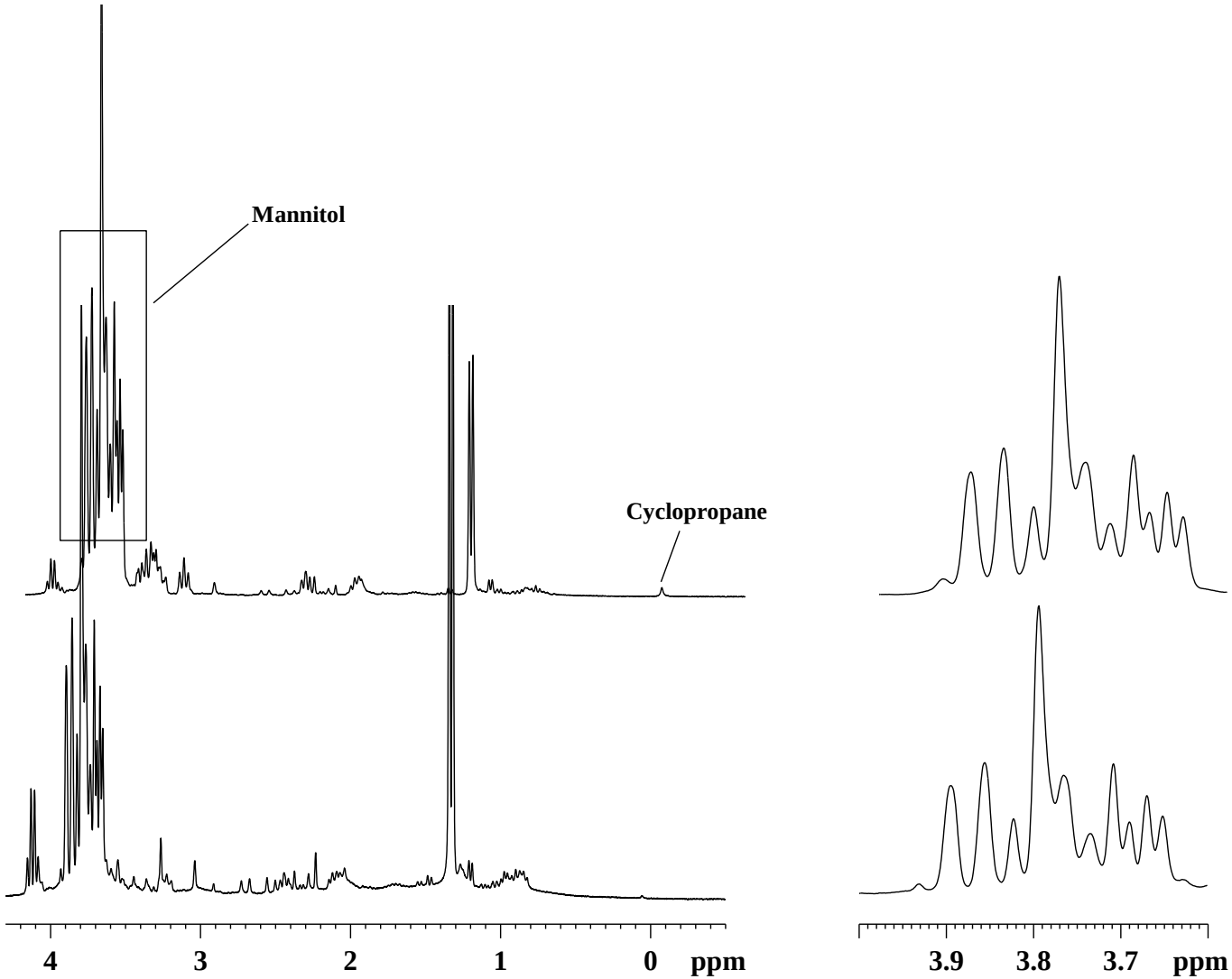

Fig. 31: Stack plot of the ^{1}H NMR spectra of representative TBM cases, highlighting the resonance assignment of mannitol.

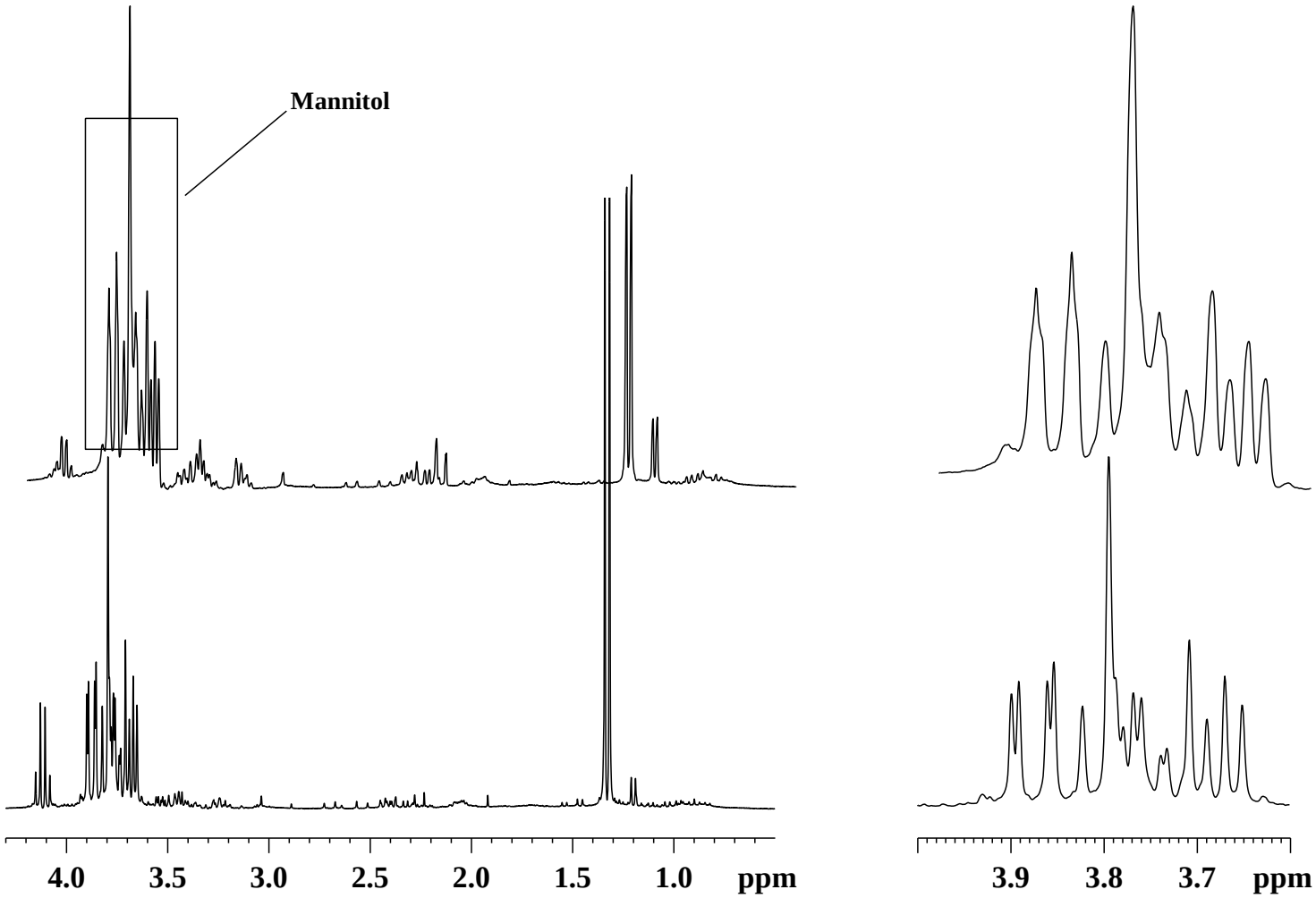

Fig. 32: Stack plot of the ^{1}H NMR spectra of representative VM cases, highlighting the resonance assignment of mannitol.

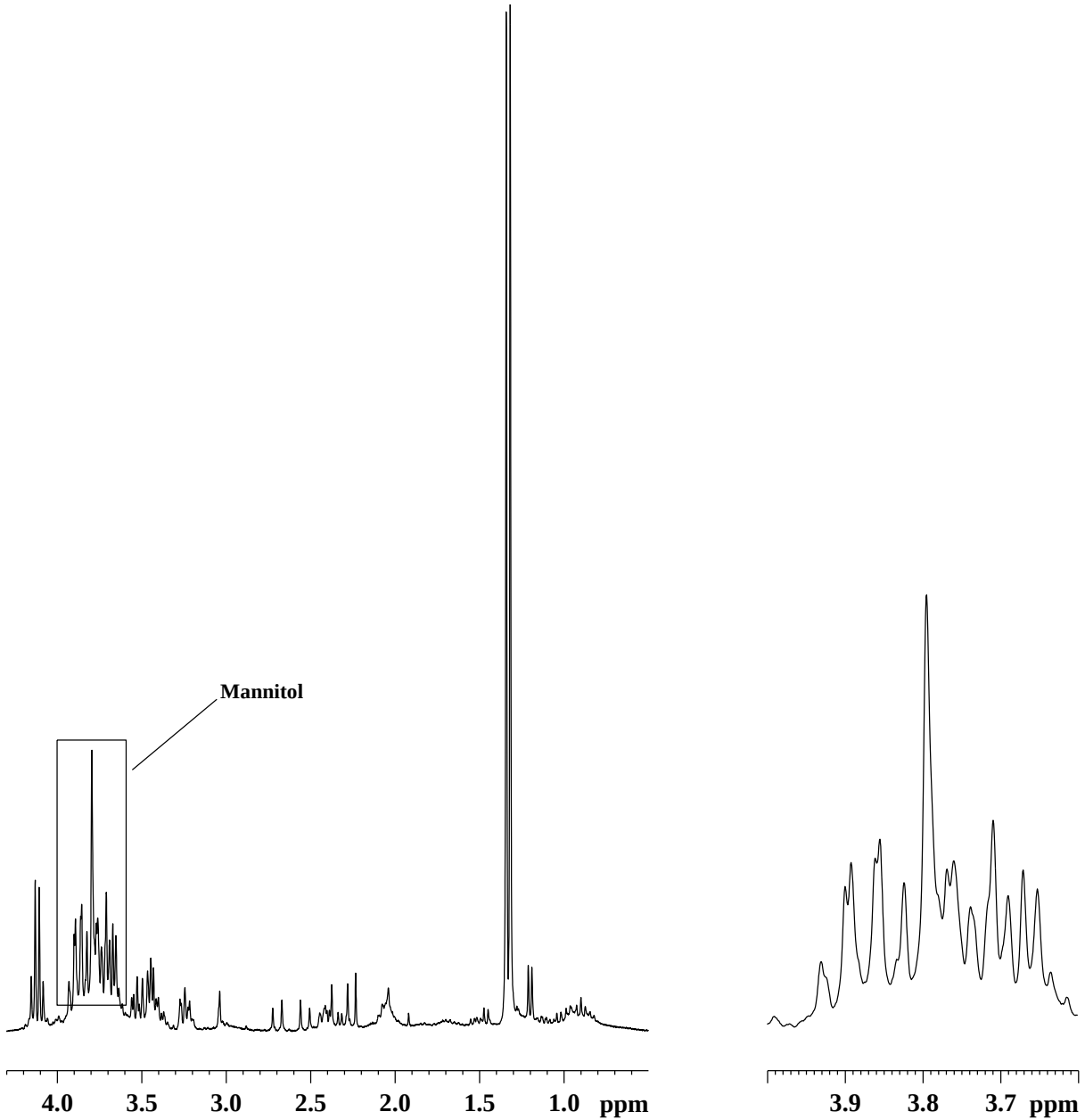

Fig. 33: ^{1}H NMR spectrum of a representative Control case, highlighting the resonance assignment of mannitol.

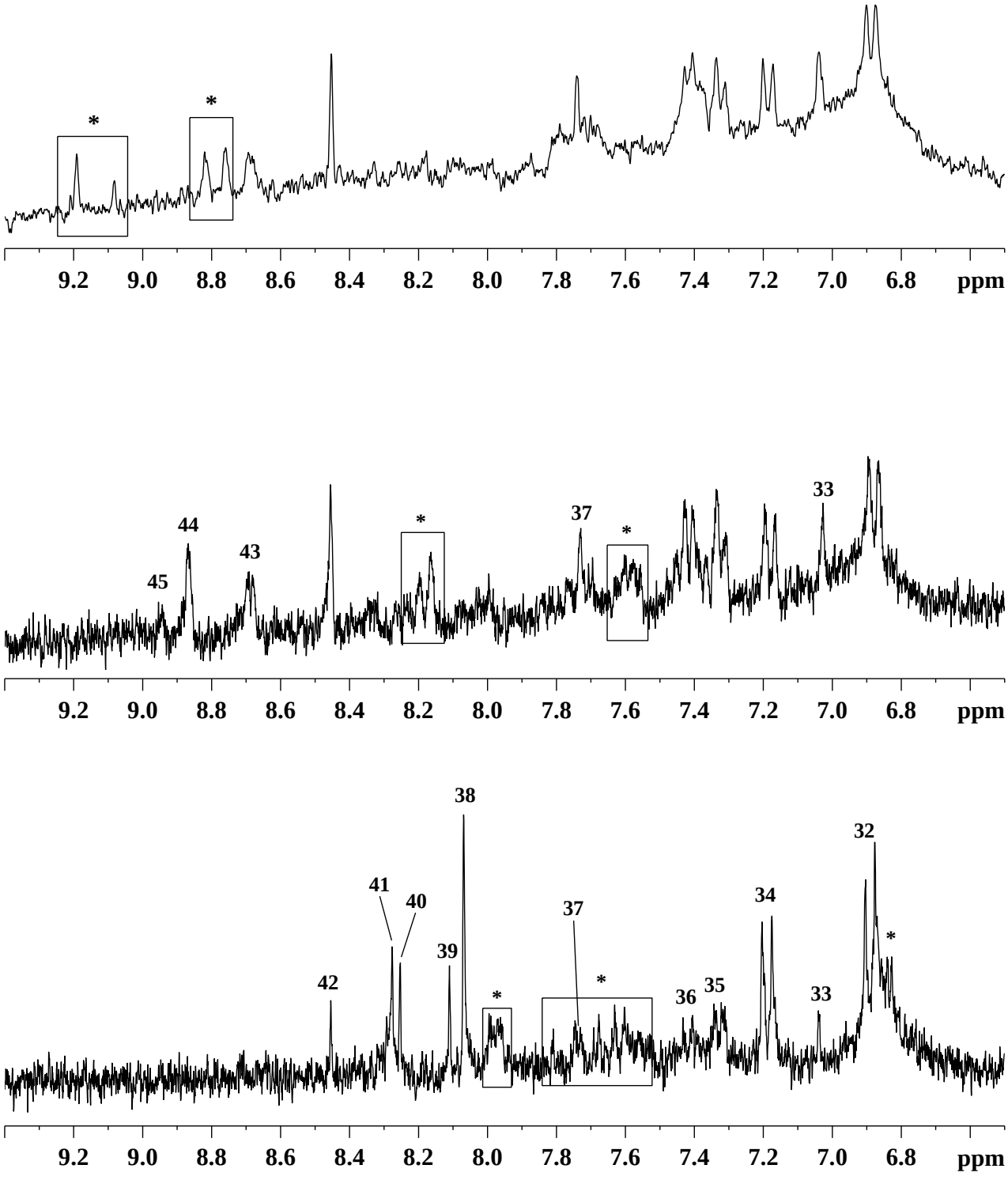

Fig. 34: Stack plot of the ^{1}H NMR spectra of representative childhood meningitis cases, highlighting the chemical shift assignments of aromatic amino acids and nucleic acid bases in CSF. The labeled assignments are as given in Table-3.

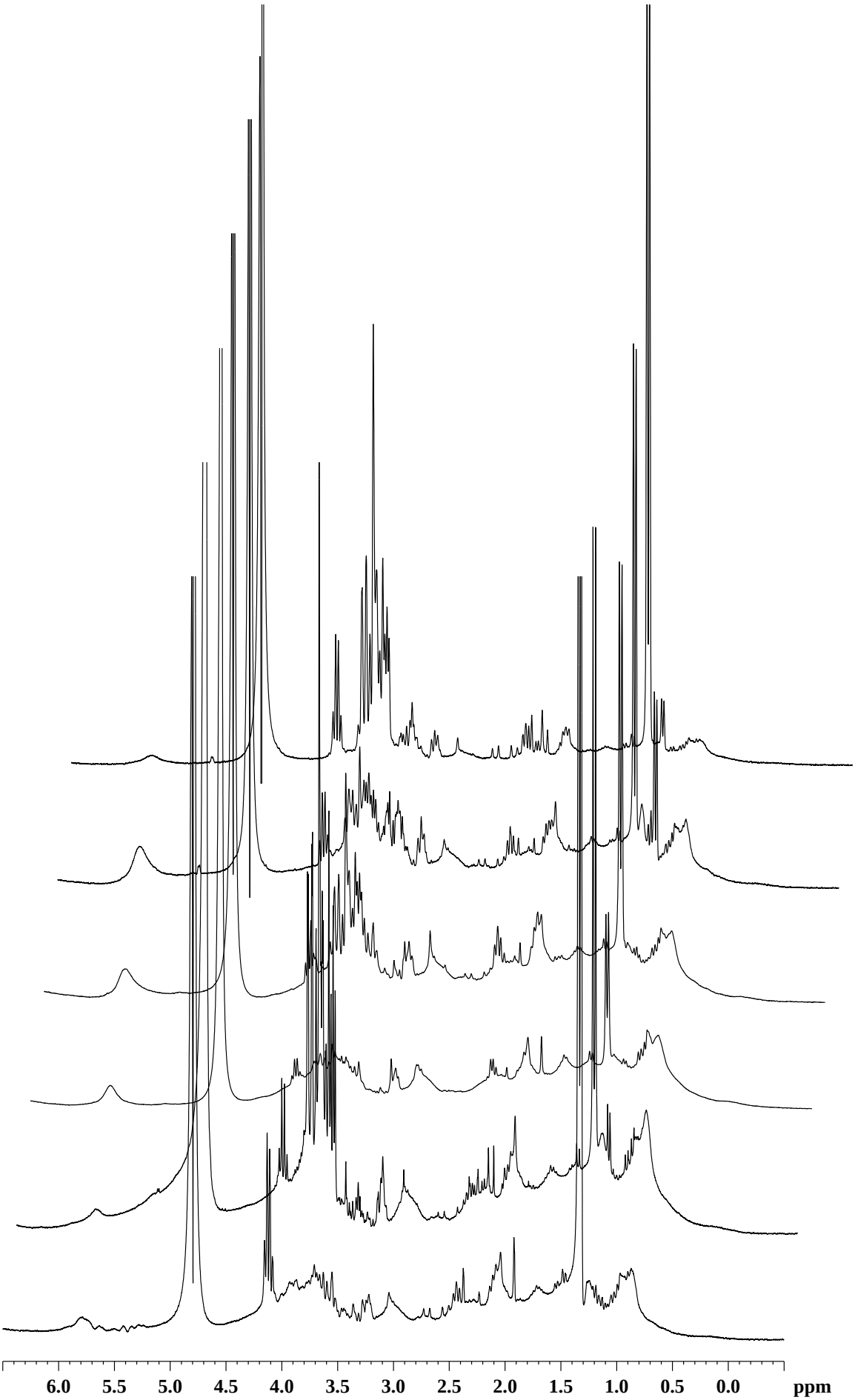

Fig. 35: Stack plot of the ^{1}H NMR spectra of representative BM cases, highlighting the protein contribution in CSF.

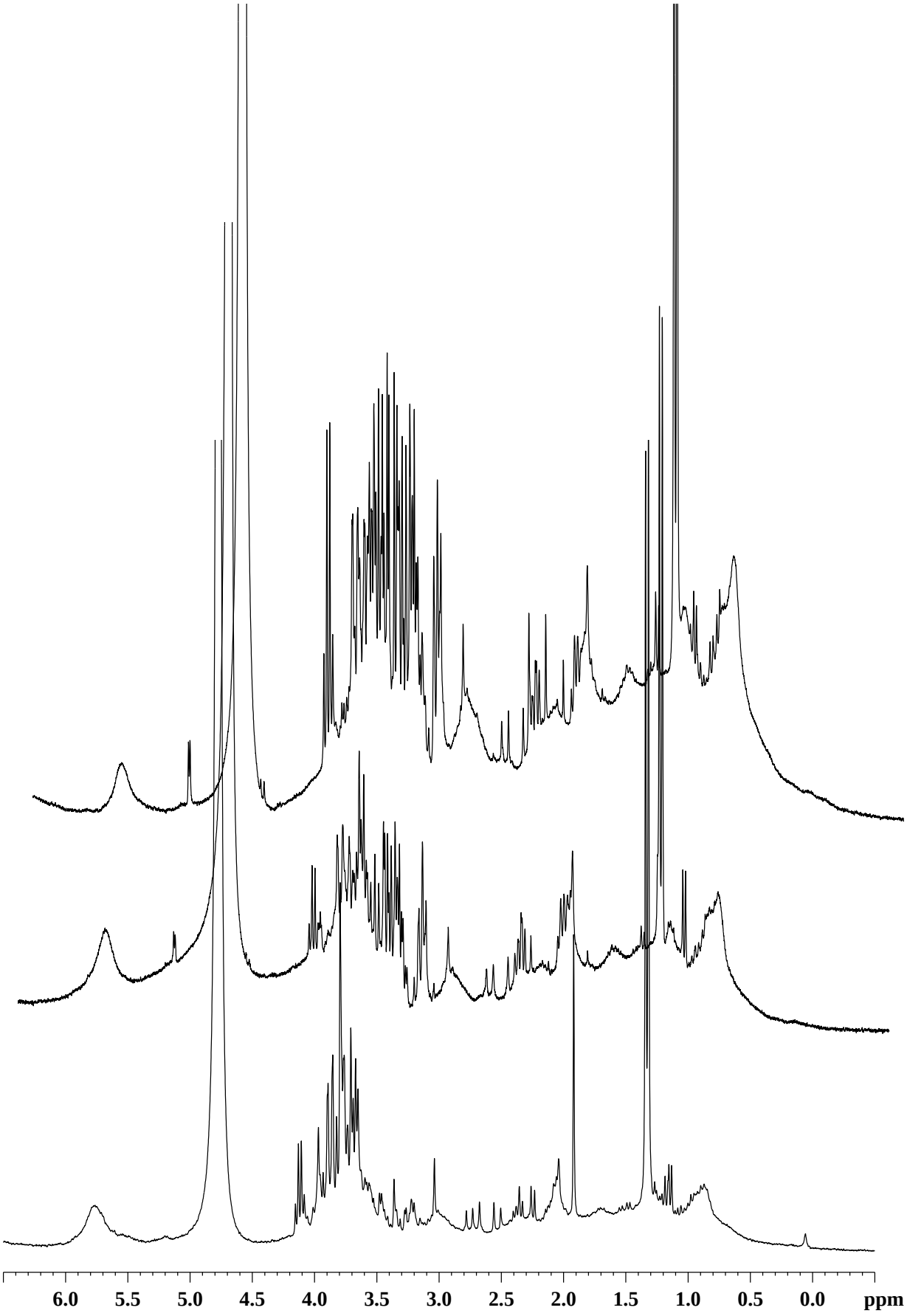

Fig. 36: Stack plot of the ^{1}H NMR spectra of representative TBM cases, highlighting the protein contribution in CSF.

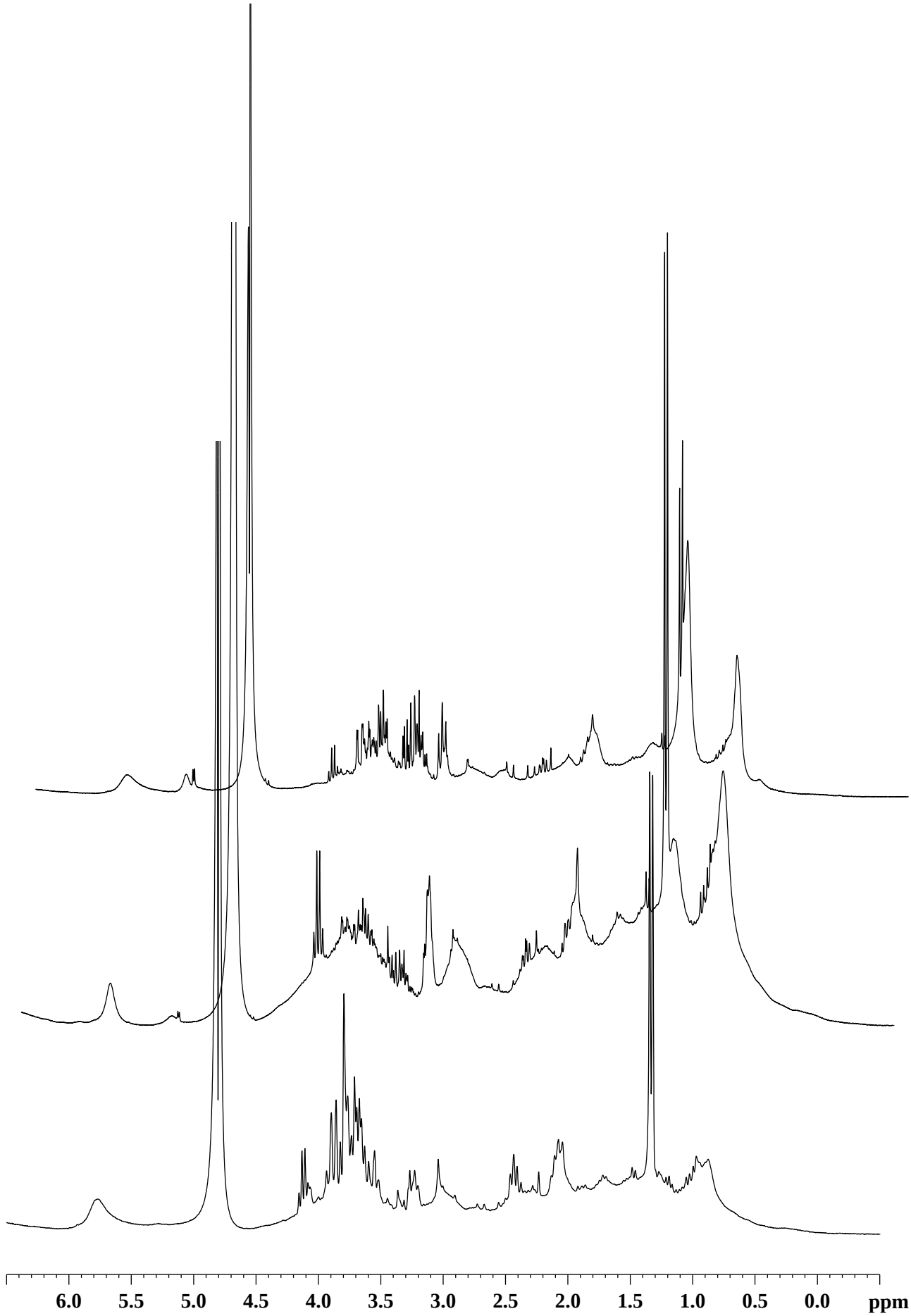

Fig. 37: Stack plot of the ^{1}H NMR spectra of representative Control cases, highlighting the protein contribution in CSF.

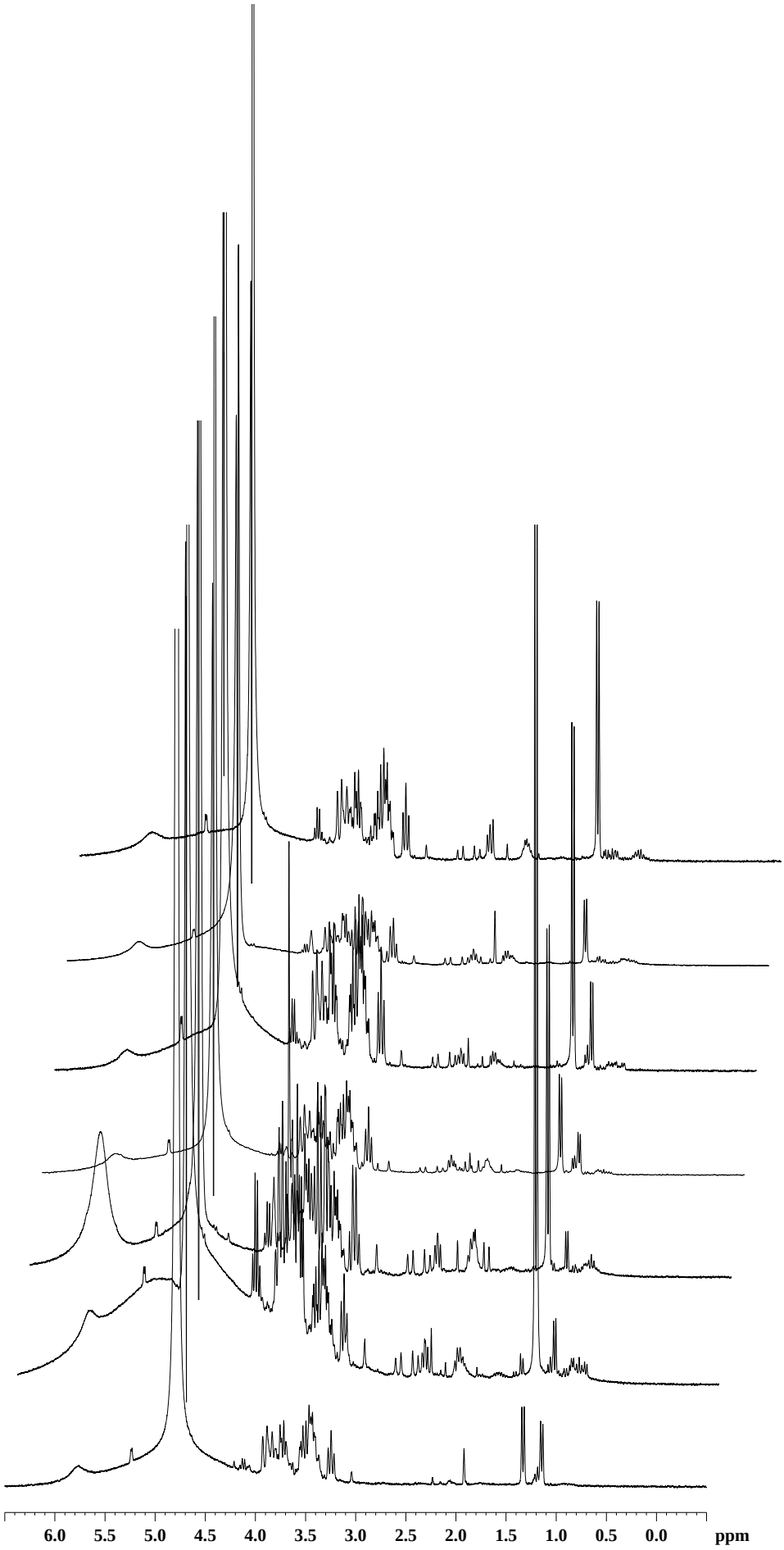

Fig. 38: Stack plot of the ^{1}H NMR spectra of representative BM cases, highlighting the coagulum contribution in CSF.

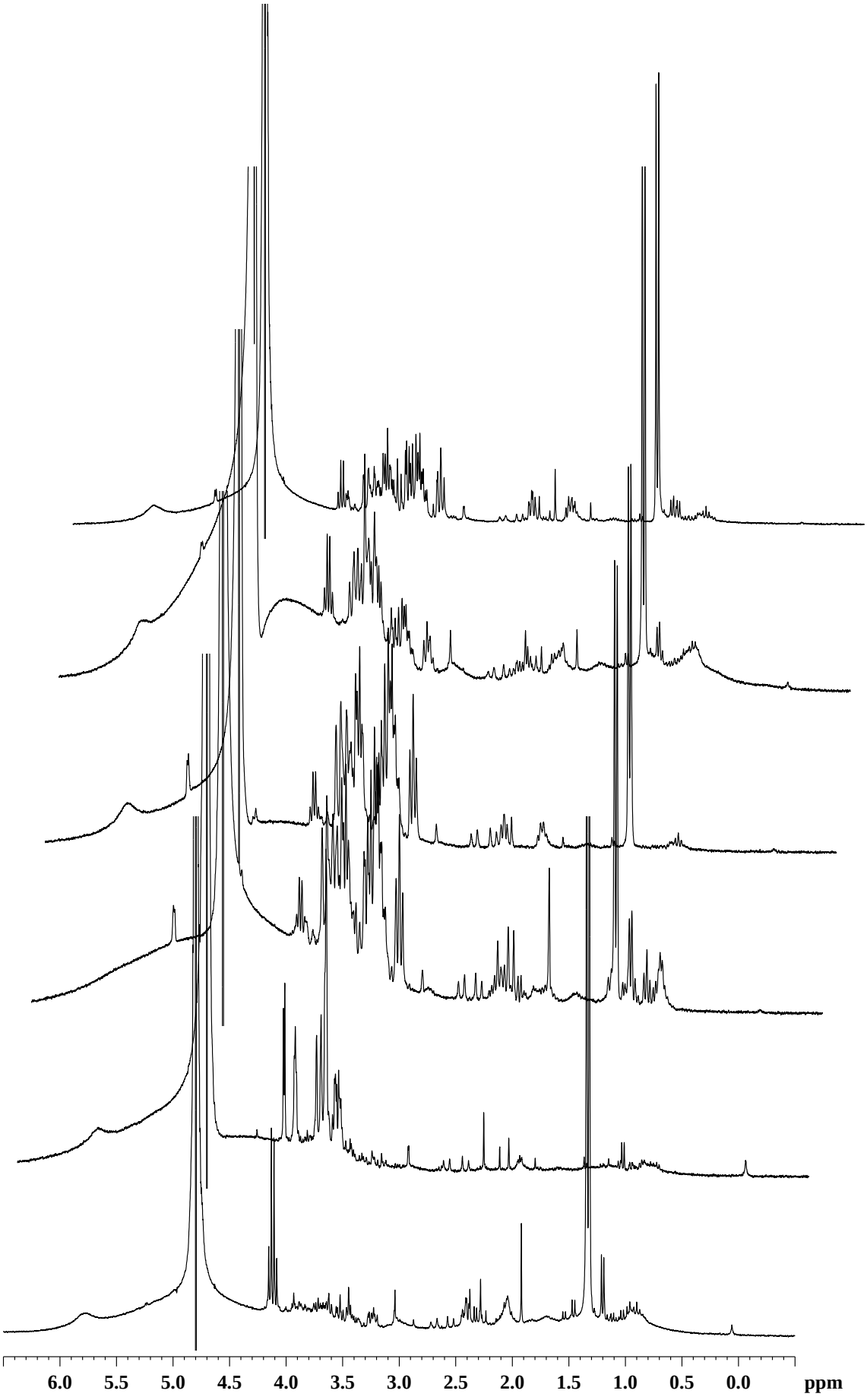

Fig. 39: Stack plot of the ^{1}H NMR spectra of representative TBM cases, highlighting the coagulum contribution in CSF.

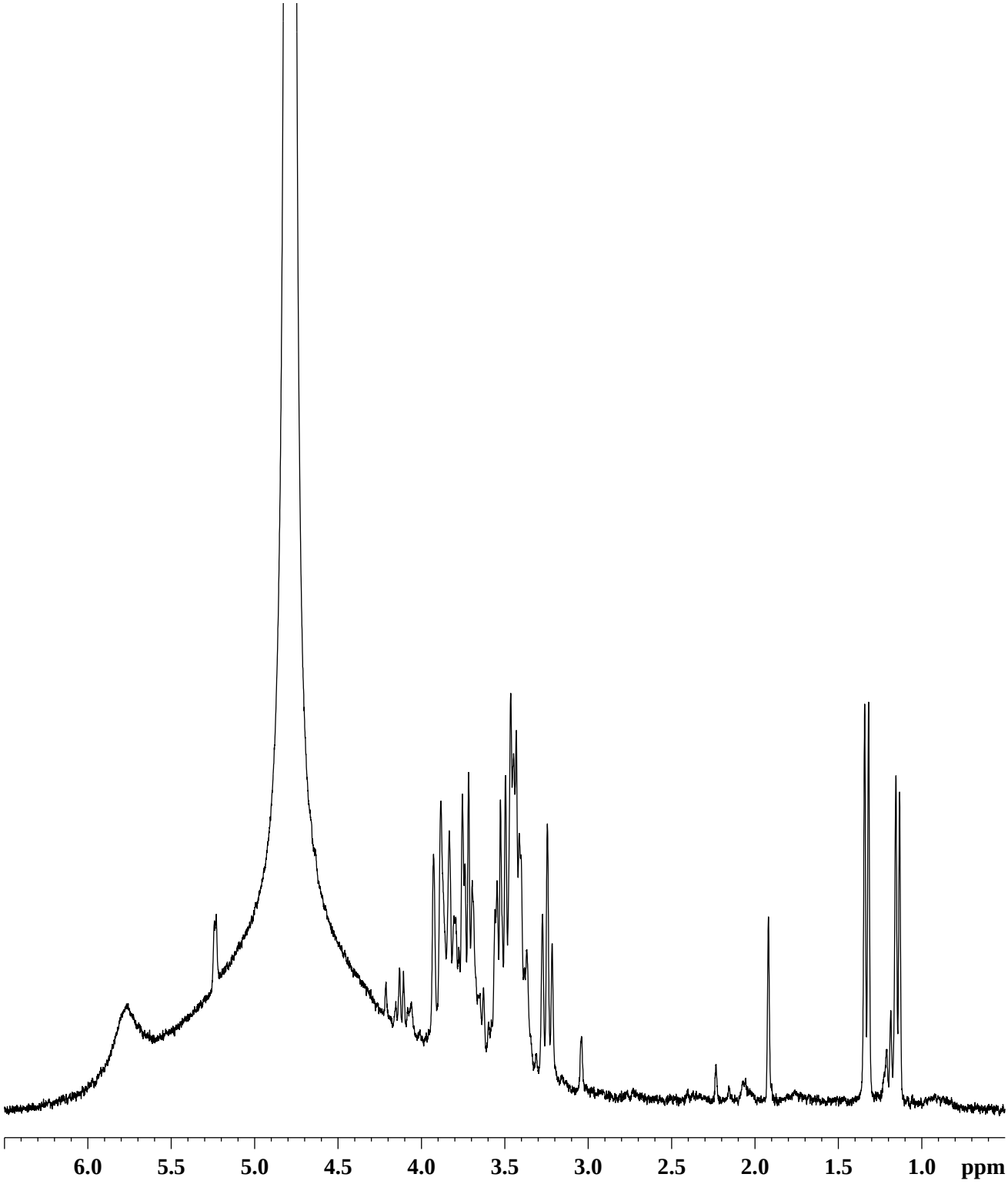

Fig. 40: ^{1}H NMR spectra of a representative Control case, highlighting the coagulum contribution in CSF.

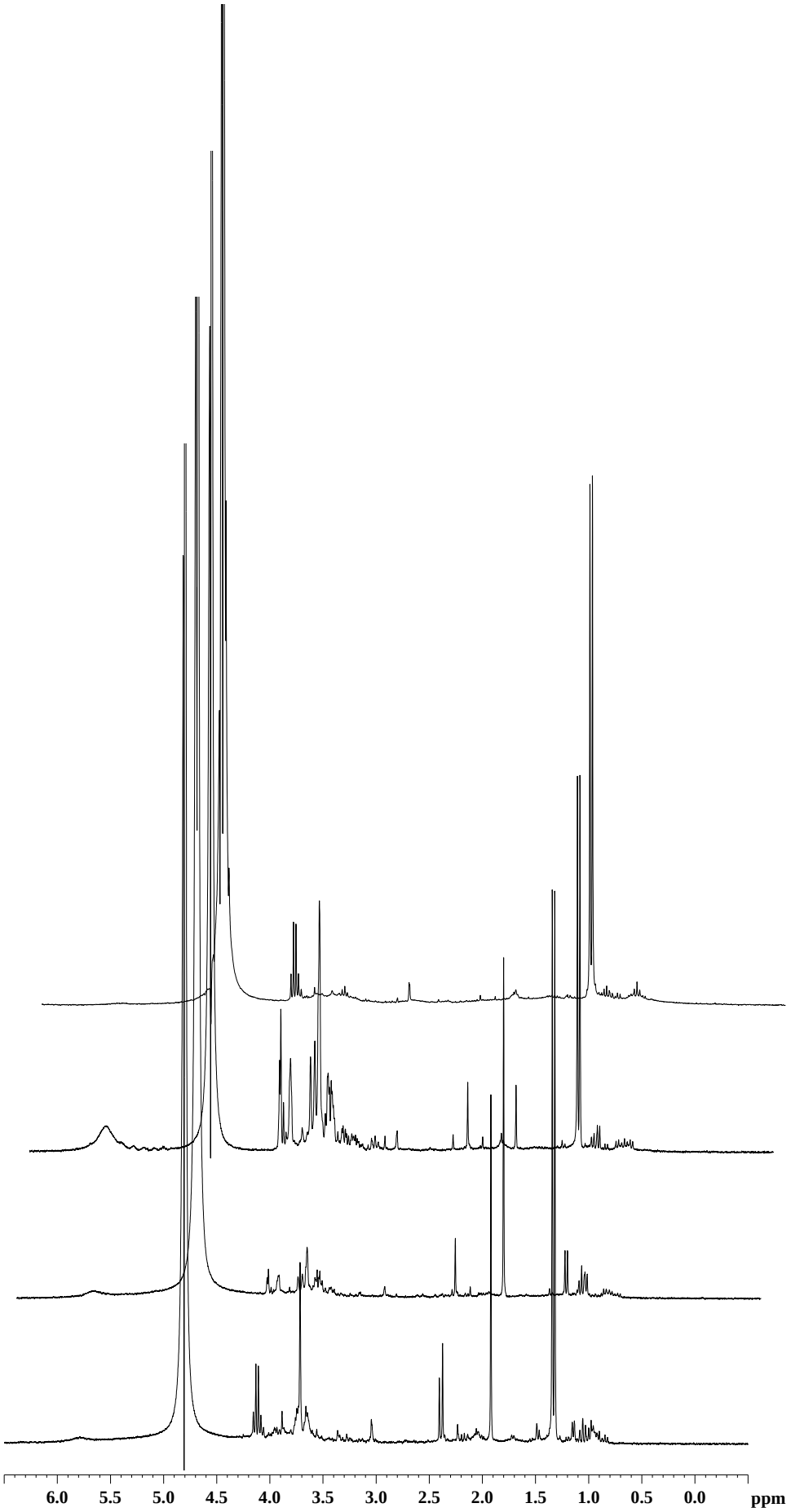

Fig. 41: Stack plot of the ^{1}H NMR spectra of representative BM cases, highlighting the abnormal metabolic profile in CSF in the form of altered levels of urea, glucose, acetate and lactate.

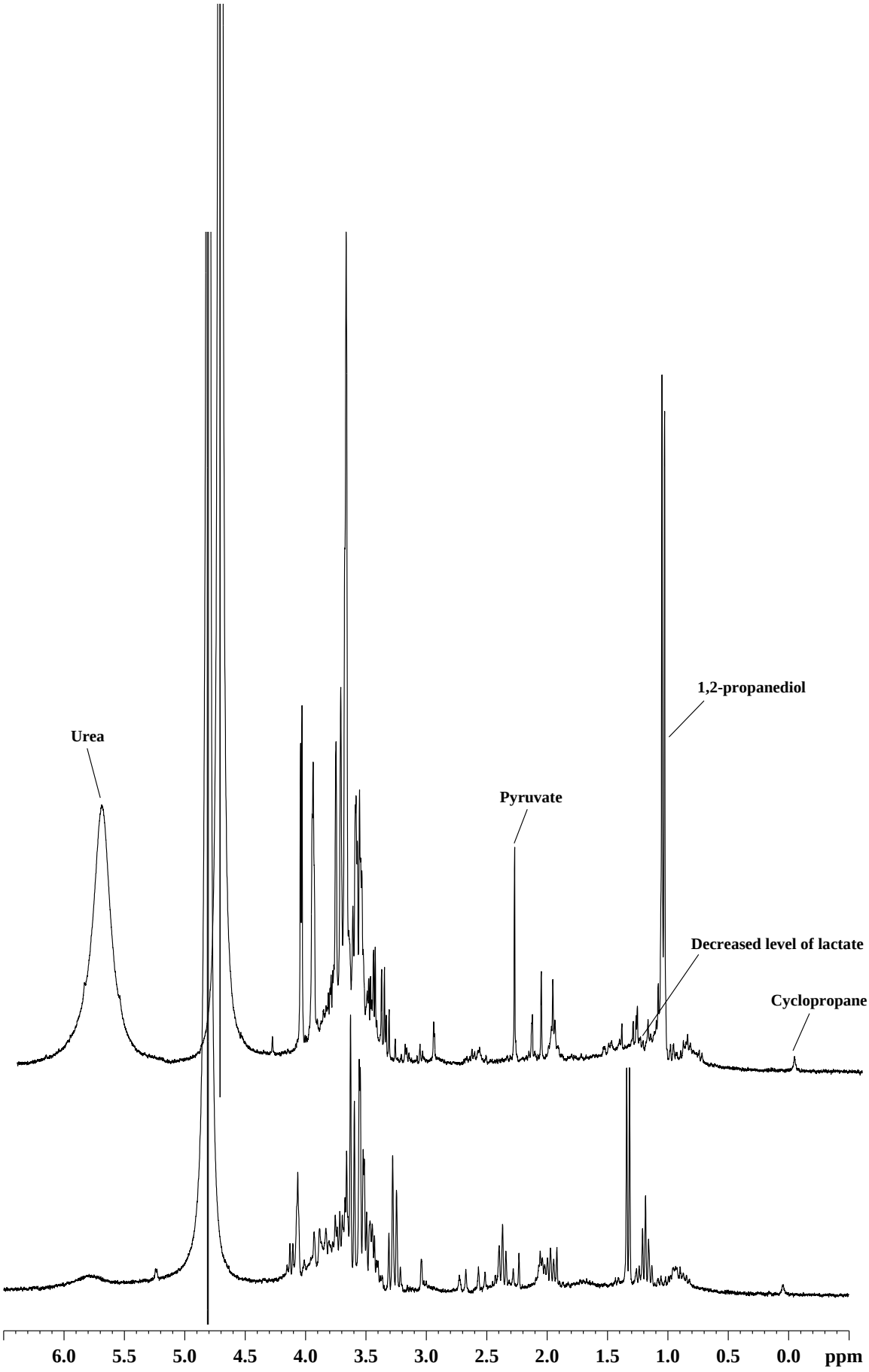

Fig. 42: Stack plot of the ^{1}H NMR spectra of representative TBM cases, highlighting the abnormal metabolic profile in CSF in the form of altered levels of urea, pyruvate, lactate and 1,2-propanediol.

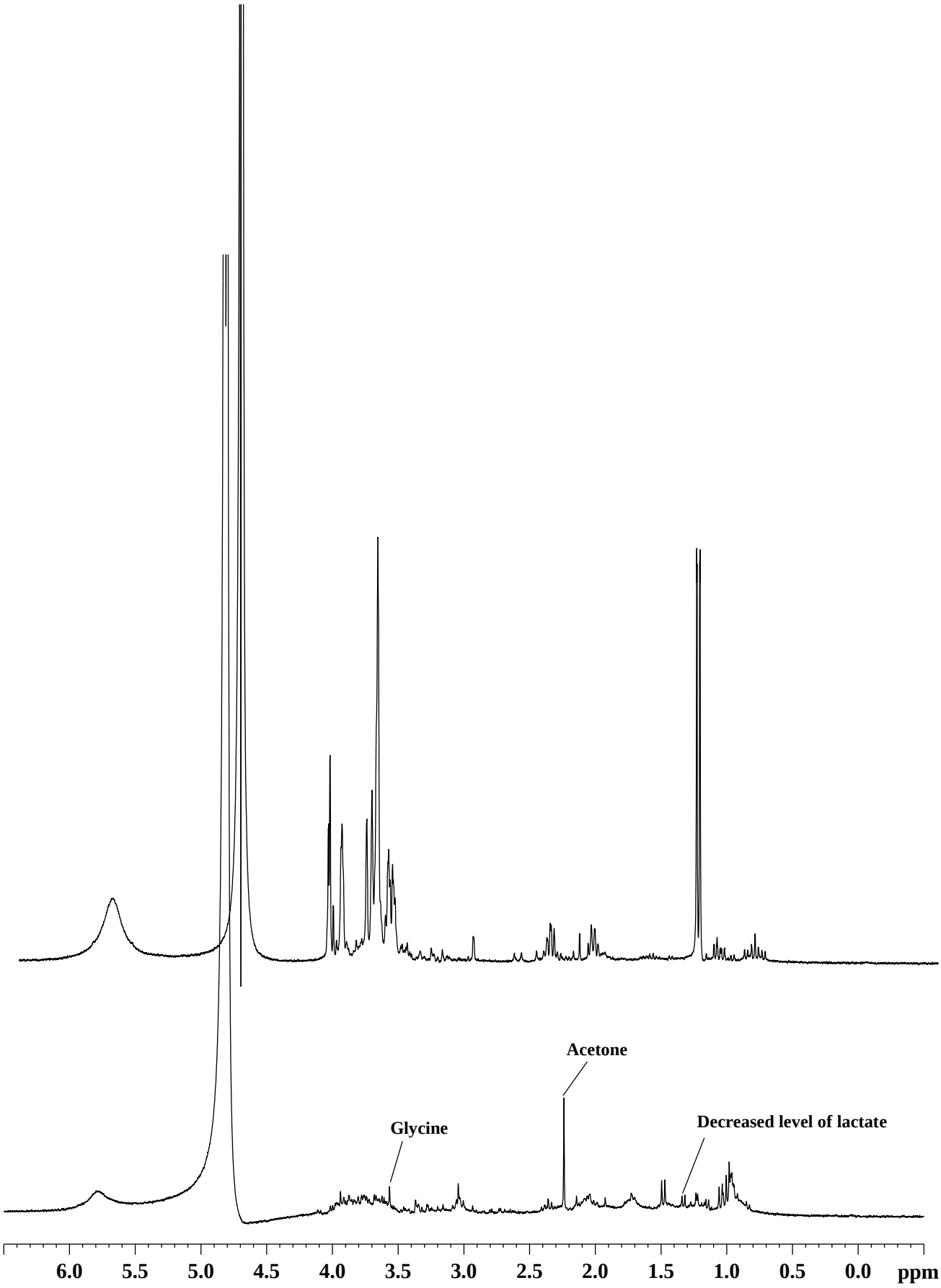

Fig. 43: Stack plot of the ^{1}H NMR spectra of representative VM cases, highlighting the abnormal metabolic profile in CSF in the form of altered levels of urea, glucose, lactate, acetone and glycine.

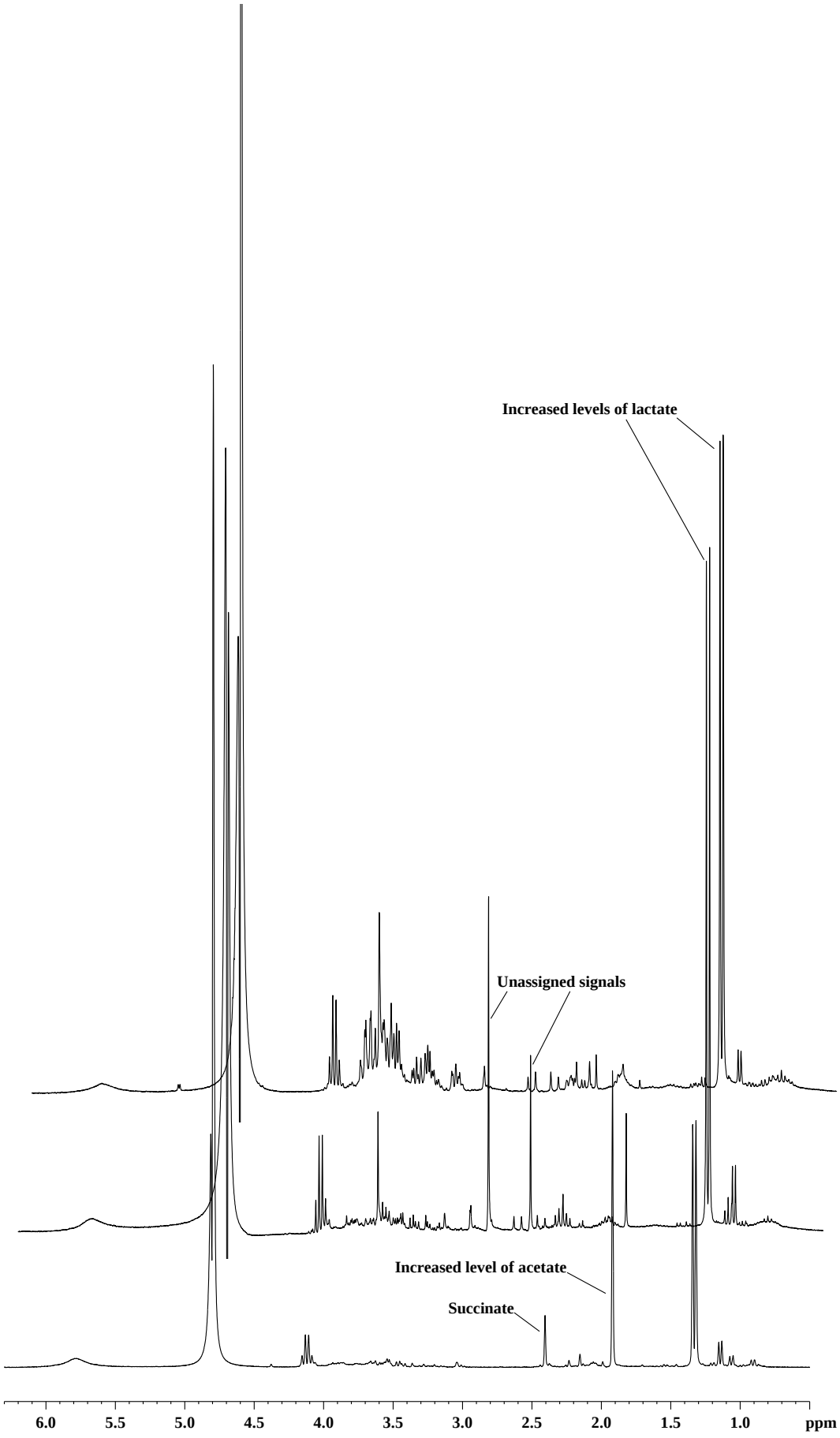

Fig. 44: Stack plot of the ^{1}H NMR spectra of representative Control cases, highlighting the abnormal metabolic profile in CSF in the form of altered levels of glucose, succinate, acetate and lactate.

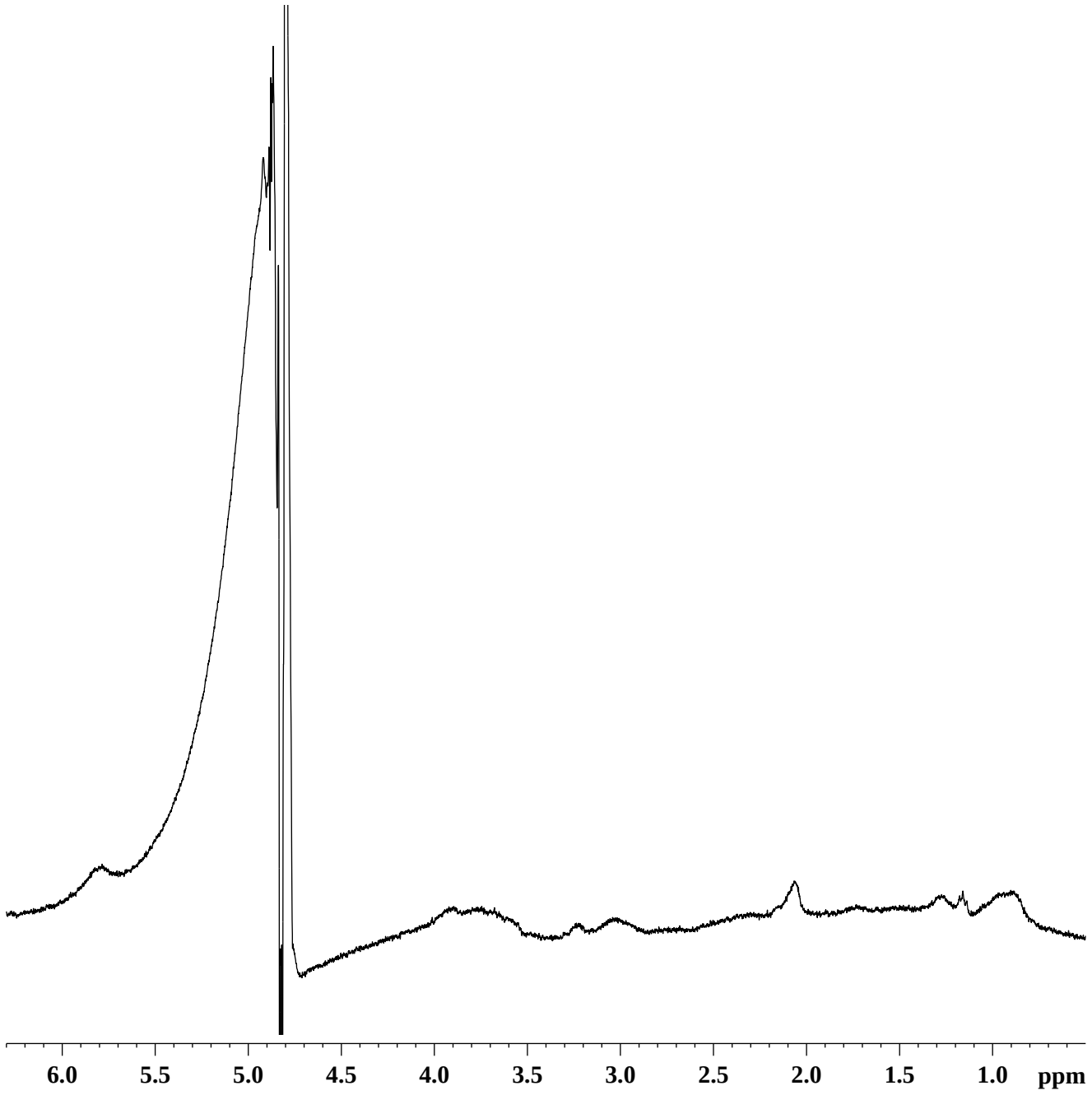

Fig. 45: ^{1}H NMR spectrum of the CSF of an abnormal case.

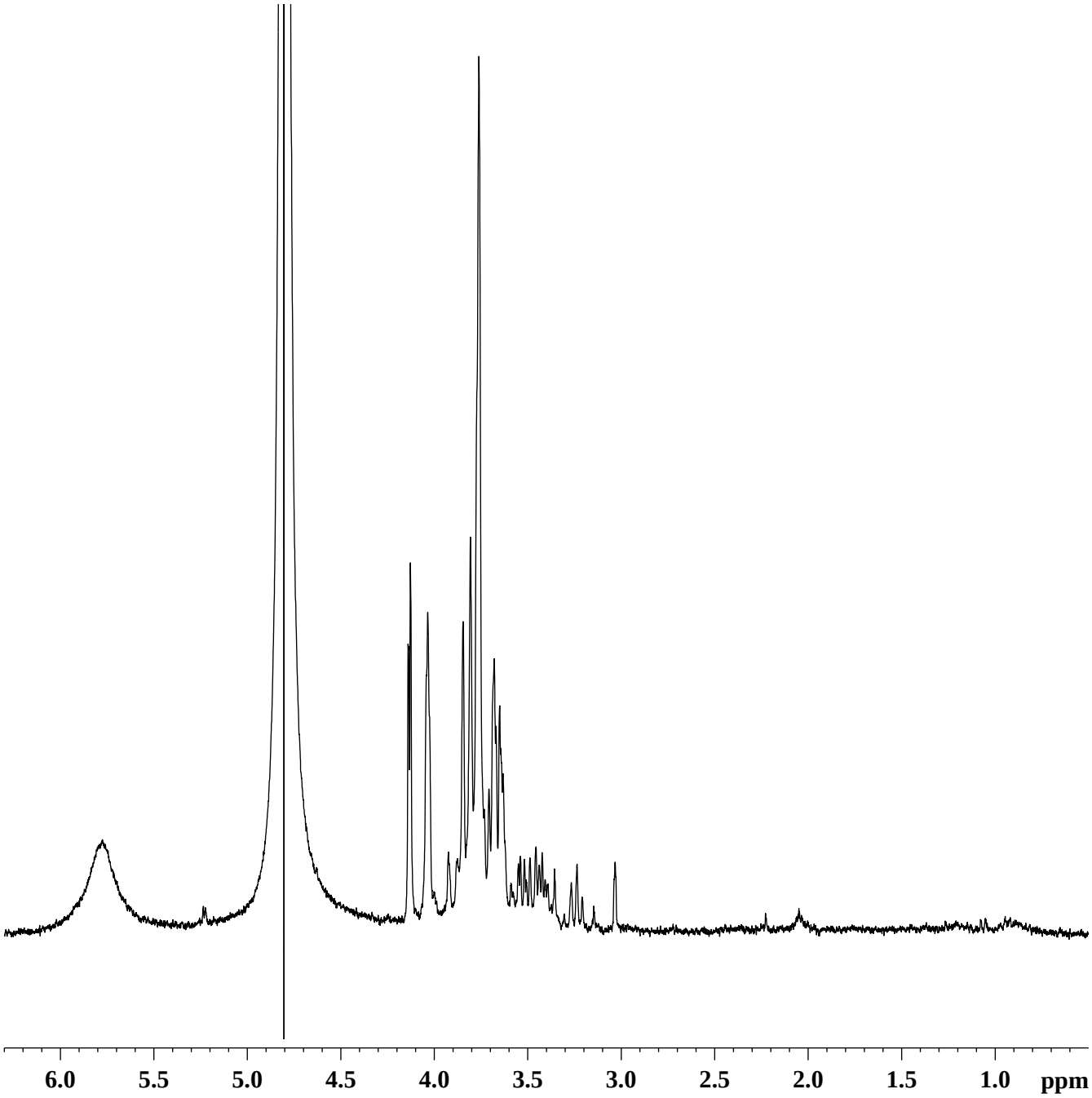

Fig. 46: ^{1}H NMR spectrum of the CSF of an abnormal case.

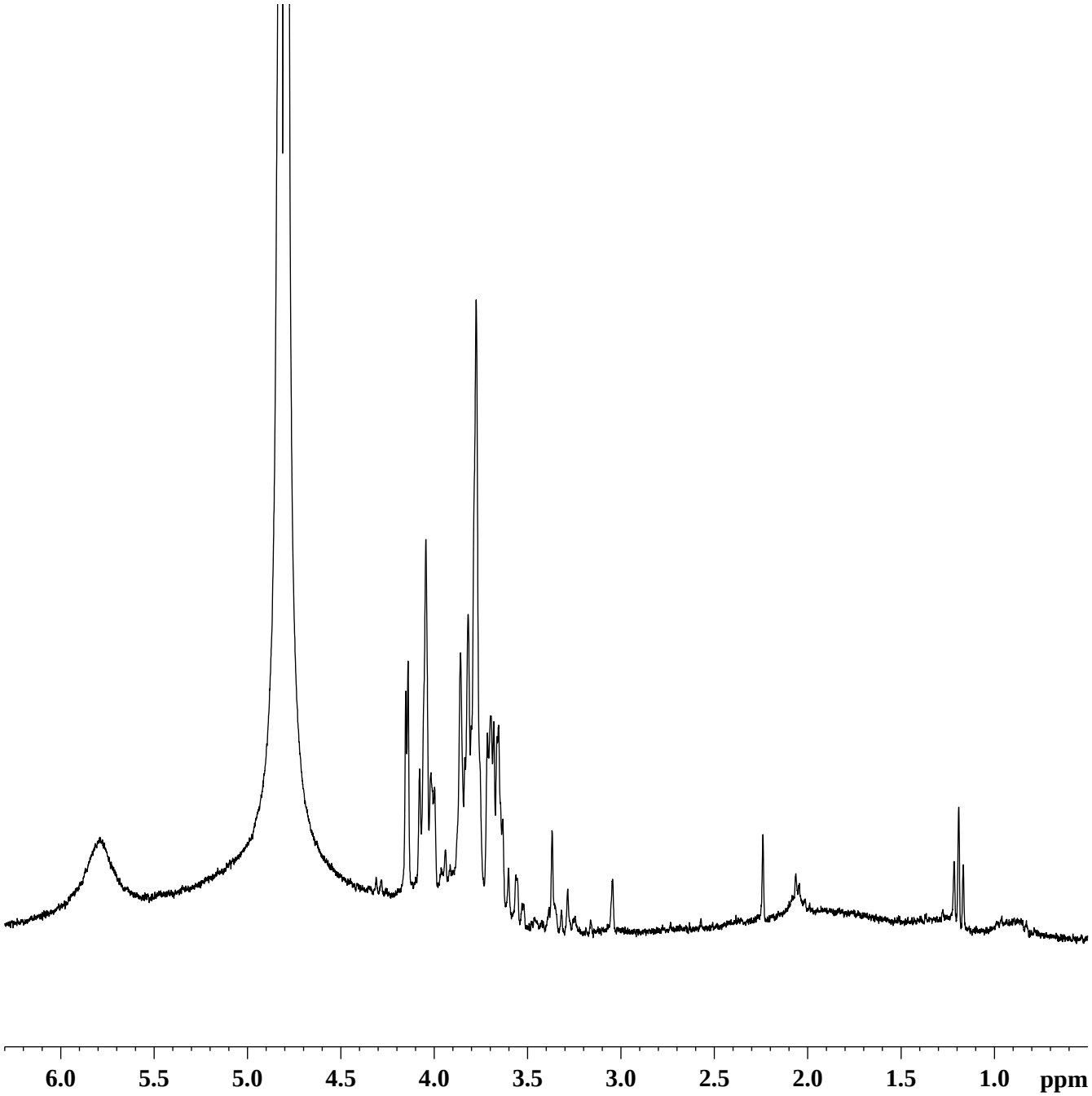

Fig. 47: ^{1}H NMR spectrum of the CSF of an abnormal case.

Since a suitable classification pattern of the disease and control data could not be achieved through univariate analysis due to severe overlapping, it became necessary for us to carry out multivariate analysis to construct a diagnostic rule. A DFA-based logistic approach was undertaken to construct training-sets with our classified database, followed by a complete re-validation of the data that involved comparing each disease category with the control group. It was further necessary to carry out a second re-validation regarding the classification of the disease groups (BM+TBM+VM) from control (non-meningitis) cases based on DFA, followed by the segregation of TBM from non-TBM cases, and finally resulting in the differentiation of BM from VM cases. It was found that disease groups could be successfully classified from the control data with an acceptable sensitivity and specificity. This second re-validation step has also provided us with the basis for the build up of the software MENEXSYS. Since untreated TBM in children may lead to permanent neurological sequealae, it was initially decided to discriminate the TBM cases with non-TBM cases followed by differentiation of the other two (BM and VM). DFA analysis defined that ten clinical symptoms excluding fever along with acetoacetate alone are predictive of distinction between the three types of meningitis (Table-5); moreover, presence of cyclopropane has further refined the results for the TBM group.

The prediction possibility of the model was checked with a 75/25 data split, by using 75% of the patients' data as training sets and the remaining 25% data as test sets (Table-6). When this 75/25 data split was further assessed for correct classifications based on the discriminant functions obtained with the training sets data, a classification of 85.7%, 66.7%, and 78.9% were obtained for the test sets groups comprising control vs. BM+TBM+VM, TBM vs. BM+VM, and BM vs. VM, respectively, followed by a classification of 94.4%, 76.2%, and 87.7% for the training sets groups, respectively. This validation has indicated that the prediction possibility of the model is almost at par with the results represented in Table-5. This fairly high prediction possibility of the model obtained based on the test data has also revealed an overall improvement in the differential diagnosis of meningitis when important clinical and NMR descriptors were combined together and taken for the analysis.

5.3. Operational Features of MENEXSYS

Table-6: Validation results obtained based on 75% training set data and 25% test set data, selected from 167 meningitis and 24 control cases. (a). Number of patients selected to form the training and test sets. (b). % Correct classifications obtained for the training and test sets data based on DFA.

(a).	**Category**	**Training Set**	**Test Set**
	Control (N=24)	24	-
	BM (N=85)	64	21
	TBM (N=47)	32	15
	VM (N=35)	26	9
(b).	**Groups for classification**	**% Correct classification obtained through DFA**	
	Control vs. BM+TBM+VM	94.4	85.7
	TBM vs. BM+VM	76.2	66.7
	BM vs. VM	87.7	78.9

The purpose of developing MENEXSYS was to simplify the analysis for the differential diagnosis of meningitis besides making it very user-friendly in the form of an easy-to-use Graphical User Interface, as handling of the statistical software for multivariate analysis may become too technical and time-consuming. The clinical symptoms observed during the time of admission and the metabolite weights obtained through NMR-based quantification serve as input variables in MENEXSYS. The prediction regarding the type of a new 'suspected to be meningitis' case is carried out based on a 'classification tree' as outlined in fig. 20, with the stages of analysis defined as: (i). Differentiation of control (non-meningitis) cases from disease cases; (ii). Differentiation of TBM from non-TBM cases (i.e., bacterial and viral meningitis); (iii). Differentiation of BM from VM cases (Appendix I).

6. Conclusions

In conclusion, it is proposed that the NMR spectroscopic information along with other routine clinical features coupled in the form of an expert system MENEXSYS may serve as an additional diagnostic tool for the differential diagnosis of meningitis in children. It is hoped that the results obtained through MENEXSYS may supplement the results of other gold-standard methods.

7. Future Scope of the Work

The work paves way for the application of Pattern Recognition statistics (e.g., Principal Component Analysis) to classify the ^{1}H NMR spectra of meningitis and control cases, so as to compare the respective group classifications obtained through Discriminant Function Analysis. Further, evaluation of the predictive and/or additional diagnostic ability of MENEXSYS remains to be carried out with new childhood meningitis cases.

References

Arditi M, Mason EO, Bradley JS, Tan TQ, Barson WJ, Schutze GE, Wald ER, Givner LB, Kim KS, Yogev R, Kaplan SL (1998) *Pediatrics* 102:1087-1097.

Armitage P, Berry G (1990) In *Statistical methods in Medical Research 2nd Edition*. Eds, P Armitage and G Berry. Oxford: Blackwell Scientific Publications, pp 472.

Auslander MC, Meskan ME (1988) *Laryngoscope* 98:940-948.

Avery ME, First LR (1994) Meningitis. In *Pediatric Medicine 2nd Edition*. Eds, ME Avery and LR First. Baltimore: William & Wilkins, 1164-1169.

Bale JF (1993) *Med Clin North Am* 77:25-41.

Behrman RE (1996) In *Nelson Textbook of Pediatrics 15th Edition*. Eds, RE Behrman, R Kliegman and HB Jenson. Philadelphia: Saunders, pp 707-716.

Bell JD, Brown JC, Sadler PJ (1989) *NMR Biomed* 2:246-256.

Berenguer J, Moreno S, Laguna F, Vicente T, Adrados M, Ortega A, Gonzalez-LaHoz J, Bouza E (1992) *The New Engl J Med* 326:668-672.

Berkley JA, Mwangi I, Ngetsa CJ, Mwarumba S, Lowe BS, Marsh K, Newton CRJC (2001) *Lancet* 357:1753-1757.

Bhargava S, Gupta AK, Tandon PN (1982) *Br J Radiol* 55:189-196.

Bock JL (1989) *Am J Clin Pathol* 91:S19-26.

Boss EA, Moolenaar SH, Massuger LF, Boonstra H, Engelke UF, De'Jong JG, Wevers RA (2000) *NMR Biomed* 13:297-305.

Campagne G, Schuchat A, Djibo S, Ousseini A, Cisse L, Chippaux JP (1999) *Bull World Health Organ* 77:499-508.

Chadwick DR (2005) *Br Med Bull* 75-76:1-14

Cherry JD (1993) Encephalitis. In *Nelson Textbook of Pediatrics 14th Edition*. Eds, RE Behrman and RM Kleigman. Pennsylvania: WB Saunders, pp 666-669.

Commodari F, Arnold DL, Sanctuary BC, Shoubridge EA (1991) *NMR Biomed* 4:192-200.

Dagan R, Jenista JA, Menegus MA (1988) *J Pediatr* 113:975-978.

De'Certaines JD (1996) *Anticancer Res* 16:1325-1331.

Ewer K, Deeks J, Alvarez L, Bryant G, Waller S, Andersen P, Monk P, Lalvani A (2003) *Lancet* 361:1168-1173.

Farinha NJ, Razali KA, Holzel H, Morgan G, Novelli VM (2000) *J Infect* 41:61-68.

Feigin RD, McCracken GH, Klein JO (1992) *Pediatr Infect Dis J* 11:785-814.

Fisher RA, Yates F (1957) In *Statistical Tables for Biological, Agricultural and Medical Research 5th Edition*. Eds, RA Fisher and F Yates. London: Oliver and Boyd, pp 126-131.

Fishman RA (1980) In *Cerebrospinal fluid in diseases of the nervous system*. Ed, RA Fishman. Philadelphia: Saunders.

Foulds J, O'Brien R (1998) *Int J Tuberc Lung Dis* 2:778-783.

Garg M, Chawla S, Prasad KN, Roy R, Sikora SS, Kumar R, Husain M, Khetrapal CL, Gupta RK (2002) *NMR Biomed* 15:320-326.

Ghauri FY, Nicholson JK, Sweatman BC, Wood J, Beddell CR, Lindon JC, Cairns NJ (1993) *NMR Biomed* 6:163-167.

Gilroy FV, Edwards MR, Norton RS, O'Sullivan WJ (1988) *Mol Biochem Parasitol* 31:107-116.

Goetghebuer T, West TE, Wermenbol V, Cadbury AL, Milligan P, Lloyd-Evans N, Adegbola RA, Mulholland EK, Greenwood BM, Weber MW (2000) *Trop Med Int Health* 5:207-213.

Govindaraju V, Young K, Maudsley AA (2000) *NMR Biomed* 13:129-153.

Gray LD, Fedorko DP (1992) *Clin Microbiol Rev* 5:130-145.

Griffin DE, Hardwick JM (1999) *Trends Microbiol* 7:155-160.

Griffin JL (2003) *Curr Opin Chem Biol* 7:648-654.

Groenen PM, Engelke UF, Wevers RA, Hendriks JC, Eskes TK, Merkus HM, Steegers-Theunissen RP (2004) *Eur J Obstet Gynecol Reprod Biol* 112:16-23.

Gupta RK, Roy R, Dev R, Husain M, Poptani H, Pandey R, Kishore J, Bhaduri AP (1996) *Magn Res Med* 36:829-833.

Heiblim DI, Evans HE, Glass L, Agbayani MM (1978) *Arch Neurol* 35:765-768.

Henry CM (2002) *Chem & Eng News* 80:66-70.

Hiraoka A, Miura I, Hattori M, Tominaga I, Kushida K, Maeda M (1994) *Biol Pharm Bull* 17:1-4.

Hoen B, Viel JF, Gerard A, Dureux JB, Canton P (1993) *Eur J Med* 2:28-32.

Hosoglu S, Ayaz C, Geyik MF, Kokoglu OF, Ceviz A (1998) *Int J Tuberc Lung Dis* 2:553-557.

Huy B, Tu H, Luan T, Lindqvist R (1994) *Am J Trop Med Hyg* 25:549-553.

Jeffery KJ, Read SJ, Peto TE, Mayon-White RT, Bangham CR (1997) *Lancet* 349:313-317.

Jinkins JR (1991) *Neurocardiol* 36:126-135.

Jodar L, Feavers IM, Salisbury D, Granoff DM (2002) *Lancet* 359:1499-1508.

Kabilan L (2004) *Indian J Pediatr* 71:707-712.

Kabilan L, Edwin N, Balashankar S, Meikandan D (2000) *Trans Roy Soc Trop Med Hyg* 94:157-158.

Kaplan SL (1999) *Infect Dis Clin North Am* 13:579-590.

Kennedy C (1995) *BMJ* 310:139-140.

Kennedy DH, Fallon RJ (1979) *JAMA* 241:264-268.

Keun HC, Ebbels TM, Antti H, Bollard ME, Beckonert O, Schlotterbeck G, Senn H, Niederhauser U, Holmes E, Lindon JC, Nicholson JK (2002) *Chem Res Toxicol* 15:1380-1386.

Kingsley DP, Hendrickse WA, Kendall BE, Swash M, Singh V (1987) *J Neurol Neurosurg Psychiatry* 50:30-36.

Kinoshita Y, Yokota A (1997) *NMR Biomed* 10:2-12.

Kirsch EA, Barton RP, Kitchen L, Giroir BP (1996) *Pediatr Infect Dis J* 15:967-978.

Klein JO, Feigin RD, McCracken GH (1986) *Pediatrics* 78:959-982.

Koedel U, Scheld WM, Pfister HW (2002) *Lancet Infect Dis* 2:721-736.

Kumar D, Watson JM, Charlett A, Nicholas S, Darbyshire JH (1997) *Thorax* 52:1060-1067.

Kumar R (2005) *Indian J Pediatr* 72:57-63.

Kumar R (1999) *Indian J Pediatr* 66:73-83.

Kumar R, Agarwal SP, Wakhlu I, Mishra KL (1991) *Indian Pediatr* 28:1525-1528.

Kumar R, Mathur A, Kumar A, Sethi GD, Sharma S, Chaturvedi UC (1990) *Arch Dis Child* 65:1227-1230.

Kumar R, Mathur A, Singh KB, Sitholey P, Prasad M, Shukla R, Agarwal SP, Arockiasamy J (1993) *Indian J Med Res* 97:9-13.

Laurichesse H, Grimaud O, Waight P, Johnson AP, George RC, Miller E (1998) *Commun Dis Public Health* 1:22-27.

Learmonth MP, Euerby MR, Jacobs DE, Gibbons WA (1987) *Mol Biochem Parasitol* 25:293-298.

Lisboa PJ, Kirby SP, Vellido A, Lee YY, El-Deredy W (1998) *NMR Biomed* 11:225-234.

Lobato M, Cummings K, Will D, Royce S (1998) *Paediatr Infect Dis J* 17:407-411.

Lutz NW, Maillet S, Nicoli F, Viout P, Cozzone PJ (1998) *FEBS Lett* 425:345-351.

Maillet S, Vion-Dury J, Confort-Gouny S, Nicoli F, Lutz NW, Viout P, Cozzone PJ (1998) *Brain Res Protocols* 3:123-134.

Mandal BK, Evan DZK, Iranside AG, Pollan BR (1972) *BMJ* 4:413-415.

Marcos MA, Martinez E, Almela M, Mensa J, De'Anta MTJ (2001) *Lancet* 357:1499-1500.

Marton KI, Gean AD (1986) *Ann Intern Med* 104:840-848.

Maxson S, Jacobs RF (1993) *Postgrad Med* 93:153-156, 159-160, 163-166.

McCracken GH (2002) *Lancet* 360:183.

McGale EHF, Pye IF, Stonier C, Hutchison EC, Aber GM (1977) *J Neurochem* 29:291-297.

McMillan DA, Lin CY, Aronin SI, Quagliarello VJ (2001) *Clin Infect Dis* 33:969-975.

Meshitsuka S, Morio Y, Nagashima H, Teshima R (2001) *Clin Chim Acta* 312:25-30.

Michal G (1998) Biochemical Pathways. In *An Atlas of Biochemistry and Molecular Biology*. Ed, G Michal. New York: John Wiley & Sons.

Misra UK, Kalita J (1998) *Electromyogr Clin Neurophysiol* 38:41-46.

Molyneux E, Walsh A, Phiri A, Molyneux M (1998) *Trop Med Int Health* 8:610-618.

Moolenaar SH, Engelke UF, Wevers RA (2003) *Ann Clin Biochem* 40:16-24.

Moosa AA, Quortum HA, Ibrahim MD (1995) *Lancet* 345:1290-1291.

Muller PD, Donald PR (1987) *Ann Trop Paed* 7:287-289.

Narain S, Singhal T, Kabra SK, Seth V (2000) *Paediatrics Today* 3:144-149.

Neuman HB, Wald ER (2001) *Clin Pediatr (Phila)* 40:595-600.

Ni H, Knight AI, Cartwright K, Palmer WH, McFadden J (1992) *Lancet* 340:1432-1434.

Nicholson JK, Wilson ID (1989) *Prog Nucl Magn Reson Spectr* 21:449-501.

Niroli F, Vion-Dury J, Maloteaux JM, Delwaide C, Confort-Gouny S, Sciaky M, Cozzone PJ (1993) *Neurosci Lett* 154:47-51.

O'Meara M, Ouvrier R (1996) *Curr Opin Pediatr* 8:11-15.

Pagliano P, Fusco U, Attanasio V, Conte M, Maturo N, Prejan A, Fescigno C, Faella FS (2001) *Infez Med* 9:246-250.

Pai M, Flores LL, Pai N, Hubbard A, Riley LW, Colford JM (2003) *Lancet Infect Dis* 3:633-643.

Panagariya A, Jain RS, Gupta S, Garg A, Sureka RK, Mathur V (2001) *Neurol India* 49:360-365.

Petroff OAC, Yu RK, Ogino T (1986) *J Neurochem* 47:1270-1276.

Pfister HW, Scheld WM (1997) *Curr Opin Neurol* 10:254-259.

Pfyffer GE (1999) *J Infect* 39:21-26.

Piotto M, Saudek V, Sklenar V (1992) *J Biomol NMR* 2:661-666.

Pole SL, Khare PM, Kelkar SS (1983) *Indian J Pathol Microbiol* 26:193-199.

Potts BCM, Deese AJ, Stevens GJ, Reily MD, Robertson DG, Theiss J (2001) *J Pharm Biomed Anal* 26:463-476.

Pui MH, Memon WA (2001) *Can Assoc Radiol J* 52:43-49.

Ribera E, Martinez-Vazquez JM, Segura RM, Pascual C (1987) *J Infect Dis* 7:603-607.

Rupprecht CE, Hanlon CA, Hemachudha T (2002) *Lancet Infect Dis* 2:327-343.

Saez'Llorens X, McCracken GH (2003) *Lancet* 361:2139-2148.

Saez'Llorens X, McCracken GH (1990) *Infect Dis Clin North Am* 4:623-644.

Saez'Llorens X, Ramilo O, Mustafa MM, Mertsola J, McCracken GH (1990) *J Pediatr* 116:671-684.

Schuchat A, Robinson K, Wenger JD, Harrison LH, Farley M, Reingold AL, Lefkowitz L, Perkins BA (1997) *N Engl J Med* 337:970-976.

Seiler N (2002) *Neurochem International* 41:189-207.

Sharma B, Malik GK, Jain AK, Agarwal DK (1982) *Pediatr* 79:225-228.

Simone IL, Federico F, Trojano M, Tortorella C, Liguori M, Giannini P, Picciola E, Natile G, Livrea P (1996) *J Neurol Sci* 144:182-190.

Singhi, PD, Singhi SC (1995) *Curr Opin Neurol* 8:150-155.

Smith AW, Bradley AK, Wall RA, McPherson B, Secka A, Dunn DT, Greenwood BM (1988) *Trans R Soc Trop Med Hyg* 82:312-320.

Spranger M, Schwab S, Krempien S, Winterholler M, Steiner T, Hacke W (1996) *Arch Neurol* 53:992-996.

Suarez I, Bodega G, Fernandez B (2002) *Neurochem International* 41:123-142.

Sweatman BC, Farrant RD, Holmes E, Ghauri FY, Nicholson JK, Lindon JC (1993) *J Pharm Biomed Anal* 11:651-664.

T'Hart BA, Vogels JT, Spijksma G, Brok HP, Polman C, Van-Der Greef J (2003) *J Neurol Sci* 212:21-30.

Thwaites GE, Chau TTH, Stepniewsak K, Phu NH, Choung LV, Sinh DX, White NJ, Parry CM, Farrar JJ (2002) *Lancet* 360:1287-1292.

Thwaites G, Chau TT, Mai NT, Drobniewski F, McAdam K, Farrar J (2000) *J Neuro Neurosurg Psychiatry* 68:289-299.

Tucci S, Pinto C, Goyo J, Rada P, Hernandez L (1998) *Clin Biochem* 31:143-150.

Tunkel AR, Scheld WM (1995) *Lancet* 346:1675-1680.

Tyler KL (2004) *Herpes* 11:A57-64.

Upadyaya GC, Tripathi BN, Shukla RK, Singh KH (1984) *Indian Pediatr* 51:633-636.

Van De'Beek D, Schmand B, De'Gans J, Weisfelt M, Vaessen H, Dankert J, Vermeulen M (2002) *J Infect Dis* 186:1047-1052.

Venetz I, Schopfer K, Muhlemann K (1998) *Int J Epidemiol* 27:1101-1104.

Vion-Dury J, Nicoli F, Torri G, Torri J, Kriat M, Sciaky M, Davin A, Viout P, Confort-Gouny S, Cozzone PJ (1992) *Biochimie* 74:801-807.

Walia R, Hoskyns W (2000) *Eur J Pediatr* 159:535-538.

Walls T, Shingadia D (2004) *J Infect* 48:13-22.

Wevers RA, Engelke UF, Moolenaar SH, Brautigam C, De'Jong JG, Duran R, De'Abreu RA, Van Gennip AH (1999) *Clin Chem* 45:539-548.

Whitley RJ (1990) *New Engl J Med* 323:242-249.

Whitley RJ, Gnann JW (2002) *Lancet* 359:507-514.

WHO Report (1998) In *Epidemic meningococcal disease: WHO Fact Sheet 105*. Geneva: World Health Organization.

Wiggelinkhoizen J, Mann M (1980) *J Pediatr* 97:843-847.

Xu Y, Zhaori G, Vene S, Shen K, Zhou Y, Magnius LO, Wahren B, Linde A (1996) *Pediatr Infect Dis J* 15:1018-1024.

Summary

The salient features of the thesis work entitled "**NMR Structural Aspects in Biological Systems: Analysis in Leishmaniasis, Tuberculosis and Meningitis**" have been summarized as follows:

NMR Structural Aspects in Leishmaniasis

The parasitic protozoan members of genus *Leishmania* are responsible for the most severe pathologies associated with visceral leishmaniasis (VL) in humans, caused by *Leishmania donovani* and *Leishmania infantum*. VL is an infection of the liver and spleen that can be fatal, which if untreated in time may cause morbidity with high rate of mortality.

Leishmaniasis occurs in approximately 90 tropical and subtropical countries around the world. It has been estimated that 12 million new cases of leishmaniasis occur each year worldwide, making it the second largest protozoal disease next to malaria. The situation in India is grave, particularly in eastern India (Bihar State) where an official estimate of more than 4,30,000 cases were reported between 1985-1996, although it is believed that the actual number of cases currently exceeds this figure by at least five folds. Recent trends indicate that there are 5,00,000 cases per year of visceral leishmaniasis, which occurs primarily in the Indian subcontinent.

It has been speculated that the increasing number of treatment failures in India might be due to the emergence of drug-resistant strains as the main cause of SAG unresponsiveness in Bihar. The mechanism of drug-resistance in kala-azar is still not well understood. Although several methods are currently employed for characterizing unresponsiveness in leishmaniasis, it is apparent that in-depth parasitological investigations and new approaches will be necessary to fully understand the exact extent of drug resistance in leishmaniasis. In addition to the current procedures, the utility of other bio-analytical techniques such as NMR spectroscopy in understanding the biochemistry of *Leishmania* has been explored in recent times.

In continuation to the earlier efforts, the present investigation has been undertaken with an objective of mapping important intracellular metabolites using ^{1}H NMR spectroscopy in the promastigote PCA extracts of six cultured strains of *L. donovani*. An attempt has been made to understand the metabolic information of the live Dd8 promastigotes (WHO reference strain) under different conditions, to arrive at any possible clues regarding the biochemical pathways in *L. donovani*.

^{1}H resonance signals occurring due to the presence of valine, lactate, alanine, arginine, citrulline, acetate, acetoacetate, glutamate, succinate, citrate, choline, α-glycerophosphorylcholine (α-GPC), betaine, mannose, tyrosine, phenyl alanine, formate, uracil, cytosine, guanine, adenine, UTP/UDP, CTP, GTP, NAD/NADH and ATP/ADP were assigned in all promastigote PCA extracts. Further, ^{1}H resonance signals arising from the ribose sugars bound to uracil, cytosine, guanine and adenine, and in the forms of UTP/UDP, CTP, GTP, NAD/NADH, ATP/ADP (as nucleotides) were found to be highly abundant in all ^{1}H NMR spectra of the promastigote PCA extracts of the *L. donovani* strains. The chemical shift assignments of these nucleic acid bases and their sugars have been demonstrated for the first time using ^{1}H NMR in the PCA extracts of *L. donovani* promastigotes.

Presence of high-energy phosphate entities and nucleotides in *L. donovani* promastigotes has been established by performing ^{31}P NMR experiment for one of the strains (Dd8). Resonance signals arising from NTP, NDP, NMP (adenosine-, guanosine-, cytidine- and uridine- mono-, di-, and tri-phosphates), pentapolyphosphate, pyrophosphate, glycerophosphorylethanolamine, glycerophosphorylcholine, inorganic phosphate, phosphorylcholine, phosphorylethanolamine, 3-phosphoglycerate, glycerol 3-phosphate and glucose 6-phosphate could be assigned during the course of the present investigation. The present investigation using ^{1}H NMR analysis of the promastigote PCA extracts of six *L. donovani* strains has indicated that all the strains have undergone similar biochemical pathways, but with different metabolic activities.

To ascertain further the details of the metabolism in *L. donovani* promastigotes, NMR experiments were done on the live cells of Dd8 strain obtained at the stationary phase of their growth. The study was divided into two categories: in the first category the live Dd8 promastigotes were suspended in normal PBS without any nutrient and subjected to the NMR studies, and in the second category the parasites were incubated with $^{13}C_1$-glucose under different buffer conditions. For the second category, the conditions involved suspending the cells in normal PBS with $^{13}C_1$-glucose, followed by the incubation with $^{13}C_1$-glucose under hypoxic (anaerobic, N_2-bubbled) and normoxic (aerobic, O_2-bubbled) conditions.

Signals pertaining to ethanol, lactate, alanine, acetate, acetoacetate, succinate, and resonances pertaining to betaine and choline-containing compounds could be readily assigned for the cells maintained under starved conditions. Resonances of the aliphatic cytosolic amino acids

such as valine, leucine and isoleucine could also be identified using 2D ^{1}H-^{1}H COSY spectrum. When the cells were maintained in normal PBS with $^{13}C_1$ glucose at 4°C, there was an increased production of acetate and succinate than the usually observed high levels of lactate as observed for the cells under starved conditions. The NMR-observable incorporation of ^{13}C-enrichment was observed to be maximum for succinate and alanine, followed by a moderate labeling of glycerol-based intermediate and acetate, and a minimum labeling of lactate.

When the live Dd8 promastigotes were subjected to anaerobic and aerobic conditions with $^{13}C_1$ glucose available as the energy-source, signals pertaining to succinate, alanine and acetate were mainly observed. The ^{1}H NMR spectrum of the live Dd8 promastigotes maintained under anaerobic conditions showed a weak lactate signal after 45 min of incubation with $^{13}C_1$ glucose, which was not ^{13}C-labeled (in the C_3 position) as observed in the HSQC spectrum. The labeling pattern of the metabolites in live Dd8 promastigotes has given an indication that glucose was most likely converted via the Embden-Meyerhof-Parnas glycolytic pathway, with the associated conversion of pyruvate to succinate, alanine and acetate. This was further supported by the ^{31}P NMR performed on the promastigote PCA extract of the Dd8 strain, wherein many of the metabolic intermediates and high-energy phosphates of the proposed pathway could be observed.

The results have indicated that lactate production was different under different conditions; when starved, the promastigotes were found to use the endogenous reserve energy-source (possibly glycogen), producing high levels of lactate followed by acetate and ethanol (figs. 5a1-c2). When the promastigotes were provided an external energy-source in the form of $^{13}C_1$ glucose, utilization of the reserve energy-source decreased; the level of lactate was decreased, while the levels of succinate and acetate were pronounced. The weak ^{13}C-labeling of lactate indicated that the parasites (in normal PBS) had utilized the external energy-source and metabolized it partially to lactate; the majority of lactate was produced by the metabolic conversion of the reserve energy-source. The cells under anaerobic conditions relied on the reserve energy-source but to a lesser extent, which was accounted for the production of lactate; they predominantly utilized $^{13}C_1$-enriched glucose as the external energy-source, and thus produced the metabolic intermediates specifically succinate and acetate. Lastly, when the cells were maintained under aerobic conditions with $^{13}C_1$-glucose, they did not produce lactate and seemed to utilize only the $^{13}C_1$-enriched glucose and not the reserve energy-source. No NMR-observable lactate was produced by the cells under aerobic conditions, which seemed to justify that the cells met their energy demands

mainly by the metabolic conversion of glucose via other biochemical pathways such as citric-acid cycle. These unique observations in *L. donovani* promastogites have indicated the possible existence of a reserve energy-source that might help the parasites for their survival under different conditions, and are to be explored further using other conventional biochemical techniques.

NMR Structural Aspects in Tuberculosis

TB still remains one of the foremost among infectious diseases in the world, which causes maximum death from a single microorganism. Approximately one third of the world's population has been infected with the causative organism *Mycobacterium tuberculosis* (MTB), eight million become sick with TB every year, and globally it accounts for almost 3 million deaths annually. Immunodeficiencies occurring under conditions of malnutrition, deterioration of general health or after the HIV infection have become responsible for an increase in the incidence of central nervous system TB.

India has been particularly hit by the dual threat of HIV and TB. Tuberculosis remains a serious public-health problem in India accounting for nearly one-third of the global burden, and it has been estimated that 3.5 million of the population are infected with TB. The re-emergence of TB is mainly due to the compromise of immune mechanisms, and particularly in HIV-infected individuals the risk is more. Not only do many developed countries face the gloomy scenario of increasing TB incidence, but also the problem of multi-drug-resistant TB that has emerged in several major urban centers of countries worldwide.

The most common clinical manifestation of tuberculosis is pulmonary disease. The extrapulmonary manifestation of tuberculosis, involving the central nervous system, is the most serious clinical manifestation of tuberculosis. Such involvement can include inflammation of the meninges (intracranial and intraspinal meningitis), as well as space-occupying lesions (tuberculomas) of the brain (cerebral or cord tuberculoma). In patients diagnosed with tuberculoma, surgery becomes essential to avoid mass effect and hydrocephalus.

Proper antitubercular treatment to patients suffering from tuberculoma of brain, if at all diagnosed by MRI, becomes an essential requirement, and ultimately in such cases the imaging modalities fail to differentiate whether it is a malignant, non-malignant or an infectious lesion. The diagnosis of tuberculomas is usually based on the characteristic histological features, which at times may overlap with other infective or non-infective granulomas, and the gold-standard culture

method is very time-consuming and is often insensitive. As a result, there is an increasing requirement for the development of newer and additional diagnostic techniques for the CNS form of TB.

The lipid components of tuberculomas as well as the causative organism have a role in assisting differential diagnosis. Earlier work has revealed that one could fingerprint the membrane lipid components of *Mycobacterium tuberculosis* in the lipid extract of intracranial tuberculomas. In order to explore further the diagnostic utility of NMR, detailed ^{1}H, ^{13}C and ^{31}P NMR studies of the lipid extract of intracranial tuberculomas have been carried out in the present investigation. The main objective was to characterize various lipid structural components in tuberculoma and to look for any possible specific diagnostic markers that may aid in the differentiation of tuberculomas from the tumors of brain.

Glycerophosphatidylcholine and sphingomyelin were identified as the two major choline-containing phospholipids in the present study, while the ethanolamine phospholipids were identified to be glycerophosphatidylethanolamine and plasmalogen. Based on the ^{1}H, ^{13}C and ^{31}P NMR experiments, the following lipid components could be identified in the tuberculoma lipid extracts: phosphatidylcholines, phosphatidylethanolamines, sphingomyelin, plasmalogen, triglycerides, phosphatidylinositol, phosphatidylserine, phosphatidylglycerol, phosphatidic acid, cholesterol and cholesterol ester (as oleate). The ^{1}H and ^{13}C NMR assignments of fatty acid chains indicated that the lipids consisted of both mono-unsaturated and poly-unsaturated fatty acids, and have been identified to be oleic acid (18:1(n-9)), linoleic acid (18:2(n-6)) and possibly arachidonic acid (20:4(n-6)).

The semi-quantitative levels of the lipid components are of importance so as to differentiate a pathological condition from healthy or other diseased states as shown by the literature evidence. This task was carried out for the tuberculoma lipid extracts in the present study, by obtaining the ratios of arbitrary integral values of lipid components from their respective ^{1}H NMR spectra. The mean levels obtained for the methylenes/methyls ratio, methylenes/di-allylic methylenes ratio, methylenes/olefinic ratio, di-allylic methylenes/mono-allylic methylenes ratio, triglycerides/phospholipids ratio and cholesterol ester/cholesterol ratio were in accordance with the reported values observed in pathological states such as cancer. Based on the observations of the present study, it could be stated that the values obtained for methylenes/methyls ratio, triglycerides/phospholipids ratio, methylenes/di-allylic methylenes ratio, methylenes/olefinic ratio

and cholesterol ester/cholesterol ratio may be of importance in differentiating tuberculomas from healthy or other pathological conditions of the brain.

The presence of ethanolamine plasmalogen in the tuberculoma lipid extracts, as observed during the course of the present investigation, may assume diagnostic significance, since literature evidence had indicated a possible role of choline plasmalogen in certain forms of tumors. While the exact role of ethanolamine plasmalogen in the disease process could not be elucidated during the present study, the relatively higher abundance of glycerophosphatidylcholine and glycerophosphatidylethanolamine, as seen in ^{1}H and ^{31}P NMR, may give an indication that the tuberculomas belong to the proliferative class and thus may mimic tumors.

The possible diagnostic value of ^{1}H NMR spectral assignments of human tuberculoma samples in the present study involved the assignments of cholesterol, cholesterol ester, phenolic glycolipids and plasmalogen. A comparative picture of cholesterol and its esterified form (identified as cholesterol oleate) in the ^{1}H NMR spectra of tuberculoma lipid extracts has indicated that the tuberculomas were of proliferative type with a relatively lower cholesterol ester/cholesterol ratio, and hence could be different from benign or low-grade tumors in which cholesterol ester has been reported to be absent.

The NMR investigations on tuberculoma lipid extracts have further highlighted the presence of phenolic glycolipids, besides cholesterol ester and ethanolamine plasmalogen. It could be reasoned that the granuloma formation by MTB infected macrophages in intracranial lesions might have resulted in the NMR observable levels of phenolic glycolipids that are constantly shed by the mycobacteria within the intracellular milieu of the host during infection. Phenolic glycolipids thus observed in the present study could be taken to represent the component of the cell wall of either living or dead mycobacteria in a granuloma.

The present study has brought out a speculation that the presence of cholesterol ester along with ethanolamine plasmalogen and phenolic glycolipids may aid in the identification of intracranial tuberculomas more authentically, and could thus differentiate them from the benign/malignant tumors of the brain. It is proposed that the presence of cholesterol ester is not only significant in case of proliferating tumors, but also in infective tuberculous granulomas of the brain. Since timely diagnosis after surgery and appropriate treatment is the cornerstone of management in intracranial tuberculomas, the present study has addressed the role of NMR as an additional diagnostic tool based on the analysis of lipid extracts.

NMR Structural Aspects in Meningitis

Meningitis is a severe acute infectious disease caused by several microorganisms, including viruses, bacteria, parasites and fungi, and is one of the most devastating infectious diseases of childhood in developing as well as in underdeveloped countries. Meningitis causes an intense headache, fever, loss of appetite, and intolerance to light and sound, rigidity of muscles especially those in the neck, and in severe cases convulsions, vomiting, and delirium finally leading to death if not properly diagnosed and treated. It is one of the major causes of childhood mortality, morbidity and disability.

The statistical features regarding the incidence of this disease are still alarming. Fatality rates associated with this disease can be as low as 2% in infants and children, and as high as 20-30% in neonates and adults. Despite the availability of several therapies, the three most common forms of meningitis, *viz*., bacterial meningitis, tuberculous meningitis and viral meningitis continue to be potentially fatal illnesses that can lead to death or permanent neurological sequelae in the child if not diagnosed at an early stage. The outcome of meningitis is strongly associated with the stage of disease presentation, with a 100% cure rate if proper diagnosis and treatment are given; otherwise it leads to 50% mortality or 80% permanent handicap. Unfortunately, because of limited economic resources and poor living conditions, many developing countries are still affected by the devastating consequences of this life-threatening systemic infection.

The cornerstone of management of meningitis in children depends on the rapid diagnosis and prompt treatment; however, the differential diagnosis of meningitis in children has been reported to be difficult due to various non-specific clinical features. Several new methodologies and techniques have been developed over the course of time such as the bromide partition test, lactate dehydrogenase assay, adenosine deaminase assay, IgG assay etc., but none has yet been stated to be a foolproof method. PCR, a relatively new technique for the diagnosis of TBM is also not foolproof, and is expensive for many developing countries. Besides all these techniques, the analysis of CSF often becomes crucial for the diagnosis of neurological disorders as the chemical components of CSF reflect the state of the CNS in healthy and diseased state.

Several reports exist in the literature, which highlight the potential role of NMR in understanding the metabolic profile of CSF under various pathological conditions. It has been well documented that NMR spectroscopy gives non-invasive, qualitative as well as quantitative

information regarding the metabolic profile and usually a metabolite concentration of greater than a few μM is detectable in the ^{1}H NMR spectra in a reasonable amount of time (^{1}H NMR; 128 scans; ca. 15 min). Taking into consideration the limitations of the currently available diagnostic techniques as well as the persistent problems regarding the timely diagnosis of childhood meningitis, the present investigation has been carried out to explore the possibility of ^{1}H NMR spectroscopy as an additional diagnostic tool based on the analysis of CSF from 191 cases.

During the present study, quantification of twelve well-separated and commonly observed CSF metabolites *viz*., *β*-hydroxybutyrate, lactate, alanine, acetate, acetone, acetoacetate, pyruvate, glutamine, citrate, creatine/creatinine, glucose (total) and urea was carried out using Bruker's NMRQUANT software with respect to a known concentration of sodium-3-(trimethylsilyl)-2,2,3,3-d_4-propionate (TSP), serving as an external reference. The assignment of urea in CSF is reported for the first time by NMR. The presence of cyclopropane observed for the first time in tuberculous meningitis overall in 85.1% of cases, acts as a fingerprint marker for the differential diagnosis. Multivariate discriminant function analysis was carried out for the proton MR-detected metabolite information and the clinical symptoms data of the meningitis and control cases to find out the important descriptors for classification, followed by a re-validation of the entire database. It was found the differentiation of control from the disease group could be successfully classified overall with a success rate of 96.4%, followed by the differential diagnosis of tuberculous meningitis with a corresponding value of 77.2%. Excluding the presence of cyclopropane, bacterial meningitis could be classified 84.4% correct and viral meningitis with a rate of 83.3%.

A new expert system MENEXSYS was developed using Microsoft Visual Basic 6.0 incorporating all the ^{1}H NMR quantitative information, and clinical symptoms data of 167 meningitis and 24 control cases. The discriminant function analysis-based weights/coefficients and the mid-point cut-off values obtained based on the multivariate analysis of the entire database of 191 cases have been incorporated in the software modules to make predictions of the 'disease type' in a new childhood meningitis patient case. The classification logic that would be responsible for any future prediction of the meningitis type has been divided into three phases as: (i). Differentiation of control (non-meningitis) from disease (meningitis) groups; (ii). Differentiation of TBM from the non-TBM cases, i.e., bacterial and viral meningitis; (iii). Differentiation of BM from VM cases.

The prediction possibility of the classification model was further checked with a 75/25 data split, by using 75% of the patients' data as training sets and the remaining 25% data as test sets, which revealed an overall improvement in the differential diagnosis of meningitis when important clinical and NMR descriptors were combined together and taken for the analysis. The purpose of developing MENEXSYS was to simplify the analysis for the differential diagnosis of meningitis besides making it very user-friendly in the form of an easy-to-use Graphical User Interface, as handling of the statistical software for multivariate analysis may become too technical and time-consuming. In conclusion, it is proposed that the NMR spectroscopic information along with other routine clinical features coupled in the form of an expert system MENEXSYS may serve as an additional diagnostic tool for the differential diagnosis of meningitis in children. It is hoped that the results obtained through MENEXSYS may supplement the results of other gold-standard methods.

Appendices

MENEXSYS Modules:

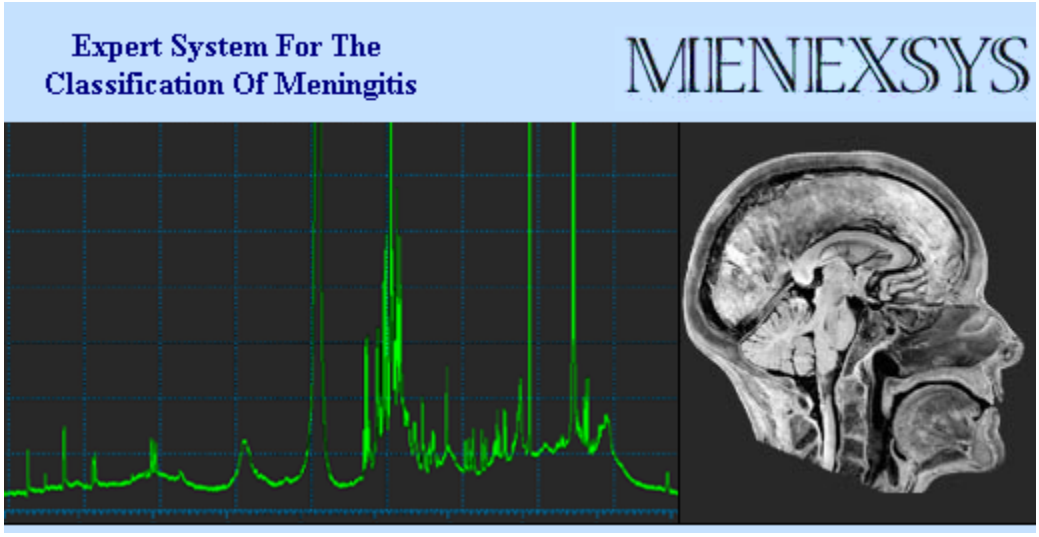

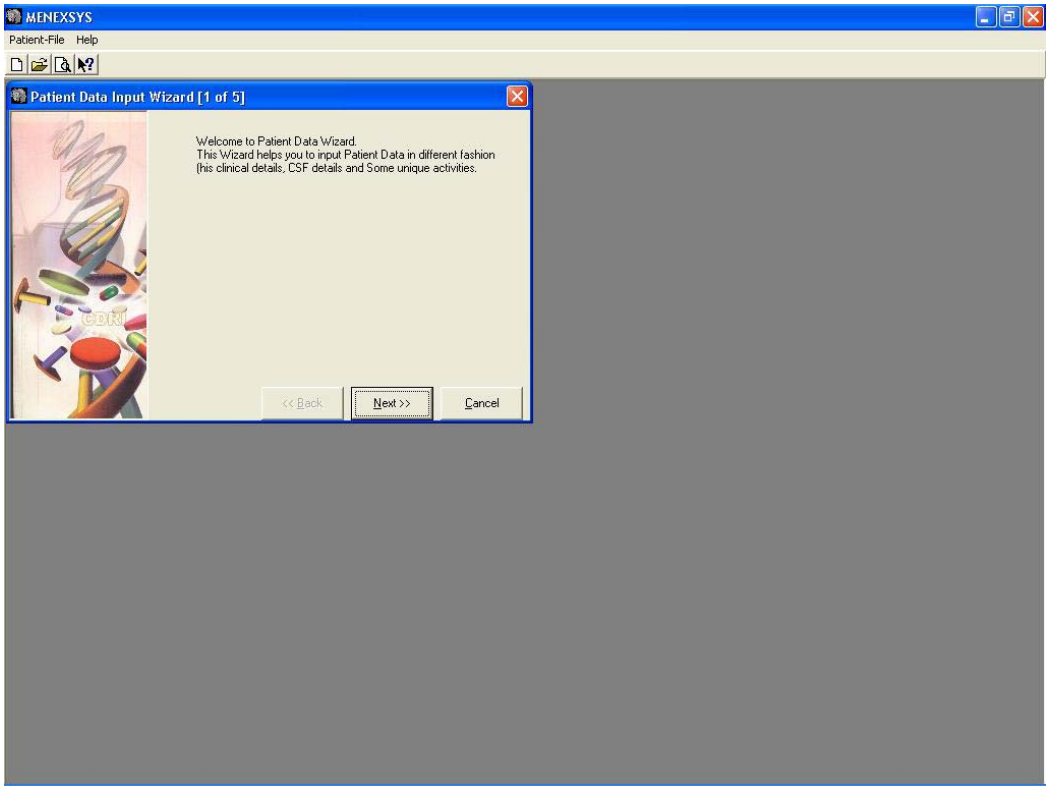

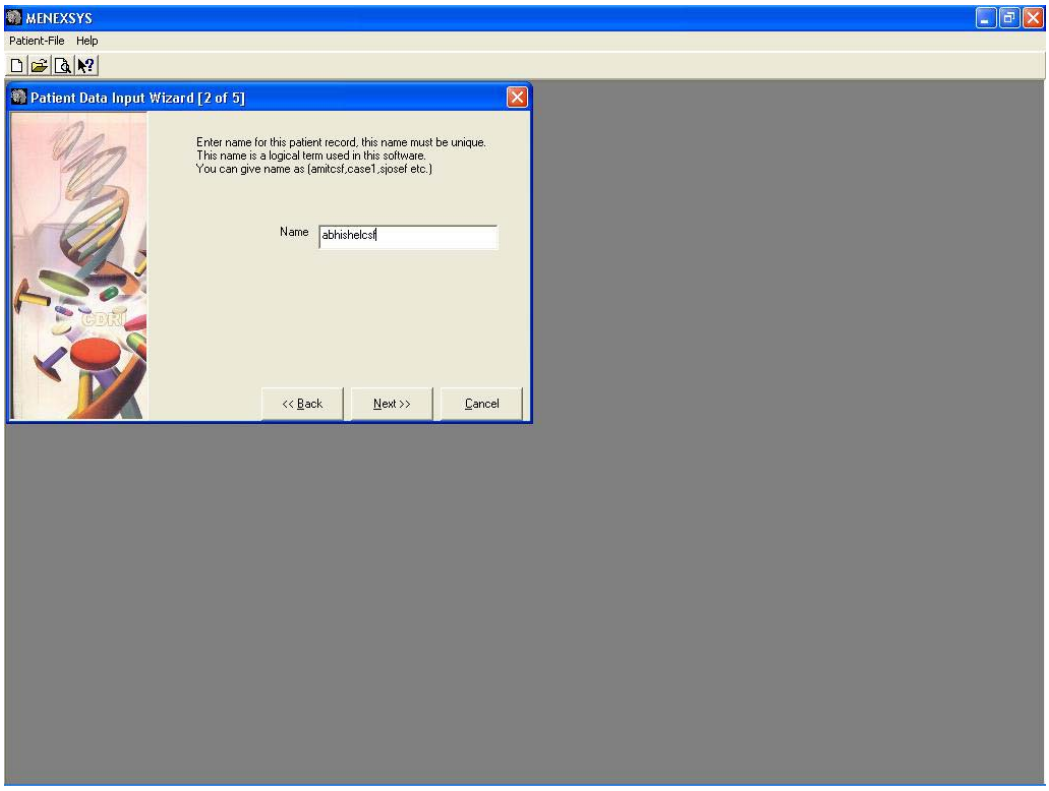
MENEXSYS
Patient-File Help
Patient Data Input Wizard [2 of 5]
Enter name for this patient record, this name must be unique.
This name is a logical term used in this software.
You can give name as (amitcsf,case1,sjosef etc.)
Name abhishelcsf
<< Back
Next >>
Cancel

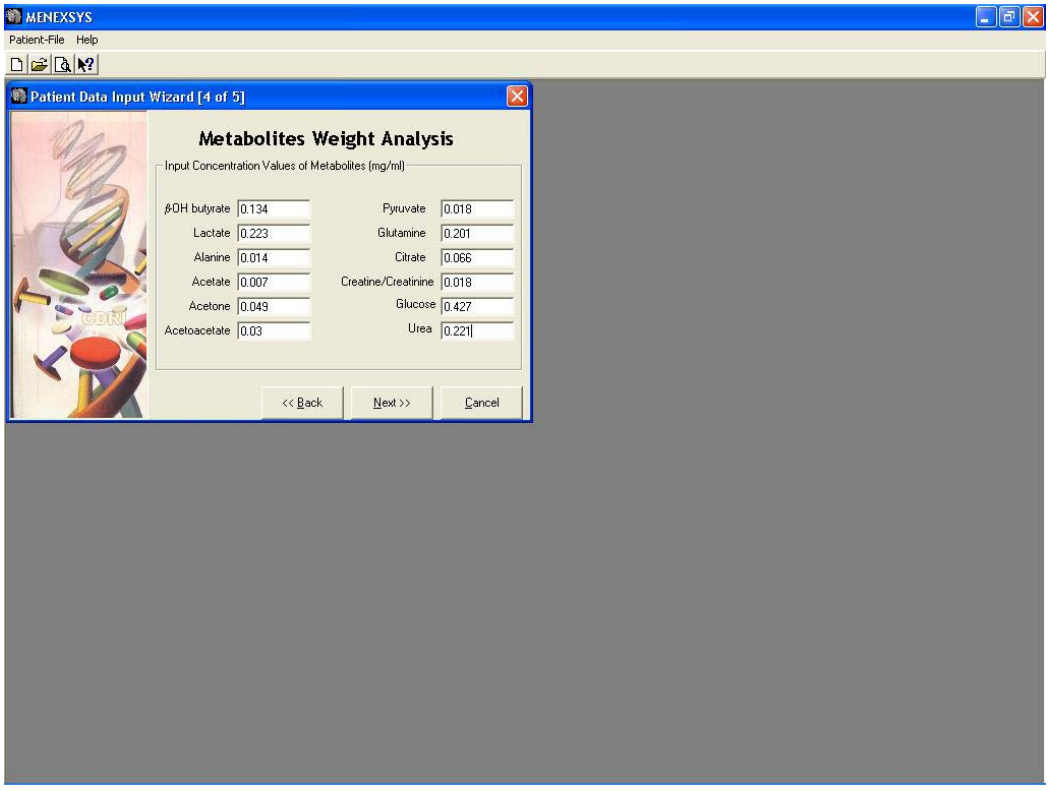
MENEXSYS
Patient-File Help
Patient Data Input Wizard [4 of 5]
Metabolites Weight Analysis
Input Concentration Values of Metabolites (mg/ml)
β-OH butyrate 0.134
Lactate 0.223
Alanine 0.014
Acetate 0.007
Acetone 0.049
Acetoacetate 0.03
Pyruvate 0.018
Glutamine 0.201
Citrate 0.066
Creatine/Creatinine 0.018
Glucose 0.427
Urea 0.221
<< Back
Next >>
Cancel

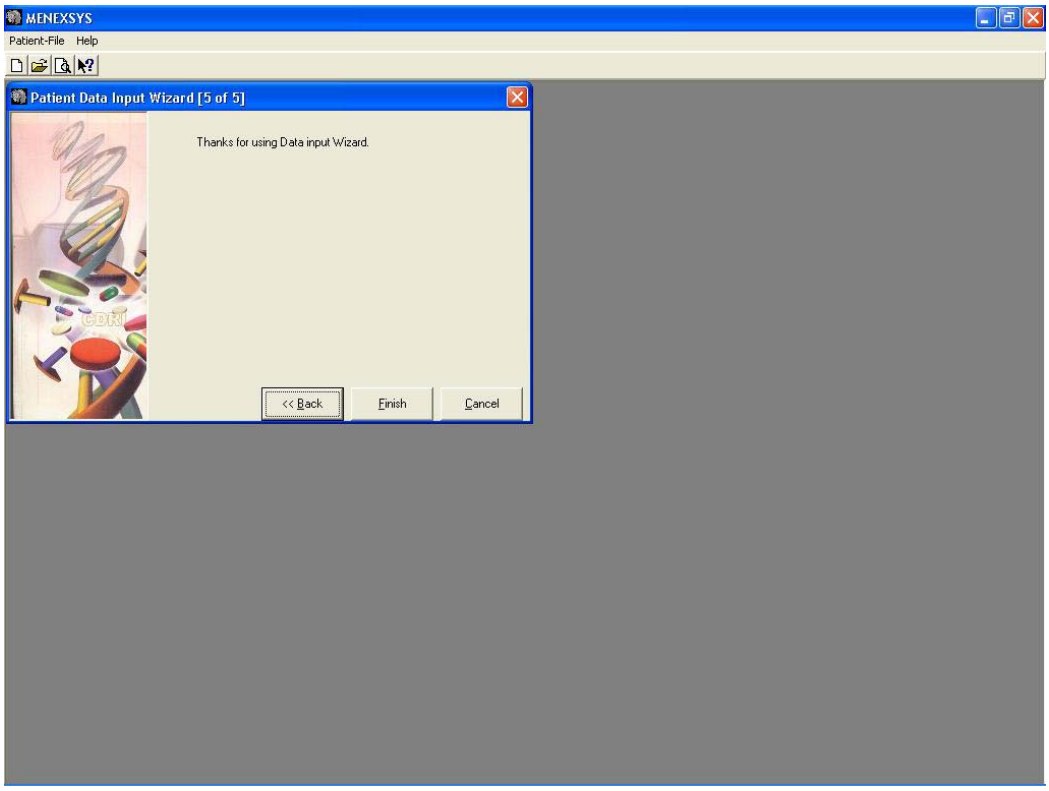
MENEXSYS
Patient-File Help
Patient Data Input Wizard [5 of 5]
Thanks for using Data input Wizard.
<< Back
Finish
Cancel

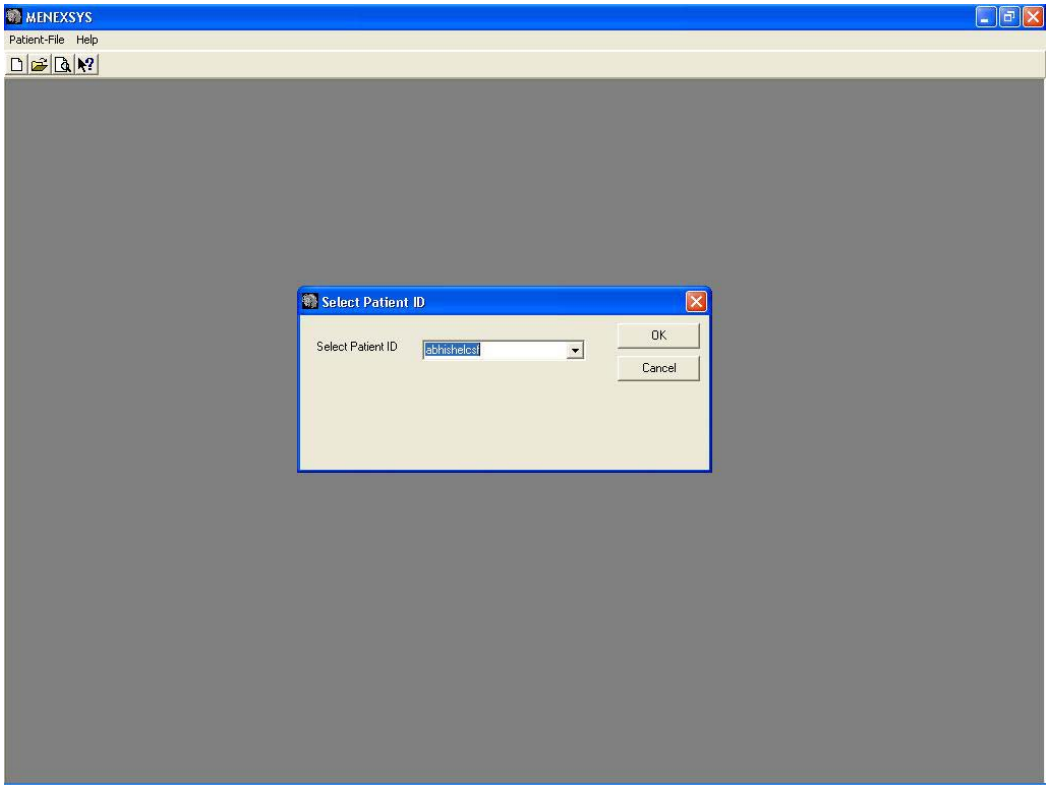
MENEXSYS
Patient-File Help
Select Patient ID
Select Patient ID
abhishekst
OK
Cancel

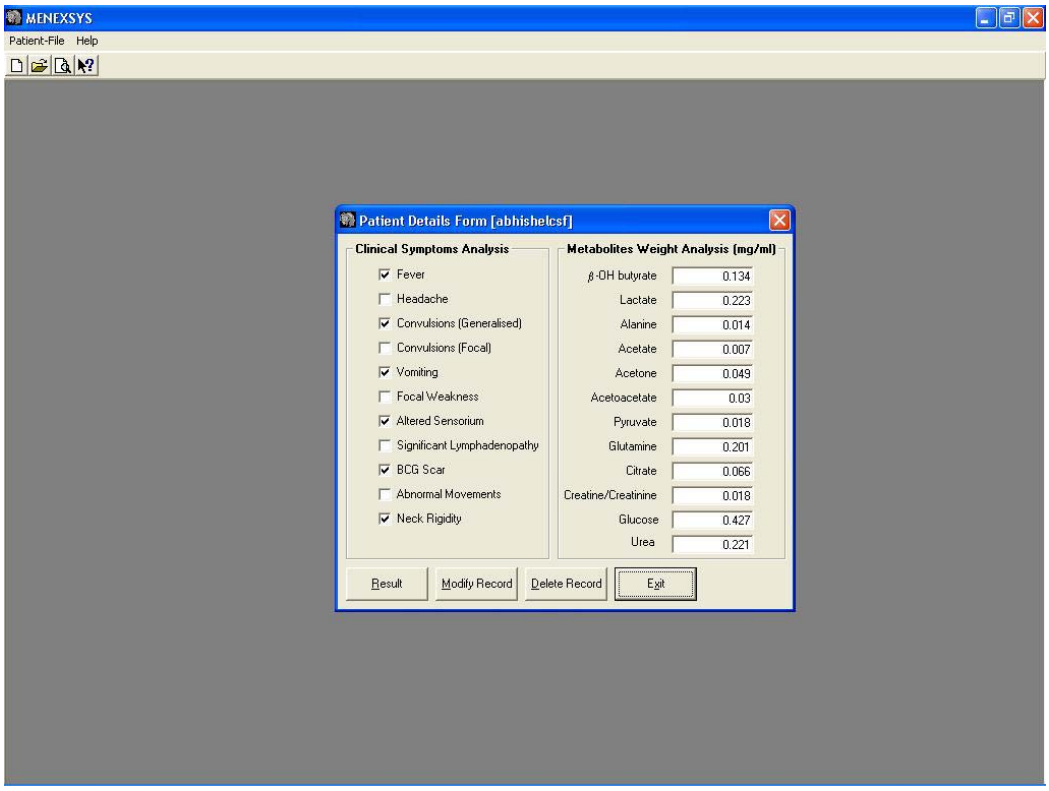
MENEXSYS
Patient-File Help
Patient Details Form [abhishekcsf]
Clinical Symptoms Analysis
Fever
Headache
Convulsions (Generalised)
Convulsions (Focal)
Vomiting
Focal Weakness
Altered Sensorium
Significant Lymphadenopathy
BCG Scar
Abnormal Movements
Neck Rigidity
Metabolites Weight Analysis (mg/ml)
β-OH butyrate 0.134
Lactate 0.223
Alanine 0.014
Acetate 0.007
Acetone 0.049
Acetoacetate 0.03
Pyruvate 0.018
Glutamine 0.201
Citrate 0.066
Creatine/Creatinine 0.018
Glucose 0.427
Urea 0.221
Result
Modify Record
Delete Record
Exit

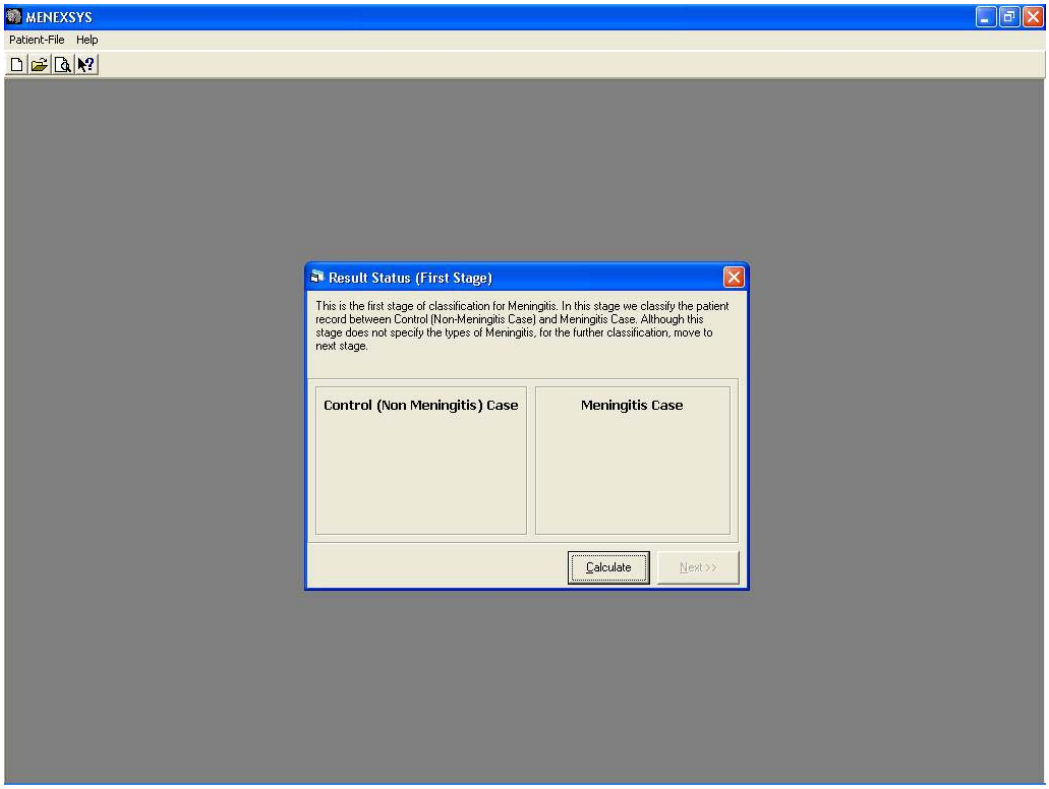
MENEXSYS
Patient-File Help
Result Status (First Stage)
This is the first stage of classification for Meningitis. In this stage we classify the patient record between Control (Non-Meningitis Case) and Meningitis Case. Although this stage does not specify the types of Meningitis, for the further classification, move to next stage.
Control (Non Meningitis) Case
Meningitis Case
Calculate
Next>>

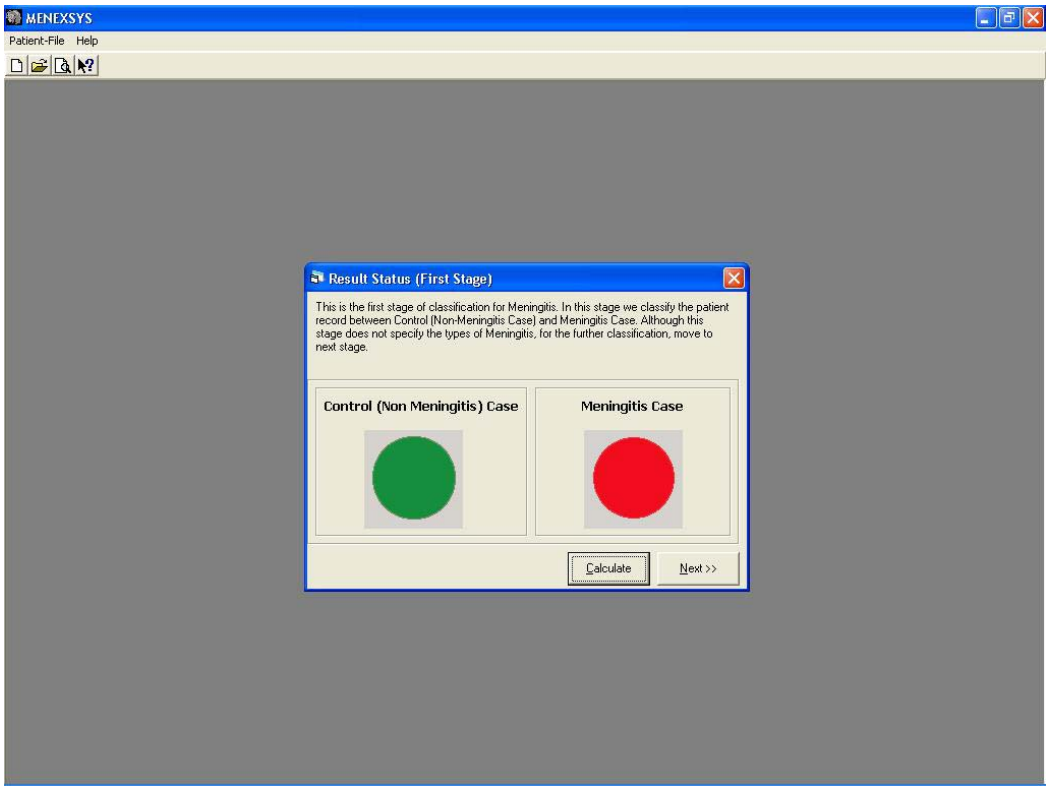
MENEXSYS
Patient-File Help
Result Status (First Stage)
This is the first stage of classification for Meningitis. In this stage we classify the patient record between Control (Non-Meningitis Case) and Meningitis Case. Although this stage does not specify the types of Meningitis, for the further classification, move to next stage.
Control (Non Meningitis) Case
Meningitis Case
Calculate
Next >>

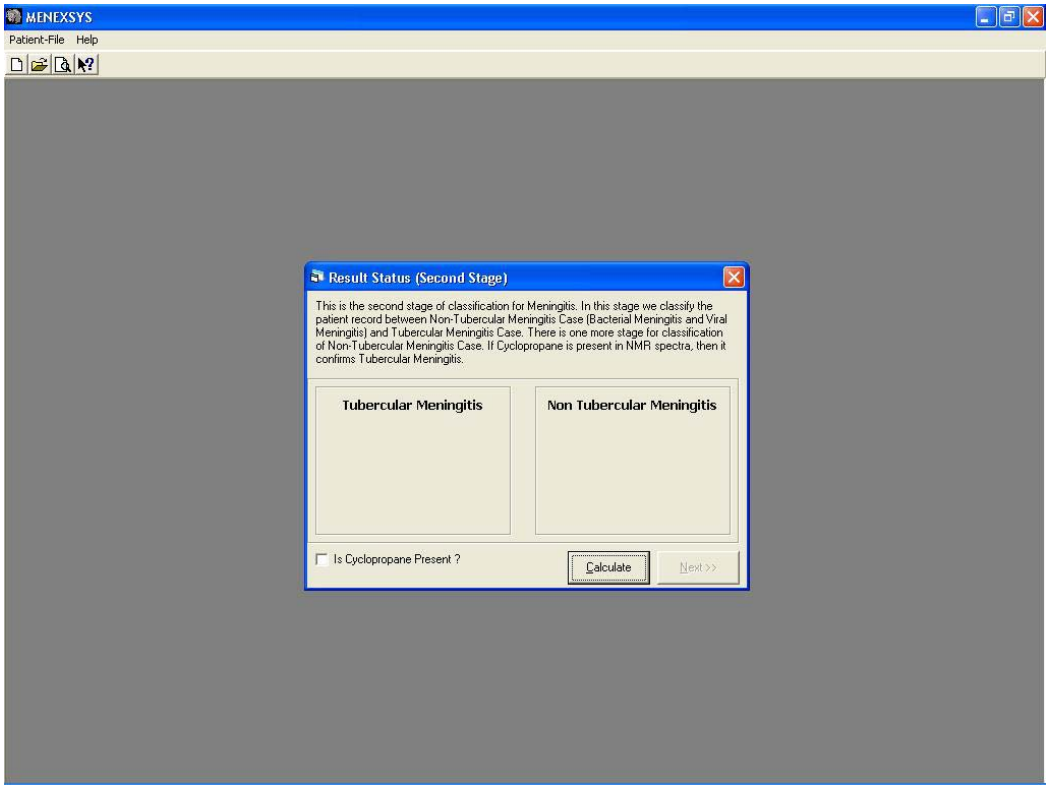
MENEXSYS
Patient-File Help
Result Status (Second Stage)
This is the second stage of classification for Meningitis. In this stage we classify the patient record between Non-Tubercular Meningitis Case (Bacterial Meningitis and Viral Meningitis) and Tubercular Meningitis Case. There is one more stage for classification of Non-Tubercular Meningitis Case. If Cyclopropane is present in NMR spectra, then it confirms Tubercular Meningitis.
Tubercular Meningitis
Non Tubercular Meningitis
Is Cyclopropane Present ?
Calculate
Next >>

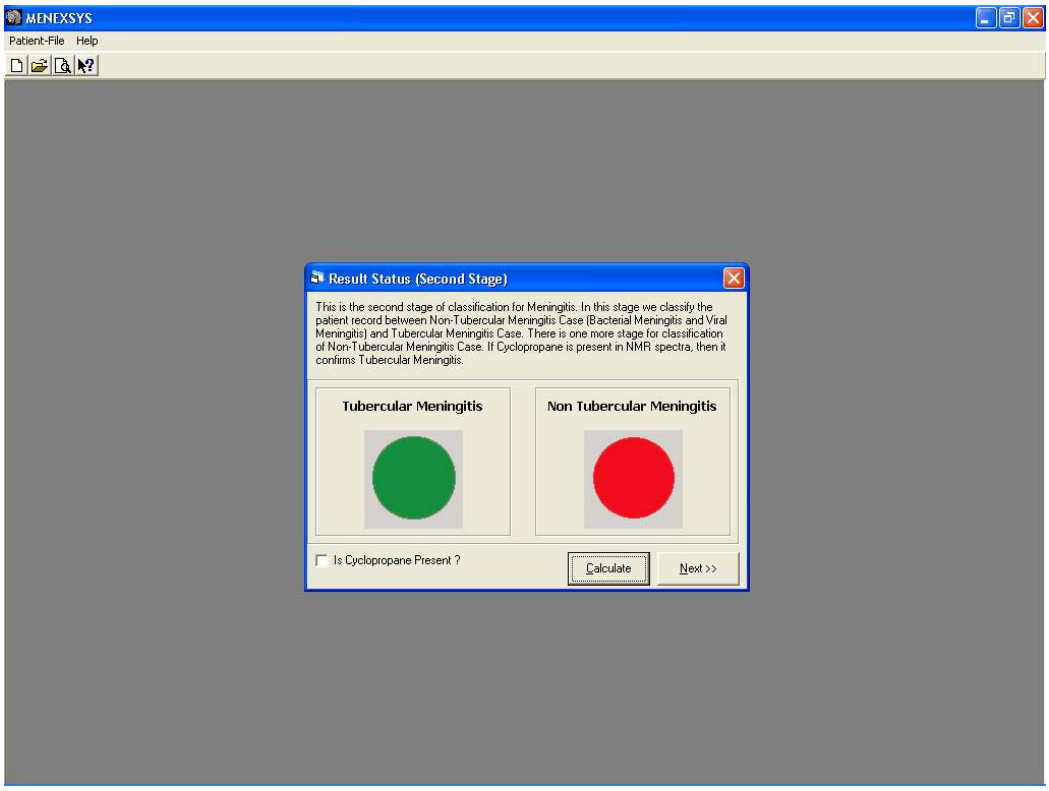
MENEXSYS
Patient-File Help
Result Status (Second Stage)
This is the second stage of classification for Meningitis. In this stage we classify the patient record between Non-Tubercular Meningitis Case (Bacterial Meningitis and Viral Meningitis) and Tubercular Meningitis Case. There is one more stage for classification of Non-Tubercular Meningitis Case. If Cyclopropane is present in NMR spectra, then it confirms Tubercular Meningitis.
Tubercular Meningitis
Non Tubercular Meningitis
Is Cyclopropane Present ?
Calculate
Next >>

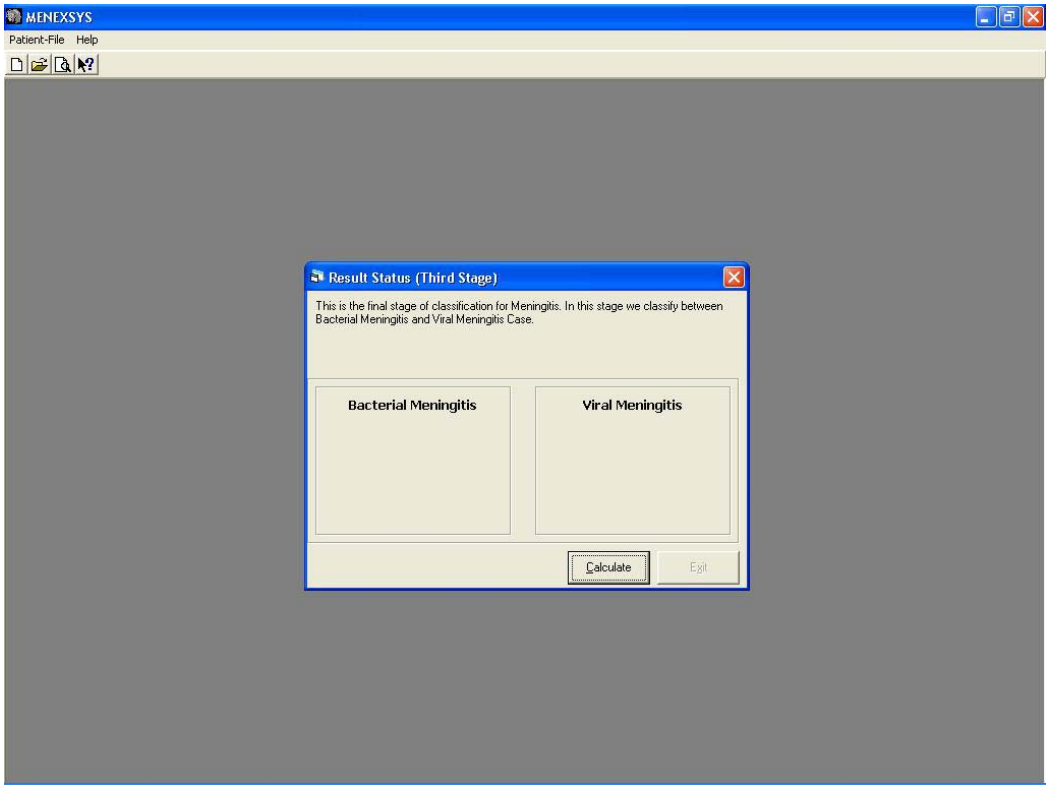
MENEXSYS
Patient-File Help
Result Status (Third Stage)
This is the final stage of classification for Meningitis. In this stage we classify between Bacterial Meningitis and Viral Meningitis Case.
Bacterial Meningitis
Viral Meningitis
Calculate
Exit

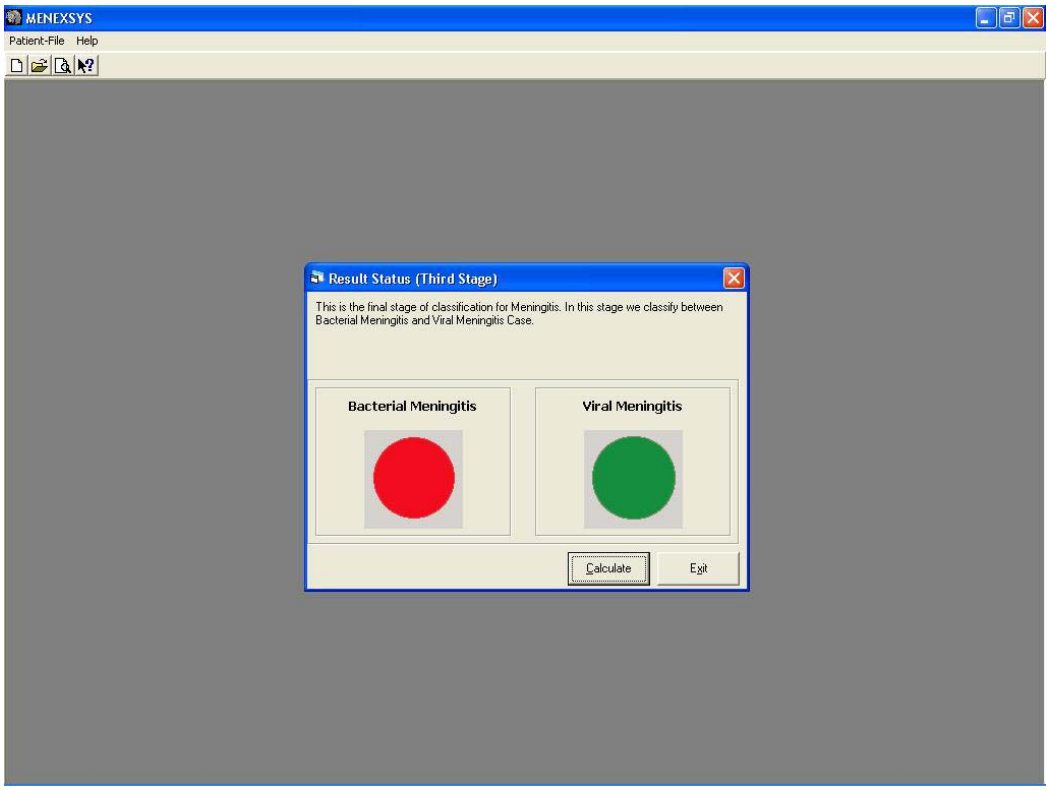
MENEXSYS
Patient-File Help
Result Status (Third Stage)
This is the final stage of classification for Meningitis. In this stage we classify between Bacterial Meningitis and Viral Meningitis Case.
Bacterial Meningitis
Viral Meningitis
Calculate
Exit

List of Publications:

A. Subramanian, A. Gupta, S. Saxena, A. Gupta, R. Kumar, A. Nigam, R. Kumar, S.K. Mandal and R. Roy. "Proton MR CSF Analysis and a New Software as Predictors for the Differentiation of Meningitis in Children", *NMR Biomed*., **18**, 213-225, 2005. [*Appeared as a Featured Article in the SpectroscopyNOW.com portal during June 2005*.]

List of Presentations:

A. Subramanian, A. Gupta, S. Saxena, A. Gupta, R. Kumar, A. Nigam, R. Kumar, S.K. Mandal and R. Roy. "Proton MR and a New Software as Predictors for the Differentiation of Meningitis in Children" (Electronic Poster), 13th International Society for Magnetic Resonance in Medicine (ISMRM) meeting held at Miami, Florida, USA from 7th May, 2005 to 13th May, 2005.

A. Subramanian, M. Srivastava, U. Roy, A.K. Rastogi, S.K. Mandal and R. Roy. "Proton NMR Analysis and Identification of Predictive Metabolite-Descriptors for the Differentiation of Unresponsive and Responsive Strains in *Leishmania donovani*" (Poster), 21st International Conference on Magnetic Resonance in Biological Systems (ICMRBS) held at Hyderabad, India from 16th January, 2005 to 21st January, 2005.

A. Subramanian, A. Gupta, S. Saxena, A. Gupta, R. Kumar, A. Nigam, R. Kumar, S.K. Mandal and R. Roy. "Proton MR CSF Analysis and a New Software as Predictors for the Differentiation of Meningitis in Children" (Poster), 21st International Conference on Magnetic Resonance in Biological Systems (ICMRBS) held at Hyderabad, India from 16th January, 2005 to 21st January, 2005.

A. Subramanian, B.S. Joshi and R. Roy. "Cholesterol Esters and Ceramide in Human Intracranial Tuberculomas" (Poster), 21st International Conference on Magnetic Resonance in Biological Systems (ICMRBS) held at Hyderabad, India from 16th January, 2005 to 21st January, 2005.

A.R. Subramanian, Abhishek Gupta, Swapnil Saxena, Anjali Nigam, R. Kumar and Raja Roy. "Development of an Expert System (MENEXSYS) for the Prediction and Classification of ^{1}H NMR Spectra of CSF of Children suffering from Meningitis" (Poster), Special Symposium on "Recent Developments in NMR Methodology & National Symposium on Magnetic Resonance" held at Indian Institute of Science, Bangalore, India from 3rd February, 2003 to 6th February, 2003.

A.R. Subramanian, U.K. Singha, Raja Roy, Uma Roy and A.K. Rastogi. "*Leishmania donovani*: First Quantitative Report on Comparative Intracellular Metabolites Profile of Eight Clinically Unresponsive, Four Responsive and One Reference (Dd8) Promastigote Strains based on Proton Nuclear Magnetic Resonance Spectroscopy" (Oral), Symposium on "Biomedical Magnetic Resonance & 8th NMRS Meeting", held at Sanjay Gandhi Post-Graduate Institute of Medical Sciences, Lucknow, India from 20th January, 2002 to 24th January, 2002.

A.R. Subramanian, Anjali Nigam and Raja Roy. "High-Resolution ^{1}H-NMR Spectroscopy of the Cerebrospinal Fluid (CSF) of Children with Meningitis" (Poster), National Symposium on "Magnetic Resonance and Biomolecular Structure and Function" held at Tata Institute of Fundamental Research (TIFR), Mumbai, India, from 17th January, 2000 to 20th January, 2000.


ATOMIC IR MRI MS NMR RAMAN UV X-RAY CHEMOMETRICS PROTEOMICS
MRI - Magnetic Resonance Imaging Resource
spectroscopyNOW.com
On Your Wavelength
brought to you by WILEY
MRI The key resource for Magnetic Resonance Imaging
search go
News & Features
Discussion Forums
Education
Training
Jobs
Links
Library & Bookshop
Conference Centre
Classifieds
About This Site
Membership Centre
Contact Us
Newsletter Sign-up
Opinion Polls
Welcome Subramanian
Logout | My Details
Only required for enhanced features
FEATURES
Proton MR CSF analysis and a new software as predictors for the differentiation of meningitis in children
27 June 2005
This article, recently published in NMR in Biomedicine, describes proton MR spectroscopic analysis of cerebrospinal fluid of 167 children suffering from meningitis. The paper proposes that the NMR spectroscopic information, along with other routine clinical features, may serve as an additional diagnostic tool for the differential diagnosis of meningitis. [More...]
Accelerating MRI by skipped phase encoding and edge deghosting (SPEED)
27 June 2005
A fast imaging method called skipped phase encoding and edge deghosting is introduced in this paper published in Magnetic Resonance in Medicine. The k-space is sparsely sampled into three interleaved datasets, each with a skip-size N and a relative shift in phase encoding. [More...]
NEW MAGAZINE
Spectroscopy Asia launched in May
Spectroscopy Asia is a controlled circulation journal which is now available Free to all qualifying spectroscopists in Asia. Sign up now to receive your complimentary copy of this new and exciting journal which is published 4 times a year.
Read more... [More...]
FEATURED BOOK
Singular transistor
Martian aurora
A molecular bunker for chromophores
Hurricanes touch base with ozone
NEWS
Latest Issue of NMR Ezine, Resonants, Now Online
01 July 2005 [More...]
MRS May Lead to Better Treatments for Parkinson's
29 June 2005 [More...]
Brain Imaging Brings New Understanding of Language and Literacy
29 June 2005 [More...]
MRI Used to Measure Myocardial Infarct Size
29 June 2005 [More...]
Feasibility of 3D proton MR Spectroscopic Imaging of Prostate Cancer Studied


ATOMIC IR MRI MS NMR RAMAN UV X-RAY CHEMOMETRICS PROTEOMICS
MRI - Magnetic Resonance Imaging Resource
spectroscopyNOW.com
On Your Wavelength
brought to you by WILEY
MRI The key resource for Magnetic Resonance Imaging
search go
News & Features
News
Features
Product News
Site News
Archive
Discussion Forums
Education
Training
Jobs
Links
Library & Bookshop
Conference Centre
Classifieds
About This Site
Membership Centre
Contact Us
Newsletter Sign-up
Opinion Polls
Welcome Subramanian
Logout | My Details
Only required for enhanced features
NEWS & FEATURES
FEATURES
Proton MR CSF analysis and a new software as predictors for the differentiation of meningitis in children
Last Updated: 27 June 2005
NMR in Biomedicine 2005, 18, 213-225
Arunachalam Subramanian, Abhishek Gupta, Swapnil Saxena, Ashish Gupta, Raj Kumar, Anjali Nigam, Rashmi Kumar, Sudhir K. Mandal and Raja Roy
This article describes proton MR spectroscopic analysis of cerebrospinal fluid of 167 children suffering from meningitis and 24 control cases. Quantification of 12 well-separated and commonly observed cerebrospinal fluid metabolites viz., β-hydroxybutyrate, lactate, alanine, acetate, acetone, acetoacetate, pyruvate, glutamine, citrate, creatine/creatinine, glucose (total) and urea was carried out using Bruker's NMRQUANT software with respect to a known concentration of sodium-3-(trimethylsilyl)-2,2,3,3-d4-propionate (TSP), serving as an external reference. The assignment of urea in CSF is reported for the first time by NMR. The presence of cyclopropane, observed for the first time in tuberculous meningitis overall in 85.1% of cases, acts as a finger-print marker for the differential diagnosis. Multivariate discriminant function analysis was carried out for the proton MR-detected metabolite information and the clinical symptoms data of the meningitis and control cases to find the important descriptors for classification, followed by a re-validation of the entire database. It was found that the control could be differentiated from the disease group with a success rate of 96.4%, followed by the differential diagnosis of tuberculous meningitis with a corresponding value of 77.2%. Excluding the presence of cyclopropane, bacterial meningitis could be classified 84.4% correct and viral meningitis with a rate of 83.3%. It is proposed that the NMR spectroscopic information, along with other routine clinical features, may serve as an additional diagnostic tool for the differential diagnosis of meningitis in children.
For more information, view the PDF Full Text article (size: 240K) from within Wiley InterScience.
Please note that the first time you access this file, you will be presented with the paper's Abstract. To view the HTML or PDF version of the full paper, simply click on the HTML or PDF link near the top of the page.
FREE ACCESS
View this issue's Table of Contents
Further information about:
NMR in Biomedicine
Magnetic Resonance in Medicine
Concepts in Magnetic Resonance Part A
Magnetic Resonance in Chemistry

Brief Biography of the Candidate, Mr. Subramanian A.R.

Mr. Subramanian A.R. hails from Chennai, Tamil Nadu. Following his higher-secondary examinations he joined BITS, Pilani for his Bachelor's degree in Pharmacy and graduated in 1996. The inspirational academic atmosphere in BITS had further led him to earn his Master's degree in Pharmacy in 1997 along with a concurrent dissertation in Medicinal Chemistry under the guidance of Dr. P. Srinivas. His quest for research continued and led him to pursue a Ph.D. when he joined BITS, Pilani as a faculty member in the Pharmacy Group in 1997.

After the sudden and untimely demise of Prof. P. Parimoo in 1998, Mr. Subramanian was given an opportunity to pursue his dreams at Central Drug Research Institute, Lucknow, as an off-campus Practice School faculty. It is here that he came across the magnetic influence of Dr. Raja Roy, Scientist-in-charge of the FT-NMR Facility at the Division of Sophisticated Analytical Instruments Facility (SAIF), and subsequently he chose to pursue a Ph.D. involving the Biomedical Applications of NMR under his guidance. He has completed his thesis work entitled "NMR Structural Aspects in Biological Systems: Analysis in Leishmaniasis, Tuberculosis and Meningitis", which is being submitted in partial fulfilment of the requirements for the degree of Doctor of Philosophy at BITS, Pilani. As part of his thesis work he has been involved in the Biomedical aspects of Magnetic Resonance with an emphasis on Visceral Leishmaniasis, Neuro-tuberculosis and Childhood Meningitis.

On the professional front, Mr. Subramanian has been involved with the Practice School program of BITS, Pilani at Central Drug Research Institute, Lucknow and Industrial Toxicology Research Center, Lucknow since 1998. He has about nine publications to his credit in peer-reviewed journals, and has also presented his works in national and international symposia. He has also contributed in the structure elucidation of novel N-confused porphyrins using NMR, and in the design and synthesis of novel bioactive molecules as potential 5-HT receptor modulators. Mr. Subramanian was awarded a fellowship to participate and present his work regarding 'Proton MR and a New Software as Predictors for the Differentiation of Meningitis in Children' in the 13th

Scientific Meeting of the International Society for Magnetic Resonance in Medicine (ISMRM) held at Miami Beach, Florida, USA during 7-13 May, 2005.

Mr. Subramanian has been affiliated to the National Magnetic Resonance Society (NMRS), India as a Life Member since 1999. His current areas of interest include *ex vivo*, *in vivo* and *in vitro* NMR of Body Fluids and Tissue Extracts, Biomedical Aspects of NMR involving Cellular Metabolism, as well as the Design and Synthesis of Novel Heterocyclic Bioactive Molecules.

Brief Biography of the Supervisor, Dr. Raja Roy, FNASc.

Dr. Raja Roy is one of the well-acclaimed NMR spectroscopists of the country, and has been involved in various aspects of Application of NMR, ranging from Chemistry, Biology and Medicine for the last twenty years.

Dr. Roy received his Master's degree in Chemistry from Lucknow University in 1982, and his Ph.D. degree in Chemistry in 1991 from Meerut University. Following his Ph.D., he has joined the Central Drug Research Institute, Lucknow as a Scientist and has been involved in the planning and implementation of several front-line projects involving NMR at this premier institute since 1988.

Dr. Roy was awarded the Bruker Young Scientist Award in 1993 for his outstanding contributions in the field of NMR, and also a fellowship under the Indo-Italian collaboration for a scientific visit to CERM Florence, Italy from 20th August 2000 to 20th October 2000. He was elected as a Fellow of the National Academy of Sciences (FNASc.), Allahabad in 2001, and was subsequently awarded the 'DS Bhakuni Prize of Indian Chemical Society' for the year 2002.

Dr. Roy has been involved in the promotion of NMR and its varied applications across the country, and has conducted a NMR workshop at Regional Research Laboratory, Jammu in 2001. He has been one of the pioneers and motivators for several young aspirants who wish to pursue a career involving Magnetic Resonance, and has been regarded for his inspirational teaching abilities. He is involved in several consultancy and teaching activities, and is one of the Program Advisory Committee Member (PAC) of the National Facility for High Field NMR at Tata Institute of Fundamental Research (TIFR), Mumbai. Dr. Roy was a Visiting Faculty of Biotechnology at Allahabad University, and is also a Visiting Faculty and Collaborator of Center of Biomedical Magnetic Resonance (CBMR), Sanjay Gandhi Post-graduate Institute of Medical Sciences (SGPGIMS), Lucknow. He has been involved as the Convener and Faculty of the 'National Summer School on NMR: From Molecules to Human Behaviour' for the last four years, and has delivered several invited lectures at various academic and research institutions across the country.

Dr. Roy has about 110 publications to his credit in peer-reviewed journals, and has supervised three Ph.D. Thesis and several M.D. and M.S. Thesis, as well as the training programs of students from premier academic institutions, including BITS, Pilani. He has been affiliated to the National Magnetic Resonance Society (NMRS), India as a Life Member since 1996.

Presently, Dr. Roy is the Scientist-in-charge of the FT-NMR Facility at the Division of Sophisticated Analytical Instruments Facility (SAIF), CDRI Lucknow, which involves overall handling responsibilities of the Bruker *Avance* 400 MHz with HR-MAS, Bruker *Avance* DRX 300 MHz, Bruker *Avance* 300 MHz and Bruker *Avance* DPX 200 MHz with sample changer units. His 'current areas of research' include the Structure Determination of Bioactive Natural Products by NMR, NMR Studies on Diversified Organic Molecules, *in vivo* NMR Studies concerning Parasite Metabolism, Magnetic Resonance in Biomedicine for Disease Diagnosis and Pathophysiology, NMR Studies regarding the Dynamics in Expanded Porphyrins, NMR Applications in Drug Discovery and Development, as well as the NMR-driven Synthetic Methodologies and Real-Time NMR for various Reaction Mechanisms of Novel Bioactive Molecules.

NMR Structural Aspects in Biological Systems: Analysis in Leishmaniasis, Tuberculosis and Meningitis

SYNOPSIS OF THE THESIS

Submitted in partial fulfilment
of the requirements for the degree of
DOCTOR OF PHILOSOPHY

By

SUBRAMANIAN A.R.

Under the Supervision of
Dr. Raja Roy, FNASc.

BIRLA INSTITUTE OF TECHNOLOGY AND SCIENCE
PILANI (RAJASTHAN) INDIA

2006

Synopsis of the Thesis

In the six decades since its theoretical origins, Nuclear Magnetic Resonance (NMR) spectroscopy has matured with unprecedented speed and revolutionized the manner in which chemists and biologists conduct structural analysis. NMR has contributed not only to investigations of molecular level structures and dynamics, important in modern chemistry and biology, but also in medicine in the form of Magnetic Resonance Imaging to study the macroscopic distribution of materials found in the human body. The structural information now available to the chemists and biologists, through pulse NMR, is probably greater and more readily obtained than by any other single technique.

The present thesis work entitled "**NMR Structural Aspects in Biological Systems: Analysis in Leishmaniasis, Tuberculosis and Meningitis**" is arranged in the form of five chapters. The first chapter addresses a brief overview regarding the historical development of NMR, followed by a description of the essential concepts in modern FT-NMR spectroscopic techniques. The second chapter deals with the applications of NMR spectroscopy pertaining to Pharmaceutical Sciences, Biochemical Sciences, Biomedical Sciences and Metabonomics, and is arranged in the form of a review of literature. The third chapter describes the work carried out involving *Leishmania donovani* promastigotes to map the important metabolites using ^{1}H and ^{31}P NMR in six cultured strains of *L. donovani* based on the perchloric acid extract method, followed by the NMR experiments on live Dd8 promastigotes to explore the cell bioenergetics under different buffer conditions. The fourth chapter deals with the ^{1}H, ^{13}C and ^{31}P NMR spectroscopy of the lipid extracts of human intracranial tuberculoma samples, and addresses the utility of NMR as a potential diagnostic tool to distinguish tuberculomas from the benign/malignant tumors of the brain. The fifth chapter describes proton MR spectroscopic analysis of cerebrospinal fluid (CSF) of 167 children suffering from meningitis and 24 control cases, and explores the utility of NMR as an additional diagnostic tool in the form of an expert system MENEXSYS to distinguish the three major forms of meningitis in children.

The salient features of the work carried out regarding the **NMR Structural Aspects in Leishmaniasis, Tuberculosis and Meningitis** have been summarized as follows:

NMR Structural Aspects in Leishmaniasis

The parasitic protozoan members of genus *Leishmania* are responsible for the most severe pathologies associated with visceral leishmaniasis (VL) in humans, caused by *Leishmania donovani* and *Leishmania infantum*. VL is an infection of the liver and spleen that can be fatal, which if untreated in time may cause morbidity with high rate of mortality.

Leishmaniasis occurs in approximately 90 tropical and subtropical countries around the world. It has been estimated that 12 million new cases of leishmaniasis occur each year worldwide, making it the second largest protozoal disease next to malaria. The situation in India is grave, particularly in eastern India (Bihar State) where an official estimate of more than 4,30,000 cases were reported between 1985-1996, although it is believed that the actual number of cases currently exceeds this figure by at least five folds. Recent trends indicate that there are 5,00,000 cases per year of visceral leishmaniasis, which occurs primarily in the Indian subcontinent.

It has been speculated that the increasing number of treatment failures in India might be due to the emergence of drug-resistant strains as the main cause of SAG unresponsiveness in Bihar. The mechanism of drug-resistance in kala-azar is still not well understood. Although several methods are currently employed for characterizing unresponsiveness in leishmaniasis, it is apparent that in-depth parasitological investigations and new approaches will be necessary to fully understand the exact extent of drug resistance in leishmaniasis. In addition to the current procedures, the utility of other bio-analytical techniques such as NMR spectroscopy in understanding the biochemistry of *Leishmania* has been explored in recent times.

In continuation to the earlier efforts, the present investigation has been undertaken with an objective of mapping important intracellular metabolites using ^{1}H NMR spectroscopy in the promastigote PCA extracts of six cultured strains of *L. donovani*. An attempt has been made to understand the metabolic information of the live Dd8 promastigotes (WHO reference strain) under different conditions, to arrive at any possible clues regarding the biochemical pathways in *L. donovani*.

^{1}H resonance signals occurring due to the presence of valine, lactate, alanine, arginine, citrulline, acetate, acetoacetate, glutamate, succinate, citrate, choline, α-glycerophosphorylcholine (α-GPC), betaine, mannose, tyrosine, phenyl alanine, formate, uracil, cytosine, guanine, adenine,

UTP/UDP, CTP, GTP, NAD/NADH and ATP/ADP were assigned in all promastigote PCA extracts. Further, ^{1}H resonance signals arising from the ribose sugars bound to uracil, cytosine, guanine and adenine, and in the forms of UTP/UDP, CTP, GTP, NAD/NADH, ATP/ADP (as nucleotides) were found to be highly abundant in all ^{1}H NMR spectra of the promastigote PCA extracts of the *L. donovani* strains. The chemical shift assignments of these nucleic acid bases and their sugars have been demonstrated for the first time using ^{1}H NMR in the PCA extracts of *L. donovani* promastigotes.

Presence of high-energy phosphate entities and nucleotides in *L. donovani* promastigotes has been established by performing ^{31}P NMR experiment for one of the strains (Dd8). Resonance signals arising from NTP, NDP, NMP (adenosine-, guanosine-, cytidine- and uridine- mono-, di-, and tri-phosphates), pentapolyphosphate, pyrophosphate, glycerophosphorylethanolamine, glycerophosphorylcholine, inorganic phosphate, phosphorylcholine, phosphorylethanolamine, 3-phosphoglycerate, glycerol 3-phosphate and glucose 6-phosphate could be assigned during the course of the present investigation. The present investigation using ^{1}H NMR analysis of the promastigote PCA extracts of six *L. donovani* strains has indicated that all the strains have undergone similar biochemical pathways, but with different metabolic activities.

To ascertain further the details of the metabolism in *L. donovani* promastigotes, NMR experiments were done on the live cells of Dd8 strain obtained at the stationary phase of their growth. The study was divided into two categories: in the first category the live Dd8 promastigotes were suspended in normal PBS without any nutrient and subjected to the NMR studies, and in the second category the parasites were incubated with $^{13}C_1$-glucose under different buffer conditions. For the second category, the conditions involved suspending the cells in normal PBS with $^{13}C_1$-glucose, followed by the incubation with $^{13}C_1$-glucose under hypoxic (anaerobic, N_2-bubbled) and normoxic (aerobic, O_2-bubbled) conditions.

Signals pertaining to ethanol, lactate, alanine, acetate, acetoacetate, succinate, and resonances pertaining to betaine and choline-containing compounds could be readily assigned for the cells maintained under starved conditions. Resonances of the aliphatic cytosolic amino acids such as valine, leucine and isoleucine could also be identified using 2D ^{1}H-^{1}H COSY spectrum. When the cells were maintained in normal PBS with $^{13}C_1$ glucose at 4°C, there was an increased production of acetate and succinate than the usually observed high levels of lactate as observed for the cells under starved conditions. The NMR-observable incorporation of ^{13}C-enrichment was

observed to be maximum for succinate and alanine, followed by a moderate labeling of glycerol-based intermediate and acetate, and a minimum labeling of lactate.

When the live Dd8 promastigotes were subjected to anaerobic and aerobic conditions with $^{13}C_1$ glucose available as the energy-source, signals pertaining to succinate, alanine and acetate were mainly observed. The ^{1}H NMR spectrum of the live Dd8 promastigotes maintained under anaerobic conditions showed a weak lactate signal after 45 min of incubation with $^{13}C_1$ glucose, which was not ^{13}C-labeled (in the C_3 position) as observed in the HSQC spectrum. The labeling pattern of the metabolites in live Dd8 promastigotes has given an indication that glucose was most likely converted via the Embden-Meyerhof-Parnas glycolytic pathway, with the associated conversion of pyruvate to succinate, alanine and acetate. This was further supported by the ^{31}P NMR performed on the promastigote PCA extract of the Dd8 strain, wherein many of the metabolic intermediates and high-energy phosphates of the proposed pathway could be observed.

The results have indicated that lactate production was different under different conditions; when starved, the promastigotes were found to use the endogenous reserve energy-source (possibly glycogen), producing high levels of lactate followed by acetate and ethanol (figs. 5a1-c2). When the promastigotes were provided an external energy-source in the form of $^{13}C_1$ glucose, utilization of the reserve energy-source decreased; the level of lactate was decreased, while the levels of succinate and acetate were pronounced. The weak ^{13}C-labeling of lactate indicated that the parasites (in normal PBS) had utilized the external energy-source and metabolized it partially to lactate; the majority of lactate was produced by the metabolic conversion of the reserve energy-source. The cells under anaerobic conditions relied on the reserve energy-source but to a lesser extent, which was accounted for the production of lactate; they predominantly utilized $^{13}C_1$-enriched glucose as the external energy-source, and thus produced the metabolic intermediates specifically succinate and acetate. Lastly, when the cells were maintained under aerobic conditions with $^{13}C_1$-glucose, they did not produce lactate and seemed to utilize only the $^{13}C_1$-enriched glucose and not the reserve energy-source. No NMR-observable lactate was produced by the cells under aerobic conditions, which seemed to justify that the cells met their energy demands mainly by the metabolic conversion of glucose via other biochemical pathways such as citric-acid cycle. These unique observations in *L. donovani* promastogites have indicated the possible existence of a reserve energy-source that might help the parasites for their survival under different conditions, and are to be explored further using other conventional biochemical techniques.

NMR Structural Aspects in Tuberculosis

TB still remains one of the foremost among infectious diseases in the world, which causes maximum death from a single microorganism. Approximately one third of the world's population has been infected with the causative organism *Mycobacterium tuberculosis* (MTB), eight million become sick with TB every year, and globally it accounts for almost 3 million deaths annually. Immunodeficiencies occurring under conditions of malnutrition, deterioration of general health or after the HIV infection have become responsible for an increase in the incidence of central nervous system TB.

India has been particularly hit by the dual threat of HIV and TB. Tuberculosis remains a serious public-health problem in India accounting for nearly one-third of the global burden, and it has been estimated that 3.5 million of the population are infected with TB. The re-emergence of TB is mainly due to the compromise of immune mechanisms, and particularly in HIV-infected individuals the risk is more. Not only do many developed countries face the gloomy scenario of increasing TB incidence, but also the problem of multi-drug-resistant TB that has emerged in several major urban centers of countries worldwide.

The most common clinical manifestation of tuberculosis is pulmonary disease. The extrapulmonary manifestation of tuberculosis, involving the central nervous system, is the most serious clinical manifestation of tuberculosis. Such involvement can include inflammation of the meninges (intracranial and intraspinal meningitis), as well as space-occupying lesions (tuberculomas) of the brain (cerebral or cord tuberculoma). In patients diagnosed with tuberculoma, surgery becomes essential to avoid mass effect and hydrocephalus.

Proper antitubercular treatment to patients suffering from tuberculoma of brain, if at all diagnosed by MRI, becomes an essential requirement, and ultimately in such cases the imaging modalities fail to differentiate whether it is a malignant, non-malignant or an infectious lesion. The diagnosis of tuberculomas is usually based on the characteristic histological features, which at times may overlap with other infective or non-infective granulomas, and the gold-standard culture method is very time-consuming and is often insensitive. As a result, there is an increasing requirement for the development of newer and additional diagnostic techniques for the CNS form of TB.

The lipid components of tuberculomas as well as the causative organism have a role in assisting differential diagnosis. Earlier work has revealed that one could fingerprint the membrane lipid components of *Mycobacterium tuberculosis* in the lipid extract of intracranial tuberculomas. In order to explore further the diagnostic utility of NMR, detailed ^{1}H, ^{13}C and ^{31}P NMR studies of the lipid extract of intracranial tuberculomas have been carried out in the present investigation. The main objective was to characterize various lipid structural components in tuberculoma and to look for any possible specific diagnostic markers that may aid in the differentiation of tuberculomas from the tumors of brain.

Glycerophosphatidylcholine and sphingomyelin were identified as the two major choline-containing phospholipids in the present study, while the ethanolamine phospholipids were identified to be glycerophosphatidylethanolamine and plasmalogen. Based on the ^{1}H, ^{13}C and ^{31}P NMR experiments, the following lipid components could be identified in the tuberculoma lipid extracts: phosphatidylcholines, phosphatidylethanolamines, sphingomyelin, plasmalogen, triglycerides, phosphatidylinositol, phosphatidylserine, phosphatidylglycerol, phosphatidic acid, cholesterol and cholesterol ester (as oleate). The ^{1}H and ^{13}C NMR assignments of fatty acid chains indicated that the lipids consisted of both mono-unsaturated and poly-unsaturated fatty acids, and have been identified to be oleic acid (18:1(n-9)), linoleic acid (18:2(n-6)) and possibly arachidonic acid (20:4(n-6)).

The semi-quantitative levels of the lipid components are of importance so as to differentiate a pathological condition from healthy or other diseased states as shown by the literature evidence. This task was carried out for the tuberculoma lipid extracts in the present study, by obtaining the ratios of arbitrary integral values of lipid components from their respective ^{1}H NMR spectra. The mean levels obtained for the methylenes/methyls ratio, methylenes/di-allylic methylenes ratio, methylenes/olefinic ratio, di-allylic methylenes/mono-allylic methylenes ratio, triglycerides/phospholipids ratio and cholesterol ester/cholesterol ratio were in accordance with the reported values observed in pathological states such as cancer. Based on the observations of the present study, it could be stated that the values obtained for methylenes/methyls ratio, triglycerides/phospholipids ratio, methylenes/di-allylic methylenes ratio, methylenes/olefinic ratio and cholesterol ester/cholesterol ratio may be of importance in differentiating tuberculomas from healthy or other pathological conditions of the brain.

The presence of ethanolamine plasmalogen in the tuberculoma lipid extracts, as observed during the course of the present investigation, may assume diagnostic significance, since literature evidence had indicated a possible role of choline plasmalogen in certain forms of tumors. While the exact role of ethanolamine plasmalogen in the disease process could not be elucidated during the present study, the relatively higher abundance of glycerophosphatidylcholine and glycerophosphatidylethanolamine, as seen in ^{1}H and ^{31}P NMR, may give an indication that the tuberculomas belong to the proliferative class and thus may mimic tumors.

The possible diagnostic value of ^{1}H NMR spectral assignments of human tuberculoma samples in the present study involved the assignments of cholesterol, cholesterol ester, phenolic glycolipids and plasmalogen. A comparative picture of cholesterol and its esterified form (identified as cholesterol oleate) in the ^{1}H NMR spectra of tuberculoma lipid extracts has indicated that the tuberculomas were of proliferative type with a relatively lower cholesterol ester/cholesterol ratio, and hence could be different from benign or low-grade tumors in which cholesterol ester has been reported to be absent.

The NMR investigations on tuberculoma lipid extracts have further highlighted the presence of phenolic glycolipids, besides cholesterol ester and ethanolamine plasmalogen. It could be reasoned that the granuloma formation by MTB infected macrophages in intracranial lesions might have resulted in the NMR observable levels of phenolic glycolipids that are constantly shed by the mycobacteria within the intracellular milieu of the host during infection. Phenolic glycolipids thus observed in the present study could be taken to represent the component of the cell wall of either living or dead mycobacteria in a granuloma.

The present study has brought out a speculation that the presence of cholesterol ester along with ethanolamine plasmalogen and phenolic glycolipids may aid in the identification of intracranial tuberculomas more authentically, and could thus differentiate them from the benign/malignant tumors of the brain. It is proposed that the presence of cholesterol ester is not only significant in case of proliferating tumors, but also in infective tuberculous granulomas of the brain. Since timely diagnosis after surgery and appropriate treatment is the cornerstone of management in intracranial tuberculomas, the present study has addressed the role of NMR as an additional diagnostic tool based on the analysis of lipid extracts.

NMR Structural Aspects in Meningitis

Meningitis is a severe acute infectious disease caused by several microorganisms, including viruses, bacteria, parasites and fungi, and is one of the most devastating infectious diseases of childhood in developing as well as in underdeveloped countries. Meningitis causes an intense headache, fever, loss of appetite, and intolerance to light and sound, rigidity of muscles especially those in the neck, and in severe cases convulsions, vomiting, and delirium finally leading to death if not properly diagnosed and treated. It is one of the major causes of childhood mortality, morbidity and disability.

The statistical features regarding the incidence of this disease are still alarming. Fatality rates associated with this disease can be as low as 2% in infants and children, and as high as 20-30% in neonates and adults. Despite the availability of several therapies, the three most common forms of meningitis, *viz*., bacterial meningitis, tuberculous meningitis and viral meningitis continue to be potentially fatal illnesses that can lead to death or permanent neurological sequelae in the child if not diagnosed at an early stage. The outcome of meningitis is strongly associated with the stage of disease presentation, with a 100% cure rate if proper diagnosis and treatment are given; otherwise it leads to 50% mortality or 80% permanent handicap. Unfortunately, because of limited economic resources and poor living conditions, many developing countries are still affected by the devastating consequences of this life-threatening systemic infection.

The cornerstone of management of meningitis in children depends on the rapid diagnosis and prompt treatment; however, the differential diagnosis of meningitis in children has been reported to be difficult due to various non-specific clinical features. Several new methodologies and techniques have been developed over the course of time such as the bromide partition test, lactate dehydrogenase assay, adenosine deaminase assay, IgG assay etc., but none has yet been stated to be a foolproof method. PCR, a relatively new technique for the diagnosis of TBM is also not foolproof, and is expensive for many developing countries. Besides all these techniques, the analysis of CSF often becomes crucial for the diagnosis of neurological disorders as the chemical components of CSF reflect the state of the CNS in healthy and diseased state.

Several reports exist in the literature, which highlight the potential role of NMR in understanding the metabolic profile of CSF under various pathological conditions. It has been well documented that NMR spectroscopy gives non-invasive, qualitative as well as quantitative information regarding the metabolic profile and usually a metabolite concentration of greater than

a few μM is detectable in the ^{1}H NMR spectra in a reasonable amount of time (^{1}H NMR; 128 scans; ca. 15 min). Taking into consideration the limitations of the currently available diagnostic techniques as well as the persistent problems regarding the timely diagnosis of childhood meningitis, the present investigation has been carried out to explore the possibility of ^{1}H NMR spectroscopy as an additional diagnostic tool based on the analysis of CSF from 191 cases.

During the present study, quantification of twelve well-separated and commonly observed CSF metabolites *viz*., *β*-hydroxybutyrate, lactate, alanine, acetate, acetone, acetoacetate, pyruvate, glutamine, citrate, creatine/creatinine, glucose (total) and urea was carried out using Bruker's NMRQUANT software with respect to a known concentration of sodium-3-(trimethylsilyl)-2,2,3,3-d_4-propionate (TSP), serving as an external reference. The assignment of urea in CSF is reported for the first time by NMR. The presence of cyclopropane observed for the first time in tuberculous meningitis overall in 85.1% of cases, acts as a fingerprint marker for the differential diagnosis. Multivariate discriminant function analysis was carried out for the proton MR-detected metabolite information and the clinical symptoms data of the meningitis and control cases to find out the important descriptors for classification, followed by a re-validation of the entire database. It was found the differentiation of control from the disease group could be successfully classified overall with a success rate of 96.4%, followed by the differential diagnosis of tuberculous meningitis with a corresponding value of 77.2%. Excluding the presence of cyclopropane, bacterial meningitis could be classified 84.4% correct and viral meningitis with a rate of 83.3%.

A new expert system MENEXSYS was developed using Microsoft Visual Basic 6.0 incorporating all the ^{1}H NMR quantitative information, and clinical symptoms data of 167 meningitis and 24 control cases. The discriminant function analysis-based weights/coefficients and the mid-point cut-off values obtained based on the multivariate analysis of the entire database of 191 cases have been incorporated in the software modules to make predictions of the 'disease type' in a new childhood meningitis patient case. The classification logic that would be responsible for any future prediction of the meningitis type has been divided into three phases as: (i). Differentiation of control (non-meningitis) from disease (meningitis) groups; (ii). Differentiation of TBM from the non-TBM cases, i.e., bacterial and viral meningitis; (iii). Differentiation of BM from VM cases.

The prediction possibility of the classification model was further checked with a 75/25 data split, by using 75% of the patients' data as training sets and the remaining 25% data as test sets, which revealed an overall improvement in the differential diagnosis of meningitis when important clinical and NMR descriptors were combined together and taken for the analysis. The purpose of developing MENEXSYS was to simplify the analysis for the differential diagnosis of meningitis besides making it very user-friendly in the form of an easy-to-use Graphical User Interface, as handling of the statistical software for multivariate analysis may become too technical and time-consuming. In conclusion, it is proposed that the NMR spectroscopic information along with other routine clinical features coupled in the form of an expert system MENEXSYS may serve as an additional diagnostic tool for the differential diagnosis of meningitis in children. It is hoped that the results obtained through MENEXSYS may supplement the results of other gold-standard methods.